Modèle de champ de phase pour l'étude de l'ébullition

Pierre Ruyer

THESE DE DOCTORAT DE L'ECOLE DOCTORALE DE L'ECOLE POLYTECHNIQUE

présentée par

Pierre RUYER

Ingénieur de l'Ecole Centrale de Lyon

Spécialité
Mécanique

Laboratoire d'accueil :

Commissariat à l'Energie Atomique
Direction de l'Energie Nucléaire
Département d'Etude des Réacteurs
Service de Simulation en THermohydraulique
Laboratoire de Modélisation et de Développements de Logiciels

Sujet :

Modèle de champ de phase pour l'étude de l'ébullition

Thèse dirigée par **M. Lev TRUSKINOVSKY**

Soutenue le 17 juillet 2006 devant le jury composé de :

M. Sergey GAVRILYUK, Université Aix-Marseille III	Rapporteur
M. Didier JAMET, CEA Grenoble	Ingénieur responsable
M. Samuel KOKH, CEA Saclay	Examinateur
M. Chaouqi MISBAH, Université Joseph Fourier Grenoble I	Rapporteur, Président
M. Mathis PLAPP, CNRS Ecole Polytechnique	Examinateur
M. Lev TRUSKINOVSKY, CNRS Ecole Polytechnique	Directeur de thèse

THESE DE DOCTORAT DE L'ECOLE DOCTORALE DE L'ECOLE POLYTECHNIQUE

présentée par

Pierre RUYER

Ingénieur de l'Ecole Centrale de Lyon

Spécialité
Mécanique

Laboratoire d'accueil :

Commissariat à l'Energie Atomique
Direction de l'Energie Nucléaire
Département d'Etude des Réacteurs
Service de Simulation en THermohydraulique
Laboratoire de Modélisation et de Développements de Logiciels

Sujet :

Modèle de champ de phase pour l'étude de l'ébullition

Thèse dirigée par **M. Lev TRUSKINOVSKY**

Soutenue le 17 juillet 2006 devant le jury composé de :

M. Sergey GAVRILYUK, Université Aix-Marseille III	Rapporteur
M. Didier JAMET, CEA Grenoble	Ingénieur responsable
M. Samuel KOKH, CEA Saclay	Examinateur
M. Chaouqi MISBAH, Université Joseph Fourier Grenoble I	Rapporteur, Président
M. Mathis PLAPP, CNRS Ecole Polytechnique	Examinateur
M. Lev TRUSKINOVSKY, CNRS Ecole Polytechnique	Directeur de thèse

Remerciements

Je tiens à remercier chaleureusement Monsieur Didier Jamet, ingénieur chercheur au C.E.A. et encadrant de ce travail. Ses grandes qualités scientifiques, pédagogiques et humaines m'ont apporté à la fois de nombreux enseignements, des conseils formateurs, une écoute patiente et disponible, et enfin un précieux soutien.

Je remercie également Monsieur Lev Truskinovsky, directeur de recherche au C.N.R.S. qui a assuré la direction de cette thèse. Sa rigueur et son exigence scientifique ont déterminé pour beaucoup l'orientation de ces travaux.

Je remercie particulièrement Monsieur Sergey Gavrilyuk, professeur à l'université Aix-Marseille, et Monsieur Chaouqi Misbah, professeur à l'université Joseph Fourier de Grenoble, d'avoir accepté de lire et de juger ce document en tant que rapporteurs. Je remercie également Monsieur Samuel Koch, ingénieur chercheur au C.E.A., et Monsieur Mathis Plapp chargé de recherche au C.N.R.S., pour leur participation au jury de cette thèse.

Ces travaux se sont déroulés au sein du Service de Simulation en Thermohydraulique au centre C.E.A. de Grenoble. Je remercie Messieurs Christian Chauliac et Bernard Faydide, chefs successifs de ce service, de m'avoir accueilli. Je remercie également Messieurs Fabien Boulanger et Frédéric Ducros, chefs successifs du laboratoire d'accueil, pour le soutien qu'il m'ont accordé depuis ma candidature jusqu'à ma soutenance.

Je remercie enfin toutes les personnes de l'équipe du C.E.A. Grenoble qui m'ont entouré pendant ces années de thèse. Merci aussi à Adrien Pesenti pour la collaboration qu'il apporté à ce travail lors d'un stage.

Contents

Notations

Latin letters

At	Atwood number
$\mathcal{A}$	numerical constant
c_P	specific heat capacity at constant pressure
C	constant ofintegration
e	specific internal energy
f	specific Helmholtz free energy
F	volumetric helmholtz free energy
Fr	Froude number
g	specific Gibbs free energy
G	volumetric Gibbs free energy
$\mathcal{G}$	modified pressure
$\mathscr{G}$	driving force
$\vec{g_0}$	gravity
h	specific enthalpy
h	interface thickness
$\mathcal{I}$	identity matrix
k	heat conductivity
k_x	wave number
$\mathcal{L}$	latent heat
$\mathscr{L}$	Lagrangean
L	lenght scale
$\mathbf{L}$	linear operator
M	matrix
$\vec{n}$	unitary vector along the normal to an interface
P	pressure
$\tilde{P}$	modified pressure
Pe	Peclet number
q	heat flux
r	radial coordinate
$\bar{r}$	non-dimensional coordinate
Re	Reynolds number
$\mathcal{R}_s$	Interface entropy production
s	specific entropy
St	Stefan number
t	time
T	temperature
v	specific volume
$\vec{V}$	velocity field
W	double well function
$\mathcal{W}$	rate of work
We	Weber number
(x, y, z)	cartesian coordinates
$\bar{x}$	non-dimensional abscissa

Greek letters

α	non-dimensional kinetic parameter
α_P	coefficient of thermal expansion
γ	non-dimensional number
Γ	mass transfer rate
δ	variation
$\tilde{\delta}$	variational derivative
ε	non-dimensional interface thickness
ϵ	parameter for the variation of the path
η	viscosity
θ	non-dimensional temperature difference
κ	mobility coefficient
λ	capillarity coefficient
Λ	linear operator
μ	thermodynamic potential
$\tilde{\mu}$	variational thermodynamic potential
ν	interpolation function
ξ	Lagrangean coordinate
Π	pressure level
ρ	density
σ	coefficient of surface tension
τ	stress tensor
φ	phase field variable
Φ	non-local dependence coefficient
χ_T	coefficient of isothermal compressibility
$\vec{\Psi}$	non-local dependence
ω	growth rate
Ω	volume

Introduction

Context

Boiling flows involve both two-phase fluid mechanics and phase change process. They are present in a vast variety of heat exchangers from micro-heat-pipes to large industrial facilities. The use of boiling fluids is motivated by the efficiency of the nucleate boiling regime to extract heat from a heated wall. Indeed, in boiling systems, in addition to the single phase sensible heat transport, the latent heat transport plays a major role. Moreover, the heat transfer process occurs at a quasi-constant temperature: the saturation temperature. In the nuclear industry, phase change process are of interest mainly in the study of potential accidental scenarii, where phenomena like the boiling crisis can occur. The improvement and control (mainly for safety reasons) of industrial facilities is constrained by the understanding of the boiling process. Both large scale mechanisms (averaged bubbly flow) and small scale mechanisms (at the scale of individual bubbles) play an important role in the boiling heat transfer process, *e.g.* Carey [28]. As a consequence, the study of the boiling process is scientifically challenging.

The study of industrial configurations requires the use of large scale analysis tools of the boiling process. The corresponding models are based on space and time averaged governing equations. As a consequence of this averaging procedure, the models must be supplemented by closure laws to be solved. These specific closure laws are generally based on experimental data. But these laws are often devoted to specific configurations and have a limited range of validity, which limits the accuracy and versatility of their use. There is thus a need of closure laws inherited from the study of the local scale phenomena. Experiments at the bubble scale are *(i)* complex to set-up and *(ii)* difficult to analyze because of the difficulty to get local measurements. The use of direct numerical simulation does not bear this latter limitation and is therefore a promising tool to get improved closure laws. Direct numerical simulation takes into account the whole spectrum of space and time scales. Its use is thus restricted by the computers' limitations to length scales of the order of magnitude of the centimeter and time scales of the order of magnitude of the second. As a consequence, it cannot be used directly for the study of industrial configurations. Nevertheless, it can be used to study bubble scale phenomena and then to develop validated larger scale models, for example dedicated to the boiling crisis.

Boiling crisis

The phenomenon Beyond a particular high value of the wall heat flux, called the critical heat flux, a transition of the boiling regime suddenly occurs: this is called the boiling crisis. This transition leads to a very fast and very large increase of the wall temperature. This increase can eventually lead to the melting of the wall: this is called the burnout. The physical mechanism at the origin of this transition is nowadays still not well understood. Its understanding is in itself an interesting scientific challenge. Moreover, its consequence, namely the burnout, can further lead to the destruction of the heat exchanger: boiling crisis must be thus avoided for safety reasons. In this study, we focus on this particular phenomenon of the boiling process.

Study of the boiling crisis There is a long history of the study of the boiling crisis and several attempts have been made to model its mechanisms. However, there is a lack of experimental evidence that could support any of these theories. More generally, there is a large number of experimental efforts that need to be pursued in order to have a clear understanding of the phenomenon, *e.g.* Sadavisan et al. [117]. In chapter 1, we study the current understanding of the boiling crisis and identify the major physical mechanisms potentially involved. It leads us to define a target problem to study: the possible transition in the bubble growth regime at high wall heat flux. According to the physical mechanisms involved in this process, numerical simulation is proposed as the most relevant tool. This intermediate conclusion motivates the developments made in the remainder of the study.

A diffuse interface model for the numerical study of the boiling flows at the bubble scale

The goal of this part of the study is to develop a model that can be used as a numerical method for the computation of boiling flows. The different numerical methods allowing the study of a bubble growth or more generally of liquid-vapor flows with phase change at the bubble scale are presented and analyzed in chapter 2. Most of the methods are based on the Gibbs theory of the interface: the interface is sharp, *i.e.* it is modeled as a surface of discontinuity. The difficulties of the computation of boiling flows are related to the management of the interface motion especially when phase change occurs. The methods based on diffuse interface models, for which the interface is viewed as a volumetric transition layer, propose a thermodynamically consistent setting of the computed governing equations, including the liquid-vapor interface dynamics. This induces numerical methods that are easier to handle since, contrarily to the methods based on sharp interface models, no particular treatment of the interface is required. However, the physical thickness of the interface transition layer is of the order of magnitude of the Ångströms as soon as the system is far from the critical conditions. As a consequence, the direct use of the diffuse interface models is irrelevant for simulations of mechanisms at the bubble scale. We thus turn our attention toward phase field methods. The thermodynamic model used in these methods is based on the introduction of an additional abstract variable or internal parameter, called the *phase field*, to describe multi-phase or multi-component systems, as introduced by Truskinovsky [136]. Existing phase field methods are mainly devoted to the study of solid-liquid or solid-solid phase transitions. They allow to deal with an artificial but thermodynamically consistent smearing of the interface. This latter property is attractive from both modeling and computational points of view. However, the review of the existing models shows that there is a need to derive a new formulation adapted to the study of the liquid-vapor transition.

In chapter 3, we first study the phase field thermodynamic model. We propose a constitutive form for the thermodynamic potential that allows to control both the diffuse interface description and the bulk phase physical properties. The structure of the interface for the planar and spherical symmetric two-phase equilibrium cases are studied in chapters 3 and 4. In particular, it is shown that the description of spherical inclusions is consistent with the Laplace theory. We then study dynamics and introduce dissipative processes in the model in chapter 5. We thus derive the thermodynamically consistent set of governing equations that includes the model for the interface dynamics. The set of governing equations is then studied in two theoretical configurations: the stability of homogeneous states (see chapter 6) and the one-dimensional steady state phase change process (see chapter 7). In particular, we study the equivalent sharp interface model and derive its kinetic relation that is a necessary closure relation, *e.g.* Truskinovsky [134]. The use of this formalism provides a clear interpretation of the sharp limit of phase field equations. Finally, in chapter 8, we present first computations and study the ability of the model to be used for the study of bubble growth dynamics.

Chapter 1

Study of nucleate wall boiling near boiling crisis conditions: Toward a gain in understanding

Introduction

Boiling crisis (BC) is an instability of the heat transfer process between a hot wall and a boiling fluid that leads to a sudden transition in the behavior of the boiling system. The consequences of this transition can lead to wall damages (burnout). The efficiency and design of industrial heat exchangers using boiling fluids (and in particular nuclear power plants for safety reasons) is therefore constrained by the fact that the BC phenomenon must not occur to prevent the destruction of the facility, should it be partial. Despite more than 70 years of study, the mechanism leading to the BC still remains obscure. Its understanding is important from an industrial point of view and scientifically challenging. This study proposes a review of the models and experimental observations concerning the mechanisms of the BC and aims at identifying some potential triggering instabilities in the pattern of the nucleate boiling regime near the BC conditions. The goal is to deduce from this study a target problem to solve (and some ways to study it) that could help improving the understanding of the BC phenomenon. This leads us naturally to the motivation of the numerical simulation of bubble growth and the subsequent development of a numerical method dedicated to it.

This chapter is organized as follows. In section 1.1, we briefly introduce the classical description of the different regimes of boiling heat transfer. The boiling crisis is defined as the departure (transition) from the nucleate boiling regime (DNB) that occurs at large heat flux and is associated to the drying of the heating surface. In the following, we therefore focus on this regime. In section 1.2, we distinguish three different length scales for the study of the nucleate boiling regime and define the main physical mechanisms associated to each length scale. The goal is to define a framework for the analysis of the boiling crisis phenomenon as being triggered by an instability that takes place at one of these length scales. In section 1.3, we establish the state of the art of the modeling of the boiling crisis. We introduce the Zuber correlation, which is one of the most efficient correlation to predict the DNB, and we establish the main open questions concerning the nature of the BC instability. In section 1.4, we briefly report some recent experimental results attesting the existence of a specific regime in the near-wall region close to the BC conditions. We then suggest a local interpretation of the Zuber correlation consistent with these recent direct observations. In section 1.5, we review the existing models for the boiling crisis that can be related to the local interpretation of the Zuber correlation and conclude on the necessity of pursuing the analysis of the instabilities of a bubble growing over a heated wall. Due to the nature of the equations describing such a bubble growth, simplifying models allowing analytical results can be viewed as too rigid and it appears as useful to study the whole system of governing equations using numerical simulations. This last statement constitutes the motivation for the developments presented in the remainder of this study.

1.1 The boiling regimes and the boiling crisis

In this section, we present the classical description of the boiling regimes and introduce the BC phenomenon as the transition between two different boiling regimes. This section reproduces classical considerations about boiling systems and is therefore devoted to readers unaware of these questions. A more detailed presentation of the boiling process can be found in [28] or in [45] among others.

This section is organized as follows. First, we introduce the different boiling regimes with the help of the classical representation of the Nukiyama curve (section 1.1.1). Then we describe more precisely the main characteristics of the different regimes by describing the different nature of the physical processes occurring in a near wall region (section 1.1.2).

1.1.1 The Nukiyama curve

Let us consider the heat transfer process from a heated solid to a boiling fluid. In 1934, Nukiyama [103] experimentally studied the heat transfer coefficient of the process for a pool configuration and first introduced its essential features including observation of the process instabilities. The pool boiling experimental set-up consists in a boiling fluid confined in a pool and therefore does not include any external mean flow. The heating solid is either a plane plate, a wire, a ribbon or one of the bounding wall of the pool. It is required that its dimensions exceed the characteristic dimension of the vapor inclusion (typical bubble radius) in order to ignore size effects. In the remainder of this study, we consider by default the pool boiling of pure fluids with an heated horizontal wall at the bottom of the pool as represented on figure 1.1. Let us introduce the amount of heat transmitted through the solid-fluid contact area q and the mean temperature $\langle T \rangle$ of the wall. There exists a typical value of the temperature at the liquid-vapor interface at thermodynamic equilibrium at the pressure P of the system, say $T_{sat}(P)$. This temperature is considered as reached asymptotically, *i.e.* sufficiently far from the heated wall. It appears as naturally relevant, since we describe boiling systems as a heat exchange process, to characterize the wall temperature by $\langle \Delta T \rangle \triangleq \langle T \rangle - T_{sat}(P)$ instead of $\langle T \rangle$; $\langle \Delta T \rangle$ is called the wall superheat. The heat transfer coefficient of the process reads $h_{boiling} = q/\langle \Delta T \rangle$. For a given system, the Nukiyama curve is a plot of the heat flux q as a function of the mean temperature $\langle \Delta T \rangle$. A typical Nukiyama curve is reproduced on figure 1.1.

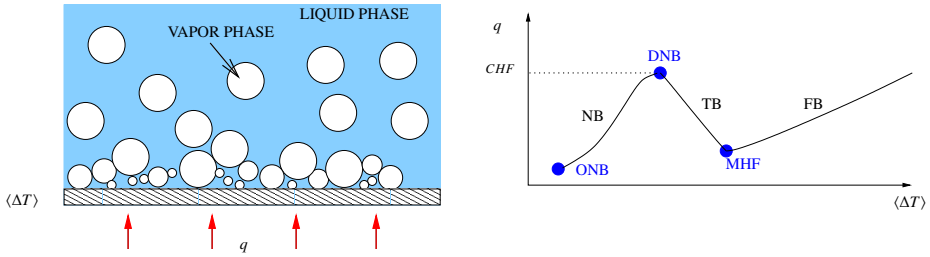

Figure 1.1: Nukiyama curve

Different portions of the curve, namely (NB), (TB), and (FB), allow to clearly identify three different boiling regimes. In the following we describe these different regimes.

Nucleate boiling regime (NB) The nucleate boiling regime corresponds to low wall superheats $\langle T \rangle$ and to a limited range of wall heat flux q. The lower limit in terms of both q and $\langle \Delta T \rangle$ is the onset of the boiling (ONB) and thus corresponds to the limit of the convective regime. ONB corresponds to a transition between the non-boiling and the boiling regimes. It is worth noting that the NB regime is a very efficient heat exchange mechanism since large amounts of heat can be extracted through a wall while keeping its temperature at low levels (*i.e.* of the order of magnitude of the saturation temperature of the boiling fluid). This explains the wide use of boiling fluids in heat exchangers. The limit of the NB regime associated to the high values of q is called departure from nucleate boiling (DNB) and corresponds to a transition between the different boiling regimes. The associated value for the heat flux is called the critical heat flux (CHF).

Film boiling regime (FB) If at DNB, the heat flux is increased above the CHF value, the system shifts to the film boiling regime (FB). The FB regime corresponds to high values of the wall superheat and to heat transfer

coefficients that are lower than in the NB regime. The transition from NB to FB is the boiling crisis BC of interest in this study. It is characterized by a very sudden and very large increase of the wall temperature. Typically the order of magnitude of this increase can reach several hundreds of Kelvin. This increase is at the origin of the potential burnout of the wall.

Transition boiling regime (TB) The lower limit of FB is characterized by the minimal heat flux (MHF) that corresponds to the transition to the third boiling regime, the transition boiling (TB). The domain of existence of TB joins the CHF and the MHF points and concerns intermediate values of wall temperature. For this regime, the local wall heat flux and/or temperature fluctuate violently around their mean values. For these reasons, TB is hard to characterize in itself and is often modeled as an unstable mix between the NB and FB regimes. It is worth noting that steady-state TB regime can be experimentally reached by imposing the wall temperature and not the heat flux. If the heat flux q is experimentally imposed, this regime is unstable and therefore unaccessible. We discuss this point in more details in section 1.1.3.

In the next section, we present more precisely the boiling process of the different regimes.

1.1.2 Vapor production and vapor release processes *versus* solid/fluid contact

In this section, we present how the regime distinction in terms of wall temperature and wall heat flux is related to different boiling flow patterns in the near wall region, where the major part of the vapor is generated. The denomination of the boiling regimes explicitly describes the corresponding near wall configuration. Figure 1.2 provides a schematic representation of near-wall boiling process for the different regimes.

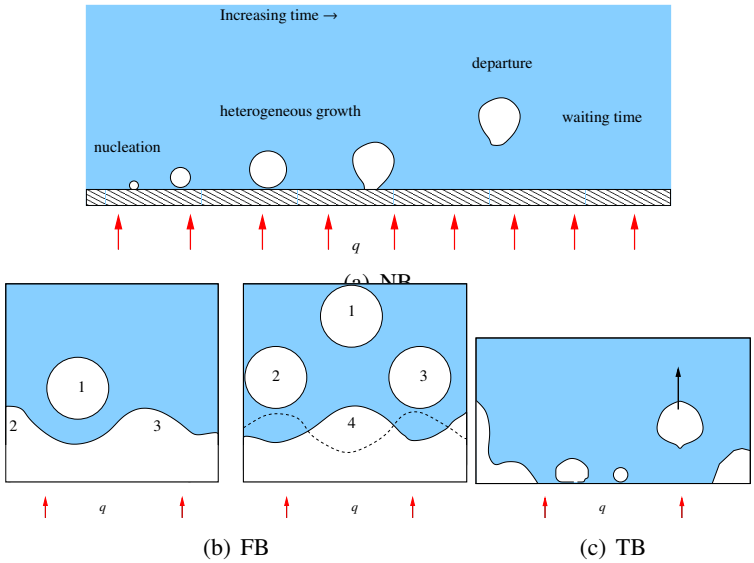

(b) FB (c) TB

Figure 1.2: Boiling regimes

NB regime The formation of the vapor bubbles in the NB regime is the result of successive nucleation events and consecutive heterogeneous bubble growth dynamics until the departure of the bubble from the wall. The major part of the wall is in contact with the liquid phase even if high void fractions can be reached right above the wall. As a consequence, the wall superheat is low (since liquid temperature cannot reach large superheats values). Due to the agitation associated with bubble growth and motion, the efficiency of the convective heat exchange is greatly enhanced with regard to a single-phase case. This basic picture of the NB regime is studied more precisely in the next sections where we focus on the large heat transfer regime.

FB regime In the FB regime, the wall is covered by a vapor film. At the liquid-vapor interface, a dynamic process of vapor generation and release occurs. Due to the Rayleigh Taylor instability (RTI), the surface of the vapor film is wavy and is the location of a cyclic process of bubble formation as represented on figure 1.2(b). The heat flux is transmitted from the wall to the liquid-vapor interface (whose temperature can be approximated by the saturation temperature) through a combination of radiative, conductive and convective transfers across the

vapor layer. The low value of the vapor thermal diffusivity (with regard to the liquid one), explains the higher wall temperature in the FB regime than in the NB regime.

TB regime At the MHF, while decreasing $\langle \Delta T \rangle$ and coming from the TB regime, the film configuration becomes unstable and locally breaks (*i.e.* locally some liquid comes into contact with the wall). As a consequence, wetted (covered by the liquid phase) area appears on the solid surface. In the transition boiling regime, the fluid/solid contact surface is the place of large and intermittent wetting and drying dynamics, *i.e.* it is covered alternatively by the liquid (wet) or the vapor (dry) phases. These hydrodynamic events are related to the large fluctuations of $\langle \Delta T \rangle$ and q.

Distinction of the boiling regimes in terms of the nature of wall-fluid contact As a consequence of their above classical descriptions, the main boiling regimes can be characterized by the ratio of the wetted solid/liquid area with the total wall surface. We can thus associate each regime transition (DNB and MHF) with a drying transition. DNB (and therefore BC) corresponds to the appearance of large dry areas whereas MHF corresponds to the collapse of a vapor film over the wall.

1.1.3 A few remarks about the boiling regimes and the boiling transition

In this section, we provide to the reader a set of remarks about the validity of the very general presentation of the boiling regimes made in the sections 1.1.1 and 1.1.2 using the pool boiling as a representation of a typical boiling system.

In the following, we consider several singularities of the pool-boiling configuration considered and discuss briefly their influence on the NB features. Most of the experimental facilities considered in the remainder of this study are built such that a steady-state uniform heat flux q is imposed at the wall. The influence of such an experimental set-up is discussed concerning

- ⋆ the wall temperature field,
- ⋆ the existence of the TB regime,
- ⋆ the fact that transient heat conditions are not taken into account,
- ⋆ and the neglect of the influence of more realistic characteristics of an industrial heat exchanger on the NB features (such that the heater orientation and geometry or the existence of a mean fluid flow, currently inside a loop)

Wall heat flux controlled and wall temperature In most of the experimental facilities considered, the heat flux q is imposed as being spatially and temporally constant. The boiling process takes place in the near wall region. On the one hand, the temperature at the liquid-vapor interface of a growing bubble is close to the equilibrium temperature $T_{sat}(P)$, this interface is locally in contact with the wall (at the so-called triple line region) where it imposes the temperature. On the other hand, in the surrounding liquid, and due to heat conduction, the temperature is larger than $T_{sat}(P)$. As a consequence, the wall temperature is neither uniform nor constant in time. This explains why we choose to introduce the notation $\langle \Delta T \rangle$ for the wall temperature thus explicitly referring to a mean (in space and time) temperature. Experimental data (*e.g.* [130]) show that the wall temperature in the NB regime can encounter large fluctuations (up to several tens of Kelvin near the BC conditions); this will be discussed in more details in section 1.4.

Transition Boiling regime When the heat flux is imposed, the TB regime is unstable and therefore unobservable. The boiling curve thus reduces to the two regimes of NB and FB, the transition from one regime to another being still defined by the same CHF and MHF points. Let us consider a cyclic (supposed quasi-steady for the sake of simplicity) in terms of evolution of the heat flux q where the maximum, resp. minimum, value say q_{max}, resp. q_{min}, is larger, resp. lower, than CHF, resp. MHF. The evolution of the system is typically a hysteresis phenomenon since the sequence over a period $q_{min} \rightarrow q_{max} \rightarrow q_{min}$ reads

- ⋆ NB regime on $q_{min} \rightarrow$ CHF

- ⋆ FB on CHF $\rightarrow q_{max}$ and $q_{max} \rightarrow$ MHF
- ⋆ NB on MHF $\rightarrow q_{min}$

It is worth noting that experiments of pool boiling with a controlled wall temperature can also be performed (*cf.* [44] or [7] whose experimental results are partially reported in section 1.4). In this case, the whole Nukiyama curve, including the TB regime is accessible. It is observed that the space and time variations of the temperature at the heater-fluid interface are rather small (of the order of $1K$ maximal) but that the corresponding space and time variations of the wall heat flux q can be very large.

Transient conditions The third point concerns the validity of the study of the BC mechanism for industrial situations. In an industrial situation, the heat flux is not necessarily steady and the BC condition is often reached under transient conditions. The value of the CHF should depend on the characteristic time of this transient. Let us note that the value of the transient CHF is classically considered as being larger than or equal to the steady-state value, *e.g.* [14]. The study of the CHF under transient conditions is not considered in this study. However, in the context of the heat exchange with a fluid that does not boil in the nominal condition (of interest for the targeted applications concerning the study of nuclear power plants safety), this tendency needs to be studied more carefully for very rapid transients as stated by Berthoud [14] and according to the results of the experimental study of Sakurai [118] briefly presented in section 1.3.4. In the following we will not consider such very rapid transients but only BC that may occur from less rapid transients, those latter conditions being quite relevant as well for many accidental situations in the study of nuclear power plants safety.

Industrial configuration In the industrial situation where the boiling system is a heat exchanger, the boiling fluid flows inside a loop and the heating element consists in one part of the loop. This situation is different from the pool boiling experimental facility. However, the two regimes of NB and FB are still observed, as well as the transition that takes place at the BC. The question that arises reads: Does the nature of the experimental facility have an influence on the BC? Experimentally the value of the CHF differs for different facilities. Nevertheless the mechanism leading to the BC is not necessarily different. Indeed if a similar BC mechanism is valid for any facility, the difference between the CHF values can be attributed to secondary effects of the facility on the NB process. The assumption of a single mechanism for the BC is made in the following and will be justified in more details in section 1.3.4. It is also interesting to mention that the geometry of the heating element as well as its orientation with respect to the gravitational direction have at least a parametric influence on all the phenomena considered. Nevertheless their influence is secondary since they are not considered as the primary parameters that are at the origin of the BC.

Concluding remarks We have briefly considered a few remarks concerning the *a priori* validity of the following developments. We have clarified the real nature of the variables q and $\langle T \rangle$ used to parameterize the boiling curve by specifying their meaning in two experimental configurations: wall heat flux or wall temperature controlled. Then we have mentioned that our study does not apply for very rapid transients conditions (such situation can also lead to BC and eventually corresponds to certain scenarii of accidents). Finally we have introduced the problematic of the existence of a single mechanism for the BC , *i.e.* that should not depend on the experimental configuration investigated. We assume that the BC mechanism corresponding to the pool-boiling configuration studied in the following corresponds to the mechanism in other configurations as well. This point will be justified in more details in section 1.3.4.

In the remainder of this study, we consider by default the pool boiling configuration with a horizontal plane heater and with a controlled heat flux q at steady state. The reader will be explicitly informed when other configurations are considered.

1.1.4 Conclusion on the presentation of the boiling regimes

The different boiling regimes, as well as the different transitions between these regimes, have been introduced from the classical representation of the heat exchange process between a hot wall and a boiling fluid. Then, we have described the near-wall process for the different regimes. We have identified the boiling crisis (BC) as being related to a drying transition at the wall. We have determined the validity of our study of the BC mechanism in

the particular pool boiling configuration by assuming a single (independent from the configuration) mechanism for the BC .

It is worth noting that, despite more than a half century of studies devoted to its understanding, the BC mechanism is nowadays still not well understood.

In the following, we reduce our attention to the study of the pool boiling at conditions near the BC, *i.e.* the NB regime at high heat flux.

1.2 Length scales and physical mechanisms

Let us first study the main physical mechanisms of the NB process at high heat fluxes. The goal of this study is to introduce the different physical mechanisms liable to the BC. To study these physical mechanisms, we first introduce three different length scales as determining three levels of description of the NB process. For each scale we then identify the major physical mechanisms that have been associated to a possible BC mechanism. We will then in section 1.3, on the basis of a review of the previous models for the BC, study the pertinence of considering these physical mechanism as being at the origin of the BC phenomenon.

This section is organized as follows. First in section 1.2.1, we introduce and motivate the classification of the NB mechanism according to three different length scales. Then in section 1.2.2, we present the first length scale denoted "two-phase flow" scale and that corresponds to the most idealized model for the NB process. In section 1.2.3, we study the "mean bubble growth" scale that corresponds to a more rich and more local description of the NB process with regard to the "two-phase flow" scale. We introduce the main physical mechanisms that are taken into account at this level of description. Finally, in section 1.2.4 we present the most precise level of description of the NB process that refers to the "local" length scale. We determine the main additional physical mechanisms considered at this scale with regard to the two other levels of description.

1.2.1 The three different scales

An exhaustive description of the NB mechanism in view of the study of the single BC mechanism At this stage, it seems important to expose the motivations for the exhaustive presentation of the NB mechanisms, whereas only the study of BC is targeted. This exhaustive presentation is justified by a currently recognized experimental observation: the value of the CHF is influenced by all the parameters of the NB process regardless the nature of this parameter (from the micro-structure of the wall to the intensity of the convective flow far above the wall), *e.g.* Sadavisan et al. [117]. Therefore, no physical phenomenon involved in the NB regime can be *a priori* disregarded to determine the potential instability mechanism related to the BC. It also means that some more precise information, than the above mentioned single knowledge of the influence of a parameter on the value of CHF, is required to conclude on the nature of the instability. Such a more precise information could lie, for example, on the knowledge of the sequence of events associated to the drying of the wall or on the analysis of successful correlation for the value of the CHF. We will indeed in section 1.4 study some recent experimental observations that provide a way to improve the actual understanding of the NB regime process at high heat flux and as a consequence can be used to determine the BC mechanism.

The classification of the mechanisms according to three levels of description In the following, we define three different levels of description of the NB process, each of this level being related to a different typical length scale for the bubble description. For each scale different physical mechanisms can be identified. Let us briefly introduce the different scales considered.

In the previous section, we have clearly distinguished the different regimes of the pool boiling by considering the process in a near wall region. The typical size of this region is of the order of magnitude of a few bubble diameters. This sets the bubble as the natural basic element of the NB process. The three different length scales can be defined from three different levels of modeling bubbles. At the first level of description, denoted "two-phase flow scale", (see section 1.2.2), the bubbles are considered as fixed in geometry and size. This is mainly relevant far from the wall, *i.e.* when the main part of the bubble growth is achieved. This level of description therefore ignores the bubble growth dynamics. At the second level of description, denoted "mean bubble growth scale", (see section 1.2.3), the bubble are considered as fixed in geometry but not in size. For instance the bubble is assimilated to a sphere whose size depends on time, the dynamics of bubble formation is therefore taken into

account. At the third level of description, denoted "local scale", (see section 1.2.4), both the geometry and size of the bubble are considered as time dependent. The dynamics of bubble formation is therefore described more precisely (with more degrees of freedom) than at the "mean bubble growth scale". An illustration of these three levels of description of the NB process is provided on figure 1.3.

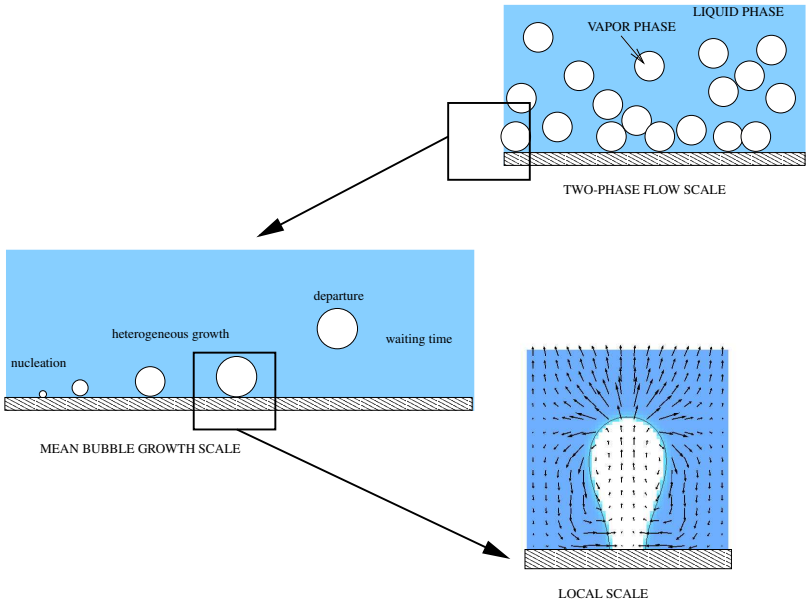

Figure 1.3: Three different levels of description, the "two-phase flow scale", the "mean bubble growth" scale and the "local scale"

In our attempt to identify a mechanism of instability in the NB process, the classification of the different mechanisms according to the scale they refer lies on a formal scale separation hypothesis. Let us note however that this scale separation is not inconsistent with the above mentioned sensitivity of the value of the CHF with all scales parameter.

This classification constitutes, to our own point of view, a gain in understanding for the analysis of the potential mechanism for the BC by allowing to provide a grouping of phenomena that could directly interact.

Sadavisan et al. [117] proposed an interesting study of the physical mechanisms that are relevant for the study of NB regime at high heat flux. The goal pursued by Sadavisan et al. [117] is to "*highlight specific areas on which [they] believe experimental efforts should focus to obtain improved mechanistic models of CHF*". The authors defined three categories related to three main "actors" of the nucleate pool boiling process, namely, the fluid, the heater, and the heater-fluid interface. In our own study of the physical mechanisms of the NB regime that are supposed to be related to the BC, we consider a similar set of mechanisms however with a different classification. The difference between these classifications lies on the goal pursued. The goal pursued in [117] is somewhat different from our goal since by considering the same set of actors of the NB process we indeed also try to identify the potential BC mechanism.

Let us consider one by one the different scales and the mechanisms of the NB related to the corresponding level of description.

1.2.2 Two-phase flow scale

This scale is the largest one in our classification and is associated to the most idealized level of the modeling of the NB process. The basic picture considers a population of bubbles coming from the wall and having constant size and geometry. Mean space and time frequencies of bubble emission are modeled. The rate of vapor incoming from the wall is related to the value of the wall heat flux q. It is worth noting that this scale does not actually "see" the wall. At this level, instability in the boiling process refers to a hydrodynamic instability in the two-phase flow generated by these bubbles as presented in section 1.3. This kind of large scale analysis of the boiling flows has been used for example by Zuber [157] to derive a correlation for the low heat transfer NB regime ("region of isolated bubbles" where bubbles do not interact with each other). At larger heat flux, bubbles become

so numerous that their interactions are no longer negligible. The large number of individual bubbles generated in the near wall region coalesce each other and somewhat form big masses of vapor flowing away from the wall. These big masses can be idealized by a somewhat continuous vapor channel, the vapor columns. The model of the two-phase flow far above the wall is therefore idealized by a counter-current flow of vapor inside these channels and of liquid around those columns. Since this large scale is only roughly considered in the following study of BC mechanisms, we deliberately do not describe more precisely the details of the two-phase flow formulation. The reader interested by this approach can refer to Carey [28].

1.2.3 "Mean bubble growth" scale

In this section, we study the physical mechanisms related to the level of description at the "mean bubble growth" scale. These physical mechanisms are potentially related to the mechanism of the BC itself, as it will be shown in the review of the BC models in section 1.3. The goal of this section is therefore to introduce these main mechanisms of the NB regime in view of this review.

Presentation of the scale At this scale, the near wall NB process is described in such a way that the bubble formation is evaluated through modeling. From the study of the bubble growth process, several heat-exchange mechanisms can be identified and evaluated. The global correlation $q = \mathrm{f}(\langle T \rangle)$ is then recovered by integration of these mechanisms. The influence of physical phenomena occurring in a near wall region (that were ignored at the "two-phase flow" scale) are therefore entering the model.

At this level of description the NB process is idealized as a set of sub-phenomena. The main one is the cyclic process of bubble formation near the heated wall. It is idealized by a sequence of events (nucleation, growth and departure). Each of these sub-phenomena have been the object of specific studies, either based on analytical models or on correlation issued from experimental observations. In the following we present the main sub-phenomena and provide to the reader interested the corresponding main references.

Description of the heat transfer process of the NB regime Let us consider the description of the global heat transfer process of the NB regime. The wall heat flux contributes to different sub-heat transfer mechanisms, the partition between these heat transfer mechanisms being a function of the wall heat flux, *e.g.* Dhir [45]. The most specific heat transfer mechanism of the boiling process is the latent heat transport which corresponds to the amount of heat necessary to create the bubbles that will flow outward the wall carrying this amount of heat. In addition to the latent heat transport, two different heat transfer processes can be identified. The first one is the classical convective heat transfer. It is worth noting that in absence of any mean convective flow (as in the pool boiling configuration) the fluid motion is essentiallly driven by the bubbles motion. The second one is specific of the NB regime and corresponds to a transient heat transfer mechanism associated to the process of bubble formation and departure. As the bubble leaves the wall, the thermal boundary layer that has formed above the wall is destroyed and colder liquid is brought into contact with the heated wall: the bubble motion in the near wall region acts as a pump that mixes hot liquid of the near wall thermal boundary layer with cold liquid far from the wall. This dynamics is at the origin of a transient heat conduction mechanism. Both latent heat transport and transient heat conduction are clearly related to the process of bubble formation. It is hard to actually determine the partition between these different heat transfer mechanisms. It is however classically assumed that at high heat fluxes NB regime the latent heat transport is dominant.

As a partial conclusion, the NB regime heat transfer process is mainly determined by the bubble growth dynamics. Let us now consider the idealization of this latter process at the "mean bubble growth scale".

The models for the bubble formation This bubble formation is considered as a sequence of events occurring at the wall. Let us first consider the model for the space location of the event of bubble formation.

Nucleation site density At least at low heat flux NB regime, the bubbles are experimentally observed as generated on preferential locations of the wall, the so-called nucleation sites. This phenomenon has been modeled through the definition of a nucleation site density, NSD, for a given wall. The surface of a given wall is characterized by a discrete set of cavities being of specific size and shape. Models for the activation as a nucleation site of a given size of shape of cavity can be found in Hibiki and Ishii [61]. NSD has also been studied

experimentally, *e.g.* the experimental study of Benjamin and Balakrishnan [12]. For a given wall, NSD is a function of the wall superheat (and as a consequence of the wall heat flux).

As a partial conclusion, the NSD characterizes the space location of the bubble formation events for a given wall heat flux.

The bubble formation cycle at a given nucleation site Bubble are thus considered as being generated from given locations. The cyclic process occurring at a given activated nucleation site is the following: the bubble first nucleate, then it grows and finally it departs from the wall, a delay exists between the departure of the bubble and the next nucleation event.

Let us first consider the models for the bubble growth. It is classically modeled as being made of two different stages, the growth being first inertially controlled and then thermally controlled, *e.g.* Mikic et al. [93]. During these stages, the bubble is idealized as having constant geometry, being first hemispherical (inertially controlled) and then spherical (thermally controlled). As a consequence the growing bubble is described with the help of a single parameter: its radius. In [93], the classical models for the growth rate for the two stages are derived that reduce to the time evolution of the bubble radius R. More complex models including the effect of a liquid micro-layer underneath the bubble on the thermally controlled stage have been later developed by Cooper and Lloyd [40] among others.

The end of the bubble growth process in the near wall region corresponds to the departure of the bubble. Classically the size of the bubble (its radius) at departure is modeled using a force balance[1]. The most classically and widely used model is due to Fritz [55] but let us also refer to the most recent review proposed by Thorncroft et al. [132]. It is worth noting that the departure of the bubble from the wall is thus classically modeled as independent from the growth dynamics.

As the bubble departs from the wall, there exists, at low heat flux at least, a delay before a new nucleation occurs, this delay is called the "waiting time", *e.g.* the model of the NB regime proposed by Kolev [79]. This waiting time enters the whole bubble formation cycle such that together with the bubble growth rate and the size at departure, the frequency of bubble emission from a given activated site is defined. Together with the NSD, we therefore have a complete description of the bubble formation process of the NB regime.

Interaction between bubble formations process at neighboring sites Let us note that the previously described bubble growth formation mechanisms are valid as long as each nucleation site can be considered as isolated from its surrounding. The interaction between sites has been also investigated, *e.g.* the interesting experimental work of Zhang and Shoji [154]. The interaction can be considered as being of three types: thermal, hydrodynamic, or coalescence. The relative effect and its nature (as being either promotive or inhibitive) of each interaction on the bubble departure frequency depends on the spacing between the sites as well as on the wall heat flux. However let us note that too little is known on these interactions at high heat fluxes.

Conclusion on the main physical phenomena of the description of the NB regime at the "mean bubble growth" scale The list of table 1.1 summarizes the main physical phenomena associated to the "mean bubble growth" scale. From all these "sub"-models it then possible to model the whole NB heat transfer, as it has been done for example by He et al. [60].

As a partial conclusion, we have introduced the main physical mechanisms corresponding to the description of the NB regime at the "mean bubble growth" scale. The bubble formation cycle has been shown to be the key phenomenon of the NB regime process at this level of description. The corresponding models for the bubble growth and dynamics are however still rigid since the bubbles are described as being either spherical or hemispherical. As a consequence, the models at the "mean bubble growth" scale do not bear the ability to describe a spreading of the bubble. We will refer in the following to these bubbles as "regular" bubbles. *A priori*, none of the mechanisms determining the NB regime can be disregarded as being at the origin of the BC.

[1]Let us mention the interesting attempt of Buyevich and Webbon [22] to introduce less rigid description of the bubble shape (two parameters, namely bubble volume and wall contact area of the bubble foot, instead of the single bubble radius in the classical models) to evaluate the bubble growth dynamics. The model studied is very interesting since it includes the departure mechanism as a fully consistent part of the whole bubble growth process. Due to its ability to consider a time evolution of the geometry of the bubble, this model is in fact at the boundary between the "mean bubble growth" scale and the "local" scale. In this model, the surface tension is shown to promote the departure of the bubble. There still exists an open debate about the role of surface tension as either promoting or impeding the departure *e.g.* [45]. Let us note that numerical simulations appear as a possible relevant tool for improving this understanding.

1. partition of the wall heat flux between different heat transfer processes
   (a) latent heat transport (evaporation) (eventually two parts around bubble and micro-layer contribution)
   (b) transient conduction
   (c) natural convection
2. spatial frequency of the bubble formation process, the nucleation site density NSD, NSD($\langle T \rangle$)
3. bubble growth rate
4. bubble departure size
5. waiting time
6. bubble interactions: thermal, hydrodynamic, and coalescence

Table 1.1: Physical mechanisms at the "mean bubble growth" scale

It is worth noting that from all these mechanisms, it is possible to imagine a variety of possible events leading to the BC mechanisms. The review of the corresponding models is provided in section 1.3.

1.2.4 Local bubble description

The previous level of description at the "mean bubble growth" scale describes the bubble growth on an idealized way which is relevant for the description of the mean bubble formation process at least at low heat flux NB regime. However, as it is shown in the section 1.4, at the high heat fluxes NB regime, there exists a population of bubbles whose behavior is apparently very different from this regular behavior: these bubbles are more spread over the wall before their departure. This irregular bubble dynamics will be shown to be potentially related with the BC event, and is therefore of interest in this study. The model of NB process at the "mean bubble" scale is too rigid to describe such a behavior (according to the fact that the bubble shape is imposed to be either spherical or hemispherical). We must therefore consider a smaller level of modeling of the NB process. The present level of description takes into account the fully time and space dependent bubble shape. It is worth noting that the amount of modeling is therefore quasi-vanishing since we now consider the full set of non-isothermal Navier-Stokes equations and interface jump conditions (*cf.* our presentation of the interface jump conditions in the appendix A.2). In the list 1.2, we consider the main physical mechanisms that are taken into account at this "local" scale in addition to the physical mechanisms considered at the "mean bubble growth scale" and provide some references. To take into account the whole set of mechanisms and the complex time dependent geometry of the bubble at this level of description, it is required to use numerical methods. Several numerical simulations of bubble growth dynamics using different numerical methods can be found in the literature, *e.g.* Son et al. [128] for the level-set method, Welch and Wilson [147] for the VOF method, Juric and Tryggvason [69] for the front tracking method (the application proposed in the two latter mentionned article only concern the FB regime), Yang et al. [151] for Lattice-Boltzmann model based numerical method or Fouillet and Jamet [54] for diffuse interface model based numerical method.

As a partial conclusion, in order to describe certain features of the NB regime at high heat fluxes, it is necessary to consider the full problem of the bubble growth as having time dependent geometry.

1.2.5 Conclusion on the analysis of the different mechanisms related to NB regime near BC conditions

In this section we have studied the main physical mechanisms of the NB mechanisms in view of the determination of the BC mechanism.

1. Local curvature of the bubble and capillary forces
2. Pressure recoil at the interface: the jump in pressure $[\![P]\!] = -\Gamma^2[\![1/\rho]\!]$ where Γ is the local mass transfer rate (*cf.* our study of the jump conditions in appendix A.2)
3. Triple line dynamics (static-dynamic contact angle) and associated quasi-singular heat transfer (*cf.* Anderson and Davis [3] or Mathieu et al. [92])
4. Gravity: effect of the hydrostatic pressure gradient on the bubble shape and consequently on its departure dynamics (*cf.* Shikhmurzaev [125] whose model considers the time dependent shape of the bubble and also includes a model for the contact line dynamics)
5. Local heat conduction problem inside the area of contact between wall and vapor at the dry foot of a bubble (*cf.* Blum et al. [16])

Table 1.2: Physical mechanisms at the local scale

To do, we have first introduced a classification of the different mechanism according to different levels of descriptions of the NB regime process. At the largest scale, the "two-phase flow scale", the near wall process are not considered but rather the mean bubbly flow above it. At the "mean bubble growth" scale, the NB process is described as a sum of bubble growth events. Each bubble growth event is described with the help of semi-rigid models allowing to consider the time dependent size of the bubble. The physical mechanisms corresponding to this level of description are summarized on table 1.1. However, this level of description is not sufficient in order to describe some irregular bubble growth events that could be associated with the BC mechanism. To describe these irregular bubbles it is required to use the level of description at the "local" scale. At this scale of analysis, the whole set of Navier-Stokes equations as well as the interface jump conditions are considered. As a consequence, additional physical mechanisms can be taken into account in the model of the bubble growth and therefore explain the irregular bubble growth. These physical mechanisms are summarized on table 1.2.

Now that the main physical mechanisms of the NB regime have been introduced, it is possible to consider the different models for the BC mechanisms.

1.3 Models of the boiling crisis mechanism

Introduction

The question about the BC that arises from our presentation of the physical mechanisms at different scales is the following: At which scale does the triggering mechanisms of the DNB[2] transition take place ? However, other open issues about the nature of the BC phenomenon can be identified. They are briefly discussed in the last part of this section.

In this section we study the different models that have been proposed to explain the mechanism of the BC. The goal is to provide, through the analysis of these models, an analysis of the potential mechanisms for the boiling crisis. This analysis will help us to justify the fact we disregard some mechanisms as being actors of the BC and finally redirect our investigation on a specific scale. We therefore deliberately report the extended field of research devoted to the study of the BC mechanism.

The different models for the BC are grouped according to the scale to which belong the physical mechanism considered as being at the origin of the BC. Our presentation is not exhaustive but deliberately contains a large amount of information and illustrates the wide range of possible mechanisms for the BC. This analysis will then be used to determine what we believe to be the most relevant elementary target problem. Our main goal is thus not to present each model in detail but rather to identify, for each model, what are the main NB mechanisms considered as being at the origin of the BC. The reader interested on a specific model can refer to the references

[2]It is worth noting that whatever the initial scale of the mechanism its consequences have an influence mainly on the near-wall process where it leads to a total dry-out.

provided for each model or on more general articles that propose a review of the BC modeling like [45] or [74] among others.

This section is organized as follows. First in section 1.3.1 we present and analyze the Zuber's model and its consequent correlation for the CHF. Then in section 1.3.2 we present the BC mechanisms related to the NB mechanisms considered at the "mean bubble growth" scale (*cf.* their presentation in section 1.2.3). In section 1.3.3 we present the model for the BC mechanism that require the more precise level of description of the NB regime related to the "local" scale. Finally in section 1.3.4, from the analyze of all these models, we determine our motivation to investigate more precisely the BC mechanisms related to the "local" scale and propose the analyze of some experimental results (provided in section 1.4) as a way to gain in understanding of the NB regime at high heat fluxes.

1.3.1 Boiling crisis' mechanisms at the "two-phase flow" scale: the hydrodynamic theory and the Zuber's correlation

In this section, we study the hydrodynamic theory, that is, to our knowledge, the only mechanism for the boiling crisis that considers that the mechanism of the BC takes place at the "two-phase flow" scale defined in section 1.2.2.

In a first part, we present the main lines of the hydrodynamic theory developed by Zuber [156] including the idealization of the NB process and of the BC phenomenon. It leads us to introduce the Zuber's correlation (1958) which is still today one of the most efficient predictive correlation for the CHF. In a second part, we show that the hydrodynamic model for the BC is not attested experimentally. In a third part, we draw our own conclusions about the interpretation of the Zuber's results.

The Zuber model and the Kutateladze correlation Zuber [156] proposed a model of the NB process at high heat flux that allows to derive a correlation for the CHF[3]. Experimental observation of the NB process at high heat flux in pool boiling indicates that, above the wall, a large amount of vapor almost covers the surface. It is worth noting that in the original context "covers the surface" meant covers the wall; in section 1.4, we analyze at which level of description this picture is actually relevant. Such a large amount of vapor is modeled by Zuber as a continuum of vapor, say a film. Vapor bubbles escape from the film and flows in the pool away from the wall. The Rayleigh-Taylor instability (RTI) is relevantly supposed to describe dynamics of the upper surface of the vapor film. The typical size of the bubbles is assumed to equal the most unstable wavelength of the RTI, say λ_{RTI}. The flow made of the train of bubbles thus created is idealized by a net of discrete vertical channels, called columns. Such a representation of the NB process is reproduced on figure 1.4. The characteristic scale of these columns and of their spacing is supposed to be λ_{RTI} (λ_0 on the figure). Each column, as an idealization of the train of bubbles, is idealized as a vapor jet bearing a wavy surface, the wave number being given by the characteristic bubble size λ_{RTI}. The vapor flows across a liquid which, because of the density contrast, is supposed to be at rest. The wavy liquid-vapor interface is subject to the Kelvin-Helmholtz instability. Therefore there exists a critical vapor flow rate for which the wave destabilizes. This two-phase flow instability corresponds to the limit of validity of the (idealized picture of the) NB process and is associated to the BC. For higher mass flow rates than the critical one, the NB process can no longer be sustained. Since the vapor flow rate is obviously related to the wall heat flux, it allows to determine the value of the CHF. The model does consider that the wall heat flux is totally transmitted to the fluid through latent heat transport (*i.e.* formation of vapor), which appears in fact as a good approximation for the NB regime at high heat flux[4]. The resulting expression for the CHF reads

$$q_{CHF\,Zuber} = \frac{\pi}{24}\mathcal{L}\rho_v \sqrt[4]{\frac{\sigma g(\rho_l-\rho_v)}{\rho_v^2}}\sqrt{\frac{\rho_l+\rho_v}{\rho_l}} \tag{1.1}$$

where $\mathcal{L}$ is the latent heat of evaporation, σ the surface tension coefficient, ρ the density of the phases denoted $_v$ for the vapor and $_l$ for the liquid, and g the gravity. The present writing of the Zuber formula is dimensional, but it seems justified to present it in this form since it corresponds, to our knowledge, to the most widely used one.

[3] It is worth noting that, using a model of the NB process, Zuber recovered the results derived initially by Kutateladze [82] using a non-dimensional analysis.

[4] This does mean that, in this model, the wall-fluid thermal interaction is not considered as a limiting mechanism of the NB process.

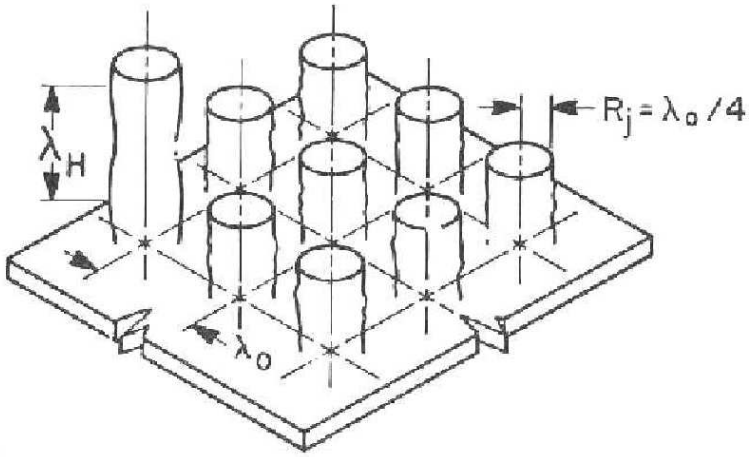

Figure 1.4: Schematic representation of the NB process in Zuber's model for the BC

This model is called the hydrodynamic model and has been, thereafter, improved and adapted to include a dependence on parameters that do not appear in the original formula (for example the shape and orientation of the heater, the static wetting properties of the fluid on the heater ...). For a more detailed presentation on these improvements of the initial Zuber's model, the interested reader can refer to the work of Moissis and Berenson [95] or of Lienhard and Dhir [87, 86].

It is worth noting that the Zuber formula, despite its simple expression, provides a good predictive tool for the value of the CHF in many different situations. Zuber's correlation is most often retained in classical presentations of the CHF. This correlation is one of the most important gain in the analysis of the BC because of the efficiency of such a simple expression as a predictive tool (with regard to the number of physical mechanisms of the NB regime). Indeed, it allows to identify the main key physical mechanisms that play a role in the instability of the NB regime. This formula is analyzed in this sense in section 1.4.2.

An unrecognized two-phase flow instability Despite the wide use and attested efficiency of the Zuber correlation, scepticism exists about the validity of the Zuber model to describe the real process of the BC phenomenon. Experimental observations (such as those reported by Chung and No [37], for instance that are presented in section 1.4) more accurate than the ones Zuber had at his disposal when he developed his model[5], do not provide any experimental evidence of any instability in the bubbly two-phase flow at BC conditions far from the very near wall region.

Katto and Otokuni [75] performed experiments that simulate the bubbly vapor flow above the wall in high heat flux NB regime using discharges of air. No abrupt change is observed in the two-phase flow pattern with air, even though the velocity of the air coming out from the wall is "*increased considerably beyond the magnitude corresponding to CHF condition*". The authors concluded that there should not be any hydrodynamic instability of the escaping vapor flow at the origin of the BC.

In a report on the actual observations concerning the boiling crisis in sub-cooled[6] flow boiling, Celata et al. [31] reported "*no evidence of a macroscopic change of the bulk flow pattern if the boiling crisis occurs*".

As a conclusion, there is no experimental evidence of the two-phase flow instability predicted by Zuber (or any other one) at CHF conditions. As a consequence, we disregard in the following of this study the hypothesis of a BC mechanism at the "two-phase flow" scale.

Conclusion In this section we have studied the hydrodynamic theory for the mechanism of the BC with the help of the Zuber model. This model considers that the mechanism of the BC takes place at the "two-phase flow" scale. We have briefly describe the main hypothesis used by Zuber in order to deduce the Kutateladze formula from a schematic representation of the NB two-phase flow. We have outlined the efficiency of the Zuber

[5]Namely the work of Westwater and Santangelo [148]. It appears clearly in this article that the information about the near-wall processes of the NB regime at high heat fluxes was still poor compared to the experimental observations we now have at our disposal.

[6]Sub-cooled refers to the fact that the mean temperature of the convective flow is below the saturation temperature.

correlation as a predictive tool for the CHF. According to the above statements, it is worth noting that the Zuber correlation allows to predict the value CHF very well even though the pre-supposed mechanism used to justify the formula is inconsistent with experimental observations. In the following, we therefore consider that the BC mechanism is not associated to any two-phase flow instability at the "two-phase flow" scale. The main question suggested by these statements is the following: How can Zuber's formula catch the correct scaling of the CHF, *i.e.* of an instability whose nature is different from the large scale instability from which his formula has been initially derived?

We present in section 1.4 an interpretation of the Zuber formula at the local scale that could answer this question.

1.3.2 Boiling crisis' mechanisms at the "mean bubble growth" scale

In this section, we present a few models that consider mechanisms occurring at the "mean bubble growth" scale as being at the origin of the BC.

A large number of models for the BC that are related to this scale exist in the literature; however some of them are only different versions of the same original idea. In this section, we provide to the reader one example of each main family of models since it is sufficient in order to analyze the pertinence of the BC mechanism considered. For another review of models at this scale, let us refer to Celata [30] that includes the description of other models of a given family than the one described in the following. Celata [30] retained mainly three categories of models, namely

1. The vapor removal limit and the near-wall bubbles crowding theory: turbulent motion of individual bubbles and high density of bubbles in a near wall region become so important near the BC conditions that liquid can supposedly no longer reach the wall, leading to its dry-out.

2. Liquid sublayer dry-out model: As a thin vapor blanket (elongated bubble) flows over the wall, the liquid trapped between the wall and the bubble evaporates. For sufficiently high heat flux, *i.e.* at BC conditions, the liquid disappears leading to the dry-out of the film.

3. Super-heated layer vapor replenishment model: this model is only devoted to boiling systems where a sub-cooled convective flow exists. In this case, there exists a layer above the wall of a given thickness where vapor bubbles can exist (because of the sub-cooling far above the wall), the so-called super-heated layer. The vapor generated at the wall accumulates in a big bubble inside this layer. BC occurs when the vapor generation is so high that this bubble reaches the wall.

To our point of view, the following list does not consider the whole set of relevant models for the BC at this "mean bubble growth" scale. In the following, we present also some (often more recent than the review proposed in [30]) models related to other categories of models for the BC mechanism.

BC mechanism based on a critical NSD, illustration of the near-wall bubble crowding theory Ha and No [59, 58] proposed a phenomenological model for the dry-out of the wall at high heat flux NB (and subsequently for the BC) based on the limited liquid resupply of the near wall region due to the increasing nucleation site density (NSD). This limitation is due to a local accumulation of vapor bubbles that limits the liquid feeding of the zone and therefore induces a local dryness of the wall. The authors consider a statistical distribution of nucleation sites and model the activation of each site. They introduce a maximum value for the number of activated sites on a given sub-area of the heater that induces a local dryness and therefore a limitation of the wall heat flux possibly extracted. As a consequence, the efficiency of the NB regime is limited at high heat fluxes and there exists a maximum heat flux that the regime can extract from the wall, the CHF.

The limitation of the liquid resupply in the very near wall region is often called upon to explain the drying transition that occurs at the BC. If apparently intuitive, there exists, to our knowledge, no experimental evidence of this phenomenon. Moreover, as it will be shown in section 1.4, there already exists, at heat flux lower than the value of the CHF, a very large accumulation of vapor above the wall, that obviously does not prevent the liquid to reach the wall[7]. Moreover local precursor drying events observed in [130] before the CHF is reached occur

[7]Let us note that due to the large density difference between vapor and liquid it is hard to experimentally visualize the path of the liquid through a bubble layer. However, since the wall will be shown to be still wet even when a large accumulation of bubbles exists above the wall, the liquid is always able to flow across this layer downward the wall.

preferentially in regions previously not populated with active bubble sites.

As a partial conclusion, the origin of a local dryness associated with a critical local value of the NSD is not attested experimentally. To our point of view, the phenomenological mechanisms based on a drying transition initiated by a critical value for the NSD are questionable because inconsistent with the experimental observations reported in [130].

BC mechanism based on a critical coalescence Bang et al. [9] proposed a model that can be linked up with the family of ideas mentioned by Celata [30] and reported in the introduction of the present section. According to Bang et al. [9], coalescence phenomena in a very near wall region increase with the heat flux and cause local dryness of the heater at sufficiently high heat flux. The presence of a large vapor bubble over the wall is supposed to hinder significantly the liquid flow toward the wall. The combination of these two effects leads to the existence of a critical value for the heat flux at which the heater dries out.

Even if NSD is not called upon for this mechanism, the main idea is a bit similar to the model of Ha and No [59] discussed previously. In the model of Bang et al. [9] the coalescence is said to promote local dryness of the wall. The effect of coalescence on the dryness of the wall is in itself an open question: either, as for example Bang et al. [9] proposes, it promotes the dryness by promoting the existence of large vapor masses in a near wall region, or, as for example Zhao et al. [155] proposes (see in section 1.3.3 the presentation of the corresponding model), it promotes the departure of this larger vapor mass (with regard to the initial bubble size) and as a consequence impedes wall dryness. Too little is known concerning the effect of coalescence on the dryness of the wall. Nevertheless, according once again to the experimental results reported in [130], the local dryness of the wall is associated to an irregular bubble growth event which is independent of any coalescence event (because it occurs preferentially in regions not previously populated by bubbles).

As a partial conclusion, the initiation of a local dryness of the wall associated to either bubble coalescence or accumulation of bubbles is questionable, because not attested experimentally.

BC mechanism based on an instability of the bubbles flowing in the liquid This model is contemporary of the Zuber' s model. Chang [32] studied the stability of the NB regime, by considering that the heat transfer is limited by a maximum rate of bubbles generated per unit area. The latent heat transport is assumed as the dominant heat transfer mode. The instability of the bubbles is related to the stability of a plane interface (Helmholtz stability). Such an instable bubble is said to break up into several smaller bubbles of various size. The dry-out of the wall is then postulated to be related to the fact that, when this instability occurs near the heater, small bubbles will partially flow toward the heater and cover it.

The author performed a force balance on a growing bubble to determine its characteristic size at departure, say R. A critical velocity (Helmholtz stability) for the bubbles flowing in the liquid is determined using the postulate that the surface tension force ($\simeq \sigma R$ where σ is the surface tension coefficient) stabilizes the bubble while the dynamic force ($\rho V^2 R^2$ where V is the "*resultant velocity at which the liquid pushes the bubble*", that is evaluated differently by the author according to the intensity of the convective flow) destabilizes it. From these considerations, it is possible to estimate the critical heat flux corresponding to the triggering of this instability. It is interesting to note that the author recovered exactly the same formula as Zuber (*i.e.* as Kutateladze *cf.* equation (1.1)). We discuss this remark in section 1.4.2.

Nevertheless such a bubble instability in a near wall region has never been, to our knowledge, observed experimentally. As a consequence, this mechanism for the BC is not, to our point of view, considered as realistic and is therefore disregarded in the following of this study.

BC mechanism based on a limitation of the NB heat transfer mode Kolev [79] considered an original phenomenological model of the pool boiling NB regime based on the idea that the heat transfer is related to the turbulence induced by bubble growth and departure in a near wall boundary layer. The turbulent length scale is assumed to be of the order of the RTI wavelength, λ_{RTI}. The author derived a model for the NB heat transfer process, *i.e.* the relation $q(\langle T \rangle)$ between the wall heat flux q and the wall temperature $\langle T \rangle$. The other ingredients of this model are more common and include classical models for the NSD, bubble growth rate, bubble departure size, and a waiting time (time between departure of a bubble from a given nucleation site and next nucleation event). From these models, the author derives the expression for $q(\langle T \rangle)$, that has a maximum value for q, associated to the CHF. Let us now consider the mechanism for this limitation of the NB regime at high heat

fluxes. The mechanism identified by the author for this limitation reads as follows: as the wall temperature $\langle T \rangle$ increases, the NSD increases sharply that leads to a decrease of both the size and time of the bubbles at departure. More comprehensively, it can be shown from an analysis of the correlation $q(\langle T \rangle)$ obtained that this limitation of the NB regime efficiency is associated to a sharp increase, at high wall temperature, of the ratio of the waiting time with the growth time at a given site. Indeed, this sharp increase yields that the bubble production rate at a given site is limited. While we suppose that the waiting time is always negligible with regard to the growth time, the limitation disappear.

The experimental results of Theofanous et al. [130] do not attest the existence of such a limiting effect of a waiting time for the bubble formation at high heat flux NB process. It is indeed observed that the bubble emission frequency at a given site monotonously increase with the heat flux even in conditions near the CHF. As a consequence, even though the model of Kolev [79] actually allows to predict well the NB process, the mechanism associated to its limitation at high heat flux (that is associated to the BC by the author) is not attested experimentally and will be in the following disregarded.

Partial conclusion on the study of the BC mechanisms at the "mean bubble growth" scale We have studied the main families of models for the BC mechanism inherited from a description of the NB regime at the "mean bubble growth" scale. It has been shown that the phenomenological BC mechanisms proposed at this level of description cannot be attested experimentally. Moreover, they are contradictory with the experimental results of Theofanous et al. [130]. As a main consequence, it appears as essential to pursue the experimental observation of the BC phenomenon in order to attest the pertinence of these models.. As a consequence for the present study, we try in the following to identify BC mechanisms that are consistent with experimental observations. The lack of experimental evidence as well as the contradiction with the experimental observations reported in [130] is therefore sufficient to ignore the hereinabove studied BC mechanisms as good subjects of study.

As a partial conclusion, there is a lack of experimental results to support BC mechanisms at the "mean bubble growth" scale. Therefore we consider that none of the hereinabove studied models for the BC are sufficiently consistent with experimental observations to pursue their analysis in the present work.

1.3.3 Boiling crisis' mechanisms at the "local" scale

In this section we study the BC mechanisms related to the description of the NB regime at the "local" scale. Keeping in mind our goal to identify a potential mechanism for the BC that is consistent with experiments, we review the corresponding models and analyze the proposed BC mechanisms as being related to attested experimental observations.

In the previous models, the BC mechanism was associated either to phenomenological sequence of events (coalescence, limit of the liquid resupply) or to an instability of the bubbles itself as it flows inside the liquid (*cf.* the models of Zuber [156] or Chang [32]) At the level of description corresponding to the "local" scale, the BC mechanism is evaluated using a quantitative model of the bubble growth dynamics when it is still pinned to the wall. In other words, the "local" scale BC models are based on the evaluation of local balances (thermal, mechanical or both) that determine the bubble growth dynamics inside the near wall region as it is still pinned to the wall. The value of the wall heat flux q enters the balance considered. When a critical value of the wall heat flux q is reached, it leads to the transition to another mode for the bubble growth. This irregular mode for the bubble growth will be shown to lead to its spreading along the wall and therefore to a drying transition. The origin of the BC mechanisms considered is thus associated to this specific bubble growth mode. Since it is initiated by a critical wall heat flux value, it indeed determines the CHF.

Recoil instability I Based on experimental observations of the dynamics of the interface of bubbles at high heat fluxes (*cf.* [71]), Kandlikar [70] proposed a model for the CHF based on a force balance on the interface of a bubble at departure. This model follows approximatively the same idea as that developed by Sefiane et al. [120] and that leads to the model reviewed in the next paragraph.

According to the author, at the contact line, the recoil force tends the bubble to spread along the wall, whereas other forces acting on the bubble tend to make the bubble become spherical and/or depart from the heater, letting the liquid re-wet the heater. Indeed the recoil force tends locally the vapor to push the liquid away and is an increasing function of the local mass transfer rate. As a consequence, when the recoil force dominates, the

bubble grows preferentially in the normal direction to the interface where the mass transfer rates is the largest. Since the region of high mass transfer rates is near the foot of the bubble, the recoil force is postulated to globally result in a force that tends the bubble to grow tangentially to the wall, and consequently to spread (*i.e.* to enlarge its dry area). The author considers a balance of forces acting on a bubble at departure conditions taking into account the recoil, surface tension and gravity forces. The bubble at departure is initially considered as spherical. The bubble size at departure is assumed to be given by the most unstable wavelength of the RTI, λ_{RTI}. The mass transfer rate at the interface used to evaluate the recoil force is supposed to be related to the wall heat flux through the definition of an influence area of the heater around a bubble where the bubble removes the heat as it grows. The CHF is associated to the condition at which the recoil force becomes larger than the sum of the gravitational and surface tension forces. For a horizontal heater and a contact angle of $\pi/2$, the resulting expression for the CHF is equivalent to the Zuber correlation. The interesting property of the model to allow to recover the Zuber correlation will be analyzed in section 1.4.2.

The development of the model is based on an interesting analysis of experimental observations of the dynamics of spreading of vapor on a hot wall. The model proposed for the BC mechanism considers the spreading of a bubble to be governed by a balance of momentum. Nevertheless this balance of momentum is performed using an evaluation of the bubble size at departure as equal to λ_{RTI}. This evaluation is not *a priori* realistic since, according to the experimental results reported in section 1.4, the typical size at departure of the bubbles is less by an order of magnitude at least from λ_{RTI}.

As a partial conclusion, even though the mechanism of spreading initiated by a critical value of the wall heat flux is an interesting mechanism for the BC, the model of Kandlikar [70] in itself is nevertheless, to our point of view, not satisfactory because it is not based on a realistic evaluation of the mechanical balance.

Recoil instability II This model is more or less of the same spirit as the Kandlikar's model presented in the previous paragraph. The main difference, to our point of view, comes from the description of the geometry of the bubble, which is less rigid. Following the idea developed by Sefiane et al. [120], Nikolayev and Beysens, [101, 100] proposed the mechanism of the BC to be related to an instability (the so-called recoil instability) at the liquid-vapor interface of a growing bubble pinned to the wall.

The recoil instability is related to the pressure jump condition at an interface undergoing a mass transfer (*cf.* the study of the jump conditions in the appendix A.2) and has been successfully used by Palmer [106] to describe the de-stabilization of plane evaporation fronts in the study of steady rapid evaporation at reduced pressure. In the context of the BC, Sefiane et al. [120] proposed the same destabilizing mechanism to explain the occurrence of the BC. Let us consider a bubble growing on a hot plate. The mass transfer rate is known to be locally more intense in a near wall region in the vicinity of the triple line. Thus, the maximum effect of the recoil pressure on the momentum balance at the interface is located in this region. The destabilizing effect of the recoil pressure is then supposed to induce, above a critical value of the mass transfer rate (obviously related to a critical wall heat flux), a centrifugal force on the interface that tends to make the bubble spread instead of keep a quasi-spherical form (which is the case when the effect of capillary forces is dominant). This is supposed to initiate a spreading dynamics (formation of a large "dry spot" under the bubble), leading to a drying transition and therefore to be the mechanism of the BC.

According to the complex geometry of a realistic description of such a bubble dynamics, it is not possible (contrarily to the initial work of Palmer [106] for plane fronts) to get any result analytically. Nikolayev et al. [100] therefore use numerical simulations of the interface balances of momentum and energy coupled with the liquid thermal problem. These calculation, performed without gravity, actually reproduce the dynamics of spreading of such a growing bubble and moreover establish an important dependence of this spreading dynamics on the wall heat flux value.

However and according to the authors these numerical simulations allow to show "*that at some typical time the dry spot under the bubbles begins to grow rapidly under the action of the vapor recoil. Such a bubble can eventually spread into a vapor film that can separate the liquid from the heater thus triggering the boiling crisis (critical heat flux)*". Therefore the numerical simulations, proposed to illustrate the model, do not allow to reproduce the drying transition that occurs at DNB, but only a supposed precursor event. Indeed, since the two-phase flow is not taken into account in these numerical simulations, there do not exist any departure mechanism that would impede this spreading dynamics. To our point of view, the model therefore proposes an interesting mechanism for a precursor event of the drying transition that should be supplemented by taking into account the

coupling with the bulk phases fluid mechanics to balance the spreading by a departure mechanism. The condition of BC would therefore be the one for which the dynamics of spreading prevails on the dynamics of departure.

The original idea of Sefiane et al. [120] for the BC mechanism is based on the irregular bubble growth at high heat fluxes leading to a partial dryness of the wall and finally, above a critical value for the heat flux to the BC itself. The consistency of this hypothesis will be discussed as we report experimental observations of the near wall NB process at high heat fluxes in section 1.4.

BC mechanism based on the evaporation of the liquid entrapped under a bubble In the model of Zhao et al. [155], the mechanism of the BC is associated to the dry out of the micro-layer of liquid trapped between the bubble and the heater. The bubble growth is decomposed into two stages: a first thermal stage followed by a second mechanical stage. A classical calculation of the initial growth of the bubble based on the micro-layer evaporation constitutes the first and in fact determines the initial profile (radial thickness) for the micro-layer. During the second stage of evolution of the bubble, the micro-layer is supposed to be formed and a competition between inertial, gravity and capillary forces (including a model of vertical coalescence with a large bubble layer over the growing bubble) determines the dynamics of the bubble growth until its departure. During the two stages, the total evaporation of radial crowns of the micro-layer at high heat flux causes a dryness under the bubble. This evaporation is evaluated using an energy balance at the liquid-vapor interface of the micro-layer. Let us note that, in this model, coalescence with a larger bubble is said to promote the departure of the bubble and thus to prevent the wall from a possible dry-out, which is actually far from the ideas of the models based on a critical coalescence. The unknown of this model is the typical size of a bubble after the initial stage of growing (thermal growth). Zhao et al. [155] obtain a relation for the heat flux q as a function of local superheat and this bubble size to describe the NB regime at high heat flux. It has a maximum in q and therefore allows to predict the CHF as the limitation of this idealized NB regime.

In this model, and by difference with the previous other models, the mechanics determines the departure of the bubble, whereas the spreading of the dry area is only associated with an energy balance inside the micro-layer. The first stage of the dynamics of the bubble is only phenomenologically described. As a consequence, the size of the bubble after its initial growth, which appears as a key parameter in the final correlation, is unknown. To our point of view, this study needs to be supplemented by a more accurate model for this initial stage in order to actually attest the validity of such a two-stage bubble growth dynamics and thereafter of the suggested BC mechanism. Moreover the fact that the second stage of bubble growth is only governed by mechanics is subject of question since it actually contradicts the most recognized model for the last stage of bubble growth which is said to be heat-transfer controlled (*e.g.* [28]).

As a partial conclusion, this model for the BC mechanism is questionable according to the validity of the two-stage bubble growth idealization on which it lies.

Purely thermal model of the BC Blum et al. [16] proposed a model for the CHF based on an initial idea of van Ouwerkerk [145]. They postulate that the instability of the NB regime is governed by the thermal problem of a growing dry area over a heated plate. The following thermal problem is studied. They consider the heating element as a plate of given thickness. At the lower part of the plate, a constant heat flux, namely q, is imposed. The upper part of the plate is in contact with the boiling fluid and is locally either dry or wet. This local state of the wall-fluid interface is modeled by its temperature with the help of a limit value, say $T_{w/d}$ for the wet-dry transition. The surface is dry, resp. wet, if $T > T_{w/d}$, resp. $T < T_{w/d}$. The heat exchange coefficient of the wet, resp. dry, area is considered as given by the NB, resp. FB, part of the Nukiyama curve. In the course of time, a point of the upper surface can pass from wet to dry or reversely according to its temperature. Now, consider an initial circular dry area of a size D. This represents a typical foot of a bubble growing on a wall. By performing thermal calculation inside two-dimensional plates, the authors show that there exists a critical value for q such that the initial dry area grows without any limit. This critical value is therefore associated to the CHF.

This model actually highly differs from the previous ones because no bubble growth dynamics is considered by the authors. Even though the use of the global correlation (either the one of the NB or the one of the FB regime according to the local dryness of the wall) for the heat exchange coefficient appears as an interesting idealization of the local heat transfer process, the neglect of any fluid mechanics is to our point of view, the major default of this model. Indeed, it is classically recognized that the mechanism of departure and therefore of re-wetting of a dry zone is mainly governed by fluid mechanics (*e.g.* Buyevich and Webbon [22]). Moreover this model fails

to explain the drying transition that still occurs at DNB for temperature controlled experiments (for the same CHF value of the mean heat flux extracted from the wall). Indeed in this latter case, no local increase of the wall temperature at the location of dry areas exist. According to the model considered, no drying transition should therefore occur. As a consequence the model is not able to explain this drying transition. In the temperature controlled case, (if, as the authors suggested, only the very near wall process determines the drying transition mechanism) only the mass transfer rate existing at the liquid-vapor interface and the consequent growth of the bubble is able, to our point of view, to explain the drying transition and therefore the DNB mechanism.

As a partial conclusion, the purely thermal model of the BC mechanism is unable to explain the drying transition that occurs at DNB. Indeed this drying transition results to either the BC for a heat-controlled system or the transition toward TB regime for a temperature-controlled system. The model of Blum et al. [16] for the BC mechanism fails to explain this latter situation although the mechanism of the drying transition at DNB should be unique.

Thermal balance inside a dry spot and critical level of temperature Bricard et al. [20] proposed to investigate the models of Kirby et al. [78] and Fiori and Bergles [50] for the study of the BC mechanism in sub-cooled flow boiling. The model of Fiori and Bergles [50] considers the influence, in convective flow boiling conditions, of the existence of a large vapor mass on the persistence of a dry area on the wall. It is not considered in the following presentation of the work of Bricard et al. [20] since it appears only as a parametric effect on the BC mechanism itself. The model of Kirby et al. [78] considers that in the NB regime, a nucleus of vapor is left on the wall at each bubble departure having the form of a flat film. The subsequent dry area is then re-wetted. Kirby et al. postulate that, at the BC, the local increase of the wall temperature at a dry location is such that liquid is no longer able to wet this zone and that, moreover, conditions are such that the dry zone spreads over the wall. Bricard [19] studied this model, developed a criterion for this critical wall temperature level based on an analogy of the physical situation with the Leidenfrost phenomenon [8] and finally provided a CHF calculation based on a heat balance in the wall under a dry patch. The Leidenfrost temperature is, according to the author, a rough approximation for the critical value of the temperature for the dry regions since the actual situation is obviously different. The order of magnitude is however suggested to be still valid, for water on classical steels, it is estimated as being equal to $T_{sat} + 150°$.

The same criticism as for the previous purely thermal problem can apply to this model. Indeed the Leidenfrost temperature is far from being reached for temperature-controlled experiments when the drying transition occurs. Such purely thermal models will therefore be disregarded in the following.

A critical heat flux for the drying of the liquid film at the boundary of a large dry area Yagov [150] developed a model based on the idea that the efficient heat transfer that exists at the boundary of the dry area at the bubbles' foot both explain the efficiency of the NB regime and "*bears the possibility of terminating the nucleate boiling*". According to Yagov [150], the origin of large dry spots is associated to the lateral coalescence of the bubbles due to the increase of the NSD. The author considered a balance between the liquid inflow at the boundary of such a large dry spot and the evaporation mass transfer rate at this same boundary. The author determined the heat flux necessary to evaporate the entire film at the dry spot boundary. As the wall heat flux reaches this critical value, the dry-out of the heater is assumed and therefore we are in conditions of the BC.

The main differences between this model and the models based on the recoil instability, are first that the dry spot are said to originate from a lateral coalescence and secondly that the spreading of the dry spot is supposedly governed by the balances of mass and energy and is therefore independent from the balance of momentum. The main default of this model is that it does not consider any departure mechanism that should impede the initiated spreading, which is, to our point of view unrealistic.

Conclusion concerning the analysis of the BC mechanisms related to the "local" scale NB mechanisms We have presented the models for the BC mechanisms that considers some irregular bubble growth events as the origin of the drying transition. The models of Kandlikar [70] and Nikolayev et al. [100] based on a spreading

[8] This phenomenon is also commonly known as the calefaction. Leidenfrost [84] first brought to light this effect: a small liquid drop deposited over a sufficiently hot wall does not fall and wet the wall but rather levitates over it. The evaporation flow at the surface of the drop that faces the hot wall forms an air-cushion between the wall and the drop. The reader interested can refer to the excellent article of Biance et al. [15] for more details.

of bubbles initiated by the recoil instability (original idea of Sefiane et al. [120]) as well as the model proposed by Yagov [150] have been shown to be not sufficiently complete. Indeed no mechanism of departure is considered that should balance the initiation of the spreading of such an irregular bubble. The relevance of the main hypothesis (mechanical instability leading to the spreading of the bubble) with regard to the experimental observation of the NB regime at high heat fluxes will be studied in the following section. The models of Blum et al. [16] or Bricard [19] based on purely thermal criterion for the initiation of spreading of a dry area have been shown to fail to explain the drying transition at DNB and that leads to the transition toward the TB regime. Since the DNB transition is the more general phenomenon that leads to the BC in the case of heat controlled experiments, the models related to such a thermal criterion are disregarded in the following of this study.

1.3.4 Conclusion on the presentation of the models for the BC mechanism

Some other open questions We have deliberately presented first the NB process in the context of a pool boiling set-up with an imposed wall heat flux q. It is worth noting that this configuration differs from industrial heat exchangers mainly because of the non-existence of any transient phenomenon in the power supply and of the absence of any convective flow. The validity of the previous developments lies indeed on an important modeling hypothesis. In other words there exists another open question about the nature of the BC phenomenon: Is the BC independent of the flow configuration?
The fact that different instabilities could trigger the drying of the wall according to the set of dominant physical mechanisms at play in the NB process is indeed not trivial to answer. Our point of view is that the mechanism is unique. This assumption is based on the following argument. Let us consider the evolution of the CHF with regard to a given parameter, say Z (such that for example the convective mass flow rate, the mean void fraction, the wetting properties of the fluid on the hot wall, or the sub-cooling). The curve CHF(Z) is relatively smooth and of constant slope (*cf.* chapter 12.5 of [28] or the review of the parametric trends of the CHF value by Celata [30] based on 2000 data points). If one assumes that the *mechanism* is modified by changing the configuration, one would have expected a clear modification of these curve: discontinuity of the value of of the slope. Such a modification is not observed.

According to our hypothesis of the existence of a single mechanism for the BC, the pool boiling configuration is the most relevant and simple configuration to study to understand the BC.

***A parte* for the sake of generality** It is worth noting that Sakurai [118] proofed the existence of two mechanisms for the transition toward TB in experiments of transient heating (increasing wall heat inputs, exponential in time, in pool boiling). In this case the parameter Z considered is the characteristic time τ of the heat input ($q \simeq e^{t/\tau}$). However, the existence of two mechanisms is attributed to the fact that, according to the characteristic time τ , we observe either a direct transition from a non-boiling state to TB (which corresponds to small values of τ) or a "double transition", first from non-boiling to NB and then to the transition from NB to TB, of interest in this study (which corresponds to larger values of τ).

Toward the motivation for an analysis of the local scale phenomena The issues associated to the understanding of the BC mechanism has been until this point, deliberately widely open. It has been illustrated by the variety of types of mechanisms in the NB process and subsequently of the types of models developed for the BC mechanism, that a lot of questions about the BC are still open. Indeed it has been shown by the analyze of the BC models that a vast majority of the supposed mechanisms are not attested experimentally or even contradictory with some experimental results. It is worth noting that a better understanding of the BC phenomenon is constrained by an improvement of the knowledge of the process through experimental observations as it has been stated by Sadavisan et al. [117] among others.

In the following, we present our analysis of a model of the CHF as being related to an instability at the local scale. Let us justify our choice to focus on the analysis of the local scale models instead of any other choice among all the tracks that need to be pursued. Recently there has been an important improvement in the observation of the near wall process (reported in section 1.4). The re-examen of the local scale mechanisms for the BC in view of these results is therefore necessary. Such a work should provide an improved understanding of the different models for the BC. As mentioned by Chung and No [37]: "*The current CHF models are mainly based on the postulation on the CHF phenomena without physical observation. The new CHF models need to be*

consistent with the direct observation on CHF. Also, as several investigators suggested [59, 117], *a realistic CHF model would be the one that gives a natural outcome for the description of the high-heat flux nucleate-boiling region in contrast to the traditional view of CHF as independent phenomena distinct from the nucleate boiling*". We therefore begin by reporting some experimental observations of the near wall process that could help us to determine such a model.

1.4 Report of experimental observations

In this section, we present some recent results of experimental observations that allow to get a more precise knowledge of the NB regime at large heat fluxes (*i.e.* close to the BC conditions). These results focus mainly on the description of a very near wall region that is very difficult to visualize without any advanced experimental techniques. The reader interested by this experimental problematic can refer to the work of Kenning [76].

Based on these observations, we then present an analysis, of a near wall mechanism of instability that is

- ⋆ consistent with these experimental observations
- ⋆ a potential mechanism for the BC
- ⋆ consistent with the successful Zuber's correlation

This section is organized as follows. In a first part (see section 1.4.1), we report some experimental observations, which provides a representation of the NB process in pool boiling near BC conditions[9]. It is shown that the hypothesis of scale separation between the two-phase flow scale and the bubble production zone is justified. Then we report the observation of some local drying events that occur for wall heat fluxes less than the CHF and that are identified as precursor events of the drying dynamics that leads to the BC. It is then shown that these drying events are associated with irregular behavior during the bubble growth process at the wall. In a second part (see section 1.4.2), we postulate that these observations actually correspond to the BC mechanism. This leads us to consider the mechanism for the BC to be related to the "local" length scale and we discuss an interpretation of the Zuber correlation at this scale.

1.4.1 NB regime at high heat fluxes

In this section, we report some experimental observations that allow to determine the validity of the scale separation hypothesis made for the classification of the BC mechanisms. They allow above all to specify the near wall NB process at BC conditions. In a first part, we report lateral visualization of the NB process. Different layers are clearly distinguished. Then we supplement the description of these layers by the report of void fraction measurements. In a second part, we report experimental observations of the local dryness of the wall near BC conditions using different experimental techniques and/or heating modes (q or T_w controlled). Finally we provide a synthesis of these observations that allows to describe the NB process near BC conditions. This will be used to deduce an elementary target problem whose study can provide a gain in understanding of the BC mechanism.

The basic picture from a lateral visualization

Comments on the nature of the pool boiling experiments for the two first experiments reported In the first two parts, we present the NB process at high heat flux observed in pool boiling experiments using refrigerants as the boiling fluids. According to the low density contrast between their liquid and vapor states ($\rho_l/\rho_v \simeq 200$ to be compared to water at atmospheric pressure $\rho_l/\rho_v \simeq 1000$), these fluids allow an easier visualization of the NB process. Special caution has been taken by the authors so that their boiling apparatus (the heated wall is very reduced in its lateral dimension) does not induce specific mechanisms and that the observed value of the CHF is actually well predicted by the Zuber correlation.

[9] It is worth noting that some other very interesting results about the local mechanisms of the NB process are presented by Rule and Kim [116], Yaddanapudi and Kim [149], Demiray and Kim [44] among others. They are not reported here because they do not concern the near BC conditions of interest in this study.

Near wall NB process A lateral picture of the NB process is obtained by Nishio et al. [102] that is reproduced on figure 1.5. Those pictures correspond to the NB process at a heat flux closed to the CHF ($q = 0.92\,CHF$). One the left hand side (LHS) picture, a sequence of several snapshots (taken at 1000 frames/s) of the NB process are represented, the time between them being given under each snapshot in milliseconds. On each snapshot, the vapor bubbles can be identified as the black forms over a white frame (continuum of liquid). At the bottom part of each picture, the wavy black line corresponds to a liquid-vapor interface, the liquid phase being on the upper side of this line. By considering the sequence of snapshots, it can be seen that several big bubbles are generated from a quasi-continuous film of vapor that exists above the wall. It is worth noting that these big bubbles, by their size and spatial spacing, can be identified as being generated by a Rayleigh-Taylor instability on the surface of the vapor film. This part of the picture is therefore consistent with the idealization made by Zuber for the generation of bubbles. Let us now consider the right hand side (RHS) picture. It corresponds to a close-up picture of the LHS process in a region very close to the wall. The scale is such that the upper part of the RHS picture corresponds more or less to the unclear dark region at the bottom of the LHS pictures. The white continuum on top of the RHS picture is therefore the big vapor mass (film-wise bubble on the picture) whose upper boundary is the wavy thin black line on the LHS pictures and whose bottom boundary is the thick black line on the RHS picture. Under this big vapor mass, there exists a liquid film, that itself contains bubbles like the one clearly identified by the arrow. Therefore, even though from a far point of view (LHS pictures), vapor covers the wall, there still exists a continuous liquid film in contact with the wall. Inside this liquid film, numerous bubbles are generated that coalesce to form the vapor film. In a following paragraph we study the nature of the fluid-solid contact for such an high heat flux.

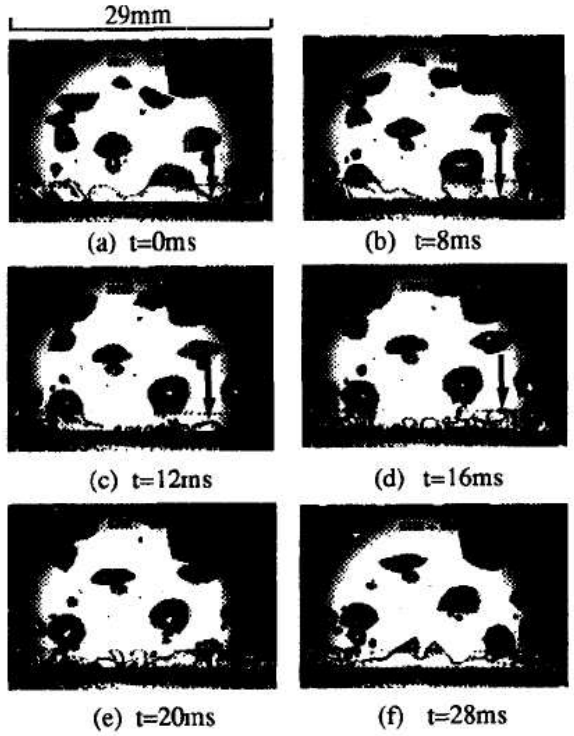

Fig. 14. Dynamic behavior of filmwise bubble ($W = 0.5$ mm, $H = 2$ mm, $q = 0.92q_{CHF}$).

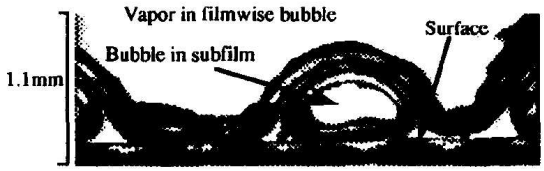

Fig. 15. Close-up picture of liquid film under filmwise bubble ($W = 0.5$ mm, $H = 2$ mm, $q = 0.92q_{CHF}$).

Figure 1.5: Lateral visualization of the NB process reproduced from [102]

As a consequence of these observations, the big bubbles that can be observed as flowing outward the wall are not the bubbles generated in the very near wall region. Indeed, as they detach from the wall, the bubbles first coalesce with each other and form a big vapor mass above the wall. This vapor mass is not a continuum since liquid is still able to reach the wall. From this big vapor mass, and due to the RTI, big bubbles actually flow

outward the wall[10]. Moreover the growth of the bubble pinned to the wall actually appears as independent of the above bubbly two-phase flow which justifies the scale separation.

Two-phase flow scale at CHF Let us now consider the experimental results of Chung and No [37] who somewhat used a similar boiling apparatus and visualization technique. Their study provide somewhat similar lateral visualizations of the NB process to the LHS pictures of figure 1.5 described in the previous paragraph. However, their study provides also a visualization of the boiling process before, when and after the CHF is reached (*cf.* figures 1.6). It is worth noting that the visible transition in the boiling process takes place rather in the near-wall region than in the two-phase flow scale region. No noticeable change can be identified between post- and pre-CHF observations of the two-phase flow configuration above the vapor "film" that could attest any regime transition at this scale. This result therefore contradicts the hydrodynamic theory and confirms the near wall region as being the location of the BC mechanism.

Void fraction measurements In order to attest the validity of the previous observations, it seems interesting to compare those results with those obtained by Auracher and Marquardt [7] with other fluids such as the refrigerant FC-72 and the isopropanol and in other experimental conditions. In this case, lateral observations of the flow are, to our knowledge, not available. The authors provide void fraction measurements at high heat-fluxes up to the CHF. It is worth noting that contrarily to the previous results, the wall temperature $\langle T \rangle$ is imposed (instead of the heat flux q) and that they actually observed the TB and thus the drying transition that occurs at DNB. Their results attest the existence of a layer in the very near wall region that is must richer in liquid (corresponding by analogy to the liquid film with bubbles in the previously presented results) than the layer just above it that is very rich in vapor (corresponding by analogy to the vapor "film"). This attests therefore the validity of the picture of the NB process at high heat fluxes proposed in [102] or in [37].

BC and precursor local drying events In the following, we report experimental observations about the nature of the fluid-solid contact during pool boiling experiments in the NB regime near and at CHF. It is worth noting that such drying events have been reported by experimentalists from a long time (*cf.* [56], [145], or [152] among others). Here we refer to experimental observations obtained using more recent techniques, that provide a more quantitative and accurate description of these events.

Theofanous et al. [130, 131] studied experimentally the pool boiling of water at atmospheric pressure. Using a sub-micron metallic film deposited on a glass as a heater, the authors have been able to visualize, among other quantities, the wall temperature field, *i.e.* T instead of $\langle T \rangle$, using infrared thermographic techniques. Such maps of the temperature field are reproduced on figure 1.7(a) for different wall heat fluxes q (namely from left to right $q = 406,\ 536,$ and $807\, kW\, m^{-2}$, whereas the CHF value is about $1\, MW\, m^{-2}$ in these conditions). Black, resp. white, regions concerns low, resp. high, levels of wall temperature. The nucleation and bubble growth events can be identified by low temperature regions of circular form as it can be seen on the LHS picture of figure 1.7(a). The low temperature is associated with the very efficient heat transfer process of the phase change phenomenon that takes place as the bubble forms and grows. To our point of view, one of the most interesting results of this study is the observation of the temperature field under a growing bubble at wall heat fluxes near BC conditions. In these conditions, it can be seen (*cf.* the RHS graph on figure 1.7(a)), at the center of the low temperature region (associated to a bubble growth event), a circular zone of very high temperature that has been clearly identified with a dry region (*cf.* the study in [130]). On figure 1.7(b) is reproduced a sequence of such a bubble growth event. At the beginning (LHS top picture) the dark region is the cooling associated to the beginning of the bubble growth event. At the center of this low temperature region it can be seen on the next pictures a white circle (high temperature) that first grows and then shrinks before the bubble finally departs (last picture bottom RHS). The graph on the RHS represents the time evolution of the temperature at the center of the hot and dry zone. The particularly high levels of temperature (up to $T_{sat} + 130°$) reached at this point allow to clearly identify this region as being dry. The authors reported the dynamics of such dry spots and their analysis allows to draw the following conclusion:

- ⋆ Such drying events occur more frequently as the wall heat flux increases and as the wall temperature is initially locally higher and not surrounded by previous bubble nucleation events

[10] As a consequence, the evaluation of the bubble size at departure from the wall made by Kandlikar [70] appears actually as irrelevant.

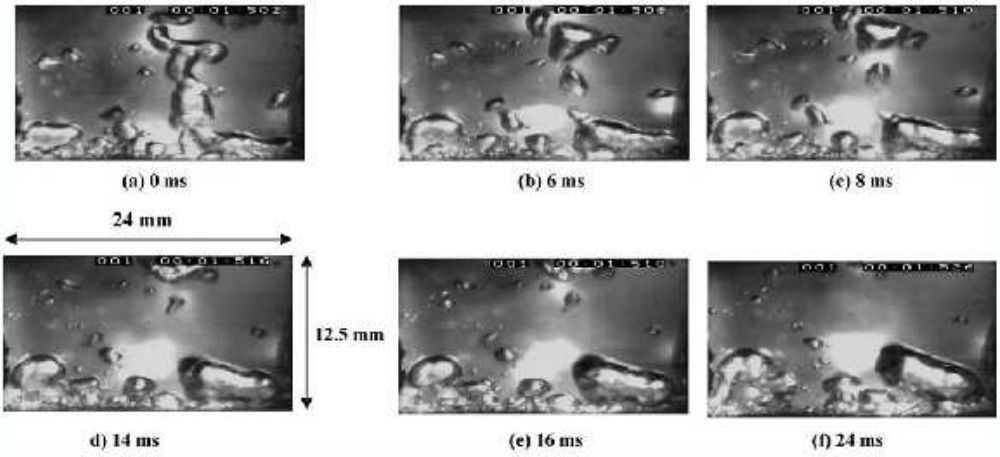

Fig. 9. Side views of bubble structures at local vapor film regimes ($q = 0.9q_{CHF}$).

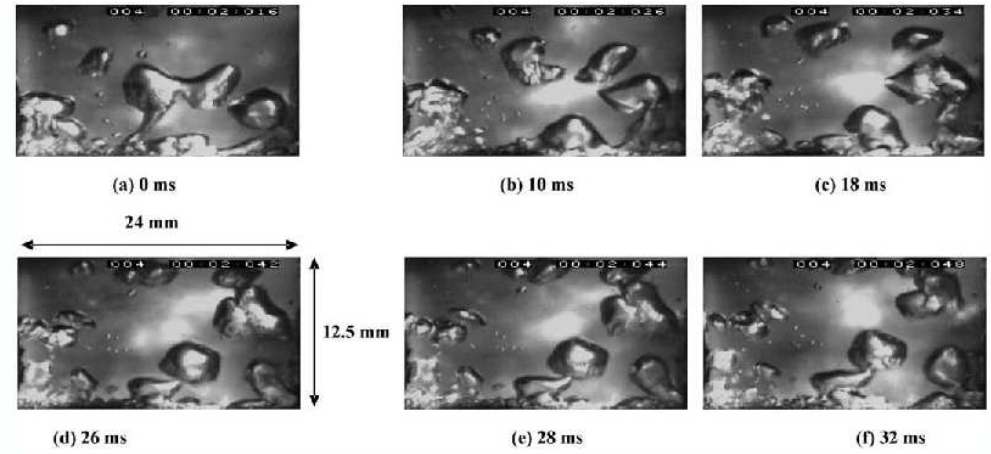

Fig. 12. Side views of dynamic behavior of bubbles at CHF.

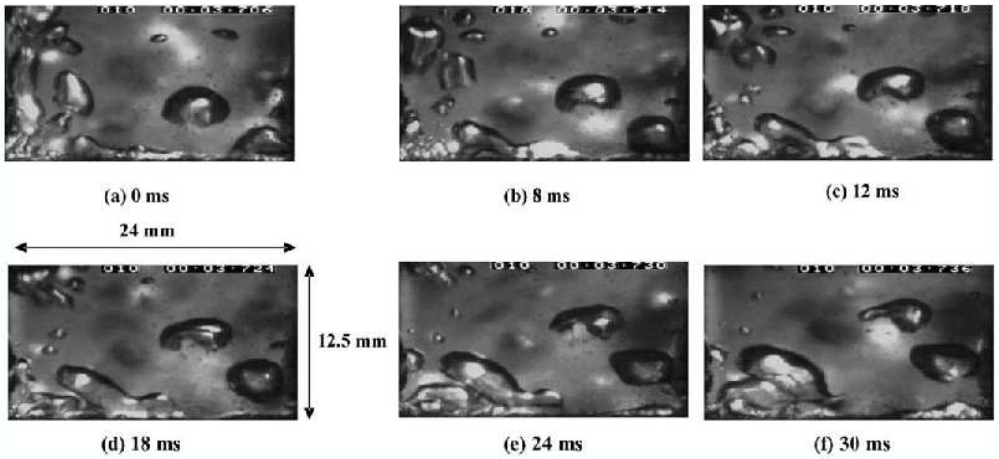

Fig. 13. Side views of dynamic behavior of bubbles just after CHF ($q = 1.06q_{CHF}$).

Figure 1.6: Lateral visualization of the CHF reproduced from [37]

- ⋆ For (relatively) low heat fluxes, the spreading-shrinking dynamics of the dry area follows the mean bubble cycle.
- ⋆ At higher wall heat fluxes, some of the drying events are much more violent and, even though they finally do not lead to the dry-out of the wall, their characteristic life time and size are no longer correlated to the mean bubble cycle, *i.e.* drying events have their own dynamics.
- ⋆ At the CHF, such a dry spot begins to spread without limit, finally leading to the burnout of the wall. Such a behavior is reproduced on figure 1.7(c).

In the following, we consider other experimental results that attest the validity of these observations with different boiling configurations.

The boiling apparatus used by Chung and No [37] allows to get information about the wetting of the wall through optical measurements. The boiling fluid is a refrigerant and the heated wall is a sapphire plate covered by a transparent electro-conducted film. The authors also report that they identified the dry spots events with nucleation events.

Buchholz et al. [21] performed pool boiling experiments with saturated iso-propanol[11]. Contrarily to all the previous experiments (except [7]), the wall temperature $\langle T \rangle$ (instead of the heat flux q) is controlled. Time dependent temperature fields are calculated using a net of thermocouples installed inside the heater. It is worth noting that, before CHF is reached, large drying events can be identified through the temperature fields measurements. Since temperature is controlled, the nucleation points, resp. the dry areas, correspond to slightly lower, resp. higher temperature regions than in the experiments of [130, 131] (of the order of 1K with respect to the mean temperature value instead of few tens of Kelvins) but are still clearly identifiable.

Conclusion about these experimental observations The NB process at high heat fluxes has been described in more details using experimental observations of pool boiling experiments. The near-wall region has been shown to consist in

- ⋆ a thin liquid layer in contact with the wall where nucleation events and bubble growth take place;
- ⋆ a very rich vapor layer created by the coalescence of the bubbles that form in the liquid film, this layer is obviously discontinuous since the feeding of the underneath liquid film is maintained.
- ⋆ above this rich vapor layer, a bubbly two-phase flow region exists, bubbles are generated by the RTI occurring at the upper surface of the vapor layer.

It has been shown that somewhat large drying events can exist before CHF, *i.e.* without leading to the DNB. The triggering of these drying events is associated with nucleation events and leads, at sufficiently high heat fluxes, to "irregular"[12] bubble growth with respect to the mean (or "regular") bubble growth events. At CHF, one or several of these dry spots suddenly spread over the wall, leading to the DNB. These irregular bubbles are not associated with bubble coalescence, since they occur preferentially in regions not previously populated by other nucleation events. These regions correspond therefore to high liquid superheat.

In the following, we interpret these experimental results to determine a potential mechanism for the BC.

1.4.2 Interpretation of the experimental results: a local interpretation of the Zuber correlation

In the following, we postulate that the experimental observations of drying events reported above are actually related to the drying transition that occurs at the BC. Let us justify this postulate. It is worth noting that even though these results have been obtained with particular experimental set-ups (especially concerning the wall thermal and aspect characteristics), the CHF is of the same order of magnitude as for more classical pool configurations (*i.e.* well predicted by the Zuber correlation). As a consequence, the specific configuration is assumed to have only a parametric effect on the CHF value, and therefore the mechanisms of the BC is assumed not to be modified by the configuration.

[11] These results correspond actually to the same set of experiments as in [7] whose void fraction measurements have been reported in the previous study of the basic picture from a lateral visualization.

[12] We here reproduce the distinction between regular and irregular bubbles introduced in [130] to characterize the experimental observations of the bubble growth processes.

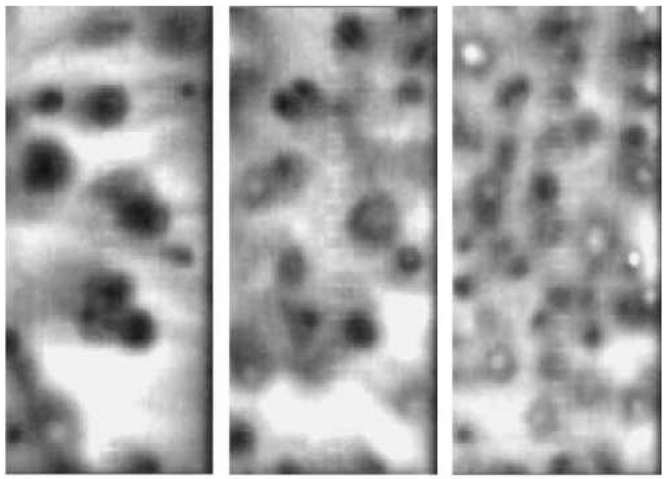

Fig. 11. IR thermometry images of a fresh heater (F1) at three different heat fluxes, $q = 406$, 536, and 807 kW/m^2.

(a) Temperature field

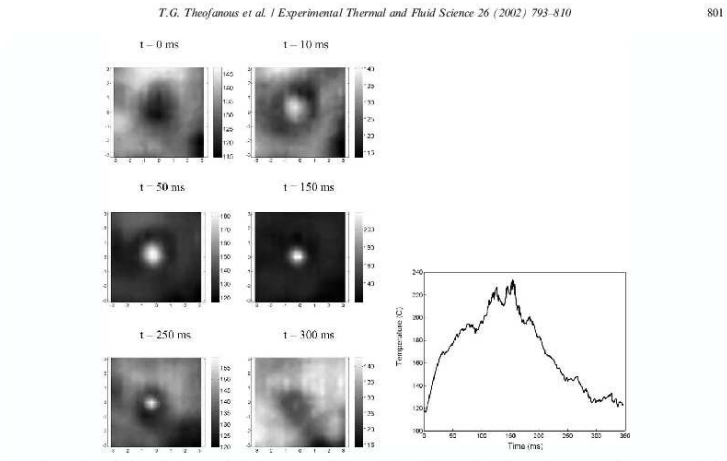

Fig. 7. Illustration of the dynamics of a reversible dryspot on a fresh heater (F1), at 800 kW/m^2. The figures show an area of 6 mm × 6 mm of the heater. The temperature scales are shown to the right of each image. The temperature transient shown on the extreme right is for the center spot of the images pictured, including intermediate frames not shown on the left.

(b) Dry spot at the center of a bubble

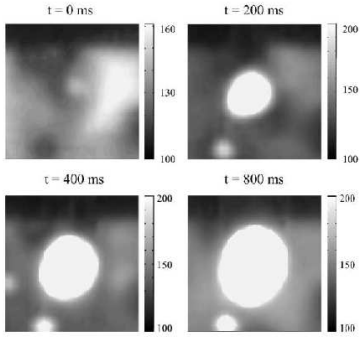

Fig. 14. Illustration of the dynamics a dryspot in the process of burning ou

(c) Burnout

Figure 1.7: Wall temperature at high heat flux NB regime, figures extracted from [130, 131]

Let us now examine the consequences of our postulate. The precursor drying events have been said to originate in a nucleation event and to be related with the growth of a bubble pinned to the wall. Therefore, the drying transition at the BC must be related to a certain mode of bubble growth on a heated wall, that is activated only for NB regime close to the DNB conditions (*i.e.* for the two types of controlled experiments considered, either wall temperature or wall heat flux imposed uniformly). This contradicts therefore the hypothesis that the dryness is associated to coalescence phenomena in a near wall region, which is the other common postulate[13].

Rewriting of the Zuber correlation For the sake of simplicity, we will not use the original Zuber formula (1.1) but rather a simplified formula that reads

$$q_{CHF\,Zuber} \simeq \frac{\pi}{24}\mathcal{L}\sqrt[4]{\sigma g \rho_l \rho_v^2} \tag{1.2}$$

Both formula (1.1) and (1.2) are equivalent as long as the density ratio satisfies $\rho_l/\rho_v \gg 1$ which is the case for the boiling fluids considered. Let us decompose this formula using the widely used energy balance at the interface (*cf.* our study of the jump conditions in the appendix A.2) $q = \Gamma\,\mathcal{L}$, where Γ is a mass transfer rate and $\mathcal{L}$ is the latent heat of vaporization. Let us also introduce, instead of the RTI wavelength λ_{RTI}, the most generic capillary length λ_{cap} defined as

$$\lambda_{cap} \triangleq \sqrt{\frac{\sigma}{\rho_l g}}$$

Thus the Zuber correlation can be written as

$$\mathcal{N}_0 = \frac{\pi}{24}$$

where the non-dimensional number $\mathcal{N}_0$ is defined as

$$\mathcal{N}_0 \triangleq \frac{\Gamma^2\,\lambda_{cap}}{\rho_v\,\sigma}$$

It is worth noting that, using this writing, it appears as natural to consider the Zuber correlation at different length scales since two of the three basic elements it is made of, namely the capillary length, and the interface energy balance, are characteristic of the analysis of any boiling system. The third one, which is the non-dimensional number $\mathcal{N}_0$, needs to be more specifically studied.

Different scales, different interpretations In the original context of the Zuber model, Γ is the mean transfer rate of the NB process and is therefore related to a *mean* vapor flow rate and thus to the velocity V_v of the vapor flow across the liquid. Let Γ reads as $\rho_v\,V_v$, then $\mathcal{N}_0$ refers to the classical non-dimensional critical parameter for the Kelvin instability. Let us now consider models at the "mean bubble growth" scale where bubbles keep their integrity in the model of the NB process. When considering a bubble instability, λ_{cap} is the bubble diameter, and $\Gamma = \rho_v\,V_v$ where V_v refers to the velocity of individual bubbles rising in the liquid. In this case $\mathcal{N}_0$ refers to the classical Weber number. It is actually a Weber number that used Chang [32] in the derivation of his correlation for the CHF, that is equivalent to the Zuber's one. When Γ is related to a local mass transfer rate at a liquid-vapor interface, the block Γ^2/ρ_v is the measure of the recoil force, which is the destabilizing force in the idea of Sefiane et al. [120]. This explains the result of Kandlikar [70]. Let us also mention the model of Mokrushin [96] (not reported here) that considered a balance of force acting on the film of liquid trapped under a growing bubble (micro-layer) as determining the occurrence of the DNB drying transition. Its resulting correlation for the value of the CHF is similar to the Zuber correlation. According to Mokrushin [96], and to our own point of view the agreement between all these expressions for the CHF "*is not surprising. It shows that the principal forces acting on the vapor bubble were accounted for in [all] cases.*".

The two interpretations of the Zuber correlation (at a global or local scale) can be represented by the two following diagrams. At the bubble scale λ_{cap} defined by the competition between surface tension, the drying

[13]There is a long history of debate on this point, already revealed in the 50's of the twentieth century by Jakob [64]: "*whether the spheroidal state is always initiated by coalescence or is spontaneously initiated will be difficult to decide*". The spheroidal state is the ability of a liquid not to contact a hot wall, *i.e.* the calefaction, (*cf.* the footnote 8 on page 21). Let us note that, in the case of rapid transients, the spheroidal state has been observed to spontaneously initiate (*cf.* Sakurai [118]). This at least proves the ability of this state not to be always induced by coalescence.

transition being governed by a competition between recoil and capillary forces, whereas the departure dynamics is governed by buoyancy and capillarity. At the flow scale the gravitational and surface energies defines the length scale λ_{RTI}. For this type of scales, at CHF a wave of typical length λ_{RTI} is destabilized by a flow of kinetic energy $m\,V^2$ (existence of a critical Kelvin or Weber number according to the fact the bubbles keep their integrity or not).

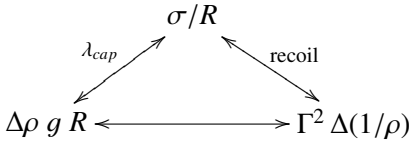

ΔP at the "local" scale

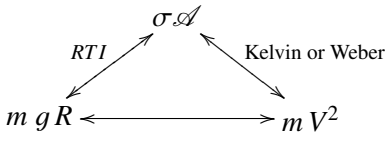

Energy scales at the "two-phase flow" scale

It has been shown how to relate the Zuber correlation to mechanisms for the BC at different scales. As a consequence, and since interesting experimental results have been shown to be related to the "local scale", it seems all the more interesting to focus on a study of the potential mechanism of the BC at this "local" scale.

1.4.3 Conclusion on the study of local observations

According to the experimental observations presented in the beginning of this section, the NB process at high wall heat flux has been specified. Some local drying events have been identified as related to irregular bubble growth events leading at CHF to the dry-out of the wall. These events have been related to a very near wall scale, and therefore it has been postulated that this scale was the scale of the BC mechanism. The Zuber correlation, that allows to predict the CHF with a good accuracy, has been related to an interpretation at different scales, including this local scale. As a consequence the Zuber correlation is not associated with the "two-phase" flow scale at which it has been initially associated. In the following, we study a way to get an improved understanding of the BC mechanism by studying the spreading dynamics of the dry area that forms under an irregular bubble.

1.5 Study of the instability of a bubble growth on an hot wall leading to the spreading of a dry spot

The goal of this section is to define an elementary target problem whose study could help to understand the basic mechanisms of the BC. Since it has been shown in the previous sections that it was justified to consider the mechanism of the BC as being related to an irregular bubble growth event, we therefore propose to study this phenomenon.

This section is organized as follows. First we define a BC mechanism at the "local" scale consistent with the experimental observations and for which the governing physical mechanisms are consistent with the Zuber's model. We analyze this model in comparison with the other BC models that have been shown in section 1.3 to be related to the dynamics of a dry area. Then we propose the numerical simulation of a bubble growing on a hot wall as an interesting subject of study in order to clarify the competition between the spreading and the departure dynamics.

1.5.1 A scenario at the DNB conditions

In order to illustrate the possible gain in understanding for the potential mechanism for the BC at the local scale, we study a BC mechanism based on the spreading of a dry area located under an irregular bubble. Several models have been reviewed in section 1.3.3 for such a BC mechanism. These models have been criticized in section 1.3.3, we consider again this criticism in view of the comparison with the model proposed and show how it allows to overcome their limitations.

A BC mechanism The corresponding BC mechanism is represented on figure 1.8. The initial configuration considers an irregular bubble (central picture of figure 1.8) that has a large dry area at his foot (as it has been observed in [130]). The origin of this irregular behavior can be related to the recoil instability as suggested by Sefiane et al. [120] and shown by the numerical results of Nikolayev et al. [100]. Its latter evolution is then

supposed to depend on the wall heat flux q. Either $q < CHF$, the bubble stops to spread and finally departs from the wall (RHS picture of figure 1.8). We are therefore still in the NB regime. Or $q = CHF$ (DNB conditions) in which case the bubble continues to spread along the wall and as a consequence begins to form a thin vapor film in contact with the wall (LHS picture). The further evolution of this film depends on the wall heating mode. If the temperature is controlled, the film locally breaks down under the action of the RTI. As a consequence we observe a succession of large drying events and of re-wetting events. This spreading dynamics is supposed to still exists for higher wall temperatures, this corresponds actually to the classical TB regime (bottom LHS picture). At MHF, the temperature of the wall is classically considered as sufficiently high in order the vapor film not to be broken by the unset of the RTI. As a consequence, if the heat flux is controlled at DNB conditions, the wall below the vapor film that establishes becomes rapidly hot (as observed in [130]) and its temperature rapidly becomes larger than the MHF's value. Therefore, the film is not destroyed by the unset of the RTI, the RTI is at the origin of a bubble release process. The wall keeps in contact with a continuum of vapor and its temperature is large. This situation corresponds to the FB regime (top LHS picture).

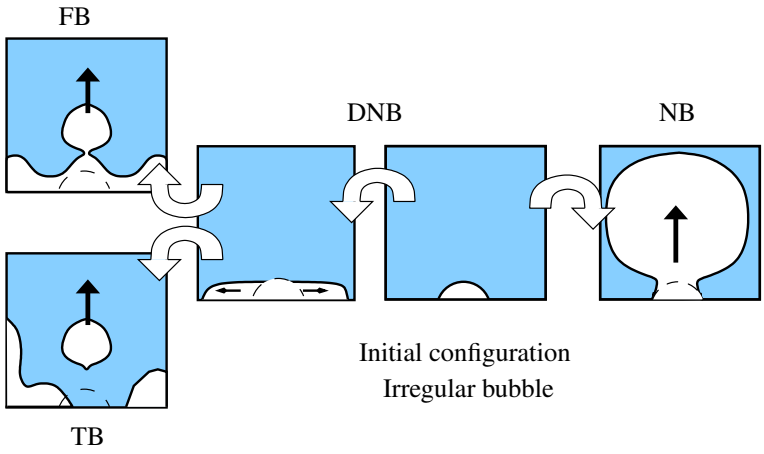

Figure 1.8: A BC mechanism at the "local" scale

Comparison of this local mechanism for the BC with regard to the previous models at the "local" scale Let us consider the main differences between the proposed BC mechanism and the models for the BC reviewed in section 1.3.3.

The explanation of the drying transition toward TB regime Let us note that the criterion of a sufficiently large wall temperature under the vapor film only concerns the stability of the drying transition (TB or FB regime) but not the drying transition itself (DNB). This hypothesis is therefore different from the ones suggested in [16] or [19] and actually allows the mechanism to explain both the transition toward FB and TB regimes as the wall heat flux reaches the value of CHF.

Departure *versus* spreading It is important to note that for this scenario of the BC mechanism, DNB conditions corresponds to the condition when the spreading dynamics is no more balanced by a departure dynamics. As a consequence, DNB conditions are not the conditions when the spreading initiates (as supposed in [100]). The interpretation of the DNB event is fully consistent with the experimental observations of Theofanous et al. [131] since drying events have been actually observed at NB conditions below the CHF.

Target problem The balance between spreading and departure of an irregular bubble has been shown in section 1.3.3, not to be captured by the previous attempts to model irregular bubble growths (namely the models studied in [70] or in [100]). As a consequence, it remains, to our point of view, of primary interest to be able to model this competition. In the following we consider a way to study this elementary target problem.

1.5.2 Numerical simulation as a way to gain in understanding for the basic mechanism occurring at DNB

It is worth noting that since "local" scale mechanism have to be taken into account and moreover since the geometry of irregular bubbles is supposed to be complex during its growth, the use of analytical models for the study of the dynamics of such an irregular bubble is out of reach. We rather propose to follow the approach of Nikolayev et al. [100] who used numerical simulations to study the initiation of the spreading dynamics. However since the numerical method used in [100] neglects the mechanisms of departure of the bubble, it needs to be supplemented. To study our target problem, we therefore need to consider a more complete model for the bubble growth that includes the whole two-phase flow dynamics. As a consequence, we turn our attention toward numerical methods able to solve the non-isothermal liquid-vapor flows with phase change at the local scale.

The use of numerical simulation is not expected to provide a gain in understanding in itself. However, once a given mechanism is supposed, numerical simulation provides an interesting tool in order to attest the validity of the assumptions. It has been said previously that performing experimental measurements at high heat flux NB is a hard and touchy task. The use of numerical simulation as numerical experiments is therefore motivated also by this limitation of use of other experiments.

To solve the problem of the bubble growth, the numerical method must obviously be based on a model for the non-isothermal liquid-vapor flows with phase-change. The main physical phenomena the numerical method should be able to reproduce read

1. two phase flow induced by recoil, buoyancy and capillarity
2. conductive and convective heat transfer at least inside the liquid phase
3. interface jump conditions
   (a) energy balance: latent heat
   (b) momentum: recoil and capillary forces
   (c) mass: phase change induced flow
4. ability to treat the triple line (contact between solid, liquid and vapor)

It is worth noting that the compressibility of the bulk phases is not considered as a key parameter for the description of the NB flows. Indeed, even though it classically plays a major role only in the nucleation stage, *e.g.* [28], compressibility of the liquid and vapor does not appear neither in the main physical mechanisms of the NB regime (*cf.* our presentation in section 1.2) nor in all the BC models considered (*cf.* in section 1.3) or more especially in the Zuber correlation for the CHF. As a consequence, and in order the numerical method not to be un-necessary complex, the ability of the model to take into account the compressibility of either the liquid or the vapor phase is not required. The neglect of compressibility of the liquid and vapor phases will be shown to lead to an interesting simplification in the numerical methods. These methods are reviewed in the following chapter in view of their application to solve the target problem defined in the present chapter.

1.6 Conclusion on the study of the BC mechanism

In section 1.1, we have defined the boiling crisis (BC) as a departure from the nucleate boiling regime and justified the interest of studying such a phenomenon. The BC mechanism is nowadays not well understood although its understanding is of primary interest for the study of the nuclear power plants safety as well as for the understanding of the boiling process at high heat flux in general. We have in section 1.2 introduced the different physical mechanisms that actually play an important role in the NB regime at conditions near the BC and that could *a priori* be related to the BC phenomenon. These different mechanisms have been classified according to three different length scales corresponding to three different levels of description of the NB regime. Indeed according to the BC mechanism considered, a different level of description of the NB regime is required. We have reviewed in section 1.3 the different BC models. The analysis of the different BC models has revealed the lack of understanding of the nature of the BC phenomenon. Indeed no experimental evidence can sufficiently support any BC model and that for each level of description of the NB regime considered. As a consequence,

experimental investigations need to be pursued in order to get a real improvement in the understanding of the BC. Nevertheless there has been recently an interesting improvement in experimental techniques that allows to gain in understanding of some NB mechanisms near BC conditions in a very near wall region. We have analyzed these mechanisms in section 1.4 in order to evaluate the consistency of the BC models with regard to experimental observations. The following conclusions have been drawn:

- ⋆ there exists actually a valid scale separation between the near wall region where bubbles first nucleate and grow as they are still pinned to the wall and a far wall region where larger bubbles flow inside a continuum of liquid and whose size is dictated by the RTI
- ⋆ local drying transitions of the wall occur in the NB regime for heat fluxes below the CHF value and have been identified as precursor events of the larger drying transition that occurs at DNB.
- ⋆ these local drying events are associated with irregular bubble growth events and are *a priori* not related to any lateral coalescence event

As a consequence the location of the BC mechanism has been related to a very near wall region where these irregular bubble growths take place. These irregular bubbles can only be modeled with the help of a high level of decription of the NB regime corresponding to our "local" scale. Moreover it has been shown that the Zuber correlation, that allows to well predict the value of the CHF and that is initially inherited from a description of the NB regime at the "two-phase flow" scale, is in fact not associated with any particular level of description of the NB regime. As a consequence, the study of the NB regime at the "local" scale has been shown to be of primary interest for the understanding of the BC phenomenon.

Based on these results, we have thus proposed to study a BC mechanism at the "local" scale that is consistent with the experimental observations reported in section 1.4. In section 1.5, we have defined such a mechanism for the BC. This mechanism is based on the competition between the spreading dynamics of an irregular bubble (that can be related to the recoil instability proposed in [70, 100, 120]) and the dynamics of departure of this bubble from the wall (that can be related to the combination of both capillary and gravity forces). It has been postulated that at DNB conditions the spreading dynamics is no more balanced by the departure dynamics, leading to a drying transition (the establishment of a thin vapor film in contact with the wall). This mechanisms has been shown to be consistent with the experimental observations and to be able to explain both the transition from the NB regime toward the TB and FB regimes. Moreover the main physical mechanisms involved are consistent with the successfull Zuber correlation.

As a consequence, to attest this BC mechanism or at least to provide a gain in understanding of the mechanisms of the high heat fluxes NB regime, the study of the growth dynamics of an irregular bubble has been proposed as an interesting target problem. Due to the complex and time dependent geometry of such a bubble, the use of numerical simulation has been proposed to study this problem adequatly. Moreover we have specified the main physical phenomena that the numerical method used should be able to reproduce. It is interesting to note that it is *a priori* not required to deal with a compressible model of the liquid and vapor phases.

In the following, we review the available numerical methods for the resolution of the liquid-vapor flows with phase-change and introduce our motivation for the development of a new method.

Chapter 2

Solving the nucleate boiling flows, a review

In this chapter, we study the different numerical methods allowing to study the dynamics of a bubble growth.

This chapter is organized as follows. First we introduce the problematic of the solving of the bubble growth dynamics. We then consider the different numerical techniques allowing to solve this dynamics (see section 2.1). Each of them has advantages and limitations. We redirect our attention on the numerical methods based on diffuse interface models and motivate this choice. In section 2.2 we consider the ability to use the classical van der Waals model for the study of the boiling flows of interest in this study. We show that the use of the van der Waals model for such a mesoscopic problem is too limited. We therefore consider another family of diffuse interface models based on the introduction of an abstract "order parameter" for the description of a two-phase system: the so-called phase field models (see section 2.3). We present the main features of these models and their ability to provide a much more useful regularization of the boiling problem than the van der Waals model as soon as mesoscopic studies are targeted. We then specify the main properties such a model should satisfy in order to envisage numerical simulations of the nucleate boiling flows. The phase field models devoted to the description of the liquid-vapor phase transition are then reviewed and it is shown that none of the existing models actually satisfies the whole set of required properties. As a consequence we propose in the next chapter to derive new phase field model devoted to the study of the nucleate boiling flows.

2.1 The boiling as a free boundary problem

In this section we study the main families of numerical methods devoted to the study of nucleate boiling flows. They are mainly of two types according to the mathematical representation (either explicit or implicit) of the liquid-vapor interface. We first consider the methods using an explicit representation of the location interface and then the one using an implicit representation of the location of the interface.

2.1.1 Necessity of a specific numerical treatment of the interface

In this section, we establish the necessity of a specific numerical treatment of the liquid-vapor interface to solve the boiling flows and introduce the main mathematical techniques for the representation of the interface.

The governing equations of the nucleate boiling flow The boiling fluid is locally either liquid or vapor. From the mathematical point of view, the two phases can be considered as a field that has two single phase regions, with moving boundaries that separate the phases. The differential equations, say the Navier-Stokes equations, hold for each of the fields separately, but cannot be applied to the whole field without violating the condition of continuity at the boundaries of each of the fields, the interface location. These boundaries, *i.e.* the geometry of the interfaces is unknown *a priori* as a function of time and space. At the interface a set of jump conditions are actually satisfied, the Rankine-Hugoniot jump conditions. These jump conditions are studied in the appendix, section A.2. The main problematic of solving the boiling flow is thus to take into account the interface as a moving boundary. Let us consider the mathematical representation of the interface.

Representation of the interface location The location of an interface $\boldsymbol{x}_i$ in a three space dimensions system can always[1] be related to the location of a surface. The mathematical description of a surface can be either explicit, *i.e.* $\boldsymbol{x}_i = f(t)$, or implicit, *i.e.* $F(\boldsymbol{x}_i, t) = 0$, where $\boldsymbol{x}_i$ denotes the position of the surface. This distinction is at the basis of two families of numerical method for the solving of the boiling flows. In the first family, the explicit representation of the interface is used which implies to track the surface along the numerical simulation. The corresponding methods are therefore denoted tracking methods. They are presented in the next section. In the second family, the implicit representation of the interface is used. The field F is not unique and only its zero iso-contour determines the location of the interface. As a consequence the location of the interface is only a part of the field F. The knowledge of the field F is sufficient to "capture" the interface location. The corresponding methods are denoted "front capturing" methods. Since the definition of F can be extended to the whole two-phase system as an Eulerian field, F can be numerically treated as any other physical main variable of the two-phase fluid description and there is no need to use a specific numerical discretization for the interface. These methods are presented in section 2.1.3 and following.

2.1.2 Explicit tracking of the interfaces

When the interface is represented explicitly, its location is tracked with the help of a moving mesh. There exists two main ways of tracking the interface dynamically. Either a part of a the discretized elements used for describing the physical domain represents the interface, or a moving additional Lagrangian grid is superposed to the fixed Eulerian grid. In the first case, the method is either purely Lagrangian or mixed (methods arbitrary Lagrangian Eulerian, ALE). In the second case, the resolution on the Eulerian grid must be coupled with the time dependent position of an additional Lagrangian grid which represents the interface. These are the so-called front-tracking methods.

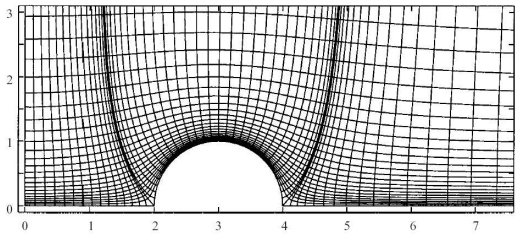

Lagrangian and ALE methods The most inconvenient feature of the purely Lagrangian methods is that the mesh becomes rapidly highly distorted. As a consequence they, are to our knowledge, not applicable to the study of the liquid-vapor phase change simulations. For the second category of method, namely the ALE methods, *cf.* [27], a particular sub-element of the mesh is associated to the interface as represented on the figure on the left. The interface being of time dependent geometry, the mesh is distorted with time. As a consequence the governing equations need to be solved on a curvilinear moving mesh. If this method allows actually a very accurate description of the interface its numerical handling is costly and complex. Moreover the ability to take into account topological transitions as well as several bubbles is really limited.

[1] *i.e.* for the two different cases where the interface is considered either as a sharp discontinuity or as a volumetric transition zone. The Gibbs' representation of the interfaces provides the formalism allowing to switch from one representation to the other one.

Front-tracking method In these methods the geometry of the interface is described with the help of a Lagrangian mesh (dots on the RHS figure) superposed on a fixed Eulerian grid (squares on the RHS figure), *e.g.* [140]. In the algorithm, the motion of the interface is an independent step of the calculation. This engenders major difficulties to apply constraints to this motion that are consistent with the main physical balances (mass, momentum, energy), *e.g.* [91]. The distortion of the Lagrangian mesh due to the motion of the interfaces requires to regularly reconstruct this mesh, *e.g.* [126] . Moreover, even though the interface is represented as a sharp surface, a necessary smearing of some source terms, like the surface tension force[2] , must be introduced in order the solving of the governing equations on the Eulerian grid takes into account the physics of the interface. This smearing is numerically controlled and its consequences on the main balances cannot be analyzed. The topological transitions are not naturally taken into account.

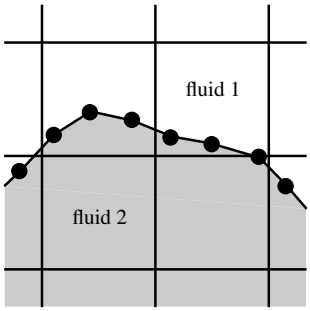

Concluding remarks As a partial conclusion, the use of an explicit representation of the interface leads to numerical difficulties for the treatment of the interface motion. As a consequence the accuracy of the main balances can be difficult to handle. Moreover even though the interface is sharply represented, it is necessary to smear its properties in order to take them into account in the physical balance equations. This smearing is numerically constrained and its consequences on the consistency of the governing equations cannot be analyzed. As a conclusion the main difficulties of dealing with these methods lies in the handling of the numerical representation of the interface. We see in the following that the difficulties are of different nature with interface capturing methods.

2.1.3 Interface capturing and diffuse interfaces

General presentation The main idea behind interface capturing methods is to use an implicit definition of a surface to describe the interface, rather than an explicit definition. This makes easier the numerical determination of the time dependent location of the interfaces. In this section 2.1.3, we provide a short presentation of the basic ideas allowing such an interface description. Two main families of such methods exist namely the level-set and diffuse interface methods. Level-set method is presented in the following. In section 2.1.4, we present the formalism of the diffuse interface models and the relevance for their use in numerical simulation.

In the implicit description, the function F is not unique, since only its zero iso-contour is relevant, but it can be smooth in the entire domain. If $\boldsymbol{V}_i$ is the speed of displacement of the surface, the motion of the surface is then described either by $d\boldsymbol{x}_i/dt = \boldsymbol{V}_i$ or by $\partial F/\partial t + \boldsymbol{V}_i \cdot \nabla F = 0$ where ∇ denotes the spatial Eulerian gradient operator. Provided that the velocity $\boldsymbol{V}_i$ defined at the surface can be continuously extended in a neighborhood around the surface [3], the latter equation is valid in the entire domain and involves only smooth functions, which is numerically much easier to handle. Moreover, the resolution of this equation is similar to any other balance equation, which makes its resolution easy and efficient (which is more especially interesting in view of three space dimensions simulations and for parallel computations). To enable this efficiency, it is therefore required to provide a well-defined smearing of the velocity of the interface. This idea is the key of interface capturing methods as opposed to interface tracking methods. Among the interface capturing methods, the most popular is the level-set method. The diffuse interface methods also belong to this class of interface capturing methods. The main difference between the level-set and diffuse interface methods is that the latter is thermodynamically consistent and is better suited for flows in which capillary phenomena cannot be neglected. F as well as the smeared velocity field $\boldsymbol{V}_i$ can be either purely numerical (level-set) or more physical (diffuse interface). The equation of evolution for F, thus determining its Lagrangian derivative (dF/dt) and the motion of the interface, is then different, even though the main idea remains the same. Let us also precise that since the time evolution of the location of the interface is implicit, the topological transitions are automatically taken into account, even though their occurrence may not always be relevant or accurate. It is worth noting that the main efforts of the interface capturing methods (with regard to the interface tracking presented in section 2.1.2), are reported on the definition and computational management of the smearing of the fields around the interface location.

[2] The surface tension is most of the time taken into account using the continuous surface force CSF method [18].

[3] For instance in a two-phase flow without interface mass transfer, the velocity field of the bulk phases can be used for such an extension. Indeed, in this case, as stated by the Rankine Hugoniot jump condition corresponding to the mass balance (*cf.* the study of the Rankine Hugoniot jump conditions in the appendix, section A.2), the bulk velocities at the interface are both equal to the interface velocity.

Level set methods This method is for sure the most popular of the interface capturing methods, *e.g.* [123]. In these methods the necessary smooth extension of the main variables around the sharp interface is made using a numerical distance function as the field F. To control the smearing of this field, it is regularly re-initialized. One of the difficulties of the level-set method is to ensure that the mass is actually conserved when the smearing of the distance function is such re-initialized. To improve the mass conservation, the coupling of the re-initialization with a Lagrangian displacement of particles can be used, *e.g.* [48]. It is worth pointing out that the use of the so-called "ghost-fluid" method, *e.g.* Liu et al. [88], allows to accurately take into account the jump conditions in the normal direction to the interface. However the accurate taking into account of the surface tension is still a challenging problem.

2.1.4 General presentation of the diffuse interface models

Let us consider a two-phase system where the bulk phases are separated by an interface. In diffuse interface models, the interface is considered as a continuous transition zone. The main issue is then to describe the behavior of fluid particles that are located within the transition region. To do that, the two-phase system is first studied thermodynamically and the corresponding equations of motion are then derived. In this chapter and in chapter 3, we focus only on the thermodynamic modeling; the corresponding equations of motion are derived and analytically studied in chapter 5.

In this section we present the basic formalism of the diffuse interface thermodynamic modeling and introduce the main diffuse interface models.

Thermodynamic modeling using local dependence with regard to the "order parameter" Let X be the main thermodynamic variable that allows to distinguish the bulk phases of the system, say the local mass density ρ for liquid-vapor phases of a pure substance or the local mass fraction for two non-miscible phases (water and oil for instance). The values of X within the bulk phases are different (by definition) and these values are thus characteristic of the bulk phases (for instance, $\rho \simeq \rho_v^{sat}$ in the vapor phase and $\rho \simeq \rho_l^{sat}$ in the liquid phase for a liquid-vapor system). X is therefore an intensive variable. The spatial average of the X field over the system volume is meaningful and defines the mean value $\langle X \rangle$ for X. As classically done in diffuse interface modeling, the variable X is called the order parameter of the phase transition, even though the use of this concept can be viewed as abusive. Let us also consider that the entire system can be described by a single energy functional E depending, as a first modeling step, on the local value of X, say $E = E_0(X)$ (for instance the Helmholtz free energy $F(\rho)$ for the liquid-vapor system)[4]. Let us present an E_0 function allowing to describe a two-phase system. Let us denote 1 and 2 the two different phases. E_0 is convex around the characteristic bulk values for X, say X_1 and X_2, such as illustrated on figure 2.1. Let us remark that, for a range of intermediate values of X where $E_0(X)$ is non-convex, such as $\tilde{X}$ on figure 2.1, the system cannot exist as a homogeneous single-phase state because it is thermodynamically unstable. Therefore only a given range of X values is locally accessible, which corresponds to the convex parts of the function $E_0(X)$. For instance, let us consider a system where the mean value $\langle X \rangle$ of X is such that $\langle X \rangle = \tilde{X}$. This means that the mean $\langle X \rangle$ value cannot correspond to any local X value. The system is therefore separated in domains, say the bulk phases, where the local values of X belong to the ranges where the function $E_0(X)$ is convex. The continuous energetic description $E_0(X)$ is therefore sufficient to model the phase separation process. Moreover between two bulk domains, X cannot adopt the intermediate values corresponding to the non-convex part of E_0. The field X undergoes thus a jump at the boundary between the bulk domains. The function E_0 provides therefore the description of the interface as a sharp discontinuity. As a partial conclusion, the thermodynamic modeling of a multi-phase system based on an energy functional depending solely on the local value of the "order parameter" allows to model the phase separation process with a sharp interface description. Since this latter characteristic is not the one desired, let us go a step further in our thermodynamic modeling of the two-phase system considered.

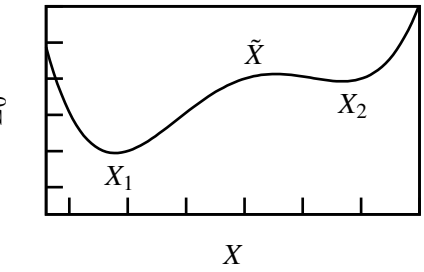

Figure 2.1: Original energy functional

[4] the dependence with any other relevant thermodynamic variables is omitted for the sake of simplicity

Thermodynamic modeling of the structure for the interface as a volumetric transition layer Across an interface, X varies continuously on a small length scale, defining a volumetric transition zone, actually sharp from a macroscopic point of view. The states of the particles inside this transition layer are not modeled by $E_0(X)$. In order to model the structure of this layer with the help of a purely conservative model (or more generally with the conservative part of the constitutive model, *i.e.* without considering any dissipative effect), a length scale is introduced in the energy functional that we have imagined to originally reduce to $E = E_0(X)$. The simplest non local generalization refers to the van der Waals' theory of capillarity [142] (1894) and reads

$$E(X, \nabla X)$$

Let us briefly illustrate how this dependence leads to define a thickness to the interface structure. In order to be more specific, let us consider the following expression for E

$$E(X, \nabla X) = E_0(X) + e_1 (\nabla X)^2$$

where $E_0(X)$ represents the original model and e_1 is a positive parameter (the capillarity coefficient in the liquid-vapor transition). The description of the homogeneous states, *i.e.* where $\nabla X = 0$, is not concerned by the additional non-local contribution. The single-phase model of the system is therefore unaffected by the existence of the non local contribution. Let us study the modification of the two-phase states of the system. In order to illustrate, we consider again the system of given X mean value $\langle X \rangle = \tilde{X}$ (*i.e.* corresponding to an unstable homogeneous state). Let us study the state that minimizes the total energy of the system. Since E is composed of two parts, namely the, say local, contribution E_0 and the non-local $e_1 (\nabla X)^2$, let us begin by considering each part separately. As already expressed, under the constraint $\langle X \rangle = \tilde{X}$, the system should be made of separated bulk phases in order to minimize E_0. The nonlocal contribution $e_1 (\nabla X)^2$ introduces an energetic penalty for the non-homogeneous states. Between the bulk phases, the field X can therefore not undergo a sharp jump that would induce an infinite local value for the square gradient term, but rather a smooth variation. With the single $e_1 (\nabla X)^2$, the state minimizing the energy of the system is the homogeneous $X = \langle X \rangle$ field. The two different states minimizing each energy contribution are thus incompatible while $\langle X \rangle = \tilde{X}$. Let us consider that the non local contribution tends to smooth the X variations between the bulks. In the region where X varies from the bulk values X_1 and X_2, X takes locally some values penalizing the E_0 energy part. Therefore a large spatial extent of this transition region is energetically penalizing. The final state corresponds to an optimization of the extent of this layer, therefore defining a thickness for the transition layer.

Thus, the dependence of the energy functional with respect to X and ∇X provides a model for the coexistence of bulk phases together with a model for the structure of an interface layer. All the diffuse interface models are based on such a thermodynamic modeling, using basically the same formalism. Let us note that the nonlocal contribution term ∇X to the energy of the system can be justified by a study of the interaction particle using the mean field theory, *e.g.* Rowlinson and Widom [115].

The main diffuse interface models For the liquid-vapor phase transition, the corresponding diffuse interface model is the so-called van der Waals' model inherited from the theory of capillarity of van der Waals [142]. In this case, the density ρ is the natural "order parameter". The presentation of this model, also called second-gradient, in the scope of our targeted numerical applications is the subject of the section 2.2. For binary mixtures, the local mass fraction of one component of the mixture is the natural "order parameter". The corresponding diffuse interface model is due to the work of Cahn and Hilliard [26, 25]. For further details, Anderson et al. [4] provide a review of diffuse interface methods in fluid mechanics. The phase field models are diffuse interface models where an abstract "order parameter" is used. They are widely used in materials science while studying solid-solid or solid-liquid phase transitions. For a detailed presentation of phase field methods in materials science, we can refer to Emmerich [47]. Phase field methods are presented and reviewed in view of our application in section 2.3.

2.1.5 Diffuse interface models *versus* sharp interface models

The main difference between the the sharp and diffuse interface models lies on the original (say physical) representation of the interface. But this has not only consequences on the compared relevance of the physics modeled but also on its computation. Let us consider the problematic for solving the temporal evolution of a multi-phase system.

Sharp interface methods presented in sections 2.1.2 and 2.1.3 are based on the Gibbs' theory of interfaces. The interfaces are thus modeled as sharp discontinuities possibly endowed with interface properties (such as surface quantities). The Gibbs' theory does not consider the fine structure of an interface layer as in diffuse interface models presented hereinabove. This theory therefore provides an interesting simplification of the more complete diffuse interface one. However, from a numerical point of view, the sharp modeling induces some complexity in the algorithms as mentioned in section 2.1.2. The introduction of a diffuse interface layer provides a physically inherited smearing of the interface allowing the use of more easily handleable algorithms, say a computational simplification (*cf.* 2.1.3). Therefore two simplifications of different nature can be considered while comparing the two models. It allows to consider the multi-phase model under the two different angles

- ⋆ the physical problem of the interface layer
- ⋆ the mathematical problem of dealing with free boundaries and the associated computational problem

We therefore propose to present in the following the sharp and diffuse interface models in view of these different angles. This defines the relevance of use of these models for different applications.

Physical relevance of the description of an interface as diffuse As stated hereinabove an interface has a characteristic physical thickness, denoted h in the following. The typical value of h far from the critical point lies between the nanoscopic and the microscopic scale. Let us consider a physical process where other physical length scales L are involved (typically the extent of the bulk phases). The Gibbs' theory provides a way to avoid the complex problem of determining the fine structure of an interface in the case where $h \ll L$. Therefore the sharp interface model is relevant for the description of mesoscopic physical processes, such as the dynamics of one or several developed inclusions whose size L satisfies $h \ll L$. This is the case while dealing with boiling flows including several bubbles or drops, say of mesoscale in the following.

The scale separation $h \ll L$ constitutes a limit for the physical relevance of the use of diffuse interface models. Diffuse interface methods are required when, for example, the extent of bulk phases (either the distance separating two interfaces or the radius of curvature of an inclusion) is locally of the order of magnitude of the interface thickness. It is then required to determine the governing equations for the fluid particles inside the interface layer (the diffuse interface model provides such a description of the fluid). This is the case while dealing with coalescence (reconnection, merging ...), break-up (pinch-off, fragmentation ...), appearance (phase separation, *i.e.* nucleation or spinodal decomposition) or disappearance (collapse) of one or several inclusion(s). Conditions close to the critical point are also concerned by this relevance since the interface thickness undergoes mesoscopic values while approaching the critical conditions, say $h \simeq L$. Let us also mention the moving contact line problem (triple line, contact angle, wetting ...) addressing the description of a fluid-fluid interface in contact with a solid, *i.e.* the common boundary of three different phases (*e.g.* [62, 111, 112]).

We have therefore presented the physical relevance of the use of either diffuse or sharp model for an interface. It is based on the relevance of determining the fine structure of the interface layer. While the internal dynamics of the structure can be considered as not interacting with the rest of the physical process the simplification of the sharp theory is justified.

Numerical relevance of diffuse interface models out of the domain of its physical relevance Let us consider a mesoscale physical process for which the physical relevance of the description of the interface layer does not hold *i.e.* $L \gg h$. As mentioned in section 2.1.3, the implicit description of the interface is numerically attractive. Diffuse interface models enable this implicit formulation, adding the interesting property of thermodynamic consistency for the description of the diffuse layer. However the use of the physical model of the interface layer can be numerically irrelevant. Indeed, in numerical simulations, a third length scale exists (apart from L and h): the size of the mesh cells discretizing the system under study, say Dx. It is obvious that the condition $Dx < L$ must be satisfied. The interface layer needs to be captured by the mesh, which imposes that the condition $Dx \leq h$ must also be satisfied. The scale separation between the mesoscale of the system and the micro-scale h induces an unreasonable (and unreachable) number of mesh cells, say $L >> h \Rightarrow Dx << L$. Indeed, let us for instance consider the thickness for the interface takes the typical value of 10 Å (Ångströms) and a physical system of size $L = 10\,\mu m$. This implies the size of the mesh cell Dx to satisfy $L/Dx \simeq L/h \simeq 10^4$ and for three dimensional computations, the required number of cells is of the order of magnitude of 10^{12}. Therefore while the physical

relevance of the diffuse interface models does not hold, the scale separation induces an irrelevant number of cells in order to capture the fine interface structure. Even though the use of the natural diffuse interface model is in this case numerically irrelevant, the use of a diffuse interface model is numerically attractive. Let us consider in the following how it is possible to deal with a numerical diffuse interface model out of its physical relevance.

Diffuse interface models with an artificial interface thickness To use a diffuse interface, the interface thickness must approach a reasonable size Dx of a mesh cell. In this case the interface thickness is no longer constrained by the physics but rather by the numerics. It requires to develop a model for an artificial diffuse interface; this can be called a diffuse interface method.

Since we aim at determining a set of equations of motion fully compatible with the desired smearing, this smearing should be based on first physical principles. The main idea is then to use the formalism developed to describe the physical structure of the interface layer in order to develop the diffuse interface method. In this regard, diffuse interface models appear as a particularly well-suited framework. At this point, it is clear that the smearing of the interfaces is not physical and thus artificial but nevertheless it originates from a physically consistent description. Two possible paths can be followed to develop a diffuse interface method:

- ⋆ adaptation of an existing physical diffuse interface model, like the Cahn-Hilliard or the second-gradient models.
- ⋆ development of a diffuse interface model equivalent to the sharp interface model, like the phase field models.

As a conclusion for mesoscopic numerical simulations it is possible to deal with diffuse interfaces whose artificial structure is numerically tractable and obtained from a physically consistent model.

Advantage of a theoretical framework for the diffuse interface computation As mentioned in the previous sections, most of the numerical methods dealing with free boundary problems, induce an effective and numerical smearing of the interfaces. The lack of a theoretical framework allowing to analyze this smearing constitutes a major difference compared to the diffuse interface methods. Indeed, the theoretical framework of the diffuse interface models can be very helpful and inspiring to design numerical algorithms. As an example, let us mention the issue of parasitic currents that exists in all current numerical methods dealing with capillary flows. To illustrate this issue, let us consider the basic problem of a bubble in a closed box without any external force. At equilibrium, the bubble should be spherical and the entire fluid should be at rest. However, the corresponding numerical result shows the persistence of a flow made of several currents concentrated at the interface. These are the so-called “parasitic currents”. For some physical problems, the intensity of these parasitic currents can be larger than that of the main physical flow. In such cases, these numerical methods cannot be applied. For instance, for the study of nucleate boiling, they can dominate the convective heat transfer process in the vicinity of the interface and therefore lead to an unrealistic estimation of the phase transition process. Jamet et al. [68] proposed a numerical scheme to reduce these parasitic currents to round-off using the second gradient model. The analysis framework of this work is provided by the ability to control the energy exchanges in the entire computational domain. Therefore, to obtain such a result, it is necessary that the interface zone is energetically consistent. Thus, the formalism of the diffuse interface models provides an efficient analysis tool that can give the benefit to the other methods.

Conclusions on the use of diffuse interface models for the numerical simulation As a first conclusion, from a computational point of view, diffuse interface models provide an attractive (because continuous and thermodynamically consistent) set of governing equations for a free boundary problem. However, the direct use of the original diffuse interface models for mesoscopic applications is irrelevant. A well suited thermodynamic description must be used in order the solving of the structure of the interface layer being actually relevant and numerically tractable. This thermodynamic model is based on the formalism of the diffuse interface models but induces an artificial interface thickness. The resulting structure of the interface layer needs then to be carefully studied in order to control the consequences of the artificial smearing on the interface properties. However the thermodynamic consistency of the smearing induces an interesting framework for the study of the numerical scheme and the comparison with (and eventual improvements of) the other numerical methods based on a sharp interface model.

Conclusion on the numerical methods for the simulation of nucleate boiling

Different numerical methods that can be used to study the nucleate boiling flows have been presented. The main difference between the diffuse interface methods and the other methods lies on the nature of the difficulty of their use. The interface tracking methods have been shown to have mainly difficulties to manage the interface displacements. The level set methods have difficulties to take into account a consistent smearing of the distance function. In the diffuse interface methods the difficulty lies on the necessary thermodynamic description of the interface layer. However, the gain in consistency with regard to the other method and its ability to model naturally the topological transitions provides some supplementary advantages. For this reason, it appears as benefit to use a numerical method based on this formalism. Its analysis should brings some interesting results for the other numerical methods. In the following of this study of simulation of boiling flows, we therefore choose to use a diffuse interface method. As mentioned by Sethian [123] in his review of the level set methods when presenting the different techniques for computing problems with moving interfaces, *(...) the strict delineations between various approaches is not meant to imply that the various techniques have not influenced each other. (...) Good numerics is ultimately getting things to work; the slavish and blind devotion to one approach above all others is usually a sign of unfamiliarity with the range of troubles and challenges presented by real applications.*

Let us review the existing diffuse interface models for the liquid-vapor flows with phase change.

2.2 The second gradient method

2.2.1 From a diffuse interface model to a numerical method

The most natural diffuse interface model dedicated to liquid-vapor flows with phase change is the second gradient model. This model comes from the van der Waals theory of capillarity [142]. In this theory, the fluid density ρ is considered as the natural "order parameter" for the liquid-vapor phase transition. The dependence of the fluid free energy with respect to the non local field $(\nabla\rho)^2$ is justified using a mean field theory in order to describe the particle interaction inside the interface layer, *e.g.* Rowlinson and Widom [115]. The capillary stress tensor depends on both the density ρ and the local gradient of density $\nabla\rho$ as shown by Korteweg [80]. This model is currently used for the theoretical study of the liquid-vapor phase transition, *e.g.* [111, 127]. This model can be used as a numerical method to simulate liquid-vapor flows with phase change, *e.g.* [104, 97]. However, while dealing with boiling flows far from the critical point, the direct use of this method leads to prohibitive computational costs due to the very small interface thickness compared to the typical radius of the bubbles. Jamet [66] proposed a modification of the thermodynamic closure relations allowing to go beyond this numerical limitation while keeping the main features of the liquid-vapor fluid description. This modification of the thermodynamic behavior is briefly presented in section 2.2.3. Two-dimensional computations of isothermal two-phase flows, namely bubble coalescence and contact line motion, are provided by Jamet et al. [67] using this modification. Fouillet [53] more particularly studied the second gradient method in the context of wall nucleate boiling simulations (which corresponds to our own goal). This study provided qualitatively satisfactory numerical results. But it revealed also quantitative limitations for the use of the method for high wall heat fluxes and subsequent large superheats of the liquid bulk phase. In section 2.2.2, we recall the basic features of the original model allowing to understand the induced numerical problems. The possible modifications considered to get rid of some of the numerical limitations and the subsequent changes in the fluid macroscopic properties are presented in section 2.2.3. These induced changes finally renders the method inapplicable for the targeted applications as stated in section 2.2.3.

2.2.2 The thermodynamic model

The model is based on the van der Waals [142] theory of capillarity. The Helmholtz free energy F of the fluid is supposed to be made of two main contributions,

$$F = F_{cl}(\rho, T) + F_{cap}(\nabla\rho^2) \tag{2.1}$$

The second term of the right hand side, F_{cap}, implies that the fluid is endowed with capillarity and provides an internal structure to the interface that separates the bulk phases. The F_{cl} part of the energy corresponds to the

more widely known van der Waals equation of state (EOS_{vdW}), $P(\rho, T)$, for a pure fluid. Let us recall that $P(\rho, T)$ is defined from the Helmholtz free energy of the fluid $F_{cl}(\rho, T)$ as follows

$$P \triangleq \rho \frac{\partial F}{\partial \rho}_{|T,(\nabla\rho)^2=0} - F = \rho^2 \frac{\partial f}{\partial \rho}_{|T,(\nabla\rho)^2=0} \tag{2.2}$$

where $f \triangleq F/\rho$ is the specific Helmholtz free energy. For the sake of simplicity, let us consider an isothermal system at a temperature T_0 smaller than the critical temperature of the fluid. In the following, we first present the basic features of this equation of state. Secondly we present the description of the two-phase equilibrium, and thirdly the interface structure with the help of the van der Waals theory. Finally, we present the main reasons for the inability of the model to be used as it is for numerical simulations of boiling flows.

Single-phase states with the van der Waals equation of state For the isothermal case, the EOS_{vdW} reduces to a non-monotonic function $P(\rho)$ as plotted on the figure 2.2. The function $P(\rho)$ is made of two increasing parts

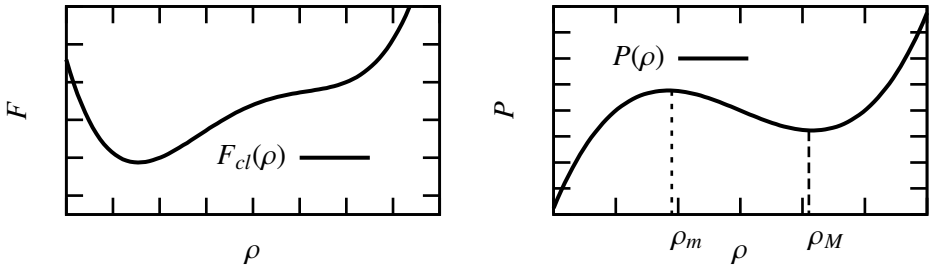

(a) Free energy (b) Pressure

Figure 2.2: Van der Waals' model

describing the two possible single-phase states, liquid and vapor. The decreasing part of the EOS_{vdW}, (*i.e.* the range of density $[\rho_m : \rho_M]$ of figure 2.2(b)), is inaccessible for homogeneous single-phase states since they are thermodynamically unstable. Let us recall that the isothermal compressibility χ_T defined as

$$\chi_T \triangleq -\frac{1}{V}\left(\frac{\partial V}{\partial P}\right)_T = \frac{1}{\rho}\frac{\partial \rho}{\partial P}_{|T} \tag{2.3}$$

must satisfy the Gibbs Duhem criterion of stability

$$\chi_T \geq 0 \tag{2.4}$$

for a single-phase state to exist, *e.g.* Papon and Leblond [107]. Using the relation (2.2) defining the pressure P from the Helmholtz free energy F and the definition of the compressibility coefficient χ_T, the unstable states correspond to a non-convex part of F_{cl} (see figure 2.3(a)).

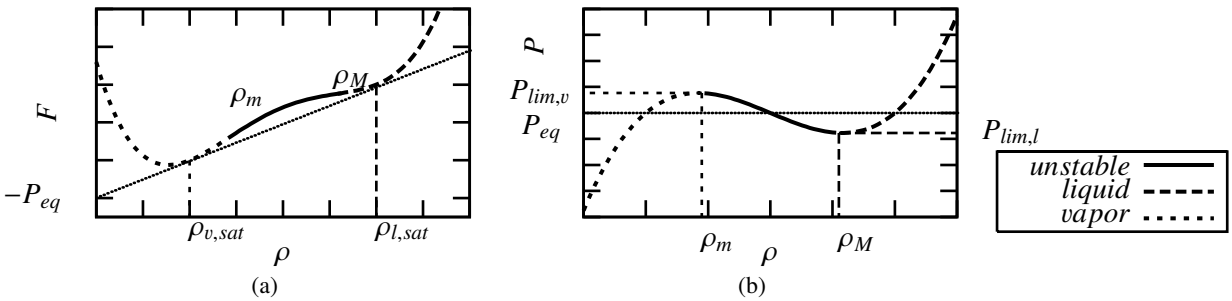

(a) (b)

Figure 2.3: Van der Waals' model

Two-phase equilibrium At two-phase thermodynamic equilibrium across a planar interface, the bulk values of the pressure and of the specific Gibbs free energy, g (also denoted the chemical potential μ in the following) are equal and take specific values (depending on the equilibrium temperature). For the van der Waals EOS_{vdW} these

equilibrium conditions are equivalent to the existence of a common tangent to the F_{cl} Helmholtz free energy at the two representative points of the single-phase states as illustrated on figure 2.3(a). The associated equilibrium value for the bulk pressure, namely the saturation pressure, is denoted $P_{eq}(T_0)$. At this pressure, the density of the single-phase states are denoted $\rho_{v,sat}(T_0)$ and $\rho_{l,sat}(T_0)$.

In order to illustrate analytically these features, let us make explicit the expression for the Helmholtz free energy part $F_{cl}(\rho)$ that is valid in vicinity of the critical point

$$F_{cl}(\rho, T_0) = A(T_0)\ W(\rho) + \mu_{sat}(T_0)\,\rho - P_{eq}(T_0) \tag{2.5}$$

where μ_{sat} is the common bulk value of the chemical potential at two-phase equilibrium and $W(\rho)$ is given by[5]

$$W(\rho) = \left(\rho - \rho_{v,sat}(T_0)\right)^2 \left(\rho - \rho_{l,sat}(T_0)\right)^2 \tag{2.6}$$

It is straightforward to show that this expression for $F_{cl}(\rho, T_0)$ satisfies the relation (2.2) for $\rho_{v,sat}(T_0)$ and $\rho_{l,sat}(T_0)$ for the same pressure $P_{eq}(T_0)$, $\mu_{sat}(T_0)$ being the slope of the common tangent of F_{cl} for these two values for the density. Therefore they correspond to the densities values at which the two-phase equilibrium condition of common tangent is satisfied.

Metastability limit The single-phase states can only exist for a given range of pressures, bounded by the maximum value $P_{lim,v}(T_0)$ for the vapor phase and by the minimum value $P_{lim,l}(T_0)$ for the liquid phase as illustrated on figure 2.3(b). This range of pressures defined here for T_0, actually depends on the temperature. For a given pressure, a corresponding range of possible temperatures for the single-phase states can be defined by bijection. Figure 2.4 provides an illustrative representation of the domain of existence of the bulk phases on a (P, T) plane.

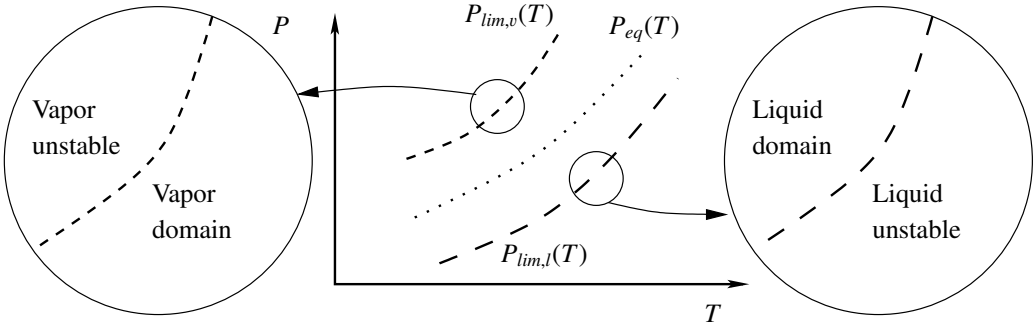

Figure 2.4: Stability domains

The bound of each bulk domain (P_{lim}) is called the limit of metastability and the corresponding curve on a (P, ρ) plane obtained by varying the temperature is called the spinodal curve. In nucleate pool boiling flows, as it has been shown in chapter 1, the liquid near the wall is locally super-heated ($T > T_{eq}(P_0)$ where P_0 is a pressure reference). When the fluid (initially liquid) locally reaches the limit of superheat the only possible state (at these conditions of pressure and temperature) is then the vapor. This leads to a bubble nucleation, *e.g.* [28]. As a consequence it is important for the two-phase flow model to control the value of this limit of superheat in order to envisage its use for quantitative numerical simulations of nucleate boiling. More particularly, if the limit of superheat of the model is too low with regard to its physical value, bubbles will naturally but undesirably nucleate in the near wall region where the liquid is the most super-heated.

It is important to note that, as shown hereinabove, the super-heat limit is closely related to the shape of the function $F_{cl}(\rho)$ between the saturation densities. Indeed ρ_m and ρ_M are the characteristic densities at which F_{cl} shifts from concave to convex and therefore at which the bulk phases shift from stable to unstable.

Interface structure and capillarity The modeling of the internal structure of the interface layer is made possible by considering the dependence of the Helmholtz free energy F with respect to the non local contribution

[5]The figure 2.3(a) is indeed obtained with such an analytic expression.

$(\nabla\rho)^2$, F_{cap}. A classical model for F_{cap} is a linear dependence in $(\nabla\rho)^2$ as

$$F_{cap} = \frac{\lambda}{2}\,(\nabla\rho)^2 \tag{2.7}$$

where λ is the capillary coefficient and is considered as constant in the remainder of this presentation. Such a fluid is said to be endowed with internal capillarity. The non local dependence introduces a specific internal length scale in the thermodynamic model related to the thickness h of the interface layer at equilibrium. Besides, an excess free energy is associated to this transition layer which is interpreted as the surface tension σ, *e.g.* Rowlinson and Widom [115]. For the definition of the excess quantities, let us refer to our presentation in appendix A.1. The physical parameter σ must be accurately modeled since it plays a major role in the boiling phenomenon.

It is worth noting that the range of values $[\rho_m : \rho_M]$ is now accessible for non-homogeneous states of the fluid, *i.e.* across the interface. Let us precise that both the surface tension and the interface thickness are defined through two features of the free energy F: its dependence with respect to $(\nabla\rho)^2$ and its dependence with respect to ρ between $\rho_{v,sat}(T_0)$ and $\rho_{l,sat}(T_0)$. This last dependence includes the range $[\rho_m : \rho_M]$ where F_{cl} is concave.

Analytical example From the given simple analytical expressions for F_{cl} (2.5) and F_{cap} (2.7), we propose to derive some illustrative examples of the previous statements. The generalized chemical potential μ_{vdW} is defined as

$$\mu_{vdW} \hat{=} \frac{\tilde{\delta}F}{\tilde{\delta}\rho} \tag{2.8}$$

where $\tilde{\delta}$ denotes the standard variational derivative

$$\frac{\tilde{\delta}}{\tilde{\delta}\ldots} = \frac{\partial}{\partial\ldots} - \nabla\cdot\left(\frac{\partial}{\partial\nabla\ldots}\right) \tag{2.9}$$

It can be shown that at two-phase equilibrium, the chemical potential μ_{vdW} is uniform (*cf.* the study of the equilibrium relations in section 3.2.2). For the given expression of F (2.1), it reads

$$\mu_{vdW} = \frac{\partial F_{cl}}{\partial\rho} - \nabla\cdot(\lambda\nabla\rho) \tag{2.10}$$

Using the particular polynomial expression for F_{cl} (2.5) yields

$$\mu_{vdW} = \mu_{sat} + 2\,A(T_0)\,\left(\rho-\rho_{v,sat}(T_0)\right)\left(\rho-\rho_{l,sat}(T_0)\right)\left(\rho-\frac{\rho_{v,sat}(T_0)+\rho_{l,sat}(T_0)}{2}\right) - \nabla\cdot(\lambda\nabla\rho) \tag{2.11}$$

In the bulk phases, $\mu_{vdW} = \mu_{sat}$. Therefore, the uniformity of the chemical potential implies that, for the specific analytical expression of F proposed, the density field ρ satisfies the following differential equation

$$2\,A(T_0)\,\left(\rho-\rho_{v,sat}(T_0)\right)\left(\rho-\rho_{l,sat}(T_0)\right)\left(\rho-\frac{\rho_{v,sat}(T_0)+\rho_{l,sat}(T_0)}{2}\right) - \nabla\cdot(\lambda\nabla\rho) = 0 \tag{2.12}$$

For a planar interface normal to an arbitrary x-axis, the ρ profile has the analytical expression

$$\rho(x) = \frac{\rho_l+\rho_v}{2} - \frac{\rho_l-\rho_v}{2}\tanh\left(\frac{\rho_l-\rho_v}{2}\sqrt{\frac{2A}{\lambda}}x\right) \tag{2.13}$$

where we have arbitrarily set the center of the profile in $x = 0$ and the liquid, resp. vapor, phases at $x = -\infty$, resp. $x = +\infty$. This profile has a characteristic thickness h that can be defined as

$$h \hat{=} \frac{\rho_l-\rho_v}{\max|d\rho/dx|} \tag{2.14}$$

From the ρ profile (2.13), one gets

$$h = \frac{4}{\rho_l-\rho_v}\sqrt{\frac{\lambda}{2A}} \tag{2.15}$$

It can be shown (*cf.* appendix A.1) that the excess Helmholtz free energy induced by the equilibrium profile $\rho(x)$ (2.13) provides the following value for the surface tension coefficient σ

$$\sigma = \frac{(\rho_l-\rho_v)^3}{6}\,\sqrt{2\,A\,\lambda} \tag{2.16}$$

The number of parameters entering the expression for F in order to recover the main physical properties required for the model of the liquid-vapor isothermal flow It has been shown with the help of a particular expression for F that the main features of the isothermal liquid-vapor equilibrium can be modeled with a set of 6 main parameters, namely

- ⋆ the bulk density values $\rho_{l,sat}$ and $\rho_{v,sat}$
- ⋆ the two parameters A and λ defining σ and h
- ⋆ the two equilibrium values for the chemical potential and pressure, P_{eq} and μ_{sat}

The compressibility coefficient of the bulk phases and their metastability limit are then consequences of these choices. Let us remark that with these 6 parameters these relations are quite simple and easy to handle [6].

The original model as a numerical method As stated in the introduction of diffuse interface models (see section 2.1.4), the use of diffuse interface models can be considered either as physically relevant or numerically relevant. The van der Waals model allows to deal with liquid-vapor flows with phase change. Let us define its domain of physical relevance and how it is related to our targeted applications of numerical simulations of nucleate boiling flows. As stated in the section 2.1.4, the physical relevance is ensured by a common length scale for both the bulk phases extension and the interface thickness. Let us mention some examples of application of the second gradient method for numerical simulation of two-phase flows. The work of Onuki [104] provides an example of use of the second gradient model for the numerical simulation of thermo-capillary flows near critical conditions in a zero gravity environment. Nadiga and Zaleski [97] studied the instability of a liquid jet at high Reynolds number and the spinodal decomposition with the help of an isothermal second gradient model.

The case of nucleate boiling flow It has been shown in chapter 1 that the study of interest in this work is the numerical simulation of a bubble growth in high heat fluxes NB regime conditions. The typical length scale for the simulation targeted is therefore of the order of a bubble diameter, *i.e.* of $1mm$. This bubble diameter has to be compared with the interface thickness h. The typical value of h far from the critical point (our own range of application for the boiling study) is of the order of magnitude of a few molecular layers, say a few tens of Ångströms. The criterion of the physical relevance of the model is not satisfied. Let us state quantitatively that the numerical use of the model is however out of reach. The necessity of solving the internal structure of the interface layer induces small mesh cells in the transition zone where about 5 discretization elements in the normal direction to the interface are required. The scale separation between the domain size and the necessary cell size is huge (of the order of 10^{-6} that has to be accounted for in the three directions). Even with the help of numerical methods for local and necessarily dynamic (since we are dealing with a free boundary problem) mesh refinement in these inhomogeneous zones, it induces a prohibitive number of cells (on the order of 10^{20}). For these reasons, the direct use of the van der Waals model as a numerical tool for boiling flows is out of reach. This justifies to consider the original van der Waals model as the basis of a more useful and artificial model that could be used for the numerical simulations of nucleate boiling flows. The presentation of the subsequent modified model is provided in the next section.

2.2.3 Modifications and associated limitation of use

The basic idea of the modification We present the numerically motivated modifications of the van der Waals model. The modified model is based on the physical original model and keeps its essential features including the mathematical structure described in the previous section. In order to overcome the limitations of use of the original model, Jamet et al. [68] proposed to artificially increase the interface thickness. Since this length scale is defined with the help of both the concave part of F with respect to ρ and its dependence with regard to $(\nabla\rho)^2$, the increase is made possible by modifying the thermodynamic description of the fluid. Let us illustrate this modification with the help of the analytical expression proposed for F_{cl} (2.5), and F_{cap} (2.7). The interface thickness h is a function of the bulk density and of the two parameters λ and A. Let us recall that the expression

[6] Even though the number of controlled parameters entering the expression of F_{cl} is increased, it can be shown that we indeed recover the same basic features presented hereinabove as well as the same limitations when dealing with a modification of the original model as presented in section 2.2.3.

for the surface tension coefficient σ implies same parameters. The surface tension and the bulk densities are essential properties of the fluid description that must be kept unchanged while enlarging artificially the interface. Therefore, in order to modify h, the ratio of the two parameters A and λ must be modified while their product must be kept unchanged.

$$\left\{\begin{array}{l} h_0 = \frac{4}{\rho_l-\rho_v}\sqrt{\frac{\lambda_0}{2A_0}} \\ \frac{\sigma_0}{(\rho_l-\rho_v)^3} = \frac{\sqrt{2A_0\lambda_0}}{6} \end{array}\right. \xrightarrow{\text{modification}} \left\{\begin{array}{l} h_{mod} = \frac{4}{\rho_l-\rho_v}\sqrt{\frac{\lambda_{mod}}{2A_{mod}}} = K\,h_0 \\ \frac{\sigma_{mod}}{(\rho_l-\rho_v)^3} = \frac{\sqrt{2A_{mod}\lambda_{mod}}}{6} = \frac{\sigma_0}{(\rho_l-\rho_v)^3} \end{array}\right. \Rightarrow \left\{\begin{array}{l} \frac{\lambda_{mod}}{A_{mod}} = K^2\frac{\lambda_0}{A_0} \\ \frac{\lambda_{mod}}{\lambda_0} = \frac{A_0}{A_{mod}} \end{array}\right. \tag{2.17}$$

$$h_{mod} = K\,h_0 \Rightarrow \left\{\begin{array}{l} \lambda_{mod} = K\,\lambda_0 \\ A_{mod} = K^{-1}\,A_0 \end{array}\right.$$

More generally, in order to keep the physical value of σ, while enlarging the interface, we get a two equations (the artificial h and the physical σ to be fixed) and two-unknowns (the two different parts F_{cl} and F_{cap} of F) problem to solve. For the analytical example provided hereinabove, these two unknowns are more precisely the parameters λ and A. This renders the thermodynamic modification doable. Such a modification is illustrated by (2.17) in the case of the simple six parameters van der Waals model presented in the previous section. We introduced a proportionality coefficient K for the ratio of the original interface thickness h_0 with the artificial thickness h_{mod}. We'd like the model to induce, $K \triangleq h_{mod}/h_0 \gg 1$. Simple calculations of (2.17) show how to get the value h_{mod} for the interface thickness while keeping the values of the bulk densities ρ_l and ρ_v and of the surface tension coefficient σ unchanged: the capillary coefficient must be multiplied by the factor K whereas the coefficient A must be divided by the same factor K, other parameters (namely $\rho_{l,sat}$, $\rho_{v,sat}$, P_{eq}, μ_{sat}) entering the expression for F_{cl} remaining unchanged. In [66], Jamet studied the consequences of such an increase of h on the dynamics of the internal structure of an interface during a liquid-vapor phase-change process. This study showed that the modification of the thermodynamic had a limited influence on this process. However it is worth emphasizing that, for the method to be numerically tractable for nucleate boiling simulations, the interface thickness must be increased by a huge factor, typically of the order of $K = 10^5$. This implies that the order of magnitude of the modification of the parameters, say the ratio A_{mod}/A_0, is of 10^{-5}. The analytical formulation is not unique and classes of functions other than the one presented can be used. Nevertheless, it turns out that one always deals with equivalent problematic.

Limitation of the modifications of the thermodynamic model

A modified limit of metastability The modification of F_{cl} necessary to artificially increase h must at least be effective on a part of the range $[\rho_{v,sat} : \rho_{l,sat}]$. As a consequence of the increase of h of a factor $K \simeq 10^5$, it has been shown that it is required the parameter A to decrease of a factor $K^{-1} \simeq 10^{-5}$. From the expression (2.5) for F_{cl} it implies the ratio of the non-linear contribution $W(\rho)$ with regard to the linear contribution $\mu_{sat}\rho$ to be decreased by the same factor K^{-1}. It therefore implies a flattening (tends to a quasi-linear function) of the variations of the function $F_{cl}(\rho)$ between the bulk densities $\rho_{v,sat}$ and $\rho_{l,sat}$. As a consequence, the curve $P(\rho)$ is also flattened as represented by the curve "$P(\rho)$ modified" on figure 2.5. This flattening has direct visible consequences on the single-phase description since it induces a higher compressibility of the fluid. In order to

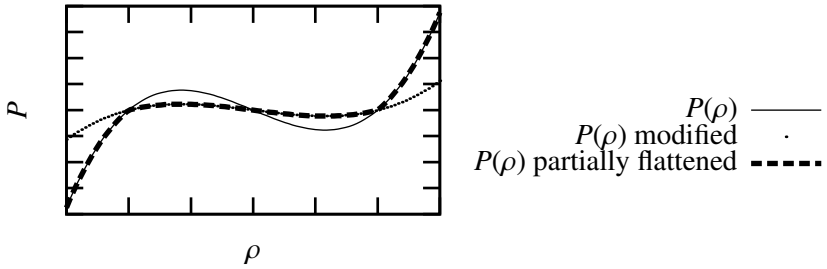

Figure 2.5: Modified van der Waals model

keep the compressibility equal to its physical value within the bulk phases, it is possible to modify the *EOS* only

on a reduced range of ρ values (as for example the "partially flattened" function $P(\rho)$ on figure 2.5). Nevertheless, the modification always affects the concave part of F_{cl}. Therefore, the limits of metastability of the bulk phases, namely the values of $P_{lim,l}(T_0)$ and of $P_{lim,v}(T_0)$, are also affected, and it can be shown that we have $|P_{lim} - P_{eq}|_{mod} = K^{-1}|P_{lim} - P_{eq}|_0$. As a partial conclusion the limit of metastability at constant temperature T_0 is reduced by a factor $K^{-1} \simeq 10^{-5}$.

Keeping unchanged the limit of superheat around a pressure value Let us consider the implication of these modifications of the limit of metastability on the limit of superheat. Indeed, an essential property of the nucleation process has been said to be the limit of superheat of the liquid. For the sake of simplicity, we here do not provide the fully explicit study of the limit of superheat as a function of the modifications envisaged but rather provide only the most important steps of the reasoning. The detailed study of the limit of superheat for the modified van der Waals model can be found in [53].

It can be shown that, when the isothermal variations of the Helmholtz free energy are given, the limit of superheat at a given pressure T_0 is defined by two functions of the temperature namely the saturation curve $P_{eq}(T)$ and the variations of the density with respect to temperature characterized by the coefficient of thermal expansion α_P of the single-phases defined as

$$\alpha_P \hat{=} \frac{1}{V}\left(\frac{\partial V}{\partial T}\right)_P = -\frac{1}{\rho}\left(\frac{\partial \rho}{\partial T}\right)_P \tag{2.18}$$

If α_P and $P_{eq}(T)$ are not modified, it turns out that if the limit of metastability is reduced by a factor K^{-1}, the limit of superheat at a given pressure is reduced by the same factor K^{-1}. This decrease of the limit of superheat for the study of nucleate boiling flows is not desirable since it leads to undesirable nucleation events in the super-heated near wall region.

In order to overcome these difficulties, Fouillet [53] proposed to modify the coefficient of thermal expansion[7] α_P to recover a correct scaling of the limit of superheat at a given reference pressure, say P_0. As a consequence for boiling systems whose pressure is always near P_0 the limit of superheat is controlled. However let us note that the limit of superheat is very sensitive with respect to the the variations of pressure.

For nucleate pool boiling flows, the range of pressure variations around a mean reference pressure, say P_0 is in fact dictated by an "external" scale: the hydrostatic pressure. As a consequence, even though the correct limit of superheat is recovered at the pressure P_0, the limit of superheat cannot be controlled for the whole range of pressures values of the boiling system. As a partial conclusion, the previous modification of the van der Waals model does not allow to control the limit of superheat and as a consequence quantitative numerical simulations of nucleate boiling flows cannot be performed with the help of this model.

We do not provide the complete set of possible modifications allowing to go further beyond some limitations which can be found in [53]. It is important to understand that whatever the way of changing h while keeping σ, it modifies the single-phase description by changing at least one of its "classical" properties, namely the density variations with (P, T), and/or the limit of stability.

Concluding remark on the attempt to modify the van der Waals model As a conclusion, there is no way to modify easily the thermodynamic description of the fluid $F(\rho, T, (\nabla\rho)^2)$ in order to deal with an artificially enlarged interface layer while keeping unchanged the main fluid properties involved in the boiling heat transfer process, *i.e.* ρ, σ, $\mathcal{L}$ and the limit of superheat. Therefore, the second gradient formulation does not allow to deal with numerical simulation of nucleate boiling flows with a diffuse interface model which is our actual goal.

2.2.4 The need for another thermodynamic model

The limitations of use of the second gradient method while dealing with boiling flows far from the critical point are induced by the necessary modifications of the thermodynamic description of the fluid. It turns out

[7] It is worth noting that the modification of the saturation curve $P_{eq}(T)$ is not possible since its slope indeed defines the latent heat of evaporation $\mathcal{L}$ that must be kept unchanged for the study of boiling flows, *cf.* the Clapeyron relation

$$\frac{dP_{eq}}{dT} = \frac{\mathcal{L}}{T\ (1/\rho_v - 1/\rho_v)}$$

This relation is studied in more details in the presentation of our model in section 3.4.

that the modifications necessary to enlarge the interface transition layer inevitably affect the single-phase state properties. Therefore the limitations are mainly attributed to the way the transition layer is modeled, namely through the use of the density dependence of the Helmholtz free energy. The fluid description appears to be too much constrained: the interface model and the bulk phase model are too closely related through the density dependence. This suggests to develop a diffuse interface model with more degrees of freedom. Since it has been shown to be impossible using the classical thermodynamic variables, say density ρ and temperature T, the introduction of an additional variable might help to solve the problem. This idea constitutes the starting direction of research of the present work. Among the diffuse interface models, the widely used phase field methods are based on the use of a purely abstract variable mainly devoted to the description of the interface layer and the local distinction of the phases. The formalism is closely related to our own problem. The following section is devoted to the presentation and review of the phase field methods.

2.3 Phase field models

In phase field models, the single-phase states of a material are associated to given and constant values of an additional and abstract thermodynamic variable, namely the phase field, denoted φ in the following. In section 2.3.1, after having presented the basic idea of the phase field models, we provide an illustrative example of the phase field thermodynamic description. In section 2.3.2, we then precise explicitly the desired features for a diffuse interface model dedicated to the numerical simulation of nucleate boiling. This allows us to review the existing phase field formulations in view of our problematic in section 2.3.3 and to conclude on the necessity to develop a specific formulation in section 2.3.4.

2.3.1 General presentation

The role of the phase field variable The phase field diffuse interface model is widely inspired by the van der Waals' theory of capillarity and indeed uses basically the same formalism. The phase field plays the role of the order parameter of the phase transition described (as the density does in the van der Waals model). This variable is devoted to the description of the interface layer. To model the structure of the interface layer, an additional nonlocal contribution to the thermodynamic potentials is introduced, most often through a dependence with respect to $\nabla\varphi$. The physical relevance of the introduction of the phase field variable for the purpose of describing the phase transition, instead of more classical physical parameters, is not always provided nor justified as mentioned by Boettinger et al. [17]. In some cases, this introduction is clearly motivated by numerical reasons and the phase field method is presented as a computational technique. As a conclusion, the introduction of the phase field variable in the thermodynamic model is unnecessary *a priori* for the description of the phase transition but useful for its use as a numerical method. We propose in the following to illustrate the subsequent advantages of this introduction. Let us refer to our presentation of the diffuse interface models in section 2.1.4 and recall that the goal of the artificial diffuse interface models is to provide a thermodynamically consistent smearing of the fields across the interface layer.

The phase field model Whatever the purpose for which φ is introduced, the numerical advantages resulting from the diffuse interface formulation, constitute an essential part of the current success of these methods. In the present section we focus only on the thermodynamic modeling the phase field models (our study of the dynamics governing equations is the subject of chapter 5). The goal is to illustrate how the introduction of a phase field thermodynamic variable provides additional degrees of freedom for the thermodynamic description of multi-phase systems.[8]. For this purpose, and since phase field models are most often devoted to the phase transition in materials science, let us consider the thermodynamic description of a solid-solid phase transition. We study in the following how we can deduce the widely used phase field formulation from a more primitive thermodynamic model of the phase transition using only classical thermodynamic variables. Let us precise that the corresponding primitive modeling of the solid-solid transition is not classical even though it is based on very general features of the thermodynamic modeling of multi-phase material.

[8] A more detailed study of the phase field formalism and of the consequences of the introduction of φ in the thermodynamic description is provided while deriving the proposed model in the section 3.2

A primitive modeling of the solid-solid phase transition Let us denote e_{cl} and s the specific energy and entropy of the material. The two single-phase states are denoted 1 and 2. In order to justify the main features of the two-phase model presented, let us refer to the van der Waals' model previously presented in section 2.2.2 and establish the following analogy

$$\begin{array}{ccc} P & \leftrightarrow & T \\ \rho & \leftrightarrow & s \\ \chi_T & \leftrightarrow & c_P \end{array} \tag{2.19}$$

Let us suppose that a continuous variation of the energy e with respect to s is meaningful. As illustrated on figure 2.6, the equation of state $T(s)$ describing the two-phase material is composed of two parts describing the single-phase states 1 and 2 and a third one referring to unstable homogeneous states. The *EOS* of the single

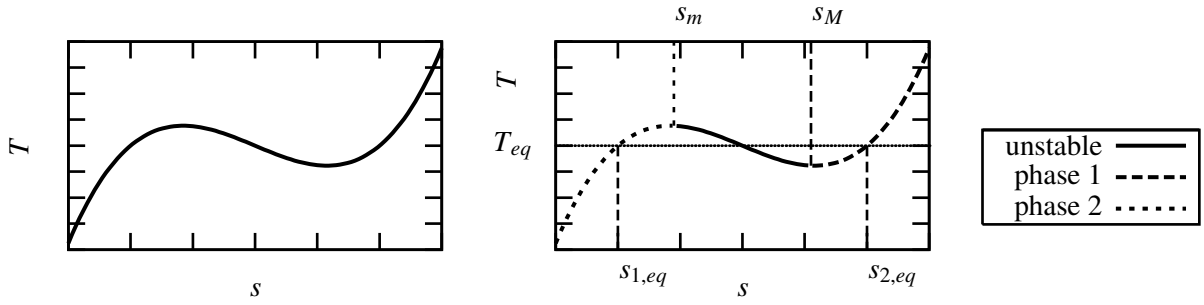

Figure 2.6: Natural *EOS* $s(T)$ shape for a solid-solid two-phase material

phase state 1, resp. 2, say $T_1(s)$, resp. $T_2(s)$, corresponds thus to the function $T(s)$ for $s \in [-\infty : s_m]$, resp. $s \in [s_M : +\infty]$. Let us recall that the third part, say T_u corresponding to $s \in [s_m : s_M]$ concerns states that can only exist in an interface layer (instable as homogeneous). Let us denote T_{eq} the temperature at which the two-phase equilibrium is possible, the two-phases being separated by a planar interface. At planar two-phase equilibrium the temperature in the bulk phases equals T_{eq} and the specific entropy jumps from $s_{1,eq}$ to $s_{2,eq}$ across the interface, *i.e.* $T_{eq} = T_1(s_{1,eq}) = T_2(s_{2,eq})$.

As a partial conclusion, we have introduced a model for the two-phase material by considering an equation of state $T(s)$ and therefore only classical thermodynamic variables.

A diffuse interface model using only classical variables Using a similar formalism than for the van der Waals model, it is possible to consider a diffuse interface modeling of this two-phase material by introducing an additional dependence of the energy

$$e = e_{cl}(s) + \lambda_s (\nabla s)^2$$

This additional energy contribution, namely a capillary contribution, "provides" the structure of the interface layer. In this case the function $T_u(s)$ is meaningful since it actually describes states inside the interface layer. However, if such a choice is made, as stated by Jamet [65], limitations appear due to the modification of the model while attempting to increase the interface thickness for numerical applications. The problem is similar to the one described for the second gradient model in section 2.2.3.

As a partial conclusion, the model using classical thermodynamic variables cannot be used with an artificial thickness.

Introduction of the phase field for the diffuse interface modeling In the phase field formulation, the dependence of the energy with respect to φ and the norm of its spatial gradient $(\nabla\varphi)^2$ is introduced[9], therefore $e(s, \varphi, (\nabla\varphi)^2)$. The values φ_1 and φ_2 are arbitrarily associated with the corresponding single-phase states. As a consequence the value φ_1 corresponds to the *EOS* $T_1(s)$ and the value φ_2 corresponds to the *EOS* $T_2(s)$. Two "classical" contributions, a double well function $W(\varphi)$ and a capillary coefficient λ allow to define the equilibrium structure of the interface layer, *i.e.* the associated thickness of the layer and the free excess energy (leading to the

[9]For the sake of simplicity, we do not consider any anisotropic dependence of the energy.

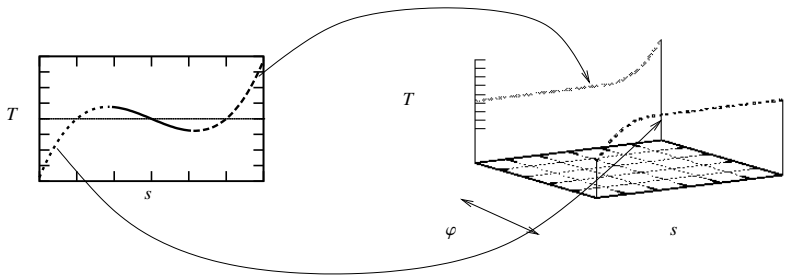

Figure 2.8: Single phase *EOS* with the phase field formulation

macroscopic surface tension). The form generally considered in the phase field models reads

$$e(s,\varphi,(\nabla\varphi)^2) = W(\varphi) + \frac{\lambda}{2}(\nabla\varphi)^2 + \tilde{e}(s,\varphi)$$

where $\tilde{e}(s,\varphi)$ will be related to the *EOS* T_1 and T_2 in the following. Let us recall that a similar capillary coefficient was considered in the non local contribution to the Helmholtz free energy F_{cap} in the van der Waals model (*cf.* section 2.2.2). The double well function W has to be related to the isothermal expression for the Helmholtz free energy F_{cl}. These energy contributions, namely the double well function and the capillary contribution, provide the structure of the interface layer. It is worth noting that it can be shown that the structure of the interface layer is not affected by the function $\tilde{e}(s,\varphi)$ (*cf.* the derivation of our thermodynamic model in chapter 3).

As a partial conclusion we have introduced two parameters, namely W and λ that are function of the single phase field variable and that define the structure of the interface layer independently of the function $\tilde{e}(s,\varphi)$.

Equation of state In the present phase field formulation, the energy contribution $\tilde{e}$ remains to be specified. Let us consider the *EOS* of the material described by the phase field formulation defined as

$$\tilde{T}(s,\varphi) \triangleq \frac{\partial e}{\partial s}_{|\varphi,(\nabla\varphi)^2} = \frac{\partial \tilde{e}}{\partial s}_{|\varphi}$$

Let us note that the *EOS* $\tilde{T}$ is a function of two variables s and φ instead of only s for the *EOS* $T(s)$ of the primitive model. This additional property, characteristic of the phase field models, provides the most important advantage of the thermodynamic description of a multi-phase system.

In order the material described by the single phase states of the phase field model $\varphi = \varphi_1$ and $\varphi = \varphi_2$ to correspond to the single phase states 1 and 2 of the primitive model it is required that

$$\begin{aligned}\tilde{T}(s,\varphi_1) &= T_1(s)\\ \tilde{T}(s,\varphi_2) &= T_2(s)\end{aligned}$$

The single equation of state $T(s)$ for the material is split into the two single-phase equations of state $T(\varphi_1,s)$ and $T(\varphi_2,s)$ with the help of the additional dimension φ. This is represented on figure 2.8.

The function $\tilde{T}(s,\varphi)$ needs then to be determined for any φ values different from φ_1 and φ_2. In order to match the correct single-phase ones, the equation of states reads

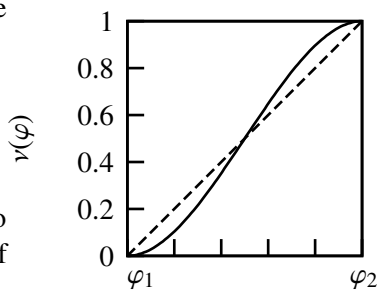

Figure 2.7: Interpolation function

$$T(s,\varphi) = T(s,\varphi_1) + (T(s,\varphi_2) - T(s,\varphi_1))\nu(\varphi) \tag{2.20}$$

where $\nu(\varphi)$ is an interpolation function taking the values 0 for φ_1 and 1 for φ_2 as represented on figure 2.7. The resulting *EOS* $\tilde{T}(s,\varphi)$ is illustrated on figure 2.9(b).

However, let us note that the introduction of the phase field in the thermodynamic description of the material and the corresponding choice of the interpolation function $\nu(\varphi)$ has consequences on the thermodynamic behavior of the material. The detailed study of the consequences of the introduction of φ is the subject of more formal

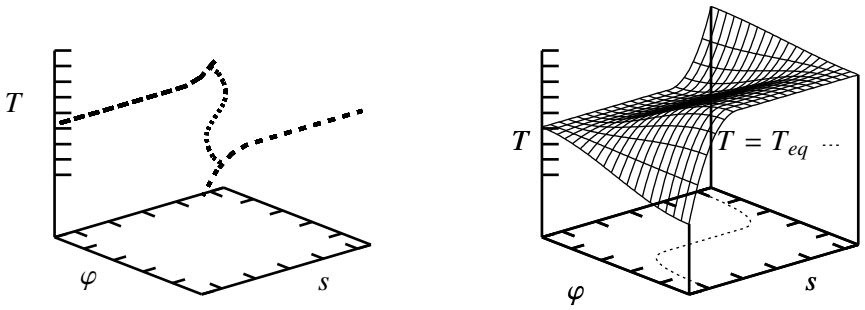

(a) (b)

Figure 2.9: The phase field $T(s,\varphi)$ *EOS*

developments in the section 3.2. In order to be more specific, let us just precise that in order that the *EOS* of the single phase states actually reduce to the *EOS* $T_1(s)$ and $T_2(s)$, some analytical properties of the interpolation function $\nu(\varphi)$ are required, the one being then determined as the most convenient numerically.

As a partial conclusion the function $\tilde{e}(s,\varphi)$ can be chosen such that the correct single phase *EOS* are recovered for the single-phase states 1 and 2.

Remarks on the modeling of the unstable homogeneous states Let us precise that, with such a diffuse interface model, the planar two-phase equilibrium is characterized by

- ⋆ a monotonic φ profile linking φ_1 and φ_2 of finite thickness and a subsequent excess free energy, both resulting from the choice of $W(\varphi)$ and λ
- ⋆ a constant and uniform temperature $T = T_{eq}$

The variation of entropy across a planar interface at equilibrium (*i.e.* at uniform temperature T_{eq}) is formally described by the function $T_{eq} = \tilde{T}(s,\varphi)$ which links the specific entropies of the single-phase states $s(\varphi_1, T_{eq}) = s_{1,eq}$ and $s(\varphi_2, T_{eq}) = s_{2,eq}$. This is represented by the transverse curve in the (s,φ) plane of equation $T = T_{eq}$ on figure 2.9(a). Let us note that as a consequence the primitive unstable part of $T_u(s)$ is not entering the phase field formulation.

Main properties of the phase field formulation The whole function $e(s,\varphi,(\nabla\varphi)^2)$ is determined using the basic ingredients $W(\varphi)$, $\nu(\varphi)$ and λ. W and λ manage the interface structure while the *EOS* is defined independently through the function $\nu(\varphi)$, including the description of the bulk phases 1 and 2. It is worth noting that the description of the single-phase state on each side of the interface is independent from the description of the interface layer. This represents an effective new degree of freedom and an advantage from the computational point of view: the interface layer can be modeled (more specifically the choice for the artificial thickness and the control of the surface tension coefficient) according to numerical constraints without modifying the *EOS*.

Phase field model for the liquid-vapor transition Let us apply the previous analysis of the phase field formulation to the liquid-vapor transition (of interest in this work). Let us recall the analogy 2.19 existing between the solid-solid transition described hereinabove and the isothermal van der Waals' model. For the isothermal liquid-vapor phase transition, a phase field φ can thus be introduced easily by analogy. For a non-isothermal thermodynamic description of the liquid-vapor transition, the basic ideas are the same.

As a partial conclusion it is *a priori* possible to use the same phase field formalism for the liquid-vapor phase transition as in the previous example for a solid-solid. As a consequence, it appears as doable using the phase field formalism to actually describe the structure of the interface layer independently from the bulk *EOS*.

Concluding remark The possibility to decouple the description of the single-phase from that of the interface layer constitutes the degree of freedom lacking while attempting to modify the van der Waals equation of state. A phase field description appears therefore as a good candidate in order to model the liquid-vapor transition for nucleate boiling simulations.

The analysis presented previously did not take special caution of the consequences of the introduction of φ in the thermodynamic model. This more complete study involves more complex and formal developments. The chapter 3 provides a more rigorous study of the derivation of the phase field models.

Several phase field models can describe the liquid-vapor phase transition, they are presented in section 2.3.3. However the specific application we aspire, namely nucleate wall boiling simulations, requires some specific constraints to be satisfied. They are presented in the next section.

2.3.2 Constraints on the diffuse interface model for the nucleate boiling simulation

The numerical advantage of dealing with a single system of governing equations for the liquid-vapor flow with phase change has a cost: it requires to capture the internal structure of the interface layer. The goal of the thermodynamic coherent description of the interface is not to deal with a more accurate description of the physical processes occurring inside this transition layer but rather to provide a coherent smearing of the equations corresponding to the classical sharp interface model, made of the Navier-Stokes equations in the bulk phases and of the Rankine-Hugoniot jump conditions. Therefore, it is required to show that the diffuse interface model provides an equivalent formulation of the two-phase flow. The model must be sufficiently generic in order to be able to deal with various assumptions concerning the thermodynamic description of the bulk phases, *e.g.* thermodynamic stability, compressibility. Moreover, the use of this diffuse interface model should not lead to additional difficulties and requires to be easily implemented and handled numerically. Let us present the main features of the diffuse interface model allowing to fulfill these requirements.

The smearing of the sharp formulation must result in controlled smooth profiles across the interface. It must be possible to define a typical thickness of the artificial transition layer compatible with an acceptable spatial discretization of the mesoscopic problem under study. The model of the interface layer should be independent of the description of the bulk phases and should be based on a simple set of parameters allowing to reproduce its macroscopic characteristic (*e.g.* surface tension ...). The model must provide the ability to include various bulk EOS. Moreover, in nucleate boiling the liquid phase undergoes local superheat and special attention must be paid on the limit of metastability induced by the formulation (since it has been shown to be a major difficulty with the second gradient method). The different constraints can be summarized as follows:

1. monotonic φ profile through an interface at equilibrium (numerical constraint)
2. monotonic density profile through an interface at equilibrium (numerical constraint)
3. easy parametric choice for the interface layer thickness (numerical constraint)
4. easy parametric choice for the excess free energy of an interface at equilibrium (physical constraint)
5. recovery of classical pressure jump conditions (physical constraint)
   (a) Laplace relation
   (b) recoil pressure
6. parametric control of the $\{P, T\}$ domains of stability and metastability of the bulk phases (physical constraint)
7. control of the equations of state of the bulk phases ($\rho(P, T)$ and $s(P, T)$) (physical constraint), for example
   (a) compressible bulk phases
   (b) incompressible bulk phases

This set of properties concerns *a priori* all the set of governing equations including the model of the dissipative process and *a fortiori* some statics features defined by the thermodynamic model. These statics features (equilibrium states) are the subject of chapter 3. The study of the dynamics is then provided in chapter 5. Following

these constraints we search for an optimal phase field model.

Diffuse interface models *versus* these constraints It has been shown that the second gradient method does not fulfill all the hereinabove constraints. Let us consider the classical phase field models for solidification. A similar list of design constraints has been used by Wang et al. [146] for the derivation of phase field models for the crystallization of a pure material from its melt. In [146] the constraint concerning the arbitrary choice of the interface thickness is however not considered even though, to our point of view, it is clearly one of the most important motivation to deal with such a diffuse description of the interface layer. Naturally the constraints more specifically related to the liquid-vapor phase transition are not considered. It is worth noting that none of the current phase field models applicable to the liquid-vapor phase transition matches all these constraints; this will be discussed in more details in section 2.3.3. This shows the necessity to develop a specific phase field model devoted to its use as a numerical method for the simulation of the liquid-vapor flows with phase change. Our main goal is to take the desired properties as constraints for the derivation of a phase field model. We believe that this modeling approach is not restricted to liquid-vapor phase transitions but can actually be applied to any other multi-phase system.

Remarks on the single-phase equations of state The last constraint (item 7) of the above list actually requires that the EOS of the bulk phases can be chosen arbitrarily, which is an important degree of freedom of the final model, especially for our application. This choice concerns the modeling of the compressibility of the fluid bulk phases. The compressible nature of the fluid (as described by the van der Waals model) induces a constraint on the maximal value for the numerical time step which induces an important computational cost[10]. Nucleate boiling flow characteristics are mostly determined by latent heat, capillarity and buoyancy as shown in chapter 1. Therefore, single-phase compressibility does not appear as a dominant factor of the boiling process. Most of the sharp interface methods devoted to the simulation of nucleate boiling deal with incompressible single-phase states, *e.g.* [69], which appears as a reasonable first order approximation of the boiling process. The possibility to model the liquid and vapor phases as incompressible in a diffuse interface model is therefore relevant (and moreover computationally interesting). The final formulation should therefore provide the possibility to deal with compressible and incompressible bulk phases. A detailed study of the single-phase equations of state compatible with a multi-phase thermodynamic description is provided in section 3.1.1.

2.3.3 Review of the phase field models dedicated to phase transitions with density difference

On the one hand, the phase field models devoted to the numerical simulations of two-phase flows (*e.g.* [8, 35, 51, 52, 63, 77, 112, 153]) most of the time do not consider phase change or non-isothermal effects. On the other hand, the phase field models devoted to phase transitions most of the time do not consider any flow or, if any, no density difference between the bulk phases is accounted for. The phase field models dedicated to the study of solidification are widely used. Only a few consider flow in the liquid phase, and even less consider a density difference. Let us consider the latter category of models. Even though these models are not dedicated to the liquid-vapor phase transition, the models actually allow to describe this transition, if one considers a large density difference and a finite viscosity in the bulk phase. Among the large number of phase field models, our review focuses on the few non-isothermal models of a pure material undergoing phase transition with flow and density difference. We only present the thermodynamic formulation proposed in view of the constraints expressed on page 53. The methods reviewed have been derived for specific applications and very few correspond to ours. Nevertheless, we analyze their possible adequateness to the study of nucleate boiling.

A phase field model dedicated to liquid-vapor flows with phase change

Caro [29] studied mathematically and numerically the system of governing equations of a diffuse interface model dedicated to the liquid-vapor transition. The phase transition is described with the help of a thermodynamic phase field variable φ. In this model, φ is introduced as an abstract order parameter supposed to be equal to 0 in the

[10] Let us note that, since, for the second gradient model, the density is considered as the order parameter of the transition, this compressibility is intrinsic to the model. The ability to model thermodynamically a two-phase system with density between two incompressible single-phase states will be studied in more details in section 3.1.1

liquid phase and 1 in the vapor phase at two-phase equilibrium. This model is therefore very closely related to ours. The proposed expression for the internal energy ($\rho\, u$) in the non-isothermal case reads

$$\rho\, u = \Big(\rho_{vap}\, u_{vap} - \rho_{liq}\, u_{liq}\Big)\varphi + \rho_{liq}\, u_{liq} + W(\varphi) + \frac{\varepsilon^2}{2}(\nabla\varphi)^2 \tag{2.21}$$

where the density ρ is given by

$$\rho = \rho_{liq} + \Big(\rho_{vap} - \rho_{liq}\Big)\varphi \tag{2.22}$$

The double well function W and the capillarity coefficient λ are introduced similarly to what has been presented in section 2.3.1. Using this model with $W = 0$ and $\varepsilon = 0$, numerical simulations of the nucleation process are provided but let us specify that, due to the nullity of both W and ε no capillary flow is taken into account.

The model provides an interesting modification of the original second gradient model using the introduction of the abstract parameter φ. In the formulation (2.21), the EOS of the single-phase states, u_{vap} and u_{liq} appear as explicitly linked through a linear dependence with respect to φ. This characteristic actually corresponds to the advantageous property of the phase field models presented in section 2.3.1. At planar equilibrium, the interface thickness and the surface tension coefficient can be chosen independently of the density difference which correspond to some required properties of the desired model. As a modification of the second gradient model, the proposed phase field formulation deals with an intrinsically compressible fluid. This property does not match the last constraint expressed in the list of section 2.3.2 and more particularly does not bring the ability of the model to deal with incompressible single-phase states.

The interpolation function chosen in this formulation is a linear dependence of both $\rho\, u$ and ρ with respect to φ. This choice has consequences on the thermodynamic behavior of the fluid out of the two-phase equilibrium conditions of a planar interface. First, the values of φ, 0 and 1, inside the bulk phases are only ensured at these equilibrium conditions. It is shown in section 3.2.3 that this property of the phase field model is actually induced by the choice of the interpolation function. Therefore, the EOS of the bulk phases are different from u_{vap} or u_{liq} and thus controlled with difficulty. Moreover, it is shown in chapter 6 that such a linear dependence does not provide any control of the thermodynamic stability domains of the bulk phases, which thus appear to be highly dependent on the choices made for the interface thickness. This reduces therefore the range of application of the model for quantitative numerical simulations of the nucleate boiling process.

As a conclusion, the phase field model proposed provides an interesting framework for dealing with liquid-vapor flows with phase change. However, the consequences of the introduction of the phase field variable on the fluid thermodynamic behavior need to be more deeply controlled such that the required properties expressed in section 2.3.2 (page 53) are satisfied. This is the subject of study of the model derivation in chapter 3.

A diffuse interface model dedicated to solid-liquid phase-change with flow, quasi-compressible formulation

Phase field models have been proposed to take into account the convective effects on the solid/liquid phase transition, *e.g.* [11, 17] or [98, 133] for monotectic alloys. These models are based on the introduction of both an external flow and a viscosity depending on φ but do not consider any density difference. Anderson et al. [5, 6] have proposed a phase field model with convection that " *incorporates in a thermodynamically consistent way the density effect in a phase field description of solidification as well as the appropriate form of the Korteweg stress term in the momentum equation"*. The corresponding specific Gibbs free energy reads

$$\begin{aligned} g(T,P,\varphi,(\nabla\varphi)^2) &= [e_0 - c_P\, T_M - \nu(\varphi)\mathcal{L} - w_m(\varphi)]\left(1 - \frac{T}{T_M}\right) \\ &\quad - c_P\, T \ln\frac{T}{T_M} + w_m(\varphi) + \frac{P - P_0}{\rho(\varphi)} + \frac{\varepsilon^2}{\rho(\varphi)}(\nabla\varphi)^2 \end{aligned} \tag{2.23}$$

where $\nu(\varphi)$ is a monotonic interpolation function that defines also the function $\rho(\varphi)$, $\mathcal{L}$ is the specific latent heat, c_P is the specific heat capacity at constant pressure common to the two-phases, T_M is the melting temperature at the pressure $P = P_0$, and $w_m(\varphi)$ is a double well function. At equilibrium of a planar interface along an arbitrary x-axis and at a given equilibrium temperature T, the differential equation governing the profile $\varphi(x)$ reads

$$\begin{aligned} &\varepsilon^2\,\varphi_{,xx} + \rho\left(\frac{\partial 1/\rho}{\partial\varphi}\right)\frac{\varepsilon^2}{2}\varphi_{,x}^2 - \rho(\varphi)\left(\frac{T}{T_M}\frac{\partial w_m}{\partial\varphi}\right) \\ &+\frac{\partial\nu}{\partial\varphi}\mathcal{L}\left(1 - \frac{T}{T_M}\right)\left(\rho(\varphi)\left(\frac{1}{\rho_S} - \frac{1}{\rho_L}\right) - \frac{(\rho_S - \rho_L)}{\rho(\varphi)}\right) = 0 \end{aligned} \tag{2.24}$$

where $\cdot_{,x}$ denotes the spatial derivative with respect to x and the subscripts $_S$, resp. $_L$, refer to the solid, resp. liquid, bulk phases. The pressure profile, determining the surface tension coefficient as shown in 3.2.4, satisfies

$$P = P_\infty - \frac{\varepsilon^2}{2}\varphi_{,x}^2 \tag{2.25}$$

the value of the bulk pressure P_∞ satisfying the following Clapeyron relation

$$(P_0 - P_\infty)\left(\frac{1}{\rho_S} - \frac{1}{\rho_L}\right) = \mathcal{L}\left(1 - \frac{T}{T_M}\right) \tag{2.26}$$

Let us comment the above relations in view of our applications.

Single-phase description Let us note that the pressure P is chosen as the main thermodynamic variable and that the density of the material is the subsequent $\rho(\varphi)$ function defined as

$$1/\rho \triangleq \frac{\partial g}{\partial P} \tag{2.27}$$

As a consequence of the linear dependence of the specific Gibbs free energy with respect to P, the density is a function of φ and actually reads

$$\rho(\varphi) = \rho_L + (\rho_S - \rho_L)\,\nu(\varphi) \tag{2.28}$$

Let us note that the single phases are incompressible, since the density ρ does not depend on the pressure. This property refers to the hypothesis of quasi-compressible liquid as introduced by Lowengrub and Truskinovsky [89], which is presented in the study of the multi-phase thermodynamic description in section 3.1. No extension of the formulation to compressible EOS is proposed.

The interpolation function ν is considered as being polynomials of degree 1 or 3. The choice of a polynomial of degree 1 implies similar consequences on the thermodynamic behavior of the fluid as presented hereinabove for the model of Caro [29]. We show in our study of the phase field interpolation functions in section 3.4.1 that the polynomial of degree 3 ensures the bulk phases to correspond to the fixed values of φ 0 and 1 even out of the two-phase equilibrium conditions $T = T_M$ and $P = P_0$. However, it is also shown in chapter 6 that the thermodynamic stability of the single-phase states is governed by the choices made for the interface thickness at $T = T_M$. As a consequence, the single-phase states can only be stable for a given range of pressure and temperature values, the extent of this range being a decreasing function of the interface thickness[11]. This limit of metastability constitutes a limitation in the use of the model since it is controlled by the *a priori* arbitrarily chosen h value[12].

Interface description Let us consider the planar equilibrium equation (2.24) for the phase field profile $\varphi(x)$. In [6], two different expressions for w_m are prescribed, one allowing to consider the interface equilibrium profile as being independent of the density ratio between the phases at $T = T_M$ and thus only parameterized by the function w_m and the capillary coefficient ε. This property is interesting since as a consequence the artificial thickness can be easily controlled (which corresponds actually to the point 3 of our own constraints).

Let us now consider the equilibrium equation (2.24) for an equilibrium temperature different from the reference temperature $T \neq T_M$. It is straightforward that in this case the second line of equation (2.24) is non-zero. As a consequence, the thickness of the interface layer at a equilibrium temperature T, $T \neq T_M$, deviates from the one obtained with an equilibrium at $T = T_M$. Since not physically motivated, this variation of the equilibrium profile is not desirable.

[11] This induces a metastability limit that does not correspond to the classical one presented with the second gradient model in section 2.2 (*i.e.* associated to the Gibbs-Duhem criterion on compressibility (2.4)). This characteristic of phase field formulation is studied in more details in chapter 6

[12] We provide in the section 6 a study of the thermodynamic stability of the single-phase states with the phase field models and present the common way to model a controlled limit of metastability (even infinite).

Concluding remarks This model shows an interesting way to take into account the density difference in a phase field model of a pure material with incompressible bulk phases. The classical Clapeyron relation, an important characteristic of the liquid-vapor phase transition, is recovered. Moreover, the interface thickness can be chosen independently of the density ratio for $T = T_M$. However some important features of the liquid-vapor phase transition are not considered, such as the possible compressible nature of the fluid or the difference of the c_P between the bulk phases. The control of the interface thickness dependence with temperature as well as the control of the metastability of the bulk phases are not ensured (points 3 and 6 of the constraints expressed on page 53). This constitutes an intrinsic limitation of use of the model for our own applications. As a conclusion, although the proposed model takes into account phase change with flow and density ratio between the phases, it cannot be used as an efficient method for the numerical study of the liquid-vapor flows with phase change in our boiling conditions. However this model already presents the main features of a phase field formulation devoted to liquid-vapor phase change. Our model constitutes a modification and extension of this formulation.

Pressure effect on the crystal growth, a compressible phase field model for liquid/solid phase transition

As mentioned by Conti [39], the phenomenology of the solidification process is not only governed by the supercooling imposed but also by density changes and associated pressure levels variations induced by the local contraction of the material. In order to model the phase transition including these effects, Conti [38] proposed a phase field model. The Helmholtz free energy density reads

$$f = \frac{W_{\rho,\varphi}(\rho,\varphi)}{\rho} + \nu(\varphi)\mathcal{L}\frac{T_m - T}{T_m} + P_{sat}(T) + \frac{\varepsilon_\rho^2}{2}(\nabla\rho)^2 + \frac{\varepsilon_\varphi^2}{2}(\nabla\varphi)^2 \tag{2.29}$$

where the function $W_{\rho,\varphi}$ reads

$$W_{\rho,\varphi} = \alpha\left(\varphi^2 + b\,(\rho-\rho_S)^2\right)\left((\varphi-1)^2 + b(\rho-\rho_L)^2\right) \tag{2.30}$$

This formulation both includes a van der Waals type EOS in order to include compressible effects (let us refer to the analytical expression for the Helmholtz free energy F_{cl} presented in 2.2.2) and the classical features of the typical phase field formulations for solidification (as presented in 2.3.1). The expression for the Helmholtz free energy (2.29) yields to the following differential equation for the φ profile at equilibrium along an arbitrary x-axis

$$\varepsilon^2\,\varphi_{,xx} - \left(\frac{\partial W_{\rho,\varphi}}{\partial\varphi} - \frac{\partial\nu}{\partial\varphi}\,\rho\,\mathcal{L}\left(\frac{T - T_{sat}(P)}{T_0}\right)\right) = 0 \tag{2.31}$$

and to the following expression for the non-dissipative part of the stress tensor $\mathbf{T}$ components (i,k)

$$T_{ik} = \delta_{ik}\left[-P + \rho\varepsilon_\rho^2\nabla^2\rho + \frac{\varepsilon_\rho^2}{2}(\nabla\rho)^2 + \frac{\varepsilon_\varphi^2}{2}(\nabla\varphi)^2\right] - \varepsilon_\rho^2\rho_{,i}\rho_{,k} - \varepsilon_\varphi^2\varphi_i\varphi_k \tag{2.32}$$

where $_{,i}$ indicates spatial derivative with respect to the coordinate x_i and δ_{ik} is the Kronecker symbol.

This model does not provide sufficiently generic formulation for the EOS in view of our application since it cannot reduce to a quasi-compressible formulation. The dependence of the formulation with respect to two non-local fields $(\nabla\rho)^2$ and $(\nabla\varphi)^2$ induces complexity in the resulting expression of the governing equations (*cf.* the expression of the non-dissipative stress tensor (2.32)). In order to model capillarity, a single dependence has been shown to be sufficient. A more adequate way to model the fact that both ρ and φ undergo strong variations across the interface should be, as made in the Caro [29] and the Anderson et al. [5] models to more deeply enslave both variations through an explicit dependence of the density with respect to the phase field φ.

As a conclusion, this model implies a useless complexity for our targeted applications and moreover cannot reduce to the description of incompressible bulk phases. It will be therefore disregarded in the following of this work.

2.3.4 Conclusion : the need for a new phase field formulation

The main properties of the phase field thermodynamic description have been presented. Specific properties of a phase field model dedicated to the simulation of nucleate boiling have been presented. A review of the existing

diffuse interface models has revealed that their properties do not match the ones required. The existing diffuse interface models do not provide for the moment a sufficiently efficient numerical method for dealing with boiling flows. In view of this previous study, the need for a new model has therefore been stated. The phase field formulation has shown to provide the most flexible way to describe the phase transition in the scope of numerical use. This solution is therefore retained in the remainder of the study. The required properties presented on page 53 are used as constraints while designing the present model.

2.4 Conclusion on the review of numerical methods for the simulation of nucleate boiling

In chapter 1, we have defined the study of a bubble growth in nucleate pool boiling configuration as a target problem of primary interest for the understanding of the mechanism of the boiling crisis. The use of numerical simulations to study this problem has been proposed. In this chapter we have thus studied the different existing numerical methods for the simulation of liquid-vapor flows with phase change. Two different families of numerical method have been considered according to two different ways to represent the liquid-vapor interface: either the interface is tracked and needs to be explicitly located, or the interface is captured (see section 2.1.1).

In section 2.1.2, we have first considered the methods using an explicit tracking of the interface. In section 2.1.3 we have then considered the main families of interface capturing methods and presented the level-set method. All these methods lie on a sharp model for the interface. This is the most relevant model from a physical point of view. However it yields some mathematical and/or numerical difficulties to ensure both an easy handling of the solving of the equations and a displacement of the interface consistent with the conservation principle of the main physical quantities.

The thermodynamic formalism of diffuse interface models allows to deal with a smeared interface layer and a local consistency of the governing equations: it guarantees local positive entropy production. It has been shown that these properties of the model are quite attractive, since there is no need of additional numerical recipes to constrain the structure of the interface layer: its smearing is naturally and physically controlled. However, the diffuse interface models are classically devoted to the fine description of the interface layer, which is not our actual goal. As a consequence, we have considered an alternative way to smear the interface: the smearing of the interface is inherited from a thermodynamic modeling but the typical thickness of the interface layer is artificial and can be chosen as numerically convenient. Therefore the formalism of diffuse interface model is used to provide a consistent regularization of an initially sharp interface model. Two ways have been defined in order to build such a model: either a classical model for the liquid-vapor phase transition (such that the van der Waals model) is modified in order to induce an enlargement of the interface thickness, or an artificial diffuse interface model is built from the primitive sharp interface formulation, the smearing of the interface being governed by the introduction of an additional abstract thermodynamic variable, the so-called phase field formulation.

In section 2.2 we have studied the ability to modify the van der Waals model. We have first recall the main features of the isothermal van der Waals model in section 2.2.2 and shown how the formulation lies on a number of 6 parameters allowing to model the physical mechanisms we'd like to take into account, namely density difference, capillarity, smearing of the interface layer. However the physical small value of the interface thickness far from the critical point has been shown to lead to an impossible use of the model for the study of nucleate pool boiling flows. In section 2.2.3 we have studied how these parameters can be modified to artificially enlarge the thickness of the interface layer while keeping unchanged the other parameters. It has been shown that this modification inevitably affect the limit of metastability. In the non-isothermal case, the limit of super-heat is as a consequence modified. It has been said that this modification is not desirable for the targeted numerical simulation of nucleate boiling flows because it induces artificial nucleation events in a near wall region that would impede a correct simulation of a single bubble growth. As a consequence, the attempt to modify a classical diffuse interface model has been shown to be unfruitful and we turned our attention toward the second possible way defined: the phase field formulation.

To introduce the phase field formulation, we have first provided in section 2.3.1 an illustrative example to show how the description of the interface layer, if thermodynamically consistent, is actually de-coupled from the thermodynamic description of the bulk phases. This property adds therefore an additional degree of freedom in the thermodynamic model of the interface layer that was lacking with the van der Waals model.

We have specified in section 2.3.2 the main desired features of the diffuse interface model in view of its use for the targeted study of nucleate boiling flows. These features have been summarized on the form of a constraints list, of page 53, that can be used to attest the validity of the phase field model.

Based on this framework for the analysis of the phase field model we have reviewed in section 2.3.3 the previously existing phase field model allowing to model a liquid-vapor phase transition. None of these models matches all the desired features for our study of the nucleate boiling flows. As a consequence, a new phase field model for the study of the liquid-vapor flows with phase change needs to be derived. This derivation is the subject of the following chapters.

Chapter 3

Phase field model: thermodynamic derivation

As stated in chapter 2, existing diffuse interface models are not well suited for the numerical simulation of nucleate wall boiling. It is necessary to develop phase field models for the study of this problem. In the present chapter, we derive the thermodynamic part of the proposed model and study its main features. The goal is to study

- ⋆ the introduction of a phase field in the thermodynamic description of the fluid, its interpretation and the consequences on the equilibrium states
- ⋆ the derivation of a generic phase field thermodynamic model
- ⋆ the subsequent main properties of the bulk phases and of the interface layer

In fact we are looking for an optimal phase field model with minimal interference between the description of the bulk phases and the one of the interface layer. This chapter is organized as follows.

In section 3.1, we study the thermodynamic modeling of a multi-phase fluid. We study the compatibility of compressible or incompressible bulk *EOS* with a multi-phase model. The choice of the main thermodynamic variables is shown to be related with this problematic of compatibility and the classical van der Waals model does not bear the ability to deal with incompressible bulk phases. It is shown that this limitation is removed while using an additional "order parameter" such as the phase field variable using the quasi compressible hypothesis. This study introduces and justifies the choice of the main thermodynamic variables used in the model presented[1]

In section 3.2, we study the introduction of the phase field as a main thermodynamic variable. The goal is to express the required properties of the model (*cf.* the list on page 53) as analytical conditions for the thermodynamic model. We first specify the meaning of the phase field variable and the goal of its introduction. We then study the conditions of thermodynamic stability of the corresponding phase field multi-phase system (see section 3.2.2). From this study, we derive analytical relations that must be satisfied by the phase field thermodynamic model in order to fulfill the equilibrium requirements expressed on page 53 of section 2.3.2. These conditions concern the ability of the model to actually control both the single-phase states *EOS* and the structure of the interface.

In section 3.3, we introduce the analytical expression for the phase field thermodynamic model proposed and compare it with the models presented in chapter 2. We first consider an isothermal case and introduce the phase field functions of our model. We then study the non-isothermal case. This model is then compared to the classical phase field models, including the widely used models for the solid-liquid phase transition that consider the density as being uniform.

In section 3.4, we show that the model proposed has actually all the required properties. More particularly, we show that the single phase states of the model are actually described by classical *EOS* and that the main classical thermodynamic relations of the description of the liquid-vapor phase transition are thus recovered. Then we show that the structure of the interface is actually easily controlled.

[1]This point has already been introduced in section 2.3.1 and is studied in more details in section 3.1.

3.1 Thermodynamic modeling of multi-phase systems

In this section, we study the possibility to construct explicit equations of state for the model of a multi-phase system and their compatibility with different classes of bulk *EOS* (*i.e.* compressible, incompressible). The goal is to present the choice of the main thermodynamic variable for our model. Therefore we focus more specifically on the thermodynamic description of phases with different densities and on the ability to deal with either compressible or incompressible bulk phases. Indeed, as expressed in section 2.3.2, we need to recover for each single-phase state described with the phase field formulation some classical equations of state and moreover to get a degree of freedom for their choice (point 7 of the list of constraints defined on page 53).

3.1.1 Single-phase state and equation of state

The single-phase *EOS* are the basic thermodynamic relations describing the behavior of the bulk phases. Let us study their main characteristics in the compressible and incompressible isothermal cases.

Thermodynamic potentials and main variable Let us denote G, (respectively F), and g, (respectively f) the volumetric and specific Gibbs (respectively Helmholtz) free energies of the fluid described. The corresponding main variable for the Gibbs, resp. Helmholtz, energies is the pressure P, resp. the density ρ. Both descriptions $F(\rho)$ and $G(P)$, are equivalent and well defined if and only if the relation linking P to ρ is a bijection. If it is the case, the switch from one description (*e.g.* $F(\rho)$) to the other (*e.g.* $G(P)$) through the associated Legendre transformation is mathematically well-posed and one gets

$$F = \rho f = G - P = \rho\left(g - \frac{P}{\rho}\right) \tag{3.1}$$

In the following, we show that if ρ is chosen as the main variable, the single-phase are characterized by the *EOS* $F(\rho)$ which defines $P(\rho)$; if P is chosen as the main variable, the single-phase are characterized by the *EOS* $G(P)$ which defines $\rho(P)$

Let us start with the case where the density ρ is the main variable. Let us recall (*cf.* equation (2.2)) that the pressure is defined from the Helmholtz free energy by

$$P = \rho\,\frac{\partial F}{\partial \rho} - F = \rho^2 \frac{\partial f}{\partial \rho} \tag{3.2}$$

The relation (3.2) is illustrated on figure 3.1(a). The equilibrium pressure P_0 at a fluid density $\rho = \rho_0$, is the opposite of the ordinate at origin of the local tangent to the curve $F(\rho)$. This description of the fluid is well defined as long as the fluid isothermal compressibility χ_T (defined by equation (2.3)) is non zero. The van der Waals' model is, for example, based on this type of fluid representation.

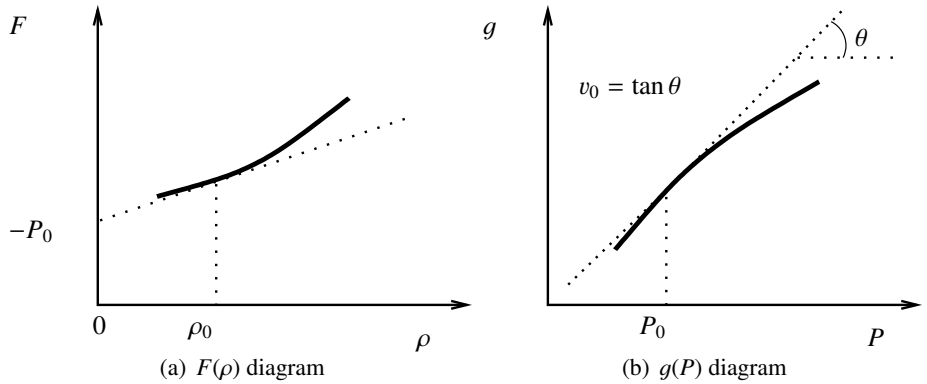

(a) $F(\rho)$ diagram (b) $g(P)$ diagram

Figure 3.1: Main thermodynamic potentials for an isothermal fluid

Let us now consider the case where the pressure P is chosen as the main variable. The corresponding thermodynamic potential is the Gibbs free energy G which variation with respect to the pressure is linked to the isothermal compressibility of the fluid through

$$\frac{\partial G}{\partial P} = 1 + G\chi_T \tag{3.3}$$

which can be expressed in terms of specific Gibbs free energy as

$$v(P) \triangleq \frac{1}{\rho}(P) \triangleq \frac{\partial g}{\partial P} \tag{3.4}$$

where v denotes the specific volume of the fluid. The relation (3.4) is illustrated on figure 3.1(b).

The main thermodynamic relations for the isothermal description of a fluid have been introduced. According to the choice for the main variable (ρ or P), two descriptions of a fluid bulk phase are possible. Let us consider two cases where one of them (*i.e.* ρ or P as being the main variable) degenerates *i.e.* when the equivalence between the choice of the density ρ or the pressure P is not satisfied:

- ⋆ the van der Waals model,
- ⋆ the incompressible case.

Van der Waals' model In the van der Waals' model, presented in section 2.2, the function $P(\rho)$ is obviously multi-valued, since for instance two different densities $\rho_{l,sat}$ and $\rho_{v,sat}$ corresponds to the same equilibrium pressure P_{eq} (*cf.* the figure 2.2(b) in section 2.2.2). The Gibbs free energy is therefore also not single-valued as

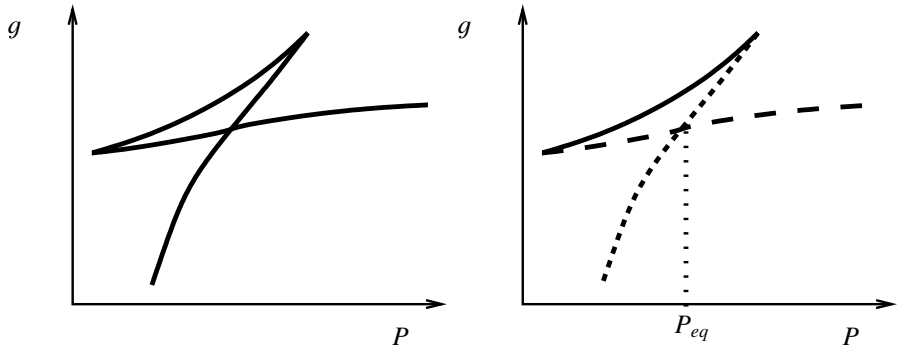

Figure 3.2: Specific Gibbs free energy for the van der Waals'model

illustrated on figure 3.2. The pressure P cannot be chosen as the main thermodynamic variable describing the fluid.

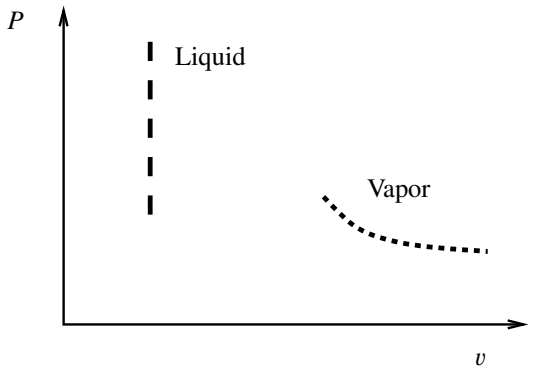

Figure 3.3: Compressible and incompressible phases on a Clapeyron diagram

The incompressible limit Let us consider the incompressible limit which we have shown in section 2.3.2 to be of interest for the model and numerical simulation of boiling flows. On the Clapeyron diagram plotted on figure 3.3, a compressible vapor phase and an incompressible liquid one ($\chi_T = 0$) are represented.

For an incompressible phase (say liquid on figure 3.3) the isothermal EOS reads

$$\rho(P) = \rho_L$$

and the pressure is obviously the main variable. Let us study the expression for the Gibbs free energy (*i.e.* the thermodynamic potential corresponding to the main variable P). We get from the relation (3.3)

$$G(P) = P - P_0$$

where P_0 is a reference pressure (constant of integration), or equivalently using the relation (3.4)

$$g(P) = \frac{P - P_0}{\rho_L}$$

The Gibbs free energy G is therefore well-defined even if $\chi_T = 0$. However, the description using the density ρ as the main variable is degenerate: it is impossible to define the Helmholtz free energy F (or the pressure P) as a function of the density ρ. F is undefined out of the line $\rho = \rho_L$.[2]

As already said in chapter 2 (point 7b of the list of constraints page 53), and according to our study of the main physical mechanisms of nucleate boiling flows in chapter 1, the possibility to describe incompressible fluids with the phase field model is targeted. In this case, the main variable is therefore the pressure and the thermodynamic description in terms of density is degenerate.

General cases More generally, the ability to get an explicit analytic expression for F or G lies on the property of bijectivity of the function linking ρ and P (in other words, it lies on the well-posedness of the Legendre transformation). We can consider three main different cases

1. $\rho(P)$ is injective but not surjective: g is well-defined and the pressure P is the main variable (incompressible case for example)
2. $\rho(P)$ is surjective but not injective: f is well-defined and the density ρ is the main variable (van der Waals' model for example)
3. $\rho(P)$ is bijective: f and g are both well-defined (ideal gas EOS for example)

Concluding remarks The main thermodynamic potentials have been introduced as well as the choice of the main variables with regard to the properties of the EOS of the bulk phases. The Gibbs G, resp. Helmholtz F, free energies describe classically the isothermal single-phase states of a fluid in the case where the pressure P, resp. the density ρ, is chosen as the main variable. For the modeling of a multi-phase system, a choice for the main thermodynamic variable must be done. As shown in the following section, this choice has consequences on the degree of freedom for the choice of the corresponding single-phase EOS.

3.1.2 Multi-phase system and equations of state: Density difference and incompressibility of the bulk phases

The goal of this section is to study the choice of the main thermodynamic variables for the model of a two-phase fluid whose phases have different densities but can either be incompressible or compressible.

Introduction to the problematic In this section, we study the thermodynamic modeling of a multi-phase system with a diffuse interface model. We show that the use of classical thermodynamic variables (*e.g.* ρ or P) for the multi-phase model leads to some restrictions on the choice of the bulk EOS. This characteristic is specific of the diffuse interface model for which the modeling of both the bulk phases and of the interface lies on a single, explicit, and continuous expression for the thermodynamic potential. In sharp interface models, this expression is not required and the bulk EOS can be chosen arbitrarily and independently of the interface properties. This difference between the two modelings can induce limitations in the use of the diffuse interface models dealing with classical thermodynamic variables (as it is the case with the van der Waals' model). However, we show in the following that, while dealing with a phase field formulation, this limitation is removed.

The section is organized as follows. We study the modeling of the liquid-vapor phase transition in both the isothermal and the non-isothermal cases. It is shown the incompatibility of the incompressible bulk EOS with

[2] Let us note that even though the pressure can no longer be defined classically from the Helmholtz free energy, it can be related to the non-dissipative stress tensor as it is shown in section 5.2.

the classical diffuse isothermal interface modeling. Then we study the multi-phase model of a phase transition using other main variables than the single density or the single pressure. We first consider the classical non-isothermal van der Waals model in order to introduce the main features of the non-isothermal description of the liquid-vapor two-phase fluid. We show then the possibility to model a non-isothermal two-phase system with density difference and incompressibility of the bulk phases as soon as the specific entropy s instead of the density ρ is considered as the order parameter of the phase transition. It leads us to introduce the quasi-compressible limit.

Incompatibility between the diffuse interface model and some bulk EOS: the illustrative example of bulk incompressibility In order to exemplify the problematic, we consider a liquid-vapor transition and study the impossibility of dealing with incompressible bulk phases together with an isothermal diffuse interface model. In this case, and since the system is isothermal, only either the pressure P or the density ρ can be considered as the main thermodynamic variable.

Let us consider the classical van der Waals' model. The isothermal van der Waals' equation of state EOS_{vdW}, presented in section 2.2.2, models a liquid-vapor system with a single function $P(\rho)$ which is injective but not surjective (*cf.* figure 2.2). As shown in the previous section, F can be expressed explicitly while G, like $\rho(P)$, can only be given implicitly since it is multi-valued. Since the density ρ is the main variable, it is not possible to degenerate it in order to get incompressible single-phase states.

Let us now consider another model of the liquid-vapor transition choosing the pressure P as the main variable. In order to consider incompressible single-phase states and a possible two-phase equilibrium, it is possible to define a specific Gibbs free energy function $g(P)$ as represented in figure 3.4. Each linear branch corresponds to a single-phase state. The specific volume ($v = 1/\rho$), defined by the Gibbs free energy first derivative (*cf.* relation (3.4)), is not continuous at the pressure P_{eq}: the phases have therefore different densities ρ_L and ρ_v. The two-phase equilibrium, characterized by the equality of the specific Gibbs free energy of each single-phase state (*cf.* the presentation of the van der Waals model in section 2.2.2), is only possible at the equilibrium pressure P_{eq}. The main features of the sharp description of the liquid-vapor transition are thus recovered. However, it is not possible to define a thermodynamic description of the fluid for values of the density ρ between its bulk values ρ_L and ρ_v. For this reason, a diffuse interface model based on such a formulation is not possible since no thermodynamic main variable is aimed to get continuous variations across the interface.

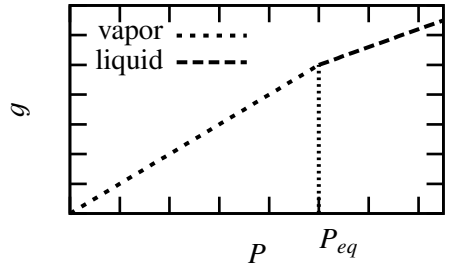

Figure 3.4: Incompressible liquid-vapor isothermal model

As a conclusion, the following set of constraints are incompatible all together

- ⋆ incompressible single-phase states
- ⋆ diffuse interface model of the liquid-vapor phase transition
- ⋆ classical and isothermal thermodynamic description, *i.e.* ρ or P as the single main variable.

It is shown in the following how this incompatibility can be removed by modifying the last statement, *e.g.* by considering a non-isothermal description and therefore by considering an additional thermodynamic variable (namely the temperature T or the specific entropy s).

Non isothermal liquid-vapor phase transition: entropy difference and arbitrary heat capacity Let us consider now the non-isothermal van der Waals' model and choose the temperature T (instead of the specific entropy s) as the second (in addition to the density ρ) main variable. The planar two-phase equilibrium is

characterized by an additional relation $T_{eq}(P_{eq})$ linking equilibrium values of the pressure and of the temperature. Let us introduce the specific entropy s of the fluid defined as

$$s \triangleq -\frac{1}{\rho}\frac{\partial F}{\partial T}_{|\rho} \tag{3.5}$$

For the liquid-vapor phase transition considered, there exists a characteristic entropy difference at two-phase equilibrium between the bulk phases. A subsequent latent heat $\mathcal{L}$ of evaporation defined as

$$\mathcal{L} \triangleq T_{eq}\ (s_{v,sat} - s_{l,sat}) \tag{3.6}$$

is associated to the phase transformation and it is important that the model recovers this feature (*cf.* our study of nucleate boiling flows in chapter 1). Let us study how this characteristic is modeled using the $F(\rho, T)$ expression. *A priori*, the entropy difference can be analytically enslaved to the density difference, since, using its definition (3.5), one can express the entropy as $s(\rho, T)$. Let us provide a basic expression for F allowing to model the latent heat. By integration of the equation (3.5), the volumetric Helmholtz free energy can be written as

$$F(\rho, T) = F(\rho, T_0) - \int_{T_0}^{T} \rho\ s(\rho, u)\ du$$

where T_0 is an arbitrary reference temperature. Thus using a Taylor expansion of F around $T = T_0$

$$F(\rho, T) \simeq F(\rho, T_0) - \rho\ s(\rho, T_0)\,(T - T_0) + O\,(T - T_0)^2 \tag{3.7}$$

For a given equilibrium temperature, say T_0, the specific entropy difference $\mathcal{L}/T_0$ is related to the function $s(\rho, T)$ through the above relations

$$s_{l,sat} = s(\rho_{l,sat}, T_0) \quad \& \quad s_{v,sat} = s(\rho_{v,sat}, T_0)$$

Therefore the specific entropy difference is formally related to the density difference. The linear dependence of the Helmholtz free energy with respect to temperature , *i.e.* the neglect of the terms of order $O\,(T - T_0)^2$ in the expression (3.7), is sufficient to model the desired entropy difference. Next (*i.e.* second) order temperature dependence of F is related to the heat capacity c_v defined as

$$c_v \triangleq T\left(\frac{\partial s}{\partial T}\right)_{\rho}$$

and once the latent heat $\mathcal{L}$ has been modeled by the linear dependency, c_v can be modeled independently using the quadratic dependency. Therefore it is possible to deal with an arbitrary (non negative, according to the Gibbs-Duhem criterion of thermodynamic stability) heat capacity c_v for the single-phase states.

We have presented the non-isothermal van der Waals' description of the liquid-vapor transition. It has been shown that the model describe well the specific entropy s difference between the bulk phases, independently of the choice for the specific heat capacity. In the following, we use the analogy (2.19) presented in section 2.3.1 in order to introduce a model for the liquid-vapor phase transition with incompressible bulk phases.

A diffuse interface model for the liquid-vapor transition with possible incompressible bulk phases Let us remark that since the specific entropy has characteristic values in the bulk phases, it can be considered as a relevant "order parameter" for the non-isothermal liquid-vapor phase transition. In order to model this transition, we therefore have the choice between two main variables the density ρ or the specific entropy s. This constitutes the main idea of the following development.

Let us recall the analogy (2.19) presented in section 2.3.1:

$$\begin{array}{rcl} P & \leftrightarrow & T \\ \rho & \leftrightarrow & s \\ \chi_T & \leftrightarrow & c_P \\ \text{or } \chi_s & \leftrightarrow & c_v \end{array} \tag{3.8}$$

Let us apply again this analogy[3] to the non-isothermal van der Waals model presented hereinabove: the entropy is considered as the order parameter of the phase transition, the pressure is chosen as the second main variable and the corresponding thermodynamic potential is chosen as the specific enthalpy $h(s, P)$. The density ρ is then defined as

$$\frac{1}{\rho} \hat{=} \frac{\partial h}{\partial P}_{|s}$$

and is therefore a function $\rho(s, P)$. It is possible to consider a density difference between the bulk phases

$$\rho_{l,sat} = \rho(s_{l,sat}, P_0) \quad \& \quad \rho_{v,sat} = \rho(s_{v,sat}, P_0)$$

such that the specific enthalpy h reads

$$h(s, P) \simeq h(s, P_0) - \frac{(P - P_0)}{\rho(s, P_0)} + O(P - P_0)^2$$

This models ensures therefore a density difference between the vapor and liquid phases and the terms of higher order in pressure define the adiabatic compressibility coefficient

$$\chi_s \hat{=} \frac{1}{\rho} \frac{\partial \rho}{\partial P}_{|s}$$

which is related to the isothermal compressibility χ_T (*cf.* its definition (2.3)) and the thermal expansion α_P (*cf.* its definition (2.18)) coefficients by

$$\chi_s = \chi_T - \alpha_P \frac{\partial T}{\partial P}_{|s}$$

As a consequence, the density difference can be considered while dealing with an arbitrary χ_s. Since χ_s can be chosen arbitrarily, it can be chosen such that $\chi_T = 0$, which implies the bulk phases to be incompressible. Let us precise that the fluid described has all the features of a non-isothermal liquid-vapor system (*i.e.* density difference, specific entropy difference, saturation curve *i.e.* the relation between the pressure and the temperature at two-phase equilibrium...).

The desired, *i.e.* incompressible, bulk *EOS* are thus compatible with a description of the liquid-vapor transition while another thermodynamic main variable is chosen as the "order parameter" (the specific entropy s in the hereinabove case) instead of the more "natural" one, the density. This description of a multi-phase system with density difference but incompressible single-phase states is known as the quasi-compressible limit which is more generally presented in the following.

The quasi-compressible limit In order to model the density variations of a fluid without taking into account the acoustic waves (*i.e.* the isothermal compressibility) a quasi compressibility (or quasi incompressibility, depending on the authors and on the context) assumption can be made. This assumption consists in considering the density as independent on the local pressure but still dependent on the other thermodynamic variable (such as the specific entropy in the hereinabove presented case).

In single-phase systems, this approximation of the compressible equations is valid at low Mach[4] number. The local value of the density variations is for instance defined from a classical perfect gas *EOS* considering the local value of the temperature field but a mean value of the pressure field, *e.g.* Paillere et al. [105].

In the diffuse interface models of a multi-phase system, the quasi-incompressible limit has been introduced by Lowengrub and Truskinovsky [89] for the study of binary fluids. In this case, the local mass fraction c of one component of the mixture is the natural "order parameter" and the main thermodynamic variable are chosen as (c, T, P). The density ρ is considered as a function $\rho(c, T)$ instead of $\rho(c, T, P)$.

More generally for the modeling of multi-phase materials, as soon as a second thermodynamic variable (like c or s) is introduced that could "play the role" of an "order parameter", the quasi-incompressible limit can be

[3] Using this analogy the isothermal van der Waals model based on $F(\rho)$ is equivalent to the incompressible model based on an energy $e(s)$ presented in the introduction of the phase field models in section 2.3.1. For instance, an analogue incompatibility exists with the $e(s)$ model: since s is the main variable of this thermodynamic model, it is not possible to deal with single-phase states with a zero heat capacity.

[4] the Mach number is the ratio of the flow velocity over the local speed of sound, itself directly related to the isothermal compressibility of the fluid

introduced. We have presented in our review of the exiting phase field models in section 2.3.3 how it has been used by Anderson et al. [5] for the study of the solidification process with a phase field formulation. In this case the main variables are chosen as (φ, T, P) and the density ρ is considered as a function $\rho(\varphi)$ (the hypothesis of a null coefficient of thermal expansion being additionally considered). Therefore in our phase field model for the liquid-vapor phase transition, a similar hypothesis is made possible by choosing the main thermodynamic variables as being (φ, P, s) or (φ, P, T).

We have presented the quasi-(in)compressible assumption in different fields of application. This assumption allows to filter out the acoustic waves of a physical process while considering the density as varying. This is made possible by considering the pressure as the main thermodynamic variable instead of the density (which can then be considered as independent on the pressure).

Conclusion on the model of a two-"incompressible"-phase fluid with density difference We have shown that this model is not possible as soon as the choice of the density as the "order parameter" of the phase transition is made. We have then introduced using analogy the model of the non-isothermal liquid-vapor phase transition where the specific entropy is the "order parameter" and that can deal with incompressible single phase. We have presented the more generic hypothesis of quasi-compressible fluid which concerns the model of fluid with non-uniform density but zero compressibility. Since it has been shown in chapter 1 that compressibility is not a primary physical mechanism of the nucleate boiling flows and since moreover a gain in numerical handling exists while dealing with incompressible fluids, the phase field model derived must be able to deal with quasi-compressibility.

3.1.3 The main variables of the phase field model

Let us consider now the model we derive for the study of the liquid-vapor phase transition with the help of the phase field method and define its main thermodynamic variables. The first main variable considered is the phase field φ.

Compressibility Let us consider the choice between either P or ρ as one of the main variable. We have shown in the previous sections that both are possible if we wish model a density difference between the bulk phases and that the choice is dictated by the desired model for the compressibility of the bulk phases. The "or" is therefore not *a fortiori* inclusive. Since the general formulation depending of φ must reduce to the single-phase EOS to be modeled, we must be able to write both (liquid and vapor EOS) in terms of the same variables. The following table presents the type of general EOS (f or g or b for both or $\emptyset$ for none) we can model with the phase field description of a liquid-vapor system.

liquid \ vapor	$\rho(P)$ not injective	$\rho(P)$ not surjective	$\rho(P)$ bijective
$\rho(P)$ not injective	$f(\rho, \varphi)$	$\emptyset$	$f(\rho, \varphi)$
$\rho(P)$ not surjective	$\emptyset$	$g(P, \varphi)$	$g(P, \varphi)$
$\rho(P)$ bijective	$f(\rho, \varphi)$	$g(P, \varphi)$	b

This table seems a bit naive but actually shows that it is possible to construct a quasi-compressible formulation, or to introduce the same kind of metastability limit than in the van der Waals' model for both phases ($P(\rho)$ injective but not surjective). However it also shows that we cannot model one incompressible phase and a second "van der Waals" type phase with a single phase field model. If the quasi-compressible limit of the formulation is targeted, the density ρ cannot be considered as a main thermodynamic variable, the pressure P is considered as being the corresponding main variable. This choice is therefore made in the remainder of this study and especially in the analytical and numerical studies presented in the chapters 5 and 8.

Non-isothermal description In order to deal with more classical description of the liquid-vapor transition, we consider the temperature T as the second main thermodynamic variable instead of its conjugate variable s. Moreover, for numerical application the choice of a main variable that is uniform at thermodynamic equilibrium, (like the temperature T in our phase field model according to the equilibrium relation (3.28a) shown in the following of this chapter), is accurate. Let us recall that for a phase transition, the entropy is multi-valued (*cf.*

the latent heat $\mathcal{L}$) at the equilibrium temperature. Therefore, classically, the function $s(T)$ cannot be analytically explicitly expressed. This should justify the choice of s as the main thermodynamic variable (like it should lead to the same statement concerning the density ρ). However, the introduction of the phase field variable allows to undergo this limitation in the model of multi-phase system as stated hereinabove and the variable T is preferred.

The thermodynamic potential corresponding to the variables (P, T) is therefore the Gibbs free energy.

Non-local dependence For isotropic reason, the non local energetic contribution must not depend on the system of coordinates, and the energy of the fluid is supposed to be a function of the norm[5] of $\nabla\varphi$. For our present study of the thermodynamic model devoted to the liquid-vapor transition, and as it is classically done in phase field models, the non local field considered is the norm associated to the Cartesian scalar product of $\nabla\varphi$, $(\nabla\varphi)^2 = \nabla\varphi \cdot \nabla\varphi$.

Specific Gibbs free energy Let us consider the primary thermodynamic potential as being the specific Gibbs free energy $g\left(\varphi, P, T, (\nabla\varphi)^2\right)$ as a function of the set of main variables: the pressure P, the temperature T, the phase field φ, and $(\nabla\varphi)^2$. The partial derivatives of g with respect to these variables are defined as follows

$$\begin{cases} \mu \triangleq & \dfrac{\partial g}{\partial \varphi} & \text{(3.9a)} \\ v \triangleq & \dfrac{\partial g}{\partial P} & \text{(3.9b)} \\ s \triangleq & -\dfrac{\partial g}{\partial T} & \text{(3.9c)} \\ \Phi \triangleq & \dfrac{\partial g}{\partial (\nabla\varphi)^2} & \text{(3.9d)} \end{cases}$$

where v is the specific volume ($v = 1/\rho$ where ρ is the density), s the specific entropy. We assume , as it is done classically in the capillary theory, that g is linear with respect to $(\nabla\varphi)^2$. Thus

$$\frac{\partial^2 g}{\partial((\nabla\varphi)^2)^2} = 0 \tag{3.10}$$

and Φ is therefore a function of (P, T, φ). The specific internal energy $u(\rho, s, \varphi, (\nabla\varphi)^2)$ is then obtained by the following double Legendre transformation (while it is valid)

$$u \triangleq g + Ts - Pv \tag{3.11}$$

Let us also define the per unit volume internal energy U by

$$U \triangleq \rho u \tag{3.12}$$

The other classical thermodynamic potential are then similarly defined from the Gibbs free energy.

Conclusion on the main variables for our phase field model of the liquid-vapor phase transition The main thermodynamic variables and the associated definitions of the thermodynamic main functions have been introduced as being $(P, T\varphi, (\nabla\varphi)^2)$ in accordance to the desired EOS for the bulk phases.

[5]This is not the most general case, and interface tension anisotropy is often considered in the solid-solid phase transitions and modeled by introducing a direction dependent non local contribution to the energy. The most general case of an energy dependence with respect to a gradient term is considered while deriving the dynamics using an Hamiltonian principle in section 5.1. It is also worth noting that another category of non-local thermodynamic constitutive forms can be considered in diffuse interface models, *e.g.* [10, 23, 34, 36] where instead of the dependence with respect to $|\nabla\varphi|^2$ of the thermodynamic potential, the non-locality is taken into account as

$$\int_{\mathbb{R}^3} J(\mathbf{x} - \mathbf{y})\,(\varphi(\mathbf{x}) - \varphi(\mathbf{y}))^2 \; d\mathbf{y}$$

where J is a smooth function.

3.2 Introduction of a phase field thermodynamic variable

The goal of this section is to study the thermodynamic description of a fluid with a phase field model in order to introduce the way the requirements presented on page 53 can actually be satisfied. In other words, we express the constraints in the form of analytical conditions applying to the thermodynamic potential g.

This section is organized as follows. In section 3.2.1 we introduce our definition of the phase field variable and specify its role. In section 3.2.2 we study the general formulation for the thermodynamic stability of the equilibrium states described with the help of our phase field formulation (Gibbs-Duhem criteria). In section 3.2.3 we use the previously derived relations to study the homogeneous equilibrium states. We deduce therefore the relations that the specific Gibbs free energy must satisfy in order the phase field single-phase states EOS to be actually controlled (point 7 of the list of constraints). In section 3.2.4 we study the structure of the diffuse interface at planar equilibrium with the help of our phase field model. In order to control the thickness of the interface and the surface tension coefficient, it is proposed that the equilibrium relations derived in section 3.2.2 reduce to a set of two simple ODEs that should be valid at any two-phase planar equilibrium conditions, *i.e.* along the saturation curve $P_{eq}(T)$.

3.2.1 A color function

The difficulty encountered with the numerical use of the van der Waals' model is mainly due to the inability to modify the characteristics of the transition layer without modifying other bulk physical properties as presented in section 2.2. The main idea behind the development of the present model is that the phase field variable φ introduced allows to describe the transition layer between single-phase states independently of the other physical properties. We consider that φ is introduced for purely numerical reasons and its role must therefore be compared to the indicator or color functions classically used in numerical methods based on sharp interface models (such as front-tracking, level-set or VOF *cf.* their presentation in sections 2.1.2). This color function takes specified and arbitrary values in the single-phase domains (where the fluid is in an homogeneous thermodynamically stable state).

Let us now consider the ability to describe single-phase states in phase field models. Since the value of φ is not in itself physically meaningful, the most simple and easy to handle interpretation of its value is the following: a particular value for φ is associated to each single-phase state. The scaling of φ is thus arbitrary and this variable is not meant to have any variation in single-phase states. Let us set

$$\begin{aligned} \varphi = 0 \quad &\leftrightarrow \quad \text{liquid phase} \\ \varphi = 1 \quad &\leftrightarrow \quad \text{vapor phase} \end{aligned}$$

The intermediate values of φ are not meant to refer to a mix between liquid and vapor but rather to states located inside the transition layer between single-phase domains (namely the diffuse interface). The thermodynamic description of the corresponding states is thus chosen adequately with the desired structure of the interface. The dependence of the thermodynamic potentials out of $\varphi = 0$ and $\varphi = 1$ (interpolation of the material properties between the bulk with the help of the φ variable) is thus dictated by this consideration.

As a consequence, the constitutive form for g must lead to classical EOS for $\varphi \in \{0; 1\}$ and to a controlled interface structure for $\varphi \in [0 : 1]$. Let us consider the single phase states to be described by the specific Gibbs free energies $g_{vapor}(P, T)$ and $g_{liquid}(P, T)$. We can introduce an intuitive pre-supposed form for the specific Gibbs free enthalpy g as

$$g = \nu(\varphi)\left(g_{vapor}(P,T) - g_{liquid}(P,T)\right) + g_{liquid}(P,T) + g_m(\varphi) + \Phi(\varphi)\ (\nabla\varphi)^2 \tag{3.13}$$

where ν is the interpolation function introduced in section 2.3.1 and g_m is zero in the liquid and vapor bulk phases ($\varphi \in \{0; 1\}$) and, together with $\Phi(\varphi)$, is mainly devoted to the model of the structure of the transition layer.

3.2.2 Gibbs-Duhem stability criterion Derivation of the equilibrium equations

In this section we study the thermodynamic stability of equilibrium states and derive the equilibrium relations corresponding to our phase field model. These equilibrium relations will then be used in the following sections to express analytically the list of constraints for the phase field model defined on page 53.

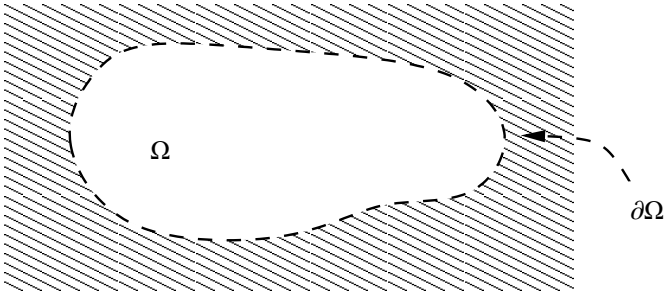

Figure 3.5: Thermodynamic system

Let us consider the equilibrium of a closed and isolated system Ω of fixed boundary $\partial\Omega$. Therefore neither exchange of energy (through work or heat transfer) nor of mass are considered through the boundary $\partial\Omega$. The Gibbs-Duhem criterion of stability states that the corresponding entropy of Ω is maximal, *e.g.* Papon and Leblond [107]. We propose to derive here the equilibrium relations using the variation of the total entropy of the system with respect to local variations δ of the main thermodynamic variables (ρ, S, φ) around the equilibrium state. We introduce L_1 and L_2 the two Lagrange multipliers associated with the two constraints of conservation of total internal energy $\int_\Omega U d\mathcal{V}$ and of total mass $\int_\Omega \rho d\mathcal{V}$ in the volume Ω. On the boundary $\partial\Omega$ we introduce an interaction energy U_b which is assumed to depend only on φ, *i.e.* on the nature of the phase in contact with the boundary. The introduction of this interaction energy is justified by the derivation of the governing dynamical equations using variational principles in section 5.1. The variation of entropy around the equilibrium state of a closed and isolated system reads thus

$$\delta\mathcal{S} \triangleq \delta \int_\Omega (S + L_1\, U + L_2\rho)\, d\mathcal{V} + \delta \int_{\partial\Omega} (L_1\, U_b)\, dA \tag{3.14}$$

where $S \triangleq \rho s$ is the entropy per unit volume. Since S is locally maximal around a stable equilibrium state, for any variation, the following relation are satisfied

$$\begin{cases} \delta\,\mathcal{S} = 0 \\ \delta^2\,\mathcal{S} \leq 0 \end{cases} \tag{3.15}$$

The first condition is the equilibrium condition of the state considered. Second order expansion provides the stability conditions of this equilibrium state. Stability of the homogeneous states is studied in section 3.2.3 in the simple case of the neglect of any non-local dependence ($\Phi = 0$) and from the complete set of governing equations in chapter 6.

Equilibrium condition Let us study the equilibrium condition

$$\delta\mathcal{S} = 0 \tag{3.16}$$

Using the definition (3.12) of the energy U, we can write

$$\delta U = u\,\delta\rho + \rho\,\delta u \tag{3.17}$$

and using the definition (3.11) of u

$$\delta U = (g - Pv)\,\delta\rho + \rho\,\delta(g - Pv) + T\,\delta(\rho s) + \rho s\,\delta T \tag{3.18}$$

The definition (3.9) of the partial derivatives of g yields

$$\delta g = v\,\delta P - s\,\delta T + \mu\,\delta\varphi + \Phi\,\delta\,(\nabla\varphi)^2 \tag{3.19}$$

Since $v\delta\rho = -\rho\delta v$, we have

$$v\,\delta P = \delta(Pv) - \frac{v\,\delta\rho}{\rho}$$

Multiplying by ρ the variation (3.19) of g and using the above relation yields the following relation between the different variations

$$-Pv\,\delta\rho + \rho\,\delta(g - Pv) + \rho s\,\delta T = \rho\left(\mu\,\delta\varphi + \Phi\,\delta\,(\nabla\varphi)^2\right)$$

And thus, using the above relation, the variation (3.18) of U reads

$$\delta U = g\,\delta\rho + \rho\left(\mu\,\delta\varphi + \Phi\,\delta\,(\nabla\varphi)^2\right) + T\,\delta(\rho s) \tag{3.20}$$

Let us link the variation of the non local field $(\nabla\varphi)^2$ to the variation of φ. The variation of the norm of $\nabla\varphi$ can be expanded as

$$\delta\,(\nabla\varphi)^2 = 2\,\nabla\varphi\,.\,\delta\nabla\varphi \tag{3.21}$$

The operator δ and ∇ commute, therefore the LHS of the above equation can be rewritten as

$$2\,\nabla\varphi\,.\,\delta\nabla\varphi = 2\,\nabla\varphi\,.\,\nabla(\delta\varphi)$$

For any scalar a and vector $\vec{b}$ fields, the following identity holds

$$\nabla\cdot\left(a\,\vec{b}\right) = a\,\nabla\cdot\vec{b} + \nabla a\cdot\ \vec{b} \tag{3.22}$$

Using this relation with $a = \delta\varphi$ and $\vec{b} = \nabla\varphi$ yields for the variation (3.21) of $(\nabla\varphi)^2$

$$\delta\,(\nabla\varphi)^2 \quad = \quad 2\,\nabla\cdot(\delta\varphi\nabla\varphi) - 2\,\nabla\cdot(\nabla\varphi)\,\delta\varphi \tag{3.23}$$

This relation implies that although φ and $(\nabla\varphi)^2$ can be considered as two independent thermodynamic variable, their evolution during a transformation δ are related. Let us now rewrite the term of the variation (3.20) of internal energy $\delta\ U$ involving this non local contribution variation

$$\rho\Phi\ \delta\ (\nabla\varphi)^2 = 2\,\rho\Phi\ \ (\nabla\cdot(\delta\varphi\nabla\varphi) - \nabla\cdot(\nabla\varphi)\,\delta\varphi) \tag{3.24}$$

Using the identity (3.22) for the first term of the right hand side yields

$$\rho\Phi\ \delta\ (\nabla\varphi)^2 = 2\ (\nabla\cdot(\rho\Phi\ \delta\varphi\,\nabla\varphi) - \nabla\,(\rho\,\Phi)\cdot(\delta\varphi\nabla\varphi) - \rho\Phi\ \nabla\cdot(\nabla\varphi)\,\delta\varphi) \tag{3.25}$$

The variation of the entropy of Ω under the energy and mass conservation constraints (3.16) can be expressed using the relations (3.20) and (3.25), uniquely in terms of variation with respect to S, ρ and φ. It reads

$$\begin{aligned}
&\int_\Omega \left[(L_1\,T + 1)\ \delta S\ + (L_2 + L_1 g)\ \delta\rho\right]\,d\mathcal{V}\\
+\int_\Omega &\left[L_1\rho\,(\mu - 2\,\Phi\,\Delta\varphi - 2\,v\,\nabla(\rho\Phi)\cdot\nabla\varphi)\right]\,\delta\varphi\,d\mathcal{V}\\
&+\int_{\partial\Omega} L_1\left(2\,\vec{n}\cdot(\rho\Phi\,\nabla\varphi) + \frac{dU_b}{d\varphi}\right)\delta\varphi\,dA \quad = \quad 0
\end{aligned}$$

where $\vec{n}$ is the local normal to $\partial\Omega$ and where we have used the divergence theorem. So since equation (3.14) must be satisfied for any variation of the independent thermodynamic variable (S, φ, ρ)

$$1 + L_1\,T \quad = \quad 0 \tag{3.26a}$$

$$(L_2 + L_1 g) \quad = \quad 0 \tag{3.26b}$$

$$L_1\rho\,(\mu - 2\,\Phi\,\Delta\varphi - 2\,v\,\nabla(\rho\Phi)\cdot\nabla\varphi) \quad = \quad 0 \tag{3.26c}$$

$$L_1\left(2\,\rho\Phi\,\vec{n}.\nabla\varphi + \frac{dU_b}{d\varphi}\right) \quad = \quad 0 \text{ on } \partial\Omega \tag{3.26d}$$

Let us denote $\tilde{\mu}$ the variational derivative of the specific Gibbs free energy with respect to φ (*cf.* the definition (2.9) of the variational derivative)

$$\begin{aligned}
\tilde{\mu} \quad &\hat{=} \quad \frac{1}{\rho}\frac{\tilde{\delta}G}{\tilde{\delta}\varphi}\\
&= \quad \frac{1}{\rho}\frac{\tilde{\delta}\rho\,g}{\tilde{\delta}\varphi}\\
&= \quad \frac{\partial g}{\partial\varphi} - \frac{1}{\rho}\nabla\cdot\left(\rho\,\frac{\partial g}{\partial\nabla\varphi}\right)\\
&= \quad \mu - 2\,\Phi\,\Delta\varphi - 2\,v\,\nabla(\rho\Phi)\cdot\nabla\varphi
\end{aligned} \tag{3.27}$$

such that the equilibrium relation (3.26c) reads $\tilde{\mu} = 0$. Thus at equilibrium

- ⋆ the specific Gibbs free energy g is uniform
- ⋆ the temperature T is uniform,
- ⋆ and the quantity $\tilde{\mu}$ is zero.

Local equilibrium relations The equilibrium conditions inside the domain read

$$\nabla T = 0 \tag{3.28a}$$
$$\nabla g = 0 \tag{3.28b}$$
$$\tilde{\mu} = 0 \tag{3.28c}$$

On the boundary of the domain, at equilibrium

$$\left(2\rho\Phi\,\vec{n}.\nabla\varphi + \frac{dU_b}{d\varphi}\right) = 0 \tag{3.29}$$

The equilibrium relation (3.28b) is non-conventional but can be related to the classical hydrostatic equilibrium relation. As it will be studied in chapter 5, in presence of capillarity, the stress tensor is not spherical, and, at equilibrium, the pressure is not uniform.

Comparison with the classical two-phase equilibrium conditions The classical multi-phase Gibbs relations for a planar interface at equilibrium are the equalities of (*e.g.* [107])

- ⋆ the temperature on each side of the interface
- ⋆ the pressure on each side of the interface
- ⋆ the specific Gibbs free energy on each side of the interface

As a consequence our equilibrium relations *a priori* differs from the classical about the equality of pressure. If the multi-phase fluid is described by a single energy functional using classical variables (*i.e.* without φ). Let us remark that thus the uniformity of g implies the uniformity of the pressure P since the Gibbs free energy g "reduces" to a function of (P, T). This does not correspond *a priori* to our own case where only the uniformity of g is recovered. However, if the phase field single-phase states correspond actually to classical single phase states (control of the EOS), the equality of pressure across a planar interface is recovered.

The thermodynamic equilibrium relation (3.28c) is additional with respect to conventional. It is actually related to φ variations.

The equilibrium conditions (3.28) are used to ensure that the φ values 0 and 1 effectively correspond to thermodynamically stable single-phase states in the following.

Boundary conditions We only briefly comment here the equilibrium boundary condition (3.29) which is studied in more details in section 5.1.2. If the interaction energy U_b does not depend on φ, the equilibrium boundary condition (3.29) yields

$$\vec{n} \cdot \nabla\varphi = 0$$

which corresponds to a static contact angle (angle between the interface and the boundary) of $\pi/2$. Otherwise the contact angle is different from $\pi/2$ and therefore express a specific affinity (*i.e.* for example $U_b(0) < U_b(1)$) of the boundary $\partial\Omega$ with respect to one of the bulk phase.

Conclusion on the derivation of the general expression for the equilibrium relations We have therefore derived the equilibrium relations of a fluid described with the help of a phase field specific Gibbs free energy $g(P, T, \varphi, (\nabla\varphi)^2)$. In addition to the classical sharp interface equilibrium relations, the nullity of the variational derivative $\tilde{\mu}$ of g with respect to φ is satisfied at equilibrium. This additional relation results directly from the fact we have considered the additional phase field thermodynamic variable. We show in the following how it can be related to the ability of the model to control the EOS of the single phase states as well as the structure of the interface.

3.2.3 Stability and equilibrium of single-phase states

In this section we consider the equilibrium condition for single-phase states and derive the analytical conditions for which the single-phase states actually correspond to $\varphi \in \{0; 1\}$

Single-phase states and the associated φ value Homogeneous states in terms of φ (*i.e.* where $\nabla\varphi = \vec{0}$) must correspond to single-phase states and satisfy the equilibrium relation (3.28c). Following our interpretation of the introduction of φ as a color function, (3.28c) must be satisfied at least for φ equals to 0 and 1. Therefore the formulation must ensure that

$$\tilde{\mu}(\varphi \in \{0; 1\}, P, T, (\nabla\varphi)^2 = 0) = 0 \tag{3.30}$$

i.e. since $(\nabla\varphi)^2 = 0$,

$$\mu(\varphi \in \{0; 1\}, P, T, (\nabla\varphi)^2 = 0) = 0 \tag{3.31}$$

As a consequence, this conditions expressed in terms of the derivative of the specific free energies reads

$$\left(\frac{\partial g}{\partial \varphi}\right)_{P,T,(\nabla\varphi)^2} (\varphi \in \{0; 1\}, P, T, (\nabla\varphi)^2 = 0) = \left(\frac{\partial f}{\partial \varphi}\right)_{\rho,T,(\nabla\varphi)^2} (\varphi \in \{0; 1\}, \rho, T, (\nabla\varphi)^2 = 0) = 0 \tag{3.32}$$

As a partial conclusion, the additional equilibrium relation induced by the introduction of φ implies the free energy to be an extrema at the specific single-phase values of the color function 0 and 1.

Stability of homogeneous states As already mentioned, since we are dealing with first order expansion around an equilibrium state, the above study of equilibrium conditions only imply S to reach an extrema. The more complete equilibrium study involves stability conditions that implies that S reaches a maxima and involves a quadratic expression in all the variations considered. In this section we restrict the study of thermodynamic stability to the desired single-phase state, namely liquid or vapor ($\varphi = 0$ or 1) and neglect any non-local dependence *i.e.* $\Phi = 0$ (*cf.* the definition (3.9) of the derivative of g with respect to $(\nabla\varphi)^2$). The equilibrium conditions derived hereinabove are supposed to be satisfied and the general stability criterion reads

$$\delta^2\mathcal{S} \leq 0 \tag{3.33}$$

and in terms of the main variations

$$\int_\Omega (1 + L_1 T)\,(\delta S)^2 + \alpha_{S\rho}\,\delta S\,\delta\rho + \alpha_{\rho\rho}(\delta\rho)^2 + \alpha_{S\varphi}\delta\varphi\,\delta S + \alpha_{\rho\varphi}\delta\varphi\,\delta\rho + \alpha_{\varphi\varphi}(\delta\varphi)^2 \leq 0 \tag{3.34}$$

where α_{XY} are coefficients that will be specified in the following. Let us study the cross variation terms including $\delta\varphi$, namely $\delta\varphi\,\delta S$ and $\delta\varphi\,\delta\rho$. The corresponding coefficient of the quadratic expression are the second order partial derivatives

$$\begin{aligned} \alpha_{S\varphi} &= L_1 \frac{\partial^2 U}{\partial\varphi\partial S} \\ \alpha_{\rho\varphi} &= L_1 \left(\rho \frac{\partial^2 u}{\partial\varphi\partial\rho} + \frac{\partial u}{\partial\varphi}\right) \end{aligned}$$

that can be rewritten using μ as

$$\begin{aligned} \alpha_{S\varphi} &= L_1 \frac{\partial\rho\mu}{\partial S} \\ \alpha_{\rho\varphi} &= L_1 \left(\rho\frac{\partial\mu}{\partial\rho} + \mu\right) \end{aligned}$$

In $\varphi = 0$ or 1, since the equilibrium condition (3.31) is supposed to be satisfied for all S and ρ values, these coefficient are null. Is is worth pointing out that this property is only valid for the equilibrium states 0 and 1. The only variation of φ remaining in the expression of $\delta^2\mathcal{S}$ is therefore $(\delta\varphi)^2$ whose coefficient is $L_1\,\rho(\partial\mu/\partial\varphi)$. We can therefore consider the φ variations independently of the other variations. Since the stability condition (3.33)

must be ensured for any set of variations, it must be satisfied if one considers only φ variations (*i.e.* when $\delta S = \delta\rho = 0$). The corresponding stability conditions reads

$$L_1 \rho \frac{\partial \mu}{\partial \varphi}_{|S,\rho} (\delta\varphi)^2 \leq 0$$

Since $1 + L_1 T = 0$ and since the temperature is positive, the Lagrange multiplier L_1 is negative and the stability condition reads

$$\frac{\partial \mu}{\partial \varphi}_{|S,\rho} \geq 0 \tag{3.35}$$

It is a straightforward calculation to show that as soon as $\mu = 0$ is ensured for $\varphi \in \{0; 1\}$ for any temperature and pressure we get

$$\frac{\partial \mu}{\partial \varphi}_{|S,\rho} (\varphi \in \{0; 1\}) = \frac{\partial \mu}{\partial \varphi}_{|T,\rho} (\varphi \in \{0; 1\}) = \frac{\partial \mu}{\partial \varphi}_{|T,P} (\varphi \in \{0; 1\})$$

Therefore we generalize the result of Umantsev [141] (that studied the stability of homogeneous states at equilibrium in incompressible phase field materials, this result is discussed in more detail in chapter 6), the adiabatic condition of thermodynamic stability coincides with the isothermal condition of thermodynamic stability and reads

$$\left(\frac{\partial^2 f}{\partial \varphi^2}\right)_{\rho,T,(\nabla\varphi)^2} (\varphi \in \{0; 1\}, \rho, T, (\nabla\varphi)^2 = 0) > 0 \tag{3.36}$$

where f denotes the Gibbs free energy. The isobaric and isothermal condition of thermodynamic stability reads

$$\left(\frac{\partial^2 g}{\partial \varphi^2}\right)_{P,T,(\nabla\varphi)^2} (\varphi \in \{0; 1\}, P, T, (\nabla\varphi)^2 = 0) > 0 \tag{3.37}$$

Condition for the phase field single phase states to correspond to $\varphi \in \{0; 1\}$ As a partial conclusion, and using the equilibrium conditions (3.32), the phase field values 0 and 1 are ensured to correspond to stable single-phase state at (P, T) if they are local minima of $g(\varphi, P, T, (\nabla\varphi)^2 = 0)$ with respect to φ. We here do not study the fact other values of φ could correspond to stable equilibrium states, this will be done in the following.

Other classical stability conditions The remaining terms of the stability conditions (3.33) for homogeneous states do not involve φ variations. They constitute thus the classical quadratic expression of the Gibbs-Duhem study and imply the classical stability conditions in terms of non negativity of the heat capacity and the compressibility coefficient, *e.g.* [107]. Since the EOS for $\varphi \in \{0; 1\}$ are supposed to be classical EOS, as soon as 0 and 1 are minima of the specific Gibbs free enthalpy, the stability conditions reduce to the classical conditions of stability.

Conclusion on the study of equilibrium and stability conditions of the single phase states $\varphi \in \{0; 1\}$ The necessary conditions for which an homogeneous state at a given φ corresponds to an homogeneous stable equilibrium states read

$$\frac{\partial g}{\partial \varphi}_{|P} = \frac{\partial f}{\partial \varphi}_{|\rho} = 0 \tag{3.38a}$$

$$\frac{\partial^2 g}{\partial \varphi^2}_{|P} = \frac{\partial^2 f}{\partial \varphi^2}_{|\rho} \geq 0 \tag{3.38b}$$

and imply the thermodynamic potentials to be minimal in this φ value. The respect of these conditions for and only for the values $\varphi = \{0, 1\}$ ensures that the only possible single-phase states correspond actually to the states described by the $EOS(P, T, \varphi = 0)$ and $EOS(P, T, \varphi = 1)$. As a consequence the stability condition of the single-phase states are equivalent to the classical conditions of stability applying to these EOS.

3.2.4 Two-phase equilibrium: capillarity and equilibrium profiles

Let us study the structure of the interface at two-phase equilibrium. We study the academic case of a planar interface. To do we introduce simple relations allowing to easily control the features of the two-phase equilibrium *i.e.* the thickness of the interface and the surface tension coefficient (points 3 and 4 of the list of constraints on page 53). The general equilibrium relations (3.28) are desired to reduce to these relations in order our model to fit these constraints.

Two parameters for the interface thickness and surface tension coefficient at planar equilibrium It is required that the model admits a solution describing the structure of an isolated planar interface between two-phases along an arbitrary direction (say an x-axis). The color function profile $\varphi(x)$, and the pressure profile $P(x)$ between the two-phases are determined by the solutions of the coupled system of differential equations (3.28b,3.28c). For numerical applications we are especially interested by the determination of the φ profile at equilibrium (*cf.* point 3 of the constraints). The surface tension coefficient is classically defined as an excess volumetric Helmholtz free energy across the interface which is in fact related to the equilibrium profile of P (*cf.* our study of the excess quantities and of the definition of the surface tension coefficient in the appendix, section A.1). As a consequence, both the pressure and phase field profiles at planar equilibrium need to be controlled in order to ensure a control of the thickness of the interface and of the surface tension coefficient.

Classically, diffuse interface models yield to simple relations for the order parameter profile and for the surface tension coefficient, *e.g.* our presentation of the isothermal van der Waals model in section 2.2.2 where these quantities have been shown to be defined with the help of a double well function $W(\rho)$ and two parameters A and the capillary coefficient λ. We therefore simply require our model to recover such simple relations in order to easily control these quantities.

Phase field profile The classical φ profiles allowing an easy parametric control in diffuse interface modeling correspond to monotonic profiles of characteristic thickness h along the x-axis normal to the interface linking the bulk φ values 0 and 1. The corresponding plot of the variations of $\varphi(x)$ and $\varphi_{,x}(x)$ (where $\cdot_{,x} = (\partial \cdot / \partial x)$) are given on figure 3.6. This is the solution of the differential equation, *e.g.* Rocard [113]

$$h^2 \, (\varphi_{,x})^2 = 2 \, W(\varphi) \tag{3.39}$$

where $W(\varphi)$ is a positive double well function satisfying

$$\left\{ \begin{array}{l} W(0) = W(1) = 0 \\ \dfrac{dW}{d\varphi}(0) = \dfrac{dW}{d\varphi}(1) = 0 \\ \displaystyle\int_0^1 \sqrt{2 \, W(\varphi)} \, d\varphi \; = \; 1 \end{array} \right. \tag{3.40}$$

and represented on figure 3.7. Let us remark that the differential equation (3.39) is equivalent to the differential equation obtained by taking the spatial derivative of (3.39) with respect to x and dividing by $\varphi_{,x}$ that reads

$$h^2 \, \varphi_{,xx} = \frac{dW}{d\varphi} \tag{3.41}$$

The widely used order 4 polynomial for W

$$W_{P4}(\varphi) = 18 \; \varphi^2 \; (\varphi - 1)^2 \tag{3.42}$$

provides a profile for a planar interface along an arbitrary $x-$axis given by

$$\varphi(x) = \frac{1}{2} \pm \frac{1}{2} \tanh\left(\frac{2\,x}{\tilde{h}}\right) \tag{3.43}$$

where the thickness $\tilde{h}$ of the profile is defined as

$$\tilde{h} \hat{=} \frac{1}{\max |\varphi_{,x}|}$$

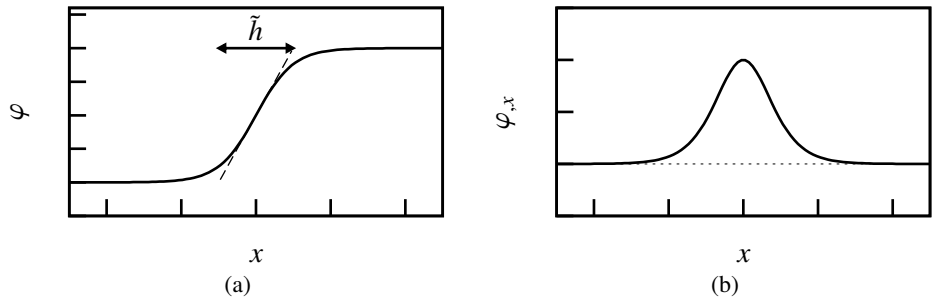

Figure 3.6: Diffuse interface profile for the phase field φ

and its relation to the parameter h is therefore

$$\tilde{h} = \frac{2}{3}\, h \tag{3.44}$$

As a partial conclusion, the differential equation (3.39) actually allows to control easily the thickness of the phase field profile at planar equilibrium and is therefore retained in the following as being a targeted equilibrium relation resulting from the constitutive expression of the thermodynamic potentials.

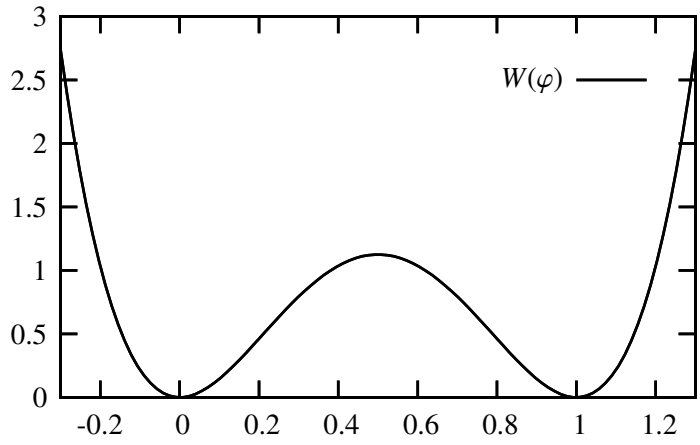

Figure 3.7: Double well function

Pressure profile and surface tension coefficient The surface tension coefficient σ (defined as an excess free Helmholtz energy) is related to the pressure profile across the interface as (*cf.* equation (A.11))

$$\sigma = \int_{-\infty}^{+\infty} P_{eq} - P(x)dx$$

For the sake of simplicity and in order the surface tension to be induced only by φ variations, we introduce the following differential equation for the pressure profile at planar equilibrium

$$P(x) = P_{eq} - \lambda\, (\varphi_{,x})^2 \tag{3.45}$$

where λ is the capillarity coefficient. Let us remark that, as soon as the differential equation (3.45) is satisfied, one recovers the classical jump condition across a planar interface at equilibrium of zero pressure jump *i.e.* $[\![P]\!] = 0$.The surface tension coefficient σ is then given by

$$\sigma = \lambda \int_{-\infty}^{+\infty} (\varphi_{,x})^2\, dx \tag{3.46}$$

Using the differential equation (3.39), the change of variable $\varphi \leftrightarrow x$, *i.e.* $d\varphi \leftrightarrow \varphi_{,x}\, dx$ and the fact that the bulk values of the phase field are attained at infinity (*i.e.* $\varphi(\pm\infty) = 0$ or $= 1$), we get

$$\sigma = \frac{\lambda}{h} \int_0^1 \sqrt{2\, W(\varphi)}\, d\varphi \tag{3.47}$$

Since $W(\varphi)$ satisfies the properties (3.40), σ is related to h and λ by

$$\sigma = \frac{\lambda}{h} \tag{3.48}$$

This relation is simple.

As a partial conclusion, as soon as the equilibrium conditions imply the relations (3.39) and (3.45) to be satisfied, the surface tension coefficient of a planar interface at equilibrium is defined by the single ratio of two parameters λ/h entering these relations. This is for sure a simple relation and actually allows to control the value of the surface tension coefficient σ induced by the phase-field formulation.

Conclusion concerning the structure of the interface at planar equilibrium In order to control the surface tension coefficient and the thickness of the interface, as required for the model (*cf.* the discussion of the section 2.3.2) the equilibrium conditions (3.28b) and (3.28c) are desired to be equivalent to the system of two differential equations (3.39) and (3.45). In addition of a double well function $W(\varphi)$ two parameters should enter the phase field formulation which are therefore λ and h. As a consequence, the thickness $\tilde{h}$ of the phase field profile and the value of the surface tension coefficient σ are simply related to these parameters. For example, when $W(\varphi)$ is the polynomial of degree 4 (3.42) we get

$$\begin{aligned} \tilde{h} &= \frac{2}{3} h \\ \sigma &= \frac{\lambda}{h} \end{aligned}$$

Let us recall that in the second gradient analytical formulation presented 2.2.2, a similar set of two parameters, namely A and λ defined the thickness and the surface tension coefficient.

3.3 Constitutive expression for the Gibbs free energy

In this section, we present the constitutive form of the thermodynamic potential of the phase field fluid that allows to fit the constraints desired for our model of the liquid-vapor phase transition.

3.3.1 Isothermal constitutive form

Let us first consider the isothermal case. The bulk phases *EOS* of the liquid $g_{liq}(P)$ and vapor phases $g_{vap}(P)$ read

$$\begin{aligned} g_{liq}(P) &\hat{=} \int_0^{P-Peq} 1/\rho_{liq}(P) + g_{eq} \\ g_{vap}(P) &\hat{=} \int_0^{P-Peq} 1/\rho_{vap}(P) + g_{eq} \end{aligned}$$

where g_{eq} is a common value of the specific Gibbs free energy at the planar two-phase equilibrium pressure P_{eq}. In the following, we assume the density ρ_{liq} and ρ_{vap} of the bulk phases to be constants thanks to the incompressibility hypothesis. The specific volume $v = 1/\rho$ of the phase field fluid is then defined as

$$v(\varphi) = 1/\rho_{liq}(P_{eq}) + \nu(\varphi)\left(1/\rho_{vap}(P_{eq}) - 1/\rho_{liq}(P_{eq})\right) \tag{3.50}$$

where ν is a monotonic interpolation function satisfying

$$\nu(0) = 0 \quad \& \quad \nu(1) = 1 \tag{3.51}$$

as the one introduced in the presentation of the phase field models in section 2.3.1 and plotted on figure 2.7. The interpolation function will be determined to ensure the thermodynamic stability of the equilibrium of the single-phase states in section 3.4.1. We now specify the dependence for g in φ and $(\nabla\varphi)^2$ such that the phase field model for the quasi-compressible case reads

$$g = v(\varphi)\left[P - P_{eq} + \frac{\lambda}{2}(\nabla\varphi)^2 + \frac{\lambda}{h^2}W(\varphi)\right] + g_{eq} \tag{3.52}$$

where $W(\varphi)$, λ and h refer to the double well function, the coefficient of capillarity and the interface thickness presented in the section 3.2.4. It is a straightforward calculation to show that the specific Gibbs free enthalpy given by equation (3.52) can be written as

$$\begin{aligned} g &= g_{liq}(P) + \nu(\varphi)\left(g_{vap}(P) - g_{liq}(P)\right) \\ &\quad + v(\varphi)\left(\frac{\lambda}{h^2}W(\varphi) + \frac{\lambda}{2}(\nabla\varphi)^2\right) \end{aligned} \tag{3.53}$$

As a consequence the single-phase thermodynamic potentials g_{liq} and g_{vap} are recovered for $\varphi = 0$ and $\varphi = 1$

$$\begin{aligned} g_{liq}(P) &= g(P, \varphi = 0, (\nabla\varphi)^2 = 0) \\ g_{vap}(P) &= g(P, \varphi = 1, (\nabla\varphi)^2 = 0) \end{aligned}$$

In the expression (3.53) for g, the interpolation function ν appears explicitly as linking the single-phase thermodynamic potentials g_{liq} and g_{vap} on the first line whereas the second line is related to the description of the interface structure.

3.3.2 Non-isothermal *EOS*

The temperature dependencies that need to be taken into account for the study of the nucleate boiling flows are the following (*cf.* the study of the nucleate boiling flows in chapter 1):

- ⋆ Equilibrium pressure as a function of temperature, *i.e.* the saturation curve $P_{eq}(T)$ since it leads to the definition of the latent heat of evaporation $\mathcal{L}$
- ⋆ Specific heat capacities of the single-phase states at constant pressure c_P since it is a primary parameter for the convective heat transfer in the bulk phases

Let us note that the introduction of a non-zero coefficient of thermal expansion α_P of the single-phase states will be related to the model of the specific heat capacity in section 3.4.2.

It is worth pointing out that the model could also take into account the possible dependence of the surface tension coefficient with respect to temperature that induces the Marangoni effect, *e.g.* [28] and a possible dependence of the interface thickness with temperature that could become infinite at a critical temperature. Since these physical phenomena are not considered as associated to primary physical mechanism of the nucleate boiling flows at high heat fluxes, they are not considered in the following.

Constitutive form for the specific Gibbs free energy The expression for the specific Gibbs energy $g(\varphi, P, T, (\nabla\varphi)^2)$ in the quasi compressible case reads as follows

$$g(\varphi, P, T, (\nabla\varphi)^2) = v\varphi, T)\left(P - P_{eq}(T) + \lambda\left(\frac{W(\varphi)}{h^2} + \frac{(\nabla\varphi)^2}{2}\right)\right) + g_{eq}(T) \tag{3.55}$$

where, in comparison with the isothermal case formulation (3.52), P_{eq} is now the saturation pressure $P_{eq}(T)$, the specific volume of the bulk phases given by $v(\varphi, T)$ is now the specific volume of the fluid that reads

$$v(\varphi, T) = v_{liq}(T) + \left(v_{vap}(T) - v_{liq}(T)\right)\nu(\varphi) \tag{3.56}$$

where v_{liq} and v_{vap} can thus eventually depend on the temperature T and are interpolated by the same interpolation function $\nu(\varphi)$. Moreover the specific Gibbs free energy at planar two phase equilibrium $g_{eq}(T)$ is supposed to

depend on temperature. This dependence will be related to the specific heat capacity at constant pressure in section 3.4.2. All the variations of g with respect to φ are equivalent to the isothermal case.

The relevant physical parameters for the thermodynamic description are the bulk phase value of the pressure and of the temperature, they define the bulk value for the specific Gibbs free energy $g(P, T, \varphi \in \{0; 1\}, (\nabla\varphi)^2 = 0)$. The level of the specific Gibbs free energy as well as the level of the pressure are not in them self meaningful. We therefore introduce a measure of their shift to the equilibrium value, that is temperature dependent, with the help of the starred variables

$$g^* \triangleq g - g_{eq}(T) \tag{3.57a}$$
$$P^* \triangleq P - P_{eq}(T) \tag{3.57b}$$

such that the specific Gibbs free energy (3.55) now reads

$$g^* = v(\varphi, T)\left[P^* + \frac{\lambda}{h^2}W(\varphi) + \frac{\lambda}{2}(\nabla\varphi)^2\right] \tag{3.58}$$

It is worth noting that since at equilibrium both temperature and specific Gibbs free energy are uniform, the quantity g^* is uniform as well. This writing will be used in the following.

Comparison with the model of Anderson et al. [5] Let us consider the difference of the proposed phase field model with the analogous model of Anderson et al. [5] that has been studied in section 2.3.3. The expression for the specific Gibbs free energy considered in [5] reads (*cf.* equation (2.23))

$$g(T, P, \varphi, (\nabla\varphi)^2) = \tilde{v}(\varphi)\left[P - P_{eq}(T)\xi_\nu(\varphi) + \lambda(T)\left(\frac{W(\varphi)}{h(T)^2} + \frac{(\nabla\varphi)^2}{2}\right)\right] + g_{eq}(T)$$

where for the sake of legibility we have used our own writing for the set of parameters and functions and where $\xi_\nu(\varphi)$ reads

$$\xi_\nu(\varphi) = \left[\left(1 - \frac{\rho_l}{\rho_v}\right) + \left(2 - \frac{\rho_v}{\rho_l} - \frac{\rho_l}{\rho_v}\right)\nu(\varphi)\right]\nu(\varphi)$$

$\tilde{v}(\varphi)$ reads

$$1/\tilde{v}(\varphi) = \rho_l + (\rho_v - \rho_l)\ \nu(\varphi)$$

and $g_{eq}(T)$ reads

$$g_{eq}(T) = [e_0 - c_P\, T_0]\left(1 - \frac{T}{T_0}\right) - c_P\, T \ln\frac{T}{T_0}$$

Let us also note that we have used the Clapeyron relation in order to express the formulation in terms of $P_{eq}(T)$ instead of $\mathcal{L}$.

Our model is different from the model of Anderson et al. [5] according to three respects:

1. the density instead of the specific volume is interpolated by the function $\nu(\varphi)$ which is chosen as a polynomial of degree 3
2. the existence of a function $\xi_\nu(\varphi)$ as soon as $\rho_l \neq \rho_v$
3. the existence of a temperature dependence of the coefficients h and λ

Concerning the point 1 of the above list, it is worth noting that since only derivatives of the interpolation function will be shown to be of interest in order to control the single phase states as being always 0 and 1, the choice of either the specific volume or the density as being a polynomial has no consequences on the main properties of the model. Nevertheless the choice of a polynomial of degree 3 will be shown to be insufficient in order to control the stability of the bulk phases (*cf.* section 3.4.1 or the chapter 6). Moreover it will be shown in chapter 4 that the choice of a polynomial of degree 3 has also undesirable consequences on the physical behavior of small spherical inclusions.

Concerning the point 2 of the above list of differences, it is worth pointing out that in our case the function ξ_ν reduces to 1. In this latter case, and only in this case, the phase field profile and the surface tension coefficient can be easily controlled along the whole saturation curve, which has been already said to be of primary interest

for our applications (points 3 and 4 of the list of constraints for the model expressed on page 53). The third point concerns the ability to make both the surface tension coefficient and the interface thickness vary along the saturation curve and can be of interest for an easy control only in the case where $\xi_\nu = 1$. This feature is of no interest for our targeted applications

As a conclusion, the constitutive form of our model mainly differs from the model of Anderson et al. [5] by the fact we consider no additional function (ξ_ν) of φ in front of the saturation pressure $P_{eq}(T)$. This additional function has no *a priori* physical meaning and moreover induces a variation of the planar equilibrium profiles along the saturation curve (*cf.* our presentation of the model considered in [5] in section 2.3.3). This additional property of the model is therefore not desirable for our applications and it justifies therefore our constitutive form as being more accurate for the study of the liquid-vapor flows with phase change.

Comparison with the standard phase field models for solid-liquid transitions We propose to compare the degeneracy of our model when the density difference between the bulk phases is set to zero to the widely used form of the phase field models for the study of the solid-liquid phase transition.

For the sake of simplicity, let us first consider the density, as being independent of the temperature T and of the pressure T, and without any loss of generality. We therefore consider the quasi compressible form of our model where v_{eq} reduces to a function of φ. The specific Gibbs free energy reads

$$g(\varphi, P, T, (\nabla\varphi)^2) = v(\varphi)\left(P - P_{eq}(T) + W(\varphi) + \frac{\lambda}{2}(\nabla\varphi)^2\right) + g_{eq}(T)$$

The solid liquid transition can be described by assuming the density difference between the bulk phases equals 0. However it is not equivalent as simply replacing $v(\varphi)$ by a constant since, according to the Clapeyron relation the product $\delta v\, dP_{eq}/dT$ equals $\mathcal{L}(T)/T$ which is non-zero even if $\delta v = 0$. Indeed from $s = -\partial g/\partial T$ we have

$$v(\varphi)(P_{eq}(T) - P_{eq}(T_0)) + g_{eq}(T_0) - g_{eq}(T) = \int_{T_0}^{T} s(\varphi, \tau)\, d\tau$$

From this expression, we identify the part associated to the description of the liquid state and rewrite left and right hand side of the above equation as follows

$$\begin{gathered}\nu(\varphi)\,\delta v\,(P_{eq}(T) - P_{eq}(T_0)) + g_{eq}(T_0) - g_{eq}(T) + v_{liquid}\,(P_{eq}(T) - P_{eq}(T_0)) \\ = \\ \nu(\varphi)\int_{T_0}^{T}(s_{vapor}(\tau) - s_{liquid}(\tau))\,d\tau - \int_{T_0}^{T} s_{liquid}(\tau)\,d\tau\end{gathered}$$

and thus the specific Gibbs free energy reads

$$\begin{aligned} g(\varphi, P, T, (\nabla\varphi)^2) \quad = \quad & v(\varphi)\left(P - P_{eq}(T_0) + W(\varphi) + \frac{\lambda}{2}(\nabla\varphi)^2\right) + g_{eq}(T_0) \\ & -\nu(\varphi)\int_{T_0}^{T}(s_{vapor}(\tau) - s_{liquid}(\tau))\,d\tau - \int_{T_0}^{T} s_{liquid}(\tau)\,d\tau \end{aligned}$$

It is then possible to assume $v_{eq}(\varphi)$ as being the specific constant volume of the material considered v_0 and to recover the classical phase field formulation for the specific free energy, *e.g.* [1]

$$f(T, \varphi, (\nabla\varphi)^2) = W(\varphi) + \frac{\lambda}{2}(\nabla\varphi)^2 + g_{eq}(T_0) - \nu(\varphi)\int_{T_0}^{T}\frac{\mathcal{L}(\tau)}{\tau}\,d\tau - \int_{T_0}^{T} s_{solid}(\tau)\,d\tau \tag{3.59}$$

where $\mathcal{L} \hat{=} T\left(s_{liquid} - s_{solid}\right) > 0$ is the latent heat of the phase transition. Let us note that *solid* substitutes *liquid* in the context of solid-liquid phase transition since its entropy is the lowest one.

As a conclusion, the proposed phase field model is a generalization of the classical phase field model for solidification allowing to consider a density difference between the single-phase states.

3.4 Properties of the constitutive form of the thermodynamic potentials

The goal of this section is to show that the constitutive form for the Gibbs free energy introduced in the previous section actually satisfy the set of constraints defined on page 53. We therefore use the analytical conditions derived in section 3.2 in order to analyze the expression (3.55) for g.

We first show that as soon as the interpolation function is chosen adequately, the phase field values $\varphi \in \{0; 1\}$ always correspond to stable equilibrium homogeneous states (see section 3.4.1). Then we study the meaning of g_{eq} as being related to the bulk specific heat capacities $c_{P,liq}$ and $c_{P,vap}$ (see section 3.4.2) as well as the expression for the latent heat of evaporation $\mathcal{L}$ (see section 3.4.3), both being important parameters for the study of the nucleate boiling flows. Finally we show that the differential equations (3.39) and (3.45) allowing to control the structure of the interface are actually satisfied at planar two-phase equilibrium (see section 3.4.4).

3.4.1 Single-phase states

Let us study the stability and equilibrium relations for the homogeneous states corresponding to the phase field values 0 and 1. We first introduce the more widely used expressions for the interpolation function $\nu(\varphi)$. We then study how the choice for the interpolation function is related to the description of the single phase states in phase field models.

The interpolation function Let us present the most current interpolation functions ν used in phase field models. They are polynomials of degree 1, 3 and 5, namely

$$P_1(\varphi) = \varphi \tag{3.60a}$$
$$P_3(\varphi) = \varphi^2 (3 - 2\varphi) \tag{3.60b}$$
$$P_5(\varphi) = \varphi^3(6\varphi^2 - 15\varphi + 10) \tag{3.60c}$$

They are represented on figure 3.8. All these interpolation functions (P_1, P_3, P_5) satisfy (3.51).

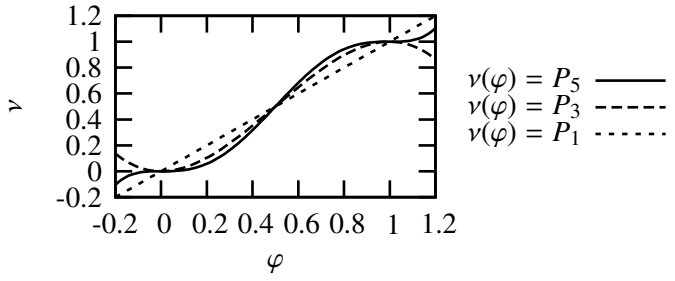

Figure 3.8: Interpolation function

Equilibrium and stability Let us state how the interpolation function choice is related to the equilibrium and stability relations (3.38a,3.38b) that ensure the single-phase states to be associated to the discrete values 0 and 1 of φ.

Equilibrium condition The equilibrium condition (3.38a) reads

$$\frac{\partial g}{\partial \varphi}_{|P,T(\nabla\varphi)^2}(\varphi \in \{0; 1\}, P, T, (\nabla\varphi)^2 = 0) = 0$$

Using the constitutive form (3.55) for g and using the properties (3.40) of the function $W(\varphi)$ this condition reads

$$\frac{d\nu}{d\varphi}(\varphi \in \{0; 1\})\Big(P - P_{eq}(T)\Big)\Big(1/\rho_{vap}(T) - 1/\rho_{liq}(T)\Big) = 0$$

As a consequence only the derivative of the interpolation function ν is concerned by the condition for $\varphi \in \{0;1\}$ to correspond to equilibrium single-phase states.

It is worth pointing out that as soon as $P \neq P_{eq}(T)$ the choice $\nu = P_1$ does not allow to satisfy this condition. This choice will therefore be disregarded in the following. Otherwise the choices P_3 and P_5 actually allows the states $\varphi = 0$ and $\varphi = 1$ to always correspond to equilibrium states.

Stability condition The stability condition (3.38b) reads

$$\frac{\partial^2 g}{\partial \varphi^2}_{|P,T,(\nabla\varphi)^2}(\varphi \in \{0;1\}, P, T, (\nabla\varphi)^2 = 0) \quad = \quad 0$$

Therefore using the expression (3.55) for g as well as the properties (3.40) and the fact that $\varphi \in \{0;1\}$ are equilibrium states (*i.e.* as shown hereinabove that $(d\nu/d\varphi)(0;1) = 0$), the stability condition reads

$$\begin{aligned} \frac{d^2\nu}{d\varphi^2}(0;1)\Big(P - P_{eq}(T)\Big)\Big(1/\rho_{vap}(T) - 1/\rho_{liq}(T)\Big) \\ + \frac{d^2W}{d\varphi^2}(0;1)\frac{\lambda}{h^2}\, v(0;1,T) \\ \geq 0 \end{aligned} \tag{3.61}$$

Since the double well function $W(\varphi)$ is minimal at $\varphi = 0$ and 1, we have

$$\frac{d^2W}{d\varphi^2}(0;1) > 0$$

Since the specific volume of the phase is positive, all the second line of equation (3.61) is positive.

Let us now consider the influence of the choice for the interpolation function. P_3, that ensures that (3.38a) is satisfied, ensures (3.38b) to be satisfied only for a given range of P, T values introducing in a way a metastability limit. This metastability limit depends on λ/h^2 *i.e.* on σ/h and on the density of the bulk phases. As a consequence it is a decreasing function of the interface thickness h other parameters being fixed. This property is not desirable for our application. The use of P_3 as the interpolation function limits therefore the range of use of the model. This point will be studied in more details in chapter 6.

P_5 ensures both (3.38a) and (3.38b) to be satisfied for any values of (P, T). This is the motivation for choosing P_5 as an interpolation function, following the choices made in most of the phase field models dedicated to liquid-solid transitions.

Density or specific volume as polynomials It is worth noting that only the derivative of the interpolation function at $\varphi = 0$ or 1 are involved in the equilibrium and stability of the single phase states. We have first considered that the function $\nu(\varphi)$ that interpolates the specific Gibbs free energy as well as the specific volume was polynomials P_n, n= 1, 3, 5. It is a straightforward calculation to show that 0 and 1 are still single phase states if the density ρ instead of the specific volume v is chosen as the polynomial P_5. In this case, the density reads

$$\rho(\varphi) = \rho_l + (\rho_v - \rho_l)\ P_n(\varphi)$$

and the interpolation function $\nu(\varphi)$ is then given by

$$\nu(\varphi) = \frac{P_n}{\rho_l/\rho_v + (1 - \rho_l/\rho_v)\ P_n}$$

For the study of the spherical symmetric case (*cf.* chapter 4) and the study of the stability of homogeneous states (*cf.* chapter 6) , the density will be considered as being interpolated by polynomials.

Other possible equilibrium states In the previous study of the ability to control the EOS of the single phase states, we have only considered the conditions for which $\varphi = 0$ and $\varphi = 1$ are equilibrium solutions. It is worth pointing out that other equilibrium solutions (solutions of uniform φ of the equation (3.38a) $\mu = 0$) than 0 and 1 exists as soon as $P \neq P_{eq}(T)$. Since they do not correspond to desirable single phase states it is required that

the model leads to their instability. Let us study these other solutions. Their stability is studied in more details in chapter 6.

We study the value of the phase-field φ as a function of the specific Gibbs free energy g^* for the homogeneous states. Therefore we precise the relation between these parameters at equilibrium. To do this, we study the equilibrium relation of an homogeneous state $\mu = 0$. It reads

$$\frac{\partial v}{\partial \varphi}\left[P^* + \frac{\lambda}{h^2}W(\varphi)\right] + v\,\frac{\lambda}{h^2}\frac{dW}{d\varphi} = 0$$

where P^* is viewed as a parameter for the equilibrium state. And therefore multiplying by ρ and using the quantity g^*, it is a straightforward calculation that the equilibrium equation is equivalent to

$$-\frac{\partial \rho}{\partial \varphi}\, g^* + \frac{\lambda}{h^2}\,\frac{dW}{d\varphi} = 0 \tag{3.62}$$

where g^* is viewed as a parameter for the equilibrium state. This writing of the equilibrium equation is attractive since it is less complex than the primitive one. For the sake of simplicity, we consider that $\alpha_P = 0$ and we do not consider the case where the specific volume v is interpolated by polynomials, but only the case when the density ρ is interpolated by polynomials. However the results are, if not quantitatively, qualitatively exactly similar in both cases.

We then introduce a non-dimensional writing of the equilibrium equation (3.62) using the non-dimensional number $\mathfrak{g}$ that reads

$$\mathfrak{g} \triangleq \frac{(\rho_l - \rho_v)\, h^2\, g^*}{\lambda} = \frac{(\rho_l - \rho_v)\, h\, g^*}{\sigma} \tag{3.63}$$

Since $\rho(\varphi)$ reads

$$\rho(\varphi) = \rho_l + (\rho_v - \rho_l)\, P_n(\varphi)$$

n being one of the following values 1, 3, or 5, the equilibrium equation (3.62) reads

$$\mathfrak{g}\,\frac{dP_n}{d\varphi} + \frac{dW}{d\varphi} = 0 \tag{3.64}$$

Let us note that $\mathfrak{g}$ has the same sign than g^* and that $\mathfrak{g} = 0$ corresponds to the planar interface equilibrium condition. This parameter will be used in the following to characterize the equilibrium solution instead of g^* which is the classical physical parameter describing the state. It is worth pointing out that when the physical parameters ρ_l, ρ_v, g^* and σ are fixed, $\mathfrak{g}$ is a function of the artificial thickness h. As a consequence, the equilibrium phase field solutions of equation (3.64) corresponding to fixed physical parameters are functions of the artificial thickness h. This influence of the artificial parameter h on the fluid description must be controlled and we show in the following how it affects the equilibrium solutions.

We consider that the double well function $W(\varphi)$ is given by (3.42). Therefore, by construction, 0 , resp. 1, the value of the phase field associated with the liquid, resp. vapor, phase, is solution of the equation (3.64) for $\mathfrak{g} = 0$. Figure 3.9 illustrates the solution of the equilibrium equation (3.64) in the cases where ρ is interpolated by one of the three polynomials considered. Let us note that the solutions are odd with respect to $\varphi - 1/2$ (central symmetry of center $(\mathfrak{g} = 0; \varphi = 1/2)$).

Polynomial of degree 1 Let us consider the case when ρ is interpolated by P_1. In this case $(dP_1/d\varphi)^{hs} = 1$. For small values of the parameter $\mathfrak{g}$ we can approximate solutions for φ around the bulk phase values 0 or 1 (corresponding to the planar two-phase equilibrium value *i.e.* $\mathfrak{g} = 0$) as follows

$$\varphi \simeq 1/2 \pm 1/2 - 36\,\mathfrak{g} \tag{3.65}$$

and around the center of the spinodal region (1/2)

$$\varphi \simeq 1/2 + 18\,\mathfrak{g} \tag{3.66}$$

More generally, there exists a finite range of possible values for $\mathfrak{g}$ for each case:

- ⋆ $\varphi \in [-\infty; 1/2 - \sqrt{3}/6]$, *i.e.* "liquid" phase corresponds to $\mathfrak{g} \in [-2\sqrt{3}; +\infty]$

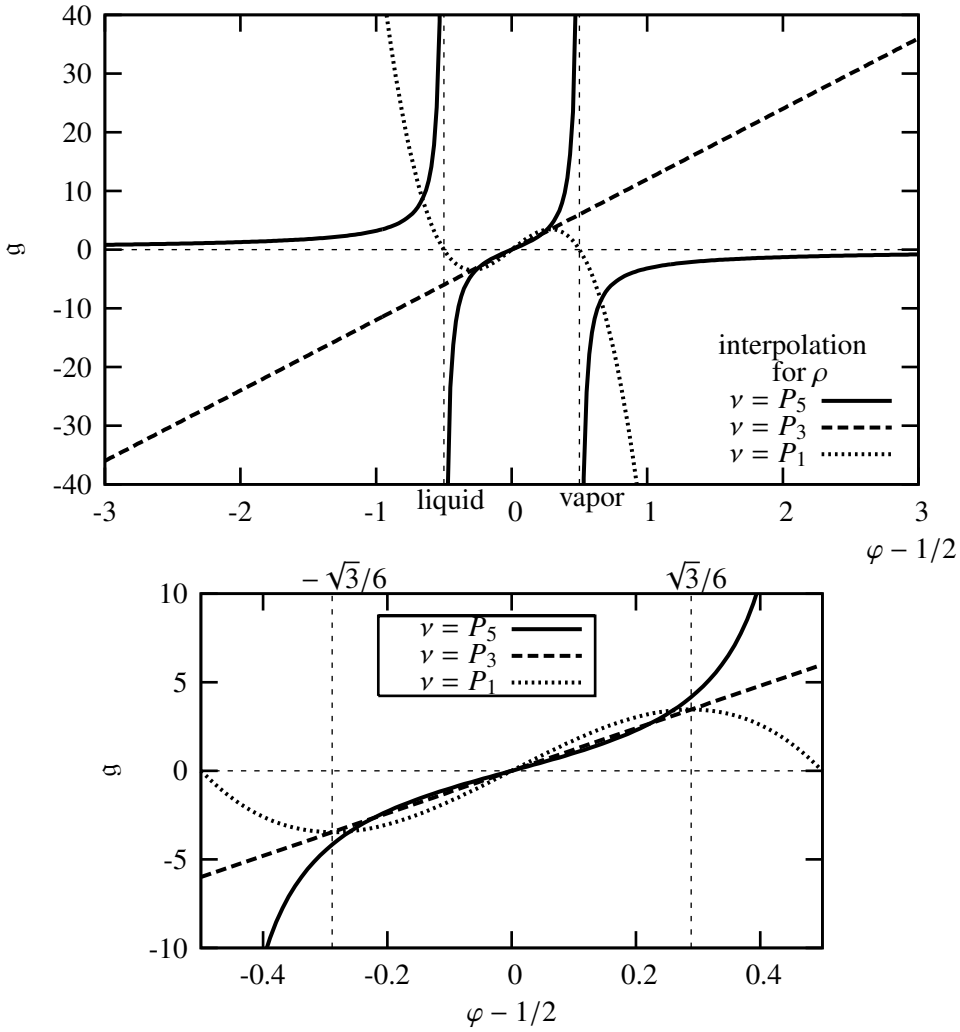

Figure 3.9: Solutions of equation (3.64), the lower picture proposes a zoom in the interval $\varphi \in [0 : 1]$

- ⋆ $\varphi \in [1/2 - \sqrt{3}/6; +\infty]$, *i.e.* "vapor" phase corresponds to $\mathfrak{g} \in [-\infty; 2\sqrt{3}]$
- ⋆ $\varphi \in [1/2 - \sqrt{3}/6; 1/2 + \sqrt{3}/6]$, *i.e.* "spinodal" phase corresponds to $\mathfrak{g} \in [-2\sqrt{3}; 2\sqrt{3}]$

The existence (the equilibrium condition is satisfied) of solutions for a given phase (say liquid or vapor) only for a given range of $\mathfrak{g}$ values is similar to the classical model of phase transitions (*cf.* the van der Waals' model for example, where for a given value of the pressure P, either one or two stable states can exist, see section 2.2.2). Let us remark that, the density of the equilibrium state deviates from the value desired and controlled (*i.e.* corresponding to $\varphi = 0$ or $\varphi = 1$) as soon as $\mathfrak{g} \neq 0$, *i.e.* as soon as equilibrium conditions deviates from planar case. Moreover since $\mathfrak{g}$ is an increasing function of the artificial thickness h, all other physical parameters being fixed, that deviation is emphasized when h is artificially increased. The metastability limit (range of values of g^* around zero for which a phase can exist at equilibrium) is also a decreasing function of the artificial thickness h. This dependence of the metastability limit is therefore equivalent to the one of the modified van der Waals' model presented in section 2.2.3 and is not desirable for the applications targeted. When ρ is linear with respect to φ, the model reproduces the van der Waals' model.

Third order polynomial Let us consider the case where ρ is interpolated by P_3. For the sake of clarity, we have omitted to represent the solutions 0 and 1 on the figure 3.9, but they are solutions for any value of the parameter $\mathfrak{g}$. Since $(\mathfrak{g}\, dP_3/d\varphi + dW/d\varphi)$ is a third degree polynomial, there exists a single other solution of (3.64) for any value of $\mathfrak{g}$, this solution satisfies

$$\varphi = 1/2 - \frac{\mathfrak{g}}{12}$$

and it varies linearly with respect to the parameter $\mathfrak{g}$. As a consequence, it diverges from the values 0 and 1 as soon as $|\mathfrak{g}|$ increases, or equivalently when physical parameters are fixed, when the artificial thickness h increased.

Fifth degree polynomial Let us consider the case where ρ is interpolated by P_5. It is worth noting that there are actually 4 solutions for φ for a given value of $\mathfrak{g}$. For the sake of legibility, we omitted to represent on figure 3.9 the set of solutions 0 and 1. The two other solutions satisfy

$$\mathfrak{g}\, 5\,\varphi\ (\varphi - 1) + 12\ (\varphi - 1/2) = 0$$

and are of two types whether φ is inside or outside the interval $[0:1]$. Solutions outside this interval diverge as $\mathfrak{g}$ tends to zero and approach the values 0 or 1 only as $|\mathfrak{g}|$ tends to infinity. The solutions inside the interval $[0:1]$ are close to the center ($\varphi = 1/2$) of the "spinodal" region for low values of $\mathfrak{g}$ and approach the values 0 or 1 only as $|\mathfrak{g}|$ tends to infinity. This corresponds to a property exactly opposite to what is obtained for the two other polynomials considered where the solution φ diverges from the solution 0 and 1 as $|\mathfrak{g}|$ tends to infinity. As a consequence, when the interface thickness h is increased, the phase field value φ corresponding to a given value of g^* tends to one of the two values 0 and 1.

Conclusion on the study of the single-phase states

We have shown the choice of the polynomial for the interpolation function $\nu(\varphi)$ to have consequences on the equilibrium value φ for a given value of the parameter g^*. If $\rho(\varphi)$ is chosen to be linear , the values 0 and 1 are solution of the equilibrium relation (6.2) only at conditions of planar two-phase equilibrium (*i.e.* $g^* = 0$). For other values of g^* the value of the phase field is different from 0 and 1 and as a consequence the physical properties of this equilibrium state also change from the targeted value, this variations being more important as the artificial thickness h increases.

When the interpolation function is chosen as being P_3 or P_5, the values 0 and 1 are equilibrium solutions for *any* value of g^* and moreover are stable for *any* g^* values if the interpolation function is chosen as the polynomial P_5 of degree 5. This choice will thus be retained in the following. The mapping of the other equilibrium solutions differs between the two polynomials: the solution diverges from the solutions 0 and 1 in the P_3 case but converges to these solutions in the P_5 case. We study the stability condition of these other possible equilibrium states in details in chapter 6 where we study the stability of the homogeneous states from the system of equations including the out-of-equilibrium processes.

3.4.2 Specific heat capacity at constant pressure c_P

Let us study the specific heat capacity at constant pressure of the single phase states of our model. The expression (3.55) for g is determined for a given fluid if one can easily determine the functions $P_{eq}(T)$ and $g_{eq}(T)$. Since $P_{eq}(T)$ can be found in classical tables, let us examine the case of $g_{eq}(T)$ and show it is related to the specific heat capacity at constant pressure c_P of the phases. c_P is defined by

$$c_P \triangleq T\,\frac{\partial s}{\partial T}_{|P,\varphi,(\nabla\varphi)^2} \tag{3.67}$$

From the definition (3.9c) of the specific entropy s, c_P reads

$$c_P = -T\,\frac{\partial^2 g}{\partial T^2} \tag{3.68}$$

Therefore using the expression (3.55) for the specific Gibbs free energy g in the non-isothermal quasi-compressible case, we get $c_P(\varphi, P, T, (\nabla\varphi)^2)$

$$c_P = -T\left(\frac{d^2 g_{eq}}{dT^2} + \frac{\partial^2}{\partial T^2}\left[v(\varphi,T)\left(P - P_{eq}(T) + \frac{\lambda}{h^2}W(\varphi) + \frac{\lambda}{2}(\nabla\varphi)^2\right)\right]\right) \tag{3.69}$$

So in a phase, say liquid *i.e.* when $\varphi = 0$, and $(\nabla\varphi)^2 = 0$, using the expression (3.56) for v and since $W(0) = 0$ (*cf.* equation (3.40)), we get

$$c_{P,liquid} = -T\left(\frac{d^2 g_{eq}}{dT^2} + \frac{d^2 v_{liquid}(T)\,\left(P - P_{eq}(T)\right)}{dT^2}\right) \tag{3.70}$$

Since $v_{liquid}(T)$ and $P_{eq}(T)$ are given, $g_{eq}(T)$ defines the value of the c_P of the fluid.

c_P difference between the phases Let us note that the c_P is interpolated by the same $\nu(\varphi)$ interpolation function. The difference of c_P between the single-phase states, namely δc_P reads

$$\delta c_P(P,T) = \frac{\partial^2}{\partial T^2}\left(\delta v(T)\left(P - P_{eq}(T)\right)\right) = \frac{d^2\delta v}{dT^2}\left(P - P_{eq}(T)\right) - 2\frac{d\delta v}{dT}\frac{dP_{eq}}{dT} - \delta v\frac{d^2P_{eq}}{dT} \tag{3.71}$$

where $\delta v(T) \hat{=} v_{vap}(T) - v_{liq}(T)$ At planar two-phase equilibrium, where both bulk pressures equal $P_{eq}(T)$, we get therefore

$$\delta c_P(P_{eq}(T),T) = -2\frac{d\delta v}{dT}\frac{dP_{eq}}{dT} - \delta v\frac{d^2P_{eq}}{dT} \tag{3.72}$$

Therefore δc_P is, like for more classical EOS, related to the temperature variation of both P_{eq} and $\delta v(T)$. As a consequence, the difference between specific heat capacities is clearly related to the coefficient of thermal expansion α_P of the liquid and vapor phases that determines $\delta v(T)$. For the sake of simplicity, we will consider in section 5.3.3 that the saturation pressure is linear with respect to temperature, as a consequence, a non-zero difference between the bulk heat capacities lies on a non zero α_P.

3.4.3 Latent heat and Clapeyron relation

In this section we study the specific density difference at planar two phase equilibrium and relate it to the saturation curve $P_{eq}(T)$.

At two phase planar equilibrium, the two bulk pressures are equal to $P_{eq}(T)$. The specific entropy s of the fluid in each bulk phase ($\varphi \in \{0;1\}$) reads therefore (*cf.* the definition (3.9c) of the specific entropy s and the expression (3.55) of the specific Gibbs free energy g with the fact that $W(0) = W(1) = 0$ according to equation (3.40) and that $\nu(0) = 0$ and $\nu(1) = 1$ according to equation (3.51))

$$\begin{aligned} s(\varphi = 0, P_{eq}(T), T, (\nabla\varphi)^2 = 0) &= v_{liq}(T)\frac{dPeq}{dT} - \frac{dgeq}{dT} \\ s(\varphi = 1, P_{eq}(T), T, (\nabla\varphi)^2 = 0) &= v_{vap}(T)\frac{dPeq}{dT} - \frac{dgeq}{dT} \end{aligned}$$

Let us introduce the latent heat $\mathcal{L}(T)$ of the liquid-vapor phase transition (*cf.* equation (3.6))

$$\mathcal{L}(T) \hat{=} T\left(s(\varphi = 1, P_{eq}(T), T, (\nabla\varphi)^2 = 0) - s(\varphi = 0, P_{eq}(T), T, (\nabla\varphi)^2 = 0)\right)$$

As a consequence, we have

$$\mathcal{L}(T) = T\left(\delta v\frac{dPeq}{dT}\right)$$

That can be rewritten on a more classical form

$$\frac{dP_{eq}(T)}{dT} = \frac{\mathcal{L}}{T\,\delta v} \tag{3.73}$$

This relation is the classical Clapeyron relation, *e.g.* [107] that is thus recovered by our model.

3.4.4 Structure of an equilibrium planar interface

Let us study the interface structure at planar equilibrium and show that the equilibrium relations reduce to the basic different differential equations (3.39) and (3.45) presented in 3.2.4.

Let us refer to the planar interface along an arbitrary x-axis as introduced in 3.2.4. The equilibrium conditions of interest in this study are the nullity of $\tilde{\mu}$ (*cf.* equation (3.28c)) and the uniformity of g (*cf.* equation (3.28b)). The temperature is uniform (*cf.* the equilibrium equation (3.28a)). Let us consider the expressions for g and $\tilde{\mu}$ one by one and show that if the differential equations (3.39) and (3.45) are satisfied the equilibrium conditions are actually recovered.

Uniformity of g Let us consider the expression (3.55) of the specific Gibbs free energy g. It is a straightforward calculation to show that if the phase field and pressure profiles satisfy the differential equations (3.39) and (3.45), we get

$$g\left(\varphi, P = P_{eq}(T) - 2\,\frac{\lambda}{h^2}W(\varphi), T, (\nabla\varphi)^2 = 2\,\frac{\lambda}{h^2}W(\varphi)\right) \quad = \quad g_{eq}(T)$$

which is actually uniform.

As a consequence the equilibrium relation (3.28b) is satisfied if the differential equations (3.39) and (3.45) are satsified which was required in order to control easily the thickness of the interface and the surface tension coefficient. It is worth noting that as a consequence of the uniformity of both g and T, g^* is uniform as well, and moreover null.

Nullity of the variational derivative $\tilde{\mu}$ Using the expression (3.58) for g^* a straightforward calculation leads to the following expression for the variational derivative $\tilde{\mu}$ (*cf.* equation (3.27))

$$\tilde{\mu} \quad = \quad \frac{1}{\rho}\left[-g^*\,\frac{d\rho}{d\varphi} + \frac{\lambda}{h^2}\left(\frac{dW}{d\varphi} - h^2\varphi_{,xx}\right)\right] \tag{3.74}$$

Since $g^* = 0$ at planar two phase equilibrium, the equilibrium equation $\tilde{\mu} = 0$ yields

$$\frac{dW}{d\varphi} - h^2\varphi_{,xx} = 0 \tag{3.75}$$

that is actually the differential equation (3.41) equivalent to the differential equation (3.39) targeted.

Concluding remark As a conclusion, the equilibrium conditions (3.28) admit the differential equations (3.39) and (3.45) as solutions. As a consequence, the different constraints our model must satisfy are recovered at planar two phase equilibrium along the whole saturation curve $P_{eq}(T)$ (*cf.* the list on page 53), *i.e.* :

- ⋆ the phase field profile is monotonic (point 1)
- ⋆ the density profile is monotonic (point 2) (since it is enslaved to the φ profile through the function $\nu(\varphi)$)
- ⋆ the thickness of the phase field profile is controlled (point 3)
- ⋆ the surface tension coefficient is controlled (point 4)

3.5 Conclusion about the derivation of the constitutive form of a phase field model for the liquid-vapor flows with phase change

In this chapter, we have derived the constitutive form of the phase field model. The following conclusion can be drawn.

It has been shown that it was possible to deal with a diffuse interface model of the liquid-vapor phase transition with an arbitrary density difference between incompressible single-phase states using the quasi-compressible hypothesis. This hypothesis has been related to the ability to consider another order parameter for the phase transition instead of the density (see section 3.1) which is actually the case with phase field model. The thermodynamic variables of our model are then $(\varphi, P, T, (\nabla\varphi)^2)$.

We have then studied the introduction of a phase field as a thermodynamic variable (see section 3.2). Its meaning has been specified as follows

1. the phase field is a purely abstract field whose introduction is devoted to the ability to decouple the description of the structure of the interface from the description of the single phase states

2. according to this role the most simple choice is therefore to associate discrete values of the phase field to the single phase states and we set

   (a) $\varphi = 0 \quad \leftrightarrow$ liquid phase

   (b) $\varphi = 1 \quad \leftrightarrow$ vapor phase

In order to analytically express the required properties of our phase field model (*cf.* the list on page 53), we have then derived the equilibrium equations of the phase field thermodynamic description of the liquid-vapor fluid. In addition to the classical equilibrium relations, an additional equilibrium relation, specific of the phase field formulation, is the nullity of the variational derivative $\tilde{\mu}$ of g with respect to φ.

In order the single phase states, as stable equilibrium states, to actually correspond to the values 0 and 1 of the phase field, it has been shown that the specific Gibbs free energy must be minimal for these values for any (P, T) value. In order to allow an easy control of the structure of the interface, simple relations for the interface thickness and for the surface tension coefficients have been introduced. These relations are inspired by the classical equilibrium relations in diffuse interface model. The equilibrium relations of the model reduce to these relations at planar two-phase equilibrium.

The corresponding constitutive form of the phase field model is based on the classical features of the phase field models *i.e.*

1. an interpolation function $\nu(\varphi)$

2. a double well function $W(\varphi)$

3. a nonlocal contribution in $(\nabla\varphi)^2$

It is worth pointing out that the two functions W and ν are required to be non-linear in order the properties targeted of the phase field model to be satisfied. The phase field specific Gibbs free energy reads

$$g(\varphi, P, T, (\nabla\varphi)^2) \quad = \quad v(\varphi)\left(P - P_{eq}(T) + \frac{\lambda}{2}(\nabla\varphi)^2 + \frac{\lambda}{h^2}W(\varphi)\right) + g_{eq}(T)$$

where $v(\varphi)$ is the specific volume of the fluid as an interpolation by the function $\nu(\varphi)$ of the corresponding bulk phase values. The parameters h and λ determine the thickness of the interface as well as the surface tension coefficient at planar equilibrium.

By comparison with the quasi-compressible model of Anderson et al. [5], our model considers a most simple analytical dependence with respect to the phase field which allows to more easily control the structure of the interface along the saturation curve. It has been shown that our model reduces to the widely used phase field model for the study of the solid-liquid phase transition when the density difference between the bulk phases is set to zero.

The model has actually all the following required properties:

1. the liquid and vapor phase states are actually represented by the phase field values 0 and 1and their EOS can be chosen independently from the structure of the interface. This property has been related to an accurate choice for the interpolation function $\nu(\varphi)$ which has been proposed to be the polynomial of degree 5 $P_5(\varphi)$ (*cf.* equation (3.60c))

2. at planar two phase equilibrium

   (a) the profiles of the density and of the phase field are monotonic and of controlled thickness

   (b) the surface tension coefficient is easily parameterized

   (c) it is worth pointing out that at planar two phase equilibrium, the interpolation function ν does not interfere with the description of the interface structure

3. the classical Clapeyron relation is valid for our phase field model

We now need to study the model in other configurations than the simple and academic cases of equilibrium single phase states and planar two-phase equilibrium. We first study in the next chapter the spherical symmetric case.

Chapter 4

Study of the spherical symmetry problem

Introduction

The goal of this study is to investigate the ability of the model to deal with multi-dimensional liquid-vapor flows with phase-change. For this purpose, we consider a spherical symmetric two-phase system and study the equilibrium of a spherical inclusion. Since our model aims at being a consistent regularization of the sharp interface model with incompressible phases, two main points need more particularly to be studied:

- ⋆ Does the model allow to recover a description of the spherical inclusions consistent with the sharp description ?
- ⋆ Does the model, like any other diffuse interface formulation, provide the ability to describe very small spherical inclusions (nucleation process) ?

These two questions will drive the following study of the spherical inclusions. This chapter is organized as follows. We first briefly review the previous studies of the spherical equilibrium using diffuse interface models (see section 4.1). In section 4.2, we derive the equilibrium conditions characteristic of a spherical inclusion. We formally define the equivalent sharp interface model and define the criteria of evaluation of our model. We define specifically the equivalent sharp radius of the inclusion, the surface tension coefficient, and the pressure jump. To quantitatively determined these features it is required to solve a unique ordinary differential equation (ODE) for the phase field profile $\varphi(r)$, say the equilibrium equation of a spherical inclusion. In section 4.3, we first analyze the ODE using a classical analogy with a standard problem of particle mechanics. Then we solve the equilibrium profile in an infinite domain using approximations for the interpolation function $\nu(\varphi)$ and for the double well function $W(\varphi)$. Then we solve numerically the equilibrium equation for a domain of finite extent using finite difference method. We get phase field profiles at equilibrium and consequently evaluate the equivalent sharp interface properties (surface tension coefficient, pressure jump and radius of the inclusion). These results are compared to those obtained with other more classical diffuse interface models and the sharp interface model. They show that the model allows to compute consistently spherical inclusions and moreover constitutes a first step toward numerical simulations of out of equilibrium dynamics of spherical symmetric systems.

4.1 Review of the study of spherical equilibrium with diffuse interface models

The equilibrium of spherical inclusions using diffuse interface models has been studied by several authors. The study of spherical liquid-vapor inclusions at equilibrium using the van der Waals diffuse interface model has been already extensively studied, *e.g.* Truskinovsky [135] for theoretical developments and Dell'Isola et al. [43] for numerical applications. In these studies, the surface tension coefficient and a sharp equivalent radius of the diffuse interface profiles are studied as a function of the value of the chemical potential: it allows to characterize the relation between the sharp Laplace formula and the van der Waals model of capillarity. Identical study with our phase field model should therefore provide an interesting way to study the relation of our model both with the sharp model and with the classical diffuse interface model. Lowengrub and Truskinovsky [89] studied the equilibrium of a spherical inclusion using a quasi-incompressible model dedicated to binary fluids with density difference. This quasi-incompressible model is much closer to our own model since, contrarily to the

van der Waals model, the bulk phases are supposed to be incompressible. In [89], the equilibrium solutions are studied analytically using piece-wise quadratic approximations for the Helmholtz free energy in the case where the density difference is zero and numerically in presence of density difference. A physical behavior of small spherical inclusions similar to the one obtained with the van der Waals model is recovered: the effective surface tension varies with curvature which impedes the pressure at the center of a spherical inclusion to diverge for vanishing spherical inclusion (as predicted by the Laplace formula). As a consequence, and contrarily to the sharp interface models, diffuse interface models can deal with vanishing interfaces. Mainly because of the additional non-linearity of the specific Gibbs free energy with regard to the phase field φ (associated to the interpolation function $\nu(\varphi)$), the property of the spherical inclusion with our phase-field model is somewhat different to the one obtained with the hereinabove mentioned models. For example, the value of the order parameter in the bulk phase outside, resp. inside, the inclusion are shown to be independent, resp. weakly dependent[1], of the equivalent sharp radius of the inclusion. This property is considered as an important feature of the present model. Indeed it actually corresponds to the property of the classical sharp interface model with incompressible bulk phases. Let us recall that our model claims to be a thermodynamically consistent regularization of this sharp model. To our knowledge, studies of spherical symmetry case with phase field models of two-phase fluids with density difference only studied the recovery of the Laplace formula for large inclusions (or the Gibbs-Thomson formula in the solid-liquid case), *e.g.* [6, 24, 94]. The present study allows to investigate more deeply the consequences of the phase field formulation on the description of spherical inclusions.

4.2 General study of a spherical inclusion at equilibrium

In this section, we study the general features of a spherical inclusion at equilibrium described by the phase-field model derived in chapter 3.

4.2.1 Equilibrium relations

General form of the equilibrium relations Let us refer to the system of equilibrium relations (3.28) derived from our study of the thermodynamic model in section 3.2.2. The equilibrium condition (3.28a) is trivial and leads to a uniform value for the temperature field, say $T = T_{eq}$. In the following of this study, we suppose that the temperature is uniform and neglect all temperature dependences in the expressions used. The equilibrium temperature T_{eq} is a parameter of the solution. The remaining (isothermal) equilibrium conditions read

$$\tilde{\mu} = 0 \tag{4.1a}$$

$$\rho \nabla g = 0 \tag{4.1b}$$

$$\Leftrightarrow$$

$$\nabla \cdot (P \mathcal{I} + \rho \Phi \nabla\varphi \otimes \nabla\varphi) = 0 \tag{4.1c}$$

where the equivalence between the two expressions for the conservative stress tensor has been shown in section 5.1.2. According to the relation (4.1b), the specific Gibbs free energy is uniform. Its value at equilibrium, say g, is therefore introduced as a second parameter. We show in the following that once one of the two parameters, either g or T_{eq}, is known, it is more convenient to use the uniform quantity $g^* \triangleq g - g_{eq}(T_{eq})$ to parameterize the equilibrium (we recall that $g_{eq}(T)$ is the equilibrium value of the specific Gibbs free energy at planar equilibrium).

Main parameter of the problem Let r be the radial coordinate and denote $\cdot_{,r} \triangleq \partial \cdot / \partial r$. Using the compact notation *, we recall that our quasi compressible model reads (*cf.* equation (3.58))

$$g^* = \frac{P^* + (\lambda/h^2) W(\varphi) + (\lambda/2)\ (\varphi_{,r})^2}{\rho(\varphi)} \tag{4.2}$$

and that as a consequence, the variational derivative $\tilde{\mu}$ reads using non-dimensional radial coordinates $\bar{r} \triangleq r/h$ (*cf.* equation (3.74))

$$\tilde{\mu} = \frac{1}{\rho}\left[-g^* \frac{d\rho}{d\varphi} + \frac{\lambda}{h^2}\left(\frac{dW}{d\varphi} - h^2 \varphi_{,xx}\right)\right]$$

[1] at least as long as the ratio of the radius of the inclusion with the artificial thickness h is larger than 1, see section 4.3.3.

In this chapter, we consider that the density is interpolated by the degree 5 polynomial P_5, therefore it is straithforward to show that the equilibrium equation $\tilde{\mu} = 0$ is equivalent to

$$\mathfrak{g}\,\frac{dP_5}{d\varphi} + \frac{dW}{d\varphi} - \varphi_{,\bar{r}\bar{r}} - 2\,\frac{\varphi_{,\bar{r}}}{\bar{r}} = 0 \tag{4.3}$$

where $[\mathfrak{g}\,(dP_5/\varphi) + (dW/d\varphi)]$ is a polynomial of degree 4. This equation is parameterized by the single non-dimensional parameter $\mathfrak{g}$ (introduced in the derivation of the model, *cf.* equation (3.63)).

The boundary conditions to use to solve this differential equation are the following

$$\forall n \in \mathbb{N}^*,\ \varphi_{,r^n}(r = \infty) = 0 \tag{4.4a}$$

$$\varphi_{,r}\ (r = 0) = 0 \tag{4.4b}$$

The equation (4.3) allows to determine the phase field profile $\varphi(r)$. It is worth noting that the single parameter for this profile is $\mathfrak{g}$. Moreover, when $\mathfrak{g} \to 0$, this differential equation tends to the equilibrium equation for the planar two-phase equilibrium (3.41). The writing of this differential equation is quite simple and it must be compared to the classical equilibrium equation for spherical inclusions with the van der Waals model, *e.g.* [135], [43]

$$g(\rho) - g(\rho_L) - \lambda\left(\rho_{,r^2} + \frac{2}{r}\rho_{,r}\right) = 0$$

which has already been investigated by several authors (Rocard [113], Cahn and Hilliard [26], ...).

As a partial conclusion the equilibrium of a spherical inclusion is governed by a single ordinary differential equation (ODE) in the phase field φ of order two with non-constant coefficients. This differential equation is parameterized by only one non-dimensional number $\mathfrak{g}$. This equation contains fourth degree polynomials in φ and cannot be solved analytically. Let us now study phase field and pressure values inside and outside the spherical inclusion.

4.2.2 Phase field and pressure values inside and ouside the spherical inclusion

In this part we study the phase field and pressure values inside and outside the spherical inclusion by letting r tends to zero and infinity in the equilibrium equation (4.3). We compare these results with the relations of the sharp interface model and study their dependence with respect to the parameter $\mathfrak{g}$.

State at infinity Let us first study the state of the fluid in the outer phase, say in $r = \infty$. Let us denote $\varphi_\infty \triangleq \varphi(r = \infty)$. Using the differential equation (4.3) for $\varphi(r)$ and the boundary condition (4.4a), the phase field value at infinity satisfies

$$\mathfrak{g}\,\frac{dP_5}{d\varphi}(\varphi_\infty) + \frac{dW}{d\varphi}(\varphi_\infty) = 0 \tag{4.5}$$

This equation is actually equivalent to the equation (3.64) that governs the equilibrium of a homogeneous state. Its general solutions have been studied in section 3.4.1 and their stability in section 6.5. Using the results of these sections, the state at infinity corresponds to one of the two possible stable single phase states, namely $\varphi_\infty = 0$ or 1. We remind that this result is valid for *any* value of the parameter $\mathfrak{g}$. It will be shown in the following that the value of φ_∞ (0 or 1) is in fact fully determined by the sign of the parameter $\mathfrak{g}$ in the case of non uniform solutions.

It is worth pointing out that the fact that the outer state always corresponds to one of the bulk phases is very attractive. It allows the diffuse interface formulation not to induce a variation of the bulk phase properties outside a spherical inclusion. This result is non-classical in diffuse interface models where the state at infinity is a function of the equilibrium state, *e.g.* [43] for the van der Waals model or [89] for the Cahn-Hilliard model. This result is however fully consistent with the sharp model with incompressible bulk phases, for which the same result holds.

State at the center of the inclusion The spherical symmetry of the system yields that at the center of the inclusion $\varphi_{,r}(r = 0) = P_{,r}(r = 0) = 0$. It is obvious $\varphi = \varphi_\infty$ and $P^* = P^*_\infty \triangleq P^*(r = \infty)$ is a trivial solution

of the problem (*cf.* the equilibrium relations (4.3) and (4.1c)). We now search for non trivial solutions that we characterize by

$$\begin{aligned} \varphi(r=0) &\triangleq \varphi_0 \\ P^*(r=0) &\triangleq P_0^* \end{aligned}$$

Let us consider the phase field value at the center of the inclusion φ_0. According to the boundary condition (4.4b), it satisfies the following equilibrium relation (*cf.* equation (4.3))

$$\mathfrak{g}\,\frac{dP_5}{d\varphi}(\varphi_0) + \frac{dW}{d\varphi}(\varphi_0) = \varphi_{,\bar{r}^2}(r=0)$$

The LHS of the above equation is non-zero $\varphi_{,\bar{r}^2}(r=0) \neq 0$ and since the bulk values are solution of this equation for a zero LHS, this equilibrium relation yields that the phase field value at the center of the inclusion is different from the bulk phases value, $\varphi_0 \neq 0$ or 1. However, as soon as the radius of the spherical inclusion (*i.e.* the typical radius where the transition layer is located) is sufficiently large (which remains to be specified, which is done in section 4.3), the value of $\varphi_{,\bar{r}^2}(r=0)$ tends to zero, and therefore φ_0 tends to the bulk values at planar equilibrium.

In the sharp interface model with incompressible bulk phases, the value of the density inside a spherical inclusion is considered to be equal to that of the bulk phases. This approximation is physically relevant as long as the inclusion is sufficiently large[2]. In our model, this should correspond to $\varphi_0 = 0$ or 1. We therefore need to investigate the dependence of the value φ_0 with respect to the spherical inclusion considered, *i.e.* with respect to $\mathfrak{g}$ and more especially for large values of this parameter (*i.e.* small inclusions).

Pressure jump and pressure profile Let us study the pressure profile at equilibrium. The integration between r and ∞ of the equilibrium condition (4.1c) yields

$$P(r) = P_\infty - \lambda\left((\varphi_{,r})^2 + 2\int_\infty^r \frac{(\varphi_{,r})^2}{\eta}d\eta\right) \tag{4.6}$$

where we have used the boundary condition (4.4a) and the identity $(\varphi_{,r}^2)_{,r} = 2\,\varphi_{,r^2}\varphi_{,r}$. Evaluating the above relation at $r = 0$ and using the boundary condition (4.4b) implies that

$$P_0 = P_\infty + 2\,\lambda\int_0^\infty \frac{(\varphi_{,r})^2}{r}dr$$

Therefore, using the jump notation ($[\![\cdot]\!] = \cdot(r=0) - \cdot(r=\infty)$), the above equation reads

$$[\![P^*]\!] = [\![P]\!] = 2\,\lambda\int_0^\infty \frac{(\varphi_{,r})^2}{r}dr \tag{4.7}$$

It is worth noting that $[\![P]\!]$ is strictly positive. Moreover it can be shown that its value is always finite, even for vanishing spherical inclusions (*cf.* the footnote 4 on page 96). Moreover equations (4.6) and (4.7) show that the knowledge of the phase field profile $\varphi(r)$ is sufficient to determine the pressure profile $P(r)$ and the pressure jump $[\![P]\!]$.

Relation between φ_∞ and g^* Using the expression (4.2) for g^* in $r = 0$ and $r = \infty$ yields

$$v_0\,\left(P_0^* + \lambda\frac{W_0}{h^2}\right) = v_\infty\,P_\infty^* = g^* \tag{4.8}$$

where we have used that $\varphi_\infty = 1/2 \pm 1/2$ and the boundary conditions (4.4) and where $W_0 \triangleq W(\varphi_0)$. Using the pressure jump $[\![P]\!]$, we deduce from the above relation, the following relation for g^*

$$g^* = \frac{v_0 v_\infty}{v_\infty - v_0}\left([\![P]\!] + \frac{\lambda}{h^2}\,W_0\right) = \frac{[\![P]\!] + \frac{\lambda}{h^2}\,W_0}{[\![\rho]\!]} \tag{4.9}$$

[2]The inside pressure of the center of the inclusion must be sufficiently close to the saturation pressure, otherwise the influence of the compressibility (namely the validity of the relation $\rho(P) \simeq \rho(P_{eq})$) on the inside state can no longer be neglected. In this study, we do not target any quantitative study of the nucleation process, and we therefore consider that this approximation is valid

Let us note that since both $[\![P]\!]$ and W_0 are strictly positive (*cf.* the equation (4.7) for the pressure jump and the property (3.40) satisfied by the double well function W), the sign of g^* is thus fully determined by the sign of $[\![\rho]\!]$. Since $\rho(\varphi)$ (interpolated by the polynomial $-P_5$) is a monotonic decreasing function, the sign of $[\![\rho]\!]$ is determined by the sign of $[\![\varphi]\!]$ and therefore by the value of φ_∞. Therefore, as soon as the equilibrium solution is not the trivial solution $\varphi(r) = \varphi_\infty$ (in which case $[\![\rho]\!] = 0$ and it is obvious from equation (4.9) that the determination of the value g^* degenerates), the value of φ_∞ is determined by the single sign of the parameter g^* or equivalently by the sign of $\mathfrak{g}$.

As a partial conclusion, the sign of the parameter $\mathfrak{g}$ determines the value of the phase field at infinity φ_∞ as being one of the two possible bulk phase values 0 or 1:

$$\begin{aligned} g^* > 0 \quad &\Leftrightarrow \quad \varphi_\infty = 1 \\ g^* < 0 \quad &\Leftrightarrow \quad \varphi_\infty = 0 \end{aligned}$$

Pressures at the center of the inclusion and at infinity *versus* the pressure jump From equation (4.8) and (4.9) it is straightforward to show that

$$\left\{ \begin{array}{lcl} P_0^* & = & \dfrac{v_\infty}{v_\infty - v_0} \left([\![P]\!] + \dfrac{v_0}{v_\infty} \dfrac{\lambda}{h^2} W_0 \right) \qquad (4.10a) \\ P_\infty^* & = & \dfrac{v_0}{v_\infty - v_0} \left([\![P]\!] + \dfrac{\lambda}{h^2} W_0 \right) \qquad (4.10b) \end{array} \right.$$

From the above expressions of P_0^* and P_∞^* we then distinguish two cases

- ⋆ Bubble at equilibrium:
  In this case $v_\infty = v_{liq}$, (*i.e.* $\varphi_\infty = 0$), $v_0 \simeq v_{vap} > v_\infty$: we have $P_{0,\infty}^* < 0$ and $g^* < 0$
- ⋆ Drop at equilibrium:
  In this case $v_\infty = v_{vap}$, ($\varphi_\infty = 1$), $v_0 \simeq v_{liq} > v_\infty$: we have $P_{0,\infty}^* > 0$ and $g^* > 0$

As a consequence, in the bubble, resp. drop case, the absolute values of the pressure in the phases and of the specific Gibbs free energy are smaller, reps. larger than the value corresponding to a planar equilibrium. For the classical sharp interface model with incompressible bulk phases, the corresponding formula giving the expressions for the pressure inside and outside a spherical inclusion have been derived from the Rankine-Hugoniot jump conditions in the appendix (see section A.2, equation (A.25)). It is worth noting that with our phase field model, these values (*cf.* equations (4.10)) are fully consistent with the sharp relations as soon as φ_0 is sufficiently close to the bulk values (*i.e.* the quantity $(\lambda/h^2)\, W_0$ is small compared to $(\rho_l/\rho_v)\, [\![P]\!]$). As a consequence the study of the value of φ_0 as a function of the parameter $\mathfrak{g}$ is of primary interest and more especially for large values of $|\mathfrak{g}|$ (since when $\mathfrak{g} \simeq 0$, we have shown that φ_0 actually tends to the bulk phase values).

4.2.3 Surface tension and Laplace formula

In the sharp interface formulation, in addition to the hereinabove studied relation between the values of the pressures and the pressure jump, the equilibrium of a spherical inclusion is characterized by two other features, namely the radius of the inclusion and the value of the pressure jump. The pressure jump is given by the Laplace relation

$$[\![P]\!] = \frac{2\,\sigma}{R_{sharp}} \qquad (4.11)$$

where σ is the surface tension coefficient[3] and R_{sharp} is the radius of the inclusion. The expression for the jump in pressure in our model has already been formally derived (*cf.* equation (4.7)). The goal of this section is to define the relation between this pressure jump, the surface tension coefficient and the radius of the interface with our model in order to compare it with the Laplace relation. Let us now define the radius and the effective surface tension of our phase field model for a spherical inclusion at equilibrium.

[3] It is worth noting that this value of σ corresponds to the value of the excess Helmholtz free energy at planar two-phase equilibrium recovered by our model

Radius of the inclusion Let us define arbitrarily the equivalent sharp interface position R_ρ such that the excess mass is zero, *i.e.*

$$\rho^{ex}_{R_\rho} \hat{=} \frac{1}{R_\rho^2}\left[\int_0^{R_\rho} (\rho-\rho_0)\, r^2\, dr + \int_{R_\rho}^{\infty} (\rho-\rho_\infty)\, r^2\, dr\right] = 0 \tag{4.12}$$

where $\rho_0 = \rho(\varphi_0)$ and $\rho_\infty = \rho(\varphi_\infty)$. It is worth pointing out that, since the profile $\varphi(r)$ (and thus the profile $\rho(r)$) is parameterized by $\mathfrak{g}$, R_ρ is formally a function of the parameter $\mathfrak{g}$.

This definition is classical in diffuse interface models (*e.g.* [89]) and is moreover consistent with the sharp interface models in which the interface is considered as a non-material surface. The definition (4.12) of the sharp interface radius R_ρ does not allow to simply derive its value from a given phase field profile $\varphi(r)$ since it is obviously an implicit equation in R_ρ. Using a straightforward calculation, we get (*cf.* [89])

$$R_\rho = \left\{3\int_0^{\infty}\left[\frac{\rho(\varphi)-\rho_\infty}{\rho_0-\rho_\infty}\right] r^2\, dr\right\}^{1/3} \tag{4.13}$$

which will be used in section 4.3 to derive the value of R_ρ from the solved phase field profiles.

This is not the only interesting definition for the equivalent sharp radius to our point of view. Indeed, in the sharp interface models, the state inside the inclusion is supposed to have a density, say $\rho_{sharp}(r=0)$ independent of the radius. This is not the case with our model since it has been shown in section 4.2.1 that the value of the phase field at the center of the inclusion, and as a consequence ρ_0 depends on the parameter $\mathfrak{g}$. Therefore $\rho_{sharp}(r=0) = \rho(1-\varphi_\infty) \neq \rho_0$. As a consequence, the mass of the diffuse interface solution is not equal to the mass of the sharp system with a spherical inclusion of radius R_ρ described with the classical sharp interface incompressible model. We therefore introduce a second relevant equivalent sharp interface radius denoted Rs_ρ, defined such that the mass inherited from our quasi-compressible diffuse model and that inherited from the sharp interface incompressible model are equal, *i.e.*

$$\frac{1}{Rs_\rho^2}\left[\int_0^{Rs_\rho} (\rho-\rho(1-\varphi_\infty))\, r^2\, dr + \int_{Rs_\rho}^{\infty} (\rho-\rho_\infty)\, r^2\, dr\right] = 0 \tag{4.14}$$

As a consequence Rs_ρ is more a Laplacean measure of the radius of a spherical inclusion of given mass. It is straightforward that the two sharp radius Rs_ρ and R_ρ are related by

$$R_\rho^3\,(\rho_0-\rho_\infty) = Rs_\rho^3\,(\rho(1-\varphi_\infty)-\rho_\infty)$$

and that

$$\varphi_0 \to 1-\varphi_\infty \;\Rightarrow\; R_\rho \to Rs_\rho$$

Let us now study the surface tension coefficient corresponding to the diffuse profile at equilibrium.

Surface tension coefficient Let us consider the definition of the surface tension coefficient for a spherical inclusion at equilibrium. Using the definition of the interface location (4.12), the definition of the surface tension coefficient $\sigma_{F^{ex}}$ as an excess free energy is well defined and we get

$$\sigma_{F^{ex}} \hat{=} F^{ex}_{R_\rho} = -P^{ex}_{R_\rho} = \frac{1}{R_\rho^2}\left[\int_0^{R_\rho} (P_0-P)\, r^2\, dr + \int_{R_\rho}^{\infty} (P_\infty-P)\, r^2\, dr\right] \tag{4.15}$$

where we have used that g is uniform and that $\rho^{ex}_{R_\rho} = 0$. Using the expressions (4.6) for the pressure profile and (4.7) for the pressure jump, we get[4]

$$\begin{aligned}
\sigma_{F^{ex}} &= \frac{1}{R_\rho^2}\left[\int_0^{R_\rho} r^2 [\![P]\!]\, dr + \lambda\int_0^{\infty}\left((\varphi_{,r})^2 + 2\int_{\infty}^{r}\frac{(\varphi_{,\eta})^2}{\eta}d\eta\right) r^2\, dr\right] \\
&= \frac{R_\rho}{3}[\![P]\!] + \frac{\lambda}{R_\rho^2}\int_0^{\infty}\left((\varphi_{,r})^2 + 2\int_{\infty}^{r}\frac{(\varphi_{,\eta})^2}{\eta}d\eta\right) r^2\, dr \\
&= \frac{R_\rho}{3}[\![P]\!] + \frac{\lambda}{3\,R_\rho^2}\int_0^{\infty} r^2(\varphi_{,r})^2\, dr \\
&= \frac{\lambda}{3}\int_0^{\infty}(\varphi_{,r})^2\left(\frac{2\,R_\rho}{r} + \frac{r^2}{R_\rho^2}\right) dr > 0
\end{aligned} \tag{4.16}$$

[4]

This last expression shows that the surface tension coefficient $\sigma_{F^{ex}}$ is always positive. An expression similar to expression (4.16) has been derived in the quasi-incompressible model for Cahn-Hilliard fluids in [89]. However an interesting difference is that the expression (4.16) for $\sigma_{F^{ex}}$ does not depend on the density function $\rho(\varphi)$ and therefore on the density contrast. It is therefore a simplification.

Keeping in mind the comparison with the incompressible sharp interface model, we introduce a second definition of the surface tension denoted $\sigma_{[\![P]\!]}$ by analogy with the Laplace relation (4.11), *i.e.*

$$\sigma_{[\![P]\!]} \hat{=} [\![P]\!] \frac{R_\rho}{2} = \lambda \int_0^\infty (\varphi_{,r})^2 \frac{R_\rho}{r}\, dr \tag{4.17}$$

where we have used the expression (4.7) for the pressure jump.

Agreement of the different definitions with each other and with the Laplace formula In this paragraph, we study in which coniditions the different definitons for the sharp interface radii R_ρ and Rs_ρ and the surface tension coefficients $\sigma_{F^{ex}}$ and $\sigma_{[\![P]\!]}$ agree with each other and moreover with the Laplace formula.

It has already been said that as soon as $\mathfrak{g} \to 0$, $R_\rho \to Rs_\rho$. Let us now consider the conditions under which the different expressions for the surface tension coefficient $\sigma_{[\![P]\!]}$ and $\sigma_{F^{ex}}$ agree. Let us consider the case where the radius R_ρ is large with respect to the characteristic thickness of the transition layer. We show in the following that this case corresponds to $\mathfrak{g} \to 0$ and that in this case the characteristic thickness is of the order of h and that $R_\rho \gg h$. In this case the following approximation holds

$$\int_0^\infty r^2 (\varphi_{,r})^2\, dr \simeq R_\rho^3 \int_0^\infty \frac{(\varphi_{,r})^2}{r}\, dr \simeq R_\rho^2 \int_0^\infty (\varphi_{,r})^2\, dr$$

Therefore, according to the expression (4.7) for the pressure jump $[\![P]\!]$, we have

$$[\![P]\!] \simeq \frac{2\,\lambda}{R_\rho} \int_0^\infty (\varphi_{,r})^2\, dr$$

which yields (*cf.* the definition (4.17) of $\sigma_{[\![P]\!]}$)

$$\sigma_{[\![P]\!]} \simeq \lambda \int_0^\infty (\varphi_{,r})^2\, dr$$

and according to the expression (4.16) for $\sigma_{F^{ex}}$

$$\sigma_{F^{ex}} \simeq \lambda \int_0^\infty (\varphi_{,r})^2\, dr$$

The equivalence between the second and third line in the deriva-tion for the expression (4.16) for the surface tension coefficient $\sigma_{F^{ex}}$ is based on the following identity

$$\begin{aligned}\int_0^\infty r^2 \int_\infty^r \frac{(\varphi_{,\eta})^2}{\eta} d\eta\, dr &= \int_0^\infty \left(\frac{r^3}{3}\right)_{,r} \int_\infty^r \frac{(\varphi_{,\eta})^2}{\eta} d\eta\, dr \\ &= \left[\frac{r^3}{3} \int_\infty^r \frac{(\varphi_{,\eta})^2}{\eta} d\eta\right]_0^\infty - \int_0^\infty \frac{r^2}{3} (\varphi_{,r})^2\, dr\end{aligned}$$

and on the fact that $\mathbb{A} \hat{=} \left[\frac{r^3}{3} \int_\infty^r \frac{(\varphi_{,\eta})^2}{\eta} d\eta\right]_0^\infty = 0$. Let us show the relation $\mathbb{A} = 0$. In order to show this relation, we need to find an equivalent for $\varphi(r)$ around 0 and ∞. In $r = 0$ and $r = \infty$, we use a quadratic approximation for W and ρ (*cf.* section 4.3.2), therefore

$$\varphi(r) - \varphi_0 \underset{0}{\sim} \frac{\sinh(r)}{r} \quad \text{and} \quad \varphi(r) - \varphi_\infty \underset{\infty}{\sim} \frac{e^{-r}}{r}$$

As a consequence

$$\frac{(\varphi_{,r})^2}{r} \underset{0}{\sim} \frac{\left(\frac{\cosh(r)}{r} - \frac{\sinh(r)}{r^2}\right)^2}{r} \quad \text{and} \quad \frac{(\varphi_{,r})^2}{r} \underset{\infty}{\sim} \frac{e^{-2r}}{r^5}$$

that are both integrable functions. As a first consequence

$$0 < \int_0^\infty \frac{(\varphi_{,r})^2}{r} dr \left(= \frac{[\![P]\!]}{2\,\lambda}\right) < \infty$$

which justifies the existence of a finite pressure jump (*cf.* equation (4.7)). It justifies also that

$$\lim_{r\to 0}\left[\frac{r^3}{3} \int_\infty^0 \frac{(\varphi_{,\eta})^2}{\eta} d\eta\right] = 0$$

Using the hereinabove relation we have

$$\int_\infty^r \frac{(\varphi_{,\eta})^2}{\eta} d\eta \underset{\infty}{\sim} \frac{-e^{-2r}}{2\,r^5}$$

and as a consequence

$$\lim_{r\to\infty}\left[\frac{r^3}{3} \int_\infty^0 \frac{(\varphi_{,\eta})^2}{\eta} d\eta\right] = 0$$

and finally $\mathbb{A} = 0$.

Let us now consider the phase field profile $\varphi(r)$ (since it appears explicitly in the above relations). According to the hypothesis $R_\rho \gg h$ and the hypothesis $\mathfrak{g} \simeq 0$, we have

$$\begin{aligned} \mathfrak{g}\,\frac{dP_5}{d\varphi} &\ll \frac{dW}{d\varphi} \\ \frac{\varphi_{,\bar{r}}}{\bar{r}} &\ll \varphi_{\bar{r}^2} \end{aligned}$$

the equilibrium equation (4.1) is therefore similar to the equilibrium equation for the planar interface profile (3.41). The profile $\varphi(r)$ can thus be accurately approximated by a hyperbolic tangent (*cf.* section 3.2.4) and the surface tension coefficients can be both approximated by σ (*cf.* equation (3.46)). As a partial conclusion, using the fact that *a priori* $\mathfrak{g} \to 0 \Rightarrow \varphi_0 \to 1/2 \pm 1/2$, we have

$$\mathfrak{g} \to 0 \Rightarrow \left\{ \begin{array}{c} R_\rho \simeq R s_\rho \\ [\![P]\!] \simeq \dfrac{2\,\sigma}{R_\rho} \\ \sigma_{F^{ex}} \simeq \sigma_{[\![P]\!]} \simeq \sigma \end{array} \right. \tag{4.18}$$

Therefore, as long as the non-dimensional parameter $\mathfrak{g}$ is sufficiently small, the different equivalent sharp interface models are equivalent and moreover agree with the classical sharp interface model. The limit of validity (in terms of $\mathfrak{g}$ values) of this agreement will be studied using the equilibrium phase field profiles computed in section 4.3.

Relation between $\mathfrak{g}$ and the sharp interface radius Let us consider the relation (4.9) between $[\![P]\!]$, $[\![\rho]\!]$ and g^* in the case where the Laplace formula (4.11) is a good approximation of the relation between the equivalent sharp radius and the pressure jump (that we have associated to small values of $\mathfrak{g}$ in the above presentation). In this case, it is justified to consider $W_0 \simeq 0$ and $[\![\rho]\!] \simeq \pm(\rho_l - \rho_v)$, and, using the approximated expression (4.11) for $[\![P]\!]$, we have

$$g^* \simeq \pm \frac{2\,\sigma}{R_\rho\,(\rho_l - \rho_v)}$$

Using the definition (3.63) of $\mathfrak{g}$, we therefore have that, in this limit,

$$|\mathfrak{g}| \simeq 2\,\frac{h}{R_\rho} \tag{4.19}$$

This is fully consistent with the hypothesis made to obtain the previous result (4.18) since $\mathfrak{g} \to 0$ actually corresponds to $R_\rho \gg h$.

Concluding remarks As a partial conclusion, we have introduced two relevant measures for the surface tension coefficient, the first one being related to the excess Helmholtz free energy (*cf.* equation (4.15)) and the second one to the Laplace relation (*cf.* equation (4.17)). The parameter $\mathfrak{g}$ has been shown to be an approximation of $2\,h/R_\rho$ (*i.e.* twice the inverse of the normalized sharp radius). As a consequence, small values of $|\mathfrak{g}|$ correspond to spherical inclusion whose radius is larger than the interface thickness h. In this limit, the two definitions for the surface tension coefficient agree and the Laplace relation is satisfied. It remains therefore to study the exact limit of validity of these statements (*i.e.* to study the dependence of these relations with respect to larger values of $|\mathfrak{g}|$). This is studied in section 4.3 using the profiles $\varphi(r)$ obtained numerically.

It is worth noting that these relations cannot be solved without the knowledge of the phase field profile $\varphi(r)$ (*cf.* the definitions (4.12) and (4.14) of the sharp interface radii, the equation (4.7) for the pressure jump and the definitions (4.16) and (4.17) of the surface tension coefficients). In the following we solve the equilibrium equation (4.3) for different values of the non-dimensional parameter $\mathfrak{g}$ to determine the agreement of our diffuse interface solution with the classical sharp interface models.

4.3 Determination of the phase field profile $\varphi(r)$

The goal of this section is to solve the differential equation (4.3) to determine $\varphi(r)$ (and therefore all the quantities mentioned above) as a function of the non-dimensional parameter $\mathfrak{g}$.

Let us precise that, in this study, we are more particularly interested in the equilibrium states corresponding to large values of the parameter $|\mathfrak{g}| > 1$. Indeed they correspond to small normalized radii and therefore characterize the limit of use of the model to describe an inclusion of a given size when the artificial thickness h is increased. We use finite difference methods to solve the equilibrium ODE in a closed domain for various values of the parameter $\mathfrak{g}$. The numerical resolution is easy enough to provide the equilibrium solutions for a large range of values for the non-dimensional parameter $\mathfrak{g}$. These results are therefore used to test the validity of the *a priori* estimates made in section 4.2 about the dependence of the radius of the inclusion and of the surface tension coefficients as a function of the parameter $\mathfrak{g}$. Moreover, this study constitutes a first numerical test for the solving of dynamics case with the spherical symmetry hypothesis.

4.3.1 Analysis of the spherical symmetric equilibrium equation

The goal of this study is to analyze the equilibrium relation (4.3) using an analogy with particle mechanics.

This analysis has been already used for the study of two-phase spherical inclusions with diffuse interface models, *e.g.* Dell'Isola et al. [43] for the van der Waals' model. The structure of our ODE is very similar to the one studied in [43], the only difference being actually the particular choice for the interpolation function $P_5(\varphi)$ and $W(\varphi)$ (in [43] a set of two parameters equations of state are considered that can be related to the classical van der Waals model). Therefore, the same qualitative analysis of the equilibrium equation based on the mechanical interpretation of this equation (originally introduced by van Kampen in 1964 [144]) holds: it can be seen as the equation of a particle of mass 1 moving in the potential $-(\mathfrak{g}\,P_5(\varphi) + W(\varphi))$ with the "viscous" time dependent force $2\,\varphi_{,r}/r$, the motion starting from the "time" $r = 0$ with zero "velocity" (*cf.* the boundary condition (4.4b)) and with an initial "position" $\varphi = \varphi_0$.

Shape of the potential with our phase-field model As a consequence of this analogy it is interesting to represent the potential $-(\mathfrak{g}\,P_n(\varphi)+W(\varphi))$ and to study the influence of the particular choice P_5 for the interpolation function on the nature of this potential. A graphical representation of this potential is given on figure 4.1 for the

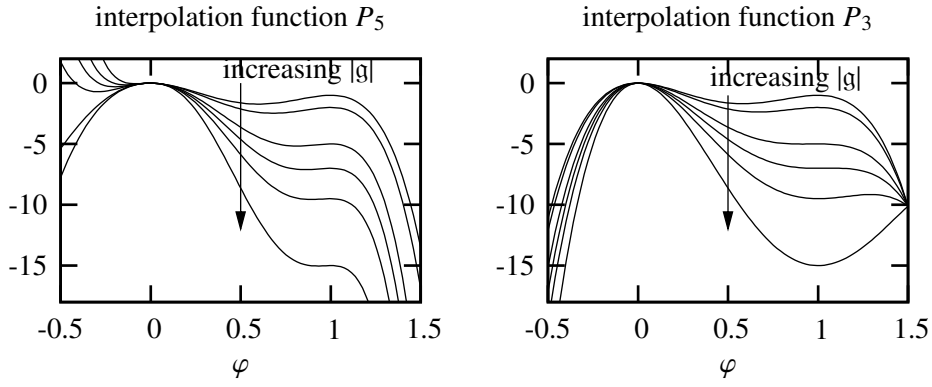

Figure 4.1: Potential $-(\mathfrak{g}\,P_n + W)$ for $\mathfrak{g} > 0$, the interpolation function P_n being either P_3 or P_5

two interpolation functions P_3 and P_5 for different values of the parameter $\mathfrak{g}$ ($\mathfrak{g} > 0$, *i.e.* drop case). Let us first note that there is no influence of the sign of $\mathfrak{g}$ on this study, indeed its sign only define the final state which is $\varphi = 1$ in the drop case and $\varphi = 0$ in the bubble case.

For both the case P_3 and P_5, the potential have the same property: the bulk values 0 and 1 are always local extrema for the potential whatever the value for $\mathfrak{g}$[5]. Since $\mathfrak{g} > 0$, the departure point (initial "time" $r = 0$) corresponds to the state $\varphi_0 \simeq 0$. The final state (infinite "time" $r = \infty$) always corresponds to $\varphi_\infty = 1$ that is an extrema of the potential. In the P_5 case, the state $\varphi = 1$ corresponds to a local maximum for any value of $\mathfrak{g}$. There exists therefore another extrema (local minimum) between the two values 0 and 1. This extrema is located

[5]This property is not satisfied by the much "simpler" choice P_1 or more generally for the other diffuse interface model such that the van der Waals' model considered in [43]. In this latter case, the density value corresponding to potential extrema changes with the value of $\mathfrak{g}$ (the chemical potential or specific Gibbs free energy μ_∞ in the original context). In the context of the van der Waals' model, this property is physically consistent and is indeed associated to the compressibility of the bulk phases.

at $\varphi = 1/2$ for $\mathfrak{g} = 0$ and tends to 1 as $\mathfrak{g}$ tends to $+\infty$. Therefore at the limit of very large $\mathfrak{g}$, the state 1 corresponds to an inflexion point. In the P_3 case, the situation is rather different. For low values of the parameter $\mathfrak{g}$, the state 1 is a maximum, and there exists, as in the P_5 case, a local minimum in the potential between 0 and 1. However, for a finite value of $\mathfrak{g}$, the location of this minimum actually reaches the value 1, which therefore becomes an inflexion point. By increasing further the parameter $\mathfrak{g}$, the state 1 is always a local minimum whereas the local maximum deviates to larger values of φ.

Finding the separatrix solution Let us now consider the use of this analogy to find the equilibrium solution $\varphi(r)$ for a given value of the parameter $\mathfrak{g}$ (which is our present goal). The solution is searched by trying to find the initial state ("position" φ_0) that actually allows to exactly reach the final state being either 0 or 1 (let us recall that according to our study of the state at infinity in section 4.2.1, we have always such a state at infinity). If the initial position is too close of the final "position" targeted, the particle won't have a sufficiently large enough initial acceleration to reach the final position and will rather fall back into the local minimum located between final and initial position. On the contrary, if the initial position is too far from the final "position" targeted, the particle will reach this position with a non-zero velocity and then fall down in the higher positions region. Using a standard dichotomy it is therefore possible to approximate the correct initial position and therefore the correct solution, the so-called separatrix solution.

We have analyzed our equilibrium ODE (4.3) using an analogy with particle mechanics. The potential corresponding to the motion of this particle has been presented. According to the choice for the interpolation function P_5, it has been shown to have different characteristics compared to the potential of more classical diffuse interface models: the final state is always a minimum for the potential. This illustrates the sensitivity of the characteristic of the spherical equilibrium with regard to the choice for the thermodynamic potential. It will be shown in section 4.3.3 that the physical properties of small spherical inclusions are indeed sensitive to the choice for the interpolation function for the density (chosen as being P_5 in our model). This analysis can be used to derive the equilibrium solution using standard shooting numerical methods, *e.g.* Dell'Isola et al. [43] for the van der Waals model or Lowengrub and Truskinovsky [89] for the Cahn-Hilliard model. However we will rather use finite difference methods to solve the equilibrium equation in a finite domain, this method turns out to be more easy to handle.

4.3.2 Analytical solving of the spherical symmetric equilibrium using piece-wise quadratic approximations

The ODE (4.3) can be solved analytically as soon as the potential is either quadratic or linear with respect to φ. This is not the general case since, at least the double well function W is classicaly modeled by a polynomial of degree 4 (in which case the potential is at least a polynomial of degree 3). In the following we therefore use piece-wise quadratic functions to approximate the potential. Such approximations have already been used in the study of the spherical symmetric equilibrium, *e.g.* Lowengrub and Truskinovsky [89] for the Cahn-Hilliard model without density difference.

In order to be able to solve analytically the ODE (4.3) in $\varphi(r)$, we prescribe a piecewise quadratic double well function denoted W_{pwP2} as an approximation of the prescribed fourth degree polynomial W_{P4} (3.42) presented in section 3.2.4. The simplest double well function W_{pwP2} satisfying the properties (3.40) and containing a non convex region is composed of three parabola and reads

$$W_{pwP2}(\varphi) = \begin{cases} \tilde{w}\,\varphi^2, & \varphi \leq \frac{1}{6}, \\ \tilde{w}\left[\frac{1}{12} - \frac{1}{2}\left(\varphi - \frac{1}{2}\right)^2\right], & \frac{1}{6} < \varphi < \frac{5}{6}, \\ \tilde{w}\,(\varphi - 1)^2, & \varphi \geq \frac{5}{6}. \end{cases} \tag{4.20}$$

where $\tilde{w} \simeq 13.02$. W_{pwP2} is a function of class C^1 and is represented on figure 4.2.

Let us also introduce a piecewise quadratic interpolation function denoted $P_{2\,pw}$ used instead of P_5 for the

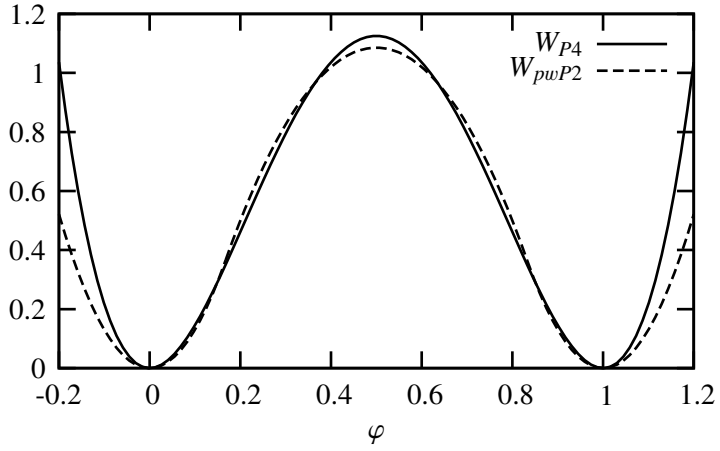

Figure 4.2: Non dimensional double well functions $W = \rho\, g_m$ satisfying (3.40) as fourth order polynomial (W_{P4}, equation (3.42)) or as piecewise quadratic (W_{pwP2}, equation (4.20))

definition of the density $\rho(\varphi)$ (that therefore reads $\rho = \rho_v + (\rho_v - \rho_l)\, P_{2\,pw}$)[6]

$$P_{2\,pw}(\varphi) = \begin{cases} 2\ \varphi^2, & \varphi \leq \frac{1}{2}, \\ -2\ (\varphi - 1)^2 + 1, & \varphi \geq \frac{1}{2}. \end{cases} \tag{4.21}$$

which is of class C^1 and is represented on figure 4.3.

The piecewise function $P_{2\,pw}$ satisfies

$$\frac{dP_{2\,pw}}{d\varphi}(1/2 \pm 1/2) = 0$$

As a consequence the condition (3.38a) is satisfied for any value of $\mathfrak{g}$, 0 and 1 are always solutions of the equilibrium equation for homogeneous states (3.64) which ensures therefore the state at infinity φ_∞ to always correspond to one of the bulk values 0 or 1 whatever the value of $\mathfrak{g}$ (*cf.* the corresponding discussion in section 4.2.1).

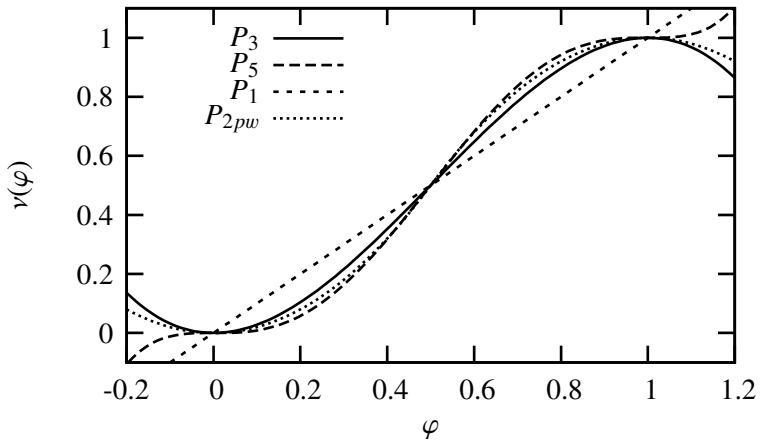

Figure 4.3: Non dimensional interpolation function for the density as a function of the phase field satisfying (3.51) as a fifth, third, or first degree polynomials (P_5,P_3 or P_1 as defined by equation (3.60)), or as piecewise quadratic (P_{2pw}, equation (4.21))

Using the expression (4.20) and (4.21), the ODE (4.3) reduces to a system of four linear equations for $\varphi(r)$ corresponding to each C^∞ domains of the three parabola for W cross those of the two parabola for ρ. It is

[6]It is worth noting that an even simpler approximation for the interpolation function would be to choose the linear interpolation function P_1. However, with this choice, we would loose the interesting property that ensures that the state at infinity is always characterized by $\varphi = 0$ or $\varphi = 1$.

straightforward[7], by matching the sub-solutions, to get the entire solution ensuring φ to be also of class C^1. The solution obtained is the following

$$\varphi(r) = \begin{cases} \varphi_\infty \pm \dfrac{R_\infty}{e\,6\,r}\, e^{-r/R_\infty}, & \varphi \leq |\varphi_\infty - \frac{1}{6}| \ , \textit{i.e. } r \in [R_\infty : \infty[\\ \varphi_\infty - \dfrac{\mathfrak{g}}{|\mathfrak{g}|}\,\dfrac{\tilde{w}/2}{\tilde{w}+8|\mathfrak{g}|} + \dfrac{\alpha_1 \sin\left(\frac{r}{R_{|\varphi_\infty-\frac{1}{2}|}}\right) + \alpha_2 \cos\left(\frac{r}{R_{|\varphi_\infty-\frac{1}{2}|}}\right)}{r/R_{|\varphi_\infty-\frac{1}{2}|}}, & \varphi \in [|\varphi_\infty - \tfrac{1}{6}| : |\varphi_\infty - \tfrac{1}{2}|] \ , \\ & \textit{i.e. } r \in [R_{|\varphi_\infty-\frac{1}{2}|} : R_\infty[\\ 1 - \varphi_\infty + \dfrac{\mathfrak{g}}{|\mathfrak{g}|}\,\dfrac{\tilde{w}/2}{\tilde{w}-8|\mathfrak{g}|} + \dfrac{\alpha_3 \sin\left(\frac{r}{R_{|\varphi_\infty-\frac{1}{2}|}}\right) + \alpha_4 \cos\left(\frac{r}{R_{|\varphi_\infty-\frac{1}{2}|}}\right)}{r/R_{|\varphi_\infty-\frac{1}{2}|}}, & \varphi \in [|\varphi_\infty - \tfrac{5}{6}| : |\varphi_\infty - \tfrac{1}{2}|], \\ & \textit{i.e. } r \in [R_{|\varphi_\infty-\frac{5}{6}|} : R_{|\varphi_\infty-\frac{1}{2}|}[\\ \varphi_0 \pm \dfrac{|\varphi_\infty - \frac{5}{6}|}{\sinh(1)}\,\dfrac{\sinh\left(r/R_{|\varphi_\infty-\frac{5}{6}|}\right)}{r/R_{|\varphi_\infty-\frac{5}{6}|}}, & \varphi \geq \tfrac{5}{6} \ , \textit{i.e. } r \in [0 : R_{|\varphi_\infty-\frac{5}{6}|} : \infty] \end{cases} \tag{4.22}$$

where, for the sake of simplicity, we have considered that the value of $\mathfrak{g}$ is sufficiently large ($|\mathfrak{g}| > \tilde{w}/8 \simeq 1.7$) so that φ_0 satisfies $1/3 < |\varphi_0 - 1/2|$ and so that, therefore, the phase field values of the profile actually crosses the four different domains. In this case the boudary and matching conditions provide a set of 8 algebraic equations parameterized by $\mathfrak{g}$ that we have to solve to determine the solution (*cf.* the footnote 7 on page 102).

Let us also note that, for any value of $\mathfrak{g}$, the state at the center is always such that $|\varphi_0 - 1/2| < 1/2$, *i.e.* $\varphi_0 \in [0 : 1]$. This latter property is satisfied for the fully non-linear problem as well.

The general solution for the profile $\varphi(r)$ is a monotonic piecewise function of r of class C^1. On figure 4.4, the solution $\varphi(r)$ corresponding to three different values of the non-dimensional parameter $\mathfrak{g}$ are represented. The first figure (top) corresponds to $\mathfrak{g} = -0.05$, and therefore to $R_\rho \simeq 10\,h$ according to the results in the limit of small values for $\mathfrak{g}$ (*cf.* the equation (4.19)). It is worth noting that $\varphi_0 \simeq 1$. The sharp equivalent radii R_ρ and Rs_ρ are both equal to $R_\rho = 10.77\,h$ which is actually close to the predicted value. Additionally to the analytical solution, the planar equilibrium profile (hyperbolic tangent) centered on the radius R_ρ is represented by the curve "tanh". It is clear that the phase field profile in the radial direction is very close to this planar profile. The second figure (bottom left) corresponds to $\mathfrak{g} = -0.5$. This figure shows that $R_\rho \simeq 1$ (actually $R_\rho = Rs_\rho = 1.08$) and still $\varphi_0 \simeq 1$. The last figure (bottom right) corresponds to a larger value of $\mathfrak{g}$, $\mathfrak{g} = -2.04$. This value is less than the upper limit -1.7 for φ_0 to be larger than $5/6$. Indeed, the value of φ_0 is approximatively 0.584. The two sharp solutions corresponding to the definition of the sharp radii R_ρ and Rs_ρ are represented on the figure. For such a relatively high value of $\mathfrak{g}$, the two definition begin to slightly disagree, R_ρ being larger than Rs_ρ. The behavior of small spherical inclusions is in fact different for different choices for the interpolation function and the influence of the piece-wise approximation on the solution is non-negligible. A deviation between the results obtained with quadratic approximations and the higher order expression for the potential has already been found in [89]. We show in section 4.3.3 that the spherical inclusions for high values of $\mathfrak{g}$ behave differently when the polynomial is

[7] In each sub-domain i, the differential equation is of the form

$$a_i\,\varphi + b_i = \left(\varphi_{,\bar{r}\bar{r}} + 2\,\frac{\varphi_{,\bar{r}}}{\bar{r}}\right)$$

where the value of the coefficients a_i and b_i depend on the parameter $\mathfrak{g}$. Therefore we introduce solutions for $\varphi_i(r)$ of the form $\varphi_i(r) = \beta_i + \sum_{j=0}^{1}\left(\alpha_{i,j}/r\right) e^{r/R_{i,j}}$ that needs to satisfy boundary (4.4) and matching conditions (continuity of the solution and of its first spatial derivative). A straightforward calculation yields

$$\begin{aligned} \beta_i &= -\frac{b_i}{a_i} \\ R_{i,j=0;1} &= \pm\sqrt{1/a_i} \end{aligned}$$

It is worth noting that, according to the sign of a_i and therefore of the value of $\mathfrak{g}$, $R_{i,j=0;1} \in \mathbb{R} \cup \mathbb{I}\mathbb{R}$. The boundary and matching conditions are used to determine the value of the coefficient $\alpha_{i,j}$ (and as a consequence the r location of the matching). In the general case, we have a set of 8 coefficients to determine, the boundary conditions (4.4) applied to the general form for the solution $\varphi_i(r)$ provide two relations whereas the three matching conditions provide 6 additional relations. We therefore have a system of 8 algebraic equations to solve. This is made using standard numerical methods.

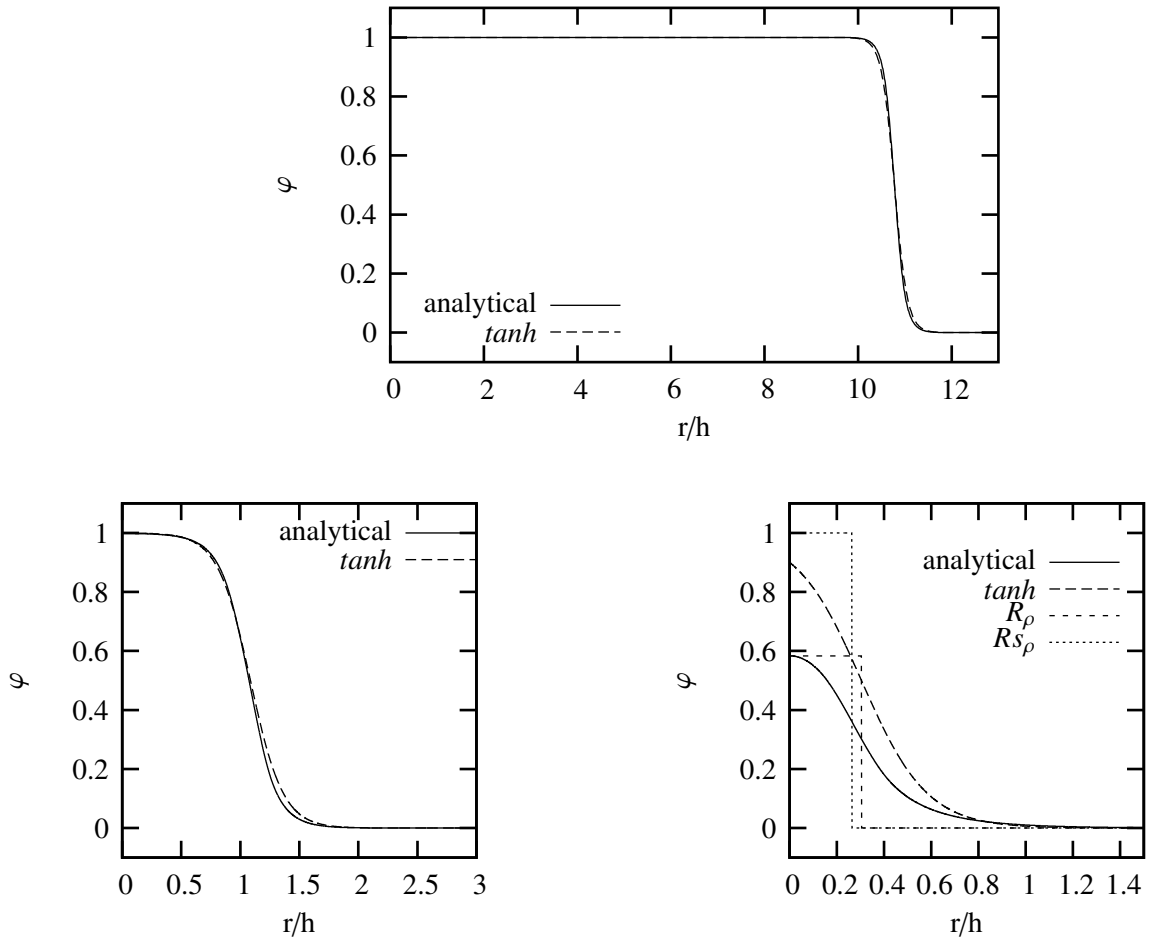

Figure 4.4: Equilibrium profiles obtained analytically using piecewise quadratic approximations.

chosen as being either P_3 or P_5. To correctly determine this behavior we therefore use finite difference methods in the following.

4.3.3 Solving of the spherical symmetric equilibrium in a closed domain using finite difference methods

The equilibrium profile $\varphi(r)$ is determined by solving the equilibrium conditions in a spherical system of coordinates and in a domain of finite extent ($20\,h$) using a non-linear solver[8]. The mass of the system is given and the profile $\varphi(r)$ is initially approximated by a hyperbolic tangent. In this study, and without any loss in generality, the vapor is considered as being at the center of the inclusion (bubble case) and the parameter $\mathfrak{g}$ is therefore always negative. The main variables of the system solved are the discretized values of the phase-field (function of r) and the specific Gibbs free energy g^* at equilibrium (real). The boundary conditions at $r = 0$ and at $r = 20\,h$ are $\varphi_{,r} = 0$. The profile is then numerically relaxed toward equilibrium. At convergence, the specific Gibbs free energy reaches a steady-state value and the norm of $\tilde{\mu}$ on the whole domain reaches the threshold of convergence. The profile is discretized by many points[9], which ensures the convergence of the solution.

In this section, we also study the influence of the choice of the particular interpolation function P_5 on the results by comparing them with those obtained when the density ρ is interpolated by the polynomial P_3 of degree 3. Indeed it will be shown that the physical behavior of the small spherical inclusions deviates from that observed with other classical (van der Waals, Cahn-Hilliard) diffuse interface models when P_5 is used instead of P_3: no increase of the equivalent sharp radius R_ρ is observed when the mass of the spherical inclusion tends to zero.

Profiles at equilibrium The profiles obtained are shown in figure 4.5 for different values of the total mass of the system. This figure shows that the equilibrium profile is very close to a hyperbolic tangent, *i.e.* the profile corresponding to a planar interface, as long as the radius of the inclusion is somewhat larger than the interface thickness. Let us now consider the density profiles. For the sake of simplicity, we have chosen to consider $\rho_v = 1$ and $\rho_l = 2$. Let us note however that the density difference modifies the results only by changing the order of magnitude of g^*, all the other parameters ($\mathfrak{g}$, σ, h) being fixed. The density profiles $\rho(r)$ provided on figure 4.5 are less diffuse than the phase-field ones, it is due to the shape of the interpolation function P_5 (*cf.* figure 4.3). On this figure, the sharp interface solution corresponding to the definition of R_ρ has been reproduced. The variation of the density value at the center of the inclusion is comparatively less pronounced for large values of $|\mathfrak{g}|$ (small radii) than the corresponding phase field value. This is due to the interpolation function shape near 0 and 1. It is worth noting that for small values of R_ρ the density at the center of the inclusion is comparatively less affected by the fact R_ρ reaches values close to h than the phase field profile. It is worth noting that the state at the extremity of the closed domain ($r/h = 20$) is always a bulk phase state (in the present case $\varphi = 0$). The state at this radius will therefore be considered as a good approximation to the state at infinity. Let us now consider the pressure profiles. To determine these profiles, we use the expression (4.2), and the non-dimensional pressure (scaled by

[8]The spatial discretization scheme is of *MAC* type, *i.e.* the scalar fields of r are located on the nodes (integer indexes $i \in \mathbb{N}$ from 1 to N, the number of cells) and the "vector" fields (such as the gradient $\nabla\varphi = \varphi_{,r}\,\vec{e}_r$) are located on the faces (indexes $i - 1/2$). The center of spherical symmetry, $r = 0$ is the face $1/2$. The spacing between nodes is constant and is denoted Δr such that the radial coordinate of a node, resp. a face, reads $r_i = i\,\Delta r + 1/2$, resp. $r_{i-1/2} = i\,\Delta r$. The numerical scheme for the discretization of the gradient operator applied on a field a simply reads

$$(\nabla a)_{i+1/2} = \frac{a_{i+1} - a_i}{\Delta r}$$

whereas the discretization of the scalar product of two vectors $b1\,\vec{e}_r$ and $b2\,\vec{e}_r$ reads

$$(b1\vec{e}_r \cdot b2\vec{e}_r)_i = \frac{r^2_{i+1/2}\; b1_{i+1/2}\; b2_{i+1/2} + r^2_{i-1/2}\; b1_{i-1/2}\; b2_{i-1/2}}{2\,r_i^2}$$

and the divergence operator of a radial vectorial field $b\,\vec{e}_r$ reads

$$(\nabla \cdot b\,\vec{e}_r)_i = \frac{r^2_{i+1/2}\; b_{i+1/2} - r^2_{i-1/2}\; bi - 1/2}{r_i^2\,\Delta r}$$

The discretized operators are thus ensured to satisfy the continuous identity for a scalar a and vector $\vec{b}$

$$\nabla \cdot \left(a\,\vec{b}\right) = a\,\nabla \cdot \vec{b} + \nabla a \;\cdot\; \vec{b}$$

that is of interest in order to ensure basic conservations of a quantity inside the domain.

[9]Let us note that the large number of discretization cells (about 500 for a domain of length $20\,h$, *i.e.* about 30 points inside the transition layer) used in the present study was introduced to ensure a very good precision for the present results. It is shown in the study of out of equilibrium dynamics that this number can actually be reduced without affecting the results significantly (*e.g.* the presentation of the dynamical numerical results in section 8.1.4).

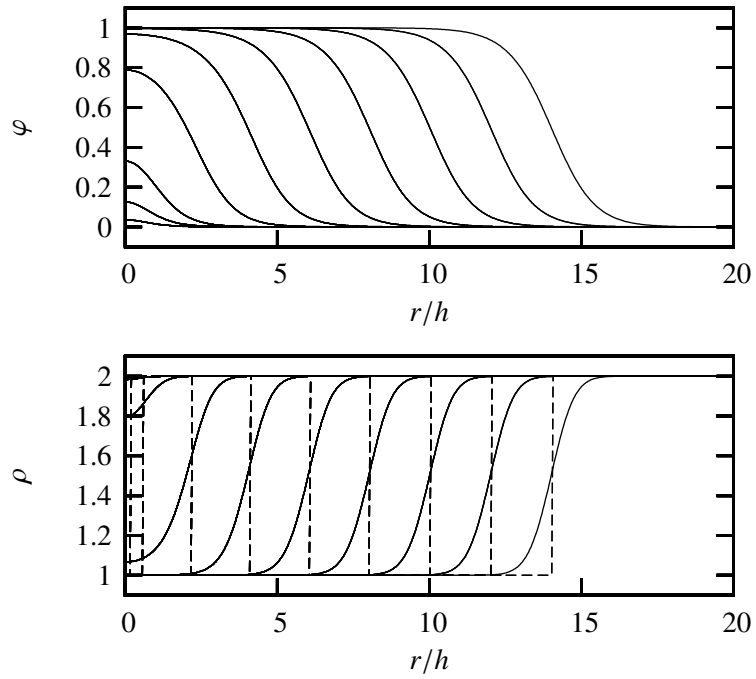

Figure 4.5: Equilibrium profiles of the phase-field and of the density for different masses of the system.

σ/h), reads

$$\begin{aligned} P^* &= \frac{\rho(\varphi)}{\rho_l - \rho_v}\,\mathfrak{g} - W(\varphi) - \frac{1}{2}\left(\varphi_{,\bar{r}}\right)^2 \\ \tilde{P}^* &= \frac{\rho(\varphi)}{\rho_l - \rho_v}\,\mathfrak{g} - \left(W(\varphi) - \frac{1}{2}\left(\varphi_{,\bar{r}}\right)^2\right) \end{aligned}$$

where $\tilde{P}^* = P^* + (\varphi_{,\bar{r}})^2$. $\tilde{P}$ corresponds to the variable homogeneous to a pressure that is uniform in the planar equilibrium case (*cf.* its introduction in section 5.3.3). The corresponding profiles are represented on figure 4.6. It can be seen that the pressure jump decreases when the bubble radius increases, which is fully consistent with

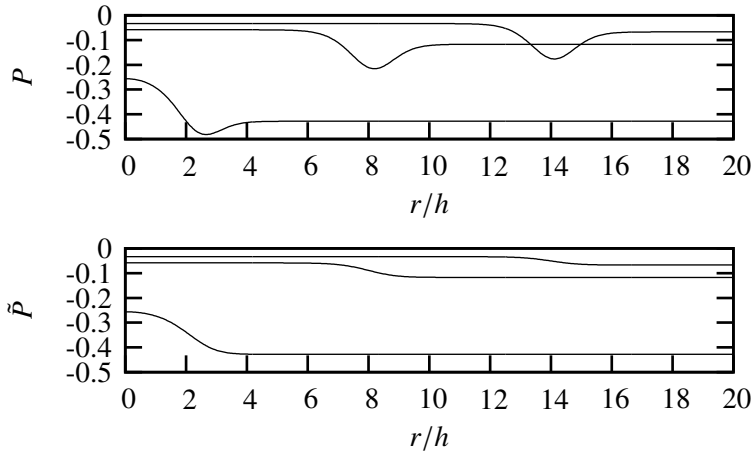

Figure 4.6: Equilibrium profiles of the pressure for different masses of the system.

the Laplace formula. Moreover, there exists a negative excess in pressure related to the positive surface tension coefficient defined as an excess Helmholtz free energy (*i.e.* minus an excess pressure, *cf.* the definition (4.15) of the surface tension coefficient $\sigma_{F^{ex}}$). The pressure $\tilde{P}^*$ is monotonic and has the same jump as the pressure P^*.

This is consistent with the equation for the profile of $\tilde{P}$

$$\tilde{P}(r) = P_\infty + 2 \int_{\bar{r}}^{\infty} \frac{(\varphi_{,\eta})^2}{\eta} d\eta$$

inherited from the pressure profile equation (4.6)[10].

Phase field value at the center of the inclusion Let us consider the variation of the phase field value at the center of the inclusion, φ_0, as a function of the sharp interface radius Rs_ρ. On figure 4.7 is represented this latter variation for the set of equilibrium profiles obtained and represented on figure 4.5. It is worth noting that the value

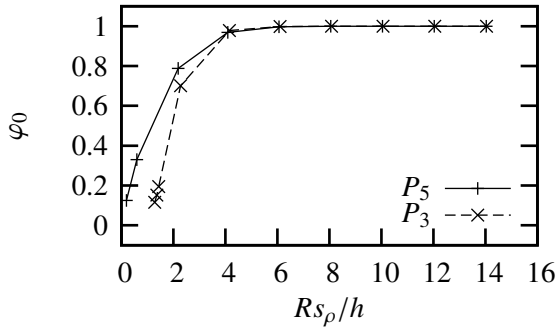

Figure 4.7: Variation of the state at the center of the inclusion as a function of its size.

φ_0 deviates significantly from the bulk value only for small normalized sharp radii, the limiting value being well approximated by $Rs_\rho/h \simeq 4$. It is worth pointing out that the total mass of the system is in fact linear with Rs_ρ^3, which precises the relevant meaning of this sharp interface radius. Below this value, the value of the phase field at the center of the spherical inclusion evolves monotonically toward the other bulk phase value corresponding to the state at infinity. The interpolation function has a weak influence on this behavior for large radii. For small radii, the evolution toward the outside state is sharper in the case of the interpolation function P_3. The deviation occurs for a relatively small value of Rs_ρ/h. This property is interesting since it means that relatively small bubbles or drops can be represented even when their size is close to the interface thickness. Let us note that, as a consequence (*cf.* our discusssion at the end of section 4.2.3), for $Rs_\rho/h > 4$, the absolute values of the pressure inside and outside the inclusion (*cf.* equation (4.10)) are actually fully consistent with the corresponding classical sharp relations equation (A.25). Let us now consider the equivalent sharp quantities of the corresponding results.

Relation between the sharp radius Rs_ρ and the non-dimensional number $\mathfrak{g}$. Let us consider the validity of the relation (4.19) that reads

$$|\mathfrak{g}| \simeq 2\, h/Rs_\rho$$

and which has been shown to be valid at least for small radii. We have represented on figure 4.8 the calculated values for $\mathfrak{g}$ and Rs_ρ for the set of profiles $\varphi(r)$ presented hereinabove. The right hand side of the curve (large values of h/Rs_ρ) corresponds therefore to the smallest inclusions. We have also represented on the RHS figure the similar results obtained when the density $\rho(\varphi)$ is interpolated by the degree 3 polynomial P_3 (*cf.* equation (3.60b)) instead of P_5 (that is the choice retained in our model). It is worth noting that the correlation (4.19) between the parameter $\mathfrak{g}$ and the sharp interface equivalent radius of the inclusion (and which has been associated to low values of $\mathfrak{g}$) holds for a larger range of large $\mathfrak{g}$ values (or equivalently of small Rs_ρ values) in the P_5 case than in the P_3 case. The deviation between the behavior with P_3 and with P_5 is analyzed in more details in the following.

As a partial conclusion, the correlation (4.19) between the parameter $\mathfrak{g}$ and the sharp interface radius Rs_ρ which has been associated to the satisfaction of the Laplace formula (*cf.* its derivation), holds for a large range of normalized (by the artificial thickness h) inclusion sizes.

[10] It is worth noting that, as a consequence, the variable $\tilde{P}$ is more spatially regular than the pressure P. This property jusitifes to choose $\tilde{P}$ or $\mathcal{G}$ as the main variables in our numerical computations as it will be introduced in section 5.3.3.

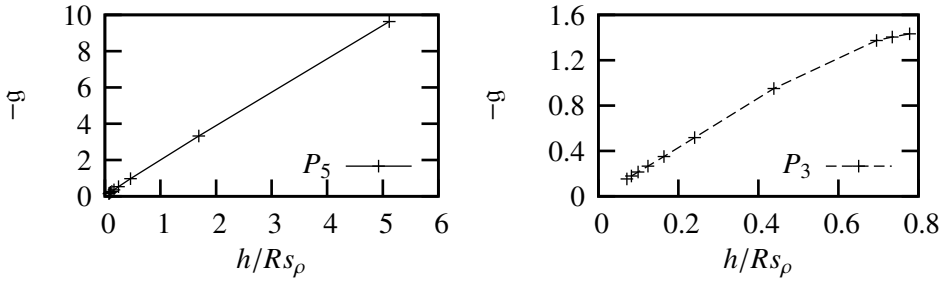

Figure 4.8: Correlation between the parameter $\mathfrak{g}$ and the normalized radius h/Rs_ρ

Sharp interface radii for spherical equilibrium solutions Let us consider the sharp interface radii R_ρ (defined by equation (4.12)) and Rs_ρ (defined by equation (4.14)). They are represented on figure 4.9 for the different equilibrium profiles already presented in the hereinabove discussion, as well as for the two interpolation functions

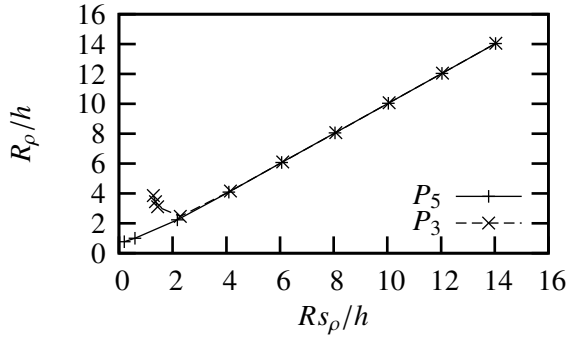

Figure 4.9: Correlation between the two different sharp radii Rs_ρ and R_ρ

P_3 and P_5 considered in the present study. For large radii (*i.e.* $Rs_\rho/h > 2$), the two definitions for the radius agree for both interpolation functions. For vanishing bubbles ($Rs_\rho \to 0$), the equivalent sharp radius R_ρ based on the nullity of the excess mass behaves differently for the P_3 and the P_5 cases. In the P_3 case, the radius R_ρ diverges from the value of the radius Rs_ρ and moreover increases with decreasing mass. Whereas in the P_5 case the agreement between the two radii is still valid for small bubbles.

The sharp increase of the normalized radius R_ρ in the P_3 case can be related to the existence of a "minimal nucleation radius"[11] in the second-gradient theory, *e.g.* Dell'Isola et al. [43]. The same behavior holds with binary fluids described with a quasi-compressible model (and an interpolation function of type P_1), *e.g.* Lowengrub and Truskinovsky [89]. Our model (with P_5) does not include such a feature. Let us note however that, if our model could reproduce a "minimal nucleation radius", the order of magnitude of this radius would be scaled by the artificial thickness h, which does not allow to recover the correct physical scale. In this sense, the results obtained with our model are consistent with the classical sharp interface model with incompressible bulk phases (that does not include such a deviatoric of the radius for small inclusions). Moreover the nucleation process can still take place with our model, that constitutes an additional advantage with regard to the sharp model. Indeed we show in the following that, with our model like with other diffuse interface models, the pressure jump does not diverge as the size of the spherical inclusion tends to zero.

Pressure jump and Laplace formula Let us consider the pressure jump $[\![P]\!]$ as a function of the inverse normalized radius h/R_ρ. According to the Laplace formula the pressure jump should be linear with respect to this inverse radius at least for large radii. The pressure jump for the different φ profiles investigated have been represented on figure 4.10. Let us first consider the case of the P_5 interpolation function. In this case, the linearity of the pressure jump with the inverse radius can be considered as valid till a critical value of the normalized radius, say $R_\rho/h \simeq 2.5 = 1/0.4$. Below this critical value, the pressure jump actually tends to

[11] "*i.e.* the minimal equilibrium radius of a bubble or a droplet necessary for nucleation in the other phase" [43]

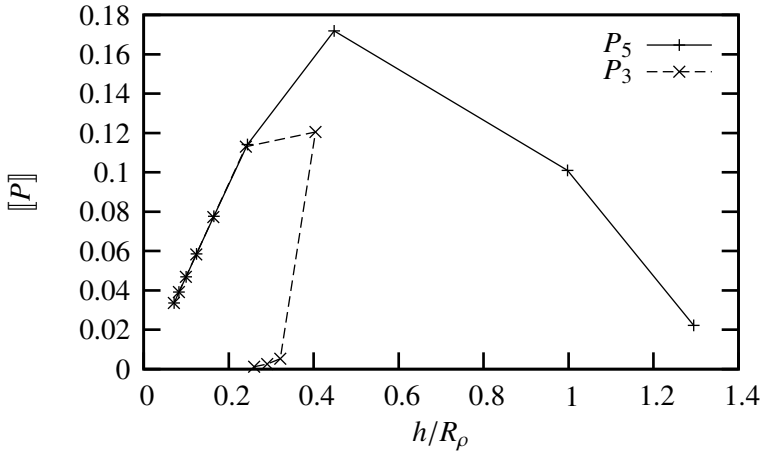

Figure 4.10: Pressure jump $[\![P]\!]$ as a function of the inverse of the normalized sharp radius h/R_ρ for the two interpolation functions considered P_3 and P_5.

zero, which is consistent with the results obtained with similar diffuse interface models. It is worth noting that the critical value at which the pressure jump deviates from the Laplace formula corresponds to larger spherical inclusions (normalized critical radius $R_\rho/h \simeq 4 = 1/0.25$) than for the P_3 case. This is an additional advantage of dealing with the interpolation function P_5.

Surface tension coefficients Let us now study the surface tension coefficients $\sigma_{F^{ex}}$ and $\sigma_{[\![P]\!]}$. The surface tension coefficient $\sigma_{F^{ex}}$ is evaluated using its original expression (4.15) with the following expression for P^{ex} (that is easier to use numerically than the integration of the expression (4.6)) inherited from the expression (4.2)

$$P^{ex} = \frac{1}{R_\rho^2}\left[\int_0^{R_\infty}\left(W(\varphi(r)) + \frac{\lambda}{2}(\varphi_{,r})^2\right) r^2\, dr - \frac{R_\infty^3}{3}\, W(\varphi(R_\infty)) - \frac{R_\rho^3}{3}\left(W_0 - \ W(\varphi(R_\infty))\right)\right] \tag{4.23}$$

where R_∞ is the radius of the finite domain, in our case $R_\infty = 20\,h$. The evolution of the surface tension coefficients as a function of the sharp interface radius R_ρ is reproduced on figure 4.11.

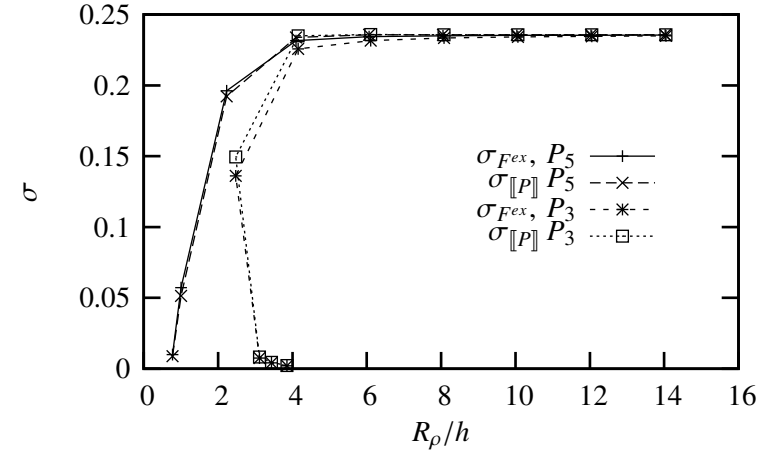

Figure 4.11: Surface tension coefficients $\sigma_{F^{ex}}$ and $\sigma_{[\![P]\!]}$ as a function of the normalized sharp radius R_ρ/h for the two interpolation functions considered P_3 and P_5.

The results corresponding to the interpolation function P_5 illustrate that the two different definitions for the surface tension coefficient agree for the entire range of radii investigated (and therefore the entire range of $\mathfrak{g}$ values). Moreover, the surface tension coefficient is very close to the planar equilibrium value σ (asymptotic value for large R_ρ) as soon as $R_\rho/h > 4$ which is a limit of use of the present model as soon as the Laplace

relation (4.11) is targeted. The surface tension actually decreases for decreasing radii below this limit, which is consistent with the classical features of diffuse interface models.

The results corresponding to the P_3 interpolation function are quite similar, except that the deviation of the surface tension coefficient $\sigma_{F^{ex}}$ slightly deviates from the asymptotic value σ for larger values of the normalized radius $R_\rho/h \simeq 10$. The two surface tension coefficients agree again when they reach lower values.

As a partial conclusion, for the interpolation function P_5 considered, the surface tension coefficients $\sigma_{F^{ex}}$ and $\sigma_{[\![P]\!]}$ agree well over the range of spherical inclusions' radii investigated. Moreover their deviation from the planar interface value σ occurs for a rather low value of the normalized radius R_ρ/h ($\simeq 4$) .

4.4 Conclusion on the study of spherical inclusions at equilibrium

In this chapter, we studied the two-phase equilibrium in a spherical symmetric system with the help of our phase-field model. This study constitutes a first step to demonstrate the ability of our model *(i)* to deal with multi-dimensional liquid-vapor systems and *(ii)* to be consistent with the classical sharp interface model of which it aims at being a regularization.

First we showed that the study of the equilibrium of a spherical inclusion lies on the solving of an ordinary differential equation (4.3) that determines the equilibrium radial phase field profile $\varphi(r)$. This equation is parameterized by a single non-dimensional number $\mathfrak{g}$. We showed that the state outside the inclusion always corresponds to one of the bulk phases ($\varphi = 0$ or $\varphi = 1$), which is consistent with the classical sharp model. We analyzed the equilibrium equation using an analogy with particle mechanics (see section 4.3.1). Due to the particular choice of the interpolation function, the initial and final "locations" of the particle are always maxima of the potential driving the motion of the particle for any value of the non-dimensional parameter $\mathfrak{g}$. Then we introduced piecewise quadratic approximations for the functions $W(\varphi)$ and $\rho(\varphi)$ entering the equilibrium equation. This allows to determine the analytical expression for the equilibrium profile. To our knowledge, this result has never been obtained for a phase field model accounting for a density difference between the bulk phases. To evaluate the limit of validity of the model for vanishing inclusions, and since the influence of the piecewise quadratic interpolation function on the description of small inclusions is non negligible, we solved the equilibrium profile in a finite domain using a standard finite difference method. As soon as the radius is a few times larger ($R_\rho/h > 4$) than the arbitrary thickness, the model allows to recover the main features of the classical sharp interface model with incompressible bulk phases, *i.e.*

- ⋆ the state inside the inclusion is a phase and does not depend on the size of the inclusion
- ⋆ the surface tension coefficient is well approximated by its planar value
- ⋆ the pressure jump is related to the surface tension coefficient through the Laplace formula

Moreover it has been shown that for spherical inclusions of radius close or less than the arbitrary interface thickness

- ⋆ the pressure jump is still related to an excess Helmholtz free energy (which proves the thermodynamic consistency of the model)
- ⋆ the pressure jump does not diverge as the size of the inclusion tends to zero, which actually allows to deal with vanishing bulk phases without any problem, a property that is not shared by the sharp model, and therefore constitutes an additional advantage of our diffuse model by allowing to take into account nucleation events
- ⋆ the equivalent sharp interface location does not diverge even for vanishing spherical inclusions

The latter result is not classical for diffuse interface models where a minimal nucleation radius exists as the size of the inclusion approaches the characteristic size of planar interface thickness, *e.g.* [43]. Our present model therefore does not take into account this phenomenon. It is actually of interest for our applications since, due to the arbitrary choice of the interface thickness h, the "minimal nucleation radius" would be scaled by h, which is physically irrelevant. It would be of interest to investigate the origin of this deviation of the physical behavior according to the choice of the expression of the specific Gibbs free energy of a fluid.

As a conclusion, the proposed phase-field model is a consistent regularization of arbitrary length h of the classical sharp interface model with incompressible bulk phases even for vanishing spherical inclusions at least as far as the equilibrium features of a spherical inclusion are concerned.

Chapter 5

Phase-field model: Derivation and study of the dynamics

In this chapter, we derive the thermodynamically consistent set of governing equations corresponding to the multi-phase system described by the phase field thermodynamic model derived in chapter 3. The goal is to derive the continuous formulation of our diffuse interface method for the numerical simulation of liquid-vapor flow with phase change by specifying the closure relations for the stress tensor and the rate of entropy production.

This chapter is organized as follows. In section 5.1, using a variational principle, we derive the form of the non-dissipative stress tensor and the boundary conditions in the compressible case. In section 5.2, using the first and second laws of thermodynamics we derive the set of governing equations for the dissipative non-isothermal dynamics of the quasi-compressible model. The study of the compressible case in section 5.1 suggests the constitutive form of the non-dissipative rate of work used in this derivation. The general consistent form of the dissipative processes in phase field models is studied. We then present the form retained in our model. In section 5.3, we derive the non-dimensional form of the governing equations. Some simplifying assumptions of the thermodynamic description are presented, which allow to recover the main features of the liquid-vapor phase transition while the corresponding writing of the equations is simplified in view of their numerical resolution. We then precise the final form of the equations of evolution for the main variables.

5.1 Dissipation free, compressible and isothermal case

In this section, we derive the set of governing equations in the compressible, isothermal, and non dissipative case using a variational principle. We suppose that the isothermal Helmholtz free energy of the fluid depends, in addition to the density ρ, on both a scalar φ and its spatial gradient $\nabla\varphi$; the phase field φ describes the local state of the fluid in the sense introduced in section 3.2. The goal of this study is to derive the form of the non-dissipative part of the stress tensor consistent with this two-phase model. However with the quasi-compressible thermodynamic model it is no longer possible to use this formalism according to the fact that the description in terms of Helmholtz free energy is degenerate (*cf.* section 3.1). The expression for the stress tensor obtained in the compressible case (present study) is used to suggest the form for the rate of work while deriving the set of governing equation in the quasi-compressible non-isothermal dissipative case (see section 5.2).

This section is organized as follows. In section 5.1.1 we introduce the main notions necessary in using variational principle. In section 5.1.2, we derive the governing equations and present the corresponding non-dissipative part of the stress tensor and the boundary conditions.

5.1.1 Presentation of the variational principle

In this section, we define the system studied, its Lagrangian and the variations considered. Then we introduce the main relations allowing to study the variation of the Lagrangian of the system. General studies of the variational principle in fluid mechanics are given in [119, 122]. Similar studies dedicated to the derivation of the dynamics of a fluid described by a compressible thermodynamic model of a diffuse interface can be found in [89, 138].

Description of the instantaneous position of material particles Let us consider material particles of current position $\vec{x}$. $\vec{x}$ is written in the form $\vec{x}(\vec{\xi}, t)$, where $\vec{\xi}$ is the initial position of the material particles $\vec{\xi} = \vec{x}(\vec{\xi}, 0)$. Let us denote $\vec{V}(\vec{\xi}, t)$ the velocity field of the particles defined by

$$\vec{V}(\vec{\xi}, t) \triangleq \frac{\partial \vec{x}}{\partial t}_{|\xi}$$

Let us consider the time derivative $\partial/\partial t_{|\xi}$ (denoted d/dt in the following for the sake of the simplicity) appearing in the above expression. The time derivative of a field a defined as a Eulerian field $a(\vec{x}, t)$ reads (since $\vec{x}(\vec{\xi}, t)$)

$$\frac{da(\vec{x}, t)}{dt}_{|\vec{\xi}} = \frac{\partial a}{\partial t}_{|\vec{x}} + \frac{\partial \vec{x}}{\partial t}_{|\xi} \cdot \frac{\partial a}{\partial \vec{x}}_{|t}$$

and therefore using the definition (5.1.1) of $\vec{V}$

$$\frac{da(\vec{x}, t)}{dt} = \frac{\partial a}{\partial t}_{|\vec{x}} + \vec{V} \cdot \frac{\partial a}{\partial \vec{x}}_{|t}$$

which corresponds to the classical relation relating the particle time derivative of a variable (*i.e.* at constant $\vec{\xi}$, or Lagrangian) to the local partial derivatives of the Eulerian field of this variable.

Thermodynamic model and expression for the Lagrangian For an isothermal flow ($T = T_0$), the unknown fields are $\vec{x}$, ρ and φ. Let us introduce $f(\rho, \varphi, \nabla\varphi)$ as the specific Helmholtz free energy at the temperature $T = T_0$ and its partial derivatives

$$\begin{aligned} \frac{\partial f}{\partial \rho} &\triangleq \frac{P}{\rho^2} \\ \frac{\partial f}{\partial \varphi} &\triangleq \mu \\ \frac{\partial \vec{f}}{\partial \nabla\varphi} &\triangleq \vec{\Psi} \end{aligned} \tag{5.1}$$

The governing equations for the dissipation free isothermal flow can be obtained from a variational principle where the Lagrangian takes the classical following form

$$\mathscr{L} = \int_{t_i}^{t_f} \int_{\Omega} \rho \left(\frac{V^2}{2} - f \right) d\mathcal{V}\, dt$$

where

- ⋆ $\Omega(t)$ is an arbitrary volume of fluid particles which is moving with the fluid (*i.e.* composed at all times of the same particles)
- ⋆ $d\mathcal{V}$ is the contraction of the three-dimensional elementary volume $d\mathcal{V} = dx_1\, dx_2\, dx_3$
- ⋆ $\dfrac{V^2}{2} \triangleq \dfrac{1}{2}\vec{V} \cdot \vec{V}$ is the specific kinetic energy
- ⋆ and t_i and t_f are endpoints (initial and final) times where the variations will be supposed to be zero (which is the framework of the Hamilton's principle followed in this study).

Definition of the variation considered In order to derive the governing equations for the flow using the fundamental d'Alembert-Lagrange variational principle, it is necessary to define the variations considered. According to the thermodynamic model of the fluid considered, we vary the path $\vec{x}$ and state φ of the material particles independently. It is shown in the following that the variation of the other main thermodynamic variables, namely the density ρ and the non-local field $\nabla\varphi$, are functions of the, say primary, variations of the state φ and path $\vec{x}$. Let us consider a set of paths $\vec{x}(\vec{\xi}, t, \epsilon)$ parameterized by ϵ, $\epsilon = 0$ being the path investigated. Let us introduce the variation δ around the path $\epsilon = 0$ by

$$\delta \triangleq \frac{\partial}{\partial \epsilon}_{|\epsilon=0, \vec{\xi}, t}$$

$\delta\vec{x}$ is thus a virtual displacement of the fluid particles from their instantaneous position $\vec{x}$. The field $\varphi(\vec{\xi},t)$ is varied independently since no conservation principle applies *a priori* on it and we thus define the set of states $\varphi(\vec{\xi},t,\epsilon)$ parameterized by the same ϵ. Now that the variation of state and path of the fluid particles have been defined, one must relate the variation of the thermodynamic variables (ρ,$\nabla\varphi$) to the two independent variations considered on $\vec{x}$ and φ.

Continuity equation Let us relate the variation of the density $\delta\rho$ to the variation of the instantaneous position of the particles $\delta\vec{x}$, *i.e.* derive the variational continuity equation. The density of the fluid $\rho(\vec{x})$ is defined by

$$\rho(\vec{\xi},t) \triangleq \frac{\rho_0(\vec{\xi})}{\det|d\vec{x}/d\vec{\xi}|}$$

where $\rho_0(\xi)$ is the initial density distribution. Let us denote J the determinant $\det|d\vec{x}/d\vec{\xi}|$. The density thus reads

$$\rho = \frac{\rho_0}{J}$$

Let us study the variation $\delta\rho$ of the density. Since ρ_0 is a function only of $\vec{\xi}$, its variation $\delta\rho_0$ satisfies $\delta\rho_0 = 0$. The variation of density $\delta\rho$ reads thus

$$\delta\rho = -\frac{\rho_0\,\delta J}{J^2} \tag{5.2}$$

Using the definition of J as a determinant, the variation δJ reads [1] where we have used the expression for $(d\vec{x}/d\vec{\xi})^{-1}_{i,j} = (d\xi_i/dx_j)$ and the commutativity of δ and $\partial/\partial\xi_j$

$$\delta J = J\,\frac{\partial\xi_j}{\partial x_i}\,\frac{\partial\delta x_i}{\partial\xi_j}$$

and thus using the operator nabla ∇:

$$\delta J = J\,\nabla\cdot(\delta x) \tag{5.3}$$

Using the above relation in the expression (5.2) for the variation of density implies that the varied motions satisfy the following continuity equation:

$$\delta\rho = -\rho\nabla\cdot(\delta\vec{x}) \tag{5.4}$$

which is actually a relation linking $\delta\rho$ to $\delta\vec{x}$.

Variation of the non-local field $\nabla\varphi$ The variation of $\nabla\varphi$, which is one of the main thermodynamic variable considered, is linked to the variations of φ and $\vec{x}$. Using vectorial identities [2] and the commutation of $(\partial/\partial\epsilon)_{|\vec{x}}$ with the nabla operator, we get

$$\delta\nabla\varphi = \nabla(\delta\varphi) - (\nabla(\delta\vec{x}))\ \nabla\varphi \tag{5.5}$$

that is effectively a relation linking $\delta\nabla\varphi$ to $\delta\vec{x}$ and $\delta\varphi$. Let us note that the second term of the RHS corresponds to a matrix vector product.

Once the variation of the main thermodynamic variables have been defined and related each other, we derive other variational relations necessary to express the variation of the Lagrangian $\mathscr{L}$.

Transport theorem We begin with using the continuity equation (5.4) to relate the variation of the integral over a given volume of a volumetric quantity (for instance the volumetric Helmholtz free energy $F = \rho f$ appearing in the Lagrangian $\mathscr{L}$) to the corresponding specific quantity (for instance f). This latter relation is known as the transport theorem. Let us $A(\vec{x},t,\epsilon)$ be an arbitrary volumetric quantity. Its volume integral

$$\int_{\Omega(t)} A(\vec{x},t,\epsilon)\,d\mathcal{V}$$

[1] *cf.* the Jacobi's formula for the derivative $\tilde{\partial}$ of a determinant of a an invertible square matrix A of adjugate matrix B, $\tilde{\partial}(\det A) = B^{i,j}\tilde{\partial}A^{i,j} = \mathrm{Tr}\left(B\tilde{\partial}A\right) = \det A\,\mathrm{Tr}\left(A^{-1}\tilde{\partial}A\right)$

[2] especially $\nabla\left(\vec{b_1}\cdot\vec{b_2}\right) = \vec{b_1}\times\left(\nabla\times\vec{b_2}\right) + \vec{b_2}\times\left(\nabla\times\vec{b_1}\right) + \left(\vec{b_1}\cdot\nabla\right)\vec{b_2} + \left(\vec{b_2}\cdot\nabla\right)\vec{b_1}$, $\nabla\times\nabla a = \vec{0}$ and $\nabla\varphi\times(\nabla\times\delta\vec{x}) + (\nabla\varphi\cdot\nabla)\,\delta\vec{x} = (\nabla\delta\vec{x})\,\nabla\varphi$

is a well-defined function of time. Let us vary this integral quantity. $\vec{\xi}$ is introduced as the new variable of integration. The corresponding volume of integration is then $\Omega_0 = \Omega(0)$ and

$$\int_{\Omega(t)} A(\vec{x},t,\epsilon)\, d\mathcal{V} = \int_{\Omega_0} A(\vec{\xi},t,\epsilon)\, J\, d\mathcal{V}_0$$

Since $d\mathcal{V} = J\, d\mathcal{V}_0$ relates the element of volume respectively in the $\vec{x}$ and $\vec{\xi}$ variables,

$$\delta \int_{\Omega(t)} A(\vec{x},t,\epsilon)\, d\mathcal{V} = \int_{\Omega_0} \left(J\, \delta A(\vec{\xi},t,\epsilon) + A(\vec{\xi},t,\epsilon)\, \delta J \right) d\mathcal{V}_0$$

Since δJ is given by (5.3), one gets

$$\delta \int_{\Omega(t)} A(\vec{x},t,\epsilon)\, d\mathcal{V} = \int_{\Omega_0} \left(\delta A(\vec{\xi},t,\epsilon) + A(\vec{\xi},t,\epsilon)\, \nabla\cdot(\delta x) \right) J\, d\mathcal{V}_0$$

Thus

$$\delta \int_{\Omega(t)} A(\vec{x},t,\epsilon)\, d\mathcal{V} = \int_{\Omega} \left(\delta A(\vec{x},t,\epsilon) + A(\vec{x},t,\epsilon)\, \nabla\cdot(\delta x) \right) d\mathcal{V}$$

If we further introduce the specific quantity $a(\vec{x},t,\epsilon) \,\hat{=}\, A(\vec{x},t,\epsilon)/\rho(\vec{x},t)$, using the continuity equation (5.4), we get

$$\delta \int_{\Omega(t)} A(\vec{x},t,\epsilon)\, d\mathcal{V} = \int_{\Omega(t)} \rho\, \delta a(\vec{x},t,\epsilon)\, d\mathcal{V} \tag{5.6}$$

This relation is known as the transport theorem. It will be used when calculating the variation of the Lagrangian $\mathscr{L}$.

Variation of the velocity field, classical continuity equation and transport theorem To express the variation of the specific kinetic energy ($V^2/2$), we study the variation of the velocity field $\vec{V}$. Using the definition (5.1.1) of $\vec{V}$ and the fact that the partial derivative with respect to ϵ, $\delta = (d/d\epsilon)_{|\vec{\xi},t,\epsilon=0}$ and to t, $(d/dt)_{|\vec{\xi}}$ applied on $\vec{x}(\vec{\xi},t)$ commute, the following identity holds

$$\delta\vec{V} = \delta\left(\frac{d\vec{x}}{dt}\right) = \frac{d\,\delta\vec{x}}{dt} \tag{5.7}$$

Let us take the benefit of having presented this commutative properties to introduce other useful relations for the study of the variation of the Lagrangian of the fluid. Let us recall that the derivation of the continuity equation was based on the commutation of partial derivatives with respect to ϵ and t of the field $\vec{x}(\vec{\xi},t)$. The reasoning that lead to the continuity equation (5.4) and the transport theorem (5.6) can be reproduced using the following analogy

$$\begin{aligned} \epsilon &\leftrightarrow t \\ \delta &\leftrightarrow \frac{d}{dt} \\ \delta\vec{x} &\leftrightarrow \vec{V} \end{aligned} \tag{5.8}$$

It leads to the classical continuity equation

$$\frac{d\rho}{dt} = -\rho\nabla\cdot(\vec{V}) \tag{5.9}$$

that is one of the main evolution equations of the fluid dynamics. Let us note that, as a consequence:

$$\frac{d}{dt_{|\xi}} \int_{\Omega} A(\vec{x},t)\, d\mathcal{V} = \int_{\Omega} \rho\, \frac{d}{dt_{|\xi}} a(\vec{x},t)\, d\mathcal{V} \tag{5.10}$$

which is a transport theorem (similar to its variational version (5.6)) that is used in the following in order to express the variation of the kinetic energy of the fluid.

Main results from the introduction of the variations of state and path We have defined the system considered as well as its Lagrangian. Then we have introduced the primary variations of the fluid path $\vec{x}$ and state φ. The main relations linking the variations of the variables of the thermodynamic model ρ and $\nabla\varphi$ to the primary variations, namely $\delta\vec{x}$ and $\delta\varphi$, have been derived. Additional variational relations, useful for the following calculations, have been also derived. Moreover, we have derived the continuity equation (5.9), which constitutes one of the governing equations for the flow. Let us now vary the Lagrangian of the system in view of applying the fundamental d'Alembert-Lagrange variational principle.

5.1.2 Derivation of the system of governing equations

We first derive the expression for the variation of the Lagrangian $\mathscr{L}$ using the relation derived in the previous section. Then, using the fundamental d'Alembert-Lagrange variational principle, we derive the dissipation free equations for the isothermal flow of the fluid described by the diffuse interface compressible thermodynamic model introduced. Thereafter, we discuss the expression for the corresponding stress tensor and boundary conditions.

First variation of the Lagrangian Let us introduce the first variation ($\delta\mathscr{L}$) of the Lagrangian $\mathscr{L}$. Using the transport theorem (5.6), this variation reads

$$\delta\mathscr{L} = \int_{t_i}^{t_f}\int_{\Omega} \rho\,\delta\left(\frac{V^2}{2} - f\right) d\mathcal{V}\,dt \tag{5.11}$$

Let us first study the term $\rho\,\delta f$. Using the definition (5.1) of the partial derivatives of the specific Helmholtz free energy f with respect to the set of main variables $(\varphi, \rho, \nabla\varphi)$, the first variation δf of f reads

$$\delta f = \frac{P}{\rho^2}\,\delta\rho + \mu\,\delta\varphi + \vec{\Psi}\cdot\delta\nabla\varphi \tag{5.12}$$

Let us relate the variation of f to the two independent primary variations considered $\delta\varphi$ and $\delta\vec{x}$ using the identities (5.4) and (5.5) derived in the previous section. Using the variational continuity equation (5.4) and the vectorial identity $\nabla\cdot\left(a\,\vec{b}\right) = a\,\nabla\cdot\vec{b} + \nabla a\cdot\,\vec{b}$, the term $(P/\rho)\,\delta\rho$ reads

$$\begin{aligned}\frac{P}{\rho}\delta\rho &= -P\,\nabla\cdot(\delta\vec{x}) \\ &= \nabla P\cdot\delta\vec{x} - \nabla\cdot(P\,\delta\vec{x})\end{aligned} \tag{5.13}$$

Let us study the term $\rho\left(\mu\,\delta\varphi + \vec{\Psi}\cdot\delta\nabla\varphi\right)$. Using once again the vectorial identity and the relation (5.5), we get

$$\begin{aligned}\rho\,\vec{\Psi}\cdot\delta\nabla\varphi &= \rho\,\vec{\Psi}\cdot(\nabla\delta\varphi - (\nabla(\delta\vec{x}))\nabla\varphi) \\ &= \nabla\cdot\left(\rho\vec{\Psi}\delta\varphi\right) - \nabla\cdot\left(\rho\vec{\Psi}\right)\delta\varphi - \nabla\cdot\left(\rho\vec{\Psi}\,(\nabla\varphi\cdot\delta\vec{x})\right) + \nabla\cdot\left(\rho\vec{\Psi}\otimes\nabla\varphi\right)\delta\vec{x}\end{aligned} \tag{5.14}$$

Let us define $\tilde{\mu}$ as follows

$$\tilde{\mu} \hat{=} \mu - \frac{\nabla\cdot\left(\rho\vec{\Psi}\right)}{\rho} \tag{5.15}$$

Using the relation (5.14) together with the definition (5.15) for $\tilde{\mu}$, we get

$$\rho\left(\mu\,\delta\varphi + \vec{\Psi}\cdot\delta\nabla\varphi\right) = \rho\,\tilde{\mu}\,\delta\varphi + \nabla\cdot\left(\rho\vec{\Psi}\otimes\nabla\varphi\right)\delta\vec{x} + \nabla\cdot\left(\rho\delta\varphi\vec{\Psi} - \rho\vec{\Psi}\,(\nabla\varphi\cdot\delta\vec{x})\right) \tag{5.16}$$

which is function only of the primary variations considered $\delta\vec{x}$ and $\delta\varphi$.

Let us remark that, in the case (considered in chapter 3) where the thermodynamic potentials, like for instance f in the present case, is supposed to depend on the isotropic non local field $(\nabla\varphi)^2$, a norm for $\nabla\varphi$, the two definitions for $\tilde{\mu}$, namely (3.27) and (5.15), are equivalent. Indeed, in this case, the following relation holds

$$\vec{\Psi} = 2\,\Phi\,\nabla\varphi$$

where we recall Φ to be defined by (3.9d) as $\Phi \triangleq \partial g/\partial\,(\nabla\varphi)^2 = \partial f/\partial\,(\nabla\varphi)^2$. In this case the quantity $\tilde{\mu}$ corresponds to the variational derivative $\tilde{\delta}$ (defined by equation (2.9)) of the specific thermodynamic potential f or g with respect to φ.

$$\tilde{\mu} = \frac{\tilde{\delta} f}{\tilde{\delta}\varphi}_{|T,\rho} = \frac{\tilde{\delta} g}{\tilde{\delta}\varphi}_{|T,P}$$

Let us now study the kinetic energy term $\rho\,\delta(V^2/2)$. Using the expression (5.7) and thereafter the distributive property for the derivative of a scalar product, we get

$$\begin{aligned} \rho\,\delta\frac{V^2}{2} &= \rho\,\vec{V}\cdot\delta(\vec{V}) \\ &= \rho\,\vec{V}\cdot\frac{d}{dt}(\delta\vec{x}) \\ &= \rho\,\frac{d}{dt}\left(\vec{V}\cdot\delta\vec{x}\right) - \rho\,\frac{d\vec{V}}{dt}\cdot\delta\vec{x} \end{aligned} \tag{5.17}$$

Using the relations (5.13), (5.16), and (5.17), we can now express the first variation of the Lagrangian $\delta\mathscr{L}$ as a function of the two independent primary variations $\delta\varphi$ and $\delta\vec{x}$. Using the divergence theorem, (5.11) reads

$$\begin{aligned} \delta\mathscr{L} = & \int_{t_i}^{t_f}\int_{\Omega} -\left(\nabla\cdot\left(\rho\vec{\Psi}\otimes\nabla\varphi\right) + \nabla P + \rho\,\frac{d\vec{V}}{dt}\right)\cdot\delta\vec{x}\,d\mathcal{V}\,dt \\ & - \int_{t_i}^{t_f}\int_{\Omega}\rho\,\tilde{\mu}\,\delta\varphi\,d\mathcal{V}\,dt + \int_{t_i}^{t_f}\int_{\Omega}\rho\,\frac{d}{dt}\left(\vec{V}\cdot\delta\vec{x}\right)\,d\mathcal{V}\,dt \\ & + \int_{t_i}^{t_f}\int_{\partial\Omega}\left[P\,\delta\vec{x} + (\nabla\varphi\cdot\delta\vec{x})\rho\vec{\Psi} - \rho\,\delta\varphi\,\vec{\Psi}\right]\cdot\vec{n}\,d\mathcal{S}\,dt \end{aligned} \tag{5.18}$$

where $\vec{n}$ is the vector unity normal to the boundary surface $\partial\Omega$ of the volume Ω. Using vectorial identities , the third line of (5.18) reads

$$\int_{t_i}^{t_f}\int_{\partial\Omega}\vec{n}\cdot\left[\left(P\,\mathcal{I} + \rho\vec{\Psi}\otimes\nabla\varphi\right)\delta\vec{x}\right] - \left(\rho\,\vec{\Psi}\cdot\delta\varphi\,\vec{n}\right)\,d\mathcal{S}\,dt$$

where $\mathcal{I}$ is the identity matrix. Using the transport theorem (5.10) the last term of the second line of (5.18) reads

$$\left[\int_{\Omega}\rho\,\left(\vec{V}\cdot\delta\vec{x}\right)\,d\mathcal{V}\right]_{t_i}^{t_f}$$

This latter quantity is identically null since variations (and more particularly $\delta\vec{x}$) cancels in t_i and t_f. The latter expression (5.18) for $\delta\mathscr{L}$ is used to derive the set of governing equations as shown in the following.

System of governing equations The fundamental d'Alembert-Lagrange variational principle states that a fluid moves in such a way that the first variation of its Lagrangian $\delta\mathscr{L}$ equals zero. From the expression (5.18) of $\delta\mathscr{L}$, and since the variations $\delta\varphi$ and $\delta\vec{x}$ are independent, the application of the d'Alembert-Lagrange principle $\delta\mathscr{L} = 0$ leads to the following set of equations governing for the flow

- ⋆ Mass balance equation

  $$\frac{d\rho}{dt} = -\rho\nabla\cdot(\vec{V})$$

  which is the continuity equation (5.9)

- ⋆ Momentum balance equation

  $$\rho\,\frac{d\vec{V}}{dt} = -\nabla\cdot\left(\rho\vec{\Psi}\otimes\nabla\varphi\right) - \nabla P \tag{5.19}$$

  where the term $\nabla\cdot\left(\rho\vec{\Psi}\otimes\nabla\varphi\right)$ of the non dissipative part of the stress tensor is the capillary (Korteweg) stress tensor

- ⋆ Thermodynamic equilibrium

$$\tilde{\mu} = 0 \tag{5.20}$$

this relation is consistent with the equilibrium relation (3.28c) derived in the analysis of thermodynamic stability of the equilibrium states in section 3.2.2.

- ⋆ Boundary conditions:
  - specification of a surface force that works on the variations of φ on $\partial\Omega$:

$$\rho\,\vec{\Psi} \tag{5.21}$$

  - surface rate of work associated to the scalar product of the virtual displacement of the boundary $\delta\vec{x}$ with the generalized non-hydrostatic dissipation free stress tensor

$$\left(P\,\mathcal{I} + \rho\,\vec{\Psi}\otimes\nabla\varphi\right) \tag{5.22}$$

In the following we discuss the boundary conditions derived and relate them to the more classical contact angle boundary condition of sharp formulations.

The equilibrium boundary condition (5.21) **and the contact angle** Let us relate the force $\rho\vec{\Psi}$ applying on φ variations on $\partial\Omega$ to the sharp interface boundary condition considering a static contact angle. Let us consider, (as introduced in section 3.2.2) an interaction energy U_b at the system boundary $\partial\Omega$ depending on the phase in contact with $\partial\Omega$, *i.e.* $U_b(\varphi)$. This dependence models the affinity of the boundary with respect to the bulk phases, then the variational principle study yields

$$\rho\vec{\Psi}\cdot\vec{n} + \frac{dU_b}{d\varphi} = 0$$

Let us consider an isotropic dependence of the specific Helmholtz free energy f, and for example prescribe $\vec{\Psi}$ as $\vec{\Psi} = (\lambda/\rho)\,\nabla\varphi$ which is actually the expression corresponding to the thermodynamic closure defined in chapter 3. Moreover and for the sake of simplicity, let us consider that U_b is linear with respect to φ. Then the boundary condition reads

$$\nabla\varphi\cdot\vec{n} = \frac{-1}{\rho\,\lambda}\,\frac{dU_b}{d\varphi}$$

It is a Neumann-type boundary condition on $\partial\Omega$. Let us consider that the length scale of spatial variations of φ reads $h = 1/|\nabla\varphi|$. Then the absolute value of $h/(\rho\,\lambda)(dU_b/d\varphi)$ is equal or less than unity and we introduce the angle ϑ such that $\cos\vartheta = -h/(\rho\,\lambda)(dU_b/d\varphi)$. The boundary condition reads

$$\frac{\nabla\varphi}{|\nabla\varphi|}\cdot\vec{n} = \cos\vartheta$$

and is the diffuse version of the sharp specification of the static contact angle ϑ at the triple line location. If U_b does not depend on φ, the boundary condition (5.21) reads

$$\nabla\varphi\cdot\vec{n} = 0$$

which specifies the contact angle as taking the value $\vartheta = \pi/2$. It is worth noting that in this case, the rate of work of the capillary stress tensor on a virtual displacement of the boundary equals zero since

$$\vec{n}\cdot\left[\left(P\;\mathcal{I}\;+\rho\vec{\Psi}\otimes\nabla\varphi\right)\delta\vec{x}\right] = \lambda\,(\nabla\varphi\cdot\delta\vec{x})\,\nabla\varphi\cdot\vec{n} = 0$$

As a conclusion the specification of the contact angle in the sharp formulation has been shown to be related to the prescription of an interaction energy that depends on φ and that represents the affinity of a surface with regard to the different phases.

Momentum balance equation and specific Gibbs free energy The specific Gibbs free energy g is defined as (*cf.* the equations (3.1) and (3.2))

$$g \triangleq f + \rho \frac{\partial f}{\partial \rho}$$

From the differential (5.1) of f, we get the following identity

$$\nabla g = \mu \, \nabla \varphi + \frac{1}{\rho} \nabla P + \vec{\Psi} \cdot \nabla \nabla \varphi$$

Using the following vectorial identity

$$\rho \vec{\Psi} \cdot \nabla \nabla \varphi = \nabla \cdot \left(\rho \vec{\Psi} \otimes \nabla \varphi \right) - \nabla \cdot \left(\rho \vec{\Psi} \right) \nabla \varphi$$

one has

$$-\nabla P - \nabla \cdot \left(\rho \vec{\Psi} \nabla \varphi \otimes \nabla \varphi \right) = -\rho \, \nabla g + \rho \tilde{\mu} \nabla \varphi$$

The momentum balance equation (5.19) can thus be re-written in the form

$$\frac{d\vec{V}}{dt} = \tilde{\mu} \, \nabla \varphi - \nabla g$$

In the non-dissipative case considered, where (5.20) applies, the momentum balance equation reads therefore

$$\frac{d\vec{V}}{dt} = -\nabla g \tag{5.23}$$

The specific Gibbs free energy g is therefore a first integral for the motion of the fluid. We therefore recover a result already stated for fluid flows with non-local free energies, *e.g.* Roshchin and Truskinovsky [114]. Let us note that this result is consistent with the equilibrium equations (3.28) derived in the study of the equilibrium states in section 3.2.2.

Conclusion on the study of the dissipation free isothermal compressible fluid dynamics with a phase-field (diffuse interface) model

A variational principle applied to a fluid has been used to derive the set of governing equations. In addition to the classical non-dissipative stress tensor $P \mathcal{I}$, a capillary (Korteweg) stress tensor exists due to the dependence of the Helmholtz free energy with respect to the non-local field $\nabla \varphi$. Specific boundary conditions have been derived and related to the classical sharp interface boundary conditions of contact angle. It is worth pointing out that this study allowed to identify the term $\nabla \cdot \left(\delta \varphi \, \rho \vec{\Psi} \right)$ appearing in the expression of the variation of the Lagrangian (*cf.* equation (5.18) where this term has been rewritten using the divergence theorem) as a rate of work. This result is a natural outcome of this study of the dissipation free dynamics, *e.g.* [138]. However for incompressible phase field models, the widely used derivation of the dissipative dynamics (*cf.* [33, 49, 109, 110]) does not identify this term as a rate of work. We consider in the following the consequences of this remark. The equilibrium relations derived in the thermodynamic study in section 3.2.2 have been shown to be consistent with the hereinabove derived set of governing equations.

5.2 Non-isothermal dynamics and dissipative processes: the quasi-compressible case

In this section, the dissipative form of the governing equations is derived by application of thermodynamic first principles. First we derive the expression for the entropy production. Then we study the dissipative processes consistent with the positivity of the entropy production.

5.2.1 Thermodynamic first principles

As shown in section 3.1, for the quasi-compressible case, the thermodynamic description of the fluid in terms of f is degenerate since

$$\frac{\partial \rho}{\partial P} = 0 \tag{5.24}$$

Due to the incomplete description in terms of Helmholtz free energy f, it is not possible to derive the set of governing equations following the variational principle presented in the previous section. As an additional consequence, the pressure P appearing in the conservative part of the stress tensor, as stated by the previous study, cannot be defined from its thermodynamic definition. However, as already stated by Lowengrub and Truskinovsky [89] in their study of quasi-incompressible binary fluids, it is possible to derive the governing equations following an approach based on the first and second laws of thermodynamics. In the following, we propose to apply the first and second thermodynamic laws to our proposed phase field model.

Thermodynamic description and suggested form for the rate of work To apply the first and second laws of thermodynamics, we define the main thermodynamic quantities characterizing a given fluid system, total energy, entropy and the surface heat transfer and work.

Let us first define the specific internal energy and entropy of the fluid. The specific Gibbs energy g as a function of $(P, \varphi, T, \nabla\varphi)$ is well-defined in the quasi-compressible case, as shown in section 3.1. Due to the quasi-compressible hypothesis (5.24), g is a linear function of the pressure P. The specific internal energy $\tilde{u}$ is defined as

$$\tilde{u} \hat{=} g + T\, s - P\, v \tag{5.25}$$

and is a function of $(P, \varphi, T, \nabla\varphi)$ where s is the specific entropy that is defined as (*cf.* equation (3.9))

$$s \hat{=} -\frac{\partial g}{\partial T} \tag{5.26}$$

Let us now define the rate of work $\mathcal{W}$ on a material volume Ω of boundary $\partial\Omega$. The study of the compressible non-dissipative dynamics in section 5.1 leads to the definition of two specific boundary conditions for the fluid flow (5.21) and (5.22). This property suggests the following expression for $\mathcal{W}$

$$\mathcal{W} = \int_{\partial\Omega} \left[-P\,\vec{V} - \left(\vec{V}\cdot\nabla\varphi\right)\rho\vec{\Psi} + \rho\vec{\Psi}\,\frac{d\varphi}{dt} \right] \cdot \vec{n}\, d\mathcal{S} \tag{5.27}$$

Let us also introduce the heat $\mathcal{Q}$ supplied to the system through $\partial\Omega$,

$$\mathcal{Q} \hat{=} -\int_{\partial\Omega} \vec{q}\cdot\vec{n}\, d\mathcal{S} \tag{5.28}$$

where $\vec{q}$ is the heat flux. We have therefore introduced the main thermodynamic definitions allowing to apply the first law of thermodynamics to the fluid system considered.

First law of thermodynamics According to the first law of thermodynamics, the time evolution of the total energy contained in a volume Ω of fluid particles is equal to the sum of the rate of work $\mathcal{W}$ and the heat flux $\mathcal{Q}$ supplied to this volume. Therefore

$$\frac{d}{dt}\int_{\Omega} \rho\left(\tilde{u} + \frac{V^2}{2}\right) d\mathcal{V} = \mathcal{Q} + \mathcal{W} \tag{5.29}$$

It is worth pointing out that in the widely used derivation of the thermodynamically consistent incompressible phase field equations (*cf.* [33, 49, 109, 110]) the rate of work $\mathcal{W}$ is not considered. In our derivation, since the previous study has allowed to identify a rate of work associated with the introduction of the nonlocal dependence of f with respect to φ (*i.e.* $\vec{\Psi} \neq \vec{0}$), we consider the corresponding terms in the expression (5.27) for $\mathcal{W}$. Let us express the corresponding evolution equation for the specific entropy of the fluid in order to apply the

Clausius-Duhem inequality. Using the transport theorem (5.10) and the partial derivative of $\tilde{u}$ resulting from its definition (5.25), the first law of thermodynamics (5.29) reads

$$\int_\Omega \rho\left(\mu\,\frac{d\varphi}{dt} + \vec{\Psi}\cdot\,\frac{d\nabla\varphi}{dt} + \frac{P}{\rho^2}\,\frac{d\rho}{dt} + T\,\frac{ds}{dt} + \vec{V}\cdot\frac{d\vec{V}}{dt}\right) d\mathcal{V} = \mathcal{Q} + \mathcal{W} \tag{5.30}$$

We now introduce the suggested expression (5.27) for $\mathcal{W}$ and use the expression (5.28) for $\mathcal{Q}$. Using the divergence theorem, the RHS of equation (5.26) reads

$$\mathcal{Q} + \mathcal{W} = \int_\Omega \nabla\cdot\left(\vec{q} - P\,\vec{V} - \left(\vec{V}\cdot\nabla\varphi\right)\rho\vec{\Psi} + \rho\vec{\Psi}\,\frac{d\varphi}{dt}\right) d\mathcal{V} \tag{5.31}$$

Let us now study the LHS of (5.29). Using the continuity equation (5.9)

$$\frac{P}{\rho^2}\,\frac{d\rho}{dt} = -\frac{P}{\rho}\,\nabla\cdot\vec{V}$$

Using the analogy (5.8), and the relation (5.14), the following identity holds

$$\rho\,\vec{\Psi}\cdot\frac{d\nabla\varphi}{dt} \;=\; \nabla\cdot\left(\rho\vec{\Psi}\frac{d\varphi}{dt}\right) - \nabla\cdot\left(\rho\vec{\Psi}\right)\,\frac{d\varphi}{dt} - \nabla\cdot\left(\left(\vec{V}\cdot\nabla\varphi\right)\rho\vec{\Psi}\right) + \nabla\cdot\left(\rho\vec{\Psi}\otimes\nabla\varphi\right)\cdot\,\vec{V}$$

Thus, using the quantity $\tilde{\mu}$ defined by (5.15) the above equation reads

$$\rho\left(\mu\frac{d\varphi}{dt} + \vec{\Psi}\cdot\frac{d\nabla\varphi}{dt}\right) = \rho\left(\tilde{\mu}\frac{d\varphi}{dt} + \nabla\cdot\left(\rho\vec{\Psi}\left[\frac{d\varphi}{dt} - \vec{V}\cdot\nabla\varphi\right]\right) + \nabla\cdot\left(\rho\vec{\Psi}\otimes\nabla\varphi\right)\cdot\vec{V}\right)$$

Using the above expression for $\rho(\mu(d\varphi/dt)+\vec{\Psi}\cdot(d\nabla\varphi/dt))$ and the expression (5.31) for $\mathcal{W}+\mathcal{Q}$, the equation (5.30) for the first law reads

$$\int_\Omega \left[\rho\tilde{\mu}\,\frac{d\varphi}{dt} + \rho T\,\frac{ds}{dt} + \vec{V}\cdot\left(\rho\frac{d\vec{V}}{dt} + \nabla P + \nabla\cdot\left(\rho\vec{\Psi}\otimes\nabla\varphi\right)\right)\right] d\mathcal{V} = \int_\Omega -\nabla\cdot\vec{q}\,d\mathcal{V} \tag{5.32}$$

In a local form, equation (5.32) yields

$$\rho T\,\frac{ds}{dt} = -\rho\tilde{\mu}\,\frac{d\varphi}{dt} - \vec{V}\cdot\left(\rho\frac{d\vec{V}}{dt} + \nabla P + \nabla\cdot\left(\rho\vec{\Psi}\otimes\nabla\varphi\right)\right) - \nabla\cdot\vec{q} \tag{5.33}$$

This equation is the evolution equation for the specific entropy of the fluid that was sought for. In the following, using the second law of thermodynamics, we derive the set of governing equations and the consistent expression for the dissipative processes.

Clausius-Duhem inequality Let us introduce the internal dissipation, or rate of entropy production, $\mathcal{R}_s$

$$\mathcal{R}_s \triangleq \rho\,\frac{ds}{dt} + \nabla\cdot\vec{q_s}$$

where $\vec{q_s}$ is an entropy flux. The second law of thermodynamics (Clausius-Duhem inequality) implies that the rate of entropy production $\mathcal{R}_s$ satisfies

$$\mathcal{R}_s \geq 0 \tag{5.34}$$

Therefore, since the temperature is positive, the latter condition implies $T\,\mathcal{R}_s \geq 0$. We assume the entropy flux $\vec{q_s}$ to be equal to $\vec{q}/T$, as classically, *e.g.* [107], therefore the condition (5.34) reads

$$\rho\,T\,\frac{ds}{dt} + T\,\nabla\cdot\left(\frac{\vec{q}}{T}\right) \geq 0$$

It is worth pointing out that in the widely used incompressible derivation of phase field models, as a consequence of the neglect of the rate of work in the application of the first principle, the entropy flux can no longer be considered as equal to $\vec{q}/T$ but rather to $(\vec{q}+\rho\,\vec{\Psi}\,(d\varphi/dt))/T$, *e.g.* Charach and Fife [33]. It has also consequences

on the consequent expression for the heat flux $\vec{q}$ (that can no more reduce to the single classical Fourier conduction term) when, as in our case, $(\partial e/\partial(\nabla\varphi)^2) \neq 0$.

Using the energy balance equation (5.33) inherited from the application of the first law of thermodynamic as an expression for the time derivative of the specific entropy, the Clausius-Duhem inequality (5.34)

$$-\rho\tilde{\mu}\frac{d\varphi}{dt} - \vec{V}\cdot\left(\rho\frac{d\vec{V}}{dt} + \nabla P + \nabla\cdot\left(\rho\vec{\Psi}\otimes\nabla\varphi\right)\right) - \nabla\cdot\vec{q} + T\,\nabla\cdot\left(\frac{\vec{q}}{T}\right) \geq 0$$

Thus

$$-\rho\tilde{\mu}\frac{d\varphi}{dt} - \vec{V}\cdot\left(\rho\frac{dV}{dt} + \nabla P + \nabla\cdot\left(\rho\vec{\Psi}\otimes\nabla\varphi\right)\right) - \frac{\vec{q}}{T}\cdot\nabla T \geq 0 \tag{5.35}$$

This inequality is the Clausius-Duhem inequality valid for the quasi-compressible fluid considered.

Remarks on the non-dissipative set of governing equations The isothermal and dissipation free dynamics is obtained by considering the temperature T as uniform, *i.e.* $\nabla T = 0$, and the internal dissipation as null, *i.e.* $\mathcal{R}_s = 0$. Considering the subsequent Clausius-Duhem inequality in the quasi-compressible case (5.35), yields the corresponding set of governing equations reads

$$\rho\frac{dV}{dt} = -\nabla P - \nabla\cdot(\rho\Psi\otimes\nabla\varphi) \tag{5.36a}$$

$$\tilde{\mu} = 0 \tag{5.36b}$$

Another equivalent form for the non-dissipative part of the stress tensor can be derived as it has been done to obtain equation (5.23) in the isothermal case, it yields

$$-\nabla P - \nabla\cdot(\rho\Psi\otimes\nabla\varphi) = -\rho\nabla g - \rho s\nabla T - \rho\nabla\tilde{\mu} \tag{5.37}$$

The use for the expression (5.27) (suggested by our study of the compressible case in section 5.1) for the rate of work $\mathcal{W}$ allows therefore to recover equivalent equations for both the compressible (equations (5.19) and (5.20)) and the quasi-compressible (5.36) isothermal and dissipation free dynamics.

Conclusion The application of the first and second laws of the thermodynamics to our phase field quasi-compressible model leads to the writing of the expression (5.35) for the rate of internal dissipation. It has been shown that the use of the expression for the rate of work suggested by the study of the compressible isothermal non dissipative case leads to a similar set of governing equations for the corresponding quasi-compressible case. In the following, we study the dissipative processes consistent with the hereinabove derived Clausius-Duhem inequality (5.35).

5.2.2 Dissipative processes

In this section, we study the kinetic equations corresponding to the hereinabove derived Clausius-Duhem inequality.

Let us introduce dissipative contribution $\bar{\bar{\tau}}^D$ for the stress tensor. This leads to the following momentum balance equation

$$\rho\frac{dV}{dt} = -\nabla P - \nabla\cdot\left(\rho\vec{\Psi}\otimes\nabla\varphi\right) + \nabla\cdot\bar{\bar{\tau}}^D \tag{5.38}$$

and to a modified expression for the rate of work $\mathcal{W}$ which, in addition to the expression (5.27), includes the work associated to the dissipative part $\bar{\bar{\tau}}^D$ of the stress tensor. The Clausius-Duhem inequality (5.35) on the rate of entropy production $\mathcal{R}_s$ therefore reads

$$-\rho\tilde{\mu}\frac{d\varphi}{dt} + \bar{\bar{\tau}}^D : \nabla\vec{V} - \frac{\vec{q}}{T}\cdot\nabla T \geq 0 \tag{5.39}$$

In the following we study the kinetic equations compatible with the condition (5.39).

Comments on the choice for the dissipative mechanisms To our knowledge, no information exists on the physical relevance of any particular choice for the dissipative processes across the liquid-vapor interface as a volumetric transition Only a "global" effect of the internal rate of entropy production can be identified experimentally. This is shown as being related to the kinetic relation defined in the appendix A. The kinetic relation resulting from our regularized model of the liquid-vapor flows with phase change is studied in the chapter 7.

General form of the isotropic kinetic relations We consider the linear approximation of the thermodynamics of the irreversible processes and begin with some simplifying assumptions concerning the nature of the dissipative mechanisms. According to this linear approximation, the Clausius-Duhem inequality in this form (5.39) corresponds to a bilinear function of the fluxes $\bar{\bar{\tau}}^D/T$, $(d\varphi/dt)/T$ and $\vec{q}/T$ by the forces $(\partial \vec{V}_i/\partial x_j)$, $-(\partial T/\partial x_i)$ and $\tilde{\mu}$. The general form for the kinetic equations satisfying the Clausius-Duhem inequality (5.39) has been studied by Roshchin and Truskinovsky [114]. In the isotropic case (relevant for our study of boiling flows) a number, say n_{kin}, $n_{kin} = 14$ of kinetic parameters needs to be defined and must satisfy some conditions in order the condition (5.39) to be fulfilled. In the remainder of this study we reduce our analysis to this isotropic case.

Let us consider a second simplifying assumption. In the remainder of this study, we do not consider any cross dependence between the dissipative processes, *i.e.* each flux/force product of the Clausius-Duhem inequality is considered independently. Separately, each product refers therefore to a classical dissipative process

$$\underbrace{-\rho\tilde{\mu}\,\frac{d\varphi}{dt}}_{\text{Phase field}} + \underbrace{\bar{\bar{\tau}}^D : \nabla\vec{V}}_{\text{Mechanical}} \quad \underbrace{-\frac{\vec{q}}{T}\cdot\nabla T}_{\text{Thermal}} \quad \geq 0$$

In the case considered of the relative independence of the dissipative mechanisms, the number n_{kin} of kinetic parameters equals (see Roshchin and Truskinovsky [114])

$$n_{kin} = \underset{\text{(Phase field)}}{1} + \underset{\text{(Mechanical)}}{5} + \underset{\text{(Thermal)}}{2} = 8$$

and let us remark that this simplifying assumptions allows therefore to reduce the number of kinetic parameters from 14 to 8. Let us note also that the non-local character of the thermodynamic variable $(\nabla\varphi)^2$ considered leads to an increased number of coefficient with regard to the classical study. Indeed in the linear approximation of the thermodynamics of the irreversible processes and when only local thermodynamic variables are considered the mechanical dissipative process is known to be described by two (the classical viscosities) parameters (instead of five in our own case) and the thermal dissipative process is know to be described by one single parameter (instead of two in our own case). This result is consistent with the results of the derivation of the dissipative mechanisms for the liquid-vapor phase transition using the van der Waals model (where the "phase- field" dissipative mechanism does not hold). With the van der Waals model $n_{kin} = 7 = (8 - 1)$ kinetics parameters have to be defined in the isotropic case and under the assumption of independence (de-coupling) of the thermal (Fourier) and mechanical (Newton) dissipative mechanisms, *e.g.* [121].

In the following, we present the most classical kinetic relations considered concerning first the phase field dissipation mechanism in the phase-field methods for phase change and then the thermal and mechanical dissipations in diffuse interface models for the phase transition processes and/or for two-phase flows.

Phase field dissipative process The "phase-field" flux/force product appearing in the Clausius-Duhem inequality does not appear in the classical study of the dissipation mechanisms for the liquid-vapor phase transition, *e.g.* [121]. This mechanism is therefore specific to the present phase-field model. Nevertheless, in the remainder of this study, we consider the possibility of taking into account the corresponding dissipation mechanism in order to study its influence on the out of equilibrium structure of the artificial diffuse interface (*cf.* the analytical study in section 7) and the resulting kinetic relation. The introduction of a phase-field dissipation mechanism has been shown to provide interesting properties for the kinetic relation (obtaining of a regularization of the Stefan problem including a kinetic Gibbs-Thomson equation, *cf.* our study of the sharp kinetic relations in section A.2)

in phase-field methods dedicated to the liquid-solid phase transition (*cf.* the analytical study of the interface structure out of equilibrium by Karma and Rappel [72]).[3]

In the case where a phase-field φ is introduced as an indicator function for phase-change problems (*i.e.* non conserved order parameter), the most widely studied and used kinetic relation corresponds to a Ginzburg-Landau type relaxation[4]. A relaxation equation or *AC* (Allen-Cahn) equation governs the evolution of the order parameter that reads

$$\frac{d\varphi}{dt} = -\kappa\tilde{\mu} \tag{5.40}$$

where κ is a positive coefficient classically called mobility. This equation represents a relaxation of the φ field toward the equilibrium condition (5.20). Two non dissipative processes are limiting cases of this relaxation process. They correspond to $\kappa \to \infty$, which yields the equilibrium relation (5.20) as a governing equation (*cf.* the system of non-dissipative equations (5.36)), and to $\kappa \to 0$, which freezes the evolution of the "order parameter". The positivity of the "phase field" dissipative term is ensured since

$$-\rho\tilde{\mu}\,\frac{d\varphi}{dt} = \rho\kappa\tilde{\mu}^2 \geq 0$$

It is worth noting that a Ginzburg-Landau relaxation mechanism has been also considered to model the dissipative processes in a near interface region using a classical thermodynamic description (*i.e.* without any phase field) of the liquid-vapor flow, *e.g.* Shikhmurzaev [124] and Pomeau [111].

In the remainder of this study, we choose to consider the *AC* equation as the possible additional dissipation mechanism in our diffuse interface model for the liquid-vapor phase transition. In chapter 7, we study analytically the consequences of the introduction of the *AC* equation on the dynamics of phase change (kinetic relation).

Viscosity and thermal conductivity Let us consider the mechanical and thermal terms of the Clausius-Duhem inequality. Let us remark that, due to the non-local terms, the introduction of viscosity and heat conductivity ("mechanical" and "thermal" dissipative mechanisms), yields to kinetic coefficients which are *a priori* tensors rather than scalars. Nevertheless, to our knowledge, no attempt has been made to introduce more complex kinetic coefficients than a generalization of the standard and scalar single-phase one, namely the Newtonian viscous stress and the Fourier heat flux

$$\bar{\bar{\tau}}^D = \eta(\nabla\vec{V} + \nabla\vec{V}^T) - \eta\,\frac{2}{3}\,\nabla\cdot\vec{V}\,\mathcal{I} \tag{5.41a}$$

$$\vec{q} = -k\nabla T \tag{5.41b}$$

where the thermal conductivity k and the dynamic viscosity η depend eventually on φ in order to match the bulk values of these dissipative coefficients. The analytical study of the φ dependence of the thermal conductivity k for the solid-liquid phase transition are provided in [1, 49]. Concerning the Newtonian viscosity coefficient, it has been considered as non-constant only for diffuse-interface models without phase change. For example, Badalassi et al. [8] studied numerically isothermal flows of binary density-matched fluids with a variable viscosity coefficient. To our knowledge there exists no analytical study of the consequences of such a choice. Let us also mention the work of Nestler et al. [98] for the study of density matched liquid-solid phase transition with a viscous liquid flow.

Contact line model with the diffuse interface models It is worth noting that similarly to the existence of a volumetric "phase-field" dissipative mechanism, it is possible to introduce a surface dissipative mechanism related to a relaxation toward the equilibrium boundary condition, *e.g.* [112] for the Cahn-Hilliard model,

$$\rho\,\vec{\Psi} + \frac{dU_b}{d\varphi} = 0$$

[3] In fact the phase-field dissipative mechanism allows to recover the classical sharp kinetic relation, the out of equilibrium Gibbs-Thomson relation (presented in section A). However it must be noted that when the entropy flux does not equal q/T it is no longer possible to relate the Gibbs Thomson equation to a kinetic relation in the sense introduced in the appendix A.2.

[4] Other dissipation mechanisms consistent with the condition (5.39) have been studied by Truskinovsky [138] but we do not consider them in the remainder of this study.

derived in our study of the non-dissipative set of governing equations in section 5.1. This boundary condition has been shown to be related to the sharp boundary condition of static contact angle. It has been experimentally attested that the model of a static contact angle is insufficient in many physical situations, *e.g.* Qian et al. [112] . However, our actual study won't consider this additional complexity, since it is not considered as a primary physical mechanism for the mechanism of the boiling crisis (*cf.* our study of chapter 1).

Final form for the set of governing equations Now that the kinetic equations considered in this model have been specified, the final form for the equations of the non isothermal dissipative fluid flow described by the quasi-compressible phase field model can be written. Let us introduce the buoyancy $\vec{F}_g$ as the single external force relevant for our targeted study of nucleate boiling flows and the associated potential energy. The system of governing equations reads

$$\frac{d\varphi}{dt} = -\kappa\tilde{\mu} \tag{5.42a}$$

$$\frac{d\rho}{dt} = -\rho\,\nabla\cdot\vec{V} \tag{5.42b}$$

$$\rho\frac{d\vec{V}}{dt} = -\nabla P - \left(\rho\vec{\Psi}\otimes\nabla\varphi\right) + \vec{F}_g + \nabla\cdot\left(\eta(\nabla\vec{V}+\nabla\vec{V}^T) - \eta\frac{2}{3}\nabla\cdot\vec{V}\,\mathcal{I}\right) \tag{5.42c}$$

$$\rho\,T\frac{ds}{dT} = \nabla\cdot(k\,\nabla T) + \rho\,\kappa\,\tilde{\mu}^2 - \vec{V}\cdot\left[\nabla\cdot\left(\eta(\nabla\vec{V}+\nabla\vec{V}^T) - \eta\frac{2}{3}\nabla\cdot\vec{V}\,\mathcal{I}\right)\right] \tag{5.42d}$$

5.3 Study of the system of governing equations, the evolution equations for the main variables

In this section, we derive the final writing of the non-dimensional system of equations corresponding to the non-isothermal quasi-compressible phase-field model dedicated to liquid-vapor phase transition. This section is organized as follows. In section 5.3.1, from the general form of the governing equations obtained in section 5.2, we derive the governing equation for the temperature T, that has been chosen as a main variable in the thermodynamic model (see section 3.1). In section 5.3.2, we study the non-dimensional form for the set of the governing equations. Then we prescribe the closure relations concerning the temperature dependences of the thermodynamic model. We introduce some assumptions allowing a more simple writing of the equations while the main physical mechanisms of the liquid-vapor phase transition necessary for the study of nucleate boiling flows are still taken into account.

5.3.1 Equation of evolution of the temperature

The temperature T is chosen as the main variable instead of the specific entropy s. In the following we thus re-write the equation of evolution of the entropy (5.33) as an equation of evolution for the temperature. In order to switch the main variable from s to T, we consider the native definition (3.9c) for s (recalled in equation (5.26)). Therefore, s is a function of $(\varphi, (\nabla\varphi)^2, P, T)$, and one has

$$\frac{ds}{dt} = -\left(\frac{\partial^2 g}{\partial T^2}\frac{dT}{dt} + \frac{\partial^2 g}{\partial T\partial\varphi}\frac{d\varphi}{dt} + \frac{\partial^2 g}{\partial T\partial\nabla\varphi}\frac{d\nabla\varphi}{dt} + \frac{\partial^2 g}{\partial T\partial P}\frac{dP}{dt}\right) \tag{5.43}$$

Let us recall that the specific heat capacity c_P is defined by (*cf.* equation (3.67))

$$c_P \triangleq -T\frac{\partial^2 g}{\partial T^2} \tag{5.44}$$

Let us also recall from (3.9) that the partial derivative of g with respect to $(\varphi, P, \nabla\varphi)$ are

$$\frac{\partial g}{\partial\varphi} = \mu$$

$$\frac{\partial g}{\partial\nabla\varphi} = \vec{\Psi}$$

$$\frac{\partial g}{\partial P} = v = \frac{1}{\rho}$$

Thus, equation (5.43) reads

$$\frac{ds}{dt} = \frac{c_P}{T}\frac{dT}{dt} - \left(\frac{\partial \mu}{\partial T}\frac{d\varphi}{dt} + \frac{\partial \vec{\Psi}}{\partial T}\cdot\frac{d\nabla\varphi}{dt} + \frac{\partial v}{\partial T}\frac{dP}{dt}\right)$$

Using the constitutive equations (5.40), (5.41a) , and (5.41b) for the dissipative mechanisms, and the hereinabove expression for ds/dt, equation (5.33) reads

$$\frac{c_P}{T}\frac{dT}{dt} = \left(\frac{\partial \mu}{\partial T}\frac{d\varphi}{dt} + \frac{\partial \vec{\Psi}}{\partial T}\cdot\frac{d\nabla\varphi}{dt} + \frac{\partial v}{\partial T}\frac{dP}{dt}\right) + \frac{1}{T\rho}\left(\bar{\bar{\tau}}^D : \nabla\vec{V} - \rho\tilde{\mu}\frac{d\varphi}{dt}\right) - \frac{\nabla\cdot\vec{q}}{T\rho}$$

Multiplying the above relation by $\rho\, T$ yields

$$\rho c_P \frac{dT}{dt} = \rho\, T\left(\underbrace{\frac{\partial \mu}{\partial T}\frac{d\varphi}{dt} + \frac{\partial \vec{\Psi}}{\partial T}\cdot\frac{d\nabla\varphi}{dt}}_{\text{phase field}} + \frac{\partial v}{\partial T}\frac{dP}{dt}\right) + \bar{\bar{\tau}}^D : \nabla\vec{V} \underbrace{-\rho\tilde{\mu}\frac{d\varphi}{dt}}_{\text{phase field}} - \nabla\cdot\vec{q} \tag{5.45}$$

Equation (5.45) actually corresponds to the evolution equation for the temperature where specific terms due to the phase-field model are specified. These terms are studied and related to the regularization of some classical sharp interface terms in section 5.3.3, where the expression for the thermodynamic potential g derived in section 3 is used. It is worth noting that the dissipative term $\rho\tilde{\mu}\,(d\varphi/dt)$ is often not taken into account in the most widely used phase-field system of governing equations (*e.g.* [72]). This neglect renders inconsistent the system of evolution equations. The consequences on the interface dissipative process are studied in section 7.3 where we consider the equivalent sharp kinetic relation of the phase-field model.

As a partial conclusion we have introduced the equation of evolution of the temperature which is one of the main variables for the description of the liquid-vapor flow with phase change. Let us now consider the main physical scales of the boiling process in order to define the non-dimensional numbers characteristic of the process.

5.3.2 Non-dimensional equations

This study is organized as follows. First we introduce the main physical scales of the nucleate boiling process. Then using the Pi theorem we introduce the set of dimensional numbers characteristic of our model of the nucleate boiling process. Using these non-dimensional numbers we then derive the scaling of the secondary parameters entering the governing equations. Finally we present the non-dimensional writing of the system of governing equations.

Relevant physical scales According to our review of chapter 1, the relevant physical scales corresponding to the description of the nucleate boiling flow with our phase-field diffuse interface model are listed below:

- ⋆ length L
- ⋆ velocity U, the time scale is then $[t] = L/U$
- ⋆ density ρ_0 (arbitrarily chosen as the vapor density for analytical convenience)
- ⋆ δv specific volume difference between vapor and liquid
- ⋆ surface tension σ
- ⋆ T_{ref} the reference level of temperature and ΔT a characteristic temperature difference
- ⋆ specific latent heat at T_{ref}: $\mathcal{L} = T\,(s_{vap} - s_{liq})$
- ⋆ specific heat capacity at constant pressure c_{P0}
- ⋆ thermal conductivity k
- ⋆ g_0, the gravitational acceleration

- ⋆ viscosity η

In addition, the following scales are more specific to our phase field model

- ⋆ the scale for the order parameter is set to 1 and has no physical meaning; for the sake of simplicity, let us recall that we assume that $\varphi = 0$ characterizes the liquid phase and that $\varphi = 1$ characterizes the vapor phase
- ⋆ interface thickness h; let us recall that, though physically consistent, this thickness has a scale dictated by numerical motivations (*cf.* the discussion on the diffuse interface methods in section 2.1.5)
- ⋆ interface dissipation associated to the Ginzburg relaxation toward the equilibrium condition $\tilde{\mu} = 0$. This is scaled by the mobility κ and will be related to the kinetic relation of the phase transition in chapter 7

We defined 14 different physical scales expressed with the help of 4 independent units (m, s, K, kg). Following the Pi theorem, we then use $14 - 4 = 10$ dimensionless numbers. Let us note that 2 physical scales are only related to the diffuse model for the interface, namely h and κ. Only two dimensional numbers will therefore be chosen as including these scales.

Non dimensional numbers and variables The following list provides the 10 non dimensional numbers used for our phase field model for the liquid-vapor phase transition.

- ⋆ Reynolds: $Re = \dfrac{U\,L\rho_0}{\eta}$
- ⋆ Stefan: $St = \dfrac{c_{P0}\,\Delta T}{\mathcal{L}}$
- ⋆ $\gamma = \dfrac{\sigma}{L\rho_0\,c_{P0}\,\Delta T}$
- ⋆ Atwood: $At = \delta v \rho_0$, $At \in [0;1[$
- ⋆ Froude: $Fr = \dfrac{U^2}{g_0\,L}$
- ⋆ $\varepsilon = \dfrac{h}{L}$
- ⋆ Weber: $We = \dfrac{\rho_0\,U^2\,L}{\sigma}$
- ⋆ Peclet: $Pe = \dfrac{\rho_0\,U\,L\,c_{P0}}{k}$
- ⋆ $\theta = \dfrac{T_{ref}}{\Delta T}$
- ⋆ $\kappa^* = \dfrac{\kappa\,\sigma\,L}{U\,h\,\rho_0}$

Let us study the different non classical numbers appearing in this list, namely γ, θ, ε, and κ^*.

The non dimensional number γ is non-classical in the study of the boiling process, it is the ratio of the latent heat to the excess energy (surface tension coefficient). Its choice for the writing of the non dimensional system lays on the necessity to scale the energy terms relative to the balance of momentum (5.36a) and to the balance of entropy (5.45), *i.e.* the kinetic energy and the thermodynamic potentials. Indeed, to our knowledge, in classical description of the boiling process, these scales are not considered as being highly coupled, the growth of the bubble being considered as either purely thermal or purely mechanical. However our model, since consistent, consider such a coupling. The introduction of γ instead of other non dimensional numbers is preferred for the induced simplified writing of the equations it induces. It can be related to the more classical Eckert number E, $E = U^2/(c_{P0}\Delta T)$ since $\gamma = E/We$. However we will see that, using the non-dimensional number γ the final form of the equation for the evolution of the temperature is much simple.

For typical saturated nucleate boiling flows, the superheat of the liquid is low and the vapor can be considered as being near the saturation temperature, the non dimensional number θ is large with respect to 1. The non dimensional number ε is specific of our phase field model and is chosen according to numerical constraints, its value being less than 1. The non dimensional number κ^* is chosen in accordance with the targeted kinetic relation as studied in chapter 7.

Let us precise how the different terms of the system of equations (5.9-5.38, 5.40-5.45), and not directly linked to the physical scales listed hereinabove, are scaled. In the following list the upper-script $\cdot^*$ denotes non dimensional quantities and the brackets $[\ \cdot\ ]$ denotes the scaling for a given quantity. The non dimensional quantity X^* is therefore related to the corresponding dimensional quantity X through $X = X^*\,[X]$. We write

- ⋆ time: $[t] = L/U$
- ⋆ spatial derivatives: $[\nabla] = 1/L$
- ⋆ capillarity coefficient λ in front of the double well function W and the non local field $(\nabla\varphi)^2$: $[\lambda] = \sigma\,h$ according to the study for the excess free energy of section 3.2.4

- ⋆ partial μ and variational $\tilde{\mu}$ derivatives of g with respect to φ: $[\mu] = [\tilde{\mu}] = \sigma/(\rho_0 h)$ their scaling is chosen in accordance to the scaling for the excess free energy, $[\sigma] = [\int F dx] = \rho_0 [g] h$ and to the fact that $[\mu] = [g]$
- ⋆ pressure: its scale is dynamic $[P] = \rho_0 U^2$ and $P^* = (P - P_{eq}(T_{ref}))/[P]$
- ⋆ saturation pressure: $P^*_{eq}(T^*) = (P_{eq}(T) - P_{eq}(T_{ref})/[\Delta P_{eq}]$ with $[\Delta P_{eq}] = \mathcal{L}\Delta T/(T_{ref}\delta v = \mathcal{L}/(\theta\,\delta v)$ since $\Delta P_{eq} \simeq \Delta T\, dP_{eq}/dT(T_{ref})$
- ⋆ equilibrium value for the Gibbs free energy $g_{eq}(T)$: since g_{eq} has been shown to be related to the specific heat capacity c_P (*cf.* equation (5.44) or section 3.4.2) , $[g_{eq}] = (\Delta T)^2\ c_{P0}/T_{ref}$

Let us precise that we use a reduced temperature defined as $T^* \triangleq (T - T_{ref})/\Delta T$.

Now that the non dimensional quantities have been defined, we use in the remainder of this study the following non dimensional form for the set of governing equations and the thermodynamic model and therefore omit the upper-script * for the sake of simplicity.

Non dimensional form for the equations Using the different scalings defined above as well as the set of non-dimensional numbers, the non-dimensional system of equations (5.42) reads:

$$\frac{d\varphi}{dt} = -\kappa\tilde{\mu} \tag{5.46a}$$

$$\rho\frac{d\vec{V}}{dt} = -\nabla P + \frac{\nabla\cdot(\tau^D)}{Re} + \frac{\rho\,\vec{g}}{Fr} - \frac{\varepsilon}{We}\,\nabla\cdot(\nabla\varphi\otimes\nabla\varphi) \tag{5.46b}$$

$$\begin{aligned}\rho\, c_P\,\frac{dT}{dt} = {} & Pe^{-1}\,\nabla\cdot(k\,\nabla T) + (\gamma We/Re)\,\tau^D : \nabla V \\ & -(\gamma We/Fr)\,\rho\, g\cdot V + (\kappa\,\gamma/\varepsilon)\,\rho\,\tilde{\mu}^2 \\ & +(\gamma We)\,\rho\,(T+\theta)\,\frac{\partial v}{\partial T}\,\frac{dP}{dt} \\ & +(\gamma\varepsilon)\,\rho\,(\theta+T)\left(\frac{\partial v}{\partial T}\,\frac{d\,(\nabla\varphi)^2}{dt}\right) \\ & +(\gamma/\varepsilon)\,\rho\,(\theta+T)\left(\frac{\partial\mu}{\partial T}\,\frac{d\varphi}{dt}\right)\end{aligned} \tag{5.46c}$$

$$\frac{d\rho}{dt} = -\rho\,\nabla\cdot V \tag{5.46d}$$

with, according to the study of chapter 3, the expressions for the quasi-compressible thermodynamic quantities $v = 1/\rho$, μ, $\tilde{\mu}$ and c_P read

$$v = (1 - At)v_{vap}(T) + At\,\delta v(T)\,\nu(\varphi) \tag{5.47a}$$

$$\mu = \frac{\partial v}{\partial\varphi}\left(\frac{\varepsilon^2}{2}(\nabla\varphi)^2 + \varepsilon\, We\left[P - \frac{P_{eq}(T)}{At\,S\,t\,\gamma\,We\,\theta}\right]\right) + \frac{\partial\,(v\,W)}{\partial\varphi} \tag{5.47b}$$

$$\tilde{\mu} = \mu - \varepsilon^2\, v\,\nabla(\nabla\varphi) \tag{5.47c}$$

$$\begin{aligned}c_P = {} & -\frac{(T+\theta)\gamma}{\varepsilon}\frac{\partial^2 v}{\partial T^2}\left[W + \frac{\varepsilon^2}{2}\,(\nabla\varphi)^2\right] - We\,\gamma\,(T+\theta)\,\frac{\partial^2 v}{\partial T^2}\,P \\ & + \frac{T+\theta}{At\,S\,t\,\theta}\,\frac{\partial^2 v\,P_{eq}}{\partial T^2} - (1 + T/\theta)\,\frac{d^2 g_{eq}}{dT^2}\end{aligned} \tag{5.47d}$$

It is worth pointing out that the scaling chosen leads to a term of order $O(\varepsilon)$ in the scaling of the "bulk part" of the specific Gibbs free energy with respect to the scaling of g

$$g = \underbrace{\varepsilon\left[v(\varphi)We\left(P - \frac{P_{eq}(T)}{At\,S\,t\,\gamma\,We\,\theta}\right) + \frac{\theta}{\gamma}\,g_{eq}(T)\right]}_{g_{liq}(P,T)+\nu(\varphi)\left(g_{vap}(P,T)-g_{liq}(P,T)\right)} + \underbrace{v\left(W + \frac{\varepsilon^2}{2}\,(\nabla\varphi)^2\right)}_{\text{structure of the interface at equilibrium}} \tag{5.48}$$

As a consequence, the parameter ε actually appears as a measure of the scaling of the equilibrium structure of the interface *versus* the classical EOS. We study in more details this scaling when we study analytically the out of equilibrium structure of the interface in section 7.

Residual closure relations We now need to prescribe the expression and/or value for the different secondary functions and coefficients appearing in the hereinabove equations, namely

Dissipative coefficients	Thermodynamic temperature dependences	
$k(\varphi)$	$\delta v(T)$	$P_{eq}(T)$, *i.e.* $\mathcal{L}(T)$
$\bar{\bar{\tau}}^D$, *i.e.* $\eta(\varphi)$	$v_{vap}(T)$	$c_P(T)$, *i.e.* $g_{eq}(T)$

The first (left) column refers to the study of the dissipative processes. These coefficients are chosen such that the classical bulk phase values are matched in $\varphi = 0$ and $\varphi = 1$, between these values, they are interpolated by classical polynomials. The influence of the choice for the function $k(\varphi)$ on the properties of the out of equilibrium interface structure is studied analytically in section 7 and numerically in section 8.1.2. The second (right) column refers to thermodynamic quantities. For a given fluid they can be found classically in thermodynamic tables. In our case, they are defined using simplifying assumptions in the following section.

5.3.3 Final writing of the governing equations

The goal of this section is to derive the final writing of the system of governing equations.

In this section we specify the complete dependence for g *i.e.* its temperature dependence. To do that we based our choice on the study of the nucleate boiling regime in chapter 1. Then we derive the final form for the evolution equation for temperature (5.46c). We then discuss the choice of a more accurate variable than the pressure P. Finally we present the final form of the system of governing equations as well as how it degenerates in the isothermal case and in the uniform density cases.

Neglect of the coefficient of thermal expansion In the nucleate boiling regime the dominant density variation to consider is the density contrast between the bulk phases. Except for one test case (*cf.* section 8.3.1) we therefore consider the density as a function of the single variable φ: its dependence in P and T are then neglected. As a consequence, $(dv/dT) = 0$, and $\delta_v(T) = v_{vap}(T) = 1$.

According to the expression (5.47a), $(\partial v/\partial\varphi)$ reads

$$\frac{dv}{d\varphi} = At\,\frac{d\nu}{d\varphi}$$

and the time derivative of v reads $(dv/dt) = At\,(d\varphi/dt)$. The continuity equation (5.9) therefore reads

$$\nabla\cdot\rho\vec{V} = -\frac{d\rho}{d\varphi}\frac{\partial\varphi}{\partial t} = \rho^2\,At\,\frac{\partial\nu(\varphi)}{\partial t} \tag{5.49}$$

or

$$\nabla\cdot\vec{V} = -v\,\frac{d\rho}{d\varphi}\frac{d\varphi}{dt} = \rho\,At\,\frac{d\nu(\varphi)}{dt} \tag{5.50}$$

The choice between the forms (5.49) and (5.50) for the continuity equation depends on the choice for the main variable between respectively $\rho\vec{V}$ and $\vec{V}$. Numerically, $\rho\vec{V}$ is chosen as the main variable. In the analytical study of the equations in the next section, the velocity field $\vec{V}$ is chosen as the main variable.

Let us now study the resulting expression for the equation of evolution of the temperature. If v is chosen as independent of T, it is a straightforward calculation to show from the expression (5.47b) for μ that

$$\frac{\partial\mu}{\partial T} = -\varepsilon/(\gamma\,\theta)\,\frac{dv}{d\varphi}\frac{dP_{eq}}{dT}\frac{1}{St}$$

Using the hereinabove simplified expressions, the equation of evolution of the temperature (5.46c) reads

$$\rho\,c_P\frac{dT}{dt} = \frac{\nabla\cdot(k\nabla T)}{Pe} + \gamma\,We\left(\frac{\bar{\bar{\tau}}^D\,:\,\nabla V}{Re} - \frac{\rho\vec{g}\cdot\vec{V}}{Fr}\right) + \frac{\gamma}{\varepsilon}\rho\kappa\tilde{\mu}^2 - \underbrace{\frac{\rho\,(1+T/\theta)}{St}\frac{dv}{d\varphi}\frac{dP_{eq}}{dT}\frac{d\varphi}{dt}}_{\Gamma\mathcal{L}} \tag{5.51}$$

and the term under-braced corresponds to a regularization of the sharp interface term $\Gamma\mathcal{L}$ (where Γ is the mass transfer rate and $\mathcal{L}$ is the latent heat) classically introduced in the sharp interface methods, *e.g.* Juric and Tryggvason [69].

As a partial conclusion we have neglected any other density variation than the one associated to the phase transition. As a consequence the continuity equation simplifies since it actually concerns the single main variable $\vec{V}$ (or $\rho\vec{V}$) and the phase field φ. Moreover the term $(\gamma/\varepsilon)\,\rho\,(\theta+T)(\partial\mu/\partial T)(d\varphi/dt)$ of the equation of evolution of the temperature has been clearly related to a regularization across the interface of the product of the latent heat by the mass transfer rate $\Gamma\mathcal{L}$.

Specific heat capacity and saturation curve From the expression (5.47d) for the specific heat capacity c_P, the independence of v with respect to the temperature T implies the independence of c_P with respect to the pressure P as well as to the non-local term $(\nabla\varphi)^2$. Its expression (5.47d) therefore reads

$$c_P = v\,\frac{T+\theta}{At\,S\,t\,\theta}\,\frac{d^2P_{eq}}{dT^2} - (1+T/\theta)\,\frac{d^2g_{eq}}{dT^2} \tag{5.52}$$

and using the expression (5.47a) for v, one gets

$$\begin{aligned} c_P \;=\; & (1-At)\frac{T+\theta}{At\,S\,t\,\theta}\,\frac{d^2P_{eq}}{dT^2} - (1+T/\theta)\,\frac{d^2g_{eq}}{dT^2} \\ & \frac{d\nu}{d\varphi}\,\frac{T+\theta}{S\,t\,\theta}\,\frac{d^2P_{eq}}{dT^2} \end{aligned} \tag{5.53}$$

The first line depends only on the temperature. The second line corresponds to the difference between the bulk values for the specific heat capacity. This difference is related to the second order derivative of the saturation pressure P_{eq} with respect to the temperature T and is independent of the density contrast modeled by the Atwood number At (*cf.* the study of section 3.4.2). As a consequence the c_P is determined by both the saturation pressure $P_{eq}(T)$ and the function $g_{eq}(T)$. Let us first consider a simple closure law for the saturation pressure $P_{eq}(T)$.

According to the Clapeyron relation (3.73), to have a non zero latent heat, it is necessary that $(dP_{eq}/dT) \neq 0$. Moreover, as shown by its expression (5.53), the specific heat capacity contrast is related to its second derivative. Therefore, the function $P_{eq}(T)$ defines main physical parameters ($\mathcal{L}$ and δc_P) of the liquid-vapor phase transformation. However in order to simplify first the numerical resolution, and since the main heat transport phenomena in nucleate boiling is assumed to be the latent heat transport (*cf.* chapter 1), the function P_{eq} is assumed to be only a linear function of the temperature. Let us note that a similar simplifying assumption has been made and justified by Fouillet [53]. Let us now consider the consequences of such a choice on the model of the specific heat capacity c_P.

In order to define the specific heat capacity c_P, it remains the temperature dependence of g_{eq} to specify (*cf.* equation (5.53)). Now that the saturation pressure has been chosen as a linear function of the temperature, it is obvious from equation (5.53) that only g_{eq} defines the specific heat capacity of the fluid. As a first approximation, we do not consider the variation of c_P with the temperature, and therefore $c_P = 1$. The expression for $g_{eq}(T)$ therefore reads

$$g_{eq}(T) = -\theta\,(T+\theta)\,(\ln(T+\theta)-1)$$

This expression is actually equivalent to the one proposed by Anderson et al. [5], *cf.* section 3.3.2. As a consequence of these choices ($d^2P_{eq}/dT^2 = 0$ and $c_P = 1$), the equation (5.51) of evolution of the temperature reads

$$\rho\,\frac{dT}{dt} = \frac{\nabla\cdot(k\nabla T)}{Pe} + \gamma\,We\left(\frac{\bar{\bar{\tau}}^D\,:\,\nabla V}{Re} - \frac{\rho\vec{g}\cdot\vec{V}}{Fr}\right) + \frac{\gamma}{\varepsilon}\rho\kappa\tilde{\mu}^2 - \frac{\rho\,(1+T/\theta)}{S\,t}\,\frac{d\nu}{d\varphi}\,\frac{d\varphi}{dt} \tag{5.54}$$

where the expression of $\tilde{\mu}$ now reads (*cf.* equation (5.47c))

$$\tilde{\mu} = \frac{dv}{d\varphi}\left(\frac{\varepsilon^2}{2}(\nabla\varphi)^2 + \varepsilon\,We\left[P - \frac{T}{At\,S\,t\,\gamma\,We\,\theta}\right]\right) + \frac{d\,(v\,W)}{d\varphi} - \varepsilon^2\,v\,\nabla(\nabla\varphi) \tag{5.55}$$

It is interesting to note that, due to the independence of v with respect to T, the main variable P only appears explicitly in the equation of evolution for the temperature (5.54) in the expression of $\kappa\tilde{\mu}^2$ which itself can be re-written as $(d\varphi/dt)^2/\kappa$ thanks to the AC equation (5.46a). Moreover the expression of $\tilde{\mu}$ is now linear with respect to both the pressure P and the temperature T which is interesting in view of the AC equation resolution.

Pressure and capillarity, the choice for another main variable Due to the existence of a capillary stress tensor, the pressure field is non uniform at equilibrium. In the following, we introduce a variable that is more numerically convenient.

The following vectorial identity holds

$$\nabla \cdot (\varphi \otimes \nabla\varphi) = \left(\nabla\left[\frac{(\nabla\varphi)^2}{2}\right] + \Delta\varphi\,\nabla\varphi\right)$$

Using the identity

$$\nabla W - \frac{d\,W}{d\,\varphi}\nabla\varphi = 0$$

the momentum balance equation (5.46b) reads

$$\rho\,\frac{d\vec{V}}{dt} = \underbrace{-\nabla\left[P + \frac{W + \frac{\varepsilon^2}{2}(\nabla\varphi)^2}{\varepsilon\,We}\right]}_{\nabla\mathcal{G}} + \underbrace{\frac{\left(\frac{dW}{d\varphi} - \varepsilon^2\Delta\varphi\right)}{\varepsilon\,We}}_{=0 \text{ at planar equilibrium}}\nabla\varphi + \frac{\nabla\cdot\bar{\bar{\tau}}^D}{Re} + \frac{\rho\,\vec{g}}{Fr}$$

At two-phase planar equilibrium, according to the simplified differential equations (3.39) and (3.45) satisfied by the present phase field model (*cf.* section 3.2.4) the under-braced terms are uniformly null. This property leads us to define another main variable instead of P, namely $\mathcal{G}$

$$\mathcal{G} \triangleq P + \frac{W + \frac{\varepsilon^2}{2}(\nabla\varphi)^2}{\varepsilon\,We}$$

$\mathcal{G}$ is uniform at planar two-phase equilibrium. The conservative part of the stress tensor in the balance of momentum is thus simplified. Let us note that the variable $\mathcal{G}$ is in fact the isothermal volumetric Gibbs free energy of the fluid, $\mathcal{G} = \rho\,(g(\varphi, P, T = T_0, (\nabla\varphi)^2) - g_{eq}(T_0))$. Using the variable $\mathcal{G}$, the expression (5.55) for $\tilde{\mu}$ reads

$$\tilde{\mu} = \frac{dv}{d\varphi}\left((At\,\varepsilon\,We)\,\mathcal{G} - \frac{\varepsilon}{St\,\gamma\,\theta}\,T\right) + v\,\left(\frac{dW}{d\varphi} - \varepsilon^2\Delta\varphi\right)$$

This writing is interesting since the term in $(\nabla\varphi)^2$ and W have disappeared; both terms can be numerically costly to evaluate implicitly due to the diffuse nature of the $(\nabla\varphi)^2$ and to the non-linearity of $W(\varphi)$. Let us note that another interesting variable could be $\tilde{P}$

$$\tilde{P} \triangleq P + \varepsilon^2\,(\nabla\varphi)^2$$

which is also uniform at planar equilibrium. This latter variable is used in the analytical study of one-dimensional phase change using the isothermal model in chapter 7.

Concluding remarks The main variables for the governing equations have been specified as being $(\varphi, T, \mathcal{G}, \rho\vec{V})$ and the expressions for all the coefficient of the thermodynamic model derived in chapter 3 have been specified. Simplifying assumptions have been made that are motivated by the necessity for the equations to be easily handled. The final writing of the equations reads

$$\frac{d\varphi}{dt} = -\kappa\left[\frac{dv}{d\varphi}\left((At\,\varepsilon\,We)\,\mathcal{G} - \frac{\varepsilon}{St\,\gamma\,\theta}\,T\right) + v\,\left(\frac{dW}{d\varphi} - \varepsilon^2\Delta\varphi\right)\right] \tag{5.56a}$$

$$\nabla\cdot\rho\vec{V} = \rho^2\,At\,\frac{\partial v(\varphi)}{\partial t} \tag{5.56b}$$

$$\rho\,\frac{d\vec{V}}{dt} = -\nabla\mathcal{G} + \frac{\left(\frac{dW}{d\varphi} - \varepsilon^2\Delta\varphi\right)}{\varepsilon\,We}\,\nabla\varphi + \frac{\nabla\cdot\bar{\bar{\tau}}^D}{Re} + \frac{\rho\,\vec{g}}{Fr} \tag{5.56c}$$

$$\rho\,\frac{dT}{dt} = \frac{\nabla\cdot(k\nabla T)}{Pe} - \frac{\rho\,(1 + T/\theta)}{St}\frac{dv}{d\varphi}\frac{d\varphi}{dt} + \gamma\,We\left(\frac{\bar{\bar{\tau}}^D\,:\,\nabla V}{Re} - \frac{\rho\vec{g}\cdot\vec{V}}{Fr}\right) + \frac{\gamma}{\varepsilon\,\kappa}\rho\left(\frac{d\varphi}{dt}\right)^2 \tag{5.56d}$$

The properties of this system of equations are the following

- ⋆ the modified pressure $\mathcal{G}$ is the isothermal volumetric Gibbs free energy. It does not appear in the equation of evolution of the temperature. The AC equation as well as the momentum balance equation are linear with respect to $\mathcal{G}$
- ⋆ the temperature T does not appear in the momentum balance equation and appears linearly in the expression for $\tilde{\mu}$ in the AC equation as well as in the evolution equation for the temperature (in the convective and in the diffusive terms)
- ⋆ the field φ defines solely the density and therefore the continuity equation relates the divergence of the momentum field to the rate of phase change ($\partial\varphi/\partial t$) independently of other variables.

In the following we write the degeneracy of this system of equations in two cases. In the first case, the density is considered as uniform, as a consequence, the continuity and momentum balance equations are trivial; this case allows to study the coupling between the thermal problem and the mass transfer rate. The system of governing equations is then equivalent to the one used for the study of the liquid-solid phase transition. In the second case, the thermal part is neglected. As a consequence the degenerated system of equation allows to study the coupling between fluid mechanics and mass transfer rate. These two elementary sub-problems will be studied analytically (see chapter 7) and numerically (see chapter 8) before we present the solving of the complete system of equations.

The system of governing equations for the study of the uniform density case reads

$$\frac{d\varphi}{dt} = -\kappa\left[-\frac{dv}{d\varphi}\frac{\varepsilon}{St\,\gamma\,\theta}T + \frac{dW}{d\varphi} - \varepsilon^2\Delta\varphi\right] \tag{5.57a}$$

$$\frac{dT}{dt} = \frac{\nabla\cdot(k\nabla T)}{Pe} - \frac{\rho\,(1+T/\theta)}{St}\frac{dv}{d\varphi}\frac{d\varphi}{dt} + \frac{\gamma}{\varepsilon\,\kappa}\left(\frac{d\varphi}{dt}\right)^2 \tag{5.57b}$$

The system of governing equations for the study of the isothermal case reads

$$\frac{d\varphi}{dt} = -\kappa\left[\frac{dv}{d\varphi}(At\,\varepsilon\,We)\,\mathcal{G} + v\left(\frac{dW}{d\varphi} - \varepsilon^2\Delta\varphi\right)\right] \tag{5.58a}$$

$$\nabla\cdot\rho\vec{V} = \rho^2\,At\,\frac{\partial v(\varphi)}{\partial t} \tag{5.58b}$$

$$\rho\,\frac{d\vec{V}}{dt} = -\nabla\mathcal{G} + \frac{\left(\frac{dW}{d\varphi} - \varepsilon^2\Delta\varphi\right)}{\varepsilon\,We}\nabla\varphi + \frac{\nabla\cdot\bar{\bar{\tau}}^D}{Re} + \frac{\rho\,\vec{g}}{Fr} \tag{5.58c}$$

The latter scaling of the equations with the set of ten non-dimensional numbers concerns their parameterization for the solving of a boundary conditions problem. It will be used in the numerical study of liquid-vapor flows with phase change in chapter 8.

5.3.4 Scaling of the system of governing equations in view of the study of the sharp interface limit

We now turn to the scaling of the equations in view of the asymptotic analysis of the system of governing equations in the limit when the interface layer is thin and isolated. This study is provided in chapter 7.

The sharp interface limit involves taking the non-dimensional parameter $\varepsilon \to 0$ where the length scale L is the typical length scale of the bulk phase processes. To have in this limit finite latent heat, surface tension, density difference, and interface entropy production, it is required to define the scaling of the different non-dimensional parameters entering the system of governing equations (5.56). In particular we set

- ⋆ the density difference (*cf.* δv) at the scale of the vapor density ρ_0, as a consequence the Atwood number reads $At = 1$
- ⋆ the typical temperature difference ΔT at the scale of the temperature level T_{ref}, as a consequence the non-dimensional number θ satisfies $\theta = 1$
- ⋆ the latent heat scale $\mathcal{L}$ at the scale of the sensible heat $c_P\,\Delta T$, as a consequence $[T] = [\mathcal{L}/c_P]$ and the Stefan number reads $St = 1$

⋆ the pressure scale at the scale of the saturation pressure, as a consequence, $[P] = [P_{sat}(T)] = [\rho_0 \mathcal{L}]$ and the velocity scale is thus $[\rho U^2] = [P] \Rightarrow [U] = [\sqrt{\mathcal{L}}]$, thus the Weber number reads $We = \rho_0 \mathcal{L} L/\sigma$

In the following we use the pressure $\tilde{P} = P + \varepsilon^2 (\nabla\varphi)^2$ as the main variable.

Two length scales can be defined from the conservative part of the model

$$h \quad ; \quad l \hat{=} \frac{\sigma}{\rho \mathcal{L}}$$

The length scale h is the typical thickness of the interface as a transition layer, whereas the length scale l is the capillary length typical of the bulk phase process. As a consequence the typical length L is chosen as equal to l and their ratio, the non-dimensional number $\varepsilon = h/l$, is considered as a parameter. As a consequence the non dimensional number γ reads $\gamma = 1$ and the Weber number reads $We = 1$. Let us now consider the dissipative processes. We now take $\kappa \sim \alpha\varepsilon^{-2}$, and $Re = \infty$. The scaling of κ is equivalent to the following restriction on the mobility $\kappa \gg 1/(U\ L)$ and is commonly considered in the studies of the phase field sharp limits, *e.g.* Karma and Rappel [72]. Let us consider a one-dimensional steady state traveling wave of speed $\mathcal{D}$ along an arbitrary X-axis carried by the normal of the interface layer. The non-dimensional abscissa x is scaled by l such that $x \hat{=} X/l$, and we denote

$$\cdot_{,x} \hat{=} \frac{\partial \cdot}{\partial x}$$

the system of governing equations reads

$$\frac{\varepsilon^2}{\alpha} (\mathcal{D} - V)\ \varphi_{,x} = \varepsilon \frac{d\nu}{d\varphi}\left(\tilde{P} - T\right) + v \left(\frac{dW}{d\varphi} - \varepsilon^2 \varphi_{,xx}\right) + \frac{d\nu}{d\varphi}\left(W - \frac{\varepsilon^2}{2}\varphi_{,x}^2\right) \tag{5.59a}$$

$$(\rho V)_{,x} = -\rho^2 \frac{\partial \nu}{\partial \varphi} (\mathcal{D} - V)\, \varphi_{,x} \tag{5.59b}$$

$$(V - \mathcal{D})\ \rho V_{,x} = -\tilde{P}_{,x} \tag{5.59c}$$

$$(V - \mathcal{D})\ \rho\, T_{,x} = \frac{(k\, T_{,x})_{,x}}{Pe} - (V - \mathcal{D})\ \rho\ (1 + T) \frac{d\nu}{d\varphi} \varphi_{,x} + (\mathcal{D} - V)^2\ \frac{\rho\varepsilon}{\alpha} (\varphi_{,x})^2 \tag{5.59d}$$

It is worth noting that the writing of the LHS of the momentum balance equation (5.59c) lies on the following identity valid for a one dimensional system

$$\left(\frac{\varphi_{,x}^2}{2}\right)_{,x} = \varphi_{,xx}\, \varphi_{,x}$$

For the canonical case of uniform density, the system reads (*cf.* the system (5.57))

$$\frac{\varepsilon^2}{\alpha} \mathcal{D}\, \varphi_{,x} = \varepsilon \frac{d\nu}{d\varphi} T - \left(\frac{dW}{d\varphi} - \varepsilon^2 \varphi_{,xx}\right) \tag{5.60a}$$

$$\mathcal{D}\, T_{,x} = \frac{(k\, T_{,x})_{,x}}{Pe} - \mathcal{D}\ (1 + T) \frac{d\nu}{d\varphi} \varphi_{,x} + \mathcal{D}^2 \frac{\varepsilon}{\alpha} (\varphi_{,x})^2 \tag{5.60b}$$

whereas for the isothermal model, it reads (*cf.* the system (5.58))

$$\frac{\varepsilon^2}{\alpha} (\mathcal{D} - V)\ \varphi_{,x} = \varepsilon \frac{d\nu}{d\varphi} \tilde{P} + v \left(\frac{dW}{d\varphi} - \varepsilon^2 \varphi_{,xx}\right) + \frac{d\nu}{d\varphi}\left(W - \frac{\varepsilon^2}{2}\varphi_{,x}^2\right) \tag{5.61a}$$

$$(\rho V)_{,x} = -\rho^2 \frac{\partial \nu}{\partial \varphi} (\mathcal{D} - V)\, \varphi_{,x} \tag{5.61b}$$

$$(V - \mathcal{D})\ \rho V_{,x} = -\tilde{P}_{,x} \tag{5.61c}$$

Conclusion on the derivation of the system of governing equations

In this chapter we have derived the system of governing equations for the liquid-vapor flows with phase change.

We have derived the expression for the non-dissipative stress tensor as well as the boundary conditions in the compressible case using an Hamiltonian principle (see section 5.1). We have identified the expression for the

rate of work. Based on this results we have derived the dissipative system of governing equations in the quasi-compressible case using the first and second principles of thermodynamics (see section 5.2). Using the linear approximation of the thermodynamics of the irreversible processes, we have specified the dissipative processes considered. In addition to the classical Fourier heat conductivity and Newtonian viscosity, we also consider a Ginzburg-Landau relaxation toward the equilibrium condition $\tilde{\mu} = 0$. This additional dissipative process will be related to the kinetic relation of the liquid-vapor phase transition in chapter 7. We have then introduced the main scales of the description of the nucleate boiling flow with the help of a phase field model (see section 5.3). The non-dimensional writing of the system of governing equations has been introduced. Finally we have specified the temperature dependences of the thermodynamic model and introduced the variable $\mathcal{G}$ which will be used instead of the pressure in the numerical study. The subsequent final writing of the system (5.56) of governing equations has been shown to be more easy to handle thanks to the simplifications considered although it allows to model the essential features of the nucleate boiling flows. It contains a set of ten non-dimensional numbers allowing to parameterize a study of nucleate boiling flow. To study the steady state mass transfer rate, we have introduced a scaling of these parameters to derive the non-dimensional system of governing equations (5.59), that in addition to the two parameters for the dissipative processes (α for the kinetics and Pe for the heat conduction), depends on the ratio of the interface thickness with the capillary length ε. We solve this system of equations using matched asymptotic expansions in chapter 7.

Chapter 6

Study of the stability of homogeneous states

The study of the stability of homogeneous states constitutes a first test of the physical behavior of our two-phase fluid model. We consider the quasi-compressible non-isothermal phase-field model for the liquid-vapor dissipative flows with phase change[1] . In this model the bulk phases liquid and vapor are considered as incompressible, and this model claims thus to be a consistent regularization of the classical sharp interface model with incompressible bulk phases. In this sharp model, since the compressibility χ_T of the fluid is zero, the liquid and the vapor are modeled as unconditionally marginally stable (*cf.* the Gibbs-Duhem criterion of stability (2.4) presented in the framework of the van der Waals' model). The goal of this chapter is to demonstrate the important properties of our model concerning its ability to recover such a description of the stability of the homogeneous states. This is indeed one of the desired properties for the model (point 6 of the requirements expressed in page 53). In particular, the choice for a fifth degree polynomial for the interpolation function $\nu(\varphi)$ will be thus fully justified.

This chapter is organized as follows. First we motivate this study of the stability of the homogeneous states by reviewing the previous and related studies of the stability of homogeneous states using diffuse interface models (see section 6.1). We show that the influence of the thermodynamic formulation on the bulk phase stability properties has been insufficiently determined. We study in section 6.2 the general set of governing equations for the problem of the stability of homogeneous phases. We derive the dispersion relation that governs the stability. Then, in section 6.3, we first derive the condition of stability for the non-isothermal dissipative case. It is shown that for most simple cases (isothermal, non-dissipative, non-heat-conducting material, or no density difference between the phases), it is also possible to provide a more precise analysis of the dynamics (than the single study of the stability condition), including the study of its dispersive nature. From the conditions of stability in all these cases is derived a definition for a $\varphi-$spinodal region: the belonging of the homogeneous state to this $\varphi-$spinodal region determines its stability. The possible equilibrium states have been studied in section 3.4.1 for different interpolation functions for the density $\rho(\varphi)$. Using these results, we first study in section 6.4 the case of the linear interpolation of the density ρ with respect to the phase field φ that illustrates the main properties of the general expression for the dispersion relation. We then study in section 6.5 the stability of the homogeneous states with higher order polynomials for the function $\rho(\varphi)$. We show how the dispersion relation, and therefore the condition of stability of the homogeneous states, is greatly modified by this choice and show how it allows to actually control the limit of metastability of the bulk phases.

6.1 Review of the study of the stability of homogeneous states using diffuse interface models

The stability of homogeneous states with a diffuse interface formulation has already been investigated by several authors. In the following we first briefly review some studies of the stability in the context of "classical" diffuse interface models. Then we focus on the special case of phase field models (as "artificial" diffuse interface models introduced to regularize a sharp interface formulation). The main difference between these two categories of

[1] whose thermodynamic expression (3.55) has been derived in chapter 3 and whose system of dynamics equations (5.56) has been derived in chapter 5

models lies indeed on the meaning of the order parameter[2]. As a consequence the thermodynamic potential has a different structure in the phase field case as in the "classical" case (dependence of the thermodynamic potential with respect to the order parameter: in our model it is the phase field φ, the dependence concerns the choice for the double well function $W(\varphi)$ and of the interpolation function $\nu(\varphi)$). It is necessary to determine the influence of this specific structure on the condition of stability of a given homogeneous state. This influence has not been, to our knowledge, fully determined, and its determination is indeed the goal of the present study.

To provide a common framework for the following review of the study of the condition of stability of homogeneous states, let us introduce a generic two-phase diffuse interface model (the non-local dependence is not considered in the following discussion and is therefore not included in this generic model even though it is a key ingredient for the diffuse interface model)

$$K(X) = K_1 + (K_2 - K_1)\ \nu_K(X) + K_m(X)$$

where

- ⋆ K is the thermodynamic potential relevant for description of the phase transition considered
- ⋆ X is the order parameter of the phase transition
- ⋆ the subscripts 1 and 2 refers to the two possible bulk states considered
- ⋆ K_m is a model for the mixture that is actually a double well function which is minimal in X_1 and X_2, $K_m(X_1) = K_m(X_2) = dK_m/dX(X_1) = dK_m/dX(X_2) = 0$
- ⋆ ν_K is an interpolation function whose value is 0 for $X = X_1$ and 1 for $X = X_2$

For the sake of simplicity we do not consider any dependence of K with respect to other thermodynamic variables.

6.1.1 Stability of homogeneous states using classical diffuse interface models

By classical diffuse interface models, we refer to diffuse interface models for which the order parameter of the phase transition is a classical thermodynamic variable, *e.g.* the density $X = \rho$ in the van der Waals' model. Let us briefly review the corresponding studies of stability of homogeneous states.

Compressible materials: a model related to the van der Waals' model Ngan and Truskinovsky [99] proposed a purely dissipative regularization to model the martensitic phase transitions (which is in fact a model similar to the non-isothermal van der Waals' model)[3]. In this model, the double well function $K_m(X)$ is the function W of our model (*cf.* equation (3.42)) and the interpolation function $\nu_K(X)$ is considered as linear. Ngan and Truskinovsky studied the stability condition for homogeneous states for viscous heat-conducting materials. The authors derived the expression of the relation dispersion that characterizes the linear stage of evolution of a perturbation of an homogeneous state. Using the Hurwitz criterion, this condition is shown to be the positivity of the isothermal acoustic velocity. This result is consistent with the classical Gibbs-Duhem criterion of stability for compressible fluids. In the case of non-heat conducting materials, the stability condition is shown to be related to the positivity of the adiabatic acoustic velocity, which is shown to be less restrictive than the isothermal stability condition. The choice for a linear interpolation function differs mainly from our actual choice of a fifth order polynomial. Moreover the incompressibility of the bulk phase considered in our model implies the classical Gibbs-Duhem criterion to be irrelevant. This study is therefore not of interest for our model. However similar results should be obtained while dealing with compressible phase field model.

[2]This differentiation between the two categories ("classical" and "artificial") of diffuse interface models has been introduced in section 2.1.5 when we presented the motivation for the development of the present phase field model.

[3]Since model studied in [99] is related to the van der Waals' model, the reader can refer to our presentation of the model in section 2.2.2: In the expression (2.5) for the thermodynamic potential, namely the Helmholtz free energy $K(X) = F_{cl}(\rho)$, the double well function F_m is $W(\rho)$ and the interpolation function ν_F is linear $\mu_{sat}(T_0)\,\rho$. This expression is actually the one considered in [99].

Quasi-incompressible fluids Lowengrub and Truskinovsky [89] proposed a quasi-incompressible Cahn-Hilliard model for the binary fluids. This quasi-incompressibility is in fact similar to the property of our model that deals with incompressible liquid and vapor phases (that we call quasi-compressibility in the context of liquid-vapor phase transition). The order parameter of the phase transition is the concentration c of one physical species and is therefore conserved, it obeys a Cahn-Hilliard evolution equation. The density of the fluid is considered as varying linearly with respect to the concentration. This linear interpolation of the density can be shown to be equivalent to a linear choice for the interpolation function $\nu_K(c)$. In [89] and [83], using this model, the stability of both homogeneous states and two-phase equilibrium solution is studied for a two-dimensional system both analytically and numerically in the isothermal non-viscous case. Since this model is closely related to our quasi-compressible phase field model, we therefore need to extend this study to the non-isothermal viscous case and moreover to study the influence of our choice of a fifth order polynomial for the interpolation function of the density.

Fully incompressible fluids Krekhov and Kramer [81] proposed an analysis of the Cahn-Hilliard and Allen-Cahn spinodal decomposition dynamics using both analytical (one-dimensional) and numerical (two-dimensional) studies of the process. In the model studied in [81], the expression of the Helmholtz free energy F can be related to our generic expression for the thermodynamic potential $K = F$ where $\nu_F(\varphi)$ is a linear function. Once again this latter choice (linearity of the interpolation function) differs of our actual choice and the consequences therefore needs to be investigated.

Let us also note that the stability of phase transition fronts with diffuse interface models has also been investigated for several models, *e.g.* Benzoni-Gavage et al. [13] for the study of the isothermal van der Waals' model. The model studied in [13] has not a prescribed expression for F_{cl} and therefore does not consider the influence of its choice on the stability.

The stability of homogeneous states using "classical" diffuse interface models *versus* the stability using phase field models In all these studies of stability of homogeneous states, the "mixture" energy K that models the states inside the spinodal region is the sum of a double well function K_m and of a linear interpolation ν_K between the bulk energies with respect to the order parameter of the transition. It is worth noting that for the latter models, the choice of a linear interpolation seems natural and justified since they deal with classical thermodynamic variables (either concentration or density) as the order parameter of the phase transition. Nevertheless, in the context of phase field models ($X = \varphi$), this linearity induces the existence of undesirable equilibrium states (phase field value different from $X_1 = \varphi_1$ or $X_2 = \varphi_2$, see section 3.4.1) that can actually be stable (see section 6.4).

6.1.2 Study of the stability of homogeneous states with the phase field models

The general choice for the interpolation function $\nu_K(\varphi)$ In phase-field models, of interest in the present work, high degree (degree 3 or 5) polynomials are commonly used as interpolation functions for the modeling of the energy of mixture, *e.g.* [146]. This choice is classically justified by the study of stability of the homogeneous states, *i.e.* corresponding to the bulk phase field values 0 and 1. The justification of the choice for fifth degree polynomials is indeed based on the single study of stability of the homogeneous states 0 and 1 using the Gibbs-Duhem stability analysis (a justification similar to the one provided in section 3.2.3), *e.g.* Wang et al. [146]. As a consequence this justification does not consider the stability of other possible equilibrium states. Moreover it does not allow to analyze the particular dynamics of the linear stage of the phase separation process.

Let us briefly review some more complete studies of the stability of homogeneous states with the help of phase field (or related) models.

Weakly non-local compressible media Roshchin and Truskinovsky [114] studied the model of a weakly non-local compressible medium by considering the internal energy u of the medium to depend, in addition to the classical thermodynamic variables (density ρ and specific entropy s) on an abstract additional degree of freedom as well as on its spatial derivatives. The latter additional dependence can thus be related to the introduction of the phase field variable considered in our model. In [114], the study of the stability of homogeneous state is considered for non-viscous, non-thermally conducting medium with a generic expression for the thermodynamic

potential. The relation dispersion that characterizes the linear stage of evolution of a perturbation of an homogeneous state is derived. However the influence of heat conductivity (that needs to be taken into account in our model) and of viscosity on the stability condition is not considered. Moreover, the influence of the choice of any particular dependence of the thermodynamic potential with respect to the phase field variable is not considered. The condition of stability derived is therefore attempted to be quite different with our phase field model where the compressibility is not taken into account but where the thermal conductivity is.

The control of the equilibrium states Umantsev [141] studied the stability condition of homogeneous states in the case of thermodynamic systems governed by the temperature and an ordering field, that can be formally related to our artificial phase field variable. This study establishes the stability conditions in both isothermal and adiabatic conditions. It is shown that the homogeneous and inhomogeneous states of equilibrium which are unstable under isothermal conditions can be stable under adiabatic conditions. This property will be studied with our model in the case of homogeneous states of equilibrium, that in addition to the Umantsev's model, takes into account a density difference between incompressible bulk phases (quasi-compressible case).

In [141], an expression for the thermodynamic potential is proposed where the interpolation function $\nu(\varphi)$ is a primitive of the square root of the double well function $\sqrt{W}$ (*i.e.* in our case where W is a polynomial of degree 4, $\nu(\varphi)$ is a polynomial of degree 3). This choice for the interpolation function provides a necessary gain in the control of the possible equilibrium states. Indeed the phase field values 0 and 1 are always equilibrium solutions (*cf.* section 3.4.1). Nevertheless it will be shown in section 6.5, that this is not sufficient to control the stability of the homogeneous states when the parameter for the interface thickness h is considered as artificial, which is the case in the present study. In the model considered in [141] there exists another possible equilibrium state in addition to the equilibrium states 0 and 1. This state is shown to be stable for temperature values out of a finite range around the two-phase equilibrium. This is not desirable for our model, since only the states 0 and 1 are actually meaningful. We will study how the choice of a fifth order polynomial, made for the interpolation function of our model, modifies the stability of such additional equilibrium states.

General remarks concerning the existence of additional equilibrium states For a phase-field model with high degree polynomials, other phase field values than 0 or 1 correspond to equilibrium states. This is in contrast with the classical sharp interface models where only two "discrete" phases are considered. For given classical thermodynamic conditions (say given pressure P and temperature T) and since these latter states do not correspond to any of the bulk phases considered, they should likely be unstable. To our knowledge, the ability of a phase field model to provide the instability of these other possible equilibrium states has never been studied in the case of a fifth order polynomial interpolation function and when a density difference between the phases is taken into account; this situation corresponds to our quasi-compressible phase field model and we therefore propose to study this point.

In order to emphasize the influence of the choice of the polynomial for the interpolation function on the dynamics of the phase separation process, we also consider the case of linear and third degree polynomial interpolations. The comparison between the stability properties of a phase field model with these different interpolation functions, allows to show the necessity of dealing with a polynomial of degree (at least) 5. Moreover the unstable processes of phase separation in the case of higher degree polynomials has similar features to the linear case and we use this similarity to characterize this dynamics.

6.2 General study of the perturbation of homogeneous states: The derivation of the dispersion relation

In this section we derive from the set of governing equations (5.42) derived in chapter 5 the expression of the dispersion relation corresponding to the linear stage of evolution of a perturbation of an homogeneous state at equilibrium.

6.2.1 System of governing equations

Let us consider the fluid to be described by the Gibbs free energy of our quasi-compressible model[4] and all the set of simplifications presented in section 5.3.3 (in particular the neglect of the thermal expansion). For the sake of generality, we consider a Ginzburg-Landau relaxation *i.e.* $\kappa \neq +\infty$. The system of governing equations for the one-dimensional problem considered (along an arbitrary $x-$axis) therefore reads (*cf.* the set of governing equations (5.56))

$$-\rho\, V_{,x} = \frac{d\rho}{d\varphi}\left(\varphi_{,t} + V\,\varphi_{,x}\right) \tag{6.1a}$$

$$\left(V_{,t} + V\,V_{,x}\right) = -g_{,x} + \tilde{\mu}\,\varphi_{,x} - s\,T_{,x} + \frac{\left(\eta\,V_{,x}\right)_{,x}}{\rho} \tag{6.1b}$$

$$\begin{aligned}\rho\, c_P\,\left(T_{,t} + V\,T_{,x}\right) &= \left(k\,T_{,x}\right)_{,x} - \rho T\,\frac{dP_{sat}}{dT}\frac{dv}{d\varphi}\left(\varphi_{,t} + V\,\varphi_{,x}\right)\\ &\quad + \rho\kappa\left(\frac{d\rho}{d\varphi}g^* + \lambda\,\left(\varphi_{,xx} - \frac{1}{h^2}\frac{dW}{d\varphi}\right)\right)^2\end{aligned} \tag{6.1c}$$

$$\frac{\rho\,\left(\varphi_{,t} + V\,\varphi_{,x}\right)}{\kappa} = \frac{d\rho}{d\varphi}g^* + \lambda\,\left(\varphi_{,xx} - \frac{1}{h^2}\frac{dW}{d\varphi}\right) \tag{6.1d}$$

where g^* is the gap between the value of the specific Gibbs free energy g with regard to its value $g_{eq}(T)$ at two-phase planar equilibrium, *i.e.* $g^* \,\hat{=}\, g - g_{eq}(T)$, V is the x component of the velocity $\vec{V}$ and where the partial derivative with respect to time t, resp. x, are denoted $\cdot_{,t}$, resp. $\cdot_{,x}$. Let us note that the expression for the non-dissipative part of the stress tensor in the momentum balance equation (6.1b) corresponds to equation (5.37).

6.2.2 Parameter of the homogeneous state at equilibrium

We study the perturbation around a *homogeneous state at equilibrium* (the corresponding equilibrium quantities are denoted $\cdot^{hs}$). Let us first define this state and then linearize the variables around this state.

According to our study of the equilibrium states, we have (*cf.* section 3.2.2)

$$\begin{aligned} g^*(x,t) &= g^{*hs}\\ \varphi(x,t) &= \varphi^{hs}\\ T(x,t) &= T^{hs}\\ V(x,t) &= V^{hs}\end{aligned}$$

For the sake of simplicity, we do not consider any overall bulk motion, *i.e.* $V^{hs} = 0$. The study of the stability of the state hs is therefore parameterized by the nature of the bulk phase considered, *i.e.* the value φ^{hs}, and the values of the classical thermodynamic variables, namely the specific Gibbs free energy g^{*hs} and the temperature T^{hs}. The parameters φ^{hs} and g^{*hs} are related by the equilibrium condition (3.28c) $\tilde{\mu} = 0$. This relation has been studied in section 3.4.1 where it has been shown that the equilibrium condition can be written as (*cf.* equation (3.62))

$$\begin{aligned}\rho^{hs}\,\mu(\varphi^{hs}, g^{*hs}) &= 0\\ &\Leftrightarrow\\ \frac{\lambda}{h^2}\frac{dW}{d\varphi}^{hs} - \frac{d\rho}{d\varphi}^{hs} g^{*hs} &= 0\end{aligned} \tag{6.2}$$

The results derived in section 3.4.1 will be used in sections 6.4 and 6.5 where we determine the stability of homogeneous states for given values of the physical parameters g^* and T.

[4] derived in chapter 3, *cf.* equation (3.55) *i.e.* from the generic expression of the diffuse interface model introduced in section 6.1, we consider the thermodynamic potential as being the specific Gibbs free energy, $K = g$. The double well function reads $g_m(\varphi) = vW$ where v is the specific volume interpolated by the function $\nu(\varphi)$ and $W(\varphi)$ is the order 4 polynomial defined by equation (3.42). The potential g is interpolated by the same function $\nu(\varphi)$. In addition, the non-local dependence considered corresponds to $\Phi = v\lambda/2$ where $\Phi = (\partial g/\partial\,(\nabla\varphi)^2)$.

6.2.3 Linear stage of perturbation

Let us linearize the system of governing equations (6.1) around the state hs by introducing small perturbations, denoted $\cdot'$, of all the fields. Since $V^{hs} = 0$, the velocity $V = V'$ is itself a perturbed quantity. The set of linearized equations reads

$$-\rho^{hs} V'_{,x} = \frac{d\rho}{d\varphi}^{hs} \varphi'_{,t} \tag{6.3a}$$

$$V'_{,t} = -s^{hs} T'_{,x} - g'_{,x} + \left(\frac{\eta}{\rho}\right)^{hs} V'_{,xx} \tag{6.3b}$$

$$(\rho c_P)^{hs} T'_{,t} = k^{hs} T'_{,xx} + \frac{T^{hs}}{\rho^{hs}} \frac{dP_{sat}}{dT} \frac{d\rho}{d\varphi}^{hs} \varphi'_{,t} \tag{6.3c}$$

$$\frac{\rho^{hs}}{\kappa} \varphi'_{,t} = -\frac{\partial \rho\mu}{\partial \varphi} \varphi' - \frac{\partial \rho\mu}{\partial g^*} g^{*'} + \lambda \varphi'_{,xx} \tag{6.3d}$$

where $g^{*'} = g' - T' \, (\rho dg_{eq}/dT)^{hs}$ and where, since $\rho\,\mu$ reads

$$\rho\mu = -\frac{d\rho}{d\varphi} g^* + \frac{\lambda}{h^2} \frac{dW}{d\varphi}$$

we have

$$\frac{\partial \rho\mu}{\partial g^*}_{|\varphi} = -\frac{d\rho}{d\varphi}^{hs} \tag{6.4a}$$

$$-\frac{\partial \rho\mu}{\partial \varphi}_{|P,T} = \frac{d^2\rho}{d\varphi^2}^{hs} g^{*hs} - \frac{\lambda}{h^2} \frac{d^2W}{d\varphi^2}^{hs} \tag{6.4b}$$

It is worth noting that the term of the balance of energy (6.1c) associated with the Ginzburg-Landau dissipation (second line of its RHS) does not appear in its linearized form (6.3c). Indeed, because it is quadratic in $\tilde{\mu}$ (and because $\tilde{\mu}^{hs} = \mu^{hs} = 0$ by definition of an homogeneous state at equilibrium) this linearized term is zero. For the same reason (because $\tilde{\mu}^{hs} = 0$ and $(\varphi_{,x})^{hs} = 0$)), the linearized expression for the stress tensor simplifies because the linearized contribution of $\tilde{\mu}\ \varphi_{,x}$ around its hs value is zero.

6.2.4 Linear system for the amplitudes

For the sake of simplicity, we consider that the system is of infinite extend. We introduce solutions proportional to $e^{\omega t + \mathbf{I} k_x x}$, where the wave number k_x is thus a real, *i.e.* $\Im(k_x) = 0$ and where ω is the angular frequency. The homogeneous state will be said to be unconditionally stable if for any wave number k_x, the angular frequency ω has a non-positive real (growth rate) part, *i.e.* $\Re(\omega) < 0$. The system of linearized equations (6.3) for the amplitudes of the perturbed solutions reads (using, for the sake of simplicity, the same notation for the coefficient as for the variable it corresponds to, *i.e.* for a variable y, $y = ye^{\omega t + \mathbf{I} k_x x}$)

$$\begin{aligned}
\omega \frac{d\rho}{d\varphi}^{hs} \varphi' & & & + \mathbf{I} k_x \rho^{hs} V' &= 0 \\
& & \mathbf{I} k_x s^{hs} T' \quad + \mathbf{I} k_x \, g' \quad + \left(k_x^2 \left(\frac{\eta}{\rho}\right)^{hs} + \omega\right) V' &= 0 \\
\omega \, \frac{T^{hs}}{\rho^{hs}} \frac{dP_{sat}}{dT} \frac{d\rho}{d\varphi}^{hs} \varphi' & - \left(\omega \, (\rho c_P)^{hs} + k_x^2 \, k^{hs}\right) T' & &= 0 \\
\alpha_{\varphi,\varphi} \, \varphi' & & + \frac{d\rho}{d\varphi}^{hs} \frac{dg_{eq}}{dT} \, T' \quad - \frac{d\rho}{d\varphi}^{hs} g' &= 0
\end{aligned} \tag{6.5}$$

where the coefficient $\alpha_{\varphi,\varphi}$ reads

$$\alpha_{\varphi,\varphi} \hat{=} \omega \frac{\rho^{hs}}{\kappa} + \lambda \, k_x^2 + \frac{\lambda}{h^2} \frac{d^2W}{d\varphi^2}^{hs} - \frac{d^2\rho}{d\varphi^2}^{hs} g^{*hs}$$

We are looking for non-trivial solutions $(\varphi', T', g', V') \neq 0$ of the linear system (6.5) of equations. Therefore, in the following, we study the conditions of nullity of the determinant of this linear system.

6.2.5 Matrix of the system of linear equations

A simple relation between the velocity and phase-field perturbations For the sake of simplicity and without any loss of generality, let us use the first equation (6.3a) of the linearized system (continuity equation) to express V' as follows

$$V' = \frac{\mathbf{I}\omega}{k_x \rho^{hs}} \frac{d\rho^{hs}}{d\varphi} \varphi' \tag{6.6}$$

This relation shows that the perturbed velocity is directly proportional to the perturbation of the phase field (and has a phase difference of $\pi/2$). This property is characteristic of the present quasi-compressible model. It is indeed due to the neglect of all compressible effects in the model [5] . As soon as compressibility is taken into account, we have $(d\rho/dt) \neq (\partial\rho/\partial\varphi)(d\varphi/dt)$ which therefore modifies the continuity equation (6.3a) by introducing an additional coupling between V', φ' and g'. In this case, the stability of an homogeneous state will also be concerned by the classical stability conditions $\chi_T > 0$ and $c_v > 0$ which are degenerated in the present model.

Matrix of the system We now use the expression (6.6) for V' (valid for any $k_x \neq 0$, which is not restrictive) in the momentum balance equation (second equation of the system (6.5)). Let us reverse the order of the equations and divide the resulting expression for the momentum balance equation by $\mathbf{I}$ for the sake of legibility and without any loss of generality. We now adopt a matrix notation for the linear system of equations which thus reads $MX = 0$ where X is the vector of unknowns (φ', T', g', V'). The matrix M reads

$$M = \begin{bmatrix} \omega\dfrac{\rho^{hs}}{\kappa} + \lambda k_x^2 + \dfrac{\lambda}{h^2}\dfrac{d^2W}{d\varphi^2}^{hs} - \dfrac{d^2\rho}{d\varphi^2}^{hs} g^{*hs} & \dfrac{d\rho}{d\varphi}^{hs}\dfrac{dg_{eq}}{dT}^{hs} & -\dfrac{d\rho}{d\varphi}^{hs} & 0 \\ \omega\,\dfrac{T^{hs}}{\rho^{hs}}\dfrac{dP_{sat}}{dT}\dfrac{d\rho}{d\varphi}^{hs} & -\left(\omega\,(\rho c_P)^{hs} + k_x^2\, k^{hs}\right) & 0 & 0 \\ \dfrac{\omega}{k_x\rho^{hs}}\dfrac{d\rho}{d\varphi}^{hs}\left(k_x^2\left(\dfrac{\eta}{\rho}\right)^{hs} + \omega\right) & k_x s^{hs} & k_x & 0 \\ \omega\dfrac{d\rho}{d\varphi}^{hs} & 0 & 0 & \mathbf{I}k_x\rho^{hs} \end{bmatrix} \tag{6.7}$$

At this point, we can determine the dispersion relation for the linear perturbation and therefore determine the conditions of stability of the homogeneous states by studying the determinant of the matrix M.

6.2.6 The dispersion relation in the general case

The determinant of the matrix M (6.7), denoted $\det M$, can be expressed as follows

$$\det M(\omega, k_x) = \mathbf{I}k_x\rho^{hs}\left[\omega\, k_x\, \frac{T^{hs}}{\rho^{hs}}\frac{dP_{sat}}{dT}\left(\frac{d\rho}{d\varphi}^{hs}\right)^2\left(\frac{dg_{eq}}{dT}^{hs} + s^{hs}\right) + k_x\left(\omega\,(\rho c_P)^{hs} + k_x^2\, k^{hs}\right)\det{}_{isoth}\right]$$

where

$$\begin{aligned} \det{}_{isoth}(\omega, k_x) &\triangleq \begin{vmatrix} \left(\omega\dfrac{\rho^{hs}}{\kappa} + \lambda k_x^2 + \dfrac{\lambda}{h^2}\dfrac{d^2W}{d\varphi^2}^{hs} - \dfrac{d^2\rho}{d\varphi^2}^{hs} g^{*hs}\right) & -\dfrac{d\rho}{d\varphi}^{hs} \\ \dfrac{\omega}{\rho^{hs}}\dfrac{d\rho}{d\varphi}^{hs}\left(\left(\dfrac{\eta}{\rho}\right)^{hs} + \dfrac{\omega}{k_x^2}\right) & 1 \end{vmatrix} \\ &= \omega^2\left[\left(\frac{d\rho}{d\varphi}^{hs}\right)^2\frac{1}{k_x^2\rho^{hs}}\right] + \omega\left[\frac{\rho^{hs}}{\kappa} - \left(\frac{d\rho}{d\varphi}^{hs}\right)^2\left(\frac{\eta}{\rho^2}\right)^{hs}\right] \\ &\quad + \lambda\left[k_x^2 + \frac{1}{h^2}\frac{d^2W}{d\varphi^2}^{hs} - \frac{d^2\rho}{d\varphi^2}^{hs}\frac{g^{*hs}}{\lambda}\right] \end{aligned} \tag{6.8}$$

[5] We do not consider any dependence of the density with respect to either P (according to the quasi compressible hypothesis) or T *i.e.* we neglect the coefficient of thermal expansion α_P defined by equation (2.18), *cf.* the set of simplifications considered in section 5.3.3.

$\det_{isoth}(\omega, k_x)$ is a polynomial expression in ω of degree 2 and will be related to the determinant of the system in the isothermal case in section 6.3.2. According to the study of the set of simplifications considered in section 5.3.3, the neglect of the dependence of the surface tension with the temperature and of the thermal expansion, yields (*cf.* the general expression (3.9c) for the specific entropy)

$$s^{hs} = \frac{1}{\rho^{hs}} \frac{dP_{sat}}{dT} - \frac{dg_{eq}}{dT}$$

Therefore, the expression for $\det M$ reads

$$\det M(\omega, k_x) = \mathbf{I} k_x^2 \rho^{hs} \left(\omega \, \frac{T^{hs}}{\rho^{2\,hs}} \left(\frac{dP_{sat}}{dT} \right)^2 \left(\frac{d\rho}{d\varphi}^{hs} \right)^2 + \left(\omega \, (\rho c_P)^{hs} + k_x^2 \, k^{hs} \right) \det_{isoth}(\omega, k_x) \right) \tag{6.9}$$

Thus $\det M$ is a third degree polynomial in ω. Since k_x only appears as quadratic, in the following, we consider only the case $\Re(k_x) > 0$ without any loss of generality. Let us introduce

$$\det M^*(\omega, k_x) \hat{=} \det M(\omega, k_x) / \left(\mathbf{I} k_x^2 \rho^{hs} \right)$$

that has the same roots as $\det M$. The dispersion relation to study reads therefore $\det M^* = 0$ and is a polynomial of degree 3 in the angular frequency ω. It is worth noting that as soon as the compressibility of the fluid is taken into account (*i.e.* $(\partial\rho/\partial P) \neq 0$) the dispersion relation of such a phase field model is a polynomial of degree 4, *e.g.* the dispersion obtained by Roshchin and Truskinovsky [114]. This difference illustrates the influence of our quasi-compressible hypothesis on the nature of the perturbation waves.

6.3 General study of the dispersion relation

In this section we study the dispersion relation $\det M = 0$ (where $\det M$ is given by (6.9)) and show how it is possible to derive from its general expression, some criteria determining the nature of the linear stage of evolution of the perturbation of the state hs.

6.3.1 Non-isothermal dissipative case: the use of the Routh-Hurwitz criterion of stability

In the non-isothermal dissipative case studied in the previous section, the study of the the linear stage of perturbation has been shown to reduce to the study of the roots ω of the third degree polynomial $\det M^*(\omega, k_x)$ as a function of k_x. Let us study the stability (*i.e.* the condition under which $\Re(\omega(k_x)) < 0$) with the help of the so called Hurwitz criterion[6] . In our case the different coefficients of the polynomial $\det M^*(\omega, k_x) = \sum_{i=0}^{3} a_i(k_x)\, \omega^i$ read

$$a_3 = \left(\frac{d\rho}{d\varphi}^{hs} \right)^2 \frac{c_P^{hs}}{k_x^2} \tag{6.10a}$$

$$a_2 = \left(\frac{k}{\rho} \right)^{hs} \left(\frac{d\rho}{d\varphi}^{hs} \right)^2 + (\rho c_P)^{hs} \left(\frac{\rho^{hs}}{\kappa} + \left(\frac{d\rho}{d\varphi}^{hs} \right)^2 \left(\frac{\eta}{\rho^2} \right)^{hs} \right) \tag{6.10b}$$

$$\begin{aligned} a_1 = {} & \frac{T^{hs}}{\rho^{2\,hs}} \left(\frac{dP_{sat}}{dT} \right)^2 \left(\frac{d\rho}{d\varphi}^{hs} \right)^2 + k_x^2 \, k^{hs} \left(\frac{\rho^{hs}}{\kappa} + \left(\frac{d\rho}{d\varphi}^{hs} \right)^2 \left(\frac{\eta}{\rho^2} \right)^{hs} \right) \\ & + (\rho c_P)^{hs} \lambda \left(k_x^2 + \frac{1}{h^2} \frac{d^2 W}{d\varphi^2}^{hs} - \frac{d^2\rho}{d\varphi^2}^{hs} \frac{g^{*\,hs}}{\lambda} \right) \end{aligned} \tag{6.10c}$$

$$a_0 = k_x^2 \, k^{hs} \, \lambda \left(k_x^2 + \frac{1}{h^2} \frac{d^2 W}{d\varphi^2}^{hs} - \frac{d^2\rho}{d\varphi^2}^{hs} \frac{g^{*\,hs}}{\lambda} \right) \tag{6.10d}$$

[6] A polynomial is said to be stable if all its roots lie in the open left half plane (*i.e.* $\Re(\omega) < 0$). A necessary condition for a polynomial $\sum_{i=0}^{n} a_i X^i$ of real coefficients a_i (which corresponds to our case) to be stable is that all these coefficients are of same sign, that is supposed to be + in the following without any loss of generality. Once this necessary condition is fulfilled, the Routh-Hurwitz criterion states a necessary and sufficient condition for the stability of the polynomial. Let us consider the $n \times n$ Hurwitz matrix of the coefficients that

The necessary condition of stability states that

all the coefficients a_i must be of same sign

When this condition is fulfilled the sufficient and necessary condition of stability reads (sign of the odd determinant Δ_3)

$$a_1\, a_2 - a_0\, a_3 > 0 \tag{6.11}$$

The necessary condition of stability The coefficient a_3 is obviously positive (*cf.* equation (6.10a)), the polynomial is thus stable only if all the other coefficients are also positive. The coefficient a_2 (*cf.* equation (6.10b)) is clearly associated with only dissipative coefficients, namely the heat conductivity k of the Fourier heat conduction, the mobility κ of the Ginzburg-Landau relaxation, and the viscosity η. The coefficient a_2 is therefore null if no dissipation is considered and strictly positive otherwise. The coefficient a_1 is only conditionally positive (*cf.* equation (6.10c)). The coefficient a_0 (*cf.* equation (6.10d)) is, like the coefficient a_1 only conditionally positive. It is worth noting that in absence of thermal dissipation (Fourier heat conductivity k^{hs} null), this coefficient is zero. The corresponding non-heat-conducting case will be considered in section 6.3.3, we assume in the following that $k^{hs} > 0$. The coefficient a_0 is thus unconditionally positive ($\forall k_x$) if and only if $(d^2W/d\varphi^2)^{hs}/h^2 - (d^2\rho/d\varphi^2)^{hs}\, g^{*\,hs}/\lambda > 0$. Otherwise, there exists sufficient low values for k_x such that $a_0 < 0$. The condition of positivity of the coefficient a_0 is more restrictive than the condition of positivity of the coefficient a_1. Therefore $a_0 > 0 \Rightarrow a_1 > 0$.

The necessary condition for the stability of the polynomial $\det M^*$ reads thus

$$a_0 > 0$$

---

reads

$$\begin{bmatrix} a_1 & a_3 & a_5 & \dots & 0 & 0 \\ a_0 & a_2 & a_4 & \dots & 0 & 0 \\ 0 & a_1 & a_3 & \dots & 0 & 0 \\ \dots & \dots & \dots & \dots & \dots & 0 \\ 0 & 0 & 0 & \dots & 0 & 0 \\ 0 & 0 & 0 & \dots & a_n & 0 \\ 0 & 0 & 0 & \dots & a_{n-1} & 0 \\ 0 & 0 & 0 & \dots & a_{n-2} & a_n \end{bmatrix}$$

and introduce the n diagonal minor determinants

$$\Delta_1 = a_1;\ \Delta_2 = \begin{vmatrix} a_1 & a_3 \\ a_0 & a_2 \end{vmatrix};\ \Delta_3 = \begin{vmatrix} a_1 & a_3 & a_5 \\ a_0 & a_2 & a_4 \\ 0 & a_1 & a_3 \end{vmatrix};\ \dots$$

For the polynomial (such that $\forall i,\ a_i > 0$) to be stable it is necessary and sufficient that

All the even determinants, Δ_{2k} be positive

$\Leftrightarrow$

All the odd determinants, Δ_{2k+1} be positive

Let us also mention a sufficient condition for a polynomial to be stable that is $a_n > a_{n-1} > \cdots > a_0 > 0$.

The necessary and sufficient condition of stability Let us consider the condition (6.11). In our case, $(a_1\ a_2 - a_0\, a_3)$ reads (*cf.* the expressions (6.10) of the coefficients of the polynomial)

$$\left(\frac{T^{hs}}{\rho^{2\,hs}}\left(\frac{dP_{sat}}{dT}\right)^2\left(\frac{d\rho}{d\varphi}^{hs}\right)^2 + k_x^2\, k^{hs}\vartheta_{diss}^{isoth}\right)a_2 + \left(\frac{(\rho\, c_P)^{hs\,2}}{k_x^2\, k^{hs}}\vartheta_{diss}^{isoth}\right)a_0$$

where the parameter ϑ_{diss}^{isoth} is defined by

$$\vartheta_{diss}^{isoth} = \frac{\rho^{hs}}{\kappa} + \left(\frac{d\rho}{d\varphi}^{hs}\right)^2\left(\frac{\eta}{\rho^2}\right)^{hs} \tag{6.12}$$

and is a measure of the isothermal dissipation. Let us note that ϑ_{diss}^{isoth} is positive and that $(a_1\ a_2 - a_0\, a_3)$ is therefore positive.

As a consequence, the necessary and sufficient condition of stability of the polynomial $\det M^*$ reads

$$a_0 > 0$$

The condition of stability expressed as the belonging of the state hs to a φ-spinodal region According to the expression (6.10d) of the coefficient a_0, we introduce the critical wave number k^c defined by

$$(k^c)^2 \triangleq -\frac{1}{h^2}\frac{d^2W}{d\varphi^2}^{hs} + \frac{d^2\rho}{d\varphi^2}^{hs}\frac{g^{*\,hs}}{\lambda} \tag{6.13}$$

such that

$$\forall k_x,\ a_0 > 0 \quad \Leftrightarrow \quad (k^c)^2 < 0$$

Let us note that k^c is either a pure real or a pure imaginary, *i.e.* $k^c \in \mathbb{R} \cup \mathbb{IR}$. If $(k^c)^2$ is positive ($k^c \in \mathbb{R}$), the lower wave number for a stable evolution of the perturbation of the state hs is therefore k^c. Otherwise ($(k^c)^2 < 0 \Rightarrow k^c \in \mathbb{IR}$) the state hs is unconditionally stable.

Let us now interpret the expression (6.13) for $(k^c)^2$ whose sign has been related to the condition of stability of the state hs. Let us relate this latter critical wave number to a thermodynamic quantity. We indeed search a definition of a "spinodal" region related to the phase-field description of the fluid. The expression for k^c indeed originates from the expression (6.4b) of the derivative of $\rho\mu$ with respect to φ:

$$\frac{\partial\rho\mu}{\partial\varphi}^{hs}_{|P,T} = \frac{\lambda}{h^2}\frac{d^2W}{d\varphi^2}^{hs} - \frac{d^2\rho}{d\varphi^2}^{hs} g^{*hs}$$

Using the fact that $\mu^{hs} = 0$ (the state hs is at equilibrium *cf.* equation (6.2)) we get using the definition (6.13) for the critical wave number k^c

$$(k^c)^2 = -\frac{\rho^{hs}}{\lambda}\frac{\partial\mu}{\partial\varphi}^{hs}_{|P,T} \tag{6.14}$$

and we define the $\varphi-$spinodal region of positivity of $(\partial\mu/\partial\varphi)^{hs}_{|P,T}$. Since, by definition, $\mu = (\partial g)(\partial\varphi)_{|P,T,\varphi^2_{,x}}$, the thermodynamic quantity $\rho^{hs}(\partial\mu/\partial\varphi)^{hs}_{|P,T}$ is clearly related to a convexity of the specific Gibbs free energy. This thermodynamic quantity can be related to its analogous in more classical thermodynamic models such as the isothermal compressibility[7] χ_T for the compressible fluids since we obviously have

$$\begin{aligned}
\varphi &\leftrightarrow \rho \\
g &\leftrightarrow F \\
\mu = \frac{\partial g}{\partial\varphi_{|T}} &\leftrightarrow P = \rho\frac{\partial F}{\partial\rho}_{|T} - F = \rho\,\mu_{vdW} - F \\
\rho\frac{\partial\mu}{\partial\varphi_{|T}} &\leftrightarrow \rho\frac{\partial\mu_{vdw}}{\partial\rho}_{|T} = \frac{\partial P}{\partial\rho}_{|T} = \frac{1}{\rho\,\chi_T}
\end{aligned}$$

[7]The condition $\chi_T > 0$ is the classical Gibbs-Duhem criterion of stability (2.4), we recall the definition (2.3) of the isothermal compressibility

$$\chi_T \triangleq -\frac{1}{V}\left(\frac{\partial V}{\partial P}\right)_T = \frac{1}{\rho}\frac{\partial\rho}{\partial P}_{|T}$$

Since the condition of stability of the state hs has been previously related to the sign of $(k^c)^2$ (*cf.* the above study of the condition of stability $a_0 > 0$), we have thus shown the condition of stability to be related to the belonging of the state hs to a convex region of the specific Gibbs free energy as a function of the phase-field φ. Let us draw a few consequences of this definition

- ⋆ a state outside the $\varphi-$spinodal region is unconditionally stable
- ⋆ a state inside the $\varphi-$spinodal region is conditionally stable, indeed it is unstable for any perturbation whose wave number k_x is less than the critical wavelength k^c defined by equation (6.13)

It is worth noting that a state hs has been said to be parameterized by the parameters $(\varphi^{hs}, g^{*hs}, T^{hs})$ (*cf.* section 6.2.2). It is therefore of interest to determine the ranges of these parameters for which the state hs corresponds actually to the $\varphi-$spinodal region.

The study of stability using the Hurwitz criterion does not allow to study more precisely the linear stage of evolution of a perturbation. In the following, we propose to consider different physical sub-cases for which the different branches of the dispersion relation (the growth rate ω as a function of the wave number k_x) can be studied analytically.

6.3.2 Isothermal case

System of governing equations in the isothermal case Let us consider the isothermal case (*i.e.* obtained by considering T' as uniformly null). The system of governing equations (6.1) reduce to the continuity equation (6.1a), the momentum balance equation (6.1b) where the non-dissipative part of the stress tensor now reduce to $(-\rho\, g_{,x} + \rho\tilde{\mu}\varphi_{,x})$ (*cf.* its expression (5.23)) derived in chapter 5), and the AC equation (6.1d) where the temperature dependence of g^* is irrelevant ($g_{eq}(T) = cste$). The system of equation reads thus

$$-\rho\, V'_{,x} = \frac{d\rho}{d\varphi}\left(\varphi_{,t} + V'\,\varphi_{,x}\right) \tag{6.15a}$$

$$\left(V'_{,t} + V'\,V'_{,x}\right) = -g_{,x} + \tilde{\mu}\,\varphi_{,x} + \frac{\left(\eta\, V'_{,x}\right)_{,x}}{\rho} \tag{6.15b}$$

$$\frac{\rho\,\left(\varphi_{,t} + V'\,\varphi_{,x}\right)}{\kappa} = \frac{d\rho}{d\varphi}g^* + \lambda\left(\varphi_{,xx} - \frac{1}{h^2}\frac{dW}{d\varphi}\right) \tag{6.15c}$$

Using the reasoning followed in section 6.2.1, the determinant of the system of linear equations for the amplitude of the perturbed variables in the isothermal dissipative case can be shown to have the same roots than the determinant $\det_{\,isoth}$ defined by equation (6.8).

Isothermal dispersion relation, the roots of $\det_{\,isoth}$ Let us consider the study of the polynomial $\det_{\,isoth}$ of degree 2 in ω. Equation (6.8) shows that the coefficient of the linear term in ω of $\det_{\,isoth}$ is the parameter ϑ^{isoth}_{diss} (defined by equation (6.12)) and is therefore related to the isothermal dissipative mechanisms, namely the Ginzburg-Landau relaxation (mobility κ) and the viscous dissipation η. Using the parameters ϑ^{isoth}_{diss} and $(k^c)^2$, $\det_{\,isoth}$ reads

$$\det_{\,isoth} = \omega^2\left[\left(\frac{d\rho}{d\varphi}^{hs}\right)^2\frac{1}{k_x^2\rho^{hs}}\right] + \omega\,\vartheta^{isoth}_{diss} + \sigma\, h\left(k_x^2 - (k^c)^2\right) \tag{6.16}$$

It is worth noting that a similar dispersion relation has been derived in [89] where, by difference with our case, $(d\rho/d\varphi)^{hs}$ is considered as constant and where ϑ^{isoth}_{diss} is related to the dissipative Cahn-Hilliard diffusivity (rather than the viscous dissipation and Ginzburg-Landau relaxation of our model). The roots $\omega_\pm$ of this second order polynomial read

$$\omega_\pm = \frac{k_x^2\rho^{hs}}{2}\left(\frac{d\rho}{d\varphi}^{hs}\right)^{-2}\left[-\vartheta^{isoth}_{diss} \pm \sqrt{\left(\vartheta^{isoth}_{diss}\right)^2 - \frac{4\,\sigma\, h}{\rho^{hs}}\left(\frac{d\rho}{d\varphi}^{hs}\right)^2\left(1 - \frac{(k^c)^2}{k_x^2}\right)}\right] \tag{6.17}$$

There exists therefore two branches ω_+ and ω_- for the dispersion relation. Let us study these two branches.

Stability of homogeneous state in the isothermal case Let us first consider the condition for which $\Re(\omega_\pm) > 0$. It is straightforward from equation (6.17) that, for all wave number k_x, we have $\Re(\omega_-) < 0$. The corresponding branch of the dispersion relation is therefore never unstable. Let us consider the root ω_+. It is worth noting that the criterion of positivity of $\Re(\omega_+)$ is exactly the criterion of stability derived in the non-isothermal dissipative case studied in section 6.3.1 using the Hurwitz criterion: as a consequence, for the isothermal case, a state *hs* outside the $\varphi-$spinodal region is unconditionally stable whereas a state *hs* inside the $\varphi-$spinodal region is unstable if $k_x < k^c$.

As a partial conclusion, the condition of stability in the isothermal case are exactly the one of the non-isothermal dissipative case.

Dispersive nature of the perturbation Let us consider the expression (6.17) in view of determining the dispersive nature of the growth rate. We therefore have to study under which condition we have $\Im(\omega_\pm) \neq 0$. This condition is sufficient in order to conclude on the dispersive nature of the branches since obviously, as soon as $\Im(\omega_\pm) \neq 0$, $\Im(\omega_\pm)$ is actually a function of the wave number k_x. Let us introduce a second critical wave number k^c_{disp} for the condition of nullity of the imaginary part of the roots, $\Im(\omega_\pm)$ that reads

$$\left(k^c_{disp}\right)^2 \triangleq (k^c)^2 \left(1 - \vartheta^{isoth\,2}_{diss} \left(\frac{d\rho}{d\varphi}^{hs}\right)^{-2} \frac{\rho^{hs}}{4\,\sigma\,h}\right)^{-1} \tag{6.18}$$

where $k^c_{disp} \in \mathbb{R} \cup \mathbb{IR}$. Let us note that $\left(k^c_{disp}\right)^2 > (k^c)^2$. Let us also introduce a critical value ϑ^c for the dissipative mechanisms that reads

$$\vartheta^c \triangleq 2 \sqrt{\frac{\sigma\,h}{\rho^{hs}}} \left|\frac{d\rho}{d\varphi}^{hs}\right| \tag{6.19}$$

Using the two expressions (6.18) and (6.19) for k^c_{disp} and ϑ^c, the roots $\omega_\pm$ therefore read

$$\omega_\pm = \frac{2\,k_x^2\,\sigma\,h}{\vartheta^{c\,2}} \left[-\vartheta^{isoth}_{diss} \pm \sqrt{\frac{\vartheta^{c\,2}\,(k^c)^2}{k_x^2}\left(k_x^2 - \left(k^c_{disp}\right)^2\right)}\right]$$

The resulting expression for the square root term appearing in $\omega_\pm$ allows therefore the determination of the conditions for the imaginary part of $\omega_\pm$ to be non-zero. It is worth noting that, as soon as the imaginary part of the roots $\omega_\pm$ is non zero, the real part of the roots $\omega_\pm$ are equal and moreover negative, *i.e.* $\Re(\omega_+) = \Re(\omega_-) < 0$. This is used in order to determine the condition for the wave to be dispersive that are illustrated by the table 6.1.

Summary of the study of the roots of $\det_{\ isoth}$ The table 6.1 determines the condition of stability as well as the existence of an imaginary part for the roots $\omega\pm$ of $\det_{\ isoth}$ as a function of the wave number k_x, the sign of $(k^c)^2$ and of the value of $\vartheta_{diss\,isoth}$. As a partial conclusion of this study of the roots of $\det_{\ isoth}$, the dispersive nature

$(k^c)^2$	> 0 *i.e. hs* inside the $\varphi-$spinodal					< 0		
ϑ^{isoth}_{diss}	$> \vartheta^c$		$< \vartheta^c$			$> \vartheta^c$		$< \vartheta^c$
$\left(k^c_{disp}\right)^2$	< 0		> 0			> 0		< 0
k_x	$< k^c$	$> k^c$	$< k^c$	$\in [k^c : k^c_{disp}]$	$> k^c_{disp}$	$< k^c_{disp}$	$> k^c_{disp}$	$\forall$
$\Im(\omega_\pm)$	$= 0$				$\neq 0$	$\neq 0$	$= 0$	$\neq 0$
$\Re(\omega_+)$	> 0	< 0	> 0	< 0				

Table 6.1: Dispersive and dissipative structure of the perturbation waves in the isothermal case

of the solutions depends both on the intensity of the dissipative effects (ϑ^{isoth}_{diss} *versus* ϑ^c) and on the belonging of

the hs state to the $\varphi-$spinodal region (sign of $(k^c)^2$). The stability condition only depends on the belonging of the hs state (like in the non-isothermal dissipative case).

Therefore, it is required to study the belonging of the state hs to the $\varphi-$spinodal region as a function of the parameters for the state hs in order to conclude on the dispersive/stable nature of a perturbation of a state hs in the isothermal case.

6.3.3 The influence of the dissipative processes on the stability of the state hs

We consider now the absence of any dissipative process, *i.e.* $k^{hs} = 0$, $\kappa = +\infty$ and $\eta = 0$. In this case the expression for the dispersion relation $\det M^* = 0$ still holds and is therefore a polynomial of degree 3. However $a_2 = 0$, $a_0 = 0$ (*cf.* their expressions (6.10b) and (6.10d)) and $\vartheta_{diss}^{isoth} = 0$ (*cf.* its definition (6.12)) which simplifies notably the study of this polynomial. According to the study of the Hurwitz criterion of the stability of $\det M^*$, the necessary and sufficient condition of stability thus reduces to the condition $a_1 > 0$ where a_1 reads (*cf.* its expression (6.10c))

$$a_1 = \frac{T^{hs}}{\rho^{hs}} \left(\frac{dP_{sat}}{dT} \right)^2 \left(\frac{d\rho}{d\varphi}^{hs} \right)^2 + (\rho c_P)^{hs} \lambda \left(k_x^2 + \frac{1}{h^2} \frac{d^2W}{d\varphi^2}^{hs} - \frac{d^2\rho}{d\varphi^2}^{hs} \frac{g^{*hs}}{\lambda} \right)$$

We introduce the critical wave number $\left(k^c_{diss=0}\right)^2$ for the positivity of a_1 defined by

$$\left(k^c_{diss=0}\right)^2 \triangleq (k^c)^2 - \frac{T^{hs}}{\lambda \rho^{3\,hs} c_P^{hs}\, h\, \sigma} \left(\frac{dP_{sat}}{dT} \right)^2 \left(\frac{d\rho}{d\varphi}^{hs} \right)^2 \tag{6.20}$$

where $k^c_{diss=0} \in \mathbb{R} \cup \mathbb{IR}$.

Since $a_0 = 0$, $\omega = 0$ is a trivial root of $\det M^*$ and the dispersion relation to study reads (*cf.* equation (6.9))

$$\frac{\det M^*(\omega, k_x)}{\omega} = \sigma\, h\, (\rho c_P)^{hs} \left(k_x^2 - \left(k^c_{diss=0}\right)^2 \right) + \omega^2 \left(\frac{d\rho}{d\varphi}^{hs} \right)^2 \frac{(\rho c_P)^{hs}}{k_x^2 \rho^{hs}} \tag{6.21}$$

Let us consider the two branches $\omega_\pm$ corresponding to the roots of this simple second order polynomial. They read

$$\omega_\pm = \pm\, k_x^2\, \sigma\, h\, \rho^{hs} \left(\frac{d\rho}{d\varphi}^{hs} \right)^{-2} \left(k_x^2 - \left(k^c_{diss=0}\right)^2 \right) \tag{6.22}$$

It is obvious that we have $\omega_+ = -\omega_-$ and that the existence of a non-zero real part is simply related to the condition $\left(k_x^2 - \left(k^c_{diss=0}\right)^2 \right) > 0$. It is worth noting that, according to equation (6.20) $\left(k^c_{diss=0}\right)^2 < (k^c)^2$. Therefore, the necessary condition of stability is less restrictive than in the dissipative case. As a consequence, any state hs that is unconditionally stable in the dissipative case is also unconditionally stable in the non-dissipative case. On the other hand, any state hs that is conditionally stable in the non-dissipative case is also conditionally stable in the dissipative case. The existence of dissipative mechanisms destabilizes thus some states that should be stable in absence of any dissipative mechanism. The crucial role of the heat conductivity on this property (with regard to the other isothermal dissipative mechanism) is shown in the next paragraph.

Let us also note that when $(d\rho/d\varphi)^{hs} = 0$ (which will be shown to be of interest when the interpolation functions for the density $\rho(\varphi)$ are either P_3 or P_5) both critical wave numbers are equal ($k^c_{diss=0} = k^c$) and therefore the existence of dissipative terms has no influence on the stability of the corresponding states. This result has already been stated by Umantsev [141] in the case where no density difference between the phases is taken into account.

In the non-dissipative case, the different cases we have to consider can be summarized by the following table

$\left(k^c_{diss=0}\right)^2$	> 0 *i.e.* hs inside the non-dissipative $\varphi-$spinodal		< 0
k_x	$< k^c_{diss=0}$	$> k^c_{diss=0}$	$\forall$
$\Re(\omega_+)$	> 0	< 0	
$\Im(\omega_\pm)$	$= 0$	$\neq 0$	

The non-heat-conducting case As soon as $k^{hs} = 0$, (since it yields $a_0 = 0$), the stability condition reads $a_1 > 0$. Therefore, for a non-heat conducting material, the critical wave number for the stability is always $k^c_{diss=0}$. However, when other dissipative mechanisms are considered ($\eta \neq 0$ and/or $\kappa \neq \infty$ *i.e.* $\vartheta^{isoth}_{diss} \neq 0$), the dispersion relation differs from the one studied hereinabove and the polynomial to study reads

$$\frac{\det M^*(\omega, k_x)}{\omega} = \omega^2 \left[\left(\frac{d\rho}{d\varphi}^{hs} \right)^2 \frac{(\rho c_P)^{hs}}{k_x^2 \rho^{hs}} \right] + \omega \left[(\rho c_P)^{hs} \vartheta^{isoth}_{diss} \right] + \sigma\, h\, (\rho c_P)^{hs} \left(k_x^2 - \left(k^c_{diss=0} \right)^2 \right)$$

and is of degree 2 in ω. It can be shown that the above results are modified as follows

- ⋆ the critical wave number for the stability is still $k^c_{diss=0}$
- ⋆ the existence of dispersive perturbations is related to the same critical wave number k^c_{disp} than in the isothermal case (*cf.* its definition (6.18) where k^c must be understood as $k^c_{diss=0}$). Moreover, since $|k^c| < |k^c_{disp}|$ and $|k^c_{diss=0}| < |k^c|$,we have $|k^c_{diss=0}| < |k^c_{disp}|$, which is similar to the isothermal case.
- ⋆ the domain of existence of dispersive perturbations is subject to the same influence of the magnitude of the dissipative mechanism than in the isothermal case (*i.e.* to the condition $\vartheta^{isoth}_{diss} < \vartheta^c$ where ϑ^c is defined by equation (6.19))

As a consequence, the structure of the perturbation can be summarized by exactly the same table than the table 6.1 holding for the isothermal case; only the value of k^c must be replaced by $k^c_{diss} = 0$.

The absence of any dissipative thermal process (non-heat-conducting material) in the non-isothermal case has therefore the single consequence to shift the wave number for the critical wave length to lower values ($|k^c_{diss=0}| < |k^c|$). As a consequence, a state inside the $\varphi-$spinodal region (unstable in the heat-conducting case) can be stable in the non-heat conducting case. The heat conductivity has therefore a destabilizing influence on the evolution of an equilibrium homogeneous state submitted to perturbations. This influence of the heat conductivity on the stability is indeed fully consistent with the results obtained by Ngan and Truskinovsky [99] where the stability of homogeneous states with a model equivalent to the van der Waals' model is studied: in the heat-conducting case the stability condition is the positivity of the isothermal compressibility ($\chi_T > 0$) whereas in the non-heat-conducting case the stability condition is the positivity of the adiabatic compressibility [8] ($\chi_s > 0$) and we have ($\chi_s > \chi_T$).

It is worth noting that as a consequence the condition of stability is no more related to the belonging of the state *hs* to the $\varphi-$spinodal region defined in the heat-conducting case. Let us study how the stability condition $k_x > \Re(k^c_{diss=0})$ can still be related to a spinodal region. To do this, we first recall the result obtained when we defined the first $\varphi-$spinodal region that reads

$$(k^c)^2 = -\frac{\rho^{hs}}{\lambda} \frac{\partial \mu}{\partial \varphi}^{hs}_{|P,T}$$

which is therefore the isothermal (at constant temperature T) derivative of the chemical potential μ with regard to the phase field variable.

Let us now consider the adiabatic derivative of the chemical potential μ. We have

$$\frac{\partial \mu}{\partial \varphi}_{|s} = \frac{\partial \mu}{\partial \varphi}_{|T} + \frac{\partial \mu}{\partial T}_{|\varphi} \frac{\partial T}{\partial \varphi}_{|s}$$

The following relations hold

$$\begin{aligned} \frac{\partial \mu}{\partial T}_{|\varphi} = -\frac{\partial s}{\partial \varphi}_{|T} &= -\frac{1}{\rho^2} \frac{\partial \rho}{\partial \varphi} \frac{dP_{sat}}{dT} \\ \frac{\partial s}{\partial T}_{|\varphi} &= \frac{T}{c_P} \end{aligned}$$

[8] The adiabatic compressibility χ_s is defined as

$$\chi_s \hat{=} -\frac{1}{V} \left(\frac{\partial V}{\partial P} \right)_s = \rho \frac{\partial \rho}{\partial P}_{|s}$$

and let us note that $(\partial s/\partial P)$ is zero in the considered case where the thermal expansion is null. Therefore, using the definition (6.20) of $k^c_{diss=0}$

$$\begin{aligned}\lambda\left(k^c_{diss=0}\right)^2 &= -\rho^{hs}\frac{\partial\mu}{\partial\varphi}^{hs}_{|P,T} - \frac{T^{hs}}{\rho^{3\,hs}c_P^{hs}\,h\,\sigma}\left(\frac{dP_{sat}}{dT}\right)^2\left(\frac{d\rho}{d\varphi}^{hs}\right)^2 \\ &= -\rho^{hs}\frac{\partial\mu}{\partial\varphi}^{hs}_{|P,T} + \rho^{hs}\frac{(\partial s/\partial\varphi)_{|T}}{(\partial s/\partial T)_{|\varphi}}\frac{\partial\mu}{\partial T}^{hs}_{|\varphi} \\ &= -\rho^{hs}\frac{\partial\mu}{\partial\varphi}^{hs}_{|P,s}\end{aligned}$$

The adiabatic $\varphi-$spinodal region, as the set of states hs for which $(\partial\mu/\partial\varphi)_{|P,s} < 0$ can thus be defined by analogy with the $\varphi-$spinodal region considered in the isothermal case. The adiabatic $\varphi-$spinodal region is less extended than the isothermal $\varphi-$spinodal region. This extends therefore the results obtained by Umantsev [141] to the case where a density difference between the phases is considered.

Conclusion concerning the study of the general form for the dispersion relation

In the dissipative non-isothermal case (see section 6.3.1), using the Hurwitz criterion of stability, we have shown that the necessary and sufficient condition of stability is the non-belonging of the homogeneous state hs to the $\varphi-$spinodal region *i.e.*

$$\frac{\partial\mu}{\partial\varphi}^{hs}_{|P,T} > 0s$$

Inside the $\varphi-$spinodal region, the homogeneous state is unstable to small wave-number perturbations, the critical value for the wave number being equal to $k^c = \sqrt{-(\partial\mu/\partial\varphi)^{hs}_{|P,T}}$.

We have then defined a set of sub-cases for which a more complete analytical study of the linear stage of evolution of the perturbation of homogeneous states is possible. Let us summarize the corresponding results. First, as soon as the heat conductivity is non-zero, the condition of stability for the state hs is exactly similar to the one corresponding to the non-isothermal dissipative case presented above. If the heat conductivity is null, the condition of stability is related to the non-belonging of the homogeneous state hs to the adiabatic $\varphi-$spinodal region *i.e.*

$$\frac{\partial\mu}{\partial\varphi}^{hs}_{|P,s} > 0$$

It has been shown that the condition of stability is indeed less restrictive than in the heat-conducting case.

Let us now consider the condition of dispersive evolution of the perturbation. It has been shown than in the isothermal case, as well as in the non-heat-conducting case, the condition of existence of dispersive waves is related to the belonging of the state hs to the $\varphi-$spinodal region as well as on the intensity of the dissipative mechanisms. The corresponding results are given on table 6.1. In the absence of any dissipative mechanism, the perturbation is dispersive as soon as it is damped.

In the following, we consider different choices for the interpolation function $\rho(\varphi)$ to study how it affects the belonging to the $\varphi-$spinodal region for given thermodynamic conditions (g^* and T) and show how the choice for the polynomial P_5 actually allows to control the stability of the single-phase states.

6.4 Stability of homogeneous states using linear interpolation

When the interpolation function $\rho(\varphi)$ is linear, $(d\rho/d\varphi) = (\rho_v - \rho_l)$ and $(d^2\rho/d\varphi^2) = 0$. $(d\rho/d\varphi)$ and $(d^2\rho/d\varphi^2)$ are independent of the state hs considered. In the following, we take advantage of this property to simplify the general expressions for the conditions under which the perturbation wave is dispersive/unstable that have been derived in section 6.3.

6.4.1 Non-isothermal dissipative case, the necessary and sufficient condition of stability

In the linear interpolation case, the expression for the critical wave number k^c simplifies and reads

$$(k^c)^2 = \frac{-(d^2W/d\varphi^2)^{hs}}{h^2}$$

The equilibrium phase field value is determined by the value of the single parameter $\mathfrak{g} = g^*\,\sigma/[h(\rho_l - \rho_v)]$ (see section 3.4.1) and equals 0 or 1 only for $\mathfrak{g} = 0$. It is straightforward to show that the $\varphi-$spinodal region corresponds to $|\mathfrak{g}| < 2\sqrt{3}$. The metastability limit of the liquid state ($\varphi < 1/2 - \sqrt{3}/6$), resp. vapor state state ($\varphi > 1/2 + \sqrt{3}/6$), is thus defined by $g^*_{lim,l} = -2\sqrt{3}\,\sigma/[h\,(\rho_l - \rho_v)]$, resp. $g^*_{lim,v} = 2\sqrt{3}\,\sigma/[h\,(\rho_l - \rho_v)]$. It is thus not controlled since h dependent.

6.4.2 Non dissipative and isothermal case

Let us express the growth rate ω in the isothermal case. Let us consider at first the case of zero dissipative processes, $\vartheta_{diss} = 0$ (*i.e.* $\kappa = \infty$ and $\eta = 0$). The growth rate reads

$$\omega_{\text{diss free}} = \pm\frac{\sqrt{\sigma/h}\,k_x}{\rho_l - \rho_v}\sqrt{(k^c)^2 - k_x^2}$$

where the critical wave length k^c has the same expression than in the previous studied general case. We have either pure imaginary ($\Re(\omega_{\text{diss free}}) = 0$, dispersive wave) or pure real (either damped or unstable) growth rates ($\Im(\omega_{\text{diss free}}) = 0$) . Let us state for which state hs, unstable growth of the perturbation can occur.

For φ^{hs} outside the spinodal region, we have $\Re(\omega_{\text{diss free}}) = 0$ and there exists only purely dispersive evolution of the perturbation. For φ^{hs} inside the spinodal region there exists a critical wave length, namely k^c, such as there exists non-dispersive unstable perturbations for $k_x < k^c$ and purely dispersive for $k_x > k^c$.

As a partial conclusion for non-dissipative isothermal cases, the states out of the spinodal region (unconditionally stable) are purely dispersive whereas in the spinodal region unstable growth rates corresponds to low values of k_x, the critical value for the wave number k^c being scaled by the inverse of the artificial thickness, namely $1/h$.

6.4.3 Dissipative isothermal case

Let us study how the isothermal linear stage of evolution is modified in presence of dissipative effects (*i.e.* $\vartheta^{isoth}_{diss} \neq 0$). For non-zero dissipative processes (*i.e.* $\kappa \neq \infty$ and/or $\eta \neq 0$), there exists two branches in the dispersion relation (*cf.* equation (6.17)) and the critical wave length for dispersive solutions is given by equation (6.18). It is worth noting that dispersive ($\Im(\omega_\pm) \neq 0$) solutions, always correspond to damped perturbations ($\Re(\omega_\pm) < 0$) whatever the initial state considered. Let us now study the states corresponding to either dispersive or non-dispersive perturbations. We refer to the table of cases presented in section 6.3.2

Let us consider a state hs outside the spinodal region. In this case, we have $k^{c\,2}_{isoth} < 0$. Non-dispersive growth rate ($\Im(\omega_\pm) = 0$) exists only if the dissipative terms ϑ_{diss} is less than ϑ^c. If this condition is fulfilled, non-dispersive growth rates are possible for large k_x ($k_x^2 > k^{c\,2}_{disp}$) where $k^{c\,2}_{disp}$ is given by (6.18).

For states inside the spinodal region, we have unstable growth rate ($\Re(\omega_+) > 0$) for $k_x < k^c$. There are two different cases according to the value of ϑ^{isoth}_{diss}. If ϑ^{isoth}_{diss} is larger than ϑ^c, solutions are always non dispersive ($\Im(\omega) = 0$). If ϑ^{isoth}_{diss} is less than ϑ^c, the non-dispersive solutions correspond for $k_x < k_{c\,disp}$.

Such a dispersion relation is illustrated on figure 6.1 where the real part of the growth rate as a function of the wave number is represented. It is worth noting that when the wave is dispersive, we have only one branch (instead of two) for the real part (*i.e.* $\Im(\omega_\pm) = 0 \Rightarrow \Re(\omega_+) = \Re(\omega_-)$).

As a conclusion for the dissipative isothermal case, states out of the spinodal region are purely dispersive for low or zero dissipation. For sufficiently large dissipation, they are purely damped for low values of the wave length $k_x < k^c_{diss}$ and dispersive otherwise. States inside the $\varphi-$spinodal region are dispersive.

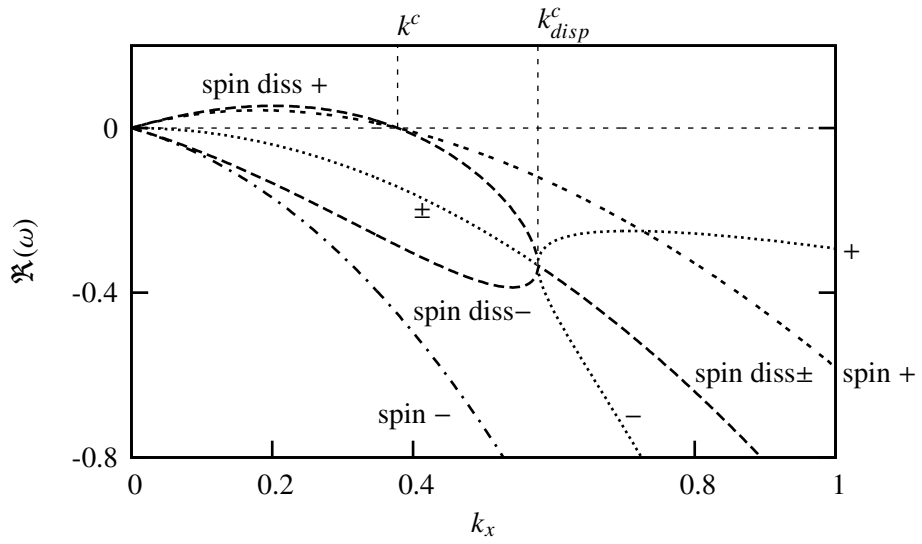

Figure 6.1: Real part of the growth rate ω . The "spin" case corresponds to the spinodal case when $\vartheta^{diss} < \vartheta^c$ while the "±" and "spin diss" cases correspond to large dissipation rate $\vartheta^{diss} > \vartheta^c$

6.4.4 Non-heat conducting case

We consider the case of zero heat conductivity, therefore $a_0 = 0$ and the dispersion relation reads (*cf.* equation (6.21))

$$\omega^2 \left[\frac{(\rho_l-\rho_v)^2}{\rho^{hs}\, k_x^2}\right] + \omega\, \vartheta_{diss} + \left[\lambda\left(\frac{1}{h^2}\frac{d^2W^{hs}}{d\varphi^2} + k_x^2\right) + \frac{T^{hs}\,(\rho_l-\rho_v)^2\;(dP_{sat}/dT)^2}{(\rho\, c_P)^{hs}\,(\rho^{hs})^2}\right] = 0 \tag{6.23}$$

For non-dissipative ($\vartheta_{diss} = 0$) processes, we get similar results than for the non-isothermal dissipation free case, *i.e.* :

- ⋆ outside the spinodal region, *hs* is unconditionally stable and we have dispersive solutions
- ⋆ inside the spinodal region the states are unstable for low wave numbers $k_x < k^c_{diss=0}$, $k^c_{diss=0}$ being lower than its isothermal value (*cf.* equation (6.20)) and dispersive otherwise. Let us note that $k^c_{diss=0}$ can even become unconditionally negative (in which case no more unstable growth is possible) for $h > \rho^{hs\,2} c_P^{hs}\,\sigma\,|Min(d^2W/d\varphi^2)|/(T^{hs}(dP_{sat}/dT)^2\,(\rho_l-\rho_v)^2)$. In the present case $|Min(d^2W/d\varphi^2)| = 18$.

It is therefore worth noting that, as h increases, the value of the critical wave number under which the spinodal phase become unstable decreases and can even reach zero. As a consequence, the stability of adiabatic homogeneous states is clearly not controlled since it is h dependent.

Let us now consider the case with zero heat conductivity but still other isothermal dissipative mechanisms. Then it is straightforward that the structure of the dispersion relation is strictly identical than in the dissipative isothermal case, and we refer to the corresponding study.

6.4.5 Conclusion on the study of the linear interpolation

The unstable and dispersive properties of the linear stage of evolution of a perturbation have been studied. For the isothermal, non-dissipative, non-heat conducting or without density differences cases, we have determined the spectrum of wavelengths of both dispersive and unstable perturbations. The $\varphi-$spinodal region corresponds in this case to a finite range of g^* values around zero, this range being a decreasing function of the artificial thickness h. The liquid and vapor states are always outside the spinodal. Their domain of existence is bounded by a limiting g^* value. At the limit $h = +\infty$, there only exists liquid phase for $g^* > 0$ and vapor phase for $g^* < 0$. It does mean that the limit of superheat is a decreasing function of the artificial thickness. This property is not desirable for our phase field model (*cf.* the corresponding discussion in the study of the limitation of the van der Waals model for the study of mesoscopic boiling systems in section 2.2). As a consequence, we disregard the choice of a linear interpolation function in the remainder of this study.

However this study has allowed to illustrate the characteristic of the general dispersion relation. These results will be used in the following to characterize the perturbation of the hs states corresponding to $\varphi \neq 0$ or 1 when the interpolation function is not linear.

6.5 Stability of homogeneous states using non-linear interpolation functions

In this case the nature of the instability differs mainly according to the fact that the initial phase field value φ^{hs} equals either the values 0 and 1 or not. We therefore first study the stability of the liquid and vapor phases in section 6.5.1. Then we study the stability of the other equilibrium solutions in section 6.5.2.

6.5.1 Liquid and vapor phase

Let us note also that all these results are still valid if the specific volume v instead of the density ρ is interpolated by either P_3 or P_5.

In the case where ρ is interpolated by either P_3 or P_5, $\varphi^{hs} = 0$ or 1 are solutions of the equilibrium condition (6.2) for any value of the parameter g^{*hs} (*cf.* section 3.4.1). In the following, we study the stability of these two possible states as a function of the parameter g^{*hs}. It is worth noting that in this case, $(d\rho/d\varphi)^{hs} = 0$. This condition considerably modifies the system of equations (6.3) linearized around the state hs and as a consequence the nature of the physical response of this state to perturbations.

A system of governing equations considerably modified In the case where $(d\rho/d\varphi)^{hs} = 0$, the linearized set of governing equations (6.3) for the perturbation reads

$$\begin{aligned}
\rho^{hs}\, V'_{,x} &= 0 \\
V'_{,t} &= -g'_{,x} - s^{hs} T'_{,x} + (\eta/\rho)^{hs}\, V'_{,xx} \\
(\rho\, c_P)^{hs}\, T'_{,t} &= k^{hs} T'_{,xx} \\
\frac{\rho^{hs}\, \varphi'_{,t}}{\kappa} &= \left(\frac{d^2\rho}{d\varphi^2}^{hs}\, g^{*hs} - \frac{\lambda}{h^2} \frac{d^2 W}{d\varphi^2}^{hs} \right) \varphi' + \lambda\, \varphi'_{,xx}
\end{aligned}$$

This set of linearized equations is very different from the set (6.3) obtained in the general case. Particularly the main variables are less-coupled: the linearized continuity equation only depends on the perturbed velocity, the energy balance equation only depends on the perturbed temperature and the AC equation only depends on the perturbed phase field. This has of course consequences on the determinant of the linear system. Introducing solutions proportional to $e^{\omega t + \mathbf{I} k_x x}$ and adopting the matrix notation used in section 6.2.5, the system reads $MX = 0$ with $X = (\varphi', T', g', V')$ and where M reads

$$M = \begin{bmatrix}
\omega \dfrac{\rho^{hs}}{\kappa} + \lambda \left(k_x^2 - (k^c)^2 \right) & 0 & 0 & 0 \\
0 & \left(\omega\, (\rho c_P)^{hs} + k_x^2\, k^{hs} \right) & 0 & 0 \\
0 & k_x s^{hs} & k_x & \left(\omega + k_x^2 \dfrac{\eta^{hs}}{\rho} \right) \\
0 & 0 & 0 & \mathbf{I} k_x \rho^{hs}
\end{bmatrix}$$

It is clear from this matrix notation that the perturbed velocity is always zero.

Dispersion relation The study of the roots of the determinant $\det M$ reduces to the study of the following polynomial in ω

$$\left((\rho\, c_P)^{hs}\, \omega + k^{hs}\, k_x^2 \right) \left(\frac{\rho^{hs}\, \omega}{\lambda\, \kappa} - (k^c)^2 + k_x^2 \right) = 0 \tag{6.24}$$

which has obviously two roots ω_1 and ω_2

$$\begin{aligned}
\omega_1 &= -\frac{k^{hs} k_x^2}{(\rho\, c_P)^{hs}} \\
\omega_2 &= -\frac{\lambda\, \kappa}{\rho^{hs}} \left(k_x^2 - (k^c)^2 \right)
\end{aligned}$$

The root ω_1 is a negative real and corresponds to a non-zero temperature perturbation as soon as $\omega_1 \neq 0$. In this case, and only in this case, the perturbed specific Gibbs free energy is non-zero, *i.e.* $g' \neq 0$. The root ω_2 of this polynomial corresponds to a non-zero phase field perturbation. It is either pure real or pure imaginary ($\omega_2 \in \mathbb{R} \cup \mathbb{IR}$). The dispersion relation (6.24) implies that unstable perturbations of the homogeneous state hs can only be achieved for a zero Fourier amplitude of the temperature field, *i.e.* $\Re(\omega) > 0 \Rightarrow \omega = \omega_2 \Rightarrow T' = 0 \,\&\, g' = 0$. Moreover since $V' = 0$ in the linear stage of the instability, the single dissipative process affecting the stability of bulk phases homogeneous states is therefore the Ginzburg-Landau relaxation. The dispersion relation (6.24) implies that unstable perturbations of the homogeneous state hs can only be achieved for low values of the wave number $k_x^2 \leq (k^c)^2$, which is fully consistent with our study of the general necessary and sufficient condition of stability in section 6.3.1. Let us note that for non-heat-conducting fluids ($k^{hs} = 0$) the stability condition is not modified, *i.e.* $k^c_{diss=0} = k^c$. In the purely non-dissipative case ($\kappa = +\infty$ and $k^{hs} = 0$), the growth rate is strictly null, $\omega = 0$. When only the Ginzburg-Landau relaxation is neglected ($\kappa = \infty$), the perturbation is always purely damped ($\omega = \omega_1$).

The stability condition Let us now study the stability condition. We therefore study the value of $(k^c)^2$ the interpolation function being either P_5 or P_3. Let us note that $(d^2W/d\varphi^2)^{hs} = 36$.

- ⋆ P_5:

  in this case $(d^2\rho/d\varphi^2)^{hs} = 0$ and thus from the expression (6.13) of k^c, we have $(k^c)^2 = -(d^2W/d\varphi^2)^{hs}/h^2 < 0$ and no perturbation can linearly destabilize the state hs

- ⋆ P_3:

  we consider two sub-cases whether $\varphi^{hs} = 0$, $hs = liquid$ or $\varphi^{hs} = 1$, $hs = vapor$

  - $hs = liquid$:
    In this case $(d^2\rho/d\varphi^2)^{liquid} = 6\,(\rho_{vap} - \rho_{liq}) < 0$, the condition of stability $(k^c)^2 < 0$ reads $36\sigma/h + 6\,(\rho_{liq} - \rho_{vap})g^{*liquid} > 0$ *i.e.* $\mathfrak{g} > -6$. As a consequence the liquid phase is unconditionally stable for any value of $g^{*liquid}$ satisfying $g^{*liquid} > -6\,(\rho_{liq} - \rho_{vap})^{-1}\sigma/h$, *i.e.* $P > P_{eq}(T_{eq}) - 6\,(1 - \rho_{vap}/\rho_{liq})^{-1}\sigma/h$.
  - $hs = vapor$:
    In this case $(d^2\rho/d\varphi^2)^{vapor} = 6\,(\rho_{liq} - \rho_{vap}) > 0$, and the vapor phase is unconditionally stable for any value of g^{*vapor} satisfying $g^{*vapor} < 6\,(\rho_{liq} - \rho_{vap})^{-1}\sigma/h$, *i.e.* $P < P_{eq}(T_{eq}) + 6\,(\rho_{liq}/\rho_{vap} - 1)^{-1}\sigma/h$.

It is worth noting that in the case when the specific volume v is chosen as a polynomial instead of the density ρ, we still have $(d\rho/d\varphi) = 0$ and for P_5 $(d^2\rho/d\varphi^2) = 0$, for P_3 the value is modified as $(d^2\rho/d\varphi^2)^{liquid} = -6\,(\rho_{liq})^2\,(v_{vap} - v_{liq}) < 0$ and $(d^2\rho/d\varphi^2)^{vapor} = 6\,(\rho_{vap})^2\,(v_{vap} - v_{liq}) > 0$, the whole analysis remaining unchanged.

The stability condition of the liquid and vapor phase in view of our applications of the model Let us comment these results. In the P_5 case, the liquid and vapor phases are unconditionally stable which is exactly the property targeted since it actually corresponds to the one of the incompressible sharp interface model. On the contrary, in the P_3 case, at a given temperature T, there exists a finite range of stable pressure values around the equilibrium pressure $P_{eq}(T)$. The liquid phase is always stable for pressures above $P_{eq}(T)$ which is fully consistent with the classical model of the stability of this phase. However, the liquid phase is also stable for a finite range of pressure below the saturation pressure. The lower limit $P_{lim,l}(T)$ of this range corresponds to the classical definition for the limit of metastability (*cf.* its presentation in section 2.2.2) and reads

$$P_{lim,l}(T) = 6\,\frac{\sigma}{h\,(1 - \rho_{vap}/\rho_{liq})}$$

As a consequence, even though this value is finite, it is possible to have a liquid phase that exists below the saturation pressure which is physically consistent. Let us consider we have access to an empirical value for $P_{lim,l}(T)$, we'd like our model to reproduce. Let us note that, in this case, the phase field model has an additional property with regard to the sharp interface model with incompressible phases. Indeed, in this sharp model, there does not exist any way to model such a limit of metastability. Let us comment this property in view of our targeted use of the model as a numerical method. In this case the artificial thickness for the interface h is dictated

by numerical constraints. As a consequence, the model is too constrained in order to be able to reproduce the correct scaling for the metastability limit $P_{lim,l}(T)$.

A similar reasoning applies concerning the stability of the vapor phase in the P_3 case. The same reasoning can also be reproduced when we consider the pressure as being fixed and study the range of temperature for which a phase is stable.

As a partial conclusion, only the choice P_5 for the interpolation function satisfies our requirements. Indeed in this case the liquid and vapor phase are unconditionally stable.

The ability to impose a fixed value for the metastability limit Let us consider again the existence of an empirical value for the metastability limit of the phases, say $P_{lim,l}(T)$, we'd like our model to reproduce. Let us consider the condition $(\partial\rho/\partial\varphi)(\varphi = 0) = 0$ satisfied. In this case, the liquid phase is actually an equilibrium solution for any value of the pressure. Therefore we arrive, following the same reasoning as in the beginning of this section to the stability condition for the liquid phase that reads

$$-6\,\frac{\sigma}{h} - (1 - \rho_{vap}/\rho_{liq})\,(P - P_{sat}(T))\,\frac{d^2\bar{P}}{d\varphi^2}(\varphi = 0) < 0$$

where we have considered the density as being interpolated by a function $\bar{P}$. The stability condition of the liquid phase is therefore related to the single value of $(d^2\bar{P}/d\varphi^2)(\varphi = 0)$. To impose a stability condition for the liquid phase as

$$P > P_{lim,l}(T)$$

where $P_{lim,l}(T) < P_{sat}(T)$ it is therefore sufficient to satisfy

$$\frac{d^2\bar{P}}{d\varphi^2}(\varphi = 0) = \frac{h\,(1 - \rho_{vap}/\rho_{liq})}{6\,\sigma\,(P_{sat}(T) - P_{lim,l}(T))} \hat{=}\, \zeta_{liq}$$

where we have introduced the non-dimensional quantity ζ_{liq} in order to simplify the writing of this condition. For the sake of simplicity, let us ignore the eventual temperature dependence of this quantity. Since the same type of relations have to be considered for the vapor phase, the function $\bar{P}$ needs to satisfy the following 6 conditions

$$\begin{aligned}
\bar{P}(0) = 0 \;\&\; \bar{P}(1) = 1 &\qquad \text{Interpolation function}\\
\frac{d\bar{P}}{d\varphi}(0) = \frac{d\bar{P}}{d\varphi}(1) = 0 &\qquad \text{Liquid and vapor always equilibrium states}\\
\frac{d^2\bar{P}}{d\varphi^2}(0) = \zeta_{liq} \;\&\; \frac{d^2\bar{P}}{d\varphi^2}(1) = \zeta_{vap} &\qquad \text{Control of the metastability limit}
\end{aligned}$$

Let us note that as soon as $P_{lim,l}(T) = P_{lim,v}(T) = \infty$, *i.e.* when we consider an unconditional stability of the liquid and vapor phases, we have $\zeta_{liq} = \zeta_{vap} = 0$ and we recover the conditions satisfied by the polynomial P_5. It is worth noting that, since 6 conditions need to be satisfied by the function $\bar{P}$, by choosing adequately $\rho(\varphi)$ as a polynomial of degree 5, it is thus possible to control and reproduce an empirical limit of metastability. Moreover this can be done for an arbitrary value of the artificial thickness h which was not possible in the P_3 case as shown in the previous paragraph.

As a partial conclusion, we have shown that it was possible to deal with a quasi-compressible phase field model, *i.e.* with incompressible bulk phases, and to reproduce an empirical limit of metastability of the bulk phases vapor and liquid. This property of the formulation must therefore be viewed as an advantage with respect to the native sharp interface model with incompressible bulk phases. Indeed the consequent phase field model constitutes a consistent regularization of this sharp interface model and in addition holds the ability to model empirically the stability of homogeneous states, and that for an arbitrary choice for the artificial thickness h of the interface.

6.5.2 Stability of homogeneous states for φ^{hs} different from 0 or 1

Determination of the sign of $(k^c)^2$, the extent of the $\varphi-$spinodal region It has been shown that the state hs is unconditionally stable if and only if $(k^c)^2 < 0$. Using the fact that φ^{hs} is a function of the non-dimensional

parameter $\mathfrak{g}$, the critical wave number $(k^c)^2$ reads (*cf.* equation (6.13))

$$(k^c)^2 = -\frac{1}{h^2}\left(\frac{d^2W}{d\varphi^2}(\varphi^{hs}(\mathfrak{g})) + \mathfrak{g}\frac{d^2P_n}{d\varphi^2}(\varphi^{hs}(\mathfrak{g}))\right)$$

It is straightforward to show that when ρ is interpolated by either P_3 or P_5, $\mathfrak{g}(d^2P_n/d\varphi^2)(\varphi^{hs}(\mathfrak{g}))$ is negative. In the P_3 or P_5 cases, $\mathfrak{g}^2\ (k^c)^2$ is therefore positive for $\varphi^{hs} \in [1/2 - \sqrt{3}/6 : 1/2 + \sqrt{3}/6]$ (where $d^2W/d\varphi^2$ is positive) but is *a priori* undetermined otherwise. The value of the non-dimensional parameter $h^2\ (k^c)^2$ as a function of the single variable $\mathfrak{g}$ is represented on the figures 6.2. We have represented the results for the P_1 case that corresponds

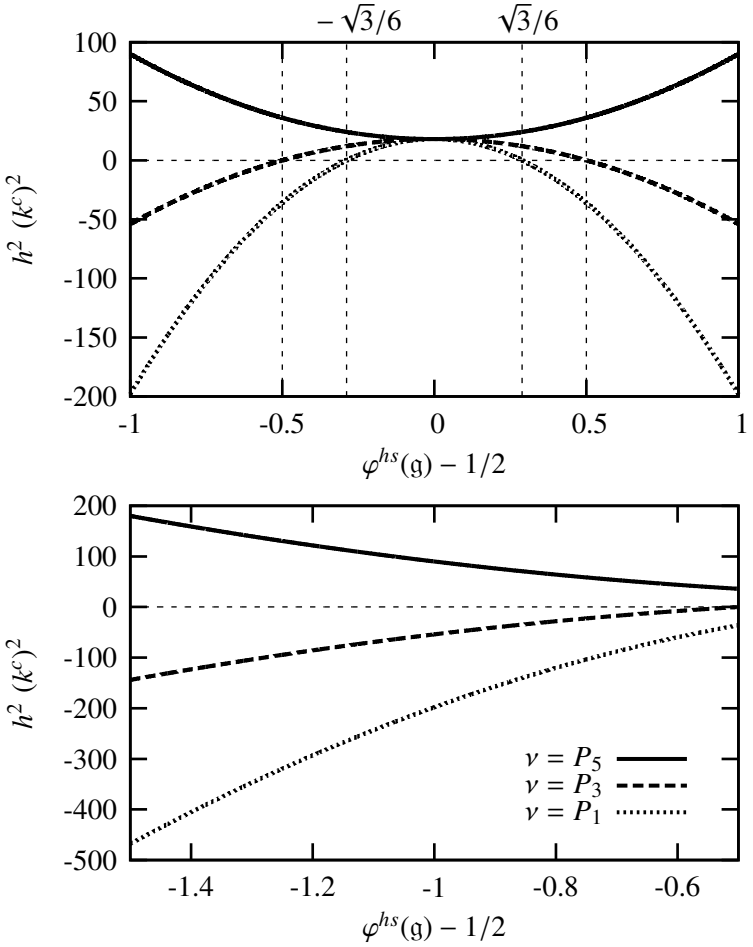

Figure 6.2: Value of $h^2\ (k^c)^2$ for the solutions $\varphi^{hs}(\mathfrak{g})$ of equation (6.2)

to the result derived in section 6.4.

Let us consider the P_3 case. As it has been previously stated, $h^2\ (k^c)^2$ is positive for $\varphi^{hs} \in [1/2 - \sqrt{3}/6 : 1/2 + \sqrt{3}/6]$. Moreover it is positive inside the whole interval $[0 : 1]$. However, as soon as $\varphi^{hs} \in]-\infty : 0[\cup]1 : +\infty[$, $h^2\ (k^c)^2$ is positive[9]. The necessary and sufficient condition of stability is therefore satisfied. The state *hs* corresponding to $|\mathfrak{g}| > 6$ (and therefore $|g^{*hs}| > 6\sigma/[h(\rho_l - \rho_v)]$ and $\varphi^{hs} \notin [0 : 1]$) is therefore unconditionally stable. Since the corresponding states do not correspond to desired stable homogeneous states, this property is not desirable. Moreover it is worth noting that the lower bound of physical values of $|g^{*hs}|$ that corresponds to these undesirable states approaches 0 as h is artificially increased.

Let us now consider the P_5 case. It is clear from figure 6.2 that $h^2\ (k^c)^2$ is strictly positive whatever the value of φ^{hs} and subsequently of g^{*hs}. The $\varphi-$spinodal region is therefore of infinite φ extent. The necessary condition of stability for any state different from 0 or 1 is therefore never satisfied as soon as the solution is different from

[9]Let us precise that the solutions 0 and 1 represented here do not correspond to the solutions 0 and 1 valid for any value of g^{*hs} considered in section 6.5.1, but to the particular case when φ^{hs} actually depends on g^{*hs}. This explains why in this case $h^2\ (k^c)^2$ is fully determined and is null for $\varphi^{hs} = 1/2 \pm 1/2$. In the previous case, where g^{*hs} was an independent parameter, the value of $h^2\ (k^c)^2$ for $\varphi^{hs} = 1/2 \pm 1/2$ actually depends on g^{*hs}.

the values 0 and 1 considered in section 6.5.1. Therefore these states are always unstable to low wave numbers perturbations[10].

As a consequence of these results, when ρ is interpolated by P_5, the states that correspond to $\varphi^{hs} \neq 0$ or 1 are always conditionally stable (unstable for low wave numbers). This is the result targeted for these states.

Sub-cases allowing an analytical study of the growth rate ω as a function of hs and k_x Let us now consider the different physical sub-cases for which the analytical expression of the growth rate ω can be easily derived. In sections 6.3.2-6.3.3, we have derived some very general features for the study of these physical sub-cases. They have been applied to the study of the stability of homogeneous states in the case of a linear interpolation function in section 6.4. In the present case, the same features are still valid, since the only modified parameter is the expression for $(k^c)^2$ which has been studied hereinabove. As a consequence, using this similarity the following conclusions can be drawn

- ⋆ in the P_5 case the hs states are always inside the isothermal $\varphi-$spinodal region. We then refer to the LHS of table 6.1 that allows to characterize the dispersive nature of the perturbation wave for states inside the isothermal $\varphi-$spinodal region. When isothermal dissipative mechanisms are taken into account, two sub-cases can be distinguished. Either the isothermal dissipation is large ($\vartheta_{diss}^{isoth} > \vartheta^c$) and the perturbation wave is never dispersive, either it is low and the perturbation wave is dispersive for large wave numbers (corresponding to dissipative waves).

- ⋆ in the P_3 case we have still two cases whether the state is inside the $\varphi-$spinodal region ($\varphi^{hs} \in [0:1]$ or $|\mathfrak{g}| \in [6:+\infty[$) or outside this region. We are therefore exactly in the same case than the one studied for the linear interpolation case, and as a consequence we refer to the study of these cases in section 6.4.

As a partial conclusion, the dispersive nature of the perturbation wave for homogeneous equilibrium states different from liquid and vapor has already been fully determined in the study of the linear interpolation case. In the P_3 case, since the state hs is either inside or outside the isothermal $\varphi-$spinodal region, the whole results obtained for the linear interpolation case is relevant. In the P_5 case, since the states hs are always inside the isothermal $\varphi-$spinodal region, only the corresponding results must be taken into account. As a consequence, in the P_5 case, dispersive perturbation waves only corresponds to large isothermal dissipation and to large wave numbers corresponding to damped perturbations.

6.6 Conclusion on the study of the stability of homogeneous states

We have studied the linear stage of evolution of the perturbations of a one dimensional homogeneous state at equilibrium using our quasi-compressible phase field model of the liquid-vapor flows with phase-change. First we have motivated this study by the desire to justify the choice for a fifth order polynomial for the interpolation function that enters the expression for the specific Gibbs free energy of the model. The study of the dynamics of a perturbation of an homogeneous equilibrium state including a discussion on the influence of the interpolation function on this dynamics has, to our knowledge, never been presented for the diffuse interface models with density contrast between the phases.

We have derived the expression for the dispersion relation for the perturbation in the non-isothermal dissipative case. Using the Hurwitz criterion, we have determined a necessary and sufficient condition of stability. We have shown that this condition is related to the belonging of the state to a $\varphi-$spinodal region defined as $(\partial^2 g/\partial\varphi^2) < 0$. We have then studied the dispersive nature of the perturbation wave for a set of relevant physical sub-cases, namely the isothermal, without density difference, non-dissipative and non heat-conducting cases. More generally, the states inside the $\varphi-$spinodal region are unstable for low wave number perturbations, whereas

[10] It is worth noting that from figure 6.2 it can be seen that h^2 $(k^c)^2$ remains positive when φ^{hs} approaches $1/2 \pm 1/2$. This could appear as inconsistent with the study of the stability of the liquid and vapor states in section 6.5.1. Indeed we have shown that for $\varphi^{hs} = 1/2 \pm 1/2$, we had $\forall \mathfrak{g}$, $(k^c)^2 < 0$. For the liquid and vapor states $\varphi^{hs} = 1/2 \pm 1/2$ we have actually $\mathfrak{g}\,(\partial^2 P_5/\partial\varphi^2) = 0$. In the present case considered we have $|\mathfrak{g}| \to +\infty \Rightarrow \varphi^{hs} \to 1/2 \pm 1/2$, as it has been shown in section 3.4.1 (*cf.* figure 3.9). However φ^{hs} is then a function of $\mathfrak{g}$ and as a consequence $(\partial^2 P_5/\partial\varphi^2)^{hs}$ is also a function of $\mathfrak{g}$. Therefore, even though we have still $|\mathfrak{g}| \to +\infty \Rightarrow (\partial^2 P_5/\partial\varphi^2)^{hs} \to 0$, we have indeed $|\mathfrak{g}| \to +\infty \Rightarrow \mathfrak{g}\,(\partial^2 P_5/\partial\varphi^2)^{hs} \to 72$ which is finite and positive and actually yields to $|\mathfrak{g}| \to +\infty \Rightarrow (k^c)^2 \to 36$ as it can be seen on figure 6.2. Since this value is positive, the states corresponding to $|\mathfrak{g}|$ as big as we want, even though they actually tend to the phase field values (of the stable liquid and vapor phases) are still unstable.

outside this region they are unconditionally stable. It has been shown that the $\varphi-$spinodal region corresponds indeed to a range of values for the physical parameter g^*.

The choice for the interpolation function determines the different possible equilibrium states and as a consequence the extend of the $\varphi-$spinodal region. When it is chosen as P_1 or P_3, it corresponds to a finite range of g^* values, this range being a decreasing function of the artificial thickness. As a consequence undesired states (*i.e.* $\varphi \neq 0$ or 1) can actually become stable. Moreover the domain of existence or stability (limit of metastability) of the liquid and vapor phase are also decreasing with the artificial thickness. As a consequence the stability of the desired states ($\varphi = 0$ or 1) is not controlled. When the interpolation function is chosen as P_5, all the equilibrium homogeneous states different from the liquid and vapor are inside the $\varphi-$spinodal region. As a consequence, apart from the liquid and vapor phases which are then unconditionally stable, all the other equilibrium states are only conditionally stable. This justifies the choice for a polynomial of degree 5 for the interpolation function. Indeed it provides an interesting property for the model since it allows actually to recover the infinite limit of metastability consistent with the incompressible nature of the bulk phase considered.

Let us note that the dynamics of phase separation in the solid-liquid case using the fifth order polynomial P_5 for the interpolation function is illustrated using two-dimensional numerical simulations in section 8.1.5.

Moreover the number of degrees of freedom determining the interpolation function with a fifth order polynomial (*i.e.* 6) has been shown to be sufficient to control the stability of the liquid and vapor states *i.e.* to impose an empirical domain of stability of g^* values for which the state is stable. The subsequent model has therefore an interesting additional property compared to the native sharp interface model for which it provides a consistent regularization: it is possible to include a limit of metastability. The consequences of such a choice for the interpolation function on the stability of the equilibrium states different from the liquid and vapor has not been investigated. It would be interesting to study it.

Chapter 7

Analytical study of one-dimensional dynamics

In this chapter, we study analytically, with our phase field model, out of equilibrium one-dimensional phase change when the transition front is a traveling wave. The goal of this analytical study is two-fold. First, this study allows to determine an approximation of the internal structure of the diffuse interface in non-equilibrium conditions. We derive approximate solutions for the profiles of the main variables in the bulk phases and within the interface transition layer. We study the dependence of these solutions on the value of the non-dimensional thickness of the interface ε. Secondly, we determine the relation between this internal structure and the larger scale phase transition process. This corresponds to the determination of the equivalent sharp interface model, or sharp interface limit of our diffuse interface model.

In a first part, we study the sharp interface model for liquid-vapor flows with phase change (see section 7.1). From the general writing of the Rankine-Hugoniot jump conditions, the interface entropy production must be specified, *e.g.* Truskinovsky [134]. The model for the interface entropy production provides a kinetic relation for the phase transition. It is shown that this kinetic relation actually defines a closure law for the interface temperature and pressure, namely an out of equilibrium Clapeyron relation (or Gibbs-Thomson equation in the uniform density case). This result is used in the following to study the sharp interface limit of our phase field model. In a second part, we derive this limit. The technique of matched asymptotic expansions is applied for the solving of the system of governing equations (5.59) for a steady state phase change process (see section 7.2). In this system, the parameter ε, defined as the ratio of the interface thickness to the capillary length l, is considered as a small parameter. The solution is the sum of an outer solution (bulk phase) and an inner solution (interface transition layer). Solutions in both the bulk phases and the interface transition layer are expanded with respect to ε and leading order terms are derived. Three canonical systems are studied. First, the density is considered as uniform and we study the coupling between the thermal and phase field parts of the model (see section 7.3). Second, we study the isothermal phase field model and the coupling between mechanics and phase field (see section 7.4). Finally, we study our phase field model dedicated to liquid-vapor flows with phase change including thermal, mechanical and phase field parts of the model (see section 7.5). All the leading order results of this study are consistent with a particular sharp interface model known as the normal growth approximation mostly justified for slow phase boundaries. In a third part (see section 7.6), we study how this latter result is in fact related to the particular choice made for the scaling of the mobility α in section 5.3.4. Using another choice for this scaling, we demonstrate the ability of the phase field model to deal with kinetic relations that are more accurate for fast kinetics.

7.1 Sharp interface models

In this section, we study the sharp interface model for the liquid vapor phase transition. The goal is to study the interface jump conditions in order to compare the sharp interface limit of the phase field model with the sharp interface model. In particular, we show how the non-equilibrium relation giving the interface temperature and pressure can be related to the interface entropy production thanks to the formalism of the kinetic relations. The detailed derivation of the following results can be found in the appendix A.2.

For the sharp interface model, a variable Y takes specific values on each side of the interface, say + and −. These values are denoted Y^+ and Y^- in the following. The Y jump and the value of Y at the interface are defined

as follows

$$\begin{aligned} [\![Y]\!] &\triangleq Y^+ - Y^- \\ \{Y\} &\triangleq \frac{Y^+ + Y^-}{2} \end{aligned}$$

7.1.1 Rankine-Hugoniot jump conditions

General writing Let us consider a one-dimensional traveling wave of constant speed $\mathcal{D}$. Integral of the Navier-Stokes equations over the interface discontinuity, yields the general form of the Rankine-Hugoniot jump conditions:

$$[\![\rho(\mathcal{D}-V)]\!] = 0 \tag{7.1a}$$

$$[\![P]\!] + [\![\rho(\mathcal{D}-V)^2]\!] = 0 \tag{7.1b}$$

$$\rho(\mathcal{D}-V)\left[\!\!\left[\frac{V^2}{2}+e\right]\!\!\right] - [\![q]\!] - [\![PV]\!] = 0 \tag{7.1c}$$

$$\left[\!\!\left[\frac{q}{T}\right]\!\!\right] - \rho(\mathcal{D}-V)[\![s]\!] = \mathcal{R}_s \tag{7.1d}$$

where V is the velocity, q the heat flux, e the specific internal energy, s the specific entropy and $\mathcal{R}_s$ the interface entropy production that satisfies the Clausius Duhem inequality

$$\mathcal{R}_s \geq 0$$

It is worth pointing out that $\mathcal{R}_s$ needs to be specified to close the problem, its study is the subject of the following developments.

Pressure and velocity jumps Let us introduce the constant mass transfer rate Γ

$$\Gamma \triangleq \frac{\mathcal{D}-\{V\}}{\{1/\rho\}} = \rho_l(\mathcal{D}-V_l) = \rho_v(\mathcal{D}-V_v)$$

where the second equality is obtained thanks to equation (7.1a) (*cf.* equation (A.15)). From the jump conditions (7.1), it is straightforward to show that the following jump conditions are satisfied

$$[\![V]\!] = -\Gamma\left[\!\!\left[\frac{1}{\rho}\right]\!\!\right] \tag{7.2a}$$

$$[\![P]\!] = -\Gamma^2\left[\!\!\left[\frac{1}{\rho}\right]\!\!\right] \tag{7.2b}$$

The latter pressure jump classically called pressure recoil. It is shown in the following study that, in the sharp limit of our phase field model, these relations are satisfied.

Kinetic relation and interface entropy production The interface entropy production $\mathcal{R}_s$ can be rewritten as a product of a flux by a force, where the flux is the mass transfer rate Γ. To show this, we transform the LHS of equation (7.1d). The detailed derivation is provided in the appendix A.2.2. Introducing the internal energy e defined as

$$e = g + Ts - \frac{P}{\rho}$$

it is straightforward to show that

$$[\![s]\!]\{T\} = [\![e]\!] - [\![g]\!] - [\![T]\!]\{s\} + \left[\!\!\left[\frac{P}{\rho}\right]\!\!\right]$$

Therefore, using the energy jump condition (7.1c) as well as the identities (7.2), the interface entropy production (7.1d) reads

$$\mathcal{R}_s\{T\} = \Gamma\left([\![g]\!] + [\![T]\!]\{s\} + \frac{[\![(V-\mathcal{D})^2]\!]}{2}\right) - [\![q]\!] + \left[\!\!\left[\frac{q}{T}\right]\!\!\right]\{T\}$$

It yields naturally to the introduction of a driving force $\mathcal{G}$ defined as (*cf.* equation (A.20))

$$\mathcal{G} \;\hat{=}\; [\![g]\!] + [\![T]\!]\{s\} + \frac{[\![(V-\mathcal{D})^2]\!]}{2} \tag{7.3}$$

such that $\mathcal{R}_s$ reads (*cf.* equation (A.21))

$$\mathcal{R}_s\,\{T\} = \Gamma\,\mathcal{G} - [\![T]\!]\left\{\frac{q}{T}\right\} + [\![q]\!]\left(\{T\}\left\{\frac{1}{T}\right\} - 1\right) \tag{7.4}$$

Two canonical sharp interface models can be considered, the process being either isothermal ($[\![T]\!] = 0$) or adiabatic $q = 0$. In these two limits, we get

$$\{T\}\,\mathcal{R}_s = \Gamma\,\mathcal{G} \tag{7.5}$$

The kinetic relation is the closure law that gives the driving force as a function of the mass transfer rate, *i.e.* $\mathcal{G}(\Gamma)$. In the following we consider the two isothermal and adiabatic limits for the phase change process and thus assume equation (7.5) to be satisfied.

7.1.2 Interface entropy production and non-equilibrium Clapeyron relations

Models for $\mathcal{R}_s$ Two simple models for the interface entropy production can be considered. The first one assumes that the interface is at equilibrium, *i.e.*

$$\mathcal{R}_s = 0$$

As a consequence, the driving force is itself zero. It is worth pointing out that, as a consequence, in the adiabatic or isothermal limits, the following jump condition is satisfied (*cf.* equation (7.1d))

$$[\![q]\!] = \Gamma\,\mathcal{L}$$

where $\mathcal{L} = T[\![s]\!]$ is the latent heat. This relation is classical in the sharp interface models.

The second model assumes that the interface entropy production is quadratic in Γ

$$\mathcal{R}_s \propto \Gamma^2$$

as a consequence, the driving force is linear in Γ

$$\mathcal{G} \propto \Gamma$$

This latter model is classically known as the *normal growth theory*.

In the following, we relate this latter theory to the models for the interface pressure and temperature.

Out of equilibrium Gibbs-Thomson and Clapeyron relations In sharp interface models of phase transition, the relation between the interface pressure and the interface temperature as a function of the mass transfer rate can be given as closure laws. These closure laws can be related to the closure law for the interface entropy production.

Let us assume that, in the evaluation of the interface jump conditions, the compressibility of the bulk phases can be neglected compared to the density difference between the bulk phases. Similarly, let us assume that the sensible heat is negligible compared to the latent heat. In appendix A.2.3, we show that these assumptions yield (*cf.* equation (A.26))

$$\mathcal{G} \simeq \Big(\{P\} - P_{eq}\Big)\,[\![1/\rho]\!] - \Big(\{T\} - T_{eq}\Big)\,[\![s]\!] \tag{7.6}$$

where P_{eq} and T_{eq} are arbitrary references for the pressure and temperature, (P_{eq}, T_{eq}) being located on the saturation curve. It is clear that the latter expression at equilibrium ($\mathcal{R}_s = 0 \Rightarrow \mathcal{G} = 0$) is a Clapeyron relation. According to the normal growth theory ($\mathcal{G} \propto \Gamma$), it is straightforward that

$$\Big(\{P\} - P_{eq}\Big)\,[\![1/\rho]\!] - \Big(\{T\} - T_{eq}\Big)\,[\![s]\!] \propto \Gamma$$

This relation is clearly non-equilibrium Clapeyron relation. Let us consider the reduction of our model in the uniform density case. Then $[\![1/\rho]\!] = 0$ and it yields

$$\Big(\{T\} - T_{eq}\Big)\,[\![s]\!] \propto \Gamma$$

The latter relation is thus the classical Gibbs-Thomson kinetic relation. For the isothermal model, we get a relation for the interface pressure level as

$$\Big(\{P\} - P_{eq}\Big)\,[\![1/\rho]\!] \propto \Gamma$$

Targeted relations As a consequence of the previous developments, the sharp interface models are closed by a model for the kinetic relation $\mathscr{G}(\Gamma)$. It has been shown that this relation defines the interface entropy production and is also related to a non-equilibrium relation between the interface pressure and the interface temperature. In the following study of the sharp limit of our phase field model, we therefore target to make these relations explicit. It is worth pointing out that with diffuse interface models we can derive rather than postulate the kinetic relation. We then compare the obtained kinetic relation with the normal growth approximation.

7.2 Matched asymptotic expansions

Let us introduce the use of matched asymptotic expansions to study steady state one-dimensional liquid-vapor phase transitions. Matched asymptotic expansions are classically used for the study of diffuse interface models (*e.g.* [1, 5, 47, 73, 49] for the phase field models dedicated to the solid-liquid phase transition and [89, 108] for the Cahn-Hilliard model dedicated to binary fluids) and more generally in fluid mechanics, *e.g.* [143]. A more detailed presentation of this formalism is provided in the appendix B.1.

Our goal is to solve the system of governing equations (5.59) for a constant speed of displacement of the interface $\mathcal{D}$ and whose main variables are $(\varphi, \tilde{P}, T, V)$. This system reads

$$\alpha\,\varepsilon^2\,(\mathcal{D}-V)\,\varphi_{,x} = \varepsilon\,\partial_\varphi\nu\Big(\tilde{P}\,-\,T\Big) + v\,\Big(\partial_\varphi W - \varepsilon^2\varphi_{,xx}\Big) + \partial_\varphi\nu\left(W - \frac{\varepsilon^2}{2}\varphi_{,x}^2\right) \tag{7.7a}$$

$$(\rho V)_{,x} = -\rho^2\,\partial_\varphi\nu\,(\mathcal{D}-V)\,\varphi_{,x} \tag{7.7b}$$

$$(V-\mathcal{D})\,\rho V_{,x} = -\tilde{P}_{,x} \tag{7.7c}$$

$$(V-\mathcal{D})\,\rho\,T_{,x} = \frac{(k\,T_{,x})_{,x}}{Pe} - (V-\mathcal{D})\,\rho\,(1+T)\,\partial_\varphi\nu\,\varphi_{,x} + (\mathcal{D}-V)^2\,\frac{\rho\varepsilon}{\alpha}\,(\varphi_{,x})^2 \tag{7.7d}$$

where we introduced the notation $\partial_\varphi f = \partial f/\partial\varphi$ for the sake of legibility. The parameter ε is the ratio of the interface thickness to the capillary length l. The two parameters α and Pe are kinetic parameters corresponding to the dissipative processes considered, namely the Ginzburg-Landau relaxation for α and the Fourier heat conductivity for Pe (*cf.* their definition in section 5.3).

$$Pe = \frac{\sigma}{\sqrt{\mathcal{L}}(k/c_P)}$$
$$\alpha = \kappa\,h\,\rho\,\sqrt{\mathcal{L}}$$

Scale separation hypothesis The fields behave qualitatively differently close and far from the interface. In the interface region they vary rapidly over distances of the order of magnitude of the interface thickness $O(h)$ (*i.e.* $O(\varepsilon)$ in non-dimensional length) while far from the interface they vary on a scale $O(l)$ (*i.e.* $O(1)$ in non-dimensional length). We denote these zones as, respectively, the inner and outer regions and there exists a valid scale separation between these regions as long as $\varepsilon \ll 1$. Therefore, it is relevant to consider and derive two sub-problems, namely the inner and outer problems. We expand the corresponding solutions (*i.e.* the profiles of the main variables) in powers of the small parameter ε. For any variable Y, the solution therefore reads

$$Y(x,\varepsilon) = Y_0(x) + \varepsilon\,Y_1(x) + O(\varepsilon^2)$$

The approximate solutions retained correspond to the leading order terms of these expansions. We assume the existence of an intermediate zone where both expansions are valid and where the inner and outer solutions match. We are thus able to define boundary conditions for both the outer and the inner problems through the assumption of continuity of the global solution; these are the matching conditions.

Outer problem Since the typical length scale of the outer problem is l, the system of governing equations is given by (7.7). Indeed, the non-dimensional form (7.7) of the system of governing equations has been derived by considering l as the relevant length scale (*cf.* section 5.3.4). The outer problem is valid on each side of the interface, *i.e.* the bulk phase domains + and −, the transition layer being viewed as a sharp discontinuity of the outer solutions. The sharp position of the interface x_i is considered as the position where $\varphi(x_i) = 1/2$; therefore $\mathcal{D} = dx_i/dt$. Let us note that another relevant definition of the interface position could be such that the excess mass is zero. However, this latter definition cannot be used in the uniform density case. Nevertheless, the definition of the interface position is somewhat arbitrary. Therefore, in the remainder of this study, we discuss, if the case arises, the dependence of the results to the definition of the interface position.

For the outer problem, the interface is viewed as a sharp discontinuity and $x_i(t)$ denotes its position. Since the solution is a traveling wave, the value of $\mathcal{D}$ is constant. In each bulk phase, this position is therefore viewed as a boundary. It is worth pointing out that the outer problem is a sharp problem. In order not to be confusing while considering the outer fields values at the interface, the position of the interface is denoted x_i^- for the bulk domain contained in $[0; x_i]$ and x_i^+ for the one in $[x_i; 1]$. The outer variable, say Y at x_i^+, resp. x_i^- is denoted Y^+, resp. Y^-.

Inner problem The inner problem concerns the study of the interface transition layer. We consider therefore the inner abscissa $\bar{x}$ defined as

$$\bar{x} \triangleq \frac{x - x_i(t)}{\varepsilon}$$

and we write

$$Y' \triangleq \frac{\partial Y}{\partial \bar{x}}$$

The bulk domains are considered as the external boundaries of the inner domain. The bulk phase contained in the domain −, resp. +, is thus reached asymptotically at $\bar{x} = -\infty$, resp. $\bar{x} = +\infty$. Using this new scaling for the abscissa, it is easy to show that the system of governing equations for the inner problem reads

$$\alpha\,\varepsilon\,(\mathcal{D} - V)\,\varphi' = \varepsilon\,\partial_\varphi\nu\left(\tilde{P} - T\right) + v\,\left(\partial_\varphi W - \varphi''\right) + \partial_\varphi\nu\left(W - \frac{(\varphi')^2}{2}\right) \tag{7.8a}$$

$$(\rho V)' = -\rho^2\,\partial_\varphi\nu\,(\mathcal{D} - V)\,\varphi' \tag{7.8b}$$

$$(V - \mathcal{D})\,\rho V' = -\tilde{P}' \tag{7.8c}$$

$$\varepsilon\,(V - \mathcal{D})\,\rho\,T' = \frac{(k\,T')'}{Pe} - \varepsilon\,(V - \mathcal{D})\,\rho\,(1 + T)\,\partial_\varphi\nu\,\varphi' + (\mathcal{D} - V)^2\,\frac{\rho\varepsilon}{\alpha}\,(\varphi')^2 \tag{7.8d}$$

It is worth pointing out that the scaling in ε of the different terms of the *AC* equation (7.8a) and of the entropy equation (7.8d) differs from the one of system (7.7) while the scaling of the momentum balance (7.8c) and continuity equations (7.8b) remains unchanged.

Matching conditions The matching conditions between inner f and outer f^{ext} solutions read

$$\lim_{x \to x_i^\pm} f_0^{ext} = \lim_{\bar{x} \to \pm\infty} f_0 \tag{7.9a}$$

$$\lim_{\bar{x} \to \pm\infty} f_0' = 0 \tag{7.9b}$$

(7.9c)

$$\lim_{x \to x_i^\pm} f_{0,x}^{ext} = \lim_{\bar{x} \to \pm\infty} f_1' \tag{7.9d}$$

$$\lim_{x \to x_i^\pm} f_1^{ext} = \lim_{\bar{x} \to \pm\infty} \left[f_1 - \bar{x} \lim_{x \to x_i^\pm} f_{0,x}^{ext} \right] \tag{7.9e}$$

$$\lim_{\bar{x} \to \pm\infty} f_0'' = 0 \tag{7.9f}$$

$$\lim_{\bar{x} \to \pm\infty} f_1'' = 0 \tag{7.9g}$$

7.3 Uniform density phase transition

In this section, we study the phase-field model for the liquid-solid phase transition. This model is easily obtained from the general model presented in the previous section by assuming that the density ρ is constant (*cf.* its presentation in section 3.3.2). It is easy to show that the corresponding system of governing equations for the outer problem reads (*cf.* equations (5.60))

$$\alpha\,\varepsilon^2\,\mathcal{D}\,\varphi_{,x} = \varepsilon\,\partial_\varphi\nu(\varphi)\,T - \left(\partial_\varphi W(\varphi) - \varepsilon^2\varphi_{,xx}\right) \tag{7.10a}$$

$$\mathcal{D}\,T_{,x} = \frac{(k\,T_{,x})_{,x}}{Pe} + \mathcal{D}\,(1+T)\,\partial_\varphi\nu(\varphi)\,\varphi_{,x} - \mathcal{D}^2\,\frac{\varepsilon}{\alpha}\,(\varphi_{,x})^2 \tag{7.10b}$$

and that the corresponding inner problem reads

$$\alpha\,\varepsilon\,\mathcal{D}\,\varphi' = \varepsilon\,\partial_\varphi\nu(\varphi)\,T - \left(\partial_\varphi W(\varphi) - \varphi''\right) \tag{7.11a}$$

$$\varepsilon\,\mathcal{D}\,T' = \frac{(k\,T')'}{Pe} + \mathcal{D}\varepsilon\,(1+T)\,\partial_\varphi\nu(\varphi)\,\varphi' - \mathcal{D}^2\,\frac{\varepsilon}{\alpha}\,(\varphi')^2 \tag{7.11b}$$

It is worth noting that this model corresponds to the most widely used phase field model devoted to the study of the liquid-solid phase transitions. The internal structure of the transition layer has been already extensively studied, *e.g.* Karma and Rappel [73]. However, the entropy equation (7.11b) corresponding to our model differs from the widely used one, since it incorporates the dissipative term associated to the Ginzburg-Landau relaxation ($-\mathcal{D}^2\varepsilon(\varphi')^2/\alpha$). We therefore determine in the following the effect of this additional term on the structure of the interface as an internal layer as well as on the resulting equivalent sharp representation of its internal dynamics.

In the following, we first solve the leading order solutions of $\varphi(x,\varepsilon)$ and $T(x,\varepsilon)$ in ε (see section 7.3.1). We then use these results to determine the leading order kinetic relation for the equivalent sharp model (see section 7.3.2) and show how it is associated to the Ginzburg Landau relaxation and to the model for the heat conductivity $k(\varphi)$.

7.3.1 Phase-field and temperature solutions

Outer phase field problem In the outer problem, and at leading order in ε, equation (7.10a) reads

$$\partial_\varphi W(\varphi_0) = 0$$

It implies the phase field value is necessarily equal to the bulk phases values (*i.e.* $\varphi^\pm = 0$ or 1). Moreover, it can be shown that this result is valid at any order in ε (*cf.* section B.2.2). As a consequence, even in non-equilibrium conditions, the bulk phase values are 0 or 1. Therefore, the jump of the phase field at the interface satisfies

$$[\![\varphi]\!] = \pm 1$$

This property is of major interest since it means that the bulk states are controlled even in out of equilibrium situations.

Inner phase field problem At leading order in ε, the *AC* equation (7.11a) reads

$$\partial_\varphi W(\varphi_0) - \varphi_0'' = 0 \tag{7.12}$$

This equation is the equilibrium equation for a planar two-phase equilibrium (3.41) (*cf.* section B.2.3). As a consequence, the phase-field inner profile φ_0 is the equilibrium profile and the inner phase field profile at leading order in ε therefore reads (*cf.* section B.2.3)

$$\varphi_0(\bar{x}) = 1/2 + ([\![\varphi]\!]/2)\ \tanh(3\ \bar{x})$$

Interface temperature and temperature jump The leading order entropy equation of the inner problem reads (*cf.* equation (7.11b))

$$\left(k(\varphi_0)\, T_0'\right)' = 0$$

This yields a uniform temperature gradient. According to the boundary conditions for the leading order solutions of the inner problem (matching condition (B.7a)),

$$\lim_{\bar{x}\to\pm\infty} T_0' = 0$$

the gradient across the interface transition layer is thus zero and the inner temperature is therefore uniform at leading order (*cf.* section B.2.4). According to the matching condition (B.7b), the outer temperature jump at the interface is therefore zero at leading order, *i.e.*

$$[\![T]\!]_0 = 0$$

The *AC* equation at first order in ε reads (*cf.* equation (B.21a))

$$\mathcal{D}\,\varphi_0' = \alpha\left[-\varphi_1'' + \partial_{\varphi^2} W(\varphi_0)\,\varphi_1 - T_0^i\,\partial_\varphi \nu(\varphi_0)\right]$$

$\varphi_0'(\bar{x})$ is solution of the homogeneous part of this differential equation in φ_1. Using the solvability condition (see section B.2.6 for detailed calculations), the integral over the transition layer ($\bar{x} \in [-\infty; = \infty]$) of the scalar product of the *AC* equation at first order in ε by φ_0' is independent of φ_1. Since φ_0 is known, it is thus possible to deduce the interface temperature. It yields (*cf.* equation (B.29))

$$T_0^i \,\hat{=}\, T_0(x_i) = \{T\}_0 = -\frac{[\![\varphi]\!]\,\mathcal{D}}{\alpha} \tag{7.13}$$

The sign of $[\![\varphi]\!]$ depends on the relative position of the solid and liquid phases in the system (*i.e.* the values $\varphi^\pm$). Since by convention, the sign of $\mathcal{D}$ depends also on the relative position of the phases , the value of T_0^i only depends on the phase transformation considered: it is positive for a solidification and negative for a liquefaction. At equilibrium ($\mathcal{D} = 0$), the interface temperature is equal to the equilibrium temperature ($T_0^i = 0$). At leading order in ε, the shift of the interface temperature with regard to the equilibrium temperature is associated to the Ginzburg-Landau internal dissipative process through the parameter α. At the limit $\alpha \to +\infty$, which corresponds to the thermodynamic equilibrium condition (equilibrium relation $\tilde{\mu} = 0$), at leading order in ε, the temperature of the interface is the equilibrium temperature even for $\mathcal{D} \neq 0$. This result is a classical result for the phase-field model dedicated to the study of liquid-solid phase transitions (*e.g.* [1, 73]) and is associated to the ability of the phase-field model to recover the classical Gibbs-Thomson relation.

$O(\varepsilon)$ phase field profile Since the interface temperature T_0^i is given by (7.13), the order $O(\varepsilon)$ *AC* equation (7.11a) reads (*cf.* (B.21a))

$$\mathcal{D}\,\varphi_0' = \alpha\left[-\varphi_1'' + \partial_{\varphi^2} W(\varphi_0)\,\varphi_1 - T_0^i\,\partial_\varphi \nu(\varphi_0)\right]$$

This equation can be integrated to derive $\varphi(\bar{x})$. This integration is derived in detail in section B.2.7 and yields (*cf.* equation (B.35))

$$\varphi_1(\bar{x}) = \frac{[\![\varphi]\!]}{24}\,\frac{\mathcal{D}}{\alpha}\,\ln(\cosh(3\,\bar{x}))\,(1-\tanh^2(3\,\bar{x})) \tag{7.14}$$

This function is represented on figure 7.1. The above relation shows that the phase-field inner profile is zero for either zero displacement ($\mathcal{D} = 0$) or infinite mobility $\alpha = +\infty$. To our knowledge, this analytical expression has not been determined in previous studies of phase-field models. As shown on figure B.2, the profile consists on a thinning of the thickness of the interface on one side and on a thickening on the opposite side. It is of interest for numerics to know this function since it provides the leading order in ε deformation of the non-equilibrium phase field profile with regard to the controlled equilibrium one .

Heat flux jump To study the heat flux jump, the order $O(\varepsilon)$ entropy equation, that reads as follows, must be integrated

$$\left(k(\varphi_0)T_1'\right)' = -\left(1+T_0^i\right)\,\mathcal{D}\,Pe\,\partial_\varphi \nu(\varphi_0)\,\varphi_0' - \frac{Pe\,\mathcal{D}^2}{\alpha}\left(\varphi_0'\right)^2 \tag{7.15}$$

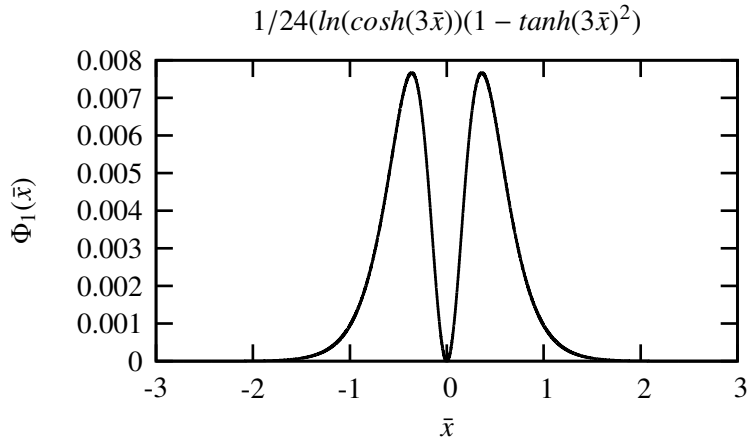

Figure 7.1: function $\varphi_1(\bar{x})$

The matching conditions yield (*cf.* equation (B.8a))

$$[\![q_0]\!] = \lim_{\bar{x}\to\infty} \left[k(\varphi_0(\bar{x}))\, T_1'(\bar{x}) - k(\varphi_0(-\bar{x}))\, T_1'(-\bar{x}) \right]$$

Using an integration of equation (7.15) between $\bar{x} = \pm\infty$ and using the expression (7.13) for T_0^i, we get (detailed calculations can be found in section B.2.8) for the leading order outer heat flux jump (*cf.* (B.40))

$$\begin{aligned} [\![q_0]\!] &= -T_0^i\, Pe\, \alpha \\ &= [\![\varphi]\!] Pe\, \mathcal{D} \end{aligned} \tag{7.16}$$

The first expression provides the interface boundary condition that, in addition to $[\![T_0]\!] = 0$, allows to solve the leading order outer thermal problem. The second writing is associated to the dimensional classical relation

$$[\![q]\!] = \mathcal{D}\,\mathcal{L}$$

where $\mathcal{L}$ is the latent heat. This relation corresponds to the jump condition of the classical Stefan problem and is thus recovered at leading order in ε by our model.

To determine the leading order terms of the kinetic relation of the sharp problem in the non-equilibrium situations where there is zero phase change but non-zero heat flux, it is required to study the equation of evolution of the temperature up to $O(\varepsilon)$. This study is the purpose of the following.

Solutions at $O(\varepsilon)$ Let us first derive the outer temperature jump at first order in ε, $[\![T_1]\!]$ (the details of the derivation is provided in section B.2.9). An integration of the entropy equation (7.15) at order $O(\varepsilon)$ yields to the introduction of the constant of integration Φ_{th} defined as

$$-\Phi_{th} \;\hat{=}\; k(\varphi_0)\, T_1' + \mathcal{D}\, Pe \left(1 + T_0^i\right) \nu(\varphi_0) + \frac{Pe\, \mathcal{D}^2}{\alpha} \int^{\bar{x}} \varphi_0'^2 d\xi \tag{7.17}$$

The matching conditions yield (*cf.* equation (B.7d))

$$\lim_{x\to x_i^\pm} T_1^{ext} = \lim_{\bar{x}\to\pm\infty} \left[T_1 - \bar{x} \lim_{x\to x_i^\pm} T_0^{ext\prime} \right]$$

Using this matching condition and the expression (7.13) for T_0^i, integration of equation (7.17) then yields (*cf.* equation (B.43))

$$[\![T_1]\!] = -\Phi_{th} \left(\frac{1}{k}\right)_0^{\bar{ex}} - Pe\, \mathcal{D} \left(\frac{\nu}{k}\right)_0^{\bar{ex}} + [\![\varphi]\!] \frac{Pe\, \mathcal{D}^2}{\alpha} \left(\frac{\nu - P_3}{k}\right)_0^{\bar{ex}} \tag{7.18}$$

where $(\cdot)_0^{\bar{ex}}$ are inner excess quantities that are evaluated with the leading order (*i.e.* equilibrium) phase field profile $\varphi_0(\bar{x})$, where P_3 is the polynomial defined by equation (3.60b) [1] and where Φ_{th} satisfies (*cf.* equation (B.41))

$$\Phi_{th} = -k(\pm)T_0^{ext'}(x_i\pm) - \nu(\pm)\,Pe\,\mathcal{D} \tag{7.19}$$

Φ_{th} represents therefore the energy flux across the interface. It is worth pointing out that the expression (7.18) for the temperature jump across the interface at order $O(\varepsilon)$ has already been derived, *e.g.* [1, 49]. However, these previous expressions do not include the last term of equation (7.18) associated to the Ginzburg-Landau relaxation. In [1], this absence is explained by the absence of non-local dependence of the energy (*i.e.* they consider $\partial s/\partial(\nabla\varphi)^2 \neq 0$ but $\partial e/\partial(\nabla\varphi)^2 = 0$, which is the contrary of our choice). In [49], both non local dependences are non-zero, but the term $\partial e/\partial(\nabla\varphi)^2$ is scaled differently from our study. Indeed, they assume that the interface profile is inherited only from $\partial s/\partial(\nabla\varphi)^2$ and not $\partial e/\partial(\nabla\varphi)^2$ (*cf.* the scaling of their parameters α, β, γ and ν [49],page 158). In our case where $\partial s/\partial(\nabla\varphi)^2 = 0$, the scaling of $\Phi = \partial e/\partial(\nabla\varphi)^2$ is unambiguously related to the interface thickness, since this the single non-local dependence that we consider (*cf.* section 5.3.2).

It is worth pointing out that the temperature jump $[\![T_1]\!]$ can be non-zero even without any mass transfer rate ($\mathcal{D} = 0$); indeed, the equality of the leading order outer heat fluxes on each side of the interface (*i.e.* $[\![q_0]\!] = 0$ and $k^+\,T_0'(x_i+) = k^-\,T_0'(x_i-) \neq 0$) yields $\mathcal{D} = 0$ (*cf.* equation (7.16)) but $\Phi_{th} \neq 0$ (*cf.* equation (7.19)). In the case of uniform heat conductivity, $(1/k)_0^{\bar{ex}} = 0$, and the Φ_{th} contribution is zero. To illustrate the case of non-uniform heat conductivity, let us consider, for the sake of simplicity, the following (natural) interpolation function $k(\varphi)$

$$k(\varphi) = k_1 + \nu(\varphi)\,(k_2 - k_1)$$

Thus, we have $(k)^{\bar{ex}} = 0$ but necessarily $(1/k)^{\bar{ex}} \neq 0$.

As a consequence, even without any mass transfer rate, the jump in temperature at order ε is non zero.

Interface temperature Let us consider the interface temperature $T_1(0)$. Its determination is based on the integration of equations (B.46) at $O(\varepsilon^2)$. The derivation of this integration is somewhat long and technical and the details are given in section B.2.13. It is found that when terms of $O(\varepsilon)$ are taken into account, the value of the interface temperature then reads (*cf.* equation (B.50))

$$\{T\}_1 = \frac{-[\![\varphi]\!]\,\mathcal{D}}{\alpha}\Phi_{th}\,\mathcal{B}_{1/k} - \mathcal{D}\,Pe\,\mathcal{B}_{\nu/k} + [\![\varphi]\!]\,\frac{Pe\,\mathcal{D}^2}{\alpha}\,\mathcal{B}_{(\nu-P_3)/k} + O(\varepsilon^2) \tag{7.20}$$

where the coefficients $\mathcal{B}$ are excess quantities that depend on the choice for $k(\varphi)$ and are zero in the case of uniform heat conductivity.

As a conclusion of the hereinabove results, the terms of $O(\varepsilon)$ *a priori* affect the temperature jump as well as the interface temperature as soon as the heat-conductivity is non-uniform. It is worth noting that Almgren [1] studied how to choose the interpolation function $\nu(\varphi)$ as well as the function $k(\varphi)$ in order to cancel these contributions. In our study of the kinetic relation, we show how these terms are related to the interface entropy production associated to the heat conduction dissipative process.

Interface temperature profile The inner temperature profile $T_1(\bar{x})$ asymptotically (*i.e.* for $\bar{x} \to \pm\infty$) tends to the first order outer profile, according to the matching condition (B.7c). As a consequence, $T_1(\bar{x})$ is asymptotically linear in $\bar{x}$ and the slope is defined by the outer interface heat flux $q_0^{\pm}$. The inner profile is given by equation (B.45)

$$\begin{aligned} T_1(\bar{x}) \;=\; & T_1(0) - \Phi_{th}\bar{x} + \left[[\![\varphi]\!]\,\frac{Pe\,\mathcal{D}^2}{\alpha} - \mathcal{D}\,Pe\right]\int_0^{\bar{x}} \nu(\varphi_0)\,du \\ & -[\![\varphi]\!]\,\frac{Pe\,\mathcal{D}^2}{\alpha}\int_0^{\bar{x}} P_3(\varphi_0)\,du - [\![\varphi]\!]\,\frac{Pe\,\mathcal{D}^2}{\alpha}\int_0^{\bar{x}} P_3(\varphi_0)\,\nu_k(\varphi_0)\,du \end{aligned}$$

[1] The presence of P_3 in the formula is inherited from the integral of $\varphi_{0\,,\bar{x}^2}$, we have indeed

$$\int_{-\infty}^{\bar{x}} \varphi_{0\,,\bar{\xi}^2}\,d\bar{\xi} = \int_1^{\varphi_0(\bar{x})} \sqrt{2\,W}\,d\varphi = P_3(\varphi_0(\bar{x}))$$

in the case of uniform heat conductivity and by equation (B.44)

$$\begin{aligned} T_1(\bar{x}) &= T_1(0) - \frac{\Phi_{th}}{k_l}\bar{x} - \Phi_{th}\,(1-1/k_l)\int_0^{\bar{x}} \nu_k(\varphi_0)\,du + \frac{1}{k_l}\left[\llbracket\varphi\rrbracket\,\frac{Pe\,\mathcal{D}^2}{\alpha} - \mathcal{D}\,Pe\right]\int_0^{\bar{x}} \nu(\varphi_0)\,du \\ &\quad -\llbracket\varphi\rrbracket\,\frac{Pe\,\mathcal{D}^2}{\alpha k_l}\int_0^{\bar{x}} P_3(\varphi_0)\,du \\ &\quad +\left[\llbracket\varphi\rrbracket\,\frac{Pe\,\mathcal{D}^2}{\alpha} - \mathcal{D}\,Pe\right](1-1/k_l)\int_0^{\bar{x}} \nu(\varphi_0)\nu_k(\varphi_0)\,du - \llbracket\varphi\rrbracket\,\frac{Pe\,\mathcal{D}^2}{\alpha k_l}\int_0^{\bar{x}} P_3(\varphi_0)\,\nu_k(\varphi_0)\,du \end{aligned}$$

in the case of variable heat conductivity. It is worth noting that this profile is determined by the leading order profile of the phase-field variable $\varphi_0(\bar{x})$ and by the choice for the interpolation function $k(\varphi)$. A graphical representation of this profile is given on figure 8.2 of section 8.1.2 where the analytical results of matched asymptotic expansions are compared with numerical results. On figure 8.3 the influence of the function $k(\varphi)$ on the inner temperature profile is represented.

7.3.2 Kinetic relation

In this section, using the results derived in the previous section, we derive the kinetic relation of the sharp interface model equivalent to our phase field model in the case of uniform density.

Leading order interface entropy production Let us study the expression for the surface entropy production (7.1d). Using non-dimensional writing[2] it reads

$$\mathcal{R}_s = \left\{\frac{1}{1+T}\right\}\llbracket q\rrbracket - Pe\,\Gamma\,\llbracket s\rrbracket + \{q\}\frac{\llbracket T\rrbracket}{\{1+T\}}\left\{\frac{1}{1+T}\right\} \tag{7.21}$$

Let us study the the interface entropy production at $O(1)$ denoted $\mathcal{R}_{s0}$. At leading order in ε, the temperature jump is zero and therefore the last term of the expression for $\mathcal{R}_{s0}$ is zero. According to our result of matched asymptotic expansion, the order $O(1)$ contribution of $\llbracket q\rrbracket$ reads (*cf.* equation (7.16))

$$\llbracket q_0\rrbracket = \llbracket\varphi\rrbracket\,Pe\,\mathcal{D}$$

Let us study the expression for $\llbracket s\rrbracket$ at leading order. In the uniform density case, the (assumed) linearity of $P_{eq}(T)$ is equivalent to the linearity of the latent heat $\mathcal{L}(T)$, *i.e.* $\mathcal{L}/T = cste = \mathcal{L}_{ref}/T_{eq}$. Therefore, according to the general expression (3.59) for the specific Helmholtz free energy f, and following the non-dimensional analysis made for g (*cf.* equation (5.48)), we get

$$f(T,\varphi,\varphi_{,\bar{x}^2}) = W(\varphi) + \frac{1}{2}\,\varphi_{\bar{x}^2} - \varepsilon\,\nu(\varphi)\,T - \varepsilon\left(\int_{T_{ref}}^{T} s_{solid}(\tau)\,d\tau + g_{eq}(T_{ref})\right)$$

where T_{ref} is a reference temperature. And the non-dimensional entropy $s = -(1/\varepsilon)\,(\partial f/\partial T)$ reads

$$s(\varphi,T) = \nu(\varphi) + s_{solid}(T) \tag{7.22}$$

Therefore

$$\llbracket s\rrbracket = \llbracket\varphi\rrbracket + \llbracket s_{solid}(T)\rrbracket$$

where $\llbracket s_{solid}(T)\rrbracket \neq 0$ if and only if $\llbracket T\rrbracket \neq 0$. Therefore, since $\llbracket T\rrbracket_0 = 0$ at leading order in ε, the entropy jump across the interface reads

$$\llbracket s_0\rrbracket = \llbracket\varphi\rrbracket$$

According to the hereinabove expressions for $\llbracket q_0\rrbracket$ and $\llbracket s_0\rrbracket$, the interface entropy production at leading order reads

$$\mathcal{R}_{s0} = \frac{Pe\,\mathcal{D}^2}{\alpha} \tag{7.23}$$

[2] where T_{ref} is chosen as equal to T_{eq}, Γ by $\rho_0\,\mathcal{D}$ and where the surface entropy production has been scaled as $[\mathcal{R}_s] = [k/L]$

Let us first remark that this expression for the leading order contribution to the interface entropy production satisfies

$$\mathcal{R}_{s\,0} \geq 0$$

This result is logical: since proportionnal to $1/\alpha$, the leading order dissipative terms are associated to the Ginzburg-Landau relaxation, whose contribution is zero in the bulk phases (where $\tilde{\mu} = 0$ since $\mu(0) = \mu(1) = 0$ by construction and since $\varphi_{,x} = 0$) and necessarily positive across the interface (according to the Clausius-Duhem inequality). Therefore, $\mathcal{R}_{s0}$ is an excess quantity of a zero jump quantity, and is therefore independent of the interface position (*cf.* our study of the excess quantities in section A.1). It is worth pointing out that such a kinetic relation is based on the classical Rankine-Hugoniot jump conditions for which the entropy flux q_s is supposed to be equal to q/T. As a consequence, this results does not hold for the most widely used phase field models where the entropy flux is defined differently (*cf.* our discussion in section 5.2). The Ginzburg-Landau relaxation equation provides a shift of interface temperature with regard to the equilibrium temperature proportional to the rate of interface mass transfer and as a direct consequence a Gibbs free energy jump (the equilibrium relation $[\![g]\!] = 0$ is not satisfied while $[\![T]\!]$ is still 0). It is worth pointing out that (since quadratic in $\mathcal{D}$) this expression is consistent with the normal growth theory or the classical Gibbs-Thomson equation (*cf.* equation (A.29)).

Next order for the dissipative terms, the dissipation associated with non-uniform thermal conductivity Let us consider the next order terms of the interface entropy production, denoted $\mathcal{R}_{s1}$. It is worth noting that in the case of infinite α or when $\mathcal{D} = 0$, we have $\mathcal{R}_{s0} = 0$ (*cf.* equation (7.23)) and $\mathcal{R}_{s1}$ corresponds to the leading order term for the interface entropy production.

According to the general expression (7.21) for $\mathcal{R}_s$, and using the fact that $[\![T_0]\!] = 0$, we get

$$\mathcal{R}_{s1} = -\{q_0\}\frac{[\![T_1]\!]}{(T_0)^2} + \frac{[\![q_1]\!]}{1+T_0} - Pe\,\Gamma\,[\![s_1]\!] \tag{7.24}$$

Let us first study $[\![s_1]\!]$. Since we have $[\![\varphi_1]\!] = 0$, equation (7.22) shows that

$$[\![s_1]\!] = [\![s_{solid,\,1}]\!] = [\![T_1]\!]\,\frac{ds_{solid}}{dT}(T_0^i) \tag{7.25}$$

To derive the expression for $[\![q_1]\!]$ it is necessary to consider the entropy equation (B.46b) at order $O(\varepsilon^2)$ that reads

$$\begin{aligned} -\mathcal{D}\,c_P(T_0^i)\,T_1' &= \frac{1}{Pe}\left(k(\varphi_0)\,T_2' + \left(\partial_\varphi k(\varphi_0)\,\varphi_1\right)'\,T_1'\right)' \\ &\quad + \mathcal{D}\left(\partial_\varphi \nu(\varphi_0)\varphi_1' + \partial_{\varphi^2}\nu(\varphi_0)\,\varphi_1\,\varphi_0'\right) + 2\,\frac{\mathcal{D}^2\,Pe}{\alpha}\,\varphi_0'\,\varphi_1' \end{aligned}$$

$[\![q_1]\!]$ is then obtained by integration of this equation, *i.e.* on a similar way than the expression (7.16) for $[\![q_0]\!]$ was obtained from equation (7.15) (see section B.2.12 for detailed calculations). It yields (*cf.* equation (B.47))

$$[\![q_1]\!] = c_P(T_0^i)\,\mathcal{D}\,Pe\,[\![T_1]\!]$$

The contribution to $\mathcal{R}_{s1}$ of $[\![q_1]\!]$ is then compared to the contribution of $[\![s_1]\!]$. According to the definition of c_P and to the simplified expression (5.52) for c_P (corresponding to the linearity of $\mathcal{L}(T)$), we have

$$c_P(T_0^i) = -\left(T_0^i + 1\right)\,\frac{d^2 g_{eq}}{dT^2} = \left(T_0^i + 1\right)\,\frac{ds_{solid}}{dT}(T_0^i)$$

It is therefore straightforward that it cancels the contribution of $[\![s_1]\!]$ to $\mathcal{R}_{s1}$. Let us now study the expression for $\{q_0\}\,[\![T_1]\!]$. According to the expression (7.19) for the constant Φ_{th} and using the identity $\{\nu\} = 1/2$, we get

$$\{q_0\} = \Phi_{th} + \frac{1}{2}\,Pe\,\mathcal{D}$$

Using the expression (7.18) for $[\![T_1]\!]$ yields

$$-\{q_0\}\,[\![T_1]\!] = \left(\Phi_{th} + \frac{Pe\,\mathcal{D}}{2}\right)\left(\Phi_{th}\left(\frac{1}{k}\right)_0^{\bar{e}x} + Pe\,\mathcal{D}\left[\left(\frac{\nu}{k}\right)_0^{\bar{e}x} - \frac{[\![\varphi]\!]\,\mathcal{D}\left(\frac{\nu-P_3}{k}\right)_0^{\bar{e}x}}{\alpha}\right]\right) \tag{7.26}$$

As already mentioned in the introduction of this paragraph, the term $\mathcal{R}_{s\,1}$ is dominant if and only if the term $\mathcal{R}_{s\,0}$ is zero *i.e.* if either $\alpha = \infty$ or if $\mathcal{D} = 0$. In the following , we consider that $\alpha = \infty$, and thus $T_0^i = 0$ and therefore

$$\mathcal{R}_{s1} = -\{q_0\}\,[\![T_1]\!]$$

i.e.

$$\mathcal{R}_{s\,1} \;=\; \Phi_{th}^2\left(\frac{1}{k}\right)_0^{\bar{ex}} + \Phi_{th}\,Pe\,\mathcal{D}\left(\frac{1}{2}\left(\frac{1}{k}\right)_0^{\bar{ex}} + \left(\frac{\nu}{k}\right)_0^{\bar{ex}}\right) - \frac{Pe^2\,\mathcal{D}^2}{2}\left(\frac{\nu}{k}\right)_0^{\bar{ex}}$$

The hereinabove relation implies that there exists a non-zero surface entropy production due to the non-uniformity of the heat conductivity. This result is consistent with the definition of $\mathcal{R}_s$ as an excess quantity (*cf.* the discussion on the equivalent sharp interface models in section A.2.4): when the heat conductivity is uniform, the sharp interface is equivalent to a medium of same heat conductivity as the surrounding bulk phases. There is no specific dissipation due to heat conductivity across the interface and the excess interface entropy production is zero. In the case of non-uniform heat conductivity the dissipation across the diffuse interface layer (a given volume) is either less or larger than the dissipation of the bulk phase extended (over the same volume) toward the sharp interface. As a consequence, there is no reason for the excess interface entropy production to be positive. $\mathcal{R}_{s1}$ is *a priori* not signed since it involves the excess quantity $(1/k)_0^{\bar{ex}}$, whose sign depends on the choice for the function $k(\varphi)$.

When $\mathcal{D} = 0$, the heat flux jump is zero $[\![q_0]\!] = 0$, and $\{q_0\} = \Phi_{th}$. Therefore, in this particular case the interface entropy production reads

$$\mathcal{R}_{s1} = (1/k)_0^{ex}\,\Phi_{th}^2$$

As a consequence, even without any mass transfer rate, the interface entropy production is non-zero. In classical phase field models, the authors try to cancel the jump in temperature $[\![T]\!]_1$ so that their model is equivalent to the classical Stefan problem. The temperature discontinuity can be interpreted as a thermal trapping effect, *e.g.* Fadden et al. [49]. Using the framework of phase field models together with a consistent definition for the entropy flux, we show that this temperature jump is related to the excess interface entropy production inside the interface.

Thus, a non-uniform heat conductivity is the source of an interface entropy production. This interface entropy production, as an excess quantity, is not *a priori* signed and its value can be controlled by choosing accurately the function $k(\varphi)$. We have related this result with the classical phase field result about the temperature jump. This provides an interpretation of this result.

Kinetic relation at next orders in ε: contribution of the Ginzburg-Landau relaxation In this paragraph, in order to focus on the single effect of the Ginzburg-Landau relaxation, we consider the heat conductivity as uniform[3]. It is worth pointing out that when the heat conductivity is uniform there is no $O(\varepsilon)$ contribution of the Ginzburg-Landau relaxation to the interface entropy production. In the following, we show that, nevertheless, the Ginzburg-Landau relaxation is not limited to a contribution of order $O(1)$ to $\mathcal{R}_s$.

The leading order term of the interface entropy production, associated to the Ginzburg-Landau relaxation, has been evaluated using the outer expressions for the temperature and heat flux interface values and jumps (*cf.* the derivation of equation (7.23) from equation (7.21) for example). However, it is also possible to express $\mathcal{R}_s$ as the integral across the interface of the local entropy production rate. This rate has been specified when we introduced the Ginzburg-Landau dissipation mechanism in section 5.2. Let us consider the consequent expression of $\mathcal{R}_s$

$$\mathcal{R}_s = \;\frac{\mathcal{D}^2\,Pe}{\alpha}\left(\varphi'^2\right)^{ex}$$

And therefore

$$\mathcal{R}_s = \;\frac{\mathcal{D}^2\,Pe}{\alpha}\left[\int_{-\infty}^{+\infty}\varphi_0'^2\,d\,\bar{x} + \varepsilon\int_{-\infty}^{+\infty}\varphi_0'\varphi_1'\,d\,\bar{x} + \varepsilon^2\int_{-\infty}^{+\infty}\left(\varphi_1'^2 + \varphi_0'\varphi_2'\right)d\,\bar{x} + O(\varepsilon^3)\right] \tag{7.27}$$

[3]Without this assumption, the contribution of both dissipative processes is more complex. Indeed, there exists a coupling between the two processes as attested by the last term of the expression (7.18) of $[\![T_1]\!]$ which is non-zero if (i) the heat conductivity is non-uniform and (ii) α is finite.

It is worth pointing out that $\varphi(\bar{x})$ depends on $\mathcal{D}$ ($\varphi_1(\bar{x})$ is proportional to $\mathcal{D}$ as shown by equation (7.14)). As a consequence, the expression for $\mathcal{R}_s$ is *a priori* not limited to quadratic terms in $\mathcal{D}$. However, since the leading order phase field profile, which is the equilibrium profile, does not depend on $\mathcal{D}$, at leading order, the rate of entropy production is quadratic in $\mathcal{D}$. Let us now draw the limit of this consistency and consider the next order contribution to the interface rate of entropy production.

The $O(\varepsilon)$ is the integral of $\varphi_{0\,,\bar{x}}\,\varphi_{1\,,\bar{x}}$. The integration over the inner region of this contribution is zero (*cf.* section B.2.12)

$$\int_{-\infty}^{+\infty} \varphi_{0\,,\bar{x}}\,\varphi_{1\,,\bar{x}}\,d\bar{x} = 0$$

It explains the absence of any Ginzburg-Landau contribution to $\mathcal{R}_{s\,1}$ as soon as the heat conductivity is uniform (*cf.* equation (7.26)).

At $O(\varepsilon^2)$, two contributions, namely $\varphi_{2\,,\bar{x}}\,\varphi_{0\,,\bar{x}}$ and $\varphi^2_{1\,,\bar{x}}$, appear in the expression for the rate of entropy production. The integral of $(d\varphi_1/d\bar{x})^2$ is non-zero as soon as $\mathcal{D} \neq 0$ and $\alpha < \infty$. It is worth noting that since φ_1 is proportional to $\mathcal{D}/\alpha$ (*cf.* equation (7.14)), the corresponding contribution to the interface entropy production scales as $\varepsilon^2\,\mathcal{D}^4/\alpha^3$.

Thus, we have shown that the Ginzburg-Landau contribution to the interface entropy production is not limited to the leading order term and moreover includes additional terms that deviate from the normal growth theory (*i.e.* not quadratic in $\mathcal{D}$) as soon as the thickness of the diffuse interface remains finite.

7.3.3 Conclusion on the study of the solid-liquid one-dimensional phase change

In this section, we studied the one-dimensional phase transition process in the case of a uniform density using matched asymptotic expansions. The leading order temperature and phase field profiles have been determined analytically (*cf.* section 7.3.1). At $O(1)$ in ε, these profiles are equivalent to equilibrium profiles (uniform temperature, and hyperbolic tangent for the phase field). Nevertheless, the order $O(1)$ rate of entropy production is non-zero and its expression is consistent with the normal growth theory. However, the expression for the rate of entropy production has been shown not to reduce to these terms. It has been shown that, as soon as the outer heat fluxes are non-zero and the heat conductivity is non uniform, there exists a contribution to the rate of entropy production associated with the Fourier heat conduction. As an excess quantity, this contribution is *a priori* not signed, and depends on the function $k(\varphi)$. Moreover, the Ginzburg-Landau relaxation generates higher order terms than the quadratic terms in $\mathcal{D}$, and therefore reduces to the normal growth theory only at the limit $\varepsilon = 0$. It is worth pointing out that as a consequence the formalism of kinetic relations provided a clear interpretation of the different leading order results.

Moreover, the outer states have been shown to correspond to the phase field values 0 and 1 even for out of equilibrium situations. This is an interesting property to control their physical properties.

7.4 Isothermal liquid-vapor flow with phase change

In this section, we study our quasi-compressible phase-field model for the liquid-vapor phase transition in the case where the system is supposed to be isothermal and where the viscous dissipation is neglected.

For the sake of legibility, only the main results are given and discussed in this section. The reader interested in the detailed derivation of these results can refer to section B.3 where all the calculations corresponding to this study are provided .

In the isothermal and inviscid case considered here, the system of governing equations for the outer problem reads (*cf.* system (5.61))

$$\alpha\,\varepsilon^2\,(\mathcal{D}-V)\,\varphi_{,x} = \varepsilon\,\partial_\varphi\nu\tilde{P} + v\,\left(\partial_\varphi W - \varepsilon^2\varphi_{,xx}\right) + \partial_\varphi\nu\left(W - \frac{\varepsilon^2}{2}\varphi^2_{,x}\right) \tag{7.28a}$$

$$(\rho V)_{,x} = -\rho^2\,\partial_\varphi\nu\,(\mathcal{D}-V)\,\varphi_{,x} \tag{7.28b}$$

$$(V-\mathcal{D})\,\rho V_{,x} = -\tilde{P}_{,x} \tag{7.28c}$$

For the inner problem, only the AC equation has a modified scaling in ε and reads

$$\alpha\,\varepsilon\,(\mathcal{D}-V)\,\varphi' = \varepsilon\,\partial_\varphi\nu\tilde{P} + v\,\left(\partial_\varphi W - \varphi''\right) + \partial_\varphi\nu\left(W - \frac{(\varphi')^2}{2}\right) \tag{7.29}$$

7.4.1 Leading orders phase-field profile

In the outer domains, the leading order *AC* equation (7.28a) reads

$$\partial_\varphi W_0 = 0$$

Therefore, as in the uniform density case we get that $\varphi^\pm$ is equal to either 0 or 1 and introduce $[\![\varphi]\!] = \pm 1$. The leading order inner *AC* equation (7.29) reads

$$v_0 \left(\partial_\varphi W_0 - \varphi_0''\right) + \partial_\varphi \nu_0 \left(W_0 - \frac{(\varphi_0')^2}{2}\right) = 0$$

where we remind that $v(\varphi)$ is the specific volume and where the function $\nu(\varphi)$ is the interpolation function used, in particular, to interpolate the density within the interface zone. Using the fact that φ equals 0 or 1 in the outer domains, it is a straightforward calculation to show (*cf.* the appendix section B.3.3) that this equation is equivalent to the leading order equation in the uniform density case studied in the hereinabove section 7.3

$$\partial_\varphi W_0 - \varphi_0'' = 0$$

Therefore, the leading order solution for the inner phase-field profile is the equilibrium profile, *i.e.* a hyperbolic tangent profile for our model that is thus independent of the density difference. At the next order in ε (*i.e.* $O(\varepsilon)$), it can be shown that the equation for the phase field profile $\varphi_1(\bar{x})$ reads

$$\varphi_1 \partial_\varphi (v\, W)(\varphi_0) - \varphi_1' v'(\varphi_0) - v(\varphi_0)\, \varphi_1'' = \frac{\Gamma\, v(\varphi_0)\, \varphi_0'}{\alpha} - \left(\mathcal{A}_1 \frac{\Gamma}{\alpha} + \frac{\Gamma^2}{2}\right) \partial_\varphi v(\varphi_0)$$

where Γ is the interface mass transfer rate and where

$$\mathcal{A}_1 \triangleq [\![\varphi]\!] \int_{-\infty}^{+\infty} \nu(\varphi_0)\, \varphi_0'^2\, d\bar{x} = 1/12 \tag{7.30}$$

The integration of this differential equation (*cf.* section B.3.5) yields the sum of two profiles, one being proportional to Γ/α and the second one being proportional to Γ^2 that reads

$$\varphi_1(\bar{x}) = \frac{\Gamma}{\alpha} \varphi_0' \int \frac{\int (G_\alpha)\, d\bar{x}}{\left(\varphi_0'\right)^2}\, d\bar{x} + \Gamma^2 \varphi_0' \int \frac{\int (G_{\alpha\infty})\, d\bar{x}}{\left(\varphi_0'\right)^2}\, d\bar{x} \tag{7.31}$$

where the functions G_α and $G_{\alpha\,\infty}$ satisfy

$$\begin{aligned} (v(\varphi_0)\, G_\alpha)' &= \left(\mathcal{A}_1 v(\varphi_0)' - v(\varphi_0)\, \varphi_0'^2\right) \\ (v(\varphi_0)\, G_{\alpha\infty})' &= \left(1/2 v(\varphi_0)' - v(\varphi_0)\, v(\varphi_0)'\right) \end{aligned}$$

The first contribution is associated to the Ginzburg-Landau relaxation and vanishes as soon as the non-dimensional mobility α is infinite. The second one is associated to the pressure recoil (*cf.* the results of the next section concerning the leading order pressure solution) and it is quadratic in the mass transfer rate Γ.

7.4.2 Leading order pressure and velocity

Velocity field At leading order in ε, the continuity equation (7.28b) reads

$$(\rho(\varphi_0) V_0)' = -\rho_0^2\, \partial_\varphi \nu(\varphi_0)\, (\mathcal{D} - V_0)\, \varphi_0'$$

Its integration simply yields

$$V_0 - \mathcal{D} = -\Gamma\, v(\varphi_0) \tag{7.32}$$

where Γ is the interface mass transfer rate.

This relation implies that the outer velocity jump reads

$$[\![V_0]\!] = -\Gamma\, [\![1/\rho]\!] \tag{7.33}$$

This condition corresponds to the sharp interface jump condition (7.2a) derived from the Rankine-Hugoniot jump conditions.

Pressure field At leading order in ε, the momentum equation (7.28c) reads

$$(V_0 - \mathcal{D})\ \rho(\varphi_0) V_0' = -\tilde{P}_0'$$

Using the expression (7.32) for the velocity, the pressure profile $\tilde{P}_0$ simply reads (*cf.* equation (B.59))

$$\tilde{P}_0 - \Pi = -\Gamma^2\, v(\varphi_0) \tag{7.34}$$

where Π is a constant of integration related to $\{P\}_0$. Its determination (see section B.3.5) is based on the use of the solvability condition for the following expression for the $O(\varepsilon)$ *AC* equation

$$\varphi_1 \left(\partial_\varphi v(\varphi_0)\, \partial_\varphi W(\varphi_0) + v(\varphi_0)\, \partial_{\varphi^2} W(\varphi_0)\right) - \partial_\varphi v(\varphi_0)\, \varphi_1'\, \varphi_0' - v(\varphi_0)\, \varphi_1'' = \frac{\mathcal{D} - V_0}{\alpha}\, \varphi_0' - \tilde{P}_0\, \partial_\varphi v(\varphi_0)$$

Multiplying this equation by φ_0' and integrating over $\mathbb{R}$ yields a quantity that is independent of $\varphi_1(\bar{x})$. Using the hereinabove derived expressions for φ_0, $\tilde{P}_0$ and V_0 allows then to determine the constant Π. We thus use exactly the same method as for the determination of the interface temperature level T_0^i in the uniform density case. It yields (*cf.* equation (B.66) and equation (B.68))

$$\Pi = \mathcal{A}_1 \frac{\Gamma}{\alpha} + \Gamma^2/2 \tag{7.35a}$$

$$\{P_0\} = \mathcal{A}_1 \frac{\Gamma}{\alpha} \tag{7.35b}$$

Using the matching condition (B.51b), equation (7.34) shows that the outer pressure jump reads

$$\left[\!\left[P_0^{ext} \right]\!\right] = -\Gamma^2 \left[\!\left[1/\rho \right]\!\right]$$

This condition corresponds to the classical sharp interface jump condition (*cf.* equation (7.2b)), which is related to the pressure recoil effect. This effect is thus recovered by our model at leading order in ε.. Thus, we showed that at leading order in ε, the jump conditions of the equivalent sharp model are the classical jump conditions (*i.e.* the jump in velocity is related to the mass conservation and the pressure jump is related to the pressure recoil). They are consistent with the jump conditions (7.2) derived from the Rankine Hugoniot jump conditions. In addition, a shift of the interface pressure from the equilibrium pressure is due to the Ginzburg-Landau relaxation. We study in the following the consequence of this out of equilibrium structure of the diffuse interface on the kinetic relation of the equivalent sharp interface model.

7.4.3 Kinetic relation

In this section, we study the kinetic relation from the leading order solutions derived in the previous section. We determine the expression for the surface entropy production $\mathcal{R}_s$ at leading order in ε and relate it to an "out of equilibrium Clapeyron relation".

It is important to note that, in the isothermal case, it is not possible to use the native expression for $\mathcal{R}_s$ (equation (7.1d)) since no direct information is available concerning either the entropy flux $q_s = q/T$ or the specific entropy s. Let us thus consider the expression for $\mathcal{R}_s$ as a function of the driving force $\mathscr{G}$ that reads (*cf.* equation (7.4))

$$\mathcal{R}_s T_{eq} = \Gamma \mathscr{G}$$

where the driving force $\mathscr{G}$ reads (*cf.* equation (7.3))

$$\mathscr{G} \hat{=} \left[\!\left[g \right]\!\right] + \left[\!\left[\frac{(V - \mathcal{D})^2}{2} \right]\!\right]$$

This latter quantity can thus be studied in the isothermal case studied. Moreover, since the relation

$$\{1/\rho\} \left[\!\left[P \right]\!\right] = -\left[\!\left[\frac{(V - \mathcal{D})^2}{2} \right]\!\right]$$

is satisfied by the $O(1)$ solutions of the pressure and velocity and, since the compressibility of the bulk phases is not considered in our phase-field model, we have thus (*cf.* equation (A.26))

$$\mathcal{R}_s\, T_{eq} = \Gamma\, \{P\}\, [\![1/\rho]\!]$$

And the study of the interface entropy production is therefore related to the study of the shift of the interface pressure with regard to the equilibrium pressure $\{P\}$. It is worth pointing out that this expression, that involves explicitly the interface pressure level $\{P\}$ is an "out of equilibrium Clapeyron relation".

Let us now derive the leading order expression for the interface entropy production. According to the leading order solution for the pressure (*cf.* equation (7.35b)), the above relation yields

$$\mathcal{R}_{s0}\, T_{eq} = \frac{\Gamma^2}{\alpha}\, \mathcal{A}_1 \tag{7.36}$$

which satisfies

$$\mathcal{R}_{s0} > 0$$

Since the only dissipative mechanism considered is the Ginzburg-Landau relaxation, interface entropy source vanishes as $\alpha \to +\infty$. Since this dissipative mechanism only exists inside the interface zone (*i.e.* zero contribution in the bulk phases), it is consistent to have a positive $\mathcal{R}_{s0}$. Since, at leading order in ε, the interface entropy source $\mathcal{R}_{s0}$ is quadratic in Γ, its expression (7.36) is consistent with the normal growth theory.

It is worth pointing out that, like in the uniform density case, the Ginzburg-Landau relaxation implies a higher contribution to the interface entropy production (*cf.* our discussion at the end of section 7.3.2). Indeed, we have $[\![1/\rho]\!]_1 = 0$ and at $O(\varepsilon)$, the value of the interface entropy production reads

$$T_{eq}\, \mathcal{R}_{s\,1} = \Gamma\, \{P_1\}\, [\![\varphi]\!]$$

where the expression for $\{P_1\}$ reads

$$\{P_1\} = \frac{2\, [\![\varphi]\!] \Gamma}{\alpha} \int_{-\infty}^{+\infty} \varphi_0'(\bar{x})\, \varphi_1'(\bar{x})\, d\bar{x}$$

We have shown that $\varphi_1(\bar{x})$ was made of two parts, the first one being scaled by Γ/α and the second one by Γ^2 (*cf.* equation (7.31)). It can be shown that the contribution to $\{P\}_1$ of $\varphi_1'\varphi_0'$ scaled by Γ^2 is zero. As a consequence only the part of φ_1' scaled by Γ/α remains and we get

$$T_{eq}\, \mathcal{R}_{s\,1} = 2\, \frac{\Gamma^3}{\alpha^2}\, [\![\varphi]\!]\, \mathcal{A}_\alpha \tag{7.37}$$

This relation shows that, at $O(\varepsilon)$, the kinetic relation deviates from the normal growth theory as soon as the mass transfer rate is sufficiently large. We have finally (*cf.* equations (7.36) and (7.37))

$$T_{eq}\, \mathcal{R}_s = \frac{\Gamma^2}{\alpha}\, \mathcal{A}_1 + \varepsilon\, 2\, \frac{\Gamma^3}{\alpha^2}\, [\![\varphi]\!]\, \mathcal{A}_\alpha + O(\varepsilon^2)$$

This study of the non-equilibrium structure of the diffuse interface in the isothermal case showed that the classical Rankine-Hugoniot jump conditions on the pressure and velocity are recovered by the equivalent sharp interface model. Besides, similarly to the uniform density case studied in section 7.3, we showed that the interface entropy production is not null and that it is due to the Ginzburg-Landau relaxation.

7.5 Non-isothermal liquid-vapor flow with phase change

In this section, we study the out of equilibrium structure of the interface in the case of a non-isothermal phase transition, which is characteristic of boiling flows. The system of governing equations corresponds to the sys-

tem (5.59) that reads

$$\alpha\,\varepsilon^2\,(\mathcal{D}-V)\,\varphi_{,x} = \varepsilon\,\frac{d\nu}{d\varphi}\left(\tilde{P}-T\right)+v\left(\frac{dW}{d\varphi}-\varepsilon^2\varphi_{,xx}\right)+\frac{d\nu}{d\varphi}\left(W-\frac{\varepsilon^2}{2}\varphi_{,x}^2\right) \tag{7.38a}$$

$$(\rho V)_{,x} = -\rho^2\,\frac{\partial\nu}{\partial\varphi}\,(\mathcal{D}-V)\,\varphi_{,x} \tag{7.38b}$$

$$(V-\mathcal{D})\,\rho V_{,x} = -\tilde{P}_{,x} \tag{7.38c}$$

$$(V-\mathcal{D})\,\rho\,T_{,x} = \frac{(k\,T_{,x})_{,x}}{Pe}-(V-\mathcal{D})\,\rho\,(1+T)\,\frac{d\nu}{d\varphi}\,\varphi_{,x}+(\mathcal{D}-V)^2\,\frac{\rho\varepsilon}{\alpha}\,(\varphi_{,x})^2 \tag{7.38d}$$

It is worth noting that, compared to the systems studied in the previous sections (uniform density and isothermal cases), these equations are only slightly modified by the coupling between thermal and mechanical physical mechanisms. For example the momentum and continuity equations are exactly similar to the one studied in section 7.4 whereas the equation of evolution of the temperature reads exactly the same than the one studied in section 7.3. In fact only the presence of both pressure and temperature in the *AC* equation makes a real difference with the previously studied equations. As a consequence, we only comment the differences for the solutions associated with this coupling (see section 7.5.1). Then, in section 7.5.2, we study in more details the expression for both the interface entropy production and the driving force of the equivalent sharp interface model.

7.5.1 Leading order solutions

The complete calculation of the leading order solutions takes advantage of the similarity of the equations with the one studied in the two degenerate cases considered (*cf.* the appendix B.4). As a consequence, we do not recall the detailed calculations that can be found in the previous sections.

The leading order solutions of the inner profiles as well as the outer jump conditions and interface values have similar expressions to those obtained in the previous sections where we studied degenerated forms of our model. They read (*cf.* the equations (B.80), (B.81b), (B.86), (B.87), (B.84) and (B.85))

$$\varphi_0(\bar{x}) = 1/2+(\llbracket\varphi\rrbracket/2)\,\tanh(3\,\bar{x}) \tag{7.39a}$$

$$\tilde{P}_0(\bar{x}) = \{P_0\}+\{v_0\}\,\Gamma^2-v(\varphi_0(\bar{x}))\,\Gamma^2 \tag{7.39b}$$

$$V_0(\bar{x}) = \mathcal{D}-\Gamma\,v(\varphi_0(\bar{x})) \tag{7.39c}$$

$$\{P_0\} = T_0^i+\Gamma\,\frac{\mathcal{A}_1}{\alpha} \tag{7.39d}$$

$$\llbracket T_0\rrbracket = 0 \tag{7.39e}$$

$$\{T_0\} = T_0^i \tag{7.39f}$$

$$\llbracket q_0\rrbracket = Pe\,\Gamma\left(1+T_0^i\right)\llbracket\varphi\rrbracket+\Gamma^2\,|\mathcal{A}_1| \tag{7.39g}$$

where $\mathcal{A}_1$ is given by (7.30).

Therefore, at leading order in ε, equations (7.39e) and (7.39f) show that the temperature is uniform and the phase field profile is the equilibrium one. Equation (7.39b) shows that the pressure satisfies the classical jump condition (pressure recoil). Equation (7.39d) shows that the pressure at the interface $\{P_0\}$ differs from the saturation pressure at the interface temperature and that the shift is proportional to Γ/α. It is worth noting that whenever the outer heat flux jump $\llbracket q_0\rrbracket$ equals zero, the mass transfer rate can still be non-zero. Indeed we have from equation (7.39g)

$$\llbracket q_0\rrbracket = 0 \Rightarrow \Gamma = Pe\,\frac{\llbracket\varphi\rrbracket}{|\mathcal{A}_1|}\left(1+T_0^i\right)$$

The corresponding mass transfer rate is actually an adiabatic phase transition process as studied in the previous section.

Thus, the leading order solution of the non-isothermal case with density difference is such that the classical jump conditions on velocity and pressure (7.2) are recovered by the equivalent sharp model. Moreover, the bulk phase field values are always 0 or 1, which allows to clearly control the physical properties of the single-phase states even in out of equilibrium conditions. The interface pressure is related to the temperature of the interface

through an "out of equilibrium Clapeyron relation". It is worth noting that this result has already been obtained by Anderson et al. [6] with the model presented in section 2.3.3. In the following, we study the consequences of this internal structure of the interface on the kinetic relation.

7.5.2 Kinetic relation

This section is organized as follows. First, we show that the leading order expression of the interface entropy production is associated only to the Ginzburg-Landau dissipative process. Then, it is shown that it is possible to derive a good approximation of the interface entropy production using an approximate expression of the interface entropy production. The use of this approximate expression is shown to be of interest since it allows to clearly relate the kinetic relation to an "out of equilibrium Clapeyron relation". We then study the next order expression of the kinetic relation and show how it is related to a non-uniform heat conductivity across the interface. Finally, we derive the expression for the kinetic relation in terms of the driving force, which is another way to interpret these results.

Leading order kinetic relation, the Ginzburg-Landau relaxation Let us study the kinetic relation at $O(1)$. According to our study of the sharp interface problem, the general expression for the interface entropy production $\mathcal{R}_s$ reads (*cf.* (7.1d))[4]

$$\mathcal{R}_s = -\{q\}\frac{[\![T]\!]}{\{1+T\}}\left\{\frac{1}{1+T}\right\} + \left\{\frac{1}{1+T}\right\}[\![q]\!] - Pe\,\Gamma\,[\![s]\!] \tag{7.40}$$

The leading order outer temperature jump is zero (*cf.* equation (7.39e)) and, as a consequence, the first term of the above expression is zero at leading order. The value of the leading order contribution to the heat flux jump is given by equation (7.39g). The only term that remains to be studied is the entropy jump.

The non-dimensional expression for the quasi-compressible Gibbs free energy reads (equation (5.48)) where we have considered that P_{eq} is linear

$$g = \varepsilon\, v(\varphi)\,[P-T] + v\left(W + \frac{\varepsilon^2}{2}(\nabla\varphi)^2\right) + \varepsilon\, g_{eq}(T)$$

Since $s = -(\partial g/\partial T)$ we get

$$s = \nu(\varphi) - \frac{dg_{eq}}{dT}$$

Thus at leading order, we get $[\![s_0]\!] = [\![\varphi]\!]$. Since $[\![T_0]\!] = 0$ and using the expression (7.39g) for $[\![q_0]\!]$ we get for the leading order of the interface entropy production (*cf.* equation (7.40))

$$\mathcal{R}_{s0} = \Gamma^2\,\frac{Pe}{\alpha}\mathcal{A}_1\frac{1}{1+\{T_0\}} \tag{7.41}$$

This expression is identical to the expression (7.36) derived in the isothermal case.

Thus, the kinetic relation of the equivalent sharp interface model at leading order is only related to the Ginzburg-Landau relaxation. As a consequence, the corresponding interface entropy production is strictly positive. Moreover, it is quadratic in Γ, which makes this relation consistent with the normal growth theory. It has been shown that a non-zero interface entropy production is at the origin of an "out of equilibrium Clapeyron relation" satisfied by the interface pressure and interface temperature.

Kinetic relation at next order The interface entropy production at $O(\varepsilon)$ is defined by equation (7.24). For the sake of simplicity, in the following, we consider only the case $\alpha = \infty$, knowing that in any other case, the leading order term of the interface entropy production associated to the Ginzburg-Landau relaxation has already been derived. $[\![q_1]\!]$ is derived from an integration of the order ε^2 equation of evolution for the temperature (see section B.4.5). In the case $\alpha = \infty$, $[\![q_1]\!]$ reads (*cf.* equation (B.94))

$$[\![q_1]\!] = c_P(T_0^i)\,\Gamma\,Pe\,[\![T_1]\!]$$

[4] $\mathcal{R}_s$, resp. s, is scaled by $[k/L]$, resp. $[\mathcal{L}/T]$.

and according to the expression (7.25) for $[\![s_1]\!]$, the contribution to the interface entropy production of $[\![s]\!]_1$ is canceled by the $[\![q_1]\!]$ contribution. It yields

$$\left(T_0^i\right)^2 \mathcal{R}_{s\,1} = -[\![q_0]\!]\,[\![T_1]\!]$$

$[\![q_0]\!]$ is given by equation (7.39g). Let us analyze the expressions for $[\![T_1]\!]$. The expression for $[\![T_1]\!]$ is derived by integration of the order ε equation of evolution for the temperature on the same way than in the uniform density case (*cf.* section B.4.3). The expression for $\tilde{\mu}$ and T_0^i being different than in the uniform density case, it yields (*cf.* equation (B.89))

$$[\![T_1]\!] = -\Phi_{th}\left(\frac{1}{k}\right)_0^{\bar{ex}} - Pe\,\Gamma\left(1+T_0^i\right)\left(\frac{\nu}{k}\right)_0^{\bar{ex}} - 2\,[\![\varphi]\!]\,\frac{Pe\,\Gamma}{\alpha}\left(\frac{\int (v\,W(\varphi_0)d\xi)}{k}(\varphi_0)\right)^{\bar{ex}} \tag{7.42}$$

It is worth pointing out that this expression is very similar to the one obtained in the uniform density case (*cf.* equation (7.18)) as involving excess quantities related to the thermal conductivity. Moreover, when α is infinite, the temperature jump has an expression similar to the one obtained with the van der Waals model (*cf.* the matched asymptotic expansions derived in [53]). Using the expression (7.39g) for $[\![q_0]\!]$, we get therefore

$$\mathcal{R}_{s\,1} = \left(Pe\,\Gamma\left(1+T_0^i\right)[\![\varphi]\!] + \Gamma^2\,|\mathcal{A}_1|\right)\left(\Phi_{th}\left(\frac{1}{k}\right)_0^{\bar{ex}} + Pe\,\Gamma\left(1+T_0^i\right)\left(\frac{\nu}{k}\right)_0^{\bar{ex}}\right)$$

Similarly to the case of uniform density (*cf.* section 7.3.2), this expression shows that $\mathcal{R}_{s\,1}$ is identically zero if the heat conductivity is uniform. This $O(\varepsilon)$ interface entropy production is related to an excess Fourier dissipation across the interface and is *a priori* not signed. We remind that this result is valid in the case $\alpha \to \infty$. The study of the $O(\varepsilon)$ interface entropy production associated to the Ginzburg-Landau relaxation is carried out in the following paragraphs.

Thus, from order ε the interface entropy production is related to the heat conduction across the interface and is *a priori* not null as soon as the heat conductivity is non-uniform. The classical kinetic relation is often presented in terms of the driving force instead of the interface entropy production. In the following paragraph, we study the expression for the driving force as a function of the mass transfer rate.

Driving force as a function of the mass transfer rate Let us study the general expression for the leading order kinetic relation as a relation between the driving force $\mathscr{G}$ and the mass transfer rate Γ. In the section 7.1), we have defined the driving force $\mathscr{G}$ such that

$$\mathcal{R}_s\,\{T+1\} = \Gamma\,Pe\,\mathscr{G} - [\![T]\!]\left\{\frac{q}{T}\right\} + [\![q]\!]\left(\{T\}\left\{\frac{1}{T}\right\} - 1\right)$$

where $\mathscr{G}$ has been scaled by V^2. Such a driving force has been shown to be defined by (*cf.* equation (7.3))

$$\mathscr{G} \,\hat{=}\, [\![g]\!] + \{s\}\,[\![T]\!] + \Gamma^2\left\{\frac{1}{\rho}\right\}\left[\!\left[\frac{1}{\rho}\right]\!\right]$$

Therefore, using the results (7.39) at leading order, we get

$$\mathscr{G}_0 = \frac{\Gamma}{\alpha}\mathcal{A}_1$$

When sensible heat is neglected with regard to the latent heat in the evaluation of $[\![g]\!]$ the approximate expression for the driving force (7.6) reads

$$\mathscr{G} \simeq \{P\}\,[\![1/\rho]\!] - \{T\}[\![s]\!]$$

Since $[\![1/\rho_0]\!] = [\![s_0]\!] = [\![\varphi]\!]$, we have

$$\{P_1\}[\![1/\rho_0]\!] - \{T_1\}[\![s_0]\!] = [\![\varphi]\!]\,(\{P_1\} - \{T_1\})$$

and the leading order of the driving force reads

$$\begin{aligned}\mathscr{G} \simeq\ & [\![\varphi]\!]\left(\{P\}_0 - \{T\}_0\right)\\ & +\varepsilon\ \left[[\![\varphi]\!]\left(\{P\}_1 - \{T\}_1\right) - \{T_0\}\ [\![s_1]\!]\right]\\ & +\mathcal{O}(\varepsilon^2)\end{aligned}$$

where $[\![s_1]\!]$ is given by (*cf.* section 7.3.2)

$$[\![s_1]\!] = [\![T_1]\!]\, c_P(T_0^i)\left(1 + T_0^i\right)$$

where $[\![T_1]\!]$ is given by equation (7.42). In the appendix section B.4.4, we study the scaling of the different terms of the *AC* equation (B.91) at order ε^2. Applying the solvability condition to this equation allows to determine the different terms entering the expression of $\{P_1\} - \{T_1\}$. Using the expressions for the leading order solution of the inner problem (7.39) for $\{P_0\}$ and $\{T_0\}$, we get

$$\begin{aligned}\mathscr{G} \simeq\ & \Gamma\frac{\mathcal{A}_1}{\alpha}\,[\![\varphi]\!]\\ & +\varepsilon\left[[\![\varphi]\!]\left(\frac{\Gamma^2}{\alpha^2}\beta_{\Gamma^2/\alpha^2} + \Phi_{th}\beta_{\Phi_{th}} + \Gamma\, Pe\,\beta_{Pe} + \frac{\Gamma^2\, Pe}{\alpha}\beta_{\Gamma^2\, Pe/\alpha} + \frac{\Gamma^3}{\alpha}\beta_{\Gamma^3/\alpha}\right)\right.\\ & \quad \left. + c_P(T_0^i)\left(1 + T_0^i\right)\left(\Phi_{th}\left(\frac{1}{k}\right)_0^{\bar{ex}} + Pe\,\Gamma\left(1 + T_0^i\right)\left(\frac{\nu}{k}\right)_0^{\bar{ex}} + [\![\varphi]\!]\,\frac{Pe\,\Gamma}{\alpha}\beta_{\Gamma\, Pe/\alpha}\right)\right]\\ & +\mathcal{O}(\varepsilon^2)\end{aligned} \tag{7.43}$$

where the coefficients β are of order unity and are excess quantities. $\beta_{\Gamma^2/\alpha^2}$ and $\beta_{\Gamma^3/\alpha}$ vanishes in the uniform density case, whereas all the other coefficients vanish for a uniform heat conductivity. The driving force is made of two different parts: the first one that depends on the mobility as $1/\alpha$ is associated to the Ginzburg-Landau relaxation, and the second one that is related to non-uniform heat conductivity is associated to the Fourier heat conduction.

In this section, we derived approximate expressions for the interface entropy production and for the driving force. They show that the non-uniformity of the heat conductivity as well as the existence of a Ginzburg-Landau relaxation determine the relation between the interface pressure and the interface temperature of the equivalent sharp interface model. At leading order, this relation is consistent with the normal growth theory (*i.e.* the interface entropy production quadratic in Γ or, equivalently, the driving force is linear in Γ), and the kinetics are associated to the Ginzburg-Landau relaxation as shown by the order 1 term of equation (7.43). However at next order, it is shown to deviate from this theory as shown by the order ε term of equation (7.43).

7.6 Sharp interface limit for far from equilibrium phase transition

In this section, we study a different sharp interface limit of our phase field model that is more accurate for far from equilibrium phase transitions. Indeed, the results obtained so far are based on a particular scaling of the mobility, *i.e.* of the dissipative coefficient associated to the Ginzburg-Landau relaxation. As a consequence, the kinetic relation reads as the linearity of the driving force with the interface mass transfer rate at leading order and that even for large mass transfer rates, *e.g.* equation (7.43). This linearity is consistent with the normal growth approximation that has been related in section 7.1 to a "close to equilibrium" model for the kinetics of phase transition. It is worth noting that an even lower level of modeling of the entropy interface production corresponds to set it to zero that corresponds in our case to set α to infinity. To deviate from the normal growth theory, we showed that it was necessary to consider higher order terms of the matched asymptotic expansion, *i.e.* the effect of a finite thickness for the interface transition layer (the so-called thin interface limit introduced by Karma and Rappel [72]). This characteristic of the kinetic relation of the model can be attractive, for example when a regularization of the Stefan model where latent heat removal is the limiting stage is targeted (as it is the case of the widely used phase field methods). Nevertheless we know that the normal growth theory is only a model for slow phase boundaries and such a linear kinetic relation could also be viewed as a limit of the model.

In the following, we derive the kinetic relation of the phase field model, considering a different scaling and show how it yields to a more complex kinetic relation. This shows how one can deal with non-linear kinetic relation as sharp interface limit as soon as the scaling of the mobility is chosen accurately. This thus demonstrates that the phase field model are not limited to a regularization of the normal growth theory but can also generate more realistic kinetic relations.

7.6.1 Leading order phase field equation and kinetic relation

We now turn our attention to the case where the normalized dissipative coefficient of the Ginzburg Landau relaxation is a fixed independent parameter, say $\bar{\alpha} = \alpha/\varepsilon$. We denote the scaling $\bar{\alpha}$, resp. α, of the mobility as the close, resp. far from equilibrium scalings. Following the far from equilibrium scaling, the system of equation (5.59) then reads

$$\bar{\alpha}\,\varepsilon\,(\mathcal{D}-V)\,\varphi_{,x} = \varepsilon\frac{dv}{d\varphi}\left(\tilde{P}-T\right)+v\left(\frac{dW}{d\varphi}-\varepsilon^2\varphi_{,xx}\right)+\frac{dv}{d\varphi}\left(W-\frac{\varepsilon^2}{2}\varphi_{,x}^2\right) \tag{7.44a}$$

$$(\rho V)_{,x} = -\rho^2\frac{\partial v}{\partial\varphi}(\mathcal{D}-V)\,\varphi_{,x} \tag{7.44b}$$

$$(V-\mathcal{D})\,\rho V_{,x} = -\tilde{P}_{,x} \tag{7.44c}$$

$$(V-\mathcal{D})\,\rho\,T_{,x} = \frac{(k\,T_{,x})_{,x}}{Pe}-(V-\mathcal{D})\,\rho\,(1+T)\frac{dv}{d\varphi}\,\varphi_{,x}+(\mathcal{D}-V)^2\,\frac{\rho}{\bar{\alpha}}\,(\varphi_{,x})^2 \tag{7.44d}$$

In order to focus on kinetics we consider a purely phase field model and thus ignore the coupling with pressure and temperature. The system of governing equations reduces therefore to the single *AC* equation (7.44a) and the single dissipative mechanism considered is thus the Ginzburg-Landau relaxation. The inner leading order *AC* equation (7.44a) is an ODE in $\varphi_0(\bar{x})$ that reads

$$\bar{\mathcal{D}}\,\varphi_0' = \left(\frac{\partial g}{\partial\varphi}\right)_0-\varphi_0'' \tag{7.45}$$

where we introduced the normalized velocity of the phase transition front $\bar{\mathcal{D}}$

$$\bar{\mathcal{D}} \triangleq \frac{\mathcal{D}}{\bar{\alpha}}$$

Equation (7.45) has already been studied by Truskinovsky [137], see also [139] in the context of kinetic relations.

Let us first analyze the out of equilibrium ODE (7.45), and reproduce the analogy used in the study of the spherical equilibrium case (*cf.* section 4.3.1). We thus consider the motion of a particle in a one dimensional system of coordinates φ, the time being associated to the abscissa $\bar{x}$. The LHS of equation (7.45) is then a viscous dissipation for the particle motion. It is worth pointing out that using the "close to equilibrium scaling" the leading order out of equilibrium ODE governing the phase field profile was non-viscous, *e.g.* equation (7.12) (zero LHS in equation (7.45)) and thus $\varphi_0(\bar{x})$ was the planar equilibrium profile. In the present case, we recover the equilibrium profile only in the limit of small $\bar{\mathcal{D}}$ where the LHS term of equation (7.45) can be neglected.

Let us now consider the kinetic relation of this model. In this case, entropy and density jumps are zero and the driving force simply reads (*cf.* its definition (7.3)).

$$\mathscr{G} = [\![g]\!]$$

and is thus equal to the specific Gibbs free energy jump across the interface transition layer. It is a straightforward calculation (multiplying by φ' and integrating over $\mathbb{R}$) to show from equation (7.45) that

$$[\![g]\!] = \bar{\mathcal{D}}\int_{-\infty}^{+\infty}\varphi'^2(\bar{x})\,d\,\bar{x} \tag{7.46}$$

This relation is the kinetic relation of the phase field model considered. It shows that at and only at equilibrium both $\bar{\mathcal{D}}$ and $[\![g]\!]$ are zero. Let us now consider the integral term. It is worth pointing out that for the "close to equilibrium" scaling of the mobility, $\varphi_0(\bar{x})$ was the planar equilibrium profile. As a consequence the integral was independent of the out of equilibrium parameter ($[\![g]\!]$ or $\bar{\mathcal{D}}$), and thus at leading order the driving force was linear in $\bar{\mathcal{D}}$. This obviously no more the case with the "far from equilibrium" scaling as illustrated in the following.

7.6.2 Illustrative example of non-linear leading order kinetic relation

As an illustrative example, let us consider a simple model for the potential $\mu(\varphi_0)$ using piecewise quadratic approximation for the specific Gibbs free energy as represented on figure 7.2. Since we consider out of equilibrium process, we have $[\![g]\!]_0 \neq 0$. At infinity, homogeneous single phase states are reached. According to the properties of our model, these single phase states correspond to the phase field values 0 and 1 as shown in chapter 6. To propose a simple model consistent with the main features of our phase field model, we set

$$\begin{aligned} \frac{\partial g}{\partial \varphi}(0) = \mu(0) &= 0 \\ \frac{\partial g}{\partial \varphi}(1) = \mu(1) &= 0 \end{aligned}$$

The piecewise potential then simply reads

$$\mu(\varphi) = \begin{cases} \varphi, & \varphi \leq \frac{1}{2}, \\ 2\,(1 + 4\,[\![g]\!])\,(\varphi - 1)\,, & \varphi > \frac{1}{2}. \end{cases} \tag{7.47}$$

and is thus discontinous at $\varphi = 1/2$. The potential μ as well as the specific Gibbs free energy g are represented on figure 7.2. To solve the ODE (7.45) we now need to solve two linear second order differential equations for

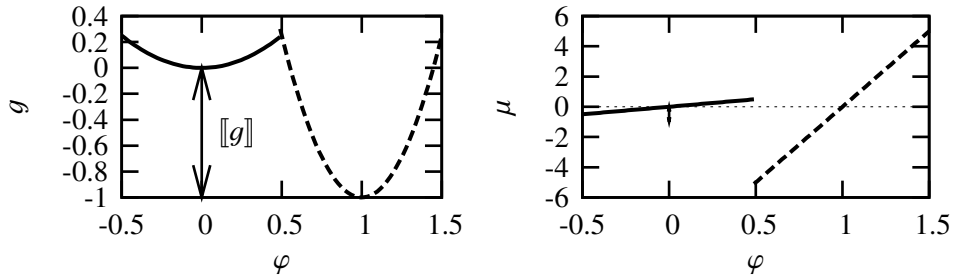

Figure 7.2: Piece wise thermodynamic potential

each domain $\varphi_0(\bar{x}) \in [0 : 1/2]$ and $\varphi_0(\bar{x}) \in [1/2 : 1]$. We set $\varphi_0(-\infty) = 0$, $\varphi_0(+\infty) = 1$ and $\varphi_0(0) = 1/2$. As a consequence the out of equilibrium ODE (7.45) has the solution

$$\varphi_0(\bar{x}) = \begin{cases} \frac{1}{2}\, e^{\,a_0\,\bar{x}}, & \bar{x} \leq 0, \\ 1 - \frac{1}{2}\, e^{-a_1\,\bar{x}}, & \bar{x} \geq 0. \end{cases} \tag{7.48}$$

where the positive coefficients a_0 and a_1 read

$$\begin{aligned} a_0 &= \frac{-\bar{\mathcal{D}} + \sqrt{\bar{\mathcal{D}}^2 + 4}}{2} \\ a_1 &= \frac{\bar{\mathcal{D}} + \sqrt{\bar{\mathcal{D}}^2 + 8\,(1 + 4\,[\![g]\!])}}{2} \end{aligned}$$

We can thus evaluate the integral entering the kinetic relation (7.46), it yields

$$\begin{aligned} \int_{-\infty}^{+\infty} \varphi_0'^2(\bar{x})\, d\,\bar{x} &= \int_{-\infty}^{0} \frac{a_0^2}{4}\, e^{\,2\,a_0\,\bar{x}}\, d\,\bar{x} + \int_{0}^{+\infty} \frac{a_1^2}{4}\, e^{-\,2\,a_1\,\bar{x}}\, d\,\bar{x} \\ &= \frac{a_0}{8} + \frac{a_1}{8} \end{aligned}$$

and thus

$$[\![g]\!] = \frac{1}{16}\,\bar{\mathcal{D}}\left[\sqrt{\bar{\mathcal{D}}^2 + 4} + \sqrt{\bar{\mathcal{D}}^2 + 8\,(1 + 4\,[\![g]\!])}\right]$$

that is obviously a non-linear relation between $\tilde{\mathcal{D}}$ and the driving force. As a consequence, the kinetic relation inherited from the "far from equilibrium" scaling for the mobility deviates from the normal growth theory for large interface mass transfer rates.

The non-linearity of the kinetic relation between the driving force and the interface mass transfer is more physically realistic than the linearity inherited from the "close to equilibrium" scaling of the mobility that is then at leading order restricted to the normal growth approximation. Nevertheless as long as a single regularization of the Stefan problem at low mass transfer rates is targeted, the "close to equilibrium" scaling is mathematically satisfying. It would be of interest to further investigate the consequences of the "far from equilibrium" scaling of the phase field equations for the model including pressure and temperature dependences.

7.7 Conclusion

In this chapter, we studied the non-equilibrium internal structure of the interface using approximate solutions (matched asymptotic expansions) of the governing equations for a steady-state one-dimensional phase change problem. The leading order profiles of the main variables have been derived. It has been shown that the equivalent sharp interface representation of our model satisfies the classical jump conditions (mass, momentum, energy). Moreover, in the outer bulk phases, the phase field value is always 0 or 1, which allows to easily control their physical properties. In addition, we have derived the kinetic relation of our model. At leading order, the interface entropy production is consistent with the normal growth theory, *i.e.* the interface entropy production is quadratic in the mass transfer rate. As a consequence, the classical Gibbs-Thomson equation is recovered for low mass transfer rates in the case of uniform density. When density difference is taken into account, a non-equilibrium Clapeyron relation has been derived. However, the kinetic relation has been shown not to reduce to the normal growth theory. Indeed, when higher order terms are taken into account, the interface entropy production is no longer quadratic in the mass transfer rate. The entropy production has been clearly shown to be made of two contributions corresponding to the two dissipative processes considered in this study. The first one is related to the Ginzburg-Landau relaxation and is non-zero as soon as the mobility is finite. Since this dissipative process only takes place inside the interface, the associated interface entropy production is positive. The second contribution is associated to heat conduction. This dissipation is non-zero both in the bulk phases and across the interface. It has been shown that the associated interface entropy production is an excess quantity that is non-zero only if the heat conductivity is non-uniform. If it is non-uniform, the sign of the interface entropy production of the equivalent sharp interface model depends on the choice for the function $k(\varphi)$. This is consistent with the fact it is an excess quantity since the dissipation associated to heat conduction that takes place across the interface can be either smaller or larger than the sum of its equivalent representation by two separated bulk domains and a sharp interface.

We note that the consistency of the leading order solutions with the normal growth approximation limits the use of the model for fast kinetics where the phase transition occurs far from equilibrium. By introducing another scaling for the mobility coefficient, we derived another sharp interface limit for a purely phase field model. With this scaling, the kinetic relations deviates from the normal growth approximation as soon as the mass transfer rate is sufficiently large and that even in a sharp interface limit (*i.e.* without considering secondary order terms in the expansion). This deviation at large mass transfer rate is more physically realistic and we therefore draw a path allowing to consider other kinetic relations for our phase field model devoted to the study of boiling process.

Let us note that we know that for boiling phase transition, in addition to heat conductivity and Ginzburg-Landau relaxation, the viscosity, as a third dissipative mechanism has to be taken into account. Due to the density difference between the single phase states, the associated interface entropy production is non-zero and visco-elasticity can actually also control the kinetics of the phase transition. It would be of interest to study this interface dissipation for our phase field model.

Nevertheless, it is worth pointing out that there is a lack of knowledge and of understanding of the kinetic relation in the case of liquid-vapor interfaces. If several models exist for the case of high mass transfer rates associated to vaporization (*e.g.* the interface resistance, *cf.* the Knudsen layer model [28]), none is consistent with the classical jump condition for the pressure recoil. As mentioned by Anderson et al. [2] it remains to have a sound target for the kinetic relation.

As a final conclusion let us remark that, to our knowledge and even though matched asymptotic expansions are widely used to study phase field models, the use of the formalism of kinetic relation has never been presented, although it allows, to our point of view, to derive a clear analysis of the properties of these models. Indeed, we showed how the relation between interface pressure and temperature ("non-equilibrium Clapeyron relation") is related to the interface entropy production.

Chapter 8

Numerical resolution of the system of governing equations

In this chapter, we solve numerically the system of governing equations corresponding to the quasi-compressible phase field model dedicated to liquid-vapor flows with phase change derived in chapter 3. The goal is to develop an algorithm for the solving of the governing equations and to study the consistency of the numerical results with the analytical developments made in the previous chapters . In particular we study the ability of the model

- ⋆ to control the stability of the liquid and vapor homogeneous states (*cf.* the corresponding analytical study of the stability of homogeneous states in chapter 6)
- ⋆ to reproduce a given kinetic relation and to recover the classical out of equilibrium jump conditions (*cf.* the corresponding analytical study of the one-dimensional phase transition dynamics in chapter 7)
- ⋆ to deal with capillarity and curvature (*cf.* the corresponding analytical and numerical study of the spherical symmetry equilibrium in chapter 4)

We propose to consider three different canonical systems of governing equations. We follow the approach used to derive the analytical results of one-dimensional phase transition. We first focus on the purely thermal part of the phase transition by studying the phase transition with uniform density and, as a consequence, without mechanics (*cf.* section 8.1). Then, we study the coupling between phase change and fluid mechanics by considering the isothermal model (*cf.* section 8.2). Finally, we study the fully non-isothermal dissipative model (*cf.* section 8.3). Let us note that, the main numerical schemes and notations used in the following numerical study are introduced in the appendix C.

8.1 Liquid-solid phase transition without mechanics

In this section, we present the numerical simulation of the phase transition in the case of uniform density for one- and two-dimensional systems. The goal is to study the coupling between the energy balance equation and the Allen-Cahn equation. The resolution of this coupling allows to take into account a major ingredient of the boiling flows: the unsteady phase transition associated to thermal effects. Indeed, the classical models of the bubble growth in nucleate boiling flows assume that the last stage of the process is governed by a thermal effects, *e.g.* Mikic et al. [93]. Moreover, the results of this section allow to illustrate some of the key ingredients of our model, namely

- ⋆ the modeling of the interfaces as transition zones of characteristic thickness h
- ⋆ the separation of the domain in single phase domains characterized by constant values of the phase-field ($\varphi = 0$ and $\varphi = 1$)
- ⋆ the ability of the model to deal with capillarity, curvature and topological changes
- ⋆ the dynamics of phase transition

- ⋆ the kinetic relation associated to the Ginzburg-Landau and thermal conductivity dissipation mechanisms (*cf.* chapter 7)

It is worth noting that, since the density is assumed to be uniform, the model corresponds to a solid-liquid phase transition. It is worth pointing out that the goal of this numerical study is to define an algorithm for the coupling between thermal and phase field parts of the model before to adress the coupling with mechanics. As a consequence we limit our study to a rather more qualitative than quantitative analysis of the results obtained. The satisfaction criteria will be based on the consistency of the results with the analytical results derived in the previous chapters. We therefore won't provide a detailed study of the phase transition without density difference such as it is done with phase field models devoted to this study.

This section is organized as follows. First, in section 8.1.1, we analyze the system and discuss the approximations introduced to develop an efficient and accurate algorithm to solve it. Then in section 8.1.2, we study one-dimensional steady-state phase change problem. We justify the main approximations used in the algorithm by a comparison with both analytical results and more accurate computations. We study the temperature and phase field profiles and compare them with the corresponding analytical results obtained in chapter 7. In section 8.1.3, we illustrate the ability of our model to deal with unsteady phase change problems. The influence of the Ginzburg-Landau relaxation on this result as well as the corresponding kinetic relation are analyzed. Two-dimensional computations are then proposed. In section 8.1.4 we first solve an unsteady phase change problem in spherical symmetry. Then in section 8.1.5, we illustrate the dynamic of phase separation and interface reconnection with our phase field model studied in chapter 6. We then study in section 8.1.6 the unsteady phase change process in a two-dimensional system that illustrates the effect of capillarity on the process.

8.1.1 Time discretization scheme

In this section, we identify the terms of the governing equations that need to be treated as implicit in time and those that can remain explicit. This identification is based on the physical anlysis of the couplings of these equations that have to be accounted for. Once these couplings are identified, a linear approximation of the terms involved is proposed as a valuable approximation. This approximation will be justified through numerical computations presented in the next section.

The system of equations The expression considered for the Helmholtz free energy corresponds to the reduction of our quasi-compressible model in the case where the bulk phase densities are equal; this expression corresponds to the classical phase-field model for solidification (*cf.* section 3.3.2). No dynamics is considered, *i.e.* it is assumed that $\vec{V}$ is uniformly null. Moreover, following the set of simplifications considered in section 5.3.3, the bulk heat capacities are assumed to be equal, and the latent heat is assumed to be a linear function of the temperature. The set of governing equations therefore reduce to the system of equations (5.57) that reads

$$\frac{d\varphi}{dt} = -\kappa\left[-\frac{d\nu}{d\varphi}\frac{\varepsilon}{St\,\gamma\,\theta}T + \frac{dW}{d\varphi} - \varepsilon^2\Delta\varphi\right] \tag{8.1a}$$

$$\frac{dT}{dt} = \frac{\nabla\cdot(k\nabla T)}{Pe} - \frac{\rho\,(1+T/\theta)}{St}\frac{d\nu}{d\varphi}\frac{d\varphi}{dt} + \frac{\gamma}{\varepsilon\,\kappa}\left(\frac{d\varphi}{dt}\right)^2 \tag{8.1b}$$

Implicit treatment of the diffusive terms We consider that the main variable of the *AC* equation 8.1a, resp. equation of evolution of the temperature 8.1b, is the phase-field variable φ, resp. the temperature T. Both equations have a purely diffusive term, namely the non-local term of the expression of $\tilde{\mu}$ in the *AC* equation, and the heat conduction term in the equation of evolution of the temperature. According to the numerical stability criteria for the solving of diffusive equations using Euler time stepping, it is required that the diffusive terms are made implicit for the scheme to be unconditionally stable. In the following, the diffusive terms are considered as implicit.

Implicit coupling and linear approximation The system of equations 8.1 contains highly non-linear terms in φ, namely $dW/d\varphi$ and $d\nu/d\varphi$ in the *AC* equation and the term $(d\nu/d\varphi)(d\varphi/dt)$ in the equation of evolution of the temperature. The implicit computation of this terms is computationally expensive, even though we observed

that it is required to preserve the accuracy of the solution. Some phase field methods use simplified expressions for the latent heat source term $(d\nu/d\varphi)(d\varphi/dt)$, the expression of the function $\nu(\varphi)$ being modified only for this term, *e.g.* [73]. This simplification allows a significant gain in numerical resolution even though the set of governing equations is thus no longer thermodynamically consistent. In this study, we choose to keep the thermodynamic consistency of our model. We thus use a simplified numerical scheme that allows to keep the expression for the interpolation function $\nu(\varphi)$ in the latent heat source term. Indeed, numerical tests showed that it is sufficient to at least partially consider the term $(d\nu/d\varphi)(d\varphi/dt)$ as implicit. Similarly, we observed that it is possible to make the non-linear functions $dW/d\varphi$ and $d\nu/d\varphi$ appearing in the *AC* equation partially implicit using Taylor expansions . The final writing of the system of equations solved reads

$$\frac{\varphi^{n+1}-\varphi^n}{Dt} = -\kappa\left[-\frac{d\nu}{d\varphi}^n \frac{\varepsilon}{St\,\gamma\,\theta}T^{n+1} + \frac{dW}{d\varphi}^n + \left(\varphi^{n+1}-\varphi^n\right)\left(-\frac{d^2\nu}{d\varphi^2}^n \frac{\varepsilon}{St\,\gamma\,\theta}T^n + \frac{d^2W}{d\varphi^2}^n\right) - \varepsilon^2\Delta\varphi^{n+1}\right] \quad (8.2a)$$

$$\frac{T^{n+1}-T^n}{Dt} = \frac{\nabla\cdot\left(k\nabla T^{n+1}\right)}{Pe} - \frac{\rho\,(1+T^n/\theta)}{St}\left[\frac{d\nu}{d\varphi}^n \frac{\varphi^{n+1}-\varphi^n}{Dt}\right] + \frac{\gamma\,\kappa}{\varepsilon}(\tilde{\mu}^n)^2 \quad (8.2b)$$

It is worth pointing out that the above system of equations is linear in $\left(\varphi^{n+1}, T^{n+1}\right)$. Efficient linear solvers can thus be used to solve it. The accuracy of the solution can be assessed by comparing it to the fully non-linear, fully implicit solution; the results reported in section 8.1.2 show good agreement between the two solutions. Numerical tests show that further simplifications (where some terms are made explicit instead of implicit) modify significantly the solution and are therefore not envisaged. When a density difference is taken into account, the expression for $\tilde{\mu}$ is more complex (*cf.* equation (5.47c)) but the terms are linearized similarly.

Numerical values of the non-dimensional parameters Since numerical simulations of nucleate boiling flows under nuclear power plant conditions are targeted, the values of the parameters are evaluated using the physical properties of pure water at the saturation pressure of 150 bar. Without taking into account any density difference, the *At*, *We*, *Re* and *Fr* numbers are irrelevant. As a consequence, the remaining non-dimensional parameters are the following

Non-dimensional number	Pe	γ	St	θ
Value	$1e^0$	$3e^{-6}$	$7e^{-2}$	$6e^2$

The non-dimensional numbers κ and ε are not specified, since, in the following, we make them vary to study their influence on the solution.

It is worth noting that the space discretization scheme is a standard *MAC* scheme where the discretization of the space derivative operators is such that the identity

$$\nabla\cdot\left(a\,\vec{b}\right) = \nabla a\cdot\vec{b} + a\,\nabla\cdot\vec{b}$$

is satisfied at the discrete level for any scalar a and vector $\vec{b}$ (*cf.* the presentation of the scheme in appendix C.2).

8.1.2 A first-test case : steady-state one-dimensional phase change

The time discretization scheme presented in the previous section is assessed on a steady-state one-dimensional phase transition problem. This problem corresponds to the analytical study performed in section 7.3 and we therefore compare the numerical results with the approximate analytical solutions derived in this study.

The numerical setting of the problem is the following. The computed domain is of non-dimensional size 1 and the value of the parameter ε, which is a measure of the interface thickness at equilibrium, is first set to 0.05. The boundary conditions is a zero heat flux at the LHS of the domain and a non-zero constant heat flux at the RHS. We impose a Neumann boundary condition for the phase-field: $\partial\varphi/\partial z = 0$. The phase field has initially an equilibrium profile at the center of the domain. The temperature is initially a piecewise linear profile satisfying the boundary conditions and having its slope break at the center of the phase field profile. The system is first solved using the fully non-linear and fully implicit system of equations and without any variation of the thermal conductivity. This solution is then compared to the solution obtained with the linearized system (8.2).

Out of equilibrium profiles Let us consider the temperature and phase field profiles after a few iterations, such that they have converged to their steady-state shape. The phase field profile is represented on figure 8.1 together with the analytical solution for the equilibrium profile (which has been shown in section 7.3 to correspond to the out of equilibrium profile at leading order in ε). It is clear that both agree. Let us remark that only a few mesh points are necessary to capture the profile (about 5). Let us now consider the temperature profile that is

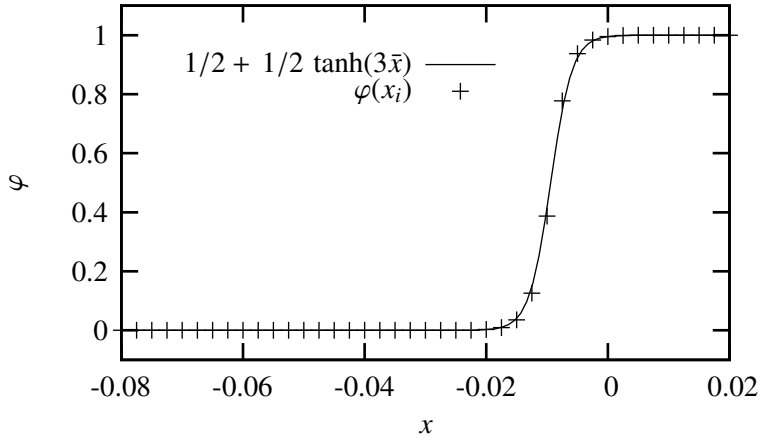

Figure 8.1: Phase field profile: numerical *vs* analytical solution (solid curve), $\varepsilon = 0.05$

represented on figure 8.2. The numerical profile is compared with the analytical solution at leading order in ε that has been derived using matched asymptotic expansions (*cf.* equation (B.45)). It is worth noting that both profiles agree.

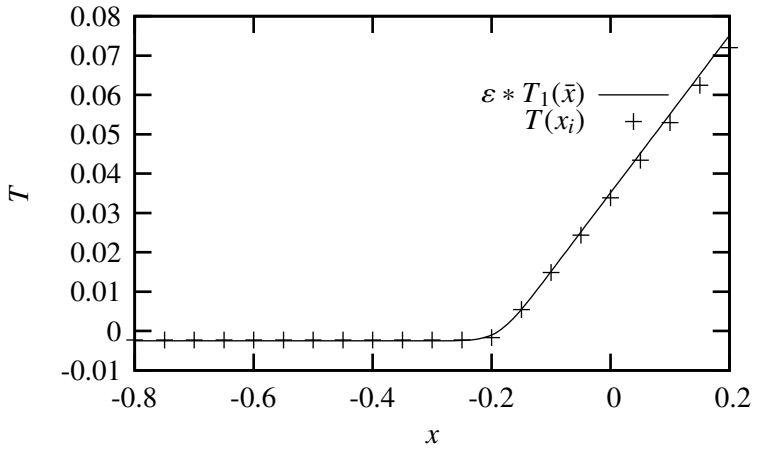

Figure 8.2: Temperature profile: numerical *vs* analytical solution (solid curve), $\varepsilon = 0.05$

	Mass transfer rate	Interface temperature	Thickness of the interface
$\kappa = 1$	**-0.00141516**	**2.9165e-05**	**0.0436395**
$\kappa = 10^2$	**-0.00141766**	**2.85051e-05**	**0.0434851**
$\kappa = 10^4$	**-0.00141782**	**2.84983e-05**	**0.0434809**
$\kappa = 10^6$	**-0.00141782**	**2.84982e-05**	**0.0434809**
$\kappa = 10^8$	**-0.00141782**	**2.84982e-05**	**0.0434809**

Table 8.1: Numerical results for the one-dimensional steady-state phase transition

The numerical value of the mass transfer rate has been evaluated using the following procedure. The location

of the center of the interface $x_i(nDt)$ at the iteration n is defined as the position where $\varphi = 1/2$. The mass transfer rate Γ, *i.e.* in this uniform density case the speed of displacement of the interface $\mathcal{D} = \Gamma$, is then the mean slope of the curve formed by the points $x_i(nDt)$. The corresponding values are given on table 8.1. The theoretical value of the mass transfer rate Γ_{theor} has been evaluated from the external boundary conditions on the heat flux q using equation (7.16)

$$\Gamma_{theor} = [\![\varphi]\!] \frac{St\,[\![q]\!]}{Pe} = -1.4\,10^{-3}$$

that has been shown to be valid for low mass transfer rates (*cf.* section 7.3). From the results of table 8.1, the numerical value of the mass transfer rate agrees with the theoretical one to a precision of about 1.2%

The numerical value of the interface temperature T^i is evaluated at the interface location using linear interpolation. It can be seen from the results of table 8.1 that its value is very close to the equilibrium temperature 0 (with regard to the order of magnitude of 1 of the temperature variations across the domain). Its value vary with regard to the mobility κ only when the mobility approaches 0. This result is characteristic of low mass transfer rates where the kinetic relation (7.13)

$$T^i = -[\![\varphi]\!]\frac{\Gamma\,\theta\,St\gamma}{\alpha} \simeq -[\![\varphi]\!]\frac{\Gamma\,\theta\,St\gamma}{\varepsilon^2\kappa} \tag{8.3}$$

derived in section 7.3 has a negligible effect on the temperature field with regard to the conductive profile.

The thickness of the interface is evaluated using the tangent of the phase field profile at $\varphi = 1/2$. The numerical value of the interface thickness must be compared with the value 0.05 of the parameter ε used in these calculations. The results reported in table 8.1 show that the interface thickness remains close to its equilibrium value for all the values of κ investigated.

Linearized solving The previous results have been obtained using a fully implicit non-linear solving of the system of equations. We show in the following that such a complex formulation is not required to get an accurate numerical solution. With the linearized system of equations (8.2) , we get the following results

	Mass transfer rate	Interface temperature	Thickness of the interface
$\kappa = 10^8$	**-0.001406**	**2.839e-05**	**0.0436**

The results obtained are thus in good agreement with those obtained with the fully implicit scheme (*cf.* table 8.1). Moreover the use of the linear system of equations, and the consequent ability to use efficient solvers, allows a noticeable gain in computational costs, of the order of at least ten, even in this simple one-dimensional calculation. It thus justifies the use the linearized approximation for the non-linear implicit terms in the computation of a phase-change problem.

These results show that the most important coupling have been identified and are accurately taken into account if they are linearized in time. In the following, we solve the linearized system (8.2) instead of the fully implicit one.

Variable heat conductivity Let us consider a contrast between the bulk values of the thermal diffusivity $k(\varphi)$. The phase field profiles and mass transfer rates presented in the previous paragraphs are still valid but the temperature profile is modified as it will be shown in the following. It has been shown in section 7.3 that the choice for the interpolation function $k(\varphi)$ has an influence on the value of the jump of the outer temperature profile at the interface (which is zero in the previous case of uniform thermal conductivity, *cf.* equation (7.18)). To emphasize the influence of the interpolation of the thermal conductivity between the bulk phases on the resulting temperature profile, we propose to consider various types of functions $k(\varphi)$ that are reproduced on the top graph of figure 8.3. For the P_3 case the thermal conductivity is interpolated by a monotonic polynomial. In the P_3^+ and in the P_3^- a non-monotonic variation is added as

$$k(\varphi) = P_3^{\pm} = (1-\delta k) + \delta k\; P_3(\varphi) \pm k_{non\ monot}\,\varphi^2\,(3-2\,\varphi)$$

In the P_3^+ case for example, for phase field values right below the liquid value (1), the heat conductivity first sharply decreases. Various amplitudes of the non-monotonicity have been considered that yield to the temperature profiles represented on the bottom graph of figure 8.3. It is worth noting that the situation differs mainly

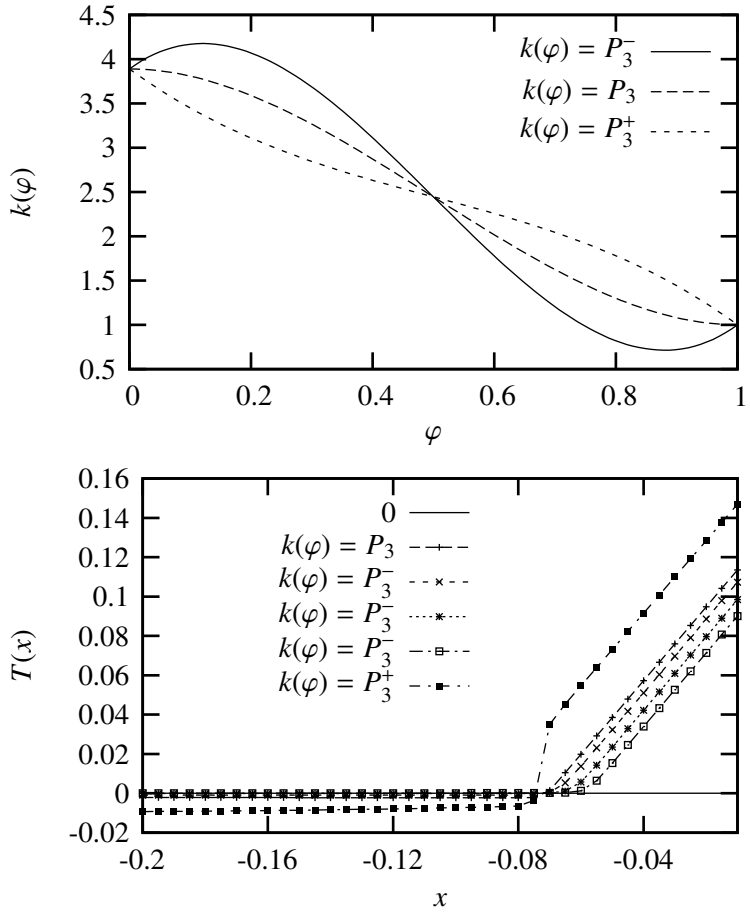

Figure 8.3: Variable thermal diffusivity and interface jump in temperature. For the three P_3^- cases, the amplitude $k_{non\,monot}$ of the non-monotonic variation is varied from first low to high.

between the different interpolation functions considered and that even though the interface position is always identical the outer profile are actually affected by the internal thermal dissipation. For the P_3^+ case for example, the heat conductivity increases more when φ becomes inferior to 1 in the P_3^- cases than in the monotonic P_3 case, and that all the more that the amplitude of the non-monotonic function is increased. As a consequence, on the RHS of the interface location where the heat flux can be considered as quasi-constant, the temperature gradient decreases rapidly. This can be clearly seen on figure 8.3. It is worth pointing out that as a consequence the jump in temperature at the interface location is non-zero: it can be seen on figure 8.3 if one considers the location of the sharp interface at $x \simeq -0.07$ and extend the linear temperature profiles in the bulk phase to this location, the jump in temperature being then null for the P_3 case, positive for the P_3^+ case and negative for the P_3^- cases. Let us recall the result derived in our analytical study (*cf.* equation (7.18))

$$[\![T_1]\!] = -\Phi_{th}\left(\frac{1}{k}\right)_0^{\bar{e}x} - Pe\,\mathcal{D}\left(\frac{\nu}{k}\right)_0^{\bar{e}x} + [\![\varphi]\!]\,\frac{Pe\,\mathcal{D}^2}{\alpha}\left(\frac{\nu - P_3}{k}\right)_0^{\bar{e}x}$$

that relates the temperature jump to the heat conductivity profile ($\varphi_0(\bar{x})$ being the equilibrium profile for the phase field) and where in our case $\Phi_{th} = 0$ (*cf.* equation (7.19)). It is worth ponting out that for the P_3 case, the excess quantities are identically zero, that is no more the case for the $P_3^\pm$ cases. The existence of a non-zero temperature jump in the corresponding computations is therefore qualitatively consistent with the analytical results: the choice for the interpolation function $k(\varphi)$ induces a particular thermal dissipation inside the transition layer that has consequences on the jump of the outer temperature at the interface.

8.1.3 Unsteady phase-transition

Setting of the problem The test case considered corresponds to a uniformly superheated liquid phase put into contact with a solid phase at saturation. The analytical solution of the sharp interface problem corresponding to this situation is known, *e.g.* Lemonnier et al. [85], and will be compared to our numerical results. The phase field profile is initialized with an equilibrium profile. The temperature is initially a discontinuous profile at the center of the interface ($\varphi = 1/2$).

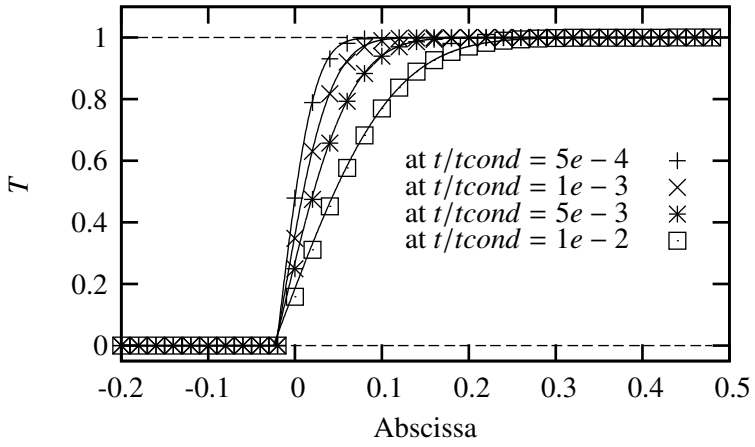

Figure 8.4: Unsteady temperature profiles at various times: numerical *vs* analytical solution (solid curves), the parameter ε equals 0.05

Comparison between numerical and analytical temperature profiles The numerical and analytical temperature profiles are represented on figure 8.4 at different times and show good agreement. However, it is important to note that such a good agreement is obtained thanks to a fine discretization of the interface layer: the interface is discretized by about 16 mesh cells. In the following, we analyze the results as a function of the spatial discretization.

Accuracy of the mass transfer rate as a function of the spatial discretization Let us consider the instantaneous mass transfer rate corresponding to this problem. The analytical expression for the time evolution of the mass transfer rate is known, *e.g.* Lemonnier et al. [85]. On figure 8.5 is represented the time evolution of both the analytical and numerical mass transfer rates for different spatial discretizations. The typical number of discretization nodes used to capture the diffuse interface varies from about 1 to about 16. The numerical mass transfer rate agrees well with the theoretical value. However it oscillates around the theoretical value for the coarser mesh ($\Delta x = 0.03333$) and that it converges toward the theoretical value when the spatial discretization is refined. More quantitative results are presented on figure 8.6 where the time evolution of the difference between the theoretical and the numerical mass transfer rates is represented. This figure shows that the numerical mass transfer rate converges to a common value as the spatial discretization is refined. The oscillations in time vanishe for $\Delta x \leq 0.002$, *i.e.* when the interface layer is discretized with about 8 mesh cells. However, at convergence (*i.e.* when $\Delta x \leq 0.002$), the error does not vanish. This is because, in the present computation, we use a finite value of κ, which implies that the interface temperature is not at equilibrium (*cf.* section 7.3). Now, in the theoretical model, the interface is assumed to be at saturation conditions. However, the effect of the Ginzburg-Landau relaxation is weak since it only affects the results by about 5%

Interface temperature and kinetic relation According to our study of the one-dimensional steady-state phase transition, the value of the interface temperature is a function of the mass transfer rate and differs from the equilibrium value 0. This result is also valid for the unsteady phase transition, as shown on figure 8.7 where the time evolution of the interface temperature is represented . This figure shows that the interface temperature converges to a monotonic function of time as the convergence in spatial discretization is reached ($\Delta x = 0.001$ for

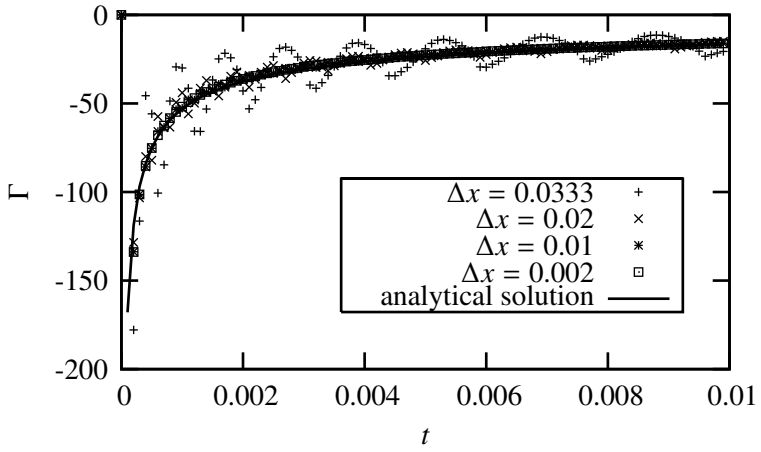

Figure 8.5: Unsteady mass transfer rate as a function of time for various spatial discretizations: numerical *vs* analytical solution (solid curve)

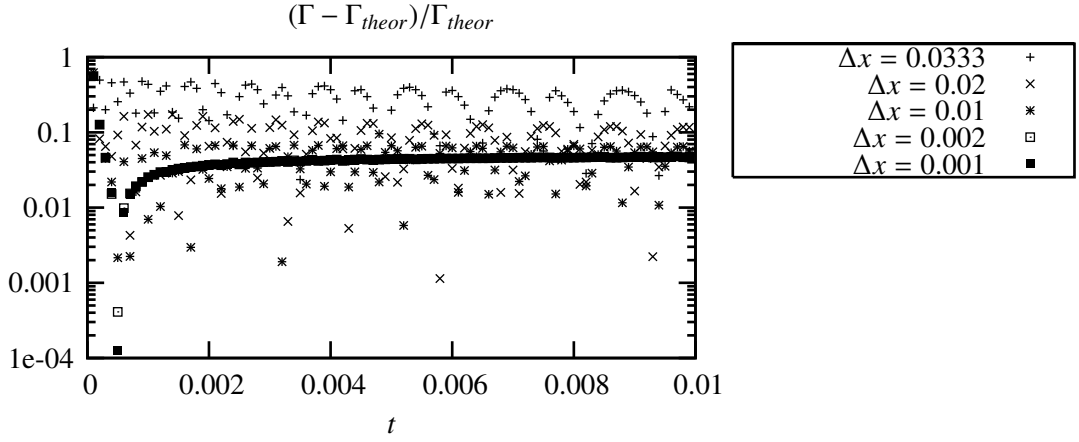

Figure 8.6: Difference between the theoretical and the numerical unsteady mass transfer rates as a function of time and for various spatial discretization

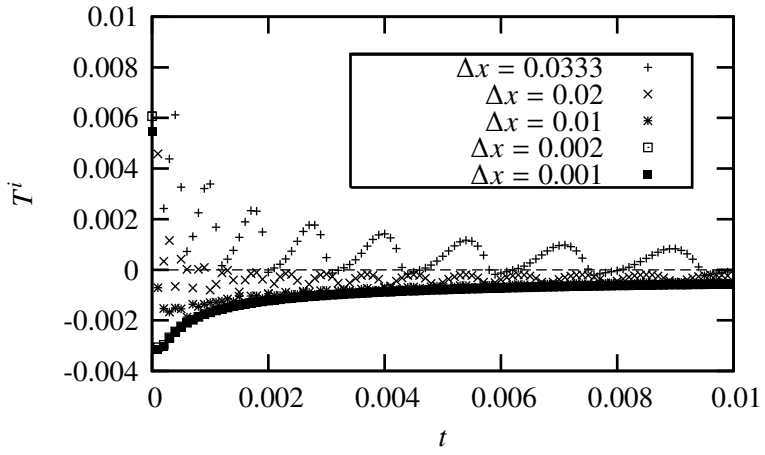

Figure 8.7: Interface temperature as a function of time for an unsteady phase transition: numerical results for various spatial discretization

example). The correlation between the intantaneous interface temperature and mass transfer rate is represented on figure 8.8 for the three finest grids. For the two finest grids ($\Delta x = 0.001$ and $\Delta x = 0.002$) the results are

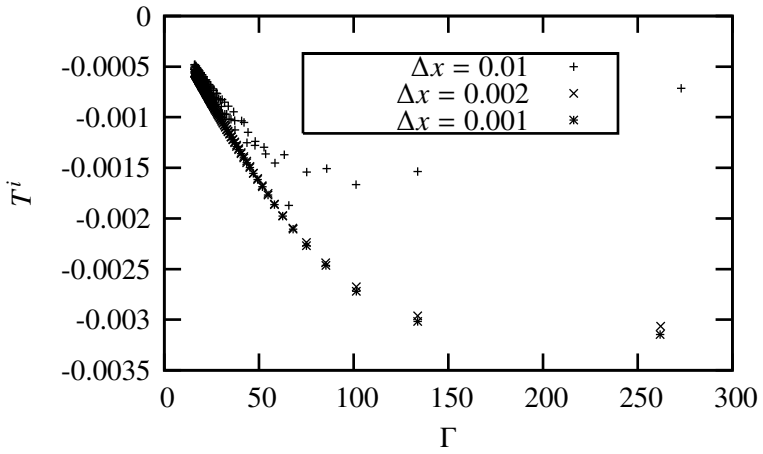

Figure 8.8: Correlation between interface temperature and mass transfer rate for unsteady phase change process and for various spatial discretization

identical even for large mass transfer rates and we consider that they actually correspond to a converged result. In the region of low mass transfer rates, the interface temperature T^i varies linearly with the mass transfer rate Γ. This is fully consistent with the leading order solution for the interface temperature derived in section 7.3.1 (*cf.* equation (8.3)). This approximation has been shown to be consistent with the normal growth theory. However, for larger mass transfer rates, the results diverge from this linear law. This confirms that the leading order results is valid for low mass transfer rates for which the phase field profile is close to the equilibrium one.

Influence of the mobility In section 7.3, we showed that the relation between the interface temperature and the mass transfer rate studied in the previous paragraph reads (*cf.* equation (7.13))

$$T_0^i = \frac{\Gamma \varepsilon^2}{\kappa}$$

and is thus scaled by the inverse of the mobility κ. Therefore, such a dependence should be captured numerically. The time evolution of the unsteady mass transfer rate for various values of the mobility is represented on figure 8.9. This figure shows that when the mobility κ tends to infinity, the phase transition process converges where the only dissipation is due to heat conduction. However, for low values of the mobility, the effect of the Ginzburg-Landau relaxation on the intensity of the mass transfer rate is non-negligible.

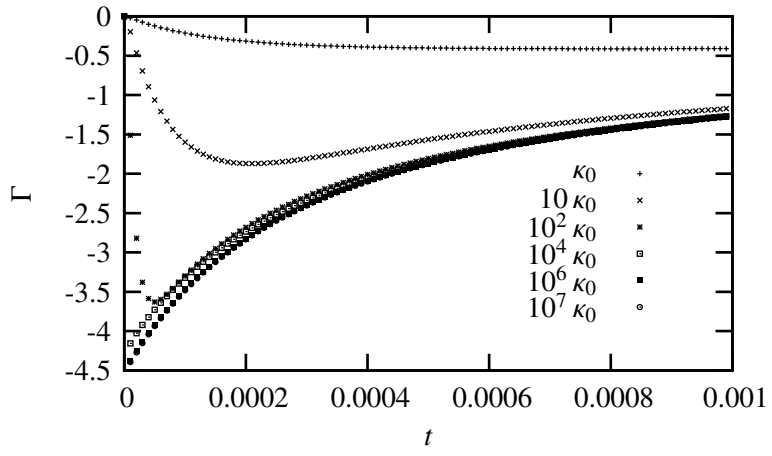

Figure 8.9: Effect of the value of the mobility on the mass transfer rate

8.1.4 Spherical symmetry

In this paragraph, we study a phase-transition process for a spherically symmetric system. The heat flux at the outer boundary is imposed constant. The equations of evolution of φ and T are solved simultaneously using an implicit scheme where the main couplings have been linearized as presented in section 8.1.1.

The profiles at the end of the simulation are shown in figure 8.10. It is worth noting that the interface is discretized by a relatively small number of mesh points *i.e.* about 5.

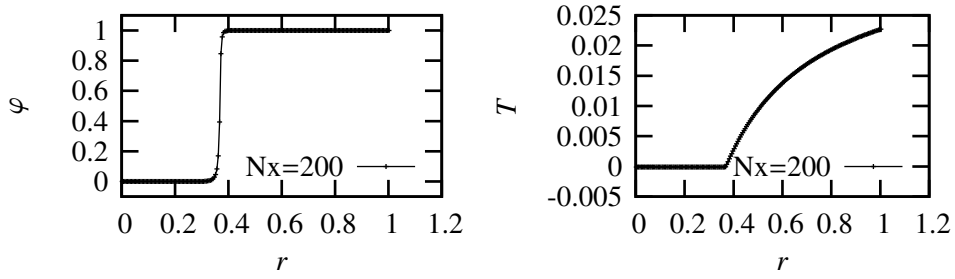

(a) Phase-field φ (b) Temperature T

Figure 8.10: Profiles at the end of the simulation.

The time evolution of the interface position, velocity, temperature and interface thickness are shown in figure 8.11. This figure shows that the interface motion is not regular (which is clearly shown by the interface velocity). This is due to the discretization in space. However, the results get smoother as the grid is refined.

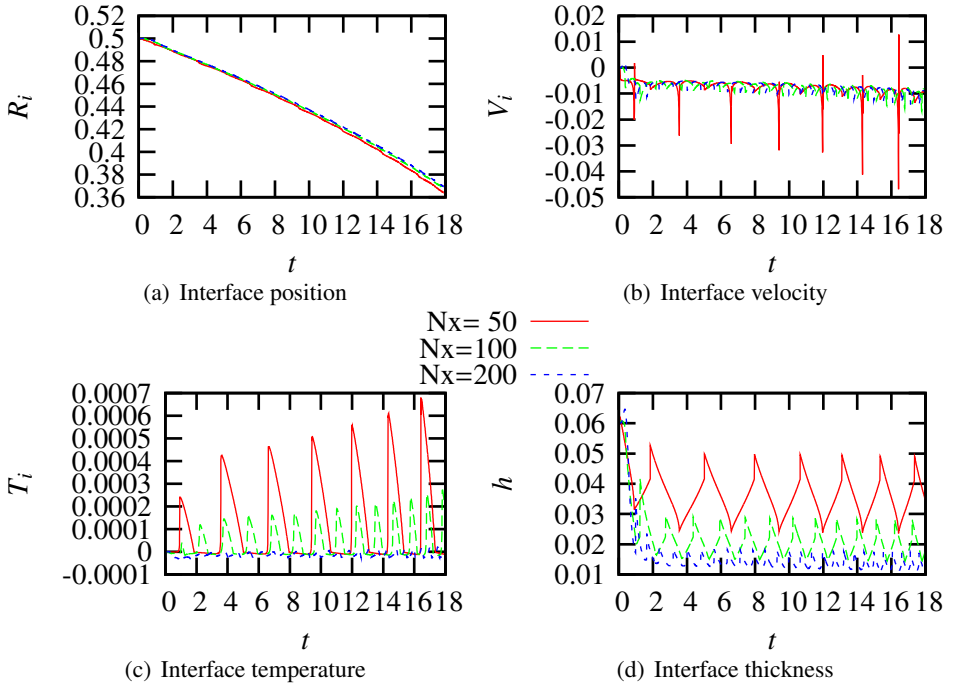

(a) Interface position (b) Interface velocity

(c) Interface temperature (d) Interface thickness

Figure 8.11: Time evolution of the interface position, velocity, temperature and thickness.

Moreover the interface temperature as well as the interface thickness converge to a fixed value as the interface is better discretized.

As a partial conclusion, the phase transition process in spherical symmetric system is qualitatitevely well predicted by the model.

8.1.5 Two-dimensional phase separation

In this section, we illustrate the phase separation process as well as the reconnection dynamics associated to our phase field model. Both phase field and temperature are initially randomly perturbed around a constant value. The values of the phase field are arbitrarily in the interval $[-1/2 : 1/2]$ (the equilibrium phase field values have been shifted of $-1/2$ from the values 0 and 1 without any consequences on the model) and the temperature field in the interval $[-0.01; 0.01]$. Zero fluxes are imposed on the external boundaries. The domain is discretized by a regular 50×50 mesh. Snapshots of the spatial phase field are represented on figure 8.12. The color scale

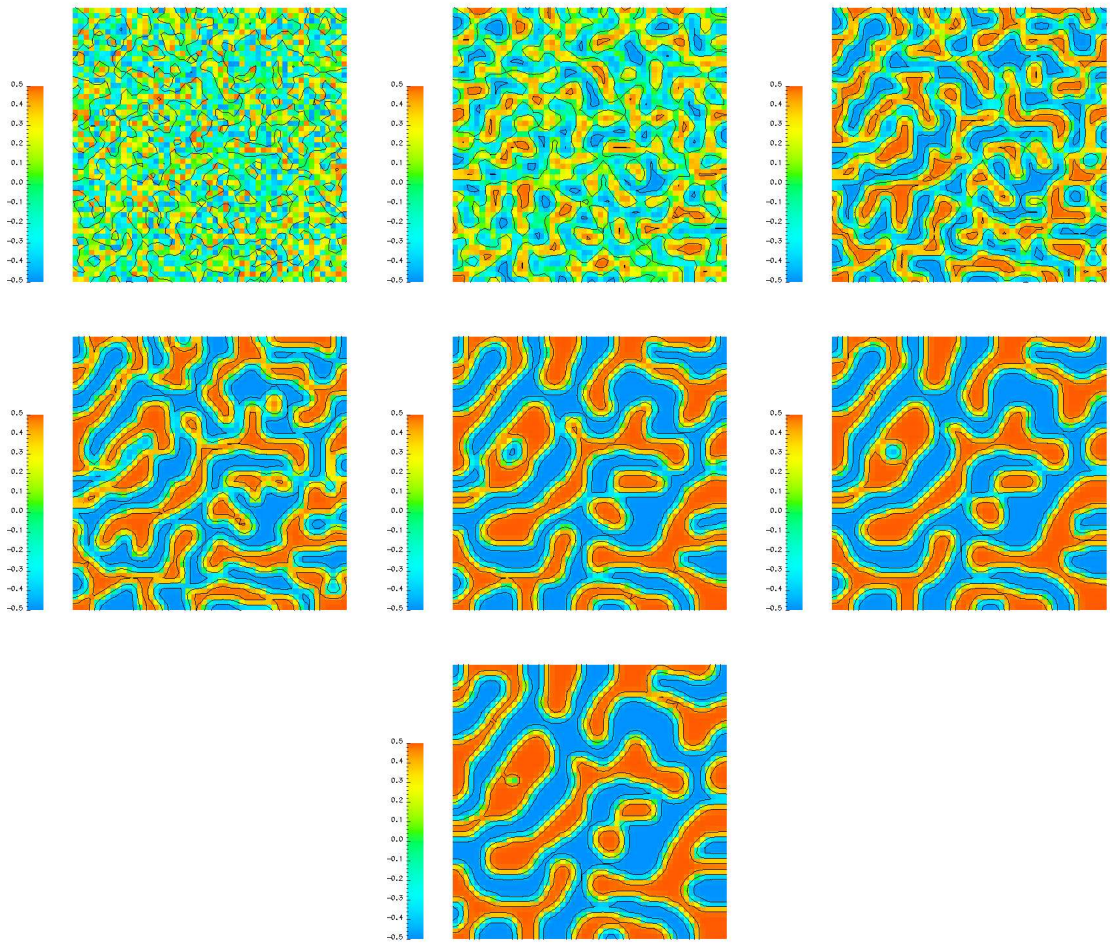

Figure 8.12: Dynamics of phase separation

varies linearly from $\varphi = -0.5$ to $\varphi = 0.5$. The black lines correspond to the iso-values -0.49, 0 and 0.49 of the phase field. This figure shows that the phase field value always remains in the interval $[-0.5 : 0; 5]$. The boundary condition $\nabla\varphi = 0$ corresponds to a contact angle of $\pi/2$, which is indeed observed on the figures. The separation of the physical domain into sub-domains characterized by $\varphi = \pm 1/2$ separated by a diffuse interface of controlled thickness can be clearly observed as time increases. Moreover the effect of capillarity on the process can be identified since high interface curvatures region tend to disappear with time.

This simulation shows the ability of the model to deal with nucleation processes even though we here considered a very large amplitude perturbation.

8.1.6 Two-dimensional solid-liquid phase transition

The following two-dimensional test cases illustrate the ability of the model to deal with two-dimensional out of equilibrium situations. The initial shape of the solid grain is deliberately considered as non-spherical to emphasize the influence of local curvature on the phase transition process.

Isolated system We consider a two-dimensional square domain. Because of symmetry, we compute only the top right quarter of the domain, symmetric conditions being imposed on the bottom and left boundaries of the computationnal domain. In this computation the heat flux is imposed null on the top and right external boundaries. A solid grain is set at the center of the domain. The solid grain is initially at the equilibrium temperature whereas the surrounding liquid is sub-cooled. The temperature varies smoothly between these two domains across the interface. The domain is discretized by a regular 100×100 mesh. Snapshots of the phase

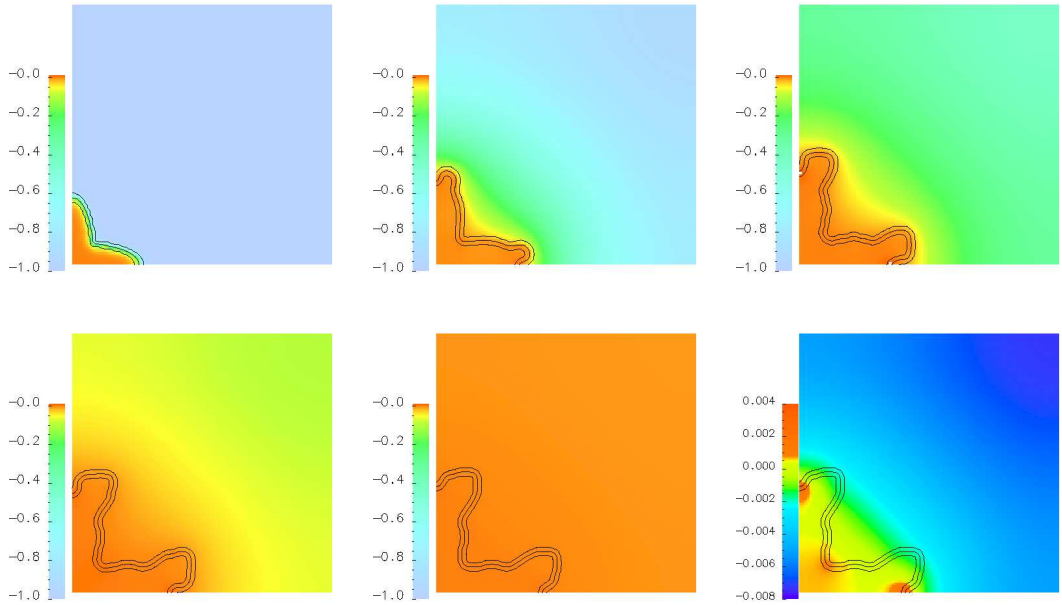

Figure 8.13: Growth of a solid grain in a sub-cooled liquid, the heat flux is imposed to be zero at the external boundary

transition process are reproduced on figure 8.13. The color field is the temperature field and the scale varies linearly between a value right above the equilibrium temperature 0.004 and the sub-cooled temperature -1, except for the last picture where the temperature scale is between 0.004 and -0.004. Black lines correspond to the iso-values 0.45, 0.5 and 0.55 of the phase field. As time increases, the temperature in both the liquid and the solid phases tends to be uniform and, as a consequence, the grain growth slows down. A change of scale of temperature on the last picture shows that the dependance of the interface temperature with the local curvature of the interface: regions of positive, resp. negative curvature, have a temperature above, resp. below the mean temperature.

This computation demonstrates the ability of the model to deal with multi-dimensional unsteady phase transitions .

Sub-cooled external temperature In this study, the temperature at the external (top and right) boundaries is imposed constant at a value lower than the equilibrium temperature. All the other parameters of the computations are identical to the previous one. Due to the square shape of the domain, the heat flux toward the interface is lower along the diagonal than along the vertical or horizontal directions. As a consequence, the grain grows faster along the axes of symmetry (bottom and left boundaries). Snapshots of the phase transition process are reproduced on figure 8.14. The color field is the temperature field and the scale varies linearly between a value right above the equilibrium temperature 0.004 and the sub-cooled temperature -1. The lines corresponds to the iso-values 0.45, 0.5 and 0.55 of the phase field. As time increases the points of the interface closest to the external boundary grow faster and faster as it approaches the external boundary . On the contrary, the point of the interface located the farthest from the boundary is quasi-immobile. It is worth noting that dendritic shapes are generated in this computation. They can be associated to the Mullins-Sekerka instability: as soon as the curvature is locally non-constant the interface temperature is non-uniform along the interface. This local variation of the interface temperature tends to emphasize the growth of regions corresponding to positive curvatures (such

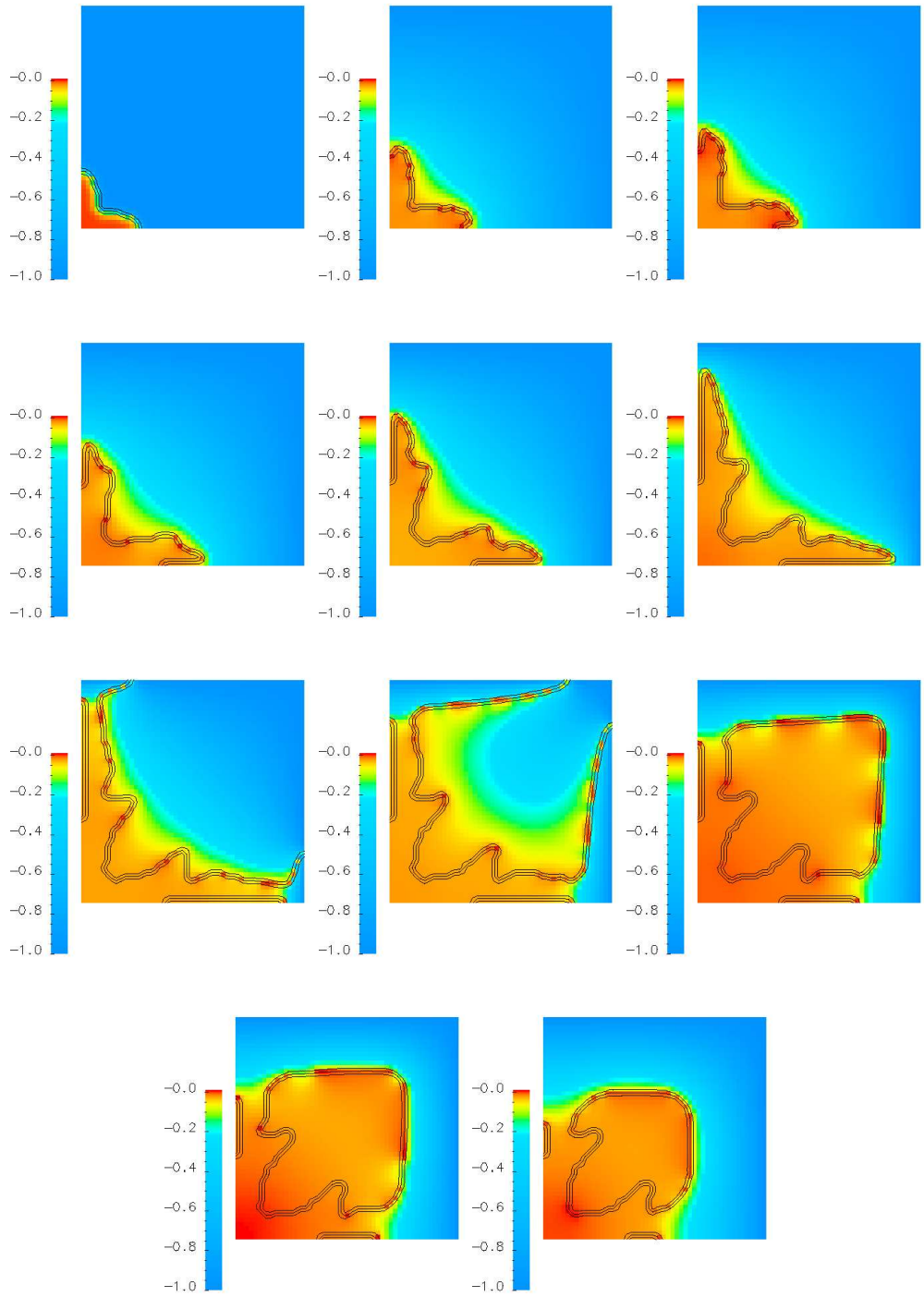

Figure 8.14: Growth of a solid grain, the temperature at the external boundary is imposed as being less than the two-phase equilibrium temperature

as the tip of the dendrites) compared to the regions of negative curvature (such as the the point of the interface located in the diagonal direction of the domain). Let us note that this tendency is deliberately emphasized by the initial shape of the grain. When the solid phase reaches the external boundary, it grows very fast along the direction tangent to this boundary, and finally reconnects at the top right angle. As a consequence, a liquid drop is trapped at the center of the domain that then progressively disappears.

This calculation demonstrates the ability of the model to deal with multi-dimensional unsteady phase transitions with reconnection.

8.1.7 Conclusions

We have numerically solved the set of governing equations of our model when the density is assumed to be uniform. It has been shown that a necessary coupling between the *AC* equation and the equation of evolution of the temperature must be taken into account in order to accurately compute the phase change process. However this coupling can be linearized, which makes the computation more efficient.

It has been shown that the analytical results derived in chapter 7 were actually recovered. As a consequence, the model is able to take into account a kinetic relation of Gibbs-Thomson type at leading order in the interface thickness ε. Moreover, the choice for the heat conductivity $k(\varphi)$ has been shown to be related to the jump in temperature at the interface, which is zero when $k(\varphi)$ is constant, which is consistent with the analytical results derived in section 7.3. In two dimensions, simulations of the phase separation process attest the results derived in chapter 6: the single-phase states domain correspond to the phase field values 0 and 1 separated by a diffuse interface of thickness ε. The simulation of the growth of a solid grain has shown the ability of the model to deal with curvature, reconnection and capillarity; the interface temperature has been shown to be correctly curvature dependent.

The numerical results presented in this section show the ability of the model to take into account the coupling between the bulk phase thermal problem and the diffuse interface dynamics. The numerical algorithm used is efficient due to the linearized terms. We did not pursue further the analysis of the uniform density case since for the targeted study it is necessary to include dynamics. In the next section we study the ability of the model to take into account the coupling between interface dynamics and two-phase fluid dynamics.

8.2 Isothermal phase change

In this section, we study isothermal liquid-vapor flows with phase change with the help of our quasi-compressible phase-field model (*cf.* its presentation in section 3.3, and the system of governing equations (5.58)). The goal is to develop a numerical method allowing to couple the phase change process with the fluid mechanics.

This section is organized as follows. We first introduce the algorithm for the solving of the coupling between the mechanics and phase field parts of the model (see section 8.2.1). In section 8.2.2, we solve a one-dimensional steady-state athermal phase transition which has been studied analytically in section 7.4. Then in section 8.2.3, a numerical simulation of the isothermal motion of a bubble in a closed two-dimensional system is investigated .

8.2.1 Resolution algorithm

The algorithm is based on the projection method.

Projection method The projection method is a widely used method for solving the coupling between continuity equation and momentum balance equations for incompressible flows. As a result of this method, a single Poisson equation on the pressure has to be solved in order to compute both the pressure and the velocity (or momentum) fields. The original method is based on the fact that the incompressibility constrains the velocity field to be divergence free. In our case of liquid-vapor flows with phase change, the divergence of the velocity fluid is non zero due to the phase transformation even though the single phase states are incompressible. Nevertheless, since the bulk phases are incompressible, the only way the density can evolve along a current line is through phase change. Phase change rate is $(d\varphi/dt)$ and since ρ is only a function of φ, it is directly linked to the field $(d\rho/dt)$. As a consequence, if we assume φ^{n+1} to be given, we get (*cf.* the continuity equation (5.56b))

$$\nabla \cdot \rho \vec{V}^{n+1} = -\frac{d\rho}{d\varphi}^{n} \frac{\varphi^{n+1} - \varphi^{n}}{Dt} \tag{8.4}$$

The momentum balance equation reads (*cf.* equation (5.56c) where for the sake of simplicity we set $Fr = \infty$ and $Re = \infty$)

$$\rho \frac{\vec{\rho V}^{n+1} - \vec{\rho V}^{n}}{Dt} + \nabla \cdot (\rho V \cdot V)^{n} = -\nabla \mathcal{G}^{n+1} + \frac{\left(\frac{dW}{d\varphi}^{n} - \varepsilon^2 \Delta \varphi^{n}\right)}{\varepsilon\, We} \nabla \varphi^{n} \tag{8.5}$$

where $\mathcal{G} = \hat{=} P + \left(W + \frac{\varepsilon^2}{2}(\nabla\varphi)^2\right)/(\varepsilon We)$. Let us now take the divergence of the momentum balance equation (8.5), it yields

$$\frac{\nabla\cdot(\rho V)^{n+1} - \nabla\cdot(\rho V)^n}{Dt} + \nabla\cdot(\rho V\cdot V)^n = -\Delta\mathcal{G}^{n+1} + \nabla\cdot\left(\frac{\left(\frac{dW}{d\varphi}^n - \varepsilon^2\Delta\varphi^n\right)}{\varepsilon We}\nabla\varphi^n\right) \tag{8.6}$$

Using equation (8.4), equation (8.6) reads thus

$$\frac{d\rho}{d\varphi}^n\frac{\varphi^{n+1}-\varphi^n}{Dt^2} - \frac{\nabla\cdot(\rho V)^n}{Dt} + \nabla\cdot(\rho V\cdot V)^n = \Delta\mathcal{G}^{n+1} - \nabla\cdot\left(\frac{\left(\frac{dW}{d\varphi}^n - \varepsilon^2\Delta\varphi^n\right)}{\varepsilon We}\nabla\varphi^n\right) \tag{8.7}$$

This is a Poisson equation in $\mathcal{G}^{n+1}$ that can thus be solved using linear solvers.

Main algorithm The main algorithm consists thus in the solving of the linear system in $(\varphi^{n+1}, \mathcal{G}^{n+1})$ made of the *AC* equation

$$\begin{aligned}\frac{\varphi^{n+1}-\varphi^n}{Dt} + \vec{V}^n\cdot\nabla\varphi^n \quad = \quad & -\kappa\left[\frac{dv}{d\varphi}^n(At\,\varepsilon We)\,\mathcal{G}^{n+1} + \frac{d^2v}{d\varphi^2}^n\left(\varphi^{n+1}-\varphi^n\right)(At\,\varepsilon We)\,\mathcal{G}^n\right.\\ & \left. + v^n\left(\frac{dW}{d\varphi}^n + \frac{d^2W}{d\varphi^2}^n\left(\varphi^{n+1}-\varphi^n\right) - \varepsilon^2\Delta\varphi^{n+1}\right)\right]\end{aligned} \tag{8.8}$$

and of the Poisson equation (8.7).

It is worth pointing out that for a closed domain, since no pressure level is imposed on the boundaries , the Poisson equation in pressure used in the projection method is ill posed. Nevertheless the system made of the equations (8.8) and (8.7) is well-posed. Indeed the presence of the pressure in the *AC* equation, that fixes its level at the interface. This point is illustrated in section 8.2.3.

In the case of open systems, an interesting simplification of the algorihtm can be introduced. Let us introduce the approximate value for the phase field φ^* that satisfies the *AC* equation (8.8) with $\mathcal{G}^{n+1} = \mathcal{G}^n$. As a consequence, equation (8.8) is a linear equation in the single variable φ^*. In the case of open systems, we assume that $\varphi^{n+1} = \varphi^*$ and we solve thus the two steps algorithm:

1. calculation of the new phase field by solving the linear equation (8.8)
2. calculation of the new modified pressure $\mathcal{G}^{n+1}$ by solving the linear Poisson equation (8.7)

The momentum field is then simply computed using the momentum balance equation (8.5) and is ensured to satisfy the continuity equation (8.4).

It is worth noting that this numerical scheme, here used for the solving of phase-field equations, is very similar to the one used in sharp methods for incompressible bulk phases (*e.g.* Juric and Tryggvason [69]). Contrarily to these methods, it is not required to smooth out the source terms associated with neither the mass transfer rate nor the surface tension.

8.2.2 One-dimensional isothermal steady state phase change

Presentation of the test case The domain is a one-dimensional system of length 1 . Initially, vapor fills the half-domain ($x \in [-0.25 : 0.25]$) and the system is supposed to be symmetric with regard to its midpoint $x = 0$. The velocity is imposed constant on the left boundary and the pressure is imposed constant on the right boundary. The pressure level inside the system (and therefore the level imposed at the right boundary) is computed such that the total mass variation of the system is twice that which corresponds to the mass variation induced by the velocity imposed on the left boundary. This condition ensures that the *computed* velocity on the right boundary is exactly opposite to that imposed on the left boundary, which thus ensures the symmetry of the system. This "trick" is used to impose a value of the pressure on one of the boundaries, which is necessary for the problem to be numerically well-posed. The numerical results of this test case are presented in the following.

Phase field and density profiles On figure 8.15 is represented the phase field profiles at various times. It shows that the phase field values are actually 0 near the external boundaries (liquid phase) and 1 at the center of the system (vapor phase). As times increases, the vapor phase disappears at the benefit of the liquid phase. The system remains symmetric about its center, which shows the validity of the algorithm to conserve mass through the particular pressure boundary condition computed. It is worth pointing out that the thickness of the diffuse

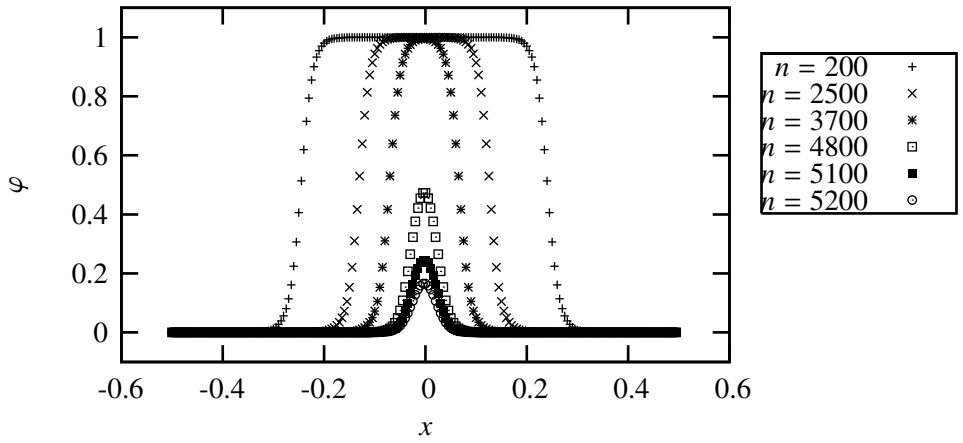

Figure 8.15: Numerical phase field profiles at various iterations n

interface remains approximatively constant throughout the computation. When the size of the vapor domain gets about the size of the interface thickness, the phase field value at the center of the domain deviates from the vapor value ($\varphi = 1$) and tends to the liquid value ($\varphi = 0$). This shows the ability of the model to deal with vanishing phases. The computation is stopped when the phase field at the center of the system approaches 0. Indeed when vapor has disappeared, and because of to the *incompressibility* of the liquid phase, the system cannot sustain the constant mass flux imposed; the system reaches the limitations of the basic formulation of our model . On

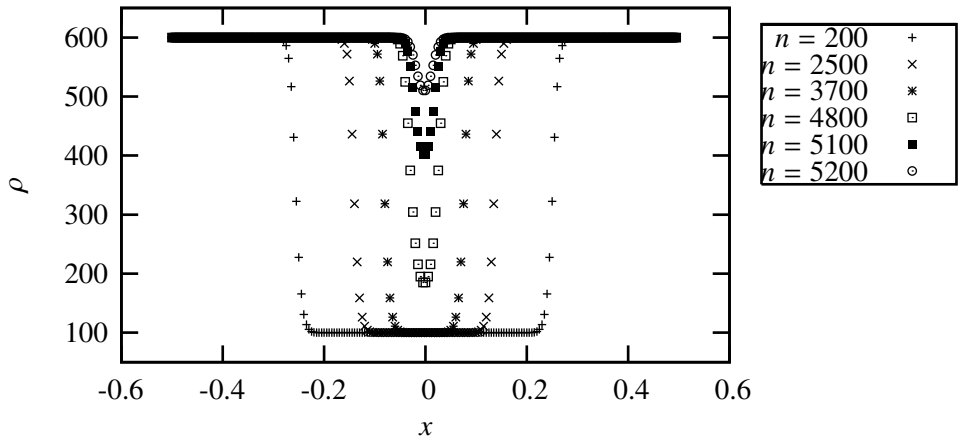

Figure 8.16: Numerical density profiles at various iterations n

figure 8.16 is represented the density field. It is worth noting that the typical thickness of the density profile across the interface is sharper than the corresponding phase field profile. This is due to the choice $\nu(\varphi) = P_5(\varphi)$ for the interpolation function for the specific volume.

Pressure and velocity profiles The main variable of the system solved is chosen to be the modified pressure $\tilde{P} = P + (\varepsilon^2/We)\,(\nabla\varphi)^2$ that is uniform at planar equilibrium. In the presence of constant mass transfer rate, it has been shown (*cf.* section 7.4.2 that the pressure jump is associated to the recoil force, *i.e.*

$$[\![\tilde{P}]\!] = \Gamma^2 [\![1/\rho]\!]$$

The theoretical value of this jump as well as the pressure profiles at different times are plotted on figure 8.17.

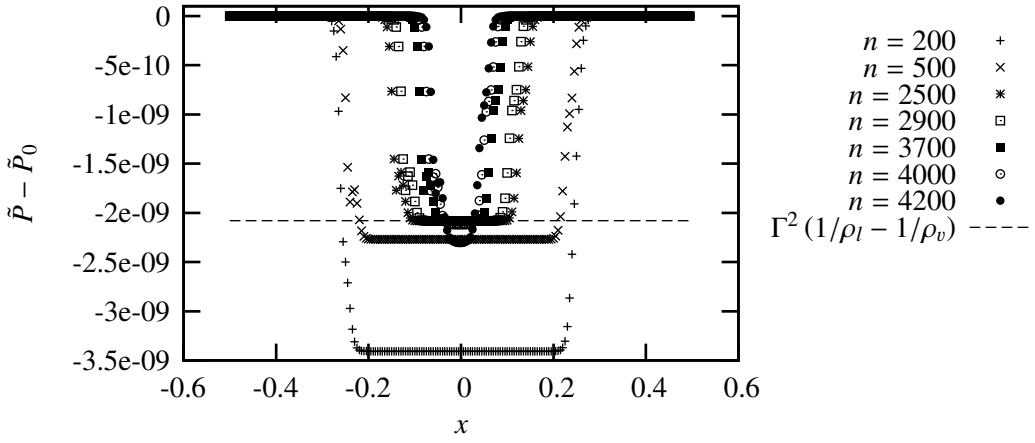

Figure 8.17: Numerical pressure profiles at various iterations n

The time dependent pressure level at the right boundary has been substracted to the pressure field for the sake of legibility. The pressure level is initially uniform. After a few thousand iterations, the jump in pressure converges to the theoretical value. When the vapor phase begins to disappear, the pressure level once again diverges from this theoretical value. The pressure profile inside the bulk phase domains is symmetric and uniform. Moreover the typical thickness of the pressure profile is of the order of magnitude of the one of the density profile, which is consistent with the approximate expression (7.34) for the pressure profile.

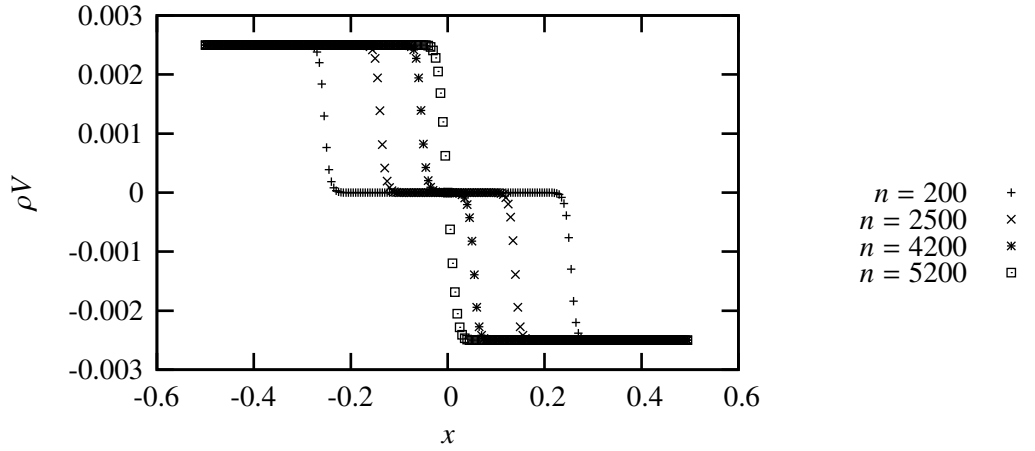

Figure 8.18: Numerical momentum profiles at various iterations n

The momentum profiles are represented on figure 8.18. It is worth noting that they are anti-symmetric. Indeed, the value at the right boundary (computed) is opposite to the value at the left boundary (imposed) and the momentum at the center of the domain (vapor phase) is zero, which is consistent with the symmetry condition. The jump in momentum as well as the momentum profiles are consistent with the corresponding analytical results (*cf.* equations (7.32) and (7.33)) *i.e.*

$$V - \mathcal{D} = -\frac{\Gamma}{\rho(\varphi)}$$

that yields

$$[\![V]\!] = -\Gamma\,[\![1/\rho]\!]$$

Isothermal kinetic relation In section 7.4.3, we showed that the interface pressure is linear in $\Gamma/\alpha = \Gamma/(\kappa\varepsilon^2)$. To study this relation and in particular its dependence in κ, we computed the previously steady-state isothermal phase change process for various values of the mobility, other parameters being fixed. The interface pressure $\tilde{P}_i$

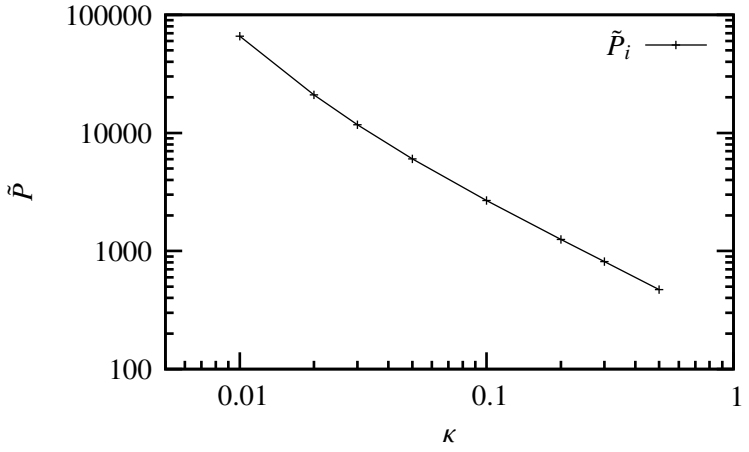

Figure 8.19: Interface pressure for a given mass transfer rate as a function of the mobility κ

is defined as

$$\tilde{P}_i = \tilde{P}(x_i)$$

where x_i is a sharp interface location such that $\varphi(x_i) = 1/2$. $\tilde{P}_i$ as a function of the mobility is represented on figure 8.19. This figure shows that the approximate relation (*cf.* equation (7.35b))

$$\tilde{P}_i \propto \frac{\Gamma}{\kappa}$$

is satisfied for sufficiently large values of the mobility κ but deviates from this approximate relation for lower values of the mobility. The numerical result is consistent with the analytical results derived in section 7.4.2.

Conclusion Using numerical simulations, we showed that the solution of a one-dimensional isothermal steady state phase change process using our phase field model is consistent with the analytical results derived in section 7.4. As a consequence, the diffuse profiles are of controlled thickness (which is of the order of the parameter ε) and the bulk phases correspond to the targeted phase field values 0 and 1. Moreover the equivalent sharp interface representation satisfies the classical jump conditions on mass and momentum. The kinetic relation is consistent with the normal growth theory as long as the ratio Γ/α is sufficiently small, which is the actual limit of validity of the normal growth theory. It means that the algorithm developed is actually satisfying for the study of one dimensional isothermal phase change process. As a consequence, we retain it in the remainder of this study to solve the coupling between phase field and mechanics.

8.2.3 Two-dimensional numerical simulation

Bubble detachment and rise To study the ability of the model to deal with two-phase flows, we study numerically the motion of a bubble inside a closed box under the action of both capillarity and buoyancy. Since the box is closed, the total mass transfer rate is zero, even though local interface mass transfer rate can occur.

Initially, a hemispherical bubble is set at the bottom of the box in contact with the bottom surface. The velocity is imposed constant and zero on all the boundaries. The phase field boundary condition corresponds to a contact angle of $\pi/2$. The numerical discretization is a two-dimensional regular Eulerian grid of 60×60 nodes.

On figure 8.20, snapshots of the numerical simulation are represented. The color field corresponds to the phase field, light color around $\varphi = 1$ (vapor) and dark around $\varphi = 0$ (liquid). The iso-value $\varphi = 0.5$ (interface) is represented by the black line. The black arrows correspond to the momentum vector field. From top left to bottom right the following sequence of events can be seen. Due to the action of buoyancy, the center of gravity

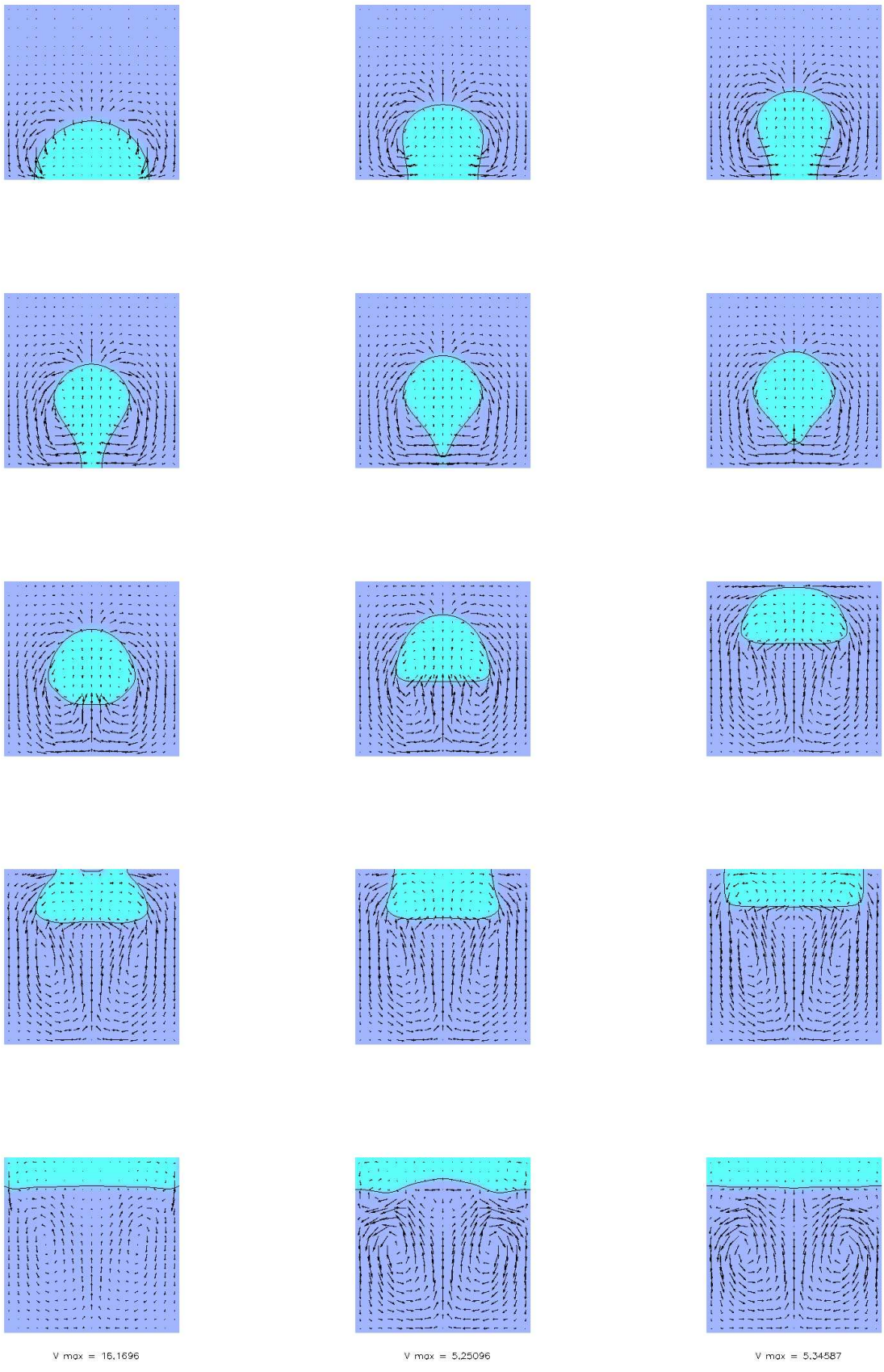

Figure 8.20: Isothermal bubble rise inside a closed box

of the bubble begins to rise. Due to the density difference between vapor and liquid, along a current line, the momentum is larger in the liquid phase than in the vapor phase, which attests the fact that the local mass transfer rate, if any, is negligible with respect to the local dynamics. As the center of gravity of the bubble rises up, the summit of the bubble keeps a quasi spherical shape under the action of the capillarity; however, at the foot of the bubble, the interface is perpendicular to the wall according to the $\pi/2$ contact angle. The surface of contact between vapor and the bottom wall continuously decreases till it vanishes (4th snapshot): at this instant the bubble departs from the wall. Under the action of capillarity, the foot part of the bubble made of a high curvature region rapidly disappears and the bubble shape gets closer to a spherical cap. As the bubble reaches the top wall, it spreads into a film whose interface progressively becomes planar, that corresponds to the final equilibrium state.

This simulation shows that the model correctly describes the dynamics of bubble departure from a wall under the action of both capillarity and buoyancy. Even though these results are only qualitative, they are important towards the study of the bubble growth dynamics (*cf.* chapter 1). It indeeds validate the use of the algorithm proposed in section 8.2.1. This algorithm has the advantage to reduce to the solving of a linear system of equations and to be well-posed in the case of closed domains.

8.3 Non-isothermal dissipative liquid-vapor flows with phase change

In this section, we solve numerically the complete set of governing equations (5.56). The goal is to study the coupling between the thermal and mechanical parts of the model , both having been studied and validated independently in the previous sections.

8.3.1 Saturation curve

Presentation of the test case The system studied is a heated and closed one-dimensional two-phase system. The goal is to study the ability of the model and of the numerical algorithm to take into account the saturation curve*i.e.* an increase of the mean pressure of a system with its mean temperature. To illustrate this point, we first consider a weak coupling between the thermal and mechanical problems . Indeed, we simplify the thermal problem by considering that the temperature is uniform is space uniform but that its value is time dependent. The remaining equations to solve are thus the *AC*, momentum balance and continuity equations. As a consequence, the system studied can be solved using an algorithm similar to that used in the isothermal case presented in the previous section: only the level of temperature is added as an additional parameter. To study the coupling with the phase change process, we consider a non-zero coefficient of thermal expansion α_P for the vapor phase. As a consequence, when the temperature of the system increases, the interface pressure follows the saturation curve, and due to mass conservation inside the closed domain (of fixed volume), the interface moves to take into account the variation of the vapor density. It is worth noting that the problem studied reproduces the physical situation of a pressure cooker.

Numerical results The time dependent interface pressure is represented on figure 8.21 together with the saturation pressure at the interface temperature. It shows that the pressure consistently follows the saturation curve. It has been shown that the quasi-compressible model allows to introduce the notion of saturation curve, this test case shows the ability of the algorithm proposed to take it into account in the computations.

Due to the non-zero coefficient of thermal expansion of the vapor phase, the volume ratio of the liquid and vapor phases inside the closed domain evolves in time. Since the temperature of the system is imposed, the time dependent position of the interface can be derived analytically. On figure 8.22 the computed interface position is compared to this analytical prediction. It shows good agreement , attesting the ability of the model to take into account a non-zero coefficient of thermal expansion.

8.3.2 Dynamic phase change in an open system

The algorithm The algorithm for the computation of the coupling between thermal, mechanical and phase field parts of the model is inspired by the algorithms developed for the studies of the uniform density and isothermal cases. It is thus based on the use of the projection method as presented in section 8.2.1. For open systems the algorithm is made of two main steps

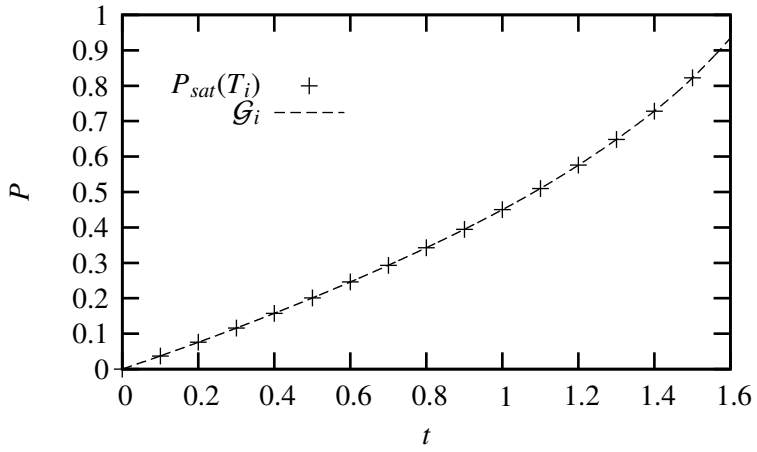

Figure 8.21: Time dependent evolution of the interface pressure *versus* the saturation curve $P_{eq}(T)$

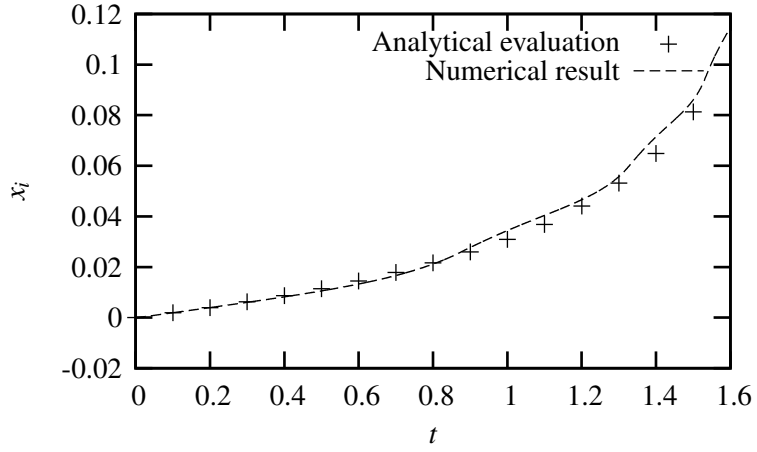

Figure 8.22: Interface position as a function of time

1. Computation of the coupling between the thermal and phase field parts, *i.e.* the *AC* equation and the equation of evolution of the temperature. In this system of equations the pressure and velocity fields are thus considered as explicit. The system is linear in (φ^{n+1}, T^{n+1}) as introduced in section 8.1.1

2. Computation of the mechanical part: The phase field being known, it thus possible to solve the Poisson equation in $\mathcal{G}^{n+1}$ and then using the momentum balance equation to compute the new momentum field.

As a consequence the whole steps of the algorithm is made of solving of linear equations and the algorithm easily degenerates to the uniform density or isothermal cases.

Presentation of the test case In this section we study a one-dimensional phase transition problem in a system that is opened on one of its boundaries. The system of governing equations is the system (5.56) where the gravity has been neglected. On the right boundary of the domain, a zero velocity and a non-zero constant heat flux are imposed. On the left boundary of the domain, the pressure and a zero heat flux are imposed. The domain is initially made of two separated bulk phases of same extent, the liquid being on the left and the vapor on the left.

Numerical results On figure 8.23 are represented the temperature profiles at various times. They clearly satisfy the boundary conditions. They are linear in each bulk phase and the derivative is discontinuous at the interface. The temperature profile is continuous across the interface, which is consistent with the hypothesis of uniform heat conductivity. On figure 8.24 are represented the phase field profiles at various times. They show that the position of the interface moves at quasi-constant velocity, which is consistent with the constant heat flux imposed at the

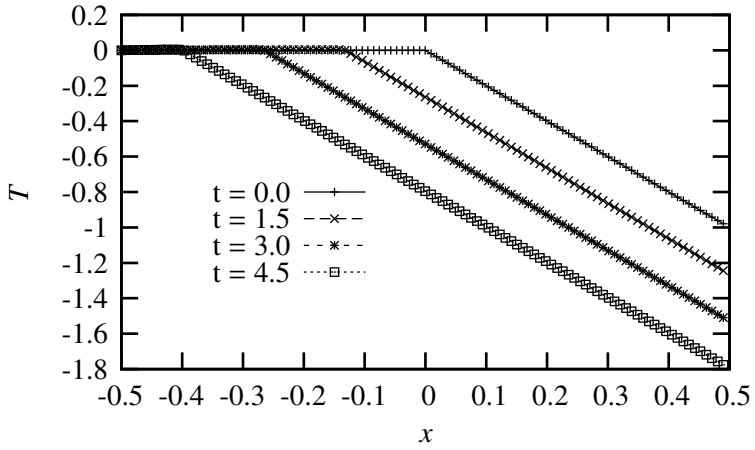

Figure 8.23: Temperature profiles at various instants

right boundary. The interface thickness is approximatively constant throughout the simulation. On figure 8.25

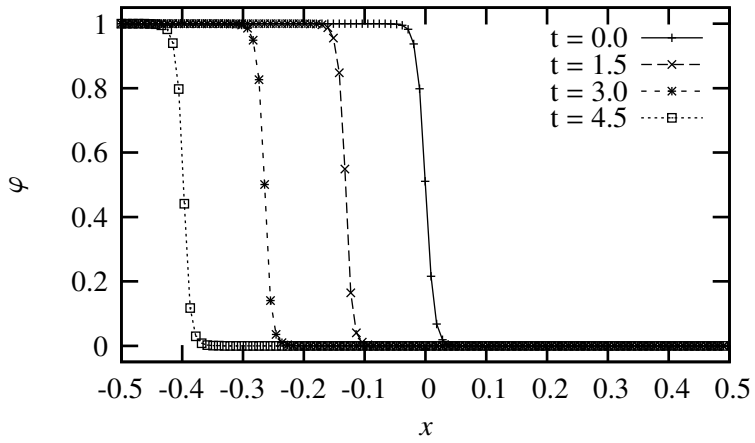

Figure 8.24: Phase field profiles at various instants

are represented the momentum profiles at various times. Initially the momentum is set to zero. The momentum is zero inside the liquid domain, which is consistent with the right boundary condition. The momentum is uniform and positive on the vapor side, which is consistent with the fact that the liquid condensates (vapor enters into the domain). However, its value is not constant in time. Indeed, as it will be seen on the pressure profile, the interface pressure varies with time whereas the interface temperature is quasi constant. The variation of the interface pressure is associated to the fact that the pressure imposed on the right boundary does not correspond to that of a steady state phase transition process. As a consequence, the mass transfer rate is not exactly constant and actually slightly decreases with time (as the boundary condition of imposed pressure gets closer to the interface).

On figure 8.26 are represented the pressure profiles at various times. The pressure jump across the interface is quasi-constant, which is consistent with the quasi-constant mass transfer rate (recoil force). The pressure is uniform in the liquid phase, which is consistent with the boundary condition imposed on the right boundary. At the left boundary, the boundary condition of constant pressure is satisfied. In the vapor phase there exists a non-zero uniform pressure gradient. This is consistent with the previously described momentum profile, the value of the pressure gradient being related to the time derivative of the momentum (*cf.* the momentum balance equation).

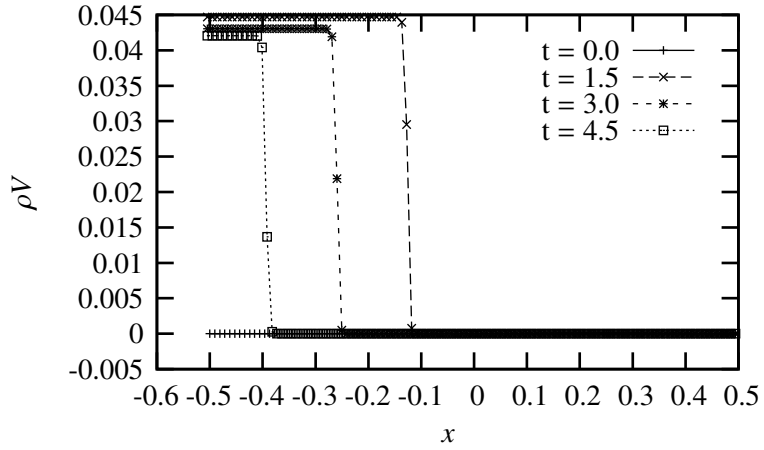

Figure 8.25: Momentum profiles at various instants

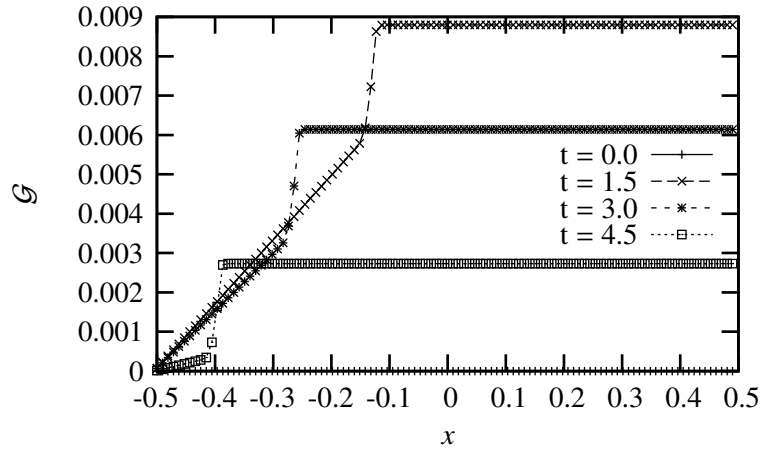

Figure 8.26: Profiles of the modified pressure $\mathcal{G}$ at various instants

Conclusion As a partial conclusion, the numerical profiles are consistent with the analytical results derived in section 7.5. Moreover these results show that the algorithm is able to taken into account the coupling between all the parts of the model.

8.3.3 Attempts to solve two-dimensional phase change problems

The one- and two-dimensional studies presented in the previous sections aimed at studying the different couplings of the equations and to validate the algorithm developped to account for these couplings. In particular, in section 8.2.3, we showed that the numerical method develop to account for the coupling between the *AC* equation and the momemtum and mass balance equations gives good qualitative results in fully multi-dimensional simulations. In section 8.3.2, we showed that the algorithm developped to solve the complete system of equations gives good both qualitative and quantitative results in one-dimension. Therefore, it is reasonnable to think that this algorithm would give good results in two dimensions as well. It turns out that we faced severe numerical difficulties in two dimensions. These difficulties are believed to be related to fundamental numerical issues and are thus reported and analyzed in this section.

To illustrate these difficulties, we analyze the numerical resolution of the one-dimensional problem of phase transition one studied in section 8.3.2. In this section, this one-dimensional system is studied using a two-dimensional system, with only a few mesh cells in the direction tangential to the interface. All the initial profiles are one-dimensional in the direction normal to the interface and the problem should therefore remain one-dimensional in this direction. However, as shown in the following, the system develops numerical instabili-

ties in the direction tangential to the interface. We describe several attempts to overcome these difficulties that, even though unfruitful, have nevertheless allowed to clearly identify the origin of the numerical difficulties of the numerical method.

Instable growth of parasitic currents The problem we have to solve is purely one-dimensional. However, by considering a two-dimensional mesh, we add degrees of freedom in the system. The corresponding setting is represented on the top graph of figure 8.27. The colored field is the phase field, or equivalently the density field. The small lines indicate the faces of the mesh elements. Vertical black lines correspond to iso-values 0.01, 0.5 and 0.99 of the phase field. Black arrows correspond to the velocity field, which is initially set to zero but rapidly converges to a mainly horizontally oriented field.

Let us now consider the two-dimensional velocity field. Since the velocity field is initially one-dimensional, we represent on figure 8.27 a modified velocity field for the sake of legibility. This velocity field is obtained by subtracting to the original velocity field the normal component of the velocity at the bottom of the domain. The corresponding snapshots correspond to the second (from top) and following (to bottom) pictures. The scale separation at the beginning of the computation between the original and modified velocity fields is huge: as it can be seen on the pictures, the norm (max) of the original momentum is 10^{11} times larger than the norm of the modified field. The tangential component of the velocity field is therefore negligible and can be attributed to numerical truncation errors. The snapshots show that the modified velocity field is made of rotating currents located in the vicinity of the interface. As a consequence, the modified velocity field, that should be zero, is not only made of numerical truncature errors, but is rather organized (even though the structure of the "flow" evolves in time as shown on figure 8.27). Since, contrarily to the physical velocity field that should be purely normal, the computed velocity field is two-dimensional, we characterize in the following this difference by considering the norm of the computed tangential component of the velocity field.

Unstable evolution of the velocity field Even though, as it has been shown in the previous paragraph, the initial tangential component of the velocity is of many orders of magnitude less than its normal component, its temporal evolution is unstable. On figure 8.28 are represented the kinetic energy contribution of both the tangential and normal components of the velocity to the total kinetic energy of the fluid as a function of the numerical iterations. This figure shows that the kinetic energy associated to the normal component of the velocity rapidly converges to a value of the order of unity. This value actually corresponds to the value of the kinetic energy of the previous one-dimensional computation. As a consequence, the normal velocity component actually converges toward the physical solution. Let us now consider the tangential component. On figure 8.28, several different numerical results are represented. They correspond to several different numerical algorithms that are discussed in the following. The computation $n^\circ 4$ corresponds to the simplest algorithm. It can clearly be seen that, in this case, the norm of the tangential component of the velocity has an exponential growth with time, which is characteristic of a numerical instability. As a consequence, the initial scale separation between the normal and tangential components of the velocity is no longer valid at a finite time (iteration 500 on the figure). Beyond this time, the computation rapidly diverges and is no longer physically meaningful. It is worth emphasizing that at this time, the interface has not moved from more than one node. As a consequence, when this instability arises, there is no way to compute any phase change process.

Attempts to stabilize the scheme In order to solve this test case problem numerically and to understand the origin of the numerical instability described above, we designed and used several different schemes. In the present study, we only propose to summarize the different learnings from these numerical tests about the origin of the instability. It is worth pointing out that capillarity should not play any physical role in this one-dimensional problem. However, it turns out that the computation of the test case in the two dimensional system is stable if one cancels the capillary part of the stress tensor. As a consequence, the observed instability is clearly related to the capillary stress tensor. Nevertheless, for a one-dimensional phase field, the capillary stress tensor should not yield to a non-zero tangential component of the velocity. It turns out that numerical truncation errors arising from the computation of the phase field is sufficient to trigger the instability. In the following we analyze the algorithm to understand the way capillary stress tensor can induce this instability.

In the original algorithm, the first step that is used to compute (φ, T) takes into acccount the velocity on an explicit way. As a consequence it does not takes into account the capillary stress tensor on an implicit way.

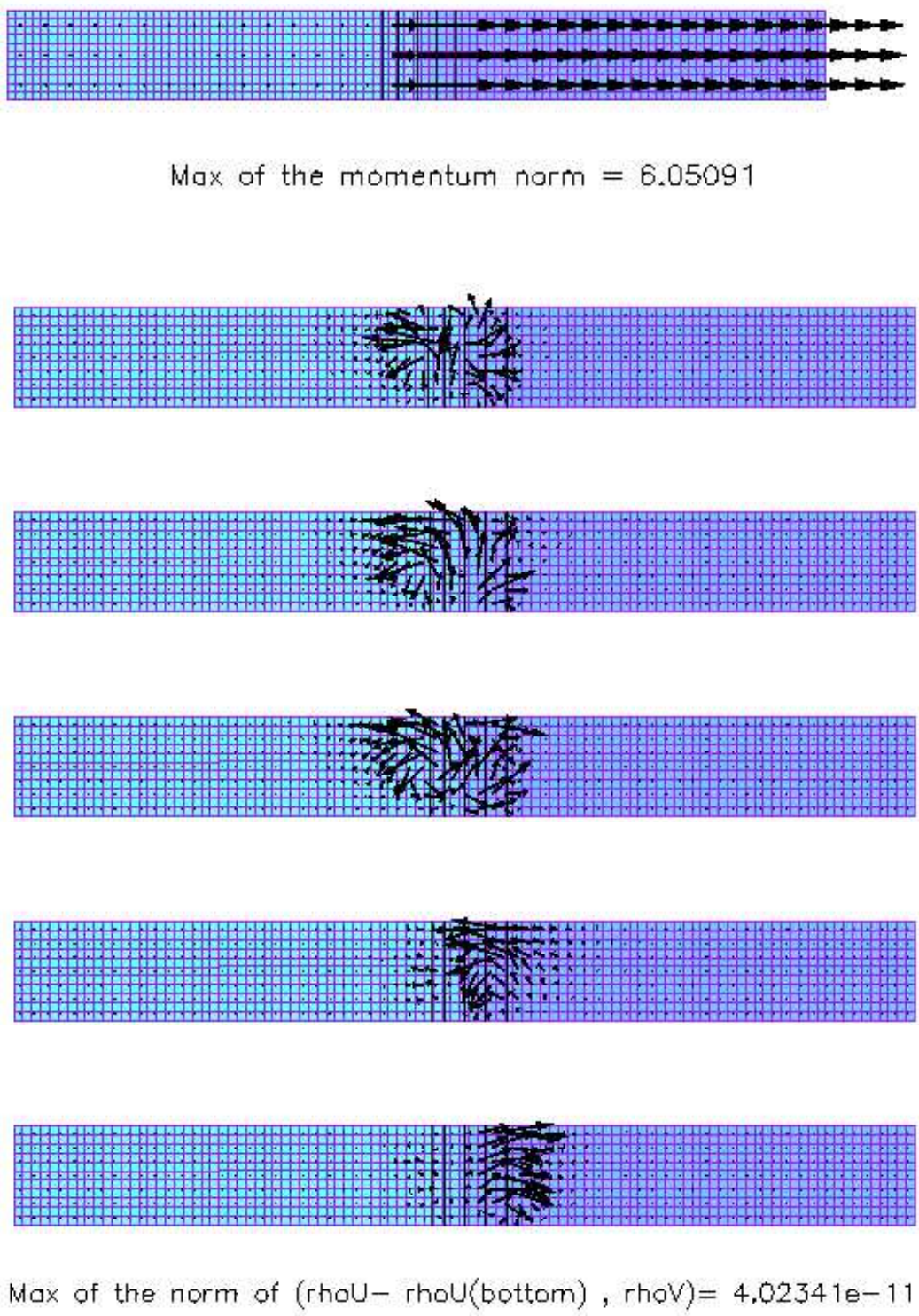

Figure 8.27: Illustration of the parasitic currents, on the top figure, the whole velocity field is represented, whereas on the other figures, the (U) component normal to the interface of the velocity field at the bottom mesh line of the domain has been substracted to the velocity field, that allows to illustrate the parasitic currents. In absence of these currents, the velocity field should not have any tangential component.

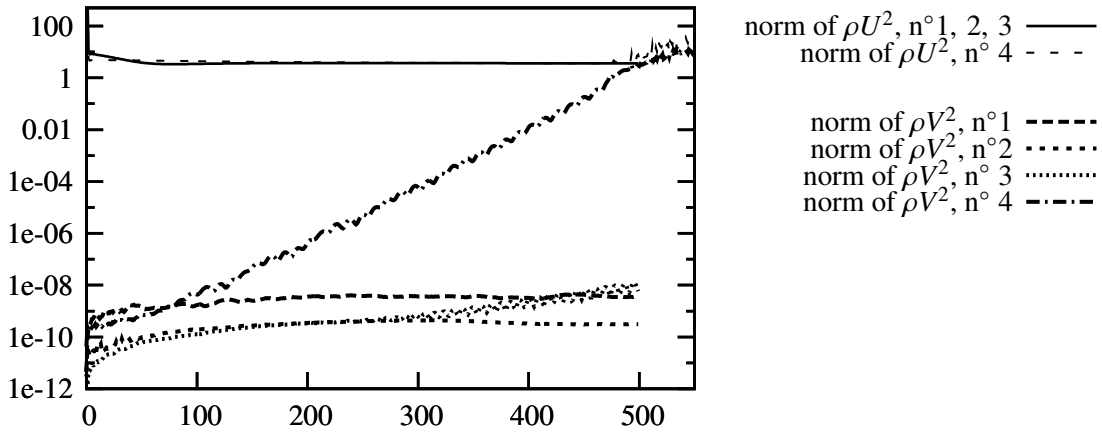

Figure 8.28: Total kinetic energy contribution of the normal U and tangent V velocity components

However this stress tensor is defined by the computed phase field. Since the instability originates from this tensor, we try in the following to develop an algorithm using different coupling between the stress tensor and the computation of the phase field φ. The first test was to more highly couple the solving of the governing equations using a loop in the algorithm: after an iteration of the algorithm, the new velocity and pressure are used in the system (φ, T) to better evaluate the explicit terms $\vec{V}^n$ and $\mathcal{G}^n$ and that till convergence. It turns out that this loop hardly converges and moreover does not significantly modify the instable growth of the parasitic currents. As a consequence, we tried to focus on the terms that are at the origin of the currents.

Origin of the instability In an attempt to understand the origin of the parasitic currents we analyzed the algorithm as follows. Let us introduce the source term $\vec{C}$ of the momentum balance equation (8.5)

$$\vec{C} = (\varepsilon\, We)^{-1} \left(\frac{\partial W}{\partial \varphi} - \varepsilon^2 \Delta\varphi \right) \nabla\varphi$$

It is worth pointing out that when $\vec{C}$ is set to zero, the computation is stable. In fact $\vec{C} = \vec{0}$ corresponds to the neglect of the capillary part of the stress tensor in the momentum balance equation ($We = \infty$). In the following we only focus on this term $\vec{C}$ and won't explicitly consider the other contributions of the momentum balance equation. Moreover we showed using numerical tests that the value of the mobility κ had no influence on the numerical instability, we thus assume infinite mobility ($\kappa = \infty$) such that the AC equation reduces to the thermodynamic equilibrium condition $\tilde{\mu} = 0$. Let us now study how the source term $\vec{C}$ induces parasitic currents. Let us introduce a decomposition of $\vec{C}$ as the sum of a gradient and a curl part as

$$\vec{C} = \nabla Y + \nabla \times \vec{Z}$$

The Poisson equation can be schematically written as

$$\Delta G^{n+1} = \nabla \cdot \vec{C} - \nabla \cdot \left(\frac{\rho\vec{V}^{n+1} - \rho\vec{V}^{n}}{Dt} + \dots \right)$$

and thus

$$\Delta G^{n+1} = \Delta Y + \nabla \cdot \left(\frac{\rho\vec{V}^{n+1} - \rho\vec{V}^{n}}{Dt} + \dots \right) \tag{8.9}$$

When $\mathcal{G}^{n+1}$ has been computed, the momentum field is then set to (*cf.* the momentum balance equation (8.5))

$$\rho\vec{V}^{n+1} = \rho\vec{V}^{n} + Dt \left(-\nabla\mathcal{G}^{n+1} + \vec{C} + \dots \right)$$

and thus, according to the Poisson equation (8.9)

$$\rho\vec{V}^{n+1} = \rho\vec{V}^{n} - Dt \left(\nabla \times \vec{Z} + \dots \right)$$

As a consequence, it appears clearly that only the component $\nabla \times \vec{Z}$ of the capillary term $\vec{C}$ contributes to the velocity field and can induce parasitic currents.

A way to stabilize the parasitic currents The basic idea is then to work on the coupling between $\nabla \times \vec{Z}$ and the computation of the phase field. To do we introduce an estimation of the velocity field $\vec{V}^*$. We ignore the other contributions than $\nabla \times \vec{Z}$ in the momentum balance equation to compute $\vec{V}^*$ and define

$$\vec{V}^* \triangleq \vec{V}^n - Dt\, \nabla \times \vec{Z}(\varphi^{n+1})$$

This velocity is used to compute (φ, T) in the first step of the algorithm instead of $\vec{V}^n$. An iterative procedure is introduced where *(i)* the phase field and temperature are first computed, *(ii)* the velocity $\vec{V}^*$ is deduced from φ, this velocity being used to improve the calculation of (φ, T) (back to step *(i)*) and so on till convergence. It is a straightforward computation to deduce $\nabla \times \vec{Z}$ from the knowledge of φ and thus of $\vec{C}$. However it remains a Poisson equation to solve, and as a consequence this step is numerically costly. Using numerical tests it has been shown that it was necessary and sufficient for the resolution to be stable to use $\vec{V}^*$ only in the phase change term of the equation of evolution of the temperature such that the step *(i)* is the solving of

$$\begin{aligned} v^n\left(\frac{\partial W}{\partial \varphi}^n - \varepsilon^2 \Delta \varphi^{n+1}\right) + \frac{\partial \nu}{\partial \varphi}^n \left((At\,\varepsilon\, We)\, \mathcal{G}^n - \frac{\varepsilon}{St\,\gamma\,\theta}\, T^{n+1}\right) & \\ + \left(\varphi^{n+1} - \varphi^n\right)\left(v^n \frac{\partial^2 W}{\partial \varphi^2}^n + \frac{\partial^2 \nu}{\partial \varphi^2}^n \left((At\,\varepsilon\, We)\, \mathcal{G}^n - \frac{\varepsilon}{St\,\gamma\,\theta}\, T^n\right)\right) &= 0 \\ \rho^n\left(\frac{T^{n+1} - T^n}{Dt} + \vec{V}^n \cdot \nabla T^n\right) - \frac{\nabla \cdot \left(k \nabla T^{n+1}\right)}{Pe} + \frac{\rho\ (1 + T^n/\theta)}{St} \frac{d\nu}{d\varphi}\left(\frac{\varphi^{n+1} - \varphi^n}{Dt} + \vec{V}^* \cdot \nabla \varphi^n\right) &= 0 \end{aligned}$$

At convergence of the loop, the fields φ^{n+1} and T^{n+1} are known. The projection method is then used to compute the fields $\mathcal{G}^{n+1}$ and $\rho \vec{V}^{n+1}$. It is worth pointing out that this algorithm, if complex, is the only way we found among numerous other attempts to stabilize the resolution. The resulting time evolution of the kinetic energy is represented on figure 8.28 calculations $n°2 - 4$. It shows that the order of magnitude of the tangential kinetic energy, even though non-zero stays very low and as a consequence, it does not interact with the physical solution. We thus managed to get rid of the instability. But the computation remains very sensitive to numerical accuracy. Moreover the first step is considerably costly and computations of larger systems, such that the one presented in section 8.2.3 were out of reach. Nevertheless, this shows that we clearly identified the origin of the parasitic currents. Since it is attributed to a non-trivial coupling (implicitation of the capillary stress tensor in the phase change term of the equation of evolution of the temperature) we face a severe numerical problem. The basic idea of the original algorithm was mainly based on the use of the projection method. Since it has been shown that the use of this method does not allow to control easily the capillary part $\vec{C}$ of the stress tensor, we propose to investigate the use of other methods to compute the momentum balance equation, such that curl-decomposition methods.

8.4 Conclusions and perspectives

In this chapter, we studied numerically the system of governing equations of our phase field model for the liquid-vapor flows with phase change. By studying one dimensional phase change problems, we showed that the numerical results are actually consistent with the analytical results derived in chapter 7. We also showed that the model was able to take into account capillarity in two-dimensional systems in the uniform density and isothermal cases. Numerical computations of bubble departure from a wall isothermal dynamics showed the model qualitatively reproduce the main physical mechanisms (capillarity and buoyancy). As a consequence the algorithm developped is able to take into account the major coupling of the models. Nevertheless, we have not been able to compute multi-dimensional non-isothermal phase transition problems with density difference. The limitation of the numerical method for such a computation has been shown to be associated to the capillary stress tensor. The use of the projection method for the solving of the momentum balance equation is potentially responsible of a numerical instability that we have not been able to avoid unless by using a costly and complex algorithm. As a consequence, we believe that another numerical method for the computation of the momentum

balance equation in the non-isothermal case should be used. In particular, we believe that the use of a method based on a curl- decomposition of the velocity field should be investigated.

Conclusion and perspectives

The study of the basic physical mechanisms occuring in boiling flows and more especially at the boiling crisis is still challenging. Indeed, despite more than 70 years of valuable scientific studies, the physical mechanisms at the origin of the boiling crisis have not been clearly identified yet. To analyze the current understanding of the boiling crisis, we proposed in chapter 1 to classify the mechanisms potentially involved in the phenomenon according to three different levels of description of the nucleate boiling regime. The first level deals with the most idealized level of description of the bubbly flow, the bubbles are modeled with the help of a mean volumetric vapor fraction. The bubbles are therefore not considered as individual entities. At the second level of description the bubbles are modeled as a set of growing spheres, they are rigid in shape but not in size. At the finest and third level of description the bubble geometry is time and space dependent. According to this classification, we studied the different existing theories for the boiling crisis. This analysis revealed the need, at each level of description, for both experimental investigation and modeling efforts to improve the understanding of the physical features of high heat flux nucleate boiling . Nevertheless, among all the mechanisms that remain to be clarified, we clearly identified one mechanism potentially related to the boiling crisis: *the "irregular" bubble growth event*. Indeed, at high wall heat flux, a bubble pinned to the wall can spread over the wall instead of departing from it. This mechanism refers to the finest level of description of the nucleate boiling regime. It has been shown, by an analysis of experimental observations as well as of the successful Zuber correlation for the prediction of the boiling crisis, that "irregular" bubble growth can indeed be at the origin of the drying transition of the hot wall that leads to the transition of the boiling regime. The bubble growth and departure from the wall processes are governed by local curvature of the bubble shape as well as local heat and mass transfer. As a consequence, the numerical simulation is the most relevant tool to study the "irregular" bubble growth dynamics. The compressibility of the liquid and vapor phases are not considered as leading physical mechanisms for this dynamics. As a consequence, the bulk phases can be modeled as incompressible. Since this assumption induces a computational simplification, the numerical method can thus take benefit of it.

In chapter 2, we analyzed the numerical methods that could be used for the computation of boiling flows and turned our attention toward diffuse interface methods. These methods are based on models that consider the interface as a volumetric transition layer across which all the physical variables have continuous variations. The set of governing equations includes, in a thermodynamically consistent way, the model for the interface dynamics. As a consequence, and contrarily to the numerical methods based on sharp interface models, there is no need to develop a specific computational treatment devoted to the interface dynamics. This constitutes an advantage from the computational point of view. Nevertheless, the physical thickness of the interface transition layer is of many orders of magnitude smaller than the typical bubble size. In order that these models can be used for the bubble scale simulation targeted, it is required to control the typical thickness of the transition layer. Indeed, the interface layer must be captured by a few mesh cells and the size of the interface must therefore be a free parameter of the model, whose typical size is that of a mesh cell. The van der Waals model is the most natural diffuse interface model for the liquid-vapor phase transition. However, it has been shown that it is not possible to increase the interface thickness from a modification of the van der Waals model without altering the description of the liquid-vapor states. For the study of the solid-liquid phase transition with a diffuse interface model, the phase field models are commonly used. These models are based on the introduction of an abstract internal parameter, called phase field, in the thermodynamic description of the system. It allows to deal with a smearing of the interface of arbitrary thickness together with a degree of freedom for the description of the physical parameters of the phase transition. This advantage was lacking when dealing with a modification of the van der Waals model and we thus choose to adapt this approach for the study of liquid-vapor flows with phase change. We first defined the properties that such a model should be endowed with to study the bubble growth dynamics. In particular, the introduction of the phase field in the thermodynamic description of the fluid should

be *only* devoted to the modeling of the internal structure of the interface layer. As a consequence, the phase field part of the model must have minimal interference with the description of the single phase states. The latter must be described by the classical thermodynamic variables, namely the pressure and the temperature. Moreover, the single phase states should be incompressible. We showed that the existing phase field models are not well suited for our applications since they do not fulfill all the required properties. We need therefore to adapt these models to our own requirements. In the remainder of the study the goal is thus to develop and study a phase field model for liquid-vapor flows with phase change.

In chapter 3, we developped the thermodynamic part of our phase-field model. We first showed that it is possible to deal with a density difference between incompressible single phase states using the *quasi-compressible hypothesis* as first introduced by Lowengrub and Truskinovsky [89]. We then studied the introduction of the phase field φ as a thermodynamic variable. We specified its role: the phase field variable has no signification outside the transition layer and it is therefore assumed *(i)* to take arbitrary fixed values in the bulk phases *(ii)* to vary smoothly between these two values across the interface transition layer. The typical thickness of this variation must be controlled for computational motivations. We then derived the equilibrium conditions to express analytically these two constraints. In comparison with the classical equilibrium relations, the nullity of the variational derivative of the specific Gibbs free energy with respect to the phase field is an additional equilibrium condition. We then considered the constitutive form of the thermodynamic potential that allows to fulfill these constraints. The expression for the phase field specific Gibbs free energy is based on the interpolation of the specific Gibbs free energies of the single phase states by a non-linear function of the phase field φ (*cf.* equation (3.53)). This interpolation is at the basis of the phase field model. The specific volume as well as the entropy are interpolated by the same non-linear function. In addition, the expression for the thermodynamic potential is made of the product of the specific volume by both a volumetric double well function of φ and a dependence in $(\nabla\varphi)^2$. The double well function is, together with the non-local dependence in $(\nabla\varphi)^2$, devoted to the description of the interface structure at planar equilibrium. The constitutive form of our phase field model yields the following property: the phase field profile of across a plnar interface equilibrium is governed by a differential equation that is independent of the physical parameters of the phase transition (saturation curve *i.e.* equilibrium conditions , density difference, specific heat capacities of the bulk phase or surface tension coefficient). Moreover, it is independent of the interpolation function. As a consequence, the thickness of the interface transition layer is easily controlled. The surface tension coefficient is simply related to the scaling of both the double well function and of the dependence in $(\nabla\varphi)^2$. We clearly related the choice of a non-linear interpolation function to the ability of the model to control the physical properties of the single phase states. Indeed we studied in chapter 6 the stability of homogeneous equilibrium states and it has been shown that using at least a polynomial of degree 5 for this interpolation function allows to have fixed phase field values associated with the liquid and vapor phases. In particular we showed that these values correspond to unconditionally stable single phase states whereas all the other phase field values either do not correspond to equilibrium states or correspond to unstable equilibrium states. This property cannot be satisfied with lower degree polynomials as interpolation functions. Moreover we showed that using polynomial of degree 5, it is possible to reproduce phenomenologically a metastability limit for the bulk phases. This study of the thermodynamic phase field model has thus allowed to clearly establish the meaning as well as the optimal expression for the phase field dependence of the thermodynamic potentials.

We then studied spherical inclusions at equilibrium in chapter 4. With our model, the equilibrium equation in the spherical symmetric case is simple enough to derive approximate analytical solutions. It is worth noting that both the double well and the interpolation function enter this equilibrium equation. As a consequence the interpolation function plays a role in the description of spherical inclusions. We have defined the equivalent sharp interface model of our diffuse model. We showed that this sharp model is consistent with the Laplace theory as soon as the radius of the spherical inclusion is a few times larger than the typical interface thickness. This result is satisfying for the studies targeted and it shows the ability of the phase field models to provide a thermodynamically consistent regularization of the sharp interface model. As the radii of the spherical inclusion decreases below the order of magnitude of the interface thickness the effective surface tension as well as the pressure jump decrease. This decrease of the pressure jump allows to model vanishing spherical inclusions that is not possible with the sharp interface model. It is worth noting that the results concerning the small radii have been shown to be sensistive to the choice for the interpolation function.

In chapter 5, we derived the dynamic system of equations corresponding to our thermodynamic model. The derivation of the governing equations has been made in two steps. First we introduced a formal compressible

isothermal phase field model. Using the fundamental d'Alembert-Lagrange principle, we derived the conservative set of governing equations. We identified the capillary part of the stress tensor and derived a constitutive expression for the rate of work. Then, using the thermodynamic first principles together with the previously suggested expression for the rate of work, the dissipative governing equations have been derived for our quasi-compressible non-isothermal model. In addition to the classical Fourier heat conduction and Newton viscosity dissipative mechanisms, we introduced a Ginzburg-Landau relaxation toward the additional phase field equilibrium condition. This introduces a phase field kinetic part in the model. As a consequence, in addition to the mass, momentum and entropy balance equations, the set of governing equations includes an Allen-Cahn equation (*cf.* the system of equations (5.42)). Using the Pi theorem, the non-dimensional form of the governing equations has been derived for the study of a boundary condition problem. We then proposed a simplification of the temperature dependence of the model: the saturation pressure is linear in temperature and the coefficient of thermal expansion is neglected. As a consequence, no difference between the heat capacities of the liquid and vapor is considered. It is worth emphasizing that this assumption is not a fundamental limitation of our model. However, it allows to simplify both the analytical and numerical studies of the governing equations and the latent heat is still non-zero. Finally, the set of governing equations contains a reduced number of non-linearities and takes into account the physical mechanisms governing the bubble growth dynamics.

We then studied our model in non-equilibrium cases in chapter 7. We first introduced the formalism of kinetic relations for the equivalent sharp interface model. We showed that the non-equilibrium Gibbs Thomson and Clapeyron relations are related to the "normal growth" theory for the interface entropy production. We then derived approximate non-equilibrium solutions for a one-dimensional phase transition when the transition front is a traveling wave. We assumed that the phase field varies mostly over a narrow transition zone (inner region) of the order of the thickness of the interface at planar equilibrium whereas in the bulk phases, the physical variables vary over larger distances (outer domains) that contain less significant variations of the phase field. Matched asymptotic expansions are then used to solve the coupled set of governing equations in both the inner and outer zones. The solutions are expanded with respect to a small parameter defined as the ratio of the typical inner length scale to the typical outer length scale. We then derived the inner profiles of the variable at the first and second leading orders. The following conclusions can be drawn from this study. At leading order, the phase transition is isothermal and the phase field profile is the equilibrium one, these results being classical with phase field models. We have derived the corresponding kinetic relation that provides a clear interpretation of these results. It has been shown that at leading order the interface entropy production is quadratic in the mass transfer rate and the driving force linear in the mass transfer rate. These results are thus consistent with the "normal growth" theory. The Ginzburg-Landau relaxation is the dissipation mechanism that governs the leading order kinetics. At next order, it has been shown that the interface temperature jump is non zero. This is commonly associated to a thermal trapping effect. We showed that it is related to an excess interface entropy production inherited from the phase field interpolation of the heat conductivity coefficient. Moreover, we showed that the leading order solutions are consistent with the classical sharp interface pressure and velocity jump conditions. We also showed that the consistency of the leading order kinetic relation with the normal growth approximation is directly related to a particular choice for the scaling of the Ginzburg Landau dissipative coefficient. By considering another scaling for this coefficient, we derived a leading order kinetic relation for a purely phase field model that deviates from the normal growth approximation at high mass transfer rates which is more physically consistent when study of fast phase boundaries is targeted.

The chapter 8 was devoted to the numerical resolution of the system of governing equations. The goal was to develop an algorithm to take into account the coupling between the thermal, mechanical, and phase field parts of the model. Successful algorithms developed to solve the coupling have been presented in two simplified cases: (i) uniform density and (ii) isothermal. The algorithms use a linear approximation of the terms that induces an improved efficiency of the solvers. The results are consistent with the analytical developments and two-dimensional computations are qualitatively satisfying. They attest the ability of the model to be at the basis of a numerical method. Based on these results, we defined an algorithm for the resolution of the complete coupling. This algorithm allows to study phase change process as attested by one-dimensional computations. However, numerical instabilities occur for two-dimensional computations. An analysis of the algorithm allowed to identify the origin of the instability as a numerical issue. Currently, we have not found a way to avoid the instability.

This study can be considered as an attempt to use phase field models for the study of boiling flows. It first provided a justification for the use of numerical simulation to improve the understanding of the boiling process,

and more particularly the boiling crisis. Secondly, we have been able to develop a diffuse interface model with a clear set of parameters and functions that allows to deal *(i)* with the main features of boiling flows and *(ii)* with controlled characteristics of the interface transition layer. In this study, we took special care of the consequences of the introduction of the phase field variable on the description of the liquid-vapor phase transition. We also provided a precise analysis of the equivalent sharp interface model and showed that our phase field model is a thermodynamically consistent regularization of the classical sharp model with incompressible bulk phases. Our numerical study, if finally unsuccessful, has drawn the first steps toward the solving of the complete model and thus the study of nucleate wall boiling.

Our study revealed that the study of the very near wall boiling processes is of primary interest for the understanding of the basic mechanisms of the boiling crisis. Experimental observation of the near wall layer (where nucleation and bubble growth take place) at near boiling crisis conditions should provide lacking information on the origin of the precursor drying events observed in [130]. This suggests the use of an experimental set-up allowing to simultaneously observe the nature of the wall-fluid contact (using for example infrared camera) and the bubble growth dynamics (using lateral visualization).

We have distinguished two categories of methods for the computation of boiling flows using an implicit tracking of the interface: the level set method that is based on a sharp interface model and the diffuse interface models. The phase field variable is formally very close to the indicator or color function used in level set methods. It allows to introduce a first formal link between the two classes of methods. It is worth pointing out that the relaxation of the distance function used in the level set methods to keep the level set function equal to a signed distance function has close similarities with our *AC* equation. In a study of the numerical computation of diffuse interface models, Glasner [57] proposed to work on a "distance" function rather than directly on the phase field variable. This change of variable makes the phase field formulation very close to the level set formulation. It would benefit to both methods to investigate more deeply the formal link between them.

The phase field model developed in this study has been deliberately devoted to the description of incompressible bulk phases. It would be of interest to derive a more generic phase field formulation for compressible bulk phases. Our quasi-compressible model should then reduce to a natural outcome of this compressible formulation. We believe that the basis of this compressible formulation should read, as our model does, as the interpolation of the bulk phase equation of states. As soon as the bulk phases are compressible, the dependence of the Gibbs free energy with respect to the pressure is non-linear. The consequences of this non-linearity on the ability to easily control the interface thickness should be investigated. It is worth pointing out that the quasi-compressible model, since taking into account a non-zero density difference between the bulk phases, can be applied to the study of the solid-liquid with convection. More generally, it would be of interest to study how the structure we proposed for the phase field model can be used for different models of multi-phase and/or multi-component systems of arbitrary equations of state. In particular, in the case of immiscible fluids, it would be also of interest to study a similar model that would have interest on the mass diffusion equation instead of our entropy equation.

The kinetic relation of our model has been derived using matched asymptotic expansions. This methods allows to get approximate solutions for the one-dimensional phase transition. It would be of interest to study the kinetic relation, *i.e.* the driving force as a function of the mass transfer rate, more accurately using numerical simulations.

It is worth noting that the choice for the interpolation function plays a particular role on the features of small inclusions: when it is not a polynomial of degree 5, the sharp interface equivalent radius diverges as the mass of the spherical inclusion vanishes (*cf.* section 4.3.3). As a consequence, this feature is not associated to a diffuse interface formulation. A better understanding of the origin of this latter phenomenon could lie on the study of the influence of the interpolation function on the spherical symmetric equilibrium equation. Moreover, still about the interpolation function, we defined a way to impose a phenomenological metastability limit even in the case of incompressible bulk phases (*cf.* section 6.5.1). We showed that it was sufficient to use a polynomial of degree 5 whose coefficients depends on the thickness of the interface layer to get this property. It yields an additional feature of the phase field model with regard to the sharp interface formulation. It would be of interest to study the consequences of this choice on the other properties of the model.

The projection method is currently used in the numerical methods for the study of two-phase flows even in presence of phase change. Nevertheless our numerical study has shown that the use of the projection method for the study of two-dimensional phase change problems with capillarity can induce severe numerical difficulties. As a consequence, it would be of interest to develop algorithms based on another resolution method for the

momentum balance equation such as the curl decomposition. Another perspective of work could be to deal with a more simplified writing of the equation, that even though it would fail to be thermodynamically consistent, would take benefit of simplifications from the point of view of computational efficiency. This pragmatic approach is commonly used with phase field methods.

Appendix A

Sharp model for the liquid-vapor flows with phase change

In this appendix we study the sharp interface models for the liquid-vapor phase transition. The goal is to study the formalism allowing to compare our phase field model with more classical models for the liquid-vapor flows with phase change. This study allows therefore to analyze the results of our phase field model as a thermodynamically consistent regularization of the sharp interface model.

First we study the model of the variables at the interface in sharp interface models and more particularly the relation between the definition of the interface location, as a moving free boundary, and the value of the jump of the variables and of excess quantities at this discontinuity (see section A.1). Then we study the Rankine-Hugoniot jump conditions that apply at the interface. We study the relation between closure laws at the interface (such that "out of equilibrium" Clapeyron relation) and the value of the interface entropy production. This study allows thus to relate the sharp closure laws to the definition of the interface dissipative processes that is made in diffuse interface models (see section A.2).

A.1 Equivalent sharp interface

A.1.1 Interface values

Equilibrium case For the sake of simplicity, let us consider a one-dimensional two phase system along an arbitrary $x-$axis. Let us specify with the superscripts $^+$ and $^-$ the phases reached at large distance from the transition layer, say respectively $+\infty$ and $-\infty$.

In the diffuse interface theory, all the variables are continuous in particular along the direction normal to the interface, say the x-axis. In the Gibbs theory of sharp interfaces, an equivalent surface (in the planar case, an abscissa x_i) models the volumetric continuous transition layer between the phases. Let us consider a variable q that is uniform in the bulk phase states + and $-$. The variable q varies continuously between the bulk phase values q^- and q^+. In the sharp interface model, the boundary condition applying at the sharp interface location

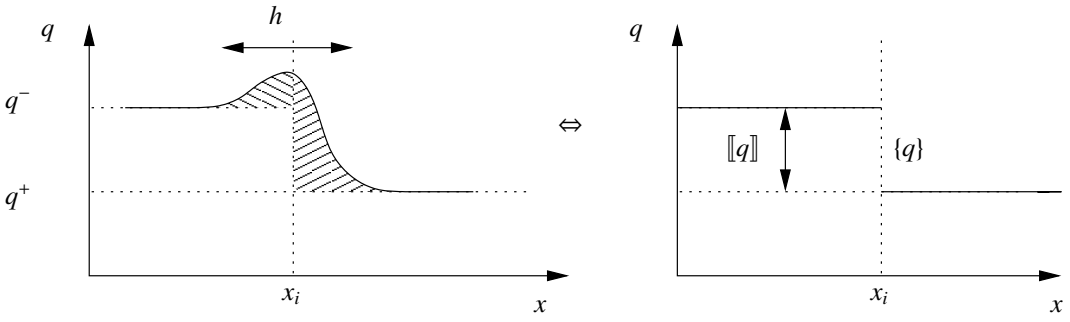

Figure A.1: Interface value and jump

x_i to the variable q can be defined thanks to a jump $[\![q]\!]$ and an interface value $\{q\}$ defined as follows

$$[\![q]\!] \triangleq q^+ - q^- \tag{A.1a}$$

$$\{q\} \triangleq \frac{q^+ + q^-}{2} \tag{A.1b}$$

These quantities are represented on figure A.1. For a zero jump we have $q^+ = q^- = \{q\} = q_i$. Let us introduce the relation

$$[\![q_1\, q_2]\!] = \{q_1\}\,[\![q_2]\!] + \{q_2\}[\![q_1]\!] \tag{A.2}$$

which is valid for any arbitrary quantities q_1 and q_2 and which is often used in the following.

It is clear from figure A.1, that in the case where q^+ and q^- can be clearly defined, $[\![q]\!]$ and $\{q\}$ are defined unambiguously and are independent from the definition of the interface location x_i. However, we see in the following that this is not the general case.

Out of equilibrium case All the previous definition are unambiguous and independent of the interface location x_i as long as the variable q takes specific values in the bulk phase domains. Let us now consider an out of equilibrium situation where the variable q, say the temperature for example, varies spatially in the direction normal to the interface over distance δ larger than the interface thickness h, say a thermal boundary layer on one side of the interface. This typical situation is represented on figure A.2 where the variable q is non-uniform on the LHS of the interface (domain $-$). On a scale of the thickness of the interface (zoom on the figure), and since $\delta \gg h$, the variation of the variable q is assumed as linear with respect to x on the LHS. This corresponds to a constant heat flux in the thermal case. On the RHS q is uniform (zero heat flux). In this case the jump and interface value of the variable q depends on the interface location. On figure A.2, three different locations are represented, for each location the jump in heat flux is the same, but it is clear that the jump and interface value differ. As a consequence, it appears that it is not sufficient to describe the physical situation in all cases with the

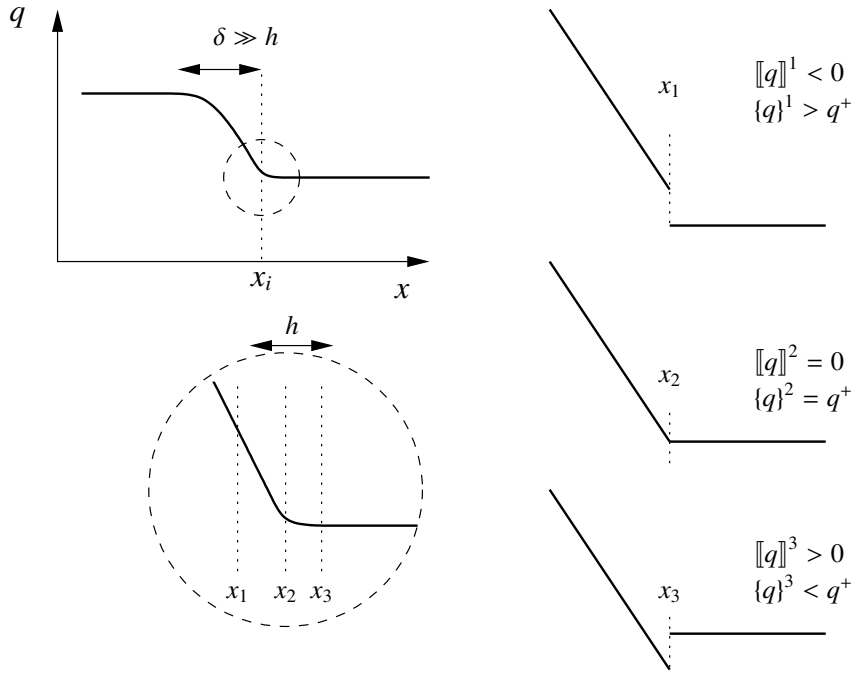

Figure A.2: Case of a non-uniform variable on one side of the interface

help of the single specification of the jump and the interface value without studying their relation to the interface location.

A.1.2 Excess quantities and interface location

Definition of excess quantities When modeling the volumetric transition layer as a surface of discontinuity, the fine description of the internal variations is neglected. However the sharp interface can bear some physical

information with the help of surface quantities also called Gibbs excesses. These surface quantities are the reflect of the internal physics of the diffuse transition layer. The reader interested to this formalism can refer to Edwards et al. [46]. Let us take the example of a volumetric physical quantity, say q, taking some specific values in the phases, say q^+ and q^-, and undergoing spatial variations inside the interface. The excess of a given volumetric quantity measures the difference between the sharp profile and the continuous one. For a given position x_i of the sharp interface, the excess quantity q^{ex} of the volumetric physical quantity q is defined as

$$q^{ex} \triangleq \int_{x_i}^{+\infty} (q(x) - q^+)\, dx + \int_{-\infty}^{x_i} (q(x) - q^-)\, dx \tag{A.3}$$

the table A.1 provides an illustrative representation of the jump and excess quantities.

Relation between interface location and excess quantities The position itself of the sharp interface must be defined through an equivalence principle whose choice is arbitrary. This can be done, as classically, by considering that the location of the sharp interface x_i is such that a given excess quantity is null. In the following we denote such a specified location x_q. The associated excess value and the location of the interface are thus interdependent. Let us consider a shift of the interface location from x_i to x_i'. It is straightforward that the new excess quantity $q^{ex'}$ becomes

$$q^{ex'} = q^{ex} + \int_{x_i'}^{x_i} (q^+ - q^-)\, dx = q^{ex} + [\![q]\!]\,(x_i - x_i') \tag{A.4}$$

If the jump is zero, the volumetric quantity q has a specific interface value that is well defined (*i.e.* independent of the choice for the interface location x_i), $\{q\} = q^+ = q^-$, and it is obvious from (A.4), that the excess quantity does not depend on the interface location. The value of an excess quantity undergoing a non-zero jump depends of the arbitrary definition of the sharp interface location x_i. Let us consider that the interface location is defined such as the excess density is zero, *i.e.* $x_i = x_\rho$. This definition is classical in sharp interface models, it leads to an interface that does not bear any mass and is a non-material surface. Let us denote by the subscript ρ the corresponding value for the excess quantities

$$q_\rho^{ex} = \int_{x_\rho}^{+\infty} (q(x) - q^+)\, dx + \int_{-\infty}^{x_\rho} (q(x) - q^-)\, dx$$

then, since by definition $q_q^{ex} = 0$, and using the relation (A.4) we have

$$q_\rho^{ex} = [\![q]\!]\,(x_q - x_\rho) \tag{A.5}$$

Let us note, that as soon as the quantity undergoes a jump across the interface, it is possible to define a location such that its excess quantity is zero, which is impossible as soon as the jump is zero.

Intrinsic excess quantities However, while considering a volumetric variable undergoing a jump across the interface, it is possible to define a physically homogeneous variable whose excess quantity is independent of the interface location, *i.e.* whose jump is zero. This excess quantity is therefore more intrinsic to the interface layer. As an example, let us consider two volumetric quantities q and Q of non-zero jump across the interface, $[\![q]\!]$ and $[\![Q]\!]$, the quantity $\tilde{Q}$ defined as

$$\tilde{Q} = Q - \frac{[\![Q]\!]}{[\![q]\!]}\, q \tag{A.6}$$

is such that $[\![\tilde{Q}]\!] = 0$. In the following we illustrate this point with the help of the definition of the surface tension coefficient for a planar interface, of interest for our applications.

A.1.3 Surface tension coefficient

The most typical excess quantity of concern for liquid-vapor phase transition is the surface tension coefficient σ. In the following we study how it is related to an excess quantity.

q_0	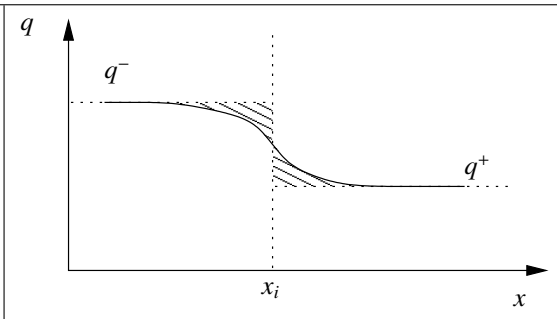	$[\![q_0]\!] = q_0^+ - q_0^-$ $q_0^{ex} = 0$ The jump is non zero but the excess quantity is zero
q_1	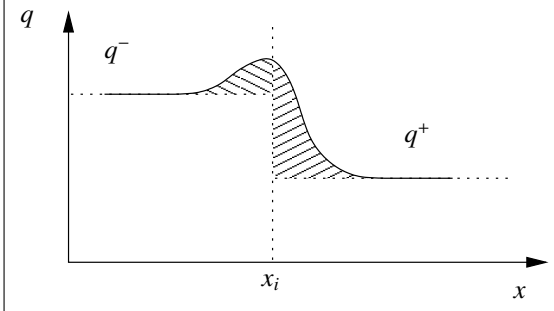	$[\![q_1]\!] = q_1^+ - q_1^-$ $q_1^{ex} \neq 0$ The jump and the excess quantity are non zero
q_2	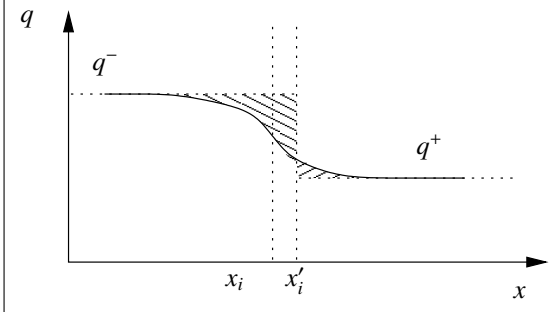	$q_2(x) = q_0(x + (x_i - x_i'))$, the interface location is shifted from x_i to x_i' $[\![q_2]\!] = [\![q_0]\!]$ but $q_2^{ex} \neq q_0^{ex}$
q_3	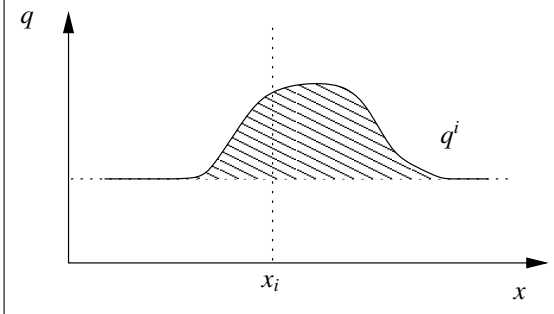	$[\![q_3]\!] = 0$ $q_3^{ex} \neq 0$ The jump is equal to zero but the excess quantity is non zero
q_4	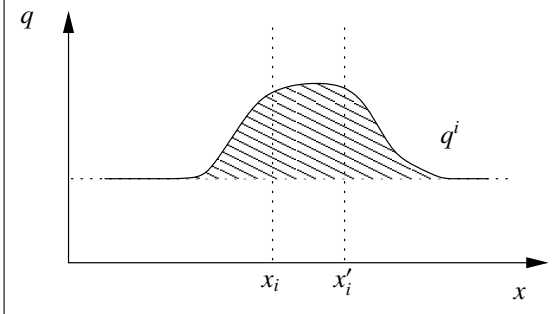	$q_4(x) = q_3(x + (x_i - x_i'))$, the interface location is shifted from x_i to x_i' $[\![q_4]\!] = [\![q_3]\!] = 0$ and $q_4^{ex} = q_3^{ex}$ the excess quantities are still equal

Table A.1: Excess quantities as a function of interface location

Surface tension as an excess volumetric free energy independent from the interface location Let us consider the volumetric quantity Helmholtz free energy in the isothermal van der Waals model as presented in 2.2.2. The planar two-phase equilibrium condition implies the existence of a common tangent to the Helmholtz free energy $F(\rho)$[1] at the two bulk densities ρ^+ and ρ^- Therefore

$$\begin{cases} \dfrac{dF_{cl}}{d\rho}^{+} \rho^+ - F_{cl}^+ = \dfrac{dF_{cl}}{d\rho}^{-} \rho^- - F_{cl}^- \\ \dfrac{dF_{cl}}{d\rho}^{+} = \dfrac{dF_{cl}}{d\rho}^{-} \hat{=} g_{eq} \end{cases} \tag{A.7}$$

where g_{eq} is the specific Gibbs free energy value at equilibrium. The first equality is a pressure equality $P^+ = P^-$ since

$$P = \frac{dF_{cl}}{d\rho}\rho - F$$

The jump in Helmholtz free energy $[\![F]\!]$ reads

$$[\![F]\!] \;=\; g_{eq}[\![\rho]\!] \tag{A.8}$$

Setting $q = F$ and $Q = \rho$, we can define the quantity $\tilde{F}$ homogeneous to the volumetric excess free energy F as

$$\tilde{F} \hat{=} F - g_{eq}\,\rho \tag{A.9}$$

and an intrinsic measure of the excess free energy, *i.e.* the surface tension coefficient σ, is

$$\sigma = F^{ex} - g_{eq}\,\rho^{ex} \tag{A.10}$$

Fouillet [53] stated that this definition is independent of the interface location x_i. This definition of σ is classically used [90].

Surface tension as an excess pressure Let us note that the pressure P has a zero jump for the planar interface case. The excess pressure can be related to the surface tension as

$$\sigma_P \;\hat{=}\; -P^{ex} \tag{A.11}$$

This definition of the free excess energy is related to the equivalent representation of the surface tension as a force (*cf.* [68]) and is also therefore classically used.

Equivalence between the two definitions in the two-phase equilibrium planar case Definition (A.11) of the surface tension is different from the definition (A.10) but is actually equivalent in the case of a planar interface. Let us state how both definitions of σ are related. Let us specify the location of the interface as the abscissa x_i by

$$\rho^{ex} = \int_{x_i}^{+\infty} (\rho(x) - \rho^+)\,dx + \int_{-\infty}^{xi} (\rho(x) - \rho^-)\,dx = 0 \tag{A.12}$$

Since $F = \rho\, g - P$, the excess Helmholtz free energy F^{ex} across a planar interface is given by

$$F^{ex} \;=\; \int_{xi}^{+\infty} (\rho(g - Pv) - \rho^+(g^+ - P^+v^+))\,dx + \int_{-\infty}^{xi} (\rho(g - Pv) - \rho^-(g^- - P^-v^-))\,dx$$

Since, as stated by (3.28b), the specific Gibbs free energy g is uniform at equilibrium, we get $g = g^+ = g^- = g_{eq}$ and F^{ex} reads

$$F^{ex} = \int_{xi}^{+\infty} (P^+ - P)\,dx + \int_{-\infty}^{xi} (P^- - P)\,dx + g_{eq}\rho^{ex}$$

Using the definition of the interface location x_i (A.12), we get

$$F_\rho^{ex} = -P^{ex}$$

And therefore

$$-P^{ex} = \tilde{F}^{ex}$$

and we get thus

$$\sigma = \sigma_P$$

The two definitions (A.9) (A.11) of the surface tension coefficient have thus been shown to be equivalent.

[1] Since $(\nabla\rho)^2 = 0$ in the bulk phases, this is indeed a common tangent to F_{cl}

A.2 Rankine Hugoniot and kinetic relations

The goal of this section is to present the classical sharp formulation for the out of equilibrium description of a liquid-vapor interface. We establish from very general relations the nature of the closure relations that need to be specified in order to determine the evolution of a sharp solution. We study the relation between the surface internal dissipation rate and the kinetic relation in form of an out of equilibrium Clapeyron relation. and consider the influence of considering incompressible bulk phases.

A.2.1 Liquid-vapor interface jump conditions

The dynamics of the two bulk phases are coupled through the mass (A.13a), momentum (A.13b-A.13c), energy (A.13d) and entropy (A.13e) jump conditions applying at the interface location. These relations are the so-called Rankine-Hugoniot jump conditions and read

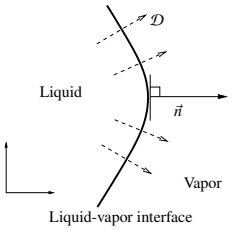

$$\llbracket \rho (\mathcal{D} - V_n) \rrbracket = 0 \tag{A.13a}$$

$$\llbracket P \rrbracket + \llbracket \rho (\mathcal{D} - V_n)^2 \rrbracket = 0 \tag{A.13b}$$

$$\rho (\mathcal{D} - V_n) \llbracket V_\tau \rrbracket = 0 \tag{A.13c}$$

$$\rho (\mathcal{D} - V_n) \left\llbracket \frac{V^2}{2} + e \right\rrbracket - \llbracket q \rrbracket - \llbracket P V_n \rrbracket = 0 \tag{A.13d}$$

$$\left\llbracket \frac{q}{T} \right\rrbracket - \rho (\mathcal{D} - V_n) \llbracket s \rrbracket = \mathcal{R}_s \tag{A.13e}$$

where $\mathcal{D}$ is the local speed of displacement of the free interface, V_n, resp. V_τ, the component of the velocity along the local normal $\vec{n}$, resp. tangent, to the interface profile, q the projection of the local heat flux along $\vec{n}$, e the specific internal energy, s the specific entropy, and $\mathcal{R}_s$ the surface entropy production associated with the interface internal dissipative effects. The tangential momentum jump condition (A.13c) is a non-slip condition implying the equality of the tangent component of the velocity field on each side of the interface, therefore $V_{\tau,l} = V_{\tau,v}$. In the following we consider that $\{V_\tau\} = 0$ and therefore $V = V_n$. Zeroes on the RHS of (A.13a,A.13d) imply that we do not consider any surface supply of mass, momentum and energy. As a consequence, the single non-zero RHS term of the jump conditions concerns the interface entropy production that remains finite even for sharp representation (vanishing thickness of the interface layer) and is related to the kinetic relation in the following.

It is worth noting that it is also possible to consider the momentum supply associated with surface tension as follows

$$\llbracket P \rrbracket + \llbracket \rho (\mathcal{D} - V_n)^2 \rrbracket = \sigma \mathcal{K} \tag{A.14}$$

where $\mathcal{K}$ is the local curvature, and σ is the surface tension coefficient,

General relations from the Rankine-Hugoniot jump conditions Since the two-phase considered are the liquid and vapor one, we also denote the phases + and − by l and v for the relations that are not function of their relative position. According to the first jump condition (A.13a), let us define the mass transfer rate Γ by

$$\Gamma \triangleq \frac{\mathcal{D} - \{V\}}{\{1/\rho\}} = \rho_l (\mathcal{D} - V_l) = \rho_v (\mathcal{D} - V_v) \tag{A.15}$$

the different equalities being obtained using the mass jump condition (A.13a). According to this convention, Γ is therefore positive for evaporation. The normal component of the velocity at the interface location in the phase $\pm$ therefore reads

$$V^\pm = \mathcal{D} - \frac{\Gamma}{\rho^\pm} \tag{A.16}$$

The jump in the normal component of the velocity field $\llbracket V \rrbracket$ appearing on the LHS of the momentum jump condition (A.13b) reads using (A.16)

$$\llbracket V \rrbracket = - \left\llbracket \frac{1}{\rho} \right\rrbracket \Gamma \tag{A.17}$$

Let us study the expression for the jump in pressure. We deduce from the momentum jump condition (A.13b) the expression for the jump in pressure

$$[\![P]\!] = [\![\rho\,(\mathcal{D} - V)]\!]\,\{V\} + \{\rho\,(\mathcal{D} - V)\}\,[\![V]\!]$$

Using the mass jump condition (A.13a) and the expression for the velocity jump (A.17), yields the expression for the pressure jump undergoing mass transfer

$$[\![P]\!] = -\Gamma^2 \left[\!\left[\frac{1}{\rho}\right]\!\right] \tag{A.18}$$

where the RHS term is classically called vapor recoil. When curvature is negligible, the bulk value of the pressure is therefore always larger in the liquid than in the vapor.

When surface tension is taken into account, the pressure jump reads

$$[\![P]\!] = -\Gamma^2 \left[\!\left[\frac{1}{\rho}\right]\!\right] + \sigma\mathcal{K} \tag{A.19}$$

where the second term on the RHS concerns the Laplace relation.

A.2.2 Interface entropy production

In this section we more specifically study the interface entropy production $\mathcal{R}_s$. We derive some general relations between $\mathcal{R}_s$ and the jump of thermodynamic quantities and introduce a driving force for the liquid vapor phase transition. We then briefly comment some basic closure laws for $\mathcal{R}_s$.

Definition of the driving force The surface entropy production $\mathcal{R}_s$ is defined by the entropy jump condition (A.13e) but needs to be specified in order to close the problem. In the case of our diffuse interface model, since the internal structure of the interface is described, we can derive an expression for $\mathcal{R}_s$. In order to compare it with classical kinetic relations, let us first write the surface entropy production $\mathcal{R}_s$ as the product of a force by the flux Γ. This force is denoted the driving force $\mathscr{G}$ in the following.

To derive the expression for $\mathscr{G}$, let us rewrite (A.13e) as

$$\mathcal{R}_s\,\{T\} = -\Gamma\,[\![s]\!]\{T\} + \left[\!\left[\frac{q}{T}\right]\!\right]\{T\}$$

Using the identity (A.2), we have

$$[\![s]\!]\{T\} = [\![T\,s]\!] - [\![T]\!]\{s\}$$

Therefore using the fact that

$$e = g + T\,s - \frac{P}{\rho}$$

we have

$$[\![s]\!]\{T\} = [\![e]\!] - [\![g]\!] - [\![T]\!]\{s\} + \left[\!\left[\frac{P}{\rho}\right]\!\right]$$

Using the latter expression and the energy jump condition (A.13d) for the expression of $[\![e]\!]$, we get thus

$$\mathcal{R}_s\,\{T\} = \Gamma\,([\![g]\!] + [\![T]\!]\{s\}) + \underbrace{\Gamma\left[\!\left[\frac{V^2}{2}\right]\!\right] - [\![P\,V]\!] - \Gamma\left[\!\left[\frac{P}{\rho}\right]\!\right]}_{mechanical}\underbrace{-[\![q]\!] + \left[\!\left[\frac{q}{T}\right]\!\right]\{T\}}_{thermal}$$

Let us now consider the "mechanical" group of terms of the above expression and relate it to a kinetic energy relative to the interface displacement. We thus use the two different identities

$$\begin{aligned}
[\![P\,V]\!] &= [\![P\;(V - \mathcal{D})]\!] + [\![P]\!]\,\mathcal{D} \\
&= \left[\!\left[\frac{P}{\rho}\,\rho\,(V - \mathcal{D})\right]\!\right] + [\![P]\!]\,\mathcal{D} \\
&= -\Gamma\left[\!\left[\frac{P}{\rho}\right]\!\right] + [\![P]\!]\,\mathcal{D} \\
&= \Gamma\left([\![V]\!]\,\mathcal{D} - \left[\!\left[\frac{P}{\rho}\right]\!\right]\right)
\end{aligned}$$

where we have used the expression (A.18) for the pressure jump and

$$\begin{aligned}\frac{\left[\!\left[V^2\right]\!\right]}{2} - \left[\!\left[V\right]\!\right]\mathcal{D} &= \left[\!\left[V\right]\!\right]\{V-\mathcal{D}\} \\ &= \left[\!\left[V-\mathcal{D}\right]\!\right]\{V-\mathcal{D}\}\end{aligned}$$

As a consequence, the interface entropy production reads

$$\mathcal{R}_s\{T\} = \Gamma\left(\left[\!\left[g\right]\!\right] + \left[\!\left[T\right]\!\right]\{s\} + \frac{\left[\!\left[(V-\mathcal{D})^2\right]\!\right]}{2}\right)\underbrace{-\left[\!\left[q\right]\!\right] + \left[\!\left[\frac{q}{T}\right]\!\right]\{T\}}_{thermal}$$

We now introduce another writing for the "thermal" part of this expression using the identity

$$\left[\!\left[\frac{q}{T}\right]\!\right] = \left[\!\left[q\right]\!\right]\left(\left\{\frac{1}{T}\right\} - \frac{1}{\{T\}}\right) - \left[\!\left[T\right]\!\right]\frac{\{q\}}{\{T\}}\left\{\frac{1}{T}\right\} + \frac{\left[\!\left[q\right]\!\right]}{\{T\}}$$

The interface entropy production now reads

$$\mathcal{R}_s\{T\} = \Gamma\left(\left[\!\left[g\right]\!\right] + \left[\!\left[T\right]\!\right]\{s\} + \frac{\left[\!\left[(V-\mathcal{D})^2\right]\!\right]}{2}\right)^2\underbrace{-\left[\!\left[T\right]\!\right]\left\{\frac{q}{T}\right\} + \left[\!\left[q\right]\!\right]\left(\{T\}\left\{\frac{1}{T}\right\} - 1\right)}_{thermal}$$

and let us note that since $\left[\!\left[T\right]\!\right] = 0 \Rightarrow \{1/T\} - 1/\{T\} = 0$, the "thermal" part cancels as soon as the temperature is continuous across the interface, *i.e.* $\left[\!\left[T\right]\!\right] = 0$.

We now define the driving force $\mathscr{G}$ as

$$\mathscr{G} \triangleq \left[\!\left[g\right]\!\right] + \left[\!\left[T\right]\!\right]\{s\} + \frac{\left[\!\left[(V-\mathcal{D})^2\right]\!\right]}{2} \tag{A.20}$$

such that the surface entropy production now reads

$$\mathcal{R}_s\{T\} = \Gamma\mathscr{G} - \left[\!\left[T\right]\!\right]\left\{\frac{q}{T}\right\} + \left[\!\left[q\right]\!\right]\left(\{T\}\left\{\frac{1}{T}\right\} - 1\right) \tag{A.21}$$

This driving force is therefore composed of a thermodynamic part $\left[\!\left[g\right]\!\right] + \left[\!\left[T\right]\!\right]\{s\}$ and a kinetic energy contribution. It refers thus to a total energy formulation.

Another writing of the driving force reads

$$\mathscr{G} = \left[\!\left[g\right]\!\right] + \left[\!\left[T\right]\!\right]\{s\} + \Gamma^2\left\{\frac{1}{\rho}\right\}\left[\!\left[\frac{1}{\rho}\right]\!\right]$$

where we have used the interface mass balance (A.16) such that

$$\begin{aligned}\frac{\left[\!\left[(V-\mathcal{D})^2\right]\!\right]}{2} &= \left[\!\left[V-\mathcal{D}\right]\!\right]\{V-\mathcal{D}\} \\ &= -\Gamma\left[\!\left[V-\mathcal{D}\right]\!\right]\{1/\rho\} \\ &= \Gamma^2\left[\!\left[1/\rho\right]\!\right]\{1/\rho\}\end{aligned}$$

As a consequence of this second writing, for phase transitions without density contrast the kinetic contribution is zero (since $\left[\!\left[1/\rho\right]\!\right] = 0$).

Closure relation for the interface entorpy production or for the driving force The interface entropy production satisfies the Clausius Duhem inequality

$$\mathcal{R}_s \geq 0$$

due to dissipative processes, and the expression (A.21) allows thus to relate this dissipation to the jump of the different thermodynamic variables across the interface. It is worth noting that the solution of the phase transition

moving free boundary problem is not unique unless $\mathcal{R}_s$ is not specified. A constitutive relation for the surface entropy production provides an additional jump condition which does not follows from the system of general jump conditions (A.13) and uniquely specifies a solution for the moving free boundary problem. A "natural" assumption for the constitutive relation is that the surface entropy production $\mathcal{R}_s$ depends on the mass flux Γ, $\mathcal{R}_s(\Gamma)$.

Let us first ignore the part of equation (A.21) related to the curvature and assume, as it is generally done that $[\![T]\!] = 0$. Thus equation (A.21) reads

$$\{T\}\,\mathcal{R}_s = \Gamma\,\mathscr{G}$$

It is straightforward that in this case, the interface entropy production is zero when the mass transfer rate is zero. We show in the study of the kinetic relation that it is not the general case: in fact, when the interface is crossed by a heat flux, it is possible to have $\Gamma = 0$ but $\mathcal{R}_s \neq 0$, and it is thus obvious from (A.21) that the dissipation leads to a non-zero temperature jump.

Let us now consider the simplest kinetic relation that ignores any interface entropy production, *i.e.* $\mathcal{R}_s = 0$. In this case, it is clear from the kinetic relation that we have also $\mathscr{G} = 0$ for any mass transfer rate Γ. As a consequence, we get

$$[\![g]\!] = -\Gamma^2 \left[\!\!\left[\frac{1}{\rho}\right]\!\!\right] \left\{\frac{1}{\rho}\right\}$$

The equilibrium relation $[\![g]\!] = 0$ is therefore recovered when $\Gamma = 0$ but also for phase transition without density contrast. It is worth pointing out that $\mathcal{R}_s = 0$ also leads to

$$[\![q]\!] = \Gamma\,\mathcal{L}$$

where $\mathcal{L}$ is the latent heat $\mathcal{L} \triangleq \{T\}[\![s]\!]$. This latter relation is classicaly used in sharp interface models.

Let us now consider the normal growth theory that models the interface entropy production as quadratic in Γ (such that the Clausius Duhem inequality is satisfied), *i.e.*

$$\mathcal{R}_s \propto \Gamma^2$$

Then the driving force is obviously linear in the mass transfer rate. In the following we establish the link between the normal growth theory and the commonly used out of equilibrium kinetic relations on the form of out of equilibrium Gibbs-Thomson and Clapeyron relations.

A.2.3 Kinetic relations and laws for the interface temperature and pressure

Isothermal model Let us consider a simple isothermal model ($[\![T]\!] = 0, \{T\} = T_{eq}$) for g in the bulk phases

$$\begin{aligned} g_l &= \int^P (1/\rho_l)\, dP \\ g_v &= \int^P (1/\rho_v)\, dP \end{aligned}$$

For the sake of simplicity and without any loss of generality, let us consider that the reference pressure is the equilibrium value for the pressure at planar equilibrium P_{eq} (*i.e.* that $g_{eq} = 0$ where g_{eq} is such that $g_{eq} = g_l(P_{eq}) = g_v(P_{eq})$). For sufficiently low values for $\left\{P - P_{eq}\right\}$ and $[\![P]\!]$, we have

$$1/\rho^{\pm}(P^{\pm}) = 1/\rho(P_{eq}) + (P^{\pm} - P_{eq}) \left(\frac{\partial \rho}{\partial P}\right)^{\pm,\, P^{\pm}=P_{eq}} + O(P^{\pm} - P_{eq})^2$$

Let us introduce a certain interpretation for the neglect of the compressibility (*i.e.* of the dependence of the specific volume $1/\rho_{l\,\mathrm{or}\,v}$ with respect to the pressure P) of the bulk phases in the context of the study of the liquid-vapor phase transition, that reads

$$\left(P_{l\,\mathrm{or}\,v} - P_{eq}\right)\left(\frac{\partial \rho}{\partial P}\right)_{l\,\mathrm{or}\,v,\, P=P_{eq}} \ll \rho_{l\,\mathrm{or}\,v}(P_{eq}) \tag{A.22}$$

Following this approximation, we get

$$[\![g]\!] \simeq (P_l - P_{eq})(1/\rho_l) - (P_v - P_{eq})(1/\rho_v) = [\![(P - P_{eq})\, 1/\rho]\!]$$

and thus we get

$$[\![g]\!] \simeq \Big(\{P\} - P_{eq}\Big)\, [\![1/\rho]\!] + [\![P]\!]\{1/\rho\} \tag{A.23}$$

Since $[\![P]\!]$ is given by equation (A.18), we get

$$[\![g]\!] \simeq \Big(\{P\} - P_{eq}\Big)\, [\![1/\rho]\!] - \Gamma^2 [\![1/\rho]\!]\{1/\rho\}$$

and therefore, from the definition of $\mathscr{G}$ by equation (A.20)

$$\mathscr{G} \simeq \Big(\{P\} - P_{eq}\Big)\, [\![1/\rho]\!]$$

As a partial conclusion, if compressibility can be neglected (in the sense of (A.22)), the driving force is proportional to the shift of the middle value of the bulk pressures with regard to the equilibrium value. Pursuing our hypothesis on the neglect of the compressibility of the bulk phases, $[\![1/\rho]\!]$ is considered as independent of the mass flux Γ. It yields for the expression of the surface entropy production $\mathcal{R}_s$

$$\mathcal{R}_s \simeq \Gamma \Big(\{P\} - P_{eq}\Big)\, [\![1/\rho]\!] \tag{A.24}$$

In this context, the normal growth theorie suggests therefore that

$$\{P\} - P_{eq} \propto \Gamma$$

The hypothesis of the neglect of compressible effects (A.22) in $[\![g]\!]$ is thus consistent with the normal growth theory, that is valid for low values of the mass flux Γ. Therefore in the scope of the normal growth theory, the shift of the middle value of the bulk pressures with regard to its equilibrium value, as well as the driving force are linear in Γ.

It is worth pointing out that this approximation is exact for incompressible bulk phases. As a conclusion, when the compressibility of the bulk phases is neglected, the normal growth theory (interface entropy production quadratic in the mass transfer rate) is equivalent to the linearity in Γ of $\{P\} - P_{eq}$.

Absolute values of the bulk pressures It is possible to deduce some very general relations about the absolute value of the bulk pressure according to the approximation (A.22). It is straightforward that

$$P^{\pm} = P_{eq} \pm \frac{[\![P]\!]}{2} + \Big(\{P\} - P_{eq}\Big)$$

From (A.23), we get the general relation

$$P^{\pm} \simeq P_{eq} + [\![P]\!] \left(\pm\frac{1}{2} - \frac{\{1/\rho\}}{[\![1/\rho]\!]}\right) + \frac{[\![g]\!]}{[\![1/\rho]\!]}$$

It is worth noting that at mechanical equilibrium ($[\![g]\!] = 0$)

$$P^{\pm} \simeq P_{eq} - [\![P]\!]\, \frac{(1/\rho)^{\mp}}{[\![1/\rho]\!]} \tag{A.25}$$

the shift of the bulk pressures with regard to the planar equilibrium value have both the same sign. As a consequence, the pressure in the vapor is always closer to the planar equilibrium value than the one of the liquid. It yields to classical results (*e.g.* Stephan [129]) for a spherical inclusion at equilibrium: let us consider the pressure jump to be given by the Laplace relation (*cf.* equation (A.14) with $\Gamma = 0$), and set $\pm$ to the liquid and vapor values then we get

$$\begin{aligned} P^l &\simeq P_{eq} + \sigma\mathcal{K}\, \frac{\rho_l}{\rho_l - \rho_v} \\ P^v &\simeq P_{eq} + \sigma\mathcal{K}\, \frac{\rho_v}{\rho_l - \rho_v} \end{aligned}$$

Out of equilibrium situations when the driving force equals zero $\mathcal{G} = 0$ (absence of dissipative process), we have $\{P\} = P_{eq}$ and the bulk pressure are equally shifted from the equilibrium value, *i.e.*

$$P^{\pm} \simeq P_{eq} \pm \frac{[\![P]\!]}{2}$$

This situation corresponds classicaly to a good model for the partition of the effect of recoil pressure on the absoulte values of the bulk pressures.

The non-isothermal case Let us now consider the non-isothermal case. We make the approximation

$$\frac{\partial s}{\partial T}_{\pm} \left(T_{\pm} - T_{eq}\right) \ll s_{\pm}$$

that is equivalent to the neglect of the sensible heat (*i.e.* the heat capacity ($c_P = T(\partial s/\partial T)$) with regard to the latent heat (associated to $[\![s]\!]$) in the expression for $[\![g]\!]$. We get

$$\mathscr{G} \simeq \left(\{P\} - P_{eq}\right) [\![1/\rho]\!] - \left(\{T\} - T_{eq}\right) [\![s]\!] \tag{A.26}$$

and therefore

$$\mathcal{R}_s \{T\} \simeq \Gamma \left(\left(\{P\} - P_{eq}\right) [\![1/\rho]\!] - \left(\{T\} - T_{eq}\right) [\![s]\!]\right) - [\![T]\!] \left\{\frac{q}{T}\right\} + [\![q]\!] \left(\{T\} \left\{\frac{1}{T}\right\} - 1\right) \tag{A.27}$$

This approximation is exact for zero bulk compressibility and specific heat capacity at constant pressure. At equilibrium $\mathscr{G} = 0$ and $[\![T]\!] = 0$ and the kinetic relation (A.27) yields the following approximation for the Clapeyron relation

$$\left(\{P\} - P_{eq}\right) [\![1/\rho]\!] = \left(\{T\} - T_{eq}\right) [\![s]\!]$$

i.e.

$$\frac{\Delta P}{\Delta T} = \frac{\mathcal{L}}{T\,(1/\rho_v - 1/\rho_l)}$$

In the context of the normal growth theory where the jump in temperature is neglected $[\![T]\!] \simeq 0$, equation (A.27) provides a generalization of the Clapeyron relation for out of equilibrium cases

$$\left(\{P\} - P_{eq}\right) [\![1/\rho]\!] - \left(\{T\} - T_{eq}\right) [\![s]\!] \propto \Gamma$$

It is worth noting that if the case is isothermal (or iso-bar), the value for P_{eq} (or T_{eq}) unambiguously refer to the value of pressure (or temperature) at planar two-phase equilibrium. For the most complete case, they refer to the reference pressure and temperature related together by the saturation curve, *i.e.* $P_{eq} = P_{sat}(T_{eq})$.

Let us assume mechanical equilibrium ($[\![P]\!] = 0$) or (equivalent) consider phase transition without density difference between the bulk phases (iso-bar approximation)[2]. In this case the kinetic relation (A.21) reads

$$\mathcal{R}_s \{T\} \simeq -\Gamma \left(\{T\} - T_{eq}\right) [\![s]\!] - [\![T]\!] \left\{\frac{q}{T}\right\} + [\![q]\!] \left(\{T\} \left\{\frac{1}{T}\right\} - 1\right) \tag{A.28}$$

For a non-zero surface entropy production, the sharp interface temperature is characterized by both a non zero jump and a shift of the middle value with respect to the equilibrium value. These two features depend on the dissipative mechanism considered and are both modeled with our phase-field model. In the classical models both can be modeled. For example Delhaye [42] derived the interface jump conditions by assuming the temperature to be continuous across the interface. The reader interested by the problematic of dealing with discontinuous temperature across the interface can refer to the theoretical work of Danescu [41].

In the context of the normal growth theory and when the contribution of the jump in temperature is neglected, this relation is consistent with the classical generalization of the Gibbs-Thomson relation for out of equilibrium situations

$$T_i - T_{eq} \propto \Gamma \tag{A.29}$$

[2]even though this case deals with a somewhat far different situation from our liquid-vapor flow with phase change problem, this corresponds to one of the possible reduction of our model and is the one of our subject of our study of the model, *cf.* the section 7.3 dedicated to the solving of stationary one-dimensional problem using matched asymptotic expansions or section 8.1 for numerical simulations

It is worth noting that from the definition for $\mathcal{R}_s$ the approximated kinetic relation (A.28) implies in the context of neglect of $[\![T]\!]$ contributions

$$\frac{[\![q]\!]}{T_i} - \Gamma\,[\![s]\!] \simeq \left(T_i - T_{eq}\right)[\![s]\!] \Rightarrow\ [\![q]\!] \simeq \Gamma\, T_{eq}[\![s]\!]$$

which is a simplified kinetic relation commonly used in sharp models of phase transition.

A.2.4 Sharp interface model inherited from the outer problem of matched asymptotic expansions

In the classical derivation of the Rankine-Hugoniot jump conditions, the interface layer is presumed to be bounded by two surfaces which are parallel to the interface but are located in the corresponding bulk phases, *e.g.* [28]. The interface entropy production $\mathcal{R}_s$ refers to the one inside the transition layer. However in the sharp interface production, the finite thickness, say δ of the transition layer is set to zero. As a consequence, the zone of thickness δ around the interface is replaced by a surface and the extension of the two bulk domains toward this surface. As a consequence, the notion itself of the layer of thickness δ disappears. The formalism derived in the previous sections can still be used since at the surface of discontinuity as well as on each side of the transition layer of thickness δ it is possible to define jump and interface values for a given variable. However the RHS of the jump conditions written as Rankine-Hugoniot jump conditions (A.13) now refers to excess quantities. Indeed, inside the bulk extensions, there exists an interface entropy production associated to the bulk phases dissipation processes. As a consequence, the surface entropy production beared by the interface is the excess quantity corresponding to the difference between the interface entropy production over the transition layer of thickness δ and the bulk entropy production over this same thickness δ. Even though both entropy production satisfy the Clausius-Duhem inequality, their difference does not.

In matched asymptotic expansions, *cf.* their presentation in appendix B, the diffuse profiles are formally separated in two parts. The first one, say the inner problem corresponds to the study of the transition layer of thickness δ. The second one, say the outer problem, corresponds to a sharp two-phase problem. Inner and outer problems are matched at the interface location and the whole solution is the sum of both sub-problems. As a consequence, the surface entropy production that can be defined with the help of the discontinuous outer fields corresponds to an excess quantity and as a consequence the Clausius-Duhem inequality does not apply to it.

A.2.5 Conclusion

In this appendix we have studied the sharp interface model and shown how the interface entropy production is related to closure laws for the interface pressure and temperature. In the analytical study of one dimensional phase transition (see chapter 7), these results are used to analyze the interface structure obtained with the phase field model proposed.

Appendix B

Matched asymptotic expansions

Introduction

In this appendix, we study analytically using matched asymptotic expansions the solutions for the one-dimensional liquid-vapor phase change problem with the help of the phase field model derived in chapters 3 and 5. In the following sections we present detailed calculations of this analytical study, the main results being summarized and discussed in chapter 7. The goal is to derive the leading orders solutions and to study their dependence with respect to the parameters specific of our model, *i.e.* the non dimensional number ε and the set of functions of the phase-field variable (namely ν and W for the conservative part of the model and $k(\varphi)$, and κ for the dissipative processes considered).

This appendix is organized as follows. In section B.1 we present the main principles of the matched asymptotic expansions. The notations are introduced as well as the identities and relations used in the following. In section B.2, we study the uniform density case and derive the phase field and temperature solutions. In section B.3 we study the phase field, velocity and pressure solutions in the quasi-compressible isothermal case. In section B.4 we then use these different results to derive the solution in the non-isothermal quasi-compressible case.

B.1 The method of matched asymptotic expansions

B.1.1 Principle

The principle of the matched asymptotic expansions can be found in van Dyke [143]. This method applies for the solving of differential equations including a small parameter. The solving domain, as a spatial domain, is separated between different regions or layers where the main variables of the system vary either rapidly or more smoothly.

The fields behave qualitatively differently close and far from the volumetric transition layer, namely the diffuse interface. In the region close to the interface they vary rapidly over distances $O(\varepsilon L)$ while far from the interface they vary on a scale $O(L)$, where L is the length-scale characteristic of the bulk phases and $\varepsilon \hat{=} h/L$, where h is the interface thickness. The parameter ε appears therefore naturally as a small parameter. We refer to these zones as respectively the inner and outer regions. We consider a one-dimensional problem. The inner and outer problems correspond to the system of governing equations obtained when abscissa is scaled either by h or L. The associated solutions are expanded in powers of the small parameter ε in order to study the influence of the artificial thickness h on the solutions. We assume the existence of an intermediate zone (as a function of the small parameter value) where both expansions are valid and where the inner and outer solutions match. We are then able to define boundary conditions for both the outer and inner problems through the assumption of continuity of the global solution.

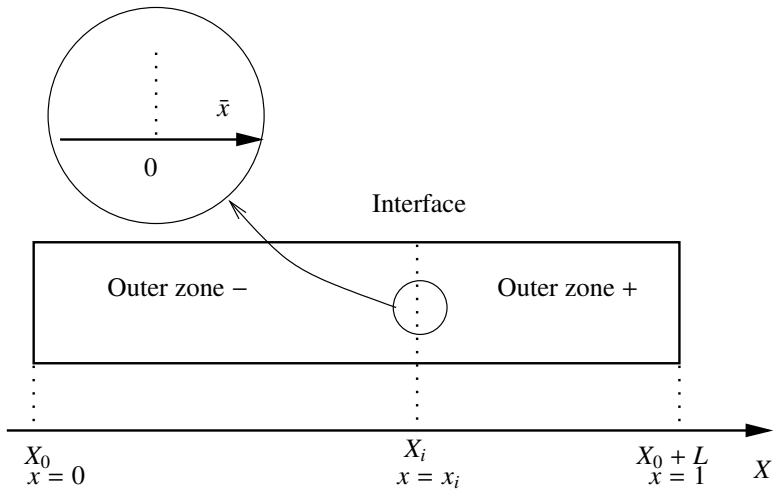

Figure B.1: system of coordinates

B.1.2 Inner and outer solutions, expansions, and matching

System of coordinates Let us consider a one-dimensional system and denote X the dimensional space variable. We introduce two non-dimensional variables x and $\bar{x}$ as

$$\begin{aligned} x &\triangleq \frac{X - X_0}{L} \\ \bar{x} &\triangleq \frac{X - X_i(t)}{h} = \frac{x - x_i(t)}{\varepsilon} \end{aligned}$$

as represented on figure B.1

Expansion of the variables Let f be a variable of the system, f^{ext} denotes the variable in the outer zone. In the inner zone, the variable $f = f(\bar{x})$ varies more smoothly than f^{ext}. The differential equations of the phase field liquid- vapor system are solved in each zone separately using Taylor expansion in the small parameter ε, *i.e.*

$$\begin{aligned} f^{ext}(x,\varepsilon) &= f_0^{ext}(x) + \varepsilon f_1^{ext}(x) + O(\varepsilon^2) \\ f(\bar{x},\varepsilon) &= f_0^{ext}(\bar{x}) + \varepsilon f_1(\bar{x}) + O(\varepsilon^2) \end{aligned}$$

Matching conditions The two different solutions have boundary conditions insuring the continuity of the solution f, these boundary (or matching) conditions applying at the interface location x_i such that

$$\begin{aligned} \lim_{x \to x_i^+} f^{ext} &= \lim_{x \to +\infty} f \triangleq f_i^+ \\ \lim_{x \to x_i^-} f^{ext} &= \lim_{x \to -\infty} f \triangleq f_i^- \end{aligned}$$

For the outer zone, the interface located in x_i is a discontinuity located either at x_i^+ or x_i- whereas in the inner zoner, the outer zones are assumed to be reached asymptotically at $\bar{x} = \pm\infty$. $f_i^\pm$ denotes the value of the variable f at the interface. Since we compare our results with classical sharp interface conditions, we introduce

$$\begin{aligned} [\![f]\!] &\triangleq f_i^+ - f_i^- \\ \{f\} &\triangleq \frac{f_i^+ + f_i^-}{2} \end{aligned}$$

Let us denote the spatial derivatives as

$$\begin{aligned} f_{,x}^{ext} &\triangleq \frac{\partial f^{ext}}{\partial x} \\ f' &\triangleq \frac{\partial f}{\partial \bar{x}} \end{aligned}$$

Using the Taylor expansions of the outer and inner expression of the f, we get the following set of matching conditions at leading orders in the small parameter ε

$$\lim_{x\to x_i^{\pm}} f_0^{ext} = \lim_{\bar{x}\to\pm\infty} f_0 \tag{B.1a}$$

$$\lim_{\bar{x}\to\pm\infty} f_0' = 0 \tag{B.1b}$$

$$\tag{B.1c}$$

$$\lim_{x\to x_i^{\pm}} f_{0,x}^{ext} = \lim_{\bar{x}\to\pm\infty} f_1' \tag{B.1d}$$

$$\lim_{x\to x_i^{\pm}} f_1^{ext} = \lim_{\bar{x}\to\pm\infty} \left[f_1 - \bar{x} \lim_{x\to x_i^{\pm}} f_{0,x}^{ext} \right] \tag{B.1e}$$

$$\lim_{\bar{x}\to\pm\infty} f_0'' = 0 \tag{B.1f}$$

$$\lim_{\bar{x}\to\pm\infty} f_1'' = 0 \tag{B.1g}$$

Steady state mass transfer rate In this study, we consider steady-state mass transfer process. As a consequence the location x_i of the interface is such that

$$\frac{dx_i}{dt} = \mathcal{D} = cste$$

where $\mathcal{D}$ is the dimensionless constant speed of displacement of the interface. As a consequence the Lagrangian time derivative of the variable f in the inner referential reads

$$\frac{\partial f}{\partial t} = -\frac{\mathcal{D}}{\varepsilon} f'$$

Function of the variable Let us consider a function $\mathcal{F}$ of a variable, say φ (such that the interpolation function $\mathcal{F} = \nu(\varphi)$ entering the expression of the thermodynamic potential of our model). The expansion of the function with respect to the small parameter ε reads

$$\mathcal{F}(\varphi) = \sum_{k=0}^{+\infty} \frac{(\varphi - \varphi_0)^k}{k!} \frac{d^k \mathcal{F}}{d\varphi^k}(\varphi_0) \tag{B.2}$$

Since

$$\varphi - \varphi_0 = \sum_{n=1}^{+\infty} \varepsilon^n \varphi_n \tag{B.3}$$

we get

$$(\varphi - \varphi_0)^k = O(\varepsilon^k) \tag{B.4}$$

So we can write

$$\begin{aligned} \mathcal{F}(\varphi) = \; & \mathcal{F}(\varphi_0) \\ & + \varepsilon \left(\varphi_1 \partial_\varphi \mathcal{F}(\varphi_0) \right) \\ & + \varepsilon^2 \left(\varphi_2 \partial_\varphi \mathcal{F}(\varphi_0) + \frac{\varphi_1^2}{2} \partial_{\varphi^2} \mathcal{F}(\varphi_0) \right) \\ & + O(\varepsilon^3) \end{aligned}$$

Let us introduce the identity valid for a given function $\mathcal{F}$ and a given profile $\varphi_0(\bar{x})$ which is used in the following calculations

$$\mathrm{f}'(\varphi_0) = \partial_\varphi \mathrm{f}(\varphi_0)\, \varphi_0' \tag{B.5}$$

Now that the main notations and relations have been introduced, let us consider the solving of the differential equations of our phase field model for the liquid-vapor phase flows with phase change. Let us note that in this study, we consider the interpolation function $\nu(\varphi)$ to be given by polynomials.

B.2 First system of equations, uniform density case

We first solve the traveling wave problem obtained by assuming that the fluid density is constant and uniform (*cf.* the system of equations (5.60))

$$\alpha\,\varepsilon^2\,\mathcal{D}\,\varphi_{,x} = \varepsilon\,\partial_\varphi\nu\,T - \left(\partial_\varphi W - \varepsilon^2\varphi_{,xx}\right) \tag{B.6a}$$

$$\mathcal{D}\,T_{,x} = -\frac{(k\,T_{,x})_{,x}}{Pe} - \mathcal{D}\,(1+T)\,\partial_\varphi\nu\,\varphi_{,x} - \frac{\varepsilon\,\mathcal{D}^2}{\alpha}\,(\varphi_{,x})^2 \tag{B.6b}$$

The system of governing equations for the inner problem reads

$$\begin{aligned}\mathcal{D}\,\varepsilon\,\varphi' &= \alpha\,\left[\partial_\varphi W(\varphi) - \varphi'' - \varepsilon\,T\,\partial_\varphi\nu(\varphi)\right]\\ -\frac{\mathcal{D}}{\varepsilon}T' &= \frac{1}{Pe\,\varepsilon^2}\,(k\,T')' + \frac{\mathcal{D}}{\varepsilon}\,\partial_\varphi\nu(\varphi)\,\varphi' + \frac{\mathcal{D}^2}{\alpha\,\varepsilon}\,(\varphi')^2\end{aligned}$$

According to the general expression for the matching conditions (B.1), the matching conditions for the thermal problem at leading orders read

$$\lim_{\bar{x}\to\pm\infty} T_0' = 0 \tag{B.7a}$$

$$\lim_{x\to x_i^\pm} T_0^{ext} = \lim_{\bar{x}\to\pm\infty} T_0 \tag{B.7b}$$

$$\lim_{x\to x_i^\pm} T_0^{ext\prime} = \lim_{\bar{x}\to\pm\infty} T_1' \tag{B.7c}$$

$$\lim_{x\to x_i^\pm} T_1^{ext} = \lim_{\bar{x}\to\pm\infty}\left[T_1 - \bar{x}\lim_{x\to x_i^\pm} T_0^{ext\prime}\right] \tag{B.7d}$$

Concerning the jump in outer heat flux, of interest for our study of the kinetic relations, we have

$$[\![q_0]\!] = \lim_{\bar{x}\to\infty}\left[k(\varphi_0(\bar{x}))\,T_1'(\bar{x}) - k(\varphi_0(-\bar{x}))\,T_1'(-\bar{x})\right] \tag{B.8a}$$

$$\begin{aligned}[\![q_1]\!] &= \lim_{x\to x_i}\left[\left(k_0\,T_1^{ext\prime} + \partial_\varphi k_0\,\varphi_1^{ext}\,T_0^{ext\prime}\right)(x+) - \left(k_0\,T_1^{ext\prime} + \partial_\varphi k_0\,\varphi_1^{ext}\,T_0^{ext\prime}\right)(x-)\right]\\ &= \lim_{\bar{x}\to\infty}\Big[k(\varphi_0(\bar{x}))\,T_2'(\bar{x}) + \partial_\varphi k(\varphi_0(\bar{x}))\,\varphi_1(\bar{x})\,T_1'(\bar{x})\\ &\qquad -k(\varphi_0(\bar{-x}))\,T_2'(\bar{-x}) - \partial_\varphi k(\varphi_0(\bar{-x}))\,\varphi_1(\bar{-x})\,T_1'(\bar{-x})\Big]\\ &\quad - \lim_{\bar{x}\to\infty}\left[\bar{x}\lim_{x\to x_i}\left(T_0^{ext\prime\prime}(x+) - T_0^{ext\prime\prime}(x-)\right)\right]\end{aligned} \tag{B.8b}$$

For the phase-field solution we have the following set of matching conditions

$$\lim_{\bar{x}\to\pm\infty} \varphi_0' = 0 \tag{B.9a}$$

$$\lim_{x\to x_i^\pm} \varphi_0^{ext} = \lim_{\bar{x}\to\pm\infty} \varphi_0 \tag{B.9b}$$

$$\lim_{x\to x_i^\pm} \varphi_0^{ext\prime} = \lim_{\bar{x}\to\pm\infty} \varphi_1' \tag{B.9c}$$

$$\lim_{x\to x_i^\pm} \varphi_1^{ext} = \lim_{\bar{x}\to\pm\infty} \varphi_1 - \bar{x}\lim_{x\to x_i^\pm} \varphi_0^{ext\prime} \tag{B.9d}$$

B.2.1 Solutions of the outer problem at order $O(1)$

We have to solve two outer problems, one on $[0; x_i(t)]$ and the other on $[x_i(t); 1]$. The first order outer problem reads

$$\begin{aligned}\partial_\varphi W(\varphi_0^{ext}) &= 0\\ \frac{dT_0^{ext}}{dt} &= \frac{\left(k(\varphi_0^{ext})T_{0,x}^{ext}\right)_{,x}}{Pe} - \partial_\varphi\nu(\varphi_0^{ext})\,\frac{d\varphi_0^{ext}}{dt}\end{aligned}$$

Solving the order parameter equation leads to a constant function φ_0^{ext} in the two bulk regions since $\partial_\varphi W$ is only locally null. These solutions are consistent with the outer boundary condition $\varphi' = 0$. From the defintion (3.42) of the double-well function W, φ_0^{ext} could only be 0, 0.5 or 1. According to our study of the stability of homogeneous bulk phases in section 6, only the value 0 and 1 correspond to thermodynamically stable phases. We therefore only consider 0 and 1 as the possible values for φ_0^{ext} and introduce the phase field jump $[\![\varphi]\!]$

$$[\![\varphi]\!] = \pm 1$$

When $\nu(\varphi)$ is either P_3 or P_5, we have

$$\partial_\varphi \nu(\varphi_0^{ext}) = W(\varphi_0^{ext}) = 0 \tag{B.10}$$

According to the above identity, the outer balance of entropy reads

$$\frac{dT_0^{ext}}{dt} = \frac{\left(k(\varphi_0^{ext}) T_{0,x}^{ext}\right)_{,x}}{Pe} \tag{B.11}$$

We therefore have to solve two coupled problems of conduction with the boundary conditions to be specified at $x = 0$ and $x = 1$ and matching conditions (B.7) at $x = x_i^-$ and $x = x_i^+$. According to the expression of these matching conditions, it is required to solve the inner problem at order $O(1)$ and $O(\varepsilon)$ has to be known.

B.2.2 Outer problem at order $O(\varepsilon)$

The system of equation reads

$$\partial_{\varphi^2} W(\varphi_0^{ext})\varphi_1^{ext} = T_0^{ext} \partial_\varphi \nu(\varphi_0^{ext}) \tag{B.12a}$$

$$\begin{aligned} \frac{dT_1^{ext}}{dt} &= \frac{1}{Pe}\left(k(\varphi_0^{ext})\, T_{1,x}^{ext} + \varphi_1^{ext} \partial_\varphi k(\varphi_0^{ext})\, T_{0,x}^{ext}\right)_{,x} \\ &\quad - \left(\partial_\varphi \nu(\varphi_0^{ext}) \frac{d\varphi_1^{ext}}{dt} + \varphi_1^{ext}\, \partial_{\varphi^2} \nu(\varphi_0^{ext}) \frac{d\varphi_1^{ext}}{dt}\right) \end{aligned} \tag{B.12b}$$

Since $\partial_{\varphi^2} W(\varphi_0^{ext}) \neq 0$ and $\partial_\varphi \nu(\varphi_0^{ext}) = 0$

$$\varphi_1^{ext} = 0 \tag{B.13}$$

Thus equation (B.12b) reads

$$\frac{dT_1^{ext}}{dt} = \frac{\left(k(\varphi_0^{ext})\, T_{1,x}^{ext}\right)_{,x}}{Pe} \tag{B.14}$$

In the following of this study, we derive the expressions for $\{T_1\}$ (*cf.* section B.2.13), $[\![T_1]\!]$ (*cf.* section B.2.9) and $[\![q_1]\!]$ (*cf.* section B.2.12) as a function of the solution at order $O(1)$ that are necessary and sufficient in order to solve this equation.

B.2.3 Order parameter profile at order $O(1)$

For the order parameter we get the following second order nonlinear differential equation in φ_0.

$$\partial_\varphi W(\varphi_0) = \varphi_0'' \tag{B.15}$$

It is worth noting that this equation is satisfied at two-phase planar equilibrium. Multiplying equation (B.15) by φ_0' and integrating over the domain leads to

$$\int \partial_\varphi W\, \varphi_0'\, d\bar{x} = \frac{\left(\varphi_0'\right)^2}{2} \tag{B.16}$$

Finally we get

$$2\left(W(\varphi_0(\bar{x})) - W(\varphi_0(\infty))\right) = \left(\varphi_0'\right)^2 - \left(\varphi_0'(\infty)\right)^2$$

As soon as the function W satisfies the set of properties (3.40), we have $W(\varphi_0(+\infty)) = W(\varphi_0(-\infty)) = 0$. Using the matching condition (B.9a) yields

$$2\,W(\varphi_0(\bar{x})) = \left(\varphi_0'\right)^2 \tag{B.17}$$

If the function W is given by (3.42), a classical integration yields

$$\varphi_0 = \frac{1 + [\![\varphi]\!]\,\tanh(3\,\bar{x})}{2} \tag{B.18}$$

where $[\![\varphi]\!]$ denotes for the outer phase field jump.

It is worth pointing out that the leading order profile for the phase field is exactly the profile at two-phase planar equilibrium. This property is numerically attractive since it allows to control the out of equilibrium phase field profile by letting ε tends to zero.

B.2.4 Temperature profile at order $O(1)$

At leading order, the equation of temperature reads

$$\left(k(\varphi_0)T_0'\right)' = 0 \tag{B.19}$$

It yields the uniformity of $k(\varphi_0)T_0'$. Using the matching condition (B.7a), $T_0(\bar{x})$ is therefore uniform and its value remains to be specified through the analysis of higher order. This uniform temperature is denoted T_0^i in the following. This result supposes that in view of the external problem, temperature is continuous. It means that using (B.7b) we get

$$\lim_{x\to x_i^+} T_0^{ext} = \lim_{x\to x_i^-} T_0^{ext} = \{T_0\} = T_0(\bar{x}) = T_0^i \tag{B.20a}$$

$$[\![T_0]\!] = 0 \tag{B.20b}$$

Equation (B.20b) specifies a part of the jump condition for the thermal outer problem at leading order. However, this is not sufficient in order to solve this problem since no information is available neither on heat flux jump nor on the value for T_0^i. Informations on these quantities can only be inherited from the study of next orders equations for the inner problem which is the subject of study of the following sections.

The main result of the resolution of the leading order inner balance of entropy is that temperature can be viewed as continuous for the equivalent sharp interface model. This result is consistent with some classical kinetic relations as studied in section 7 and has therefore important consequences on the property of the equivalent sharp interface model.

B.2.5 System of equations for the inner problem at order $O(\varepsilon)$

The corresponding system of equations read

$$\mathcal{D}\,\varphi_0' = \alpha\left[-\varphi_1'' + \partial_{\varphi^2} W(\varphi_0)\,\varphi_1 - T_0^i\,\partial_\varphi \nu(\varphi_0)\right] \tag{B.21a}$$

$$\frac{\left(k(\varphi_0)T_1'\right)'}{Pe} = -\left(1 + T_0^i\right)\mathcal{D}\,\partial_\varphi \nu(\varphi_0)\,\varphi_0' - \frac{\mathcal{D}^2}{\alpha}\left(\varphi_0'\right)^2 \tag{B.21b}$$

where we have used that according to (B.20a), $T_0' = 0$. The value of the interface temperature at leading order T_0^i, that is still undetermined, appears in equation (B.21a). This property is used in the following section in order to determine its value. Then we study in section B.2.7 the equation (B.21a) in order to determine φ_1 and thus the leading order deformation of the phase field solution with respect to the planar equilibrium solution that equals φ_0 as shown in section B.2.3. In order to be able to solve the thermal outer problem at leading order, it is necessary to determine the value for $[\![q_0]\!]$, which according to the matching condition (B.8a) is related to the knowledge of T_1'. Therefore we study in section B.2.8 the equation (B.21b) in order to determine $[\![q_0]\!]$. The leading order spatial variation of the temperature across the interface are associated to $T_1(\bar{x})$ since $T_0' = 0$. In the case of infinite α, it is shown in section 7 that the leading order interface entropy production is related to the value of $[\![T_1]\!]$ and $\{T_1\}$. Therefore we study in section B.2.9 the equation (B.21b) in order to determine $[\![T_1]\!]$. In section B.2.10 we study the leading order inner temperature profile $T_1(\bar{x})$.

B.2.6 Interface temperature T_0^i

In order to determine T_0^i independently from the knowledge of φ_1, we use some properties of equation (B.21a)[1]. Equation (B.21a) is a second order ordinary linear differential equation for φ_1. The solution of such an equation is the sum of a particular solution and a linear combination of two independent solutions of its homogeneous part. Since φ_0 satisfies (B.15), by differentiating this equation with respect to $\bar{x}$, we get

$$\varphi_0''' = \partial_{\varphi^2} W(\varphi_0)\, \varphi_0' \tag{B.22}$$

This relation shows that φ_0' is solution of the homogeneous part of equation (B.21a).

Let us define the linear operator $\mathbf{L}$ on the set of functions $\mathrm{f} : \mathbb{R} \to \mathbb{R}$ as follows

$$\mathbf{L}(\mathrm{f}) = \partial_{\varphi^2} W(\varphi_0)\, \mathrm{f} - \mathrm{f}'' \tag{B.23}$$

Equation (B.22) implies that φ_0' is in the kernel of $\mathbf{L}$. Let us define a scalar product on the domain of definition of $\mathbf{L}$ by

$$\int_{-\infty}^{+\infty} \mathrm{f}_1 \cdot \mathrm{f}_2 d\bar{x}$$

For any function f_1 in the kernel of $\mathbf{L}$ and for any function f_2 in the domain of definition of $\mathbf{L}$, the following relation is satisfied

$$\begin{aligned} \int_{-\infty}^{+\infty} \mathrm{f}_1 \cdot \mathbf{L}(\mathrm{f}_2)\, d\bar{x} &= \int_{-\infty}^{+\infty} \mathbf{L}(\mathrm{f}_1) \cdot \mathrm{f}_2\, d\bar{x} \\ &= 0 \end{aligned} \tag{B.24}$$

Thus using relation (B.24) with $\mathrm{f}_1 = \varphi_0'$ and $\mathrm{f}_2 = \varphi_1$ it is possible to determine the value of T_0^i. Indeed, let us multiply equation (B.21a) by φ_0' and integrate between minus and plus infinity. Accounting for the relation (B.24), yields

$$\int_{-\infty}^{+\infty} \mathcal{D}\, \varphi_0'^2\, d\bar{x} = -\int_{-\infty}^{+\infty} \alpha\, T_0^i\, \partial_\varphi \nu(\varphi_0)\, \varphi_0'\, d\bar{x} \tag{B.25}$$

Let us introduce the constant $\mathcal{A}$ defined by

$$\mathcal{A} \triangleq -\frac{\int_{-\infty}^{+\infty} \varphi_0'^2\, d\bar{x}}{\int_{-\infty}^{+\infty} \partial_\varphi \nu(\varphi_0)\, \varphi_0'\, d\bar{x}}$$

Equation (B.25) reads therefore

$$T_0^i = \frac{\mathcal{A}\,\mathcal{D}}{\alpha}$$

Let us now study the value of $\mathcal{A}$. Using the notation introduced while determining $\varphi_0(\bar{x})$ in section B.2.3, we write

$$\int_{-\infty}^{+\infty} \partial_\varphi \nu(\varphi_0)\, \varphi_0'\, d\bar{x} = [\![\varphi]\!]$$

Let us study the value of $\int_{-\infty}^{+\infty} \varphi_0'^2 d\bar{x}$. We introduce the change of variable valid according to the expression (B.18) for $\varphi_0(\bar{x})$

$$\begin{aligned} \bar{x} &\leftrightarrow \varphi_0 \\ \varphi_0' d\bar{x} &\leftrightarrow d\varphi_0 \end{aligned} \tag{B.26}$$

[1] This analytical handling of differential equations is currently known as the solvability theory

According to equation (B.17), we have

$$\begin{aligned}\int_{-\infty}^{+\infty} \varphi_0'^2 d\bar{x} &= \int_{-\infty}^{+\infty} \varphi_0' \left(\varphi_0' d\bar{x}\right) \\ &= [\![\varphi]\!] \int_{-\infty}^{+\infty} \sqrt{2\,W(\varphi_0)}\,\left(\varphi_0' d\bar{x}\right) \\ &= [\![\varphi]\!] \int_{\varphi_0(-\infty)}^{\varphi_0(+\infty)} \sqrt{2\,W(\varphi)}\, d\varphi \\ &= \int_0^1 \sqrt{2\,W} d\varphi\end{aligned}$$

While W satisfies (3.40), we get

$$\int_{-\infty}^{+\infty} \varphi_0'^2 d\bar{x} = 1 \tag{B.27}$$

Thus

$$\mathcal{A} \hat{=} -[\![\varphi]\!] \tag{B.28}$$

$$T_0^i = -\frac{[\![\varphi]\!]\,\mathcal{D}}{\alpha} \tag{B.29}$$

For a given transformation (say solidification or liquefaction), the sign of $\mathcal{D}$ depends on the relative position of the phases too. This finally gives a result for T_0^i dependent only of the transformation. For a solidification, T_0^i is positive and for a liquefaction it is negative. The relation (B.29) between T_0^i and $\mathcal{D}$ is not sufficient to solve the outer problem, since $\mathcal{D}$ is still undetermined. Solving the outer problem at leading order in temperature supposes to determine the jump in the first spatial derivative at the location of the interface.

B.2.7 Phase-field inner profile at order $O(\varepsilon)$, $\varphi_1(\bar{x})$

The determination of the first order phase-field profile gives an estimation of the out of equilibrium deformation of the interface and its dependence with α. In this section, we solve the differential equation (B.21a) using the variation of parameters.

Using the expression (B.29) for T_0^i yields for equation (B.21a)

$$\mathcal{D}\,\varphi_0' = \alpha\left[-\varphi_1'' + \partial_{\varphi^2} W(\varphi_0)\,\varphi_1 - \frac{\mathcal{D}\,[\![\varphi]\!]\partial_\varphi \nu(\varphi_0)}{\alpha}\right]$$

Let us take benefit of some properties of the equation already derived in the previous section while studying the value of T_0^i. Since we know that φ_0' is a solution of the homogeneous part of equation (B.21a), we introduce Y_0

$$Y_0 \hat{=} \frac{\varphi_1}{\varphi_0'} \tag{B.30}$$

Thus the equation (B.15) in φ_1 is equivalent to the following equation in Y_0

$$-\varphi_0''' Y_0 - 2\,\varphi_0'' Y_0' - \varphi_0' Y_0'' + \partial_{\varphi^2} W(\varphi_0)\,\varphi_0' Y_0 = \frac{\mathcal{D}}{\alpha}\left[\varphi_0' - [\![\varphi]\!]\,\partial_\varphi \nu\,(\varphi_0)\right]$$

where the expression (B.29) has been used to express T_0^i. Finally using (B.22)

$$-2\,\varphi_0'' Y_0' - \varphi_0' Y_0'' = \frac{\mathcal{D}}{\alpha}\left[\varphi_0' - [\![\varphi]\!]\,\partial_\varphi \nu(\varphi_0)\right] \tag{B.31}$$

Equation (B.31) is a linear ordinary differential equation in Y_0. Since the following identity holds

$$\left[\frac{1}{\left(\varphi_0'\right)^2}\right]' = -\frac{2\,\varphi_0''}{\left(\varphi_0'\right)^3}$$

a solution of its homogeneous part is

$$Y_0' = \frac{1}{\left(\varphi_0'\right)^2}$$

As a consequence, the function $\varphi_0' \int d\bar{x}/(\varphi_0')^2$ is a solution of the homogeneous part of equation (B.21a). Therefore, in order to determine a solution Y_0 of equation (B.31) let us take benefit of this result and introduce Y_1 defined as

$$Y_0' = \frac{Y_1}{\left(\varphi_0'\right)^2} \tag{B.32}$$

And the equation (B.31) reads with the unknown Y_1

$$\frac{Y_1'}{\varphi_0'} = -\frac{\mathcal{D}}{\alpha}\left[\varphi_0' - [\![\varphi]\!]\,\partial_\varphi \nu(\varphi_0)\right]$$

It is then possible to integrate this differential equation. Let us now denote $\bar{Y}_1$ as this solution. The corresponding solution of the equation (B.31) in Y_0, $\bar{Y}_0$ reads

$$\bar{Y}_0 = \int \frac{\bar{Y}_1}{\left(\varphi_0'\right)^2}\, d\bar{x}$$

and Φ_1 given by

$$\Phi_1 = \bar{Y}_0\, \varphi_0'$$

is a solution of equation (B.21a) that could be rewritten as

$$\Phi_1 = -\frac{\mathcal{D}}{\alpha}\,\varphi_0' \int \frac{\int \left(\varphi_0'^2 - [\![\varphi]\!]\,\nu'(\varphi_0)\right) d\bar{x}}{\left(\varphi_0'\right)^2}\, d\bar{x} \tag{B.33}$$

Since (i) Φ_1 is a particular solution of equation (B.21a), and (ii) φ_0' and $\varphi_0' \int d\bar{x}/(\varphi_0')^2$ are two independent[2] solutions of its homogeneous part , the solution for φ_1 is necessarily

$$\varphi_1 = \Phi_1 + \lambda_1^1\, \varphi_0' + \lambda_1^2\, \varphi_0' \int \frac{d\bar{x}}{\left(\varphi_0'\right)^2} \tag{B.34}$$

λ_1^1 and λ_1^2 are two reals whose values which are to be determined.

Let us determine these two constants Let us show that the function $\varphi_0' \int \frac{d\bar{x}}{\left(\varphi_0'\right)^2}$ does not verify the boundary condition for φ_1 in $\pm\infty$. Let us find an equivalent of $\varphi_0' \int \frac{d\bar{x}}{\left(\varphi_0'\right)^2}$. We make the change of variable defined by (B.26). Thus

$$\int \frac{d\bar{x}}{\left(\varphi_0'\right)^2} = \int \frac{d\varphi_0}{\left(\varphi_0'\right)^3}$$

Since according to equation (B.17)

$$\varphi_0' \propto \sqrt{W(\varphi_0)}$$

let us define n as

$$W(\varphi) \underset{\varphi_0(\pm\infty)}{\sim} \left(\varphi - \varphi_0^{\pm\infty}\right)^n$$

Thus

$$\int \frac{d\bar{x}}{\left(\varphi_0'\right)^2} \sim \left(\varphi - \varphi_0^{\pm\infty}\right)^{-3n/2+1}$$

and

$$\varphi_0' \int \frac{d\bar{x}}{\left(\varphi_0'\right)^2} \sim \left(\varphi - \varphi_0^{\pm\infty}\right)^{1-n/2}$$

[2] it can be shown easily by considering the integral over $\mathbb{R}$ of their product that it is nonzero

So for $n = 2$ or superior (which is the minimum required to ensure that W satisfies (3.40) *i.e.* $W(\varphi_0^{ext}) = \partial_\varphi W(\varphi_0^{ext}) = 0$), $\varphi_0' \int d\bar{x}/\left(\varphi_0'\right)^2$ has a non-zero limit in $\pm\infty$. Let us remark that in the case where the expression for W is given by (3.42) $n = 2$. According to our study of the order $O(\varepsilon)$ AC equation (B.12a) of the outer problem in section B.2.2, $\varphi_1^{ext} = 0$. Moreover, since $\varphi_0^{ext} = 1/2 \pm 1/2$, we have $\lim_{x\to x_i^\pm} \bar{x}\,\varphi_0'^{ext} = 0$. Therefore according to the matching condition (B.9d), φ_1 must satisfy $\lim_{\bar{x}\to\pm\infty} \varphi_1 = 0$. It is shown in the following that $\lim_{\bar{x}\to\pm\infty} \Phi_1 + \lambda_1^1 \varphi_0' = 0$. The function $\varphi_0' \int d\bar{x}/\left(\varphi_0'\right)^2$ does not have a zero limit in $\bar{x} = \pm\infty$ since n is obviously superior or equal to 2. This implies that $\lambda_1^2 = 0$.

Let us study the constant λ_1^1. Since

$$\varphi_0' \quad = \quad [\![\varphi]\!]\,\frac{3}{2}\,(1 - \tanh^2(3\,\bar{x}))$$

this function does not satisfy the constraint concerning the interface location, $\varphi(\bar{x} = 0) = \varphi_0(\bar{x} = 0) = 1/2$. It is shown in the following that $\Phi(0) = 0$, therefore $\lambda_1^1 = 0$. The two constants λ_1^1 and λ_1^2 are thus determined.

The next step consists in obtaining an analytical formulation for the function Φ_1 appearing on the right hand side of the general expression (B.34) for $\varphi_1(\bar{x})$. In the case where the expression for $\nu(\varphi)$ is given by P_5 (3.60c)it satisfies

$$\frac{d\nu}{d\varphi} = \frac{5}{3} W(\varphi)$$

and solving the differential equation (B.33) leads to

$$\Phi_1(\bar{x}) = \frac{[\![\varphi]\!]}{24}\,\frac{\mathcal{D}}{\alpha}\,\ln(\cosh(3\,\bar{x}))\,(1 - \tanh^2(3\,\bar{x})) \tag{B.35}$$

The even function $-\alpha\,\Phi_1/\mathcal{D}(\bar{x})$ is represented on figure B.2. Φ_1 corresponds to a thinning of the order parameter profile on the side of created phase and a thickening on the opposite side. In the case where the expression for

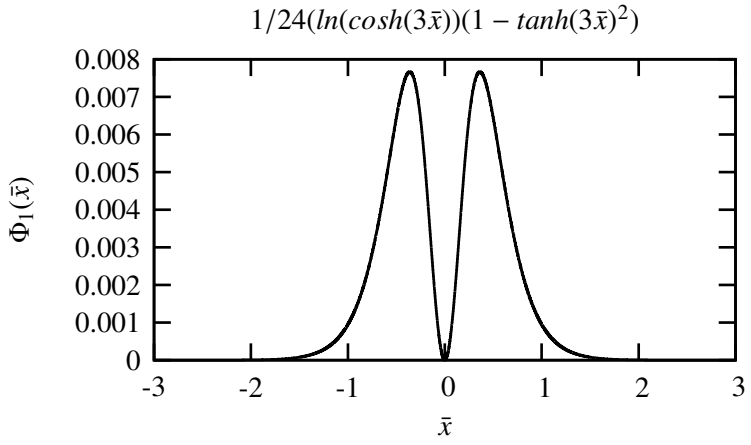

Figure B.2: function Φ_1

$\nu(\varphi)$ is given by the polynomial P_3 (3.60b) the following identity is satisfied

$$\left(\frac{dP_3}{d\varphi}\right)^2 = 2\,W \tag{B.36}$$

and therefore using (B.17) and the identity (B.5)

$$\varphi_0'^2 - [\![\varphi]\!]\,P_3'(\varphi_0) = \varphi_0'\left(\varphi_0' - [\![\varphi]\!]\,\partial_\varphi P_3(\varphi_0)\right) = [\![\varphi]\!]\,\varphi_0'\left(\sqrt{2\,W(\varphi_0)} - \partial_\varphi P_3(\varphi_0)\right) = 0$$

So equation (B.21a) becomes homogeneous and it implies that the function $\Phi_1 \equiv 0$

Introduction to the study of the order $O(\varepsilon)$ balance of entropy (equation (B.21b)) of the inner problem

In this section we study the order $O(\varepsilon)$ entropy equation (B.21b) of the inner problem in order to get an expression for $[\![q_0]\!]$ which is necessary to solve the order $O(1)$ outer thermal problem, $[\![T_1]\!]$ and $T_1(\bar{x})$ which are the leading order solutions for the inner problem as soon as $\mathcal{D} = 0$ or in the case of infinite α. The value of $\{T_1\}$ is, as well as we determined $\{T_0\}$, related to the study of next order (*i.e.* $O(\varepsilon^2)$) *AC* equation and is done in another section.

B.2.8 The leading order term for the jump in heat flux, $[\![q_0]\!]$

According to the matching condition (B.7c), the gradient of outer temperature at order $O(1)$ $T_0^{ext\prime}$ is related to the value of the gradient of inner temperature at order $O(\varepsilon)$ T_1'. Therefore it is necessary to study the order $O(\varepsilon)$ equation for the inner temperature (B.21b) in order to determine the leading order jump in heat flux $[\![q_0]\!]$. This equation reads

$$\left(k(\varphi_0)T_1'\right)' = -\left(1 + T_0^i\right)\,\mathcal{D}\,Pe\,\partial_\varphi \nu(\varphi_0)\,\varphi_0' - \frac{Pe\,\mathcal{D}^2}{\alpha}\left(\varphi_0'\right)^2$$

Let us introduce the constant of integration Φ_{th} defined as (*cf.* the integration of equation (B.21b))

$$\begin{aligned} -\Phi_{th} \quad &\hat{=} \quad k(\varphi_0)\,T_1' + \mathcal{D}\,Pe\left(1 + T_0^i\right)\nu(\varphi_0) + \frac{Pe\,\mathcal{D}^2}{\alpha}\int^{\bar{x}} \varphi_0'^2 d\xi \\ &= \quad k(\varphi_0)\,T_1' + \left(\mathcal{D}\,Pe - [\![\varphi]\!]\,\frac{Pe\,\mathcal{D}^2}{\alpha}\right)\nu(\varphi_0) + \frac{Pe\,\mathcal{D}^2}{\alpha}\int^{\bar{x}} \varphi_0'^2 d\xi \end{aligned} \tag{B.37}$$

the second expression (where $\mathcal{D}$ is used instead of T_0^i, *cf.* equation (B.29)) is used when results concerning the kinetic relation are targeted in the section 7.

Using the equality of the first expression for Φ_{th} in $\bar{x} = \pm\infty$ yields

$$k_+\,T_1'(+\infty) - k_-\,T_1'(-\infty) = -\,[\![\varphi]\!]\left(1 + T_0^i\right)\,Pe\,\mathcal{D} - \frac{Pe\,\mathcal{D}^2}{\alpha}$$

where we have used the matching condition (B.9b) and the identity (B.5) and equation (B.27). Using the matching condition (B.7c), it yields

$$k_+\,T_0^{ext\prime}(x_i^+) - k_-\,T_0^{ext\prime}(x_i^-) = -[\![\varphi]\!]\,\left(1 + T_0^i\right)\,Pe\,\mathcal{D} - \frac{Pe\,\mathcal{D}^2}{\alpha} \tag{B.38}$$

Therefore

$$[\![q_0]\!] = [\![\varphi]\!]\,\left(1 + T_0^i\right)\,Pe\,\mathcal{D} + \frac{Pe\,\mathcal{D}^2}{\alpha} \tag{B.39}$$

that is used to evaluate the expression for the interface entropy production (kinetic relation) in section 7.3. This relation is also used to provide an enclosed system of equation (*i.e.* to provide the interface boundary condition in addition to $\left[\!\left[T_0^{ext}\right]\!\right] = 0$) for the outer thermal problem at leading order. By using the equation (B.29) the undetermined constant $\mathcal{D}$ disappears, we obtain

$$[\![q_0]\!] = -T_0^i\,Pe\,\alpha \tag{B.40}$$

The hereinabove relation yields

$$[\![q_0]\!] = [\![\varphi]\!]\mathcal{D}\,Pe$$

which is the non-dimensional equivalent to the classical relation

$$[\![q]\!] = \Gamma\,\mathcal{L}$$

We are now in position to determine the spatial variations of $T_1(\bar{x})$ and therefore the value for $[\![T_1]\!]$.

B.2.9 Determination of $[\![T_1]\!]$

Let us study the expression for $T_1(\bar{x})$. Equation (B.37) provides an expression for $T_1'(\bar{x})$. Using the change of variable (B.26), and equations (B.17) and (B.36), we have

$$\int^{\bar{x}} \varphi_0'^2 d\xi = \int^{\varphi_0(\bar{x})} \varphi_0' d\varphi = \int^{\varphi_0(\bar{x})} [\![\varphi]\!] \sqrt{2\,W} d\varphi = [\![\varphi]\!] P_3(\varphi_0)$$

Let us express the constant Φ_{th} using (B.37) in $\bar{x} = \pm\infty$ and the fact that $P_3\pm = \nu\pm$

$$\Phi_{th} = -k(\pm) T_0^{ext'}(x_i\pm) - \nu(\varphi\pm)\, Pe\, \mathcal{D} \tag{B.41}$$

This equation is a balance of energy at the interface location, Φ_{th} represents therefore the energy flux at the interface. By integration of (B.37) between $\bar{x}$ and 0 we get

$$T_1(\bar{x}) - T_1(0) = -\int_0^{\bar{x}} \frac{\Phi_{th}}{k(\varphi_0)}\, du - \mathcal{D}\, Pe \int_0^{\bar{x}} \frac{\nu}{k}(\varphi_0)\, du + [\![\varphi]\!] \frac{Pe\, \mathcal{D}^2}{\alpha} \int_0^{\bar{x}} \frac{(\nu - P_3)}{k}(\varphi_0)\, du \tag{B.42}$$

Let us note that this expression for $T_1(\bar{x})$ is used in the following for the study of the T_1 profile. In order to study the jump $[\![T_1]\!]$ we use the following equation to get

$$\begin{aligned} T_1(\bar{x}) - T_1(-\bar{x}) \;=\; & -\int_{-\bar{x}}^{\bar{x}} \frac{\Phi_{th}}{k(\varphi_0)}\, du - \mathcal{D}\, Pe \int_{-\bar{x}}^{\bar{x}} \frac{\nu}{k}(\varphi_0)\, du \\ & + [\![\varphi]\!] \frac{Pe\, \mathcal{D}^2}{\alpha} \int_{-\bar{x}}^{\bar{x}} \frac{(\nu - P_3)}{k}(\varphi_0)\, du \end{aligned}$$

Using the two expressions for Φ_{th} (*cf.* equation (B.41)), we add to the RHS of the above equation

$$\pm \int_0^{\pm\bar{x}} \left(\frac{-\Phi_{th}}{k^{\pm}} - T_0^{ext'}(x_i\pm) - \mathcal{D}\, Pe \left(\frac{\nu}{k}\right)^{\pm} \right) du = 0$$

it yields

$$\begin{aligned} & T_1(\bar{x}) + \bar{x}\, T_0^{ext'}(x_i+) - T_1(-\bar{x}) - \bar{x}\, T_0^{ext'}(x_i-) \\ & = \\ & -\Phi_{th} \left[\int_0^{\bar{x}} \left(\frac{1}{k(\varphi_0)} - \frac{1}{k_+} \right) du + \int_{-\bar{x}}^{0} \left(\frac{1}{k(\varphi_0)} - \frac{1}{k_-} \right) du \right] \\ & -\mathcal{D}\, Pe \left[\int_0^{\bar{x}} \left(\frac{\nu}{k}(\varphi_0) - \frac{\nu}{k_+} \right) du + \int_{-\bar{x}}^{0} \left(\frac{\nu}{k}(\varphi_0) - \frac{\nu}{k_-} \right) du \right] \\ & + [\![\varphi]\!] \frac{Pe\, \mathcal{D}^2}{\alpha} \left[\int_0^{\bar{x}} \frac{(\nu - P_3)}{k}(\varphi_0)\, du + \int_{-\bar{x}}^{0} \frac{(\nu - P_3)}{k}(\varphi_0)\, du \right] \end{aligned}$$

Taking the limit of the hereinabove equation when $\bar{x} \to +\infty$ and using the matching condition (B.7d) and the fact that $\nu(\pm\infty) = P_3(\pm\infty)$, gives

$$[\![T_1]\!] = -\Phi_{th} \left(\frac{1}{k(\varphi_0)} \right)^{\bar{ex}} - \mathcal{D}\, Pe \left(\frac{\nu}{k}(\varphi_0) \right)^{\bar{ex}} + [\![\varphi]\!] \frac{Pe\, \mathcal{D}^2}{\alpha} \left(\frac{\nu - P_3}{k}(\varphi_0) \right)^{\bar{ex}} \tag{B.43}$$

where $\cdot^{\bar{ex}}$ denotes for inner excess quantities

$$q^{\bar{ex}}_{\bar{x}_i} \,\hat{=}\, \int_{\bar{x}_i}^{+\infty} \left(q(\bar{x}) - q^{ext}(x_i+) \right) d\bar{x} + \int_{-\infty}^{\bar{x}_i} \left(q(\bar{x}) - q^{ext}(x_i-) \right) d\bar{x}$$

where $\bar{x}_i = 0$ in the present case. It is worth noting that the expression for $[\![T_1]\!]$ is indeed dependent on the choice for $\bar{x}_i$. It has been shown that while the bulk phase values are well determined, the jump of a given quantity, such as φ_0^{ext}, is well defined. However, for a field which is non-uniform in the bulk domains, this is no more the case. The non-uniformity of $T_0^{ext}(x)$ is associated with the jump in T_1 as revealed by the matching conditions (B.7). This point is the subject of study of the last paragraph of section A.1.

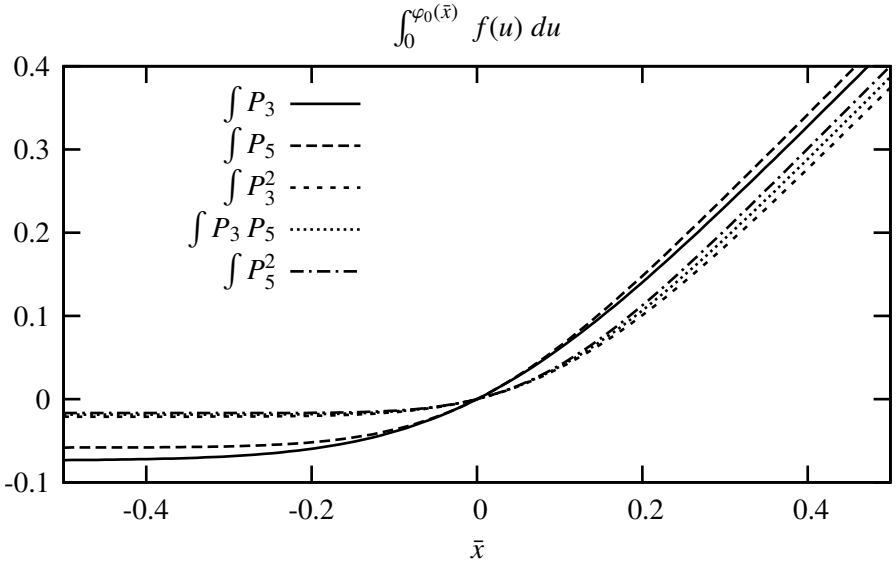

Figure B.3: Different functions entering the expression of $T_1(\bar{x})$ for different choices for ν and ν_k

B.2.10 Study of the profile of $T_1(\bar{x})$

According to the matching conditions, it is straightforward that asymptotically ($\bar{x} \to \pm\infty$), T_1 is linear in $\bar{x}$. We now illustrate the influence of the choice for $k(\varphi)$ on $T_1(\bar{x})$. Let us consider the expression (B.42) for $T_1(\bar{x})$. For the sake of simplicity, we consider the function $1/k(\varphi)$ to be interpolated by a function ν_k, *i.e.*

$$k(\varphi) = \frac{k_l}{1 + (k_l - 1)\ \nu_k(\varphi)}$$

and consider that it can be chosen either as P_3 or P_5 (*cf.* equations (3.60)). Then $T_1(\bar{x})$ reads (*cf.* equation (B.42))

$$\begin{aligned} T_1(\bar{x}) \;=\; & T_1(0) - \frac{\Phi_{th}}{k_l}\bar{x} - \Phi_{th}\,(1 - 1/k_l) \int_0^{\bar{x}} \nu_k(\varphi_0)\,du + \frac{1}{k_l}\left[\llbracket\varphi\rrbracket\,\frac{Pe\,\mathcal{D}^2}{\alpha} - \mathcal{D}\,Pe\right] \int_0^{\bar{x}} \nu(\varphi_0)\,du \\ & -\llbracket\varphi\rrbracket\,\frac{Pe\,\mathcal{D}^2}{\alpha k_l} \int_0^{\bar{x}} P_3(\varphi_0)\,du \\ & +\left[\llbracket\varphi\rrbracket\,\frac{Pe\,\mathcal{D}^2}{\alpha} - \mathcal{D}\,Pe\right](1 - 1/k_l) \int_0^{\bar{x}} \nu(\varphi_0)\nu_k(\varphi_0)\,du - \llbracket\varphi\rrbracket\,\frac{Pe\,\mathcal{D}^2}{\alpha k_l} \int_0^{\bar{x}} P_3(\varphi_0)\,\nu_k(\varphi_0)\,du \end{aligned} \tag{B.44}$$

The different functions appearing in the previous equation are represented on figure B.3 where ν_k, as well as ν have been assumed to equal either P_3or P_5. It is worth noting that this expression is simplified when the conductivity is considered as uniform ($k_l = 1$), it yields

$$\begin{aligned} T_1(\bar{x}) \;=\; & T_1(0) - \Phi_{th}\bar{x} + \left[\llbracket\varphi\rrbracket\,\frac{Pe\,\mathcal{D}^2}{\alpha} - \mathcal{D}\,Pe\right] \int_0^{\bar{x}} \nu(\varphi_0)\,du \\ & -\llbracket\varphi\rrbracket\,\frac{Pe\,\mathcal{D}^2}{\alpha} \int_0^{\bar{x}} P_3(\varphi_0)\,du - \llbracket\varphi\rrbracket\,\frac{Pe\,\mathcal{D}^2}{\alpha} \int_0^{\bar{x}} P_3(\varphi_0)\,\nu_k(\varphi_0)\,du \end{aligned} \tag{B.45}$$

These analytical results are compared with numerical results in section 8.1.2.

B.2.11 System of inner equations at order $O(\varepsilon)^2$

In order to determine $T_1(0)$, we use the next order equations. These are given by

$$\mathcal{D}\,\varphi_1' = \alpha\left[\frac{\varphi_1^2}{2}\partial_{\varphi^3}W(\varphi_0) + \varphi_2\partial_{\varphi^2}W(\varphi_0) - \varphi_2'' - T_0^i\varphi_1\partial_{\varphi^2}\nu(\varphi_0) - T_1\partial_\varphi\nu(\varphi_0)\right] \tag{B.46a}$$

$$\begin{aligned}-\mathcal{D}\,c_P(T_0^i)\,T_1' &= \frac{1}{Pe}\left(k(\varphi_0)\,T_2' + \left(\partial_\varphi k(\varphi_0)\,\varphi_1\right)'\,T_1'\right)' \\ &\quad +\mathcal{D}\left(\partial_\varphi\nu(\varphi_0)\varphi_1' + \partial_{\varphi^2}\nu(\varphi_0)\,\varphi_1\,\varphi_0'\right) + 2\,\frac{\mathcal{D}^2\,Pe}{\alpha}\,\varphi_0'\,\varphi_1'\end{aligned} \tag{B.46b}$$

B.2.12 Determination of $[\![q_1]\!]$

Let us consider the integration of equation (B.46b) between $\bar{x} = +\infty$ and $\bar{x} = -\infty$. Using the fact that

$$\lim_{\bar{x}=\pm\infty}\varphi_1 = \lim_{x=x_i\pm}\varphi_1^{ext} = 0$$

we get,

$$\begin{aligned}k(\varphi_0)\,T_2'(+\infty) - k(\varphi_0)\,T_2'(-\infty) &= c_P(T_0^i)\,\mathcal{D}\,Pe\,[T_1]_{-\infty}^{+\infty} \\ &\quad -Pe\,\mathcal{D}\int_{-\infty}^{+\infty}\left(\partial_\varphi\nu(\varphi_0)\,\varphi_1' + \partial_{\varphi^2}\nu(\varphi_0)\,\varphi_0'\,\varphi_1\right)\,d\bar{x} \\ &\quad -2\,\frac{\mathcal{D}^2\,Pe}{\alpha}\int_{-\infty}^{+\infty}\varphi_0'\,\varphi_1'\,d\bar{x}\end{aligned}$$

According to the equation (B.11) where we have taken the limit at $x \to x_i\pm$,

$$-\mathcal{D}\,c_P(T_0^i)\,T_0^{ext'}(x_i\pm) = Pe\,k(\varphi_0^{ext})\,T_0^{ext''}(x_i\pm)$$

Taking into account the matching condition (B.7d) for $T_1(\pm\infty)$ and the expression (B.8b) for $[\![q_1]\!]$ yields therefore

$$[\![q_1]\!] = c_P(T_0^i)\,\mathcal{D}\,Pe\,[\![T_1]\!] - Pe\,\mathcal{D}\int_{-\infty}^{+\infty}\left(\partial_\varphi\nu(\varphi_0)\,\varphi_1' + \partial_{\varphi^2}\nu(\varphi_0)\,\varphi_0'\,\varphi_1\right)\,d\bar{x} - 2\,\frac{\mathcal{D}^2\,Pe}{\alpha}\int_{-\infty}^{+\infty}\varphi_0'\,\varphi_1'\,d\bar{x}$$

According to our study of the even or odd property of functions φ_0 (*cf.* table B.1), φ_1 and combinations, it can be shown that the two integrals appearing on the RHS of the above expression for $[\![q]\!]_1$ are identically zero, therefore

$$[\![q_1]\!] = c_P(T_0^i)\,\mathcal{D}\,Pe\,[\![T_1]\!] \tag{B.47}$$

B.2.13 Determination of $T_1(0)$ and of $\{T_1\}$

We first determine the relation between $\{T_1\}$ and $T_1(0)$ by solving the entropy equation at order $O(\varepsilon)$ (B.42) and then determine the value of $T_1(0)$ by integration of the order $O(\varepsilon^2)$ *AC* equation (B.46a).

The mean value $\{T_1\}$ By definition, the middle value of T_1^{ext}, namely $\{T_1\}$ reads

$$\{T_1\} = \frac{T_1^{ext}(x_i+) + T_1^{ext}(x_i-)}{2}$$

Therefore using matching condition (B.7d), it reads

$$\{T_1\} = \lim_{\bar{x}\to\infty}\frac{T_1(\bar{x}) + T_1(-\bar{x}) - \bar{x}\left(T_0^{ext'}(x_i+) + T_0^{ext'}(x_i+)\right)}{2}$$

Using equation (B.42), we therefore have

$$\begin{aligned}\{T_1\} &= T_1(0) - \frac{\Phi_{th}}{2}\left[\int_0^{+\infty}\left(\frac{1}{k(\varphi_0)} - \frac{1}{k_+}\right)\,du + \int_0^{-\infty}\left(\frac{1}{k(\varphi_0)} - \frac{1}{k_-}\right)\,du\right] \\ &\quad -\frac{Pe\,\mathcal{D}}{2}\left[\int_0^{+\infty}\left(\frac{\nu}{k}(\varphi_0) - \frac{\nu}{k_+}\right)\,du + \int_0^{-\infty}\left(\frac{\nu}{k}(\varphi_0) - \frac{\nu}{k_-}\right)\,du\right] \\ &\quad +[\![\varphi]\!]\,\frac{Pe\,\mathcal{D}^2}{2\,\alpha}\left[\int_0^{+\infty}\frac{(\nu - P_3)}{k}(\varphi_0)\,du + \int_0^{-\infty}\frac{(\nu - P_3)}{k}(\varphi_0)\,du\right]\end{aligned} \tag{B.48}$$

function	odd	even	function	odd	even	function	odd	even
$\varphi_1 = \Phi_1$		✓	$\partial_{\varphi^3} W(\varphi_0)$	✓		φ_1'	✓	
φ_1^2		✓	$\varphi_1^2\, \partial_{\varphi^3} W(\varphi_0)$	✓		$\varphi_1^2\, \partial_{\varphi^3} W(\varphi_0)\varphi_0'$	✓	
$\partial_\varphi \nu(\varphi_0)$		✓	$\partial_{\varphi^2} \nu(\varphi_0)$	✓		$\varphi_1\, \partial_{\varphi^2} \nu(\varphi_0)\varphi_0'$	✓	
φ_0'		✓	$\varphi_1\, \partial_{\varphi^2} \nu(\varphi_0)$	✓		$\partial_\varphi \nu(\varphi_0)\, \varphi_0'$		✓

Table B.1: Table of even and odd properties of inner profiles

where we have used the fact that $\nu\pm = P_3\pm$.

The constant of integration $T_1(0)$ has to be determined

Determination of $T_1(0)$ In order to determine $T_1(0)$, it is necessary to study the order $O(\varepsilon^2)$ *AC* equation (B.46a). This is done in the following, where we used somewhat exactly the same method that provide us a relation between T_0^i and $\mathcal{D}$.

Let us first remark that *AC* equations of order $O(\varepsilon^2)$ (B.46a) and $O(\varepsilon)$ (B.21a) have the same homogeneous part and therefore the same homogeneous solution φ_0'. So using relation (B.24) with $f = \varphi_0'$ yields

$$\int_{-\infty}^{+\infty} \left(\mathcal{D}\,\varphi_1' - \alpha \left[\frac{\varphi_1^2}{2} \partial_{\varphi^3} W(\varphi_0) - T_0^i \varphi_1 \partial_{\varphi^2} \nu(\varphi_0) - T_1 \partial_\varphi \nu(\varphi_0) \right] \right) \varphi_0' d\bar{x} = 0 \tag{B.49}$$

We use the following properties of the different functions present in equation (B.49) and the fact that the integral of an odd function between $+\infty$ and $-\infty$ is zero. Equation (B.49) reads

$$\int_{-\infty}^{+\infty} T_1(\bar{x}) \partial_\varphi \nu(\varphi_0) \varphi_0' d\bar{x} = 0$$

Thus using the expression (B.42) for $T_1(\bar{x}) - T_1(0)$ yields (It is worth noting that since T_1 is asymptotically equivalent to $\bar{x}$, the function $\partial_\varphi \nu(\varphi_0) T_1(\bar{x})$ is equivalent to an integrable function and $T_1(0)$ is finite.)

$$\begin{aligned} T_1(0) &= -\frac{\int_{-\infty}^{+\infty} \left(T_1(\bar{x}) - T_1(0)\right) \partial_\varphi \nu(\varphi_0) \varphi_0' d\bar{x}}{\int_{-\infty}^{+\infty} \partial_\varphi \nu(\varphi_0) \varphi_0' d\bar{x}} \\ &= -[\![\varphi]\!] \int_{-\infty}^{+\infty} \left[-\int_0^{\bar{x}} \left(\frac{\Phi_{th}}{k(\varphi_0)} - \mathcal{D}\, Pe\, \frac{\nu}{k}(\varphi_0) + [\![\varphi]\!] \frac{Pe\, \mathcal{D}^2}{\alpha}\, \frac{(\nu - P_3)}{k}(\varphi_0) \right) du \right] \nu'(\varphi_0)\, d\bar{x} \end{aligned}$$

The important result is that the expression for $T_1(0)$ a linear combination of Φ_{th}, $\mathcal{D}$ and $\mathcal{D}^2$, the coefficient being related to the choices for W, ν and k. The expression (B.48) for $\{T_1\}$ reads therefore

$$\{T_1\} = \Phi_{th}\, \mathcal{B}_{1/k} - \mathcal{D}\, Pe\, \mathcal{B}_{\nu/k} + [\![\varphi]\!] \frac{Pe\, \mathcal{D}^2}{\alpha}\, \mathcal{B}_{(\nu - P_3)/k} \tag{B.50}$$

where the coefficients $\mathcal{B}$ depends on the choice for k and of the interface location. The expression for the interface temperature $T_1(0)$ has the same structure.

B.3 Isothermal approximation

In this section we study the system of equation obtained by studying the isothermal phase field model (5.61)) that reads for the outer problem

$$\begin{aligned} \alpha\, \varepsilon^2\, (\mathcal{D} - V)\, \varphi_{,x} &= \varepsilon \frac{d\nu}{d\varphi} \tilde{P} + v \left(\frac{dW}{d\varphi} - \varepsilon^2 \varphi_{,xx} \right) + \frac{d\nu}{d\varphi} \left(W - \frac{\varepsilon^2}{2} \varphi_{,x}^2 \right) \\ (\rho V)_{,x} &= -\rho^2 \frac{\partial \nu}{\partial \varphi} (\mathcal{D} - V)\, \varphi_{,x} \\ (V - \mathcal{D})\, \rho V_{,x} &= -\tilde{P}_{,x} \end{aligned}$$

and that reads for the inner problem

$$\begin{aligned}
\alpha\,\varepsilon\,(\mathcal{D}-V)\,\varphi' &= \varepsilon\,\frac{d\nu}{d\varphi}\tilde{P} + v\left(\frac{dW}{d\varphi} - \varphi''\right) + \frac{d\nu}{d\varphi}\left(W - \frac{(\varphi')^2}{2}\right)\\
(\rho V)' &= -\rho^2\,\frac{\partial \nu}{\partial \varphi}\,(\mathcal{D}-V)\,\varphi'\\
(V-\mathcal{D})\,\rho V' &= -\tilde{P}'
\end{aligned}$$

The following matching conditions determines the values for V_0^{ext} and $P_{0,x}^{\tilde{ext}}$ as a function of inner solutions.

$$\lim_{x\to x_i^{\pm}} V_0^{ext} = \lim_{\bar{x}\to\pm\infty} V_0 \tag{B.51a}$$

$$\lim_{x\to x_i^{\pm}} P_0^{\tilde{ext}} = \lim_{\bar{x}\to\pm\infty} \tilde{P}_0 \tag{B.51b}$$

$$\lim_{x\to x_i^{\pm}} P_{0,x}^{\tilde{ext}} = \lim_{\bar{x}\to\pm\infty} \tilde{P}_1' \tag{B.51c}$$

The matching conditions concerning the phase field are exactly similar to the one obtained in our previous study (*cf.* the set of matching conditions (B.9)).

B.3.1 Outer problem

The system of governing equations for the outer problem at leading order reads

$$\partial_\varphi(v\,W)(\varphi_0^{ext}) = 0 \tag{B.52a}$$

$$\frac{dV_0^{ext}}{dt} = -v(\varphi_0^{ext})\;P_{0,x}^{\tilde{ext}} \tag{B.52b}$$

$$\frac{dv(\varphi_0^{ext})}{dt} = v(\varphi_0^{ext})\;V_{0,x}^{ext} \tag{B.52c}$$

Leading order of the outer *AC* equation (B.52a) implies that φ_0^{ext} is a uniform field on each side of the interface. For the stationary solutions under study, the leading order outer continuity equation (B.52c) yields

$$V_{0,x}^{ext} = 0 \tag{B.53}$$

This solenoidal condition is due to the choice of the incompressibility of the phases. V_0^{ext} is therefore uniform in each bulk phase domain. From the steady-state hypothesis, we get from the leading order momentum equation (B.52b) that $P_{0,x}^{\tilde{ext}} = 0$ and therefore that $P_0^{\tilde{ext}}$ has a uniform value in each bulk domain. According to the set of matching conditions (B.51), the whole determination of the solutions lies on the solving of the inner problem.

B.3.2 Leading order system of governing equations of the inner problem

At order $O(1)$, we obtain the following system of governing equations for the solution of the inner problem

$$0 = v(\varphi_0)\left[\partial_\varphi W(\varphi_0) - \varphi_0''\right] + \partial_\varphi v(\varphi_0)\left[W(\varphi_0) - \frac{\left(\varphi_0'\right)^2}{2}\right] \tag{B.54a}$$

$$(V_0-\mathcal{D})\,V_0' = -v(\varphi_0)\tilde{P}_0' \tag{B.54b}$$

$$(V_0-\mathcal{D})\,v(\varphi_0)' = v(\varphi_0)V_0' \tag{B.54c}$$

The Allen-Cahn equation (B.54a) is decoupled from the mass and momentum equations (B.54b) and (B.54c) since φ_0 is the only unknown appearing in this equation. Therefore, the profile $\varphi_0(\bar{x})$ is the solution of a non-linear ordinary differential equation in φ_0 of order two that is solved in section B.3.3. The momentum equation (B.54b) shows that it is necessary to know the velocity field at leading order V_0 (determined in section B.3.4) in order to determine the pressure profile at leading order $\tilde{P}_0$ (*cf.* section B.3.5).

The system of equations of the inner problem verified at order $O(\varepsilon)$ reads

$$\varphi_1 \left[AC_0 + \partial_\varphi(v\,W)(\varphi_0)\right] - \varphi_1' v'(\varphi_0) - v(\varphi_0)\,\varphi_1'' = \frac{(\mathcal{D} - V_0)\,\varphi_0'}{\alpha} - \tilde{P}_0 \partial_\varphi v(\varphi_0) \tag{B.55a}$$

$$[(V_0 - \mathcal{D})\,V_1]' = -v(\varphi_0)\,\tilde{P}_1' - \varphi_1\,\partial_\varphi v(\varphi_0)\,\tilde{P}_0' \tag{B.55b}$$

$$V_1\,v(\varphi_0)' + (V_0 - \mathcal{D})\left(\varphi_1'\,\partial_\varphi v(\varphi_0) + \varphi_1\,\partial_\varphi v(\varphi_0)'\right) = \varphi_1\,\partial_\varphi v\,(\varphi_0)\,V_0' + v(\varphi_0)\,V_1' \tag{B.55c}$$

where AC_0 reads

$$AC_0 = \partial_\varphi v(\varphi_0)\left[\partial_\varphi W(\varphi_0) - \varphi_0''\right] + \partial_{\varphi^2} v(\varphi_0)\left[W(\varphi_0) - \frac{1}{2}\left(\varphi_0'\right)^2\right]$$

and will be shown to be zero while φ_0 satisfies the leading order *AC* equation for the inner problem (B.54a).

B.3.3 Order parameter inner profile at order $O(1)$

To solve equation (B.54a), let us multiply this equation by φ_0', assuming it is never null; we get

$$0 = \varphi_0'\,v(\varphi_0)\left[\partial_\varphi W(\varphi_0) - \varphi_0''\right] + v'(\varphi_0)\left[W(\varphi_0) - \frac{\left(\varphi_0'\right)^2}{2}\right] \tag{B.56}$$

Since φ_0 satisfies (B.54a) the following identity holds

$$\left[W(\varphi_0) - \frac{\left(\varphi_0'\right)^2}{2}\right]' = \varphi_0'\left[\partial_\varphi W(\varphi_0) - \varphi_0''\right]$$

and therefore equation (B.56) reads

$$\left\{v(\varphi_0)\left[W(\varphi_0) - \frac{1}{2}\,(\varphi_0')^2\right]\right\}' = 0$$

Therefore, φ_0 is a solution of equation (B.54a) if

$$v(\varphi_0)\left[W(\varphi_0) - \frac{1}{2}\left(\varphi_0'\right)^2\right] = cste \tag{B.57}$$

According to the equation (B.10) and to the matching condition (B.9a), $v(\varphi_0)\left[W(\varphi_0) - 1/2\,\left(\varphi_0'\right)^2\right]$ is zero at $\pm\infty$. Therefore, using equation (B.57) it is zero everywhere. Since the specific volume is strictly positive, equation (B.54a) is equivalent to equation (B.15) already solved in the solidification case. Thus φ_0 is given by (B.18) if W is defined by (3.42) and the assumption on the non nullity of φ_0' is verified *a posteriori*. Let us note that there is no influence of the curvature on this solution. The leading order inner profile of the phase field is therefore the equilibrium solution.

B.3.4 Velocity inner profile at leading order

The continuity equation (B.54c) can be integrated to give

$$V_0 - \mathcal{D} \propto v(\varphi_0)$$

Let us introduce the constant mass transfer rate Γ and rewrite

$$V_0 - \mathcal{D} = -\Gamma\,v(\varphi_0) \tag{B.58}$$

It is worth noting that this equation is fully consistent with the jump condition (A.17) inherited from classical *RH* jump conditions. Equation (B.58) provides a boundary condition for the resolution of the outer problem using the matching condition (B.51a). The determination of $\mathcal{D}$ or Γ is still not achieved and is related to the solving of the leading order outer problem.

B.3.5 Pressure inner profile at leading order

The momentum equation (B.54b) reads using the leading order velocity profile (B.58)

$$v(\varphi_0)\tilde{P_0}' = -\Gamma^2\, v(\varphi_0)\, v(\varphi_0)'$$

This yields

$$\tilde{P_0} - \Pi = -\Gamma^2\, v(\varphi_0) \tag{B.59}$$

where Π is a constant of integration that has to be determined as well as Γ. This result provides a first boundary condition for the resolution of the outer problem using the matching condition (B.51b)

$$P_0^{\tilde{ext}+} - P_0^{\tilde{ext}-} = \Gamma^2 \left(v(\varphi_0^{ext-}) - v(\varphi_0^{ext+})\right)$$

The specific volume reads

$$v(\varphi) = 1 + \nu(\varphi) \tag{B.60}$$

Therefore

$$[\![P_0]\!] = -\Gamma^2\, [\![\varphi]\!]$$

This relation shows that at leading order, the model recovers the vapor recoil effect (*cf.* equation (A.18) of our study of the sharp interface models). Let us solve the next order equations.

The AC equation at order $O(\varepsilon)$

In order to study the phase-field inner profile of order $O(\varepsilon)$, *i.e.* to determine the function φ_1, and to be able to determine the relation between the two constants Π and Γ, we follow the same formalism than in our previous study of the solid-liquid phase transition while we determined φ_1 and a relation between T_0^i and $\mathcal{D}$, *i.e.* we study the AC equation (B.55a) at order $O(\varepsilon)$. The only order $O(\varepsilon)$ terms appearing in this equation are effectively related to φ_1, other terms of order $O(1)$ being already studied and related to the constants Π and Γ. In this section, we establish the equivalence between the homogeneous part of the differential equation (B.55a) under study with the AC equation at order $O(\varepsilon)$ (B.21a) obtained in the study of the solid-liquid system.

Since φ_0 is solution of equation (B.15), the first part of equation (B.55a) (the first term $\varphi_1\ [AC_0]$) is null and the equation (B.55a) reads

$$\begin{aligned}\varphi_1 \left(\partial_\varphi v(\varphi_0)\, \partial_\varphi W(\varphi_0) + v(\varphi_0)\, \partial_{\varphi^2} W(\varphi_0)\right)& \\ - \partial_\varphi v(\varphi_0)\, \varphi_1'\, \varphi_0' - v(\varphi_0)\, \varphi_1'' \quad &= \quad \frac{\mathcal{D} - V_0}{\alpha}\, \varphi_0' - \tilde{P_0}\, \partial_\varphi v(\varphi_0)\end{aligned} \tag{B.61}$$

or using the linear differential operator $\mathbf{L}$ defined by (B.23)

$$v(\varphi_0)\, \mathbf{L}(\varphi_1) + \partial_\varphi v(\varphi_0) \left(\varphi_1\, \partial_\varphi W(\varphi_0) - \varphi_1'\, \varphi_0'\right) = \frac{\mathcal{D} - V_0}{\alpha}\, \varphi_0' - \tilde{P_0}\, \partial_\varphi v(\varphi_0) \tag{B.62}$$

This equation is decoupled from the mass and momentum balance equations at same order since only φ_1 appears as being of order $O(\varepsilon)$. Equation (B.62) is a second order differential equation in φ_1. Let us show that the homogeneous part of equation (B.62) is equivalent to the homogeneous part of the equation (B.21a) in φ_1 for which we already know the solutions. Let us define the linear operator Λ

$$\Lambda(\mathrm{f}) = -\varphi_0'\, \mathrm{f}' + \partial_\varphi W(\varphi_0)\, \mathrm{f}$$

so that the homogeneous part of differential equation (B.62) reads

$$v(\varphi_0)\, \mathbf{L}(\varphi_1) + \partial_\varphi v(\varphi_0)\, \Lambda(\varphi_1) = 0$$

Let us show that $\mathbf{L}$ is the result of the application of the linear operator $'$ to the linear operator Λ divided by φ_0'. If we apply the linear operator $'$ to the linear operator Λ, we get

$$\Lambda(\mathrm{f})' = -\varphi_0''\, \mathrm{f}' - \varphi_0'\, \mathrm{f}'' + \partial_\varphi W(\varphi_0)\, \mathrm{f}' + \partial_\varphi W(\varphi_0)'\, \mathrm{f} \tag{B.63}$$

Using the identity (B.5), we have

$$\partial_\varphi W(\varphi_0)' = \partial_{\varphi^2} W(\varphi_0)\,\varphi_0'$$

Therefore, equation (B.63) reads using equation (B.15)

$$\Lambda(\mathrm{f})' = \varphi_0'\,\mathbf{L}(\mathrm{f})$$

The kernel of the operator Λ is thus included in the kernel of operator $\mathbf{L}$.

$$\ker(\Lambda) \subset \ker(\mathbf{L}) \tag{B.64}$$

Thus since

$$\ker(v(\varphi_0)\,\mathbf{L} + \partial_\varphi v(\varphi_0)\,\Lambda) = \ker(\Lambda) \oplus \ker(\mathbf{L})$$

we get, using (B.64)

$$\ker(v(\varphi_0)\,\mathbf{L} + \partial_\varphi v(\varphi_0)\,\Lambda) = \ker(\mathbf{L})$$

The solutions of the homogeneous part of equation (B.55a) are in the kernel of the operator $v(\varphi_0)\,\mathbf{L} + \partial_\varphi v(\varphi_0)\,\Lambda$, they are therefore in the kernel of the operator $\mathbf{L}$ and thus the same than those of the homogeneous part of equation (B.21a). Using the results obtained while solving equation (B.21a) in section B.2.7, the function φ_1 reads

$$\varphi_1 = \Phi_1 + \lambda_1^1\,\varphi_0' + \lambda_1^2\,\varphi_0' \int \frac{d\bar{x}}{\left(\varphi_0'\right)^2}$$

where Φ_1 is a particular solution of equation (B.55a) that still needs to be determined (*cf.* section B.3.5 where the method of variation of parameters is used) and λ_1^1 and λ_1^2 are two reals whose values are zero for the same reasons as in section B.2.7.

Once the nature of equation (B.55a) has shown some important similarities with equation (B.21a), we determine a relation between the constant of integration Π and the mass transfer rate following a similar approach than the one used to determine the relation between T_0^i and $\mathcal{D}$ in section B.2.6.

Determination of the constant of integration Π

In order to determine a relation between Π and the mass transfer rate Γ, the same calculation as for the determination of T_0^i (*cf.* section B.2.6) is done. Using the results obtained in section B.3.5, we know that φ_0' is a solution of the homogeneous part of equation (B.55a). Thus by multiplying this equation by φ_0' and integrate between $+\infty$ and $-\infty$ we get using relation (B.24)

$$\int_{-\infty}^{+\infty} \frac{\mathcal{D} - V_0}{\alpha}\,\varphi_0'^2\,d\bar{x} = \int_{-\infty}^{+\infty} \tilde{P}_0\,v(\varphi_0)'\,d\bar{x}$$

Using the expression (B.58) for V_0 and (B.59) for and $\tilde{P}_0$ yields

$$-\frac{\Gamma}{\alpha}\int_{-\infty}^{+\infty} v(\varphi_0)\,\varphi_0'^2\,d\bar{x} + \Gamma^2 \int_{-\infty}^{+\infty} v(\varphi_0)\,v(\varphi_0)'\,d\bar{x} = \Pi \int_{-\infty}^{+\infty} v(\varphi_0)'\,d\bar{x}$$

Let us introduce the following two integral quantities $\mathcal{A}_1$ and $\mathcal{A}_2$

$$\begin{aligned}
\mathcal{A}_1 &= \frac{\int_{-\infty}^{+\infty} v(\varphi_0)\,\varphi_0'^2\,d\bar{x}}{\int_{-\infty}^{+\infty} v(\varphi_0)'\,d\bar{x}} \\
\mathcal{A}_2 &= \frac{\int_{-\infty}^{+\infty} v(\varphi_0)\,v(\varphi_0)'\,d\bar{x}}{\int_{-\infty}^{+\infty} v(\varphi_0)'\,d\bar{x}}
\end{aligned}$$

According to the definition (B.60) of $v(\varphi)$, we have

$$\int_{-\infty}^{+\infty} v(\varphi_0)'\,d\bar{x} = [\![v]\!] = [\![\varphi]\!]$$

$$\int_{-\infty}^{+\infty} v(\varphi_0)\, v(\varphi_0)'\, d\bar{x} = \left[\!\left[\frac{v^2}{2} \right]\!\right] = \{v\}\, [\![v]\!]$$

So

$$\mathcal{A}_2 = \{v\}$$

Let us study $\mathcal{A}_1$. Since $v(\varphi_0)\,\varphi_0'^2$ is a strictly positive function, $\mathcal{A}_1$ has the sign of $[\![\varphi]\!]$. Using equation (B.60), $\mathcal{A}_1$ reads

$$\mathcal{A}_1 = [\![\varphi]\!] \int_{-\infty}^{+\infty} \nu(\varphi_0)\, \varphi_0'^2$$

According to the fact that φ_0 satisfies equation (B.17), we have

$$\int_{-\infty}^{+\infty} \nu(\varphi_0)\, \varphi_0'^2\, d\bar{x} = [\![\varphi]\!] \int_{\varphi_0(-\infty)}^{\varphi_0(+\infty)} \nu(\varphi)\, \sqrt{2\, W(\varphi)}\, d\varphi = \int_0^1 \nu(\varphi)\, \sqrt{2\, W(\varphi)}\, d\varphi$$

Therefore

$$\mathcal{A}_1 = [\![\varphi]\!] \int_0^1 \nu(\varphi)\, \sqrt{2\, W(\varphi)}\, d\varphi \tag{B.65}$$

Let us consider that W is given by equation (3.42). If $\nu = P_3(\varphi)$, we get $\mathcal{A}_1 = [\![\varphi]\!]/2$ If $\nu = P_5(\varphi)$, we get $\mathcal{A}_1 = [\![\varphi]\!]/12$.

Let us recall that the sign of Γ as well as the sign of $[\![\varphi]\!]$ depend on the relative position of the bulk phases. Therefore the sign of Π depends only on the nature of the phase transformation (evaporation or condensation).

$$\Pi = \mathcal{A}_1 \frac{\Gamma}{\alpha} + \frac{\Gamma^2}{2} \tag{B.66}$$

It yields for the bulk values of the pressure, using the inner solution for the pressure (B.59) and the matching condition (B.51b)

$$P_0^{ext\pm} = \mathcal{A}_1 \frac{\Gamma}{\alpha} + \Gamma^2\, (v_\pm - \{v\}) \tag{B.67}$$

and therefore, using the fact that $\{v\} = (v^+ + v^-)/2$

$$\{P_0\} = \mathcal{A}_1 \frac{\Gamma}{\alpha} = [\![\varphi]\!] \frac{\Gamma}{\alpha} \left[\nu\, \sqrt{2\, W} \right]_0^1 \tag{B.68}$$

The sign of $\{P_0\}$ actually depends on the sign of the phase-change: it is positive for condensation and negative for evaporation. It is worth noting that in classical sharp interface models where an interface is supposed to be at local thermodynamic equilibrium $\{P\} = 0$. The fact that this term is inversely proportional to α is consistent with this approximation.

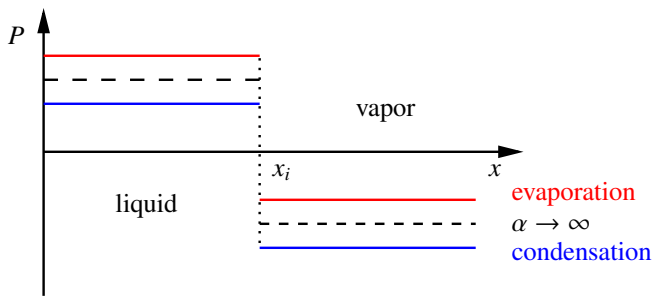

Figure B.4: Pressure profile across an interface during a steady-state phase-change.

Phase-field inner profile of order $O(\varepsilon)$, determination of $\varphi_1(\bar{x})$

The simplification of equation (B.61) in order to find a particular solution follows exactly the one done in section B.2.7. We introduce the function F defined by (B.30) and equation (B.61) becomes

$$-v(\varphi_0)\left(F''\,\varphi_0' + 2\,F'\,\varphi_0''\right) - \partial_\varphi v(\varphi_0)\left(\varphi_0'\right)^2 F' = \frac{\mathcal{D}-V_0}{\alpha}\,\varphi_0' - \tilde{P}_0\,\partial_\varphi v(\varphi_0) \tag{B.69}$$

Then we introduce G defined by (B.32) and equation (B.61) reads

$$-v(\varphi_0)\,\frac{G'}{\varphi_0'} - \partial_\varphi v(\varphi_0)\,G = \frac{\mathcal{D}-V_0}{\alpha}\,\varphi_0' - \tilde{P}_0\,\partial_\varphi v(\varphi_0)$$

In order to integrate the equation to determine G, the equation is multiplied by φ_0' and using the relation (B.5)) applied to $v(\varphi_0)$ it becomes

$$(v(\varphi_0)\,G)' = \frac{V_0-\mathcal{D}}{\alpha}\,\varphi_0'^2 + \tilde{P}_0\,v(\varphi_0)'$$

Using the solution for $\tilde{P}_0$ (B.59) and for V_0 (B.58), we get

$$(v(\varphi_0)\,G)' = \Pi\,v(\varphi_0)' - \frac{\Gamma}{\alpha}\,v(\varphi_0)\,\varphi_0'^2 - \Gamma^2\,v(\varphi_0)\,v(\varphi_0)'$$

Thus using the expression (B.66) for Π, we get

$$(v(\varphi_0)\,G)' = \frac{\Gamma}{\alpha}\left(\mathcal{A}_1 v(\varphi_0)' - v(\varphi_0)\,\varphi_0'^2\right) + \Gamma^2\,\left(1/2 v(\varphi_0)' - v(\varphi_0)\,v(\varphi_0)'\right)$$

Let us denote $G_{\alpha\infty}$ the solution of

$$(v(\varphi_0)\,G_{\alpha\infty})' = \left(1/2 v(\varphi_0)' - v(\varphi_0)\,v(\varphi_0)'\right)$$

and by G_α the solution of

$$(v(\varphi_0)\,G_\alpha)' = \left(\mathcal{A}_1 v(\varphi_0)' - v(\varphi_0)\,\varphi_0'^2\right)$$

Thus the particular solution Φ_1 reads

$$\Phi_1 = \Phi_{1\,\alpha_\infty} + \Phi_{1\,\alpha} \tag{B.70}$$

with

$$\Phi_{1\,\alpha_\infty} = \Gamma^2\,\varphi_0' \int \frac{\int (G_{\alpha\infty})\,d\bar{x}}{\left(\varphi_0'\right)^2}\,d\bar{x} \tag{B.71}$$

$$\Phi_{1\,\alpha} = \frac{\Gamma}{\alpha}\,\varphi_0' \int \frac{\int (G_{\alpha})\,d\bar{x}}{\left(\varphi_0'\right)^2}\,d\bar{x} \tag{B.72}$$

For $\Phi_{1\,\alpha\infty}$,

$$G_{\alpha\infty} = \left(1/2 - \frac{1}{2}v(\varphi_0) + \frac{C_0}{v(\varphi_0)}\right) \tag{B.73}$$

where C_0 is a constant of integration. And even if the calculation has not been made, $\Phi_{1\,\alpha_\infty}$ is a non-zero contribution to the deformation of the profile whatever the choice for ν.

B.3.6 Determination of second order inner profile for the velocity and pressure V_1 and P_1

Let us solve the balance of momentum and continuity equations (B.55b) and (B.55c). Equation (B.55c) gives

$$V_1\,v(\varphi_0)' - v(\varphi_0)\,V_1' = \varphi_1\,\partial_\varphi v(\varphi_0)\,(V_0-\mathcal{D})' - \left(\varphi_1\,\partial_\varphi v(\varphi_0)\right)'\,(V_0-\mathcal{D})$$

Let us divide by $-v(\varphi_0)^2$ and use the equation (B.58) for V_0, it reads

$$\left(\frac{V_1}{v(\varphi_0)}\right)' = -\Gamma\left(\frac{\varphi_1\,\partial_\varphi v(\varphi_0)}{v(\varphi_0)}\right)'$$

that can be integrated

$$\frac{V_1}{v(\varphi_0)} = -\Gamma\,\frac{\varphi_1\,\partial_\varphi v(\varphi_0)}{v(\varphi_0)} + C_{V1} \tag{B.74}$$

where C_{V1} is a constant of integration.

Equation (B.55b) could then be integrated.

$$[(V_0 - \mathcal{D})\,V_1]' = -v(\varphi_0)\,\tilde{P}_1' - \varphi_1\,\partial_\varphi v(\varphi_0)\,\tilde{P}_0'$$

Using the expression (B.58) for $(V_0 - \mathcal{D})$ it becomes

$$\left[\Gamma\,v(\varphi_0)\,V_1\right]' = v(\varphi_0)\,\tilde{P}_1' + \varphi_1\,\partial_\varphi v(\varphi_0)\,\tilde{P}_0'$$

Using the expression (B.59) for $\tilde{P}_0$ it becomes

$$\left[\Gamma\,v(\varphi_0)\,V_1\right]' = v(\varphi_0)\,\tilde{P}_1' - \Gamma^2\,\varphi_1\,\partial_\varphi v(\varphi_0)\,v(\varphi_0)'$$

Using the expression (B.74) for V_1 it becomes

$$\left[-\Gamma^2\,\varphi_1\,\partial_\varphi v(\varphi_0)\,v(\varphi_0) + \Gamma\,C_{V1}\,v(\varphi_0)^2\right]' = v(\varphi_0)\,\tilde{P}_1' - \Gamma^2\,\varphi_1\,\partial_\varphi v(\varphi_0)\,v(\varphi_0)'$$

that could be re-written as

$$-\Gamma^2\left[\varphi_1\,\partial_\varphi v(\varphi_0)\right]' + 2\,\Gamma\,C_{V1}\,v(\varphi_0)' = \tilde{P}_1' \tag{B.75}$$

Finally we get for $\tilde{P}_1$

$$\tilde{P}_1 = 2\,\Gamma\,C_{V1}\,v(\varphi_0) + \Gamma^2\,\varphi_1\,\partial_\varphi v(\varphi_0) + C_{P1} \tag{B.76}$$

where C_{P1} is a constant of integration to be determined.

B.3.7 Determination of $\{P_1\}$

In order to determine $\{P_1\}$ an integration of the *AC* equation at order $O(2)$ and a formalism similar to the one used in order to determine $\{T_1\}$ in section B.2.13.

However, such a complex calculation is not required since, like in this simplified isothermal and non-viscous case, the only dissipative process is associated with the Ginzburg-Landau relaxation. Indeed, in our case where the bulk compressibility are zero, we have, according to our study of the sharp jump conditions in the appendix A.2

$$\mathcal{G} = \{P\}[\![1/\rho]\!] = \frac{1}{\kappa\,\Gamma}\int_{-\infty}^{+\infty}(d\varphi/dt)^2\,dx$$

By considering our own expansion in ε of both $\{P\}$ and $\varphi(\bar{x})$, we therefore recover that at order $O(1)$

$$\{P_0\} = \mathcal{A}_1\,\frac{\Gamma}{\alpha}$$

a result that has already been established using the integration of the *AC* equation at order $O(\varepsilon)$. At order $O(\varepsilon)$ we have

$$\{P_1\} = \frac{2\,[\![\varphi]\!]\Gamma}{\alpha}\int_{-\infty}^{+\infty}\varphi_0'\,\Phi_1'\,d\bar{x}$$

The function Φ_1 has been determined in section B.3.5 as the sum of two functions, $\Phi_1 = \Phi_{1\,\alpha} + \Phi_{1\,\alpha\infty}$. From the even/odd properties of respectively $\Phi_{1\,\alpha}$ and $\Phi_{1\,\alpha\infty}$, it can be shown that

$$\int_{-\infty}^{+\infty}\varphi_0'\,\Phi_1'\,d\bar{x} = \int_{-\infty}^{+\infty}\varphi_0'\,\Phi_{1\,\alpha}'\,d\bar{x}$$

i.e. that the function $\Phi_{1\,\alpha\infty}$ does not contribute to the mid value of the interface pressure at order $O(\varepsilon)$, namely $\{P_1\}$. This implies that $\Phi_{1\,\alpha\infty}$ does not contributes to the driving force, *i.e.* to the rate of interface entropy

production. This result is fully consistent with the fact that the rate of interface production $\mathcal{R}_s = \Gamma\mathcal{G}/T$ must cancels for $\alpha = \infty$. Since $\Phi_{1\,\alpha}$ is scaled by Γ/α, we get

$$\{P_1\} = \frac{2\,\Gamma^2}{\alpha^2}\,\mathcal{A}_\alpha \tag{B.77}$$

where $\mathcal{A}_\alpha$ is of order unity.

Conclusion

We have determined the solutions for the pressure, the velocity and the phase field of the inner and outer problems at leading order in the isothermal case. These results are discussed and analyzed in section 7.4. The outer problem satisfies classical jump conditions on pressure and velocity. In particular we study the kinetic relation for the sharp model equivalent to our phase field formulation.

B.4 Liquid-vapor non-isothermal non-viscous case

In this section we study steady-state one-dimensional mass transfer rate with the non-isothermal quasi-compressible model that we derived for the study of boiling flows. The non-dimensional system of equations reads (*cf.* the system 5.59) for the outer problem

$$\alpha\,\varepsilon^2\,(\mathcal{D}-V)\,\varphi_{,x} = \varepsilon\,\frac{d\nu}{d\varphi}\Big(\tilde{P}\,-\,T\Big) + v\,\left(\frac{dW}{d\varphi} - \varepsilon^2\varphi_{,xx}\right) + \frac{d\nu}{d\varphi}\left(W - \frac{\varepsilon^2}{2}\varphi_{,x}^2\right) \tag{B.78a}$$

$$(\rho V)_{,x} = -\rho^2\,\frac{\partial\nu}{\partial\varphi}\,(\mathcal{D}-V)\,\varphi_{,x} \tag{B.78b}$$

$$(V-\mathcal{D})\,\rho V_{,x} = -\tilde{P}_{,x} \tag{B.78c}$$

$$(V-\mathcal{D})\,\rho\,T_{,x} = \frac{(k\,T_{,x})_{,x}}{Pe} - (V-\mathcal{D})\,\rho\,(1+T)\,\frac{d\nu}{d\varphi}\,\varphi_{,x} + (\mathcal{D}-V)^2\,\frac{\rho\varepsilon}{\alpha}\,(\varphi_{,x})^2 \tag{B.78d}$$

and for the inner problem

$$\alpha\,\varepsilon\,(\mathcal{D}-V)\,\varphi' = \varepsilon\,\frac{d\nu}{d\varphi}\Big(\tilde{P}\,-\,T\Big) + v\,\left(\frac{dW}{d\varphi} - \varphi''\right) + \frac{d\nu}{d\varphi}\left(W - \frac{(\varphi')^2}{2}\right) \tag{B.79a}$$

$$(\rho V)' = -\rho^2\,\frac{\partial\nu}{\partial\varphi}\,(\mathcal{D}-V)\,\varphi' \tag{B.79b}$$

$$(V-\mathcal{D})\,\rho V' = -\tilde{P}' \tag{B.79c}$$

$$\varepsilon\,(V-\mathcal{D})\,\rho\,T' = \frac{(k\,T')'}{Pe} - \varepsilon\,(V-\mathcal{D})\,\rho\,(1+T)\,\frac{d\nu}{d\varphi}\,\varphi' + (\mathcal{D}-V)^2\,\frac{\rho\varepsilon}{\alpha}\,(\varphi')^2 \tag{B.79d}$$

It is worth noting that each equation has strong similarities with the one studied in the previous sections and corresponding to the uniform density or isothermal case. The derivation of the solutions is thus made easier since we can use the results obtained in the corresponding previous studies.

B.4.1 First order inner problem

For the Allen-Cahn, momentum and continuity equations we get the same results as for the isothermal approximation. Therefore

$$\varphi_0 = 1/2 + (\llbracket\varphi\rrbracket/2)\,\tanh(3\,\bar{x}) \tag{B.80a}$$

$$\tilde{P}_0 = \Pi - \Gamma^2\,v(\varphi_0) \tag{B.80b}$$

$$V_0 = \mathcal{D} - \Gamma\,v(\varphi_0) \tag{B.80c}$$

where Π is a constant of integration that needs to be determined and Γ is the constant rate of mass transfer.

The temperature equation is at leading order exactly identical to the solidification equation. Therefore we get

$$T_0' = 0 \tag{B.81a}$$
$$[\![T_0]\!] = 0 \tag{B.81b}$$

and we denote T_0^i the value of the uniform temperature field across the interface region.

Second order resolution is necessary to determine the relation between Π, T_0^i, $\mathcal{D}$ and Γ.

B.4.2 Second order inner problem

The system of equation reads

$$\begin{aligned}
&\varphi_1 \left(\partial_\varphi v(\varphi_0)\, \partial_\varphi W(\varphi_0) + v(\varphi_0)\, \partial_{\varphi^2} W(\varphi_0)\right) \\
&\qquad - \partial_\varphi v(\varphi_0)\, \varphi_1'\, \varphi_0' - v(\varphi_0)\, \varphi_1'' = \frac{\mathcal{D} - V_0}{\alpha}\, \varphi_0' + \left(T_0^i - \tilde{P}_0\right) \partial_\varphi v(\varphi_0) && \text{(B.82a)} \\
&\qquad (V_0 - \mathcal{D})\, V_1' - V_1 V_0' = -v(\varphi_0)\tilde{P}_1' - \varphi_1 \partial_\varphi v(\varphi_0)\tilde{P}_0' && \text{(B.82b)} \\
&V_1\, v(\varphi_0)' + (V_0 - \mathcal{D}) \left(\varphi_1\, \partial_\varphi v(\varphi_0)\right)' = \varphi_1\, \partial_\varphi v(\varphi_0)\, V_0' + v(\varphi_0)\, V_1' && \text{(B.82c)} \\
&\left(k(\varphi_0)\, T_1'\right)' = -\left(1 + T_0^i\right) \frac{(\mathcal{D} - V_0)\ Pe}{v(\varphi_0)}\, \partial_\varphi \nu(\varphi_0)\, \varphi_0' \\
&\qquad - \frac{(\mathcal{D} - V_0)^2\ Pe}{\alpha}\, \frac{\varphi_0'^2}{v(\varphi_0)} && \text{(B.82d)}
\end{aligned}$$

Determination of a relation between T_0 and Π

This relation is obtained with exactly the same processes used in section B.3.5. We use the similarities between equations (B.82a)) and (B.61). Let us introduce the real constant Π_0 defined by

$$\Pi_0 = \Pi - T_0^i$$

Therefore, using equation (B.80b), the LHS of order $O(\varepsilon)$ *AC* equation for the inner problem (B.82a) reads

$$\frac{\mathcal{D} - V_0}{\alpha}\, \varphi_0' - \left(\Pi_0 - \Gamma^2\, \varphi_0\right) \partial_\varphi v(\varphi_0)$$

It is thus possible to determine the relation between Π_0 and Γ exactly by the same calculation used for Π in the isothermal case (*cf.* section B.3.5), we get

$$\Pi_0 = \mathcal{A}_1\, \frac{\Gamma}{\alpha} + \{v\}\, \Gamma^2 \tag{B.83}$$

where $\mathcal{A}_1$ is given by equation (B.65). The expression for $\tilde{P}_0$ reads therefore

$$\tilde{P}_0 = T_0^i + \mathcal{A}_1\, \frac{\Gamma}{\alpha} \{v\}\, \Gamma^2 - v(\varphi_0)\, \Gamma^2 \tag{B.84}$$

and we get

$$\{P_0\} = T_0^i + \mathcal{A}_1\, \frac{\Gamma}{\alpha} \tag{B.85}$$

that implies that

$$\{P_0\} = P_{eq}(T_0^i) + \mathcal{A}_1\, \frac{\Gamma}{\alpha}$$

or equivalently

$$\{T_0\} = T_0^i = T_{eq}(\{P_0\}) - \mathcal{A}_1\, \frac{\Gamma}{\alpha} \tag{B.86}$$

where P_{eq}, resp. T_{eq}, denotes the saturation curve. The shift of the "interface state" with regard to the two-phase planar equilibrium characterized by $\{P_0\} = P_{eq}(T_0^i)$ is there associated to the Ginzburg-Landau relaxation dissipative mechanism. It is worth noting that while the interface location is associated with the location of the zero value of the phase field (or equivalently at leading order $(\nu)_{x_\nu}^{ex} = 0$), the corresponding value of the pressure at the interface is the average of the bulk pressure values, *i.e.* $P_\nu^i = \{P_0\}$.

Leading order value for the interface jump in heat flux, $[\![q_0]\!]$

Since $V_0 - \mathcal{D}$ is given by (B.80c) equation (B.82d) reads

$$\left(k(\varphi_0)T_1'\right)' = -\Gamma\, Pe\, \left(1 + T_0^i\right)\, \partial_\varphi \nu(\varphi_0)\, \varphi_0' - \Gamma^2\, \frac{Pe}{\alpha}\, v(\varphi_0)\, \varphi_0'^2$$

By integration between $\bar{x} = +\infty$ and $\bar{x} = -\infty$ and using the matching condition (B.7c), we get

$$[\![q_0]\!] = Pe\, \Gamma \left(1 + T_0^i\right)\, [\![\varphi]\!] + \Gamma^2\, \frac{Pe}{\alpha}\, \int_0^1 \nu(\varphi)\, \sqrt{2\, W(\varphi)}\, d\varphi \tag{B.87}$$

According to the expression (B.86), the expression for $[\![q_0]\!]$ reads

$$[\![q_0]\!] = Pe\, \Gamma \left(1 + T_{eq}(\{P_0\})\right)\, [\![\varphi]\!]$$

B.4.3 Jump in outer temperature at order $O(\varepsilon)$

The determination of the $[\![T_1]\!]$ takes advantage of the very similar structure of equations (B.82d) and (B.21b) and follows exactly the same formalism than developed in section B.2.9. Therefore, it yields to the definition of Φ_{th} as the constant of integration of (B.82d) whose value is

$$-\Phi_{th} \,\hat{=}\, k(\varphi_0)\, T_1' + Pe\, \Gamma \left(1 + T_0^i\right)\, \nu(\varphi_0) + \frac{Pe\, \Gamma^2}{\alpha}\, \int^{\bar{x}} v(\varphi_0)\, \varphi_0'^2 d\xi \tag{B.88}$$

and therefore

$$[\![T_1]\!] = -\Phi_{th} \left(\frac{1}{k(\varphi_0)}\right)^{\bar{ex}} - Pe\, \Gamma \left(1 + T_0^i\right) \left(\frac{\nu}{k}(\varphi_0)\right)^{\bar{ex}} - 2\, [\![\varphi]\!]\, \frac{Pe\, \Gamma}{\alpha} \left(\frac{\int (v\, W(\varphi_0) d\xi)}{k}(\varphi_0)\right)^{\bar{ex}} \tag{B.89}$$

Moreover we deduce a somewhat compact form for the expression for $T_1(\bar{x})$, derived by analogy with the study of section B.2.10

$$\begin{aligned} T_1(\bar{x}) - T_1(0) \;=\; & \left(1 + T_0^i\right)\, Pe\, \mathcal{D} \int_0^{\bar{x}} \frac{(\nu(-\infty) - \nu(\varphi_0(x)))}{k(\varphi_0(x))} dx - T_0^{ext'}(x_i^-) \int_0^{\bar{x}} \frac{k(-\infty)}{k(\varphi_0(x))} dx \\ & -2\, [\![\varphi]\!]\, \frac{Pe\, \Gamma}{\alpha} \int_0^{\bar{x}} \frac{\int (v\, W(\varphi_0(\xi)) d\xi)}{k(\varphi_0(x))}\, dx \end{aligned} \tag{B.90}$$

B.4.4 Relation between $\{P_1\}$ and $\{T_1\}$

Let us consider the value of $\{P_1\}[\![1/\rho]\!] - \{T_1\}[\![s_0]\!]$ that is required for the expression for approximated expression of the driving force. Unfortunately, it is not possible to determine *a priori* this value in such an easy way as it has been done in the isothermal case (*cf.* section B.3.7) since different dissipative processes (namely, heat conduction and Ginzburg Landau relaxation) take place in the transition region.

In order to get its expression, it is necessary to integrate the order $O(\varepsilon)^2$ AC equation that reads

$$\begin{aligned} (\mathcal{D} - V_0)\, \varphi_1' - V_1\, \varphi_0' - \alpha\, AC_1(\varphi_1) \;=\; & \alpha \Big[\left(v(\varphi_0)\, \mathbf{L}(\varphi_2) + \partial_\varphi v(\varphi_0)\, \Lambda(\varphi_2)\right) \\ & + \left(\tilde{P}_0 - T_0^i\right) \varphi_1 \partial_{\varphi^2} v(\varphi_0) \\ & + \left(\tilde{P}_1 - T_1\right)\, \partial_\varphi v(\varphi_0) \Big] \end{aligned} \tag{B.91}$$

where $AC_1(\varphi_1)$ is given by

$$\begin{aligned} AC_1(\varphi_1) \;=\; & \frac{\varphi_1^2}{2} \Big[v_0 \partial_{\varphi^3} W_0 + 3\, \partial_\varphi v_0 \partial_{\varphi^2} W_0 + 3\, \partial_{\varphi^2} v_0\, \partial_\varphi W_0 + W_0\, \partial_{\varphi^3} v_0 \\ & - \left(\partial_{\varphi^3} v_0\, \varphi_0'^2 + \partial_{\varphi^2} v_0 \varphi_0''\right) \Big] \\ & - \varphi_1\, \varphi_1'' \partial_\varphi v_0 - \varphi_1\, \varphi_1'\, \partial_{\varphi^2} v_0\, \varphi_0' - \varphi_1'^2\, \partial_\varphi v_0 / 2 \end{aligned} \tag{B.92}$$

Let us multiply equation (B.91) by φ_0' in order to use the property (B.24). All the expressions of the quantities appearing in this equation are known at least up to a constant. Our goal is not to provide the exact calculation for $\{P_1\}[\![1/\rho]\!] - \{T_1\}[\![s_0]\!]$ but rather to scale all the terms that are entering in it.

Let us use the expression (B.76) for $P_1(\bar{x})$ and (B.90) for $T_1(\bar{x})$ and derive $\{P_1\}$ and $\{T_1\}$ by integration. According to the two functions $\Phi_{1\,\alpha}$ and $\Phi_{1\,\alpha\,\infty}$ entering the expression of $\varphi_1(\bar{x})$, the integral of $\varphi_0' AC_1(\varphi_1)$ is composed of three different terms, let say

$$\int_{-\infty}^{+\infty} \varphi_0'(\bar{x}) AC_1(\varphi_1)(\bar{x})\, d\,\bar{x} = \frac{\Gamma^2}{\alpha^2}\beta_{\Gamma^2/\alpha^2} + \frac{\Gamma^3}{\alpha}\beta_{\Gamma^3/\alpha}$$

where β are coefficients of order unity. Since $\mathcal{D} - V_0$ scales as Γ we have

$$\int_{-\infty}^{+\infty} \varphi_0'(\bar{x})\,(\mathcal{D} - V_0)\;\varphi_1'(\bar{x}) d\,\bar{x} = \frac{\Gamma^2}{\alpha}\beta_{\Gamma^2}\alpha + \Gamma^3\beta_{\Gamma^3}$$

According to equation (B.74) V_1 scales as $\Gamma\,\varphi_1$ *i.e.* according to the expression for φ_1 is made of two contributions, and therefore

$$\int_{-\infty}^{+\infty} \varphi_0'(\bar{x}) V_1(\bar{x}) d\,\bar{x} = \frac{\Gamma^2}{\alpha}\beta_{\Gamma^2/\alpha} + \Gamma^3\beta_{\Gamma^3}$$

The group of terms $\tilde{P}_0 - T_0^i$ equals $\left(\Gamma^2\, v(\varphi_0) + \Pi_0\right)$. According to the expression (B.83) it yields

$$\int_{-\infty}^{+\infty} \varphi_0'(\bar{x})\,(\tilde{P}_0 - T_0^i)\varphi_1(\bar{x})\,\partial_{\varphi^2} v(\varphi_0)(\bar{x})\; d\bar{x} = \frac{\Gamma^3}{\alpha}\beta_{\Gamma^3/\alpha}$$

According to equation (B.90) T_1 is composed of three terms that scale as Φ_{th}, $\Gamma\, Pe$ and $\Gamma^2\, Pe/\alpha$. In the expression (B.76) for $\tilde{P}_1$ the term $\Gamma^2 v(\varphi_0)\varphi_1$ yields to

$$\int_{-\infty}^{+\infty} \varphi_0'(\bar{x})\,\tilde{P}_1(\bar{x})\; d\bar{x} = \frac{\Gamma^3}{\alpha}\beta_{\Gamma^3/\,\alpha}$$

Using the different scalings of the terms of equation (B.91) and since $[\![1/\rho_0]\!] = [\![s_0]\!] = [\![\varphi]\!]$, the use of the solvability condition (B.24) yields

$$\{P_1\}[\![1/\rho_0]\!] - \{T_1\}[\![s_0]\!] = [\![\varphi]\!]\left[\frac{\Gamma^2}{\alpha^2}\beta_{\Gamma^2/\alpha^2} + \Phi_{th}\beta_{\Phi_{th}} + \Gamma\, Pe\,\beta_{\Gamma\, Pe} + \frac{\Gamma^2\, Pe}{\alpha}\beta_{\Gamma^2\, Pe/\alpha} + \frac{\Gamma^3}{\alpha}\beta_{\Gamma^3/\,\alpha}\right] \tag{B.93}$$

where the coefficients β are all of order unity.

B.4.5 Jump in heat flux at order $O(\varepsilon)$, $[\![q_1]\!]$

Let us study $[\![q_1]\!]$ of interest in the study of the interface entropy production. The order $O(\varepsilon^2)$ equation of temperature reads

$$\begin{aligned} -\mathcal{D}\, c_P(T_0^i)\, T_1' \;=\; & \frac{1}{Pe}\left(k(\varphi_0)\, T_2' + \left(\partial_\varphi k(\varphi_0)\,\varphi_1\right)' T_1'\right)' \\ & + \mathcal{D}\left(\partial_\varphi \nu(\varphi_0)\varphi_1' + \partial_{\varphi^2}\nu(\varphi_0)\,\varphi_1\,\varphi_0'\right) + 2\,\frac{\mathcal{D}^2\, Pe}{\alpha}\,\left(v(\varphi_0)\varphi_0'\,\varphi_1' + \partial_\varphi v(\varphi_0)\varphi_0'^2\,\varphi_1\right) \end{aligned}$$

An integration yields (*cf.* the study of $[\![q_1]\!]$ in the solid-liquid case in section B.2.12)

$$\begin{aligned} [\![q_1]\!] \;=\; & c_P(T_0^i)\,\Gamma\, Pe\,[\![T_1]\!] - Pe\,\Gamma\left(1 + T_0^i\right)\,\int_{-\infty}^{+\infty}\left(\partial_\varphi \nu(\varphi_0)\;\varphi_1' + \partial_{\varphi^2}\nu(\varphi_0)\,\varphi_0'\,\varphi_1\right)\,d\bar{x} \\ & - \frac{\Gamma^2\, Pe}{\alpha}\,\int_{-\infty}^{+\infty}\left(2\, v(\varphi_0)\;\varphi_0'\,\varphi_1' + \partial_\varphi v(\varphi_0)\varphi_1\,\varphi_0'^2\right)\,d\bar{x} \end{aligned}$$

Using the following identity based on the property of both φ_0 and φ_1

$$\int_{-\infty}^{+\infty}\left(\partial_\varphi \nu(\varphi_0)\;\varphi_1' + \partial_{\varphi^2}\nu(\varphi_0)\,\varphi_0'\,\varphi_1\right)\,d\bar{x} \;= \left[\partial_\varphi \nu(\varphi_0)\;\varphi_1\right]_{-\infty}^{+\infty} = 0$$

the expression of $[\![q_1]\!]$ reads

$$[\![q_1]\!] \;=\; c_P(T_0^i)\,\Gamma\, Pe\,[\![T_1]\!] - \frac{\Gamma^2\, Pe}{\alpha}\,\int_{-\infty}^{+\infty}\left(2\, v(\varphi_0)\;\varphi_0'\,\varphi_1' + \partial_\varphi v(\varphi_0)\varphi_1\,\varphi_0'^2\right)\,d\bar{x} \tag{B.94}$$

B.4.6 Concluding remarks

We have been able to derive the leading order solutions for the temperature, pressure, velocity and phase field variables. These solutions are very similar to the one obtained in the isothermal or uniform density case. These results are discussed in section 7.5 where in particular we study the sharp interface model equivalent to our phase field formulation.

Appendix C

General schemes and notations for the spatial discretization and the time stepping considered in this numerical study

In this appendix, we present the numerical schemes and the numerical algorithm used in the numerical study of liquid-vapor flows with phase change that is presented in chapter 8.

C.1 Time stepping: the Euler scheme

Let us first consider the time discretization scheme and introduce the main approximations used to solve the advance in time of the system of equation computed.

Notation The time step is considered as constant and denoted Dt. The discretization of time of a Eulerian variable X is denoted X^n where the integer upper-script n is the number of the iteration of the solver. Therefore after an iteration of the whole algorithm, the value of the variable $X(t)$ is transformed from $X(t) = X^n$ to $X(t+Dt) = X^{n+1}$.

Scheme for the advective terms Let us consider the time discretization of the partial derivative of the variable X with respect to time $(\partial X/\partial t)$. The scheme adopted in order to compute this derivative in the following numerical computation is the classical Euler scheme that reads

$$\frac{\partial X}{\partial t} \simeq \frac{X^{n+1} - X^n}{Dt}$$

Implicit and explicit source terms Let us consider a simple generic continuum equation for the evolution of the variable X

$$\frac{\partial X}{\partial t} = E(X) + I(X)$$

where E and I are two "source terms" that depends on the field X. We consider the following numerical scheme for the solving of this generic equation

$$\frac{X^{n+1} - X^n}{Dt} = E(X^n) + I(X^{n+1})$$

where the source term E is evaluated using the value of the variable X at the instant n and the source term I is evaluated using the value of the variable X at the instant $n + 1$. We denote the evaluation of the term E as explicit and of the term I as implicit.

Linear approximation of implicit source terms In the system of governing equations (5.56) some functions of the phase-field variable are non-linear (*e.g.* the double well function $W(\varphi)$ or the interpolation function $\nu(\varphi)$). These non-linearities are necessary for the properties of the phase field model, *e.g.* the control of the bulk phase physical properties for the non-linear function ν (*cf.* chapter 3). Some of these terms are required to be taken into account on an implicit way to preserve the accuracy of the solution (*cf.* section 8.1.2). Since the computation of non-linear terms is numerically costly, we introduce a quasi-implicit evaluation of these terms using an expansion of the advance in time that reads

$$I(X^{n+1}) \simeq \frac{\partial I}{\partial X}^{n} \left(X^{n+1} - X^{n}\right)$$

The consequence of this approximation on the numerical computation of the system of governing equations is of interest, since it allows the use of solvers of linear systems that are more performing than the non-linear ones.

C.2 Spatial discretization scheme

The MAC scheme In this numerical study we use the classical MAC scheme, that is represented on figure C.1. The physical domain is split in squared cells (for two dimensional simulations) of constant size Dx. The scalar

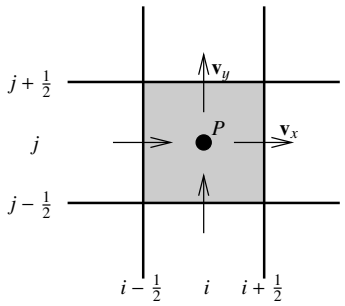

Figure C.1: Schematic representation of the MAC space discretization scheme

fields (pressure, temperature and phase field) are discretized at the center of the cells (black nodes indexed by integers) whereas the vectors ($\vec{V}$, $\nabla\varphi$, ...) are discretized on the faces of the cell (black arrows indexed by integers plus or minus a half). The faces are directed along the directions $\vec{e_x}$ and $\vec{e_y}$. The decomposition of a vector on the basis $(\vec{e_x}, \vec{e_y})$ is denoted $\vec{V} = V_x\,\vec{e_x} + V_y\vec{e_y}$ in the following. This scheme allows to easily control some vectorial identites as shown in the following.

Discretization of the spatial derivatives operators The discretization of the gradient ∇a of a scalar a is naturally

$$\begin{aligned}(\nabla a)_x\,(i+1/2;j) &= \frac{a(i+1;j)-a(i;j)}{Dx}\\ (\nabla a)_y\,(i;j+1/2) &= \frac{a(i;j+1)-a(i;j)}{Dx}\end{aligned}$$

The scalar product of two vectors $\vec{b_1}$ and $\vec{b_2}$ reads

$$\begin{aligned}\left(\vec{b_1}\cdot\vec{b_2}\right)(i;j) &= \frac{b_{1x}(i-1/2;j)b_{2x}(i-1/2;j)+b_{1x}(i+1/2;j)b_{2x}(i+1/2;j)}{2}\\ &+ \frac{b_{1y}(i;j-1/2)b_{2y}(i;j-1/2)+b_{1y}(i;j+1/2)b_{2y}(i;j+1/2)}{2}\end{aligned}$$

The divergence of a vector $\vec{b}$ reads

$$\nabla\cdot\vec{b}_{i;j} = \frac{b_x(i+1/2;j)-b_x(i-1/2;j)}{Dx} + \frac{b_y(i;j+1/2)-b_y(i;j-1/2)}{Dx}$$

As a consequence, our numerical scheme allows the continuous vectorial identity for any scalar a and vector $\vec{b}$

$$\nabla \cdot \left(a\,\vec{b}\right) = \nabla a \cdot \vec{b} + a\,\nabla \cdot \vec{b}$$

to be satisfied by the discrete scheme. This vectorial identity is of interest for our diffuse interface model since its satisfaction is a key element in the study of the consistency of the balance of discrete energy, *e.g.* Jamet et al. [68].

C.3 Solving alogorithm

Let us present the algorithm used in the numerical study of the system of governing equations. This algorithm is based on the projection method that is widely used in numerical simulations of incompressible flows (including two-phase flows with phase change) and that has been adapted to our quasi-compressible phase-field model for liquid-vapor flows with phase change.

The numerical algorithm is split into two main parts:

1. Evaluation of the mass transfer rate: φ^{n+1} and T^{n+1}
2. Computation of the dynamics: $\mathcal{G}^{n+1}$ and $\vec{V}^{n+1}$

Calculation of the mass transfer rate In the numerical algorithm proposed, the mass transfer rate is calculated using the coupling between the equation of evolution of the temperature (5.56d) and the *AC* equation (5.56a). In the uniform density case, since the governing equations reduce to these two equations (*cf.* system (5.57)), the algorithm reduces to this step. In the isothermal case, this step reduces to the solving of single *AC* equation. This equation takes into account both pressure (appearing in the expression of $\tilde{\mu}$) and velocity (appearing in the convective part of $d\varphi/dt$) on an explicit way. The main variable of this system is therefore $(\varphi(\vec{x}), T(\vec{x}))$ reducing to $\varphi(\vec{x})$ in the isothermal case. Once the new phase field $\varphi^{n+1}$is known, the phase change rate of the corresponding time step is given and one is able to use the projection method.

Projection method The projection method is a widely used method for solving the coupling between continuity equation and momentum balance equations for incompressible flows. As a result of this method, a single Poisson equation on the pressure has to be solved in order to compute both the pressure and the velocity (or momentum) fields. The original method is based on the fact that the incompressibility constrains the velocity field to be divergence free. In our case of liquid-vapor flows with phase change, the divergence of the velocity fluid is non zero due to the phase transformation even though the single phase states are incompressible. Nevertheless, since the bulk phases are incompressible, the only way the density can evolve along a current line is through phase change. Phase change rate is $(d\varphi/dt)$ and since ρ is only a function of φ, it is directly linked to the field $(d\rho/dt)$. As a consequence, since φ^{n+1} is given, we set (*cf.* the continuity equation (5.56b))

$$\nabla \cdot \rho\vec{V}^{n+1} = \frac{d\rho}{d\varphi}^{n} \frac{\varphi^{n+1} - \varphi^{n}}{Dt} \tag{C.1}$$

Let us now take the divergence of the momentum balance equation (5.56c), (where for the sake of simplicty we set $Fr = \infty$ and $Re = \infty$) it yields

$$\frac{\nabla \cdot (\rho\, V)^{n+1} - \nabla \cdot (\rho\, V)^{n}}{Dt} + \nabla \cdot (\rho V \cdot V)^{n} = -\Delta\mathcal{G}^{n+1} + \frac{\left(\frac{dW}{d\varphi}^{n+1} - \varepsilon^2 \Delta\varphi^{n+1}\right)}{\varepsilon\, We} \nabla\varphi^{n} \tag{C.2}$$

Using equation (C.1), equation (C.2) is a Poisson equation in $\mathcal{G}^{n+1}$ that can thus be solved using linear solvers.

It is worth noting that this numerical scheme, here used in the solving of phase-field equations, is very similar to the one used in sharp methods for incompressible bulk phases (*e.g.* Juric and Tryggvason [69]). Contrarily to these methods, it is not required to smooth out the source terms associated with neither the mass transfer rate nor the surface tension.

Résumé en français

Introduction

Dans ce mémoire, nous étudions un modèle de champ de phase dédié à l'étude de l'ébullition. Cette partie constitue un résumé en français de cette étude.

Contexte

L'étude des écoulements liquide vapeur avec changement de phase concerne à la fois la mécanique des fluides diphasique et la dynamique de transition de phase. Les écoulements bouillants sont rencontrés dans une large gamme d'échangeurs de chaleur depuis les micro-caloducs jusqu'à de grandes structures industrielles. L'utilisation de fluides bouillants est motivée par la grande efficacité du transfert de chaleur procurée par le régime dit d'ébullition nucléée. En effet, lorsqu'un fluide bout, le transport de chaleur latente, permettant de convecter de grandes quantités de chaleur, vient s'ajouter au phénomène de transport de chaleur sensible. De plus, le processus de changement de phase s'effectue à température quasiment constante : la température de saturation. Dans l'industrie nucléaire, les phénomènes de changement de phase sont plus principalement impliqués lors de l'étude des situations incidentelles pendant lesquelles des phénomènes tels que la crise d'ébullition peuvent se produire. L'amélioration et le contrôle (principalement pour des raisons de sûreté) des installations industrielles est ainsi contraint par la compréhension du processus d'ébullition. Les mécanismes impliqués dans ce processus couvrent une large gamme d'échelle spatiale depuis l'échelle des écoulements moyennés jusqu'à l'échelle de la bulle elle-même, *e.g.* Carey [28]. Pour cette raison, l'étude des écoulements bouillants reste de nos jours un défi scientifique.

L'étude des installations industrielles passe par l'utilisation d'outils d'analyse des grandes échelles des écoulements bouillants ; les modèles correspondants sont basés sur une représentation moyennée en temps et en espace de l'écoulement. Il est alors nécessaire de renseigner certains termes à l'aide de modèles pour représenter la physique se passant à des échelles inférieures à celle de la moyenne. Ces modèles, ou encore lois de fermeture, sont généralement issus de travaux expérimentaux. Mais ces lois sont trop souvent établies pour des configurations spécifiques, ce qui limite le domaine de validité de leur usage. Ainsi, il reste à ce jour un réel besoin de lois de fermeture concernant les phénomènes à petite échelle. Les expériences à cette échelle sont *(i)* difficile à mettre en œuvre et *(ii)* difficiles à interpréter de par la difficulté d'obtenir certaines mesures localement. L'utilisation de la simulation numérique n'est pas limitée par ces dernières contraintes et cet outil apparaît ainsi comme une source complémentaire d'information. La simulation numérique directe prend en compte le spectre complet d'échelles de temps et d'espace. Les limitations actuelles des moyens de calcul ne permettent pas d'envisager la résolution d'un tel spectre pour des systèmes de la taille d'une installation industrielle. On peut par contre envisager l'étude de systèmes de la taille de l'ordre du centimètre et ce pour des temps physiques de l'ordre de la seconde (qui correspondent à des systèmes contenant une population de bulles durant l'ensemble de leur phase de croissance). Ainsi l'utilisation de la simulation numérique directe est tout à fait adaptée au développement et à la validation de modèles de lois de fermeture, ainsi que de modèles de mécanisme de phénomènes tels que la crise d'ébullition.

Crise d'ébullition

Le phénomène Au delà d'une certaine valeur du flux de chaleur pariétal, appelée flux critique, se produit une transition soudaine de régime d'ébullition : la crise d'ébullition. Cette transition induit une élévation brusque et très importante de la température pariétale ; cette élévation peut entraîner la fonte de la paroi. Le mécanisme

physique à l'origine de cette transition est à ce jour mal compris. Sa compréhension est en soi un défi scientifique. Ses conséquences, en particulier l'embrasement de la paroi, peuvent causer des dommages irrémédiables concernant l'intégrité de l'échangeur de chaleur : dans une installation nucléaire la crise d'ébullition doit être évitée pour des raisons de sûreté. Ceci justifie l'intérêt industriel de son étude.

Dans notre étude des écoulements bouillants au chapitre I, nous nous intéresserons plus particulièrement à ce phénomène.

Étude de la crise d'ébullition La crise d'ébullition est un sujet d'étude depuis plusieurs décennies et de nombreuses tentatives ont été faites afin de la modéliser. En raison d'un manque de preuves expérimentales, aucune n'a pu à ce jour être retenue. De manière plus générale, il reste beaucoup à attendre d'observations expérimentales afin de comprendre plus clairement le phénomène comme l'a souligné Sadavisan et al. [117]. Le premier chapitre de cette étude est ainsi dédié à la présentation et à l'étude de la compréhension actuelle de la crise d'ébullition en vue d'identifier les mécanismes physiques susceptibles d'être à son origine. Ceci nous permet entre autre de définir un problème dont l'étude est propre à éclairer notre connaissance de la crise d'ébullition : une transition dans le régime de croissance de bulle en paroi pour des conditions de fort flux pariétal. Étant donnés les phénomènes physiques impliqués dans cette dynamique, la simulation numérique est considérée comme l'outil d'étude le plus pertinent. Cette conclusion intermédiaire sert alors de motivation pour le reste de notre étude.

Un modèle d'interface diffuse pour la simulation numérique des écoulements bouillants à l'échelle de la bulle

Le but de cette partie est de développer un modèle à même d'être utilisé pour la simulation numérique d'écoulements bouillants et plus particulièrement la dynamique de croissance de bulles en paroi. Les différentes méthodes numériques permettant l'étude d'écoulements liquide vapeur avec changement de phase à l'échelle de la bulle sont présentées et analysées au chapitre II. La plupart de ces méthodes se basent sur un modèle de type Gibbs des interfaces : l'interface est dite étroite *i.e.* est modélisée comme une surface de discontinuité. Les difficultés rencontrées dans les méthodes se basant sur ce formalisme sont principalement associées à la difficulté de gérer numériquement le déplacement de cette frontière libre, d'autant plus lorsqu'elle est le lieu d'une transition de phase. Les méthodes basées sur les modèles d'interface diffuse, pour lesquels l'interface est vue comme une zone de transition volumique, proposent un système d'équations continues thermodynamiquement cohérent incluant la description du mouvement des interfaces. Par conséquent le traitement numérique de l'écoulement polyphasique s'en trouve simplifié puisque, contrairement aux méthodes évoquées précédemment, il n'est pas requis d'utiliser une gestion spécifique de l'interface. Néanmoins l'épaisseur caractéristique de la zone de transition correspondant à l'interface a un ordre de grandeur de quelques Ångströms aussitôt que l'on s'éloigne du point critique. L'utilisation d'un tel modèle pour l'étude de phénomènes à l'échelle de l'ordre du millimètre, comme une croissance de bulle, perd alors toute sa pertinence. Ce constat nous amène à considérer les modèles de type champ de phase. Le modèle thermodynamique utilisé dans ces méthodes est basé sur l'introduction d'une variable additionnelle et abstraite, un paramètre interne à la zone de régularisation, appelé *champ de phase*, qui permet de décrire un système multiphasique ou multi-composant, comme introduit par Truskinovsky [136]. Les modèles de champ de phase préexistants sont pour majeure partie dédiés à la transition de phase solide-liquide ou solide-solide. Selon notre interprétation, ces modèles permettent de régulariser l'interface de manière artificielle mais néanmoins thermodynamiquement cohérente. Cette dernière propriété est particulièrement attractive tant du point de vue de la modélisation que du point de vue de la résolution numérique. Pour autant, notre revue bibliographique des modèles existants montre le besoin de développer une nouvelle formulation de modèle de champ de phase adaptée à l'étude de la transition de phase liquide-vapeur, les phases étant supposées incompressibles.

Au chapitre III, nous étudions dans un premier temps le modèle thermodynamique de champ de phase. Nous proposons une expression pour le potentiel thermodynamique permettant à la fois de contrôler les propriétés physiques des phases et la description de la zone interfaciale. La structure de l'interface à l'équilibre dans les cas plan et de symétrie sphérique est étudiée aux chapitres III et IV respectivement. En particulier, nous montrons que le modèle est cohérent avec la théorie de Laplace. Nous étudions alors des situations hors équilibre et introduisons des mécanismes dissipatifs dans le modèle au chapitre V. Nous établissons le système d'équations thermodynamiquement cohérent qui inclut la modélisation de la dynamique de l'interface. Ce système d'équations est ensuite étudié dans deux configurations théoriques : la stabilité des états homogènes (*cf.* chapitre VI) et le

changement de phase stationnaire mono-dimensionnel (*cf.* chapitre VII). En particulier nous étudions le modèle discontinu équivalent et déduisons sa relation cinétique qui est une relation de fermeture nécessaire, *e.g.* Truskinovsky [134]. L'utilisation de ce formalisme apporte une interprétation claire des équations de type champ de phase. En dernier lieu, au chapitre VIII, nous présentons le développement d'un algorithme de résolution de ce modèle ainsi que les premières simulations numériques réalisées. Nous étudions ainsi la capacité du modèle à être utilisé à plus long terme pour l'étude de la dynamique de croissance de bulle.

I Étude de la crise d'ébullition

Nous étudions dans cette partie le phénomène de crise d'ébullition. Il s'agit d'une instabilité dans le processus d'échange de chaleur entre un élément chaud et un fluide bouillant. Cette instabilité est à l'origine d'une élévation brutale de la température de l'élément chauffant ce qui peut fortement l'endommager. La crise d'ébullition est un des phénomènes envisagés dans les scenarii incidentels se rapportant à l'étude de la sûreté des centrales nucléaires. A ce jour, l'origine physique de la crise d'ébullition est mal comprise. Le but de la présente partie du mémoire est de définir, à partir des connaissances actuelles, un objet d'étude permettant d'améliorer la connaissance de ce phénomène. Pour ce faire, on propose une étude critique de la modélisation de la crise d'ébullition permettant d'identifier les aspects de l'ébullition les plus pertinents à éclaircir.

I.1 Crise d'ébullition et régimes d'ébullition

On considère dans la suite de cette étude l'ébullition en vase d'un fluide pur. Ainsi on ne considère pas d'écoulement moyen. Nous proposons tout d'abord de reprendre la présentation générale de l'ébullition en vase. Nukiyama [103] a étudié le transfert de chaleur entre un élément chauffant et un fluide environnant, introduisant le premier ses principales caractéristiques.

Considérons premièrement que la paroi inférieure du vase est l'élément chauffant. Nous notons q le flux de chaleur transmis au fluide par cette plaque et $\langle \Delta T \rangle \triangleq \langle T - T_{sat} \rangle$ l'écart moyen de température de la paroi par rapport à la température de saturation[1]. Ces deux grandeurs caractérisent le régime d'ébullition considéré comme nous le voyons par la suite. L'ébullition en vase est caractérisée par trois différents régimes d'ébullition. La figure C.2 donne l'allure des variations du flux q échangé à travers la paroi en fonction de sa température $\langle \Delta T \rangle$. Cette courbe est appelée courbe de Nukiyama et on y distingue clairement les trois différents régimes NB, TB, FB par les trois différentes portions de courbe.

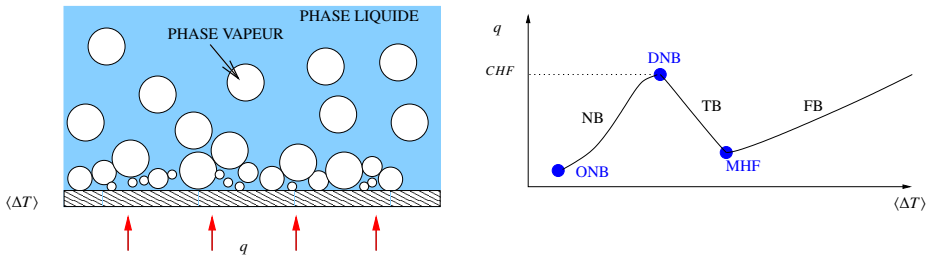

Figure C.2: Courbe de Nukiyama

Différents régimes d'ébullition

Ébullition nucléée Considérons premièrement le régime d'ébullition nucléée (NB sur la figure C.2). Ce régime est caractérisé par de faibles valeurs de la surchauffe pariétale $\langle \Delta T \rangle$. Pour cette raison, l'ébullition nucléée est un processus efficace de transfert de chaleur. Ceci explique l'usage répandu de fluides bouillants dans les échangeurs industriels. Ce régime se déclenche à la suite du régime de convection naturelle (point ONB). Des bulles de vapeur se forment alors en proche paroi avant de s'en détacher et de s'écouler dans la partie liquide supérieure. L'ébullition nucléée connaît une limite aux forts flux de chaleur q (point DNB). La valeur du flux correspondant à cette limite est le flux critique (CHF). Il est important de noter que, contrairement aux autres régimes d'ébullition, la paroi est couverte par une couche quasiment continue de liquide.

Ébullition en film Dans le régime d'ébullition en film, un film de vapeur couvre entièrement la paroi. On considère que l'interface du film en contact avec le liquide est à la température de saturation. Cette interface liquide vapeur est le lieu d'un processus cyclique de formation (croissance puis départ) de bulles gouverné par l'instabilité de Rayleigh Taylor. Il s'agit aussi du lieu de la transition de phase liquide-vapeur. Le flux de chaleur

[1] La température de saturation est la température à laquelle le liquide et sa vapeur sont à l'équilibre thermodynamique.

pariétal traverse ainsi une couche de vapeur avant d'atteindre l'interface où il est le "moteur" de la transition de phase. La diffusivité thermique de la vapeur étant bien moindre que celle du liquide, ce régime est caractérisé par des valeurs élevées de la température de paroi.

Lorsque le flux critique, CHF, est atteint, le système opère une transition entre le régime d'ébullition nucléée et le régime d'ébullition en film. Cette transition est caractérisée par une soudaine et importante élévation de la température de paroi pouvant atteindre plusieurs centaines de degrés Kelvin. La crise d'ébullition est cette même transition ; étant donnée la description précédente des régimes d'ébullition, la crise d'ébullition est associée à un assèchement total de la paroi.

Ébullition de transition Lors d'une ébullition en régime de transition, la paroi chaude est alternativement asséchée puis remouillée. Ce régime est difficile à modéliser en tant que tel et on l'associe le plus souvent à une superposition des régimes d'ébullition nucléée et en film. Ce régime est instable lorsque le flux de chaleur q est imposé et ne peut être observé que si la température moyenne de la paroi est imposée. Du fait des assèchements intermittents les valeurs locales instantanées du flux et de la température varient fortement.

Précisions et remarques

Transitoire Dans une situation industrielle, la crise d'ébullition se produit en conditions transitoires. En présence de transitoires très rapides, il est justifié, comme souligné par Berthoud [14], de considérer des mécanismes de crise d'ébullition différents. Dans la suite de cette étude, nous considérons donc le cadre de transitoires lents, au sens précisé par l'étude expérimentale de Sakurai [118].

Écoulement moyen Les échangeurs industriels sont le plus souvent des boucles au sein desquelles le fluide calo-porteur s'écoule, la partie chauffante ne constituant qu'une portion de cette boucle. Cette situation est donc en de nombreux points différentes de la configuration plus académique de l'ébullition en vase. Néanmoins, l'influence des "paramètres" de configuration sur la crise d'ébullition peut être considérée comme secondaire : la valeur du flux critique dépend de la configuration mais le mécanisme physique peut être similaire. Nous revenons plus en détail sur cette hypothèse lorsque nous abordons plus précisément les principaux mécanismes potentiellement en jeu lors de la crise d'ébullition (*cf.* section I.3).

Conclusion Le processus d'ébullition a été introduit comme un mécanisme de transfert de chaleur dont l'efficacité est grande tant que l'on observe le régime d'ébullition nucléée, *i.e.* tant que la paroi chaude est recouverte de liquide. La transition de régime correspondant à un assèchement partiel ou total de la paroi est un phénomène violent appelé crise d'ébullition pour lequel nous supposons que le mécanisme physique ne dépend pas de la configuration de l'écoulement bouillant.

I.2 Mécanismes physiques

Après avoir introduit les principales caractéristiques de l'ébullition en vase, nous nous intéressons de plus près à l'ébullition nucléée dans des conditions proches de la crise d'ébullition. Par l'étude des phénomènes qui s'y rapportent, nous souhaitons identifier les causes potentielles de la crise d'ébullition.

Un premier constat motive plus précisément notre approche : tout paramètre (la micro-structure de la paroi aussi bien que l'intensité de l'écoulement convectif dans la conduite) ayant une influence sur l'ébullition nucléée modifie la valeur du flux critique. Ceci justifie donc l'étude exhaustive des phénomènes ayant trait à l'ébullition nucléée à fort flux. Une meilleure compréhension du phénomène doit ainsi permettre d'identifier les mécanismes ayant un effet paramétrique sur la crise d'ébullition de ceux qui en sont la cause même.

On distinguera les différents phénomènes de l'ébullition en paroi selon trois différents niveaux de description du processus. Chaque niveau de description se rapporte à une échelle spatiale caractéristique : ainsi cette classification permet de considérer les phénomènes pouvant effectivement interagir, initier une instabilité du régime et donc finalement être à l'origine de la crise d'ébullition. La cellule de base du phénomène d'ébullition est la bulle et les échelles caractéristiques de chaque niveau de description se définissent naturellement par rapport au diamètre caractéristique d'une bulle.

Échelle de l'écoulement diphasique Ce niveau de description est le moins détaillé, et par là même le plus idéalisé des trois niveaux considérés. Il correspond à une vision moyennée du système liquide-vapeur. L'échelle caractéristique est supérieure à celle de la bulle, cette dernière n'étant pas considérée comme une entité à part entière. Le flot de bulles généré en proche paroi est vu comme un canal de vapeur et les phénomènes proche paroi comme la dynamique de croissance des bulles sont ignorés. A ce niveau d'analyse on considère principalement les phénomènes hydrodynamiques diphasiques. Par la suite on s'intéresse peu à ce niveau de description et on ne détaille donc pas plus les principaux phénomènes lui étant associés.

Échelle de la bulle moyenne L'échelle caractéristique de ce niveau de description est celle de la bulle. Cette dernière est considérée comme étant de géométrie fixée mais de taille variable. Ainsi on modélise sa phase de croissance en paroi. Ceci permet de modéliser plus finement les différents phénomènes jouant un rôle dans l'échange de chaleur fluide/paroi. On distingue notamment le transport de chaleur latente ainsi que l'influence de la présence de bulles sur l'intensité des échanges convectifs. La création de bulles est modélisée comme un mécanisme cyclique localisé (sur des sites) constitué d'une suite d'événements : nucléation, croissance, départ, attente. En outre certains modèles considèrent l'interaction inter-sites. Cette échelle d'analyse regroupe une grande palette de phénomènes pouvant être associés à un scenario hypothétique de la crise d'ébullition comme nous le montrons au paragraphe 1.2.3. Leur énumération est reprise dans la liste suivante. On remarquera en particulier la nature très variée des phénomènes, thermiques, mécaniques, géométriques.

1. répartition du flux de chaleur pariétal parmi différents mécanismes de transfert de chaleur
   (a) transport de chaleur latente (évaporation) (éventuellement deux sous-contributions : localisé dans une micro-couche de liquide coincée entre bulle et paroi *versus* autour de la bulle)
   (b) conduction transitoire
   (c) convection naturelle
2. fréquence spatiale du processus de croissance de bulle, concept de densité de site de nucléation (NSD fonction de la surchauffe pariétale)
3. taux de croissance des bulles
4. taille des bulles au départ de la paroi
5. temps d'attente entre deux formations de bulle sur un même site
6. interaction entre bulles (thermique, hydrodynamique, coalescence)
7. agitation et instabilité des bulles

Table C.1: Mécanismes physiques à l'échelle de la bulle

Échelle locale Ce niveau de description est le plus fin, l'échelle caractéristique des phénomènes considérés étant inférieure à celle de la bulle. Ainsi la géométrie complète de la bulle est prise en compte, c'est à dire la description fine de la position de l'interface liquide-vapeur. À ce niveau d'analyse l'ensemble des équations de Navier-Stokes doivent être résolues au sein de chaque phase (liquide ou vapeur), phase dont les frontières (interface) sont libres. Cette résolution nécessite d'avoir recours à des méthodes numériques. Les phénomènes physiques à cette échelle sont repris dans la liste C.2. Ce niveau de description peut-être nécessaire pour décrire certaines instabilités dans le processus de croissance de bulle en paroi qui, nous le verrons, peuvent être à l'origine de la crise d'ébullition et qui ne sont pas captées aux échelles supérieures de modélisation.

1. Courbure locale de la bulle et force capillaire
2. Pression de recul à l'interface : le saut de pression vaut $[\![P]\!] = -\Gamma^2[\![1/\rho]\!]$ où Γ est le taux de transfert de masse local (*cf.* notre étude des conditions de saut à l'interface en section VII.1)
3. Dynamique de la ligne de contact (angle de contact statique-dynamique) et flux de chaleur singulier associé (*cf.* Anderson and Davis [3] ou Mathieu et al. [92])
4. Pesanteur : effet du gradient de pression hydrostatique sur la forme de la bulle et conséquemment sur sa dynamique de départ (*cf.* Shikhmurzaev [125] dont le modèle prend en compte une forme de bulle dépendant du temps ainsi qu'un modèle spécifique pour la dynamique de la ligne de contact)
5. Conduction transitoire locale au sein de l'aire de contact entre la paroi et la vapeur en pied de bulle (*cf.* Blum et al. [16])

Table C.2: Mécanismes physiques à l'échelle locale

I.3 Modélisation de la crise d'ébullition

La question induite par notre présentation du régime d'ébullition nucléée est la suivante : quel niveau de description de l'ébullition est à même de capturer le mécanisme physique à l'origine de la crise d'ébullition ? D'autres questions ouvertes concernant la crise d'ébullition sont abordées dans cette étude. Précisons que nous considérons la crise d'ébullition comme un mécanisme à l'origine d'un assèchement en paroi se produisant au point de DNB, et ce indépendemment du type de conditions thermiques (flux ou température imposé). Ainsi un même mécanisme est supposé pouvoir expliquer la crise du régime d'ébullition nucléée qui initie une transition vers soit le régime d'ébullition en film, soit le régime d'ébullition de transition.

Dans cette partie de l'étude, nous étudions les différents modèles proposés dans la littérature pour expliquer le mécanisme de la crise d'ébullition. Ils sont regroupés selon le niveau de description auquel ils se réfèrent. Le but de cette présentation est d'utiliser les diverses informations que nous proposent ces modèles afin de définir un problème élémentaire dont la résolution permettrait d'améliorer la compréhension du phénomène de crise d'ébullition. Cette analyse permettra plus particulièrement de définir un cahier des charges pour le modèle de la transition de phase liquide-vapeur que nous étudions dans les chapitres suivants.

Modèle hydrodynamique de Zuber La corrélation de Zuber [156] permet d'obtenir une estimation de la valeur du flux critique dont la validité est relativement bonne. Zuber [156] a proposé un mécanisme pour la crise d'ébullition associé á l'échelle de l'écoulement moyen. L'étude de l'excitation de l'instabilité de type Kelvin-Helmoltz par la longueur d'onde la plus instable de Rayleigh-Taylor au sein de l'écoulement à bulles permet de déduire l'expression suivante du flux critique :

$$q_{CHF\,Zuber} = \frac{\pi}{24}\mathcal{L}\rho_v \sqrt[4]{\frac{\sigma g(\rho_l-\rho_v)}{\rho_v^2}}\sqrt{\frac{\rho_l+\rho_v}{\rho_l}} \tag{I.3}$$

où $\mathcal{L}$ est la chaleur latente associée au changement de phase liquide-vapeur, σ est la tension interfaciale, ρ est la masse volumique des phases liquide ($_l$) et vapeur ($_v$), et g est la gravité. Néanmoins, le modèle de Zuber, s'il permet effectivement de déduire une bonne approximation du flux critique, n'est pas basé sur une description réaliste des événements relatifs à la crise d'ébullition comme le montre, par exemple, l'étude expérimentale de Katto and Otokuni [75]. Nous verrons par la suite comment il est possible d'interpréter le succès de la formule (I.3) (déduite d'une analyse à l'échelle de l'écoulement moyen) en considérant que l'instabilité se produit à l'échelle locale.

Limite des mécanismes associés à l'échelle de la "bulle moyenne" Dans la partie 1.3.2, nous étudions en détail différents modèles pour la crise d'ébullition rattachés à une modélisation de l'ébullition nucléée à l'échelle

de la bulle moyenne. Cette étude montre la variété de mécanismes pouvant mener à une instabilité du régime d'ébullition nucléée. Ainsi la transition de régime est alternativement associée à des instabilités thermiques (*cf.* Kolev [79]), hydrodynamiques (*cf.* Chang [32]), ou encore à une trop forte densité de population de bulles en proche paroi donnant lieu à des phénomènes de coalescence (*cf.* Bang et al. [9]). Néanmoins, il apparaît clairement qu'aucun de ces phénomènes (et *a fortiori* de ces scenarii) ne peut être soutenu par des observations expérimentales de l'ébullition nucléée à des conditions proches de celles du DNB. En outre, certains aspects de ces modèles sont contradictoires avec des observations fines de l'ébullition en paroi comme celles rapportées par Theofanous et al. [131]. Notre analyse ne retient donc aucun mécanisme de crise d'ébullition pouvant être décrit à l'échelle de la bulle moyenne et soutenu par l'expérience. Ces conclusions nous amènent à considérer les phénomènes associés à l'échelle locale.

Mécanismes locaux pour la crise d'ébullition Cette famille de modèles regroupe des scenarii pour lesquels la transition de régime d'ébullition est contrôlée par la dynamique d'une bulle isolée lors de sa phase de croissance en proche paroi. On distingue notamment différentes sous catégories de modèles.

- ⋆ Modèles basés sur l'instabilité de recul. Le saut de pression à l'interface comprend un terme, dit de recul, quadratique en le taux de transfert de masse. Les modèles de Kandlikar [70] ou Nikolayev et al. [100], suivant l'idée de Sefiane et al. [120], supposent qu'aux conditions du flux critique la pression de recul constitue la force dominante du bilan de quantité de mouvement à l'interface. Elle induit une dynamique d'étalement de la zone sèche correspondant au pied d'une bulle, cette dynamique menant finalement à la crise d'ébullition.

- ⋆ Modèles basés sur un bilan thermique au sein de la zone sèche. L'idée repose sur l'hypothèse qu'au delà d'un certain flux critique, la paroi en contact avec la vapeur sous le pied d'une bulle devient suffisamment chaude pour empêcher tout re-mouillage ultérieur. On cite par exemple les modèles de Bricard et al. [20] ou de Blum et al. [16]. Ces modèles ne sont pas considérés comme réalistes car ils ne permettent pas d'expliquer la transition du régime d'ébullition nucléée vers l'ébullition de transition qui correspond pour autant à une dynamique d'assèchement local similaire à la crise d'ébullition mais se produisant pour des températures de paroi faibles. Dans ce cas la dynamique d'assèchement ne résulte donc pas d'une température très élevée au sein de la zone sèche.

En ce qui concerne les modèles basés sur l'instabilité de recul, nous avons montré dans la section 1.3 que les résultats obtenus ne sont pas suffisamment probants car il leur manque la prise en compte d'un mécanisme de départ de la paroi à même de contrebalancer la dynamique d'amorçage de l'étalement décrite.

Conclusion sur l'étude de la modélisation actuelle de la crise d'ébullition Nous avons montré par cette étude qu'il est important de considérer la crise d'ébullition comme étant une conséquence logique de la description de l'ébullition nucléée plutôt qu'un phénomène indépendant de ce dernier. En effet, dans ce cadre de travail, il est possible de discriminer un modèle d'un autre en se basant sur des observations expérimentales du régime d'ébullition nucléée à fort flux, ce qui demeure impossible sinon.

I.4 Un mécanisme pour la crise d'ébullition à l'échelle locale

Croissance instable d'une bulle en proche paroi Dans la partie 1.4 du mémoire nous reportons et analysons des observations expérimentales (en particulier les travaux de Theofanous et al. [130, 131]) des phénomènes proche paroi dans des conditions de flux critique. Les conclusions suivantes en sont tirées

1. La séparation d'échelle utilisée lors de notre présentation des mécanismes du régime d'ébullition nucléée est attestée expérimentalement même à très fort flux : quelle que soit la quantité de vapeur formée une fine couche de liquide couvre la paroi, au sein de cette couche se produit une ébullition nuclée intense. Au dessus de cette couche liquide, les bulles formées coalescent et forment de grosses masses de vapeur dont la taille caractéristique semble déterminée par l'instabilité de Rayleigh Taylor. La couche liquide est toujours approvisionnée et les phénomènes s'y produisant peuvent être considérés indépendamment de la description du reste de l'écoulement diphasique.

2. Dans des conditions de fort flux pariétal la dynamique de croissance de bulle dans cette couche liquide peut être "irrégulière" : cette irrégularité correspond à un assèchement local en pied de bulle qui modifie grandement les échelles et temps caractéristiques des bulles ainsi formées. La fréquence d'apparition de ces phénomènes irréguliers est d'autant plus importante qu'on s'approche des conditions du flux critique. Au flux critique, il a été observé qu'une des taches sèches ainsi formée s'étale, menant finalement à une transition de régime.

Ainsi nous avons montré à l'aide de résultats expérimentaux que la crise d'ébullition peut être vraisemblablement associée à des phénomènes à l'échelle dite "locale".

Un scénario pour l'instabilité du régime d'ébullition nucléée Nous proposons un mécanisme pour la crise d'ébullition basé sur une instabilité dans la croissance de bulle en proche paroi. Comme représenté sur la figure C.3, on s'intéresse à l'évolution d'une bulle ayant initialement une grande surface de contact avec la paroi (image de la configuration initiale). Cette configuration "étalée" correspond à une première phase dans le scénario d'instabilité cohérent avec le modèle de Nikolayev et al. [100] : la pression de recul domine la pression capillaire et le pied de bulle s'étale. Dans le régime d'ébullition nucléée, les forces capillaire et hydrostatique promeuvent suffisamment l'élévation de la bulle pour engendrer finalement la formation d'une bulle ressemblant à un gros champignon quittant la paroi (image de droite sur la figure C.3). Aux conditions du DNB au contraire, sous l'action de la pression de recul, la bulle continue de s'étaler en un film de vapeur. Suivant les conditions thermiques en paroi, ce film de vapeur est stable (flux imposé supérieur au flux critique, transition vers l'ébullition en film, image en haut à gauche) ou instable (température imposée correspondant au DNB et donc inférieure au MHF, régime d'ébullition de transition, image en bas à gauche). Ce scénario permet donc de décrire la crise d'ébullition comme une instabilité dans le régime d'ébullition nucléée qui conduit naturellement vers les autres régimes d'ébullition. Nous montrons en outre au paragraphe 1.4.2 que ce scénario est cohérent avec la corrélation de Zuber (I.3) pour le flux critique. En effet les grandeurs physiques caractéristiques de ce mécanisme sont celles de la corrélation. Même si cette dernière a pu être déduite d'une étude à l'échelle de l'écoulement diphasique, nous montrons donc qu'elle peut être interprétée à l'échelle locale.

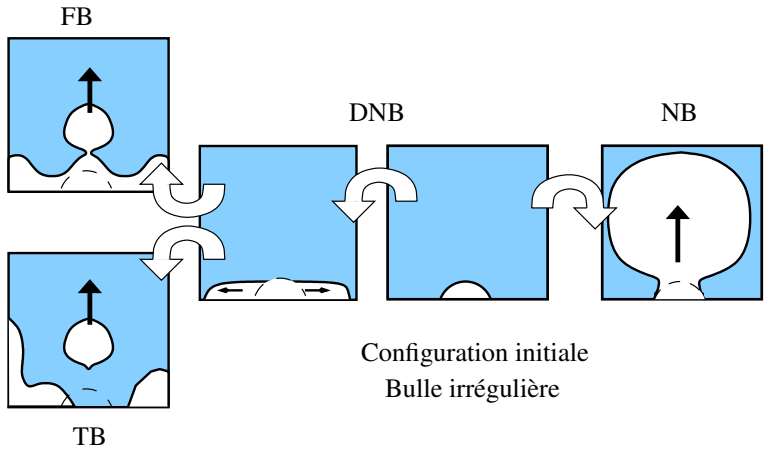

Figure C.3: Un mécanisme de la crise d'ébullition à l'échelle "locale"

L'étude de la dynamique de croissance d'une bulle Pour étudier la dynamique de la croissance de bulle correspondant au scénario instable décrit par la figure C.3, il est nécessaire de résoudre un problème à frontière libre (l'interface liquide-vapeur) et de prendre en compte les phénomènes suivants :

- ⋆ courbure locale et force capillaire
- ⋆ pression de recul
- ⋆ effet de la pression hydrostatique sur la dynamique de départ d'une bulle (*cf.* les travaux de Shikhmurzaev [124])

- ⋆ conduction de la chaleur dans le liquide en proche paroi, chaleur latente de changement d'état

Il est important de noter que la compressibilité des phases liquide et vapeur n'apparaît pas en tant que paramètre physique dans la corrélation de Zuber (I.3) ni comme un mécanisme prépondérant dans notre scenario ou dans tout autre des scenarii que nous avons analysé. Ainsi on suppose dans la suite de cet étude que l'hypothèse d'incompressibilité des phases liquide et vapeur est justifiée pour l'étude du mécanisme de crise d'ébullition. Ainsi, même si les effets compressibles jouent un rôle important dans l'initiation de la croissance d'une bulle (phase de nucléation et début de croissance, *e.g.* Mikic et al. [93]), son rôle est supposé comme non déterminant en ce qui concerne le scénario d'instabilité proposé. Étant donné la géométrie complexe de l'interface, ainsi que la nécessité de prendre en compte des couplages entre des phénomènes thermiques (conduction et chaleur latente) et mécanique (pression de recul, capillaire), l'utilisation d'une approche numérique pour résoudre cet écoulement diphasique s'impose.

I.5 Conclusion de notre étude de la crise d'ébullition

Après avoir présenté de manière générale les écoulements bouillants, nous avons introduit la problématique de la crise d'ébullition, phénomène limitant l'efficacité du transfert de chaleur et dont le mécanisme reste à ce jour mal compris. Nous avons alors analysé l'état de l'art de la modélisation de la crise d'ébullition : cette étude a révélé que la principale faiblesse de ces modèles est liée au manque d'informations expérimentales à même de les avérer. Notre analyse d'observations récentes des phénomènes proche paroi en ébullition nucléée à fort flux nous a permis d'identifier une instabilité dans le dynamique de croissance de bulle. Nous en avons déduit un scénario pour la crise d'ébullition. Les mécanismes physiques en jeu dans cette instabilité sont cohérents avec la corrélation de Zuber pour le flux critique, corrélation permettant d'obtenir une estimation de la valeur du flux critique. Pour étudier cette dynamique, il est nécessaire d'avoir recours à la simulation numérique et nous avons clairement défini l'ensemble des phénomènes physiques nécessaires et suffisants à cette étude. En particulier, nous avons montré que la compressibilité des phases liquide et vapeur n'est pas un mécanisme physique prépondérant pour l'étude du mécanisme présupposé pour la crise d'ébullition. Par la suite nous nous intéressons aux méthodes numériques permettant une telle étude.

II Méthodes numériques pour l'étude des écoulements liquide-vapeur

II.1 Les familles de méthodes

On s'intéresse dans ce chapitre aux méthodes permettant de résoudre les écoulements bouillants à l'échelle de la bulle, *i.e.* permettant de résoudre les équations de Navier-Stokes au sein des phases liquide et vapeur en prenant en compte la frontière libre que constitue l'interface entre ces deux domaines. On distingue dans un premier temps deux descriptions mathématiques de la position $\mathbf{x_i}$ de cette interface.

- ⋆ La représentation explicite $\mathbf{x_i} = f(t)$ qui donne lieu aux méthodes purement lagrangiennes (*cf.* la méthode ALE [27]) , ou lagrangiennes mixtes (*cf.* la méthode front tracking [140]). Ces méthodes nécessitent le développement d'un traitement spécifique du maillage de l'interface. Ceci est à l'origine d'une complexité dans la méthode numérique ne permettant pas de vérifier les bilans de masse, quantité de mouvement, énergie à chaque étape de l'algorithme et notamment lors du déplacement de l'interface (*e.g.* [126]).
- ⋆ La représentation implicite *i.e.* $F(\mathbf{x_i}, t) = 0$ pour laquelle le champ F n'est pas unique qui donne lieu aux méthodes de type level set (basées sur l'utilisation d'une fonction distance à l'interface, *cf.* [123]) ou aux méthodes correspondant à l'utilisation d'une modélisation de l'interface comme diffuse. Dans ces deux cas le système d'équations continues est défini en tout point de l'espace incluant la description des interfaces ce qui constitue un avantage sur le plan de leur résolution numérique. On fera, pour cette raison, le choix d'utiliser une représentation implicite dans la suite de ce mémoire.

Dans les méthodes de type level set, il est nécessaire de définir des extensions des champs interfaciaux (comme la vitesse de l'interface ou la tension interfaciale) en les étalant numériquement. Ces méthodes ne proposent pas à ce jour une manière satisfaisante de prendre en compte la tension de surface. Contrairement aux autres méthodes les méthodes d'interface diffuse ne sont pas basées sur le modèle de Gibbs pour lequel les interfaces sont des surface de discontinuité des propriétés physiques du fluide mais elles considèrent plutôt l'interface comme une zone volumique de transition à travers laquelle l'ensemble des grandeurs varient continûment. Cette description est issue d'une modélisation thermodynamique du fluide comprenant une dépendance en des termes non-locaux (le plus fréquemment des gradients). Les équations du mouvement d'un tel fluide sont déduites de l'application des principes fondamentaux de la thermodynamique, le système d'équations permettant la représentation des phases et de l'interface est ainsi dit "thermodynamiquement cohérent". Cette caractéristique permet un contrôle plus aisé des différents bilans comme l'a montré Jamet et al. [68] pour ce qui concerne la prise en compte de la tension interfaciale. Pour ces raisons on fait le choix dans la suite de cette étude d'utiliser une modélisation de type interface diffuse pour étudier la dynamique de croissance d'une bulle.

II.2 Modèle à interface diffuse et méthode numérique

Principe des modèles à interface diffuse Les modèles à interface diffuse proposent une régularisation d'un problème discontinu basée sur une description thermodynamique particulière du fluide. Cette description repose sur deux ingrédients principaux. Supposons tout d'abord un système diphasique, une variable thermodynamique intensive X prenant une valeur caractéristique au sein de chaque phase (on peut penser naturellement à la masse volumique dans le cas liquide-vapeur). On considère alors le fluide décrit par une unique énergie fonction de X. Le premier ingrédient correspond à l'existence d'une partie non-convexe des variations de l'énergie du fluide en fonction du paramètre X entre les valeurs caractéristiques des phases. En utilisant le critère de Gibbs-Duhem, on montre que cette non-convexité induit la séparation du système en deux phases. La régularisation de l'interface entre ces phases repose sur l'introduction d'une dépendance de l'énergie en des termes non-locaux tel que ∇X. Cette contribution pénalise énergétiquement les états pour lesquels X varie fortement spatialement et n'autorise ainsi pas l'interface à être une surface de discontinuité. Une telle description thermodynamique définit l'interface comme une zone de transition ayant une épaisseur caractéristique et une énergie associée.

Par conséquent ces modèles permettent une description explicite des interfaces tout en introduisant une physique "interfaciale" supplémentaire par le biais du seul modèle thermodynamique du fluide.

II.3 Modèle de van der Waals

Pour décrire un fluide pouvant exister sous deux états liquide et vapeur et étant doué de capillarité, le modèle de van der Waals est *a priori* le plus à propos. Nous montrons ici que pour autant il n'est pas approprié à la

simulation numérique de la dynamique de croissance de bulles pour laquelle notre modèle est développé.

Un modèle complet Le modèle de van der Waals, encore appelé modèle du second gradient, est basé sur l'expression de l'énergie libre F en fonction de la masse volumique ρ. On considérera, dans un premier temps, uniquement les aspects isothermes de ce modèle.

Une épaisseur de l'interface trop faible La valeur physique de l'épaisseur de l'interface h est de l'ordre de quelques Å (Ångströms) aussitôt que les conditions thermodynamiques s'éloignent de celles du point critique. Par conséquent la taille caractéristique de la zone de transition est très largement inférieure à celle de la bulle qu'on souhaite étudier (un facteur 10^5 environ). Capturer numériquement les deux échelles nécessiterait des moyens de calcul hors de portée. En outre la pertinence de la description de phénomènes à une si petite échelle n'est pas assurée. Pour pouvoir envisager la régularisation de la description des écoulements liquide vapeur en utilisant le modèle de van der Waals Jamet [66] a proposé de modifier la valeur du paramètre h en modifiant la fermeture thermodynamique, *i.e.* l'expression analytique de $F(\rho, \nabla\rho)$. Cette modification affecte plus particulièrement la partie non-convexe de F qui décrit les états du fluide à travers l'interface. Jamet [66] s'est assuré qu'il était possible de choisir librement l'épaisseur de l'interface tout en fixant l'énergie libre en excès associée, cette dernière étant à l'origine de la tension de surface. Nous reprenons en section 2.2.3 cette analyse. Nous montrons en particulier que, si elle permet effectivement le contrôle de l'épaisseur et de la tension de surface, cette modification affecte d'autres caractéristiques du fluide.

Un modèle trop contraint En effet nous montrons, en reprenant l'analyse décrite par Fouillet [53], que toute modification de l'énergie libre induit des répercussions sur la limite de métastabilité des phases pures. La limitation de la modification vient alors qu'il n'est pas possible d'avoir conjointement *(i)* une interface d'épaisseur raisonnable, *(ii)* des phases liquide et vapeur ayant toutes les propriétés physiques nécessaires à une description fidèle des écoulements bouillants à la bonne valeur (en particulier, masse volumique, capacité calorifique courbe de saturation et limite de métastabilité, cette dernière étant intimement liée aux valeurs des coefficients de compressibilité isotherme et d'expansion thermique), et *(iii)* des fonctions thermodynamiques suffisamment régulières (des cassures trop brusques dans les variations induisent des difficultés numériques).

Nous pouvons alors retenir la conclusion suivante quant à l'utilisation du modèle de van der Waals pour l'étude des écoulements bouillants. Dans un premier temps, le modèle comprend effectivement l'ensemble des phénomènes que nous souhaitons reproduire. Néanmoins son utilisation pour l'étude numérique de la croissance de bulle de taille millimétrique ne peut être envisagée. Cette limitation est interprétée comme suit : la régularisation de l'interface est associée au rôle particulier que joue la masse volumique dans le modèle de van der Waals, disons le rôle de paramètre d'ordre ; mais la masse volumique est aussi un paramètre macroscopique d'importance pour la physique du fluide. Ainsi en essayant de modifier la description de l'interface, il n'est pas envisageable de ne pas modifier la description des phases. Cette analyse permet de mettre en évidence une piste de modélisation, il s'agit d'introduire une régularisation de l'interface de manière plus indépendante de la description des phases.

II.4 Modèles de champ de phase

Nous tournons alors notre attention sur la modélisation de type champ de phase dont nous exposons dans un premier temps le principe général.

Principe général Dans les modèles champ de phase un paramètre, appelé champ de phase, est introduit en tant que variable thermodynamique et permet à la fois de distinguer les domaines phasiques et de décrire la zone de transition. Notre interprétation d'un tel modèle va dans le sens de notre but de modélisation : cette variable doit permettre d'introduire une régularisation de la zone interfaciale et l'existence d'une variable additionnelle d'introduire suffisamment de degré de liberté dans le modèle pour que la structure de l'interface puisse être choisie indépendamment de la description des phases du système.

Nous prenons ainsi l'exemple, plus simple, de la description d'un système diphasique solide-solide. Nous introduisons alors la modélisation champ de phase de la manière suivante :

- ⋆ introduction d'une équation d'état unique pour l'ensemble du système diphasique de la forme $T(s)$

- ⋆ identification des équations d'état des phases et séparation formelle de l'équation d'état
- ⋆ introduction de la variable champ de phase pour décrire les états intermédiaires à ces états phasiques

Cette dernière partie de la modélisation se base sur un certain nombre d'ingrédients similaires à ceux du modèle de van der Waals (introduction de la séparation de phase par une non-convexité du potentiel thermodynamique, dépendance en des termes non-locaux pour régulariser la description de la zone interfaciale) et des ingrédients plus spécifiques à l'utilisation d'un paramètre d'ordre artificiel (fonction d'interpolation des propriétés physiques du matériau entre les valeurs au sein des phases). Ce dernier point permet de comprendre intuitivement le gain de liberté d'une telle modélisation car permettant de décorréler la modélisation de l'interface de celle des phases. Encore faut il s'assurer que la formulation retenue induit effectivement la description souhaitée et que l'interférence entre la description de l'interface et l'interpolation des propriétés physiques au sein d'un même modèle permet effectivement de modéliser le matériau souhaité. On s'attachera donc par la suite à comprendre quels sont les propriétés d'un tel matériau et en particulier à montrer quels sont les états monophasiques décrits par ce modèle (retrouve-t-on effectivement les phases souhaitées et n'y a-t-il pas d'autres états du matériau possibles). Nous verrons par la suite que de telles propriétés d'un modèle champ de phase reposent sur un choix judicieux des dépendances en la variable champ de phase du potentiel thermodynamique.

II.5 Liste de contraintes pour le modèle de champ de phase

Notre souhait d'utiliser un modèle de type interface diffuse et en particulier de champ de phase pour la description des écoulements liquide-vapeur avec changement de phase est avant tout dicté par des motivations d'ordre numérique. Ainsi l'introduction de la variable champ de phase dans la description du fluide n'est pas censée interférer avec celle des états liquide et vapeur qui sont par ailleurs décrits naturellement à l'aide des variables thermodynamiques classiques (pression et température par exemple). En effet l'introduction de cette variable supplémentaire est dédiée à la régularisation du système discontinu composé des seuls états monophasiques.

Évidemment en introduisant cette nouvelle variable dans la description thermodynamique d'un fluide, nous disposons d'un large degré de liberté supplémentaire ; nous souhaitons pour autant contrôler les conséquences de cette introduction. Pour ce faire, nous proposons tout d'abord de dresser une liste des propriétés souhaitées pour le modèle, sorte de cahier des charges pour son utilisation comme base d'une méthode numérique. On distingue donc les principales propriétés du modèle comme suit

1. profil monotone de la variable champ de phase φ (contrainte numérique)
2. profil monotone de la masse volumique (contrainte numérique)
3. contrôle aisé de l'épaisseur de la zone de transition interfaciale (contrainte numérique)
4. contrôle aisé de l'énergie libre en excès pour une interface à l'équilibre (contrainte physique)
5. saut de pression à l'interface satisfaisant les relations classiques (contrainte physique)
   (a) relation de Laplace
   (b) pression de recul
6. contrôle paramétrique des domaines (en pression température) de stabilité et de métastabilité des phases liquide et vapeur (contrainte physique)
7. contrôle des équations d'état des états monophasiques ($\rho(P,T)$ et $s(P,T)$) (contrainte physique), par exemple
   (a) phases compressibles
   (b) phases incompressibles

Cette liste nous permettra par la suite de justifier des choix parfois arbitraires faits dans l'expression analytique des potentiels thermodynamiques de notre fluide "champ de phase". Notons que cette liste se limite à la description des états d'équilibre de notre modèle ; nous étudierons plus en détail les aspects dynamiques et plus particulièrement les phénomènes dissipatifs à partir du chapitre V.

II.6 Modèles de champ de phase existants

Dans la section 2.3.3 de notre étude, nous considérons différents modèles de type champ de phase décrivant deux phases de masse volumique différente. Nous analysons leur propriétés en fonction de la liste de contraintes que l'on souhaite satisfaire. Il ressort de cette étude qu'aucun des modèles existants ne permet à la fois de maîtriser aisément la description des états monophasiques (contrainte physique) et de contrôler les caractéristiques de la zone interfaciale (contrainte numérique). Pour autant le modèle de Anderson et al. [5] propose une formulation particulièrement intéressante car permettant de prendre en compte la description de deux états fluides incompressibles mais de masse volumique différente. Cette propriété est basée sur l'hypothèse de quasi-compressibilité initialement introduite par Lowengrub and Truskinovsky [89] pour la modélisation des mélanges binaires. Elle est discutée plus en détail dans la section 3.1.2. Néanmoins le choix de l'expression de l'enthalpie libre dans le modèle de Anderson et al. [5] ne permet pas, par exemple, de définir une structure unique pour l'interface à l'équilibre plan le long de la courbe de saturation, preuve d'une trop importante interférence entre les descriptions de l'interface et du matériau. D'où notre but pour la suite de cette étude de développer une formulation de type champ de phase plus adéquate à la description de la croissance de bulle.

Conclusion

Dans ce chapitre nous avons présenté notre choix d'utiliser une méthode numérique des écoulements bouillants basée sur une représentation implicite, diffuse et thermodynamiquement cohérente de l'interface liquide vapeur. Pour ce faire nous avons montré qu'il est nécessaire que le modèle du fluide permette une régularisation de la formulation discontinue dont les propriétés peuvent être choisies arbitrairement. Nous avons alors montré qu'une telle modélisation ne peut être obtenue en utilisant uniquement les variables thermodynamiques classiques pour décrire le système (*cf.* notre présentation des limitations du modèle de van der Waals). Nous nous sommes alors tourné vers la famille de modèles de type champ de phase qui se base sur l'introduction d'une variable thermodynamique supplémentaire. Nous avons alors analysé dans un premier temps le gain de modélisation que cette introduction représente. Puis nous avons dressé un cahier des charges pour le modèle que nous souhaitons utiliser *via* la liste de contraintes exprimées en page 273. Nous avons alors constaté que les modèles existants ne satisfont pas à l'ensemble de ces contraintes. Par la suite nous proposons ainsi une formulation de type champ de phase permettant de satisfaire la liste de ces contraintes

III Fermeture thermodynamique du modèle

Dans ce chapitre nous précisons la fermeture thermodynamique de type champ de phase de notre modèle. Nous montrons comment notre choix permet de contrôler à la fois et de manière indépendante les propriétés physiques de notre fluide diphasique (masse volumique, capacité thermique des phases liquide et vapeur, chaleur latente et courbe de saturation ...) et la description de la zone interfaciale (profils d'équilibre et épaisseur caractéristique). Notre but est tout d'abord (section 3.1) de justifier le choix que nous faisons pour les variables principales de notre description. Puis nous considérons les conséquences de l'introduction de la variable champ de phase sur la thermodynamique des états d'équilibre (*cf.* section 3.2). Cette étude nous permet de comprendre l'intérêt de maîtriser les variations des fonction d'état en fonction de la variable d'état φ. Enfin nous présentons (section 3.3) la formulation que nous avons développée pour la modélisation de type champ de phase de la transition liquide-vapeur.

III.1 Description thermodynamique d'un système multiphasique

Description de la compressibilité du fluide Dans un premier temps (section 3.1.1) nous nous intéressons à la problématique de la description thermodynamique d'un système multiphasique à l'aide d'une unique expression du potentiel thermodynamique. Nous considérons en particulier la description de la compressibilité isotherme χ_T du fluide donnée par

$$\chi_T \triangleq -\frac{1}{V}\left(\frac{\partial V}{\partial P}\right)_T = \frac{1}{\rho}\left(\frac{\partial \rho}{\partial P}\right)_T$$

Rappelons que notre but est entre autre de pouvoir modéliser librement ce paramètre physique et en particulier de considérer les phases liquide et vapeur comme incompressibles ($\chi_T = 0$) point 6 et 7 de la liste page 273.

En effet notre analyse de la crise d'ébullition au chapitre I suggère une telle hypothèse. Un premier choix de modélisation se pose suivant que l'on considère soit la pression P (auquel cas le potentiel thermodynamique est naturellement l'enthalpie libre G) soit la masse volumique ρ (auquel cas le potentiel thermodynamique est naturellement l'énergie libre F) en tant que variable principale. L'équivalence entre les deux descriptions n'étant valable que si une bijection relie P à ρ. Dans le cas où ρ est variable principale, la pression est donnée par (*cf.* équation (2.2))

$$P = \rho \frac{\partial F}{\partial \rho} - F = \rho^2 \frac{\partial f}{\partial \rho} \tag{III.4}$$

et la compressibilité isotherme est nécessairement non nulle. C'est le cas du modèle de van der Waals pour lequel la description avec P en tant que variable principale n'est pas possible. Dans le cas où P est variable principale, la masse volumique est donnée par

$$v(P) \triangleq \frac{1}{\rho}(P) = \frac{\partial g}{\partial P} \tag{III.5}$$

où v est le volume massique du fluide. Il est alors possible de considérer la compressibilité χ_T du fluide comme nulle, auquel cas l'enthalpie libre massique g est linéaire en P. Par contre, en l'absence d'autre variable thermodynamique pour décrire le système, nous montrons que ce modèle n'est pas utilisable pour un modèle d'interface diffuse.

Ainsi nous avons introduit la problématique du choix des variables thermodynamiques principales dans le cadre d'une description continue des propriétés d'un fluide multiphasique. En particulier nous montrons l'impossibilité de modéliser des phases incompressibles isothermes et une interface diffuse à l'aide d'un modèle isotherme du fluide n'utilisant que la variable thermodynamique classique ρ.

L'hypothèse quasi-compressible Dans un deuxième temps (section 3.1.2) nous montrons comment l'introduction d'une variable thermodynamique supplémentaire dans notre description du fluide permet de lever cet obstacle.

A titre d'exemple illustratif, nous considérons l'introduction d'effets anisothermes dans le modèle de van der Waals pour lequel on considère désormais une dépendance de l'énergie libre volumique F en fonction de la température T. On montre comment il est alors possible de modéliser la chaleur latente $\mathcal{L}$ librement, *i.e.* une différence entre les entropies liquide et vapeur à saturation tout en considérant un libre choix des capacités thermiques c_V des phases. Ce modèle est classique (*cf.* sa présentation section 2.2). Nous introduisons alors l'analogie suivante entre la description des effets compressibles et anisothermes d'un système thermodynamique

$$\begin{array}{rcl} P & \leftrightarrow & T \\ \rho & \leftrightarrow & s \\ \chi_T & \leftrightarrow & c_P \\ \text{ou } \chi_s & \leftrightarrow & c_v \end{array} \tag{III.6}$$

Nous montrons alors qu'il est possible d'inverser les variables principales du modèle T et ρ pour considérer désormais l'entropie s comme paramètre d'ordre. Tout comme avec la chaleur latente, on introduit une différence de masse volumique entre les phases liquide et vapeur dont la compressibilité peut alors être choisie librement.

Nous faisons alors le lien entre notre exemple illustratif et l'hypothèse de quasi-compressibilité du fluide introduite à l'origine par Lowengrub and Truskinovsky [89] dans le cadre des mélanges binaires. Cette hypothèse permet de considérer une description à interface diffuse d'un fluide dont les phases, bien qu'ayant des masses volumiques différentes, sont incompressibles. Pouvoir considérer cette hypothèse repose sur la possibilité de choisir une autre variable thermodynamique que la masse volumique comme paramètre d'ordre de la transition de phase : la concentration c dans le cadre originel, l'entropie s pour notre exemple illustratif, la variable champ de phase φ en ce qui concerne le modèle que nous développons. Dans le cadre de notre modèle de champ de phase nous posons cette même hypothèse et choisissons donc la pression P comme étant l'une de nos variables principales. Les autres variables principales sont la température T, variable expérimentale naturelle, et la variable champ de phase φ introduite à des fins de régularisation. Le potentiel thermodynamique correspondant à ces variables thermodynamiques est donc l'enthalpie libre G.

III.2 Introduction d'une variable thermodynamique de type champ de phase

Il s'agit d'étudier les propriétés d'un fluide décrit à l'aide d'une variable thermodynamique additionnelle de type champ de phase. Nous étudions formellement les conséquences de l'introduction d'une telle variable thermody-

namique sur la description des états d'équilibre d'un système.

Une fonction couleur Comme exposé au chapitre 3.2, l'introduction d'une telle variable est avant tout motivée par des raisons numériques. Rappelons en effet que l'ensemble de la physique nécessaire à la description des écoulements liquide-vapeur avec changement de phase est déjà décrite par le modèle de van der Waals anisotherme. Le but de cette introduction est de bénéficier de plus de souplesse dans la régularisation notamment en ce qui concerne les propriétés de la zone volumétrique de transition entre les deux phases. Par conséquent la variable champ de phase est dédiée à cette description de l'interface, et la description des domaines phasiques n'est pas censée s'en ressentir. En particulier des variations de φ au sein de ces domaines ne sont associées à aucune physique et ne sont donc pas souhaitables. Pour ce faire nous imposons qu'une valeur purement abstraite de φ soit associée à chaque phase, ainsi par un choix arbitraire nous posons

$$\begin{aligned} \varphi = 0 &\quad \leftrightarrow \quad \text{phase liquide} \\ \varphi = 1 &\quad \leftrightarrow \quad \text{phase vapeur} \end{aligned}$$

Les valeurs de φ entre ces deux valeurs sont donc implicitement associées à la zone interfaciale.

Équations d'équilibre

Une relation d'équilibre supplémentaire Dans la section 3.2.2 nous appliquons le critère d'équilibre et de stabilité de Gibbs-Duhem à un volume fluide décrit par notre modèle de champ de phase. Nous définissons tout d'abord les différents potentiels thermodynamiques comme suit

$$\begin{cases} \mu \triangleq & \dfrac{\partial g}{\partial \varphi} & \text{(III.7a)} \\ v \triangleq & \dfrac{\partial g}{\partial P} & \text{(III.7b)} \\ s \triangleq & -\dfrac{\partial g}{\partial T} & \text{(III.7c)} \\ \Phi \triangleq & \dfrac{\partial g}{\partial (\nabla\varphi)^2} & \text{(III.7d)} \end{cases}$$

où v est le volume massique ($v = 1/\rho$ où ρ est la masse volumique), s est l'entropie massique. Nous considérons, pour des raisons physiques que la dépendance en $\nabla\varphi$ est isotrope. En outre, nous supposons, comme classiquement en ce qui concerne la théorie capillaire, que g est linéaire en $(\nabla\varphi)^2$. Ainsi

$$\frac{\partial^2 g}{\partial((\nabla\varphi)^2)^2} = 0 \tag{III.8}$$

et Φ se réduit à une fonction de (P, T, φ). Nous montrons alors qu'un état d'équilibre, *i.e.* correspondant à un extremum d'entropie, satisfait les équations d'équilibre suivantes (*cf.* équations (3.28))

$$\nabla T = 0 \tag{III.9a}$$
$$\nabla g = 0 \tag{III.9b}$$
$$\tilde{\mu} = 0 \tag{III.9c}$$

où $\tilde{\mu}$ est un potentiel thermodynamique correspondant à la dérivée variationnelle $\tilde{\delta}$ du potentiel thermodynamique G par rapport à la variable champ de phase φ, *i.e.* est défini par

$$\begin{aligned} \tilde{\mu} &\triangleq \frac{1}{\rho}\frac{\tilde{\delta} G}{\tilde{\delta}\varphi} \\ &= \frac{1}{\rho}\frac{\tilde{\delta}\rho\, g}{\tilde{\delta}\varphi} \\ &= \frac{\partial g}{\partial \varphi} - \frac{1}{\rho}\nabla\cdot\left(\rho\,\frac{\partial g}{\partial \nabla\varphi}\right) \\ &= \mu - 2\,\Phi\,\Delta\varphi - 2\,v\,\nabla(\rho\Phi)\cdot\nabla\varphi \end{aligned} \tag{III.10}$$

Sur la frontière du domaine fluide considéré, la condition d'équilibre suivante est satisfaite

$$\left(2\,\rho\Phi\,\vec{n}.\nabla\varphi + \frac{dU_b}{d\varphi}\right) = 0 \tag{III.11}$$

où U_b est l'énergie d'interaction avec la frontière. La condition d'équilibre thermique (III.9a) est classique. La condition d'équilibre mécanique (III.9b) sera associée par la suite à l'expression du tenseur des contraintes non dissipatif de notre fluide. Nous montrerons en particulier qu'en plus du tenseur sphérique associé à la pression, ce terme comprend un tenseur de type Korteweg dû à la dépendance en $(\nabla\varphi)^2$ introduite. Ce dernier est à l'origine de la force capillaire. La dernière équation d'équilibre (III.9c) est une relation supplémentaire par rapport à la description classique d'un fluide (*e.g.* le modèle de van der Waals). Elle est la conséquence naturelle de l'introduction des variables supplémentaires φ et $\nabla\varphi$ dans la description du fluide. Nous montrons par la suite comment nous associons cette relation plus particulièrement à la description de la zone interfaciale, *i.e.* que nous l'interprétons comme une condition d'équilibre propre à la zone volumétrique interfaciale. On montre comment la relation d'équilibre (III.11) valable sur la frontière permet de définir un angle de contact entre une paroi et l'interface. En effet la dépendance de U_b avec φ permet d'introduire une plus ou moins grande affinité d'une surface vis à vis d'une ou l'autre des phases.

Par la suite (*cf.* section 3.2.3) nous étudions la condition d'équilibre stable d'un état monophasique (*i.e.* uniforme en φ). Nous montrons que la condition concerne les variations de g en φ (*cf.* la première partie de la relation $\tilde{\mu} = 0$). Ainsi les conditions analytiques suivantes (*cf.* équation (3.38))

$$\begin{aligned}\frac{\partial g}{\partial\varphi}_{|P} &= \frac{\partial f}{\partial\varphi}_{|\rho} = 0\\ \frac{\partial^2 g}{\partial\varphi^2}_{|P} &= \frac{\partial^2 f}{\partial\varphi^2}_{|\rho} \geq 0\end{aligned}$$

sont satisfaites pour chaque état monophasique. Ainsi, dans notre cas et suite à la discussion de la section précédente, notre modèle se doit de satisfaire ces relations pour et uniquement pour les valeurs particulières $\varphi = 0$ et $\varphi = 1$.

Une relation pour la régularisation de l'interface Considérons la relation d'équilibre supplémentaire (III.9c). il s'agit d'une équation différentielle en φ constituée de deux parties

- ⋆ La première est associée à la dépendance de g en φ. Cette variable a été introduite afin de modéliser la séparation du fluide en différentes phases. Ainsi cette partie de la relation d'équilibre peut être associée à l'introduction de variations non convexes du potentiel thermodynamique en φ. Classiquement cette non-convexité est introduite à l'aide d'une fonction double-puits $W(\varphi)$ satisfaisant les conditions analytiques suivantes

$$\begin{cases} W(0) = W(1) = 0\\ \dfrac{dW}{d\varphi}(0) = \dfrac{dW}{d\varphi}(1) = 0\\ \displaystyle\int_0^1 \sqrt{2\,W(\varphi)}\,d\varphi \;=\; 1 \end{cases} \tag{III.12}$$

  comme par exemple le polynôme de degré 4 suivant

$$W_{P4}(\varphi) = 18\;\varphi^2\;\;(\varphi - 1)^2 \tag{III.13}$$

  représenté sur la figure C.5.

- ⋆ La seconde partie est liée à l'introduction de la dépendance en des termes non-locaux. La vocation de cette dépendance est de régulariser l'interface en une zone de transition volumique. Classiquement une équation différentielle du type suivant, *e.g.* Rocard [113]

$$h^2\,(\varphi_{,x})^2 = 2\,W(\varphi) \tag{III.14}$$

est satisfaite par le profil du paramètre d'ordre à la traversée d'une interface plane selon un axe $\vec{x}$. Cette équation différentielle est paramétrée par h qui caractérise l'épaisseur $\tilde{h}$ du profil du paramètre d'ordre définie par (*cf.* figure C.4)

$$\tilde{h} \triangleq \frac{1}{\max |\varphi_{,x}|}$$

Tout comme la relation d'équilibre $\tilde{\mu} = 0$ l'équation différentielle (III.14) est constituée de deux parties, l'une concernant des variations en φ, l'autre en ses dérivées spatiales.

Nous avons introduit deux ingrédients classiques (fonction double-puits et équation différentielle) qui ont un double mérite. Le premier est de gérer la séparation des phases. Le second est de contrôler les propriétés de l'interface et en particulier son épaisseur ce qui est primordial pour les applications numériques envisagées. Ce sont les deux propriétés du modèle champ de phase recherchées. Nous souhaitons donc les satisfaire et pour ce faire nous imposons à notre modèle qu'à l'équilibre l'équation différentielle (III.14) soit satisfaite. Puisque la relation $\tilde{\mu} = 0$ est "libre d'interprétation" nous lui assignons ce rôle. Nous comprenons alors qu'il nous faut définir les variations de g en φ et en $(\nabla\varphi)^2$ de sorte que la relation $\tilde{\mu} = 0$ se réduise effectivement à l'équation différentielle souhaitée.

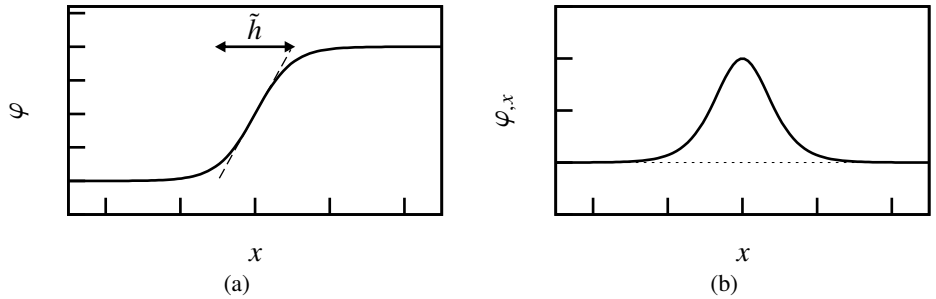

Figure C.4: Profils diffus pour la variable champ de phase φ

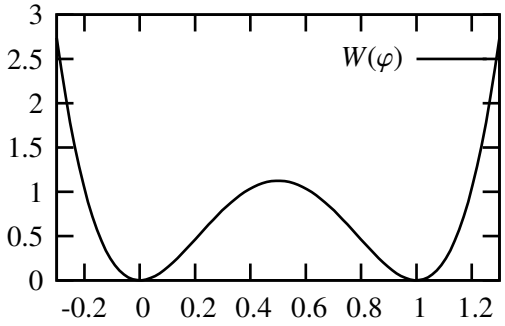

Figure C.5: Fonction double-puits

III.3 Expression de l'enthalpie libre massique

Nous avons précédemment introduit certaines spécificités que le modèle se doit de satisfaire afin de respecter les contraintes explicitées dans la liste page 273. Nous présentons la fermeture thermodynamique de notre modèle puis montrons comment elle permet effectivement de respecter ces contraintes. Dans un premier temps nous présentons la fermeture thermodynamique sous sa forme isotherme afin d'insister sur les propriétés essentielles du modèle liées à l'introduction de la variable champ de phase ainsi qu'à la modélisation de la compressibilité du fluide. Nous considérons une décomposition de l'enthalpie libre massique g en la somme de deux parties *i.e.*

$$g = g_{phase}(P, \varphi) + g_{interface}(\varphi, (\nabla\varphi)^2)$$

La première g_{phase} correspond à la description des états monophasiques et comprend uniquement des variations de g avec les variables P et φ. La seconde est dédiée à la description de la zone interfaciale et comprend uniquement des variations selon φ et $(\nabla\varphi)^2$.

Équations d'état des phases liquide et vapeur Introduisons tout d'abord les équations d'état souhaitées pour les états liquide et vapeur. Les phases étant considérées chacune comme incompressible nous introduisons les enthalpies libres massiques $g_{liq}(P)$, resp. $g_{vap}(P)$, des phases liquide, resp. vapeur, qui sont toutes deux linéaires en pression et qui sont égales entre elles à g_{eq} en la pression de saturation $P = P_{eq}$, *i.e.*

$$\begin{aligned} g_{liq} &= v_{liq}\left(P - P_{eq}\right) + g_{eq} \\ g_{vap} &= v_{vap}\left(P - P_{eq}\right) + g_{eq} \end{aligned}$$

Ces deux fonctions sont, idéalement, souhaitées être retrouvées pour les seuls états monophasiques possible du fluide, *i.e.* les valeurs $\varphi = 0$ et $\varphi = 1$ de la variable champ de phase. Nous introduisons donc une première partie g_{phase} de l'expression de l'enthalpie libre g

$$g_{phase} = g_{vap}(P)\nu(\varphi) + g_{liq}(P)\left(1 - \nu(\varphi)\right) \tag{III.15}$$

qui est simplement une interpolation des fonctions d'état par la fonction $\nu(\varphi)$. A ce stade d'analyse du modèle nous souhaitons retrouver les valeurs correctes de l'enthalpie libre pour $\varphi = 0$ et $\varphi = 1$. Ceci impose simplement que

$$\nu(0) = 0 \quad \& \quad \nu(1) = 1 \tag{III.16}$$

Nous comprenons intuitivement que nous avons alors un réel degré de liberté dans le choix de cette fonction $\nu(\varphi)$; nous verrons par la suite comment le fait que 0 et 1 soient les seuls états monophasique possibles du fluide nous guide pour déterminer cette fonction ν selon des arguments clairs.

Remarquons que le volume massique de notre fluide défini par (III.7b) s'écrit désormais à l'aide de la fonction ν apparaissant dans l'expression (III.15) de g

$$v(\varphi) = v_{vap}\nu(\varphi) + v_{liq}\left(1 - \nu(\varphi)\right) \tag{III.17}$$

Il s'agit donc d'une fonction de la seule variable champ de phase ce qui permet à la fois

- ⋆ de considérer le fluide comme incompressible
- ⋆ de considérer deux phases de volume massique différent

ce qui correspond à notre hypothèse quasi-compressible (conformément à propriété n°7.b de la liste page 273). La fonction g_{phase} permet donc de retrouver une modélisation des phases liquide et vapeur classique.

On considère désormais l'introduction des effets anisothermes dans le modèle. On considère donc simplement la dépendance des fonctions g_{liq} et g_{vap} qui s'écrivent

$$\begin{aligned} g_{liq}(P,T) &= v_{liq}\left(P - P_{eq}(T)\right) + g_{eq}(T) \\ g_{vap}(P,T) &= v_{vap}\left(P - P_{eq}(T)\right) + g_{eq}(T) \end{aligned}$$

La fonction g_{phase} fonction de (P,T,φ) s'en déduit selon une formule équivalente à (III.15). Nous avons ici supposé en outre que les volumes massiques des phases ne dépendent pas de la température. Il s'agit d'une simplification à la fois justifiée physiquement pour l'étude de la croissance d'une bulle que l'on souhaite étudier (les variations de température au sein de la vapeur sont faibles et le liquide peu dilatable) et permettant une écriture plus simple du modèle. Néanmoins il ne s'agit en aucun cas d'une limitation du modèle en lui-même. On montre alors facilement que l'introduction d'une dépendance en température de la pression de saturation $P_{eq}(T)$ permet d'introduire une chaleur latente $\mathcal{L}$ de changement d'état, *cf.* la relation de Clapeyron

$$\frac{dP_{eq}}{dT} = \frac{\mathcal{L}}{T\left(v_{vap} - v_{liq}\right)}$$

i.e. une différence entre les entropies massiques s du liquide et de la vapeur

$$s_{liq} = \frac{\partial g}{\partial T}(\varphi = 0) \quad \& \quad s_{vap} = \frac{\partial g}{\partial T}(\varphi = 1)$$

cf. équation (III.7c). En outre nous montrons (section 3.4.2) comment la dépendance de l'enthalpie libre d'équilibre $g_{eq}(T)$ permet de contrôler l'échelle des capacités calorifiques massiques.

Ainsi cette première partie g_{phase} de la fonction g permet d'introduire dans le modèle les propriétés physiques des états monophasiques liquide et vapeur qui sont nécessaires à l'étude de l'ébullition en paroi (comme démontré au chapitre I).

Modèle champ de phase pour la régularisation de l'interface Nous considérons désormais la seconde partie $g_{interface}$ de l'enthalpie libre massique. Elle se base sur notre étude des propriétés classiques des modèles à interface diffuse et on propose

$$g_{interface}(\varphi, (\nabla\varphi)^2) = v(\varphi)\lambda \left[W(\varphi) + \frac{h^2}{2} (\nabla\varphi)^2 \right]$$

où v est le volume massique du fluide champ de phase *i.e.* interpolée par la fonction $\nu(\varphi)$ (*cf.* équation (III.17), $W(\varphi)$ une fonction double-puits satisfaisant les propriétés (III.12), λ le coefficient de capillarité du fluide et h un paramètre que l'on reliera à l'épaisseur caractéristique de la zone interfaciale. Elle est donc constituée des deux ingrédients classiques, à savoir la fonction W et le terme capillaire en $(\nabla\varphi)^2$, ces deux ingrédients permettant d'introduire les phénomènes de séparation des phases ainsi que de régulariser l'interface comme une zone volumique de transition dotée de capillarité.

Ainsi l'enthalpie libre massique de notre fluide champ de phase s'écrit

$$g = v(\varphi) \left(P - P_{eq}(T) + \lambda \left[W(\varphi) + \frac{h^2}{2} (\nabla\varphi)^2 \right] \right) + g_{eq}(T) \tag{III.18}$$

La particularité essentielle de notre modèle réside dans la formulation choisie qui considère la multiplication du bloc classique par la fonction $v(\varphi)$. Cette propriété permet d'écrire l'écart g^* de l'enthalpie massique à sa valeur à l'équilibre $g_{eq}(T)$ comme

$$\begin{aligned} g^* &\triangleq g - g_{eq}(T) = v(\varphi) \left[P^* + \lambda \left(W(\varphi) + \frac{h^2}{2} (\nabla\varphi)^2 \right) \right] \\ P^* &\triangleq P - P_{eq}(T) \end{aligned}$$

i.e. sous une forme faisant apparaître le rôle particulier du volume massique comme étant en facteur de l'ensemble de la fonction g^*. Nous montrons par la suite que l'avantage majeur de cette formulation réside dans la séparation entre les descriptions des phases et de l'interface qu'elle procure.

Propriétés de la formulation

États monophasiques Nous nous intéressons aux principales propriétés de cette formulation et considérons dans un premier temps la modélisation des états monophasiques. Dans un souci de simplicité nous étudions uniquement les solutions d'équilibre (équations (III.9)) satisfaisant en outre à la condition d'uniformité de la variable champ de phase

$$\nabla\varphi = 0$$

Nous considérons les valeurs de la variable champ de phase correspondant à des états d'équilibre comme l'inconnue principale de cette étude. La fonction d'interpolation $\nu(\varphi)$ joue un rôle particulier dans cette étude et nous considérons par la suite quelques cas particuliers permettant de l'illustrer. Nous introduisons ainsi les polynômes P_1, P_3 et P_5 de degré 1, 3 et 5 définis par

$$P_1(\varphi) = \varphi \tag{III.19a}$$
$$P_3(\varphi) = \varphi^2 (3 - 2\varphi) \tag{III.19b}$$
$$P_5(\varphi) = \varphi^3(6\varphi^2 - 15\varphi + 10) \tag{III.19c}$$

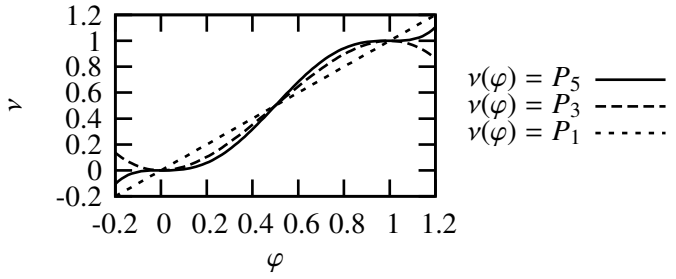

Figure C.6: Fonction d'interpolation

Ils sont représentés sur la figure C.6. et satisfaisant tous à la condition (III.16). Nous considérons alors que la masse volumique ρ est interpolée par ces polynômes, *i.e.* ce qui implique pour la fonction ν servant à interpoler le volume massique $v(\varphi)$ (*cf.* équation (III.17))

$$\nu(\varphi) = \frac{P_n(\varphi)}{\rho_l/\rho_v + (1-\rho_l/\rho_v)\ P_n(\varphi)}$$

Nous montrons tout d'abord que le seul paramètre pertinent de cette étude est l'écart à la saturation $\mathfrak{g}$ défini par

$$\mathfrak{g} \hat{=} \frac{(\rho_l-\rho_v)\ h^2\, g^*}{\lambda} = \frac{(\rho_l-\rho_v)\ h\, g^*}{\sigma} \tag{III.20}$$

(g^* étant uniforme à l'équilibre, nul aux conditions de saturation) qui permet de réduire la résolution de ce problème à l'étude de l'équation suivante écrite sous forme adimensionnelle

$$\mathfrak{g}\ \frac{dP_n}{d\varphi} + \frac{dW}{d\varphi} = 0$$

Notons d'ailleurs qu'à saturation $\mathfrak{g} = 0$ et de par les propriétés (III.12) de la fonction double-puits W, les seules et uniques solutions d'équilibre sont les valeurs 0 et 1. Hors de cette condition $\mathfrak{g} = 0$ nous montrons que les solutions diffèrent grandement suivant le choix de la fonction d'interpolation. Le choix, apparemment naturel d'une interpolation linéaire (polynôme P_1) est par exemple à exclure car il ne permet pas aux états monophasiques d'être associés aux valeurs $\varphi = 0$ et $\varphi = 1$. Ainsi les états monophasiques n'ont pas comme fonction d'état les fonction g_{liq} et g_{vap} souhaitées. Dans les deux autres cas présentés (P_3 et P_5), nous montrons que les états 0 et 1 sont effectivement des états d'équilibre monophasiques, *i.e.* des minima locaux de l'enthalpie libre massique mais

- ⋆ la stabilité de ces états d'équilibre n'a pas été établie
- ⋆ ce ne sont pas les seules solutions d'équilibre et les autres solutions se doivent d'être instables

Ainsi il apparaît comme primordial d'étudier plus en détail la stabilité des états homogènes et nous proposons par la suite de nous intéresser à ce sujet. Néanmoins comme nous souhaitons inclure dans cette étude l'influence des phénomènes dissipatifs, elle sera menée au chapitre VI. La principale conclusion à retenir de cette étude (en ce qui concerne la présente étude) est qu'afin que 0 et 1 soient des états stables, et ce sur tout les domaines de stabilité respectifs de $g_{liq}(P,T)$ et de $g_{vap}(P,T)$, et afin que ces états soient effectivement décrits par ces fonctions d'état, 6 conditions analytiques doivent être satisfaites par la fonction d'interpolation. Ces conditions impliquent que 0 et 1 soient des minima locaux de la fonction ν, conditions satisfaites par la fonction P_5. Nous montrons en outre que le choix de la fonction P_5 assure qu'aucune autre valeur de la variable champ de phase ne correspond à un état stable, condition qui n'est pas satisfaite par exemple par les fonctions P_3 ou P_1.

Profils d'équilibre En utilisant l'équation d'équilibre (III.9b), il est facile de montrer que l'équation d'équilibre (III.9c) $\tilde{\mu} = 0$ est équivalente à l'équation différentielle (III.14) dans le cas d'une interface plane ; cette propriété est

- ⋆ due à notre choix particulier de l'expression analytique de l'enthalpie libre massique g et plus précisément au fait de considérer le volume massique v en facteur dans l'expression de $g_{interface}$;

- ⋆ intéressante du point de vue de la modélisation car permettant de considérer une équation différentielle pour la gestion du profil de l'interface comme ne dépendant que des caractéristiques "champ de phase" du modèle et surtout *totalement indépendante* du reste de la description du fluide diphasique.

Nous montrons en outre que la solution diffuse en la variable champ de phase génère une tension de surface σ, définie comme une énergie libre en excès, donnée par

$$\sigma = \frac{\lambda}{h}$$

Le paramètre h étant relié à l'épaisseur de l'interface, il reste, afin de contrôler la valeur de σ le paramètre λ. Nous montrons donc que le modèle présente suffisamment de paramètres pour définir l'ensemble des paramètres physiques primordiaux des écoulements liquide vapeur avec changement de phase.

Comparaison avec les autres modèles champ de phase existants Le modèle le plus proche du nôtre est le modèle développé par Anderson et al. [5]. Nous montrons que la principale différence entre les deux modèles réside dans l'expression des variations de g avec φ. Nous avons été capables d'écrire un modèle pour lequel la fonction d'interpolation ν apparaît clairement en facteur de l'ensemble de la formulation, chose rendue impossible par le choix fait par les auteurs de [5]. Les conséquences de cette différence portent sur la possibilité de définir des propriétés de la zone de régularisation indépendamment de la description physique des états monophasiques, ce qui peut mener à des difficultés d'utilisation du modèle. En particulier l'équation gouvernant le profil de la variable champ de phase du modèle de [5] varie selon les conditions d'équilibre sans que cet effet ne soit motivé par une réalité physique. Cette variation est en fait induite par des choix relatifs à la description champ de phase du fluide. Ils ne sont pas souhaités dans notre cas et ne sont pas reproduits dans notre modèle.

En outre notre formulation possède l'avantage suivant de pouvoir se réduire à la formulation classique des modèles de champ de phase utilisés pour l'étude de la transition solide-liquide. En effet nous montrons section 3.3.2 qu'en supposant que la masse volumique des deux phases liquide et vapeur sont égales nous retrouvons une formulation identique à celle présentée par [1] par exemple. Ceci prouve qu'en utilisant la décomposition du modèle présentée précédemment nous avons été capables d'étendre son utilisation à un autre champ de la physique, les écoulements liquide-vapeur. Nous pouvons donc penser à raison qu'en utilisant le même procédé nous pourrions ainsi étendre aisément notre formulation à la modélisation d'autres écoulements pour lesquels par exemple la compressibilité des phases jouerait un rôle primordial.

Conclusion

Les caractéristiques numériques de notre modèle comme l'épaisseur de la zone de transition peuvent être choisies totalement indépendamment du reste de la modélisation physique des propriétés à l'équilibre des phases. Nous étudions plus en détail par la suite les conséquences de cette régularisation sur d'autres aspects de la modélisation des écoulements liquide-vapeur avec changement de phase, notamment les équations de la dynamique et les mécanismes dissipatifs.

IV Symétrie sphérique

IV.1 Introduction et problématique

Nous avons vu précédemment qu'une tension de surface σ était associée à la zone interfaciale dont la valeur peut être choisie librement *via* le paramètre λ de notre modèle thermodynamique (*cf.* l'expression (III.18)). La tension de surface n'agit qu'en présence de courbure. Pour les courbures d'interface typiquement rencontrées dans la dynamique de croissance de bulles décrite au chapitre 1, la relation de Laplace

$$[\![P]\!] = \frac{2\,\sigma}{R}$$

est satisfaite. Cette relation est issue de la modélisation discontinue des interfaces liquide-vapeur. Dans le cadre de cette théorie il est impossible de prédire l'apparition ou la disparition d'inclusions sphériques étant donné que, d'après la relation de Laplace, le saut de pression $[\![P]\!]$ à la traversée de l'interface diverge lorsque son rayon de courbure R tend vers zéro. Cette divergence, non physique, n'est pas observée avec les modèles à interface diffuse classiques (van der Waals ou Cahn Hilliard, *cf.* notre étude bibliographique à ce sujet en section 4.1).

L'objet de ce chapitre est d'étudier les phénomènes susmentionnés à l'aide de notre modèle champ de phase et de montrer comment ce dernier permet à la fois d'être cohérent avec la théorie de Laplace et de décrire les inclusions sphériques de faible rayon. Pour ce faire nous faisons l'hypothèse d'un système à symétrie sphérique et étudions les solutions d'équilibre pour lesquelles la variable champ de phase n'est pas uniforme.

IV.2 Équation d'équilibre

L'équation sous forme adimensionnelle Nous montrons tout d'abord que l'étude de ce problème se réduit à résoudre une équation différentielle du second ordre en $\varphi(\bar{r})$ ($\bar{r}$ étant un rayon adimensionnel $\bar{r} \triangleq r/h$) paramétrée par $\mathfrak{g}$ (qui représente l'écart adimensionnel aux conditions de saturation pour lesquelles l'équilibre diphasique est celui d'une interface plane). Cette équation se déduit des conditions d'équilibre (4.3) et s'écrit

$$\mathfrak{g}\,\frac{dP_5}{d\varphi} + \frac{dW}{d\varphi} - \varphi_{,\bar{r}\bar{r}} - 2\,\frac{\varphi_{,\bar{r}}}{\bar{r}} = 0 \tag{IV.21}$$

où P_n est un polynôme d'interpolation de la masse volumique du fluide, supposé égal à P_5 afin de contrôler les propriétés physiques des états monophasiques (*cf.* chapitre VI). Les conditions limites s'écrivent

$$\begin{aligned} \forall n \in \mathbb{N}^*,\ \varphi_{,r^n}(r=\infty) &= 0 \\ \varphi_{,r}\ (r=0) &= 0 \end{aligned}$$

La structure mathématique de ce problème est similaire à celle obtenue avec d'autres modèles à interface diffuse. Pour autant il est intéressant de noter que la structure de l'équation (IV.21) reste simple malgré le nombre de phénomènes physiques pris en compte dans le modèle. En particulier, elle n'implique qu'un seul paramètre $\mathfrak{g}$ traduisant les conditions d'équilibre et apparaissant en facteur d'un seul terme. Ceci permet d'envisager une étude synthétique des propriétés de notre régularisation de type champ de phase dans le contexte des inclusions sphériques. Ceci démontre aussi le faible degré d'interaction entre cette régularisation et la description du reste de la physique des écoulements liquide-vapeur.

Étude des états intérieurs et extérieurs, limite aux grands rayons Contrairement au cas de l'équilibre d'une interface plane, il n'est malheureusement pas possible de résoudre analytiquement l'équation différentielle (IV.21). Nous utiliserons par la suite différentes méthodes de résolution pour ce problème. Pour autant il est possible de déduire certaines informations analytiques sur la solution de (IV.21).

Valeur asymptotique de la variable champ de phase Dans la section 4.2.2, nous étudions en ce sens l'équation (IV.21) et nous montrons dans un premier temps une propriété intéressante de notre modèle : l'état atteint asymptotiquement en $\bar{r} = +\infty$ correspond soit à la phase liquide ($\varphi = 0$) soit à la phase vapeur ($\varphi = 1$) et ce qu'elles que soient les conditions d'équilibre (*i.e.* quelque soit la valeur du paramètre $\mathfrak{g}$). Il s'agit d'une spécificité recherchée pour notre modèle : nous montrons qu'elle est associée au choix particulier que nous avons

fait pour la fermeture thermodynamique, en particulier le choix de la fonction d'interpolation $\nu(\varphi)$. En effet les modèles à interface diffuse induisent communément une variation de la valeur du paramètre d'ordre en $\bar{r} = +\infty$ en fonction des conditions d'équilibre, variation justifiable physiquement tant que la valeur du paramètre d'ordre a effectivement une signification physique macroscopique ; dans notre cas nous ne souhaitons pas observer une telle variation mais au contraire conserver la description d'un état classique (liquide ou vapeur) à l'extérieur d'une inclusion sphérique. Ce résultat est cohérent avec le modèle discontinu des inclusions sphériques valable pour les échelles de bulles considérées au chapitre I et il est effectivement obtenu à l'aide de notre modèle.

A contrario, nous montrons que la valeur, notée φ_0, de la variable champ de phase en $\bar{r} = 0$ est différent de 0 ou 1 et varie selon les conditions d'équilibre. Ainsi au centre d'une inclusion on ne retrouve pas exactement un état liquide ou vapeur. Ce constat justifie l'étude de φ_0 en fonction du paramètre $\mathfrak{g}$ qui est faîte par la suite.

Pressions intérieure et extérieure Le saut et les valeurs absolues de pression de part et d'autre d'une interface courbe sont des grandeurs physiquement importantes. Notre étude analytique permet de montrer dans un premier temps que le saut de pression $[\![P]\!]$ défini par

$$[\![P]\!] \triangleq P(\bar{r} = 0) - P(\bar{r} = \infty)$$

est toujours positif ce qui est cohérent avec la relation de Laplace. En outre nous montrons que les valeurs absolues des pressions (*i.e.* l'écart à la pression de saturation[2] qui est la valeur de la pression au sein des phases dans le cas d'une interface plane à l'équilibre) sont, dans la mesure où la valeur de φ_0 est proche de 0 ou 1, cohérentes avec le résultat classique (valable pour le modèle discontinu et démontré en annexe A.2, équation (A.25)). Ainsi

- ⋆ pour une bulle à l'équilibre
  les pressions intérieure et extérieure sont inférieures à la pression de saturation
- ⋆ pour une goutte à l'équilibre
  les pressions intérieure et extérieure sont supérieures à la pression de saturation

Ce résultat dépendant de φ_0 il apparaît comme essentiel d'enrichir notre analyse d'une étude de cette valeur.

Rayon discontinu et tension de surface Nous définissons des grandeurs discontinues équivalentes associées à notre solution diffuse, en particulier deux rayons R_ρ et $R_{S\,\rho}$.

- ⋆ Le rayon R_ρ compare notre solution diffuse à une solution discontinue pour laquelle la masse en excès serait nulle tout en conservant les mêmes valeurs asymptotiques de la masse volumique

$$\rho^{ex}_{R_\rho} \triangleq \frac{1}{R_\rho^2}\left[\int_0^{R_\rho} (\rho - \rho_0)\, r^2\, dr + \int_{R_\rho}^{\infty} (\rho - \rho_\infty)\, r^2\, dr\right] = 0 \tag{IV.22}$$

  Cette définition est classique pour les modèles à interface diffuse pour lesquels la variation du paramètre d'ordre au centre de l'inclusion a une interprétation physique.

- ⋆ Le rayon $R_{S\,\rho}$ est le rayon qu'aurait une inclusion "discontinue" à l'intérieur, resp. à l'extérieur, de laquelle la valeur de la variable champ de phase vaudrait uniformément 0 ou 1 et qui porterait la même masse que la solution diffuse considérée, *i.e.*

$$\frac{1}{Rs_\rho^2}\left[\int_0^{Rs_\rho} (\rho - \rho(1 - \varphi_\infty))\, r^2\, dr + \int_{Rs_\rho}^{\infty} (\rho - \rho_\infty)\, r^2\, dr\right] = 0 \tag{IV.23}$$

  Cette définition est adaptée à la comparaison de notre modèle avec le modèle discontinu classique à phases incompressibles pour lequel les états (et donc les masses volumiques) intérieur comme extérieur sont supposés être indépendant des conditions d'équilibre (rayon de l'inclusion ou de manière équivalente valeur de l'enthalpie libre massique ou pression à l'intérieur ou à l'extérieur). Notons que l'hypothèse d'incompressibilité n'est certainement plus valide pour de très faibles rayons.

[2]Nous raisonnons par défaut à température constante, l'équilibre étant implicitement supposé isotherme (équation d'équilibre (III.9a)

Remarquons donc que la différence entre les deux rayons est indirectement une mesure de l'écart de φ_0 avec 0 ou 1, *i.e.* avec le fait qu'on retrouve effectivement une phase au centre de l'inclusion ; l'existence de ces deux définitions traduit l'ambivalence de notre modèle, bénéficiant des propriétés des modèles à interface diffuse mais se voulant à la fois une régularisation d'un modèle discontinu. Rappelons que ce modèle discontinu est satisfaisant pour la description de la physique des bulles, tant que la question numérique n'est pas considérée (*cf.* notre discussion au chapitre II).

De manière similaire nous définissons deux coefficients de tension de surface $\sigma_{F^{ex}}$ et $\sigma_{[\![P]\!]}$.

⋆ Le premier correspond à l'énergie libre volumique en excès associé à la solution diffuse

$$\sigma_{F^{ex}} \hat{=} F^{ex}_{R_\rho} = -P^{ex}_{R_\rho} = \frac{1}{R_\rho^2}\left[\int_0^{R_\rho} (P_0 - P)\, r^2\, dr + \int_{R_\rho}^{\infty} (P_\infty - P)\, r^2\, dr\right] \tag{IV.24}$$

Ce coefficient porte donc le sens premier de la tension de surface en tant que quantité portée par l'interface.

⋆ Le second est basé sur une analogie avec la relation de Laplace et s'écrit

$$\sigma_{[\![P]\!]} \hat{=} [\![P]\!]\,\frac{R_\rho}{2} = \lambda \int_0^{\infty} (\varphi_{,r})^2\,\frac{R_\rho}{r}\, dr \tag{IV.25}$$

La différence entre ces deux coefficients mesure donc l'écart de notre modèle avec une relation de type Laplace[3] *i.e.* la cohérence entre le saut de pression et l'énergie en excès portée par l'interface.

Limite aux grands rayons Nous démontrons que le paramètre $\mathfrak{g}$ peut être interprété comme l'inverse du rayon R_ρ normalisé par l'épaisseur d'une interface plane h. Nous montrons alors que lorsque le rayon de l'inclusion est suffisamment grand (environ $4\,h$) la valeur de φ_0 tend vers les valeurs phasiques 0 ou 1, les deux rayons R_ρ et $R_{s\rho}$ coïncident et la relation de Laplace est vérifiée, *i.e.*

$$\sigma_{[\![P]\!]} \simeq \sigma_{F^{ex}} \simeq \lim_{R_\rho \to \infty} \sigma_{[\![P]\!]} \simeq \frac{[\![P]\!]\, R_\rho}{2}$$

Par la suite nous souhaitons évaluer plus exactement les limites de validité de ces apprximations pour des rayons plus faibles, notamment lorsqu'ils approchent la valeur caractéristique de l'épaisseur artificielle de l'interface h, qui constitue *a priori* la limite de validité de notre modèle.

IV.3 Détermination de la solution d'équilibre

Il s'agit de résoudre l'équation différentielle (IV.21) de manière approchée.

Analyse de l'équation différentielle Nous commençons notre étude de l'équation en proposant une analogie du problème à résoudre avec un problème de mécanique du point (*cf.* section 4.3.1). Cette analogie, initialement introduite par van Kampen [144] considère le mouvement d'une particule de masse unité. La position φ de cette particule dépend du temps $\bar{r}$ et elle évolue au sein d'un champ de potentiel $-(\mathfrak{g}P_5(\varphi)+W(\varphi))$ tout en étant soumise à une force visqueuse $2\varphi_{,\bar{r}}/\bar{r}$; initialement cette particule a une vitesse nulle (condition aux limites (IV.22a) en $r = 0$). Cette analogie est utilisée afin d'illustrer la spécificité induite par notre fermeture thermodynamique : le potentiel thermodynamique est tel que, pour toute valeur de $\mathfrak{g}$, l'état $\varphi = 0$ ou 1 est un minimum local du potentiel et donc un état d'équilibre final. Cette analogie peut être utilisée pour résoudre numériquement l'équation d'équilibre en utilisant une méthode de tir. Il s'avère néanmoins que, pour les paramètres que nous avons testés, la recherche de la solution à l'aide d'une telle méthode reste très délicate. On lui préférera par la suite d'autres méthodes numériques plus proches de l'utilisation finale du modèle dans un code de mécanique des fluides.

[3] et non la relation de Laplace elle-même qui ne considèrerait pas un σ variable mais comme étant égal à la valeur pour une interface plane.

Solution analytique approchée L'équation du mouvement de la particule peut être résolue analytiquement tant que le potentiel est un polynôme de degré au plus deux. Nous considérons dans cette étude analytique des approximations des fonctions W et P_n à l'aide de fonctions par morceaux, continues à dérivée continue, constituées de polynômes de degré 2 (*cf.* les fonctions $P_{2\,pw}$ et W_{pwP2} définies par (4.20) et (4.21)). Nous montrons que

- ⋆ le potentiel en résultant conserve l'importante propriété de notre modèle : en $\bar{r} = \infty$ la variable champ de phase vaut 0 ou 1

- ⋆ l'ensemble des propriétés physiques du modèle sont reproduites par ce modèle "approché par morceaux" en particulier le contraste de masse volumique entre les deux phases ; pour autant nous ne conservons pas avec l'approximation $P_{2\,pw}$ l'ensemble des propriétés analytiques de la fonction d'interpolation permettant de maîtriser la stabilité des états monophasiques.

Le fait d'obtenir une solution analytique pour la solution d'équilibre dans l'hypothèse de symétrie sphérique n'a, à notre connaissance, jamais été obtenu dans la communauté scientifique des modèles à interface diffuse en présence d'un contraste de masse volumique entre les phases (*cf.* Lowengrub and Truskinovsky [89] pour un résultat similaire pour les mélanges binaires avec masse volumique uniforme). Ceci prouve la robustesse de notre formulation qui se "dégrade" peu avec les hypothèses simplificatrices faites pour permettre cette résolution.

Utiliser cette approximation nous a permis de déterminer la solution d'équilibre pour des rayons R_ρ de l'inclusion petits devant l'épaisseur de l'interface plane h comme illustré sur la figure C.7. Mais cette approximation est basée néanmoins sur une modification du potentiel et il apparaîtra par la suite que la solution d'équilibre reste très sensible à cette fonction.

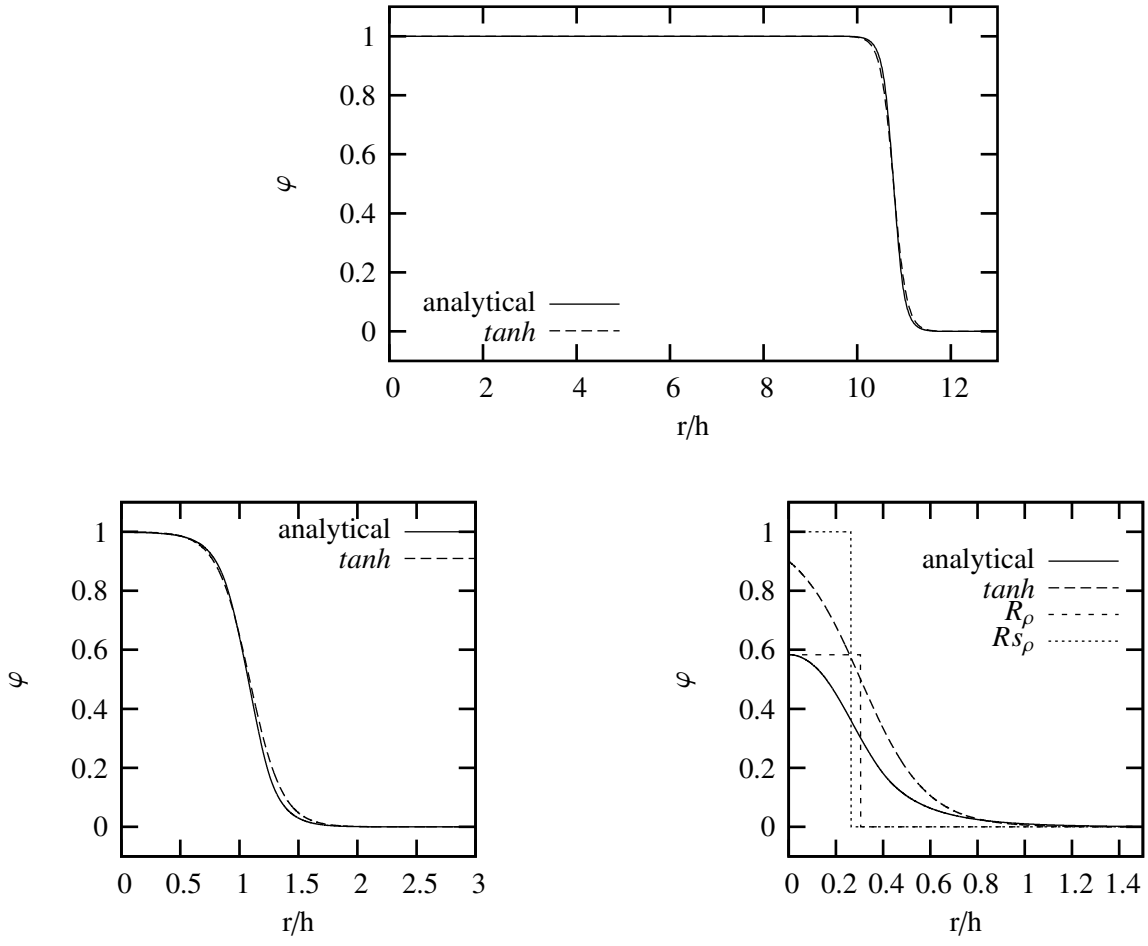

Figure C.7: Profils d'équilibre obtenus en utilisant des approximations quadratiques par morceaux

IV.4 Solution numérique pour un domaine de longueur finie

Nous étudions désormais le problème d'une inclusion sphérique à l'équilibre dans un domaine fermé[4]. Nous nous intéressons aux solutions pour lesquelles le rayon de l'inclusion est petit devant la dimension du domaine considéré, elle-même grande devant l'épaisseur caractéristique de l'interface (égale à $20\,h$). Nous résolvons alors l'équation d'équilibre en utilisant une discrétisation de type différence finie de la variable $\varphi(\bar{r})$. En outre nous utilisons un schéma particulier pour les opérateurs de dérivation spatiale permettant à la relation vectorielle $\nabla \cdot (a\,\vec{b}) = a\nabla \cdot \vec{b} + \nabla a \cdot \vec{b}$ d'être satisfaite par les champs discrets.

Profils d'équilibre La figure C.8 représente les profils radiaux à l'équilibre de la variable champ de phase, de la masse volumique et de la pression obtenus pour différentes valeurs du paramètre $\mathfrak{g}$ (négatives, cas de la bulle). Les profils de masse volumique sont plus raides que ceux de la variable champ de phase. Ceci est dû à notre choix pour la fonction d'interpolation ν. Les profils de pression illustrent à la fois le saut de pression à la traversée de l'interface, l'existence d'une pression en excès, et l'écart de la valeur absolue de la pression à la pression de saturation (on représente ici la variable réduite $P^* = P - P_{sat}(T_0)$).

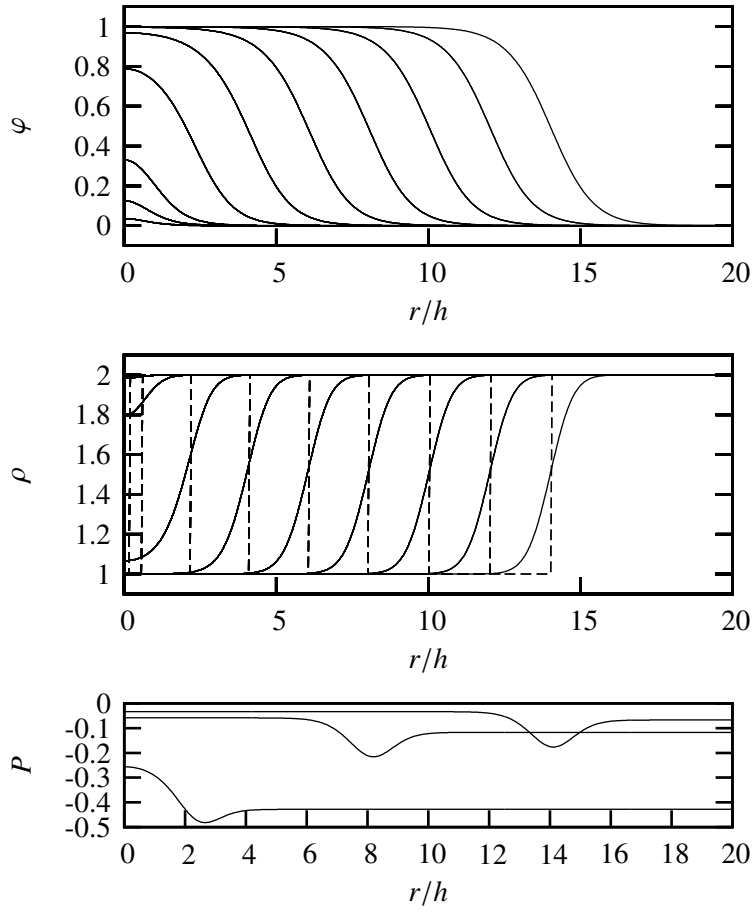

Figure C.8: Profils à l'équilibre de la variable champ de phase, de la masse volumique et de la pression pour différentes masses du système.

Ces résultats permettent de distinguer deux types de solutions. Le premier type de solution correspond à un rayon typique des variations qui est grand devant l'épaisseur de l'interface. Nous montrons que ces solutions correspondent à de faibles valeurs de $\mathfrak{g}$ et sont caractérisées par

- ⋆ un profil de φ à la traversée de l'interface proche d'une tangente hyperbolique (qui est la solution pour un rayon de courbure infini)

[4]La physique d'une telle inclusion est différente de celle précédemment décrite dans le contexte d'un domaine infini. En effet dans le cas précédent nous étudions un équilibre instable (*e.g.* Carey [28]) tandis que l'étude actuelle concerne un état d'équilibre stable.

- ⋆ une valeur de φ au centre de l'inclusion très proche de 0

Ces points montrent que notre modèle propose une régularisation satisfaisante de la description discontinue d'une bulle. Le second type de solution correspond aux faibles rayons (de l'ordre de grandeur de l'épaisseur de l'interface). Ces solutions correspondent à de grandes valeurs de $\mathfrak{g}$ et sont caractérisées par

- ⋆ un profil de la variable champ de phase qui varie continûment de celui d'une bulle de grand rayon (profil quasiment équivalent au cas d'équilibre plan) à un profil uniforme liquide
- ⋆ une valeur de φ au centre de l'inclusion qui varie continûment de 0 à 1

Ces propriétés attestent que le modèle est capable de décrire les inclusions de faible rayon, *i.e.* de reproduire les phénomènes de nucléation/collapse. Nous étudions par la suite les grandeurs intégrales de la solution discontinue équivalente se déduisant des profils diffus.

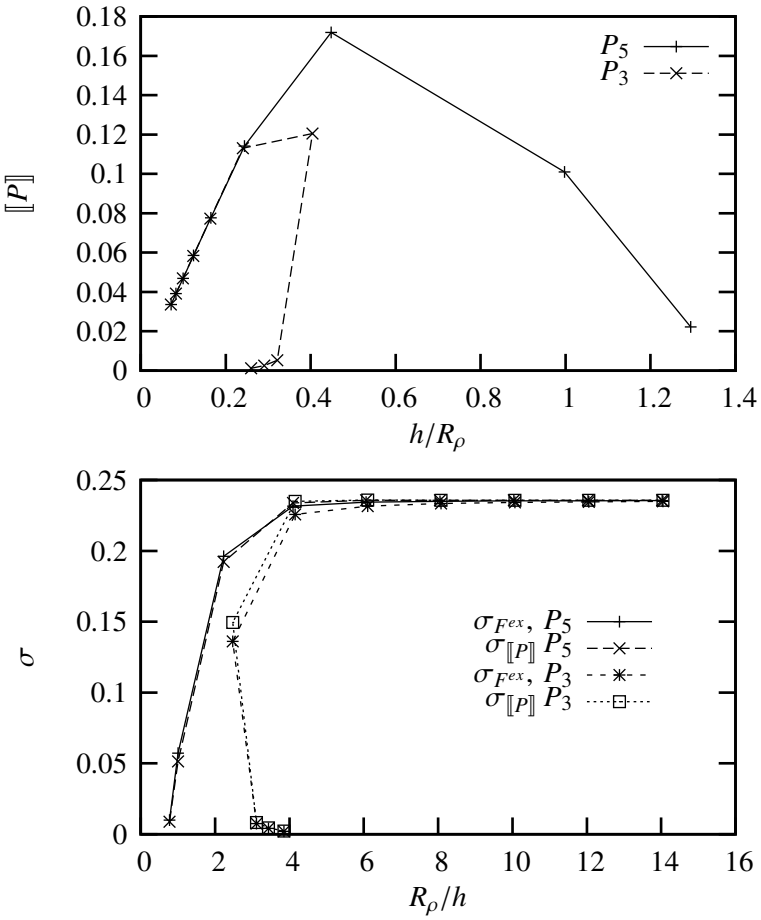

Figure C.9: Saut de pression $[\![P]\!]$ et tensions interfaciales $\sigma_{F^{ex}}$ et $\sigma_{[\![P]\!]}$ en fonction du rayon discontinu R_ρ/h pour les deux fonctions P_3 et P_5 considérées pour l'interpolation de la masse volumique

Rayon et tension interfaciale, la relation de Laplace Sur la figure C.9 est représenté le saut de pression $[\![P]\!]$ ainsi que les tensions de surface $\sigma_{[\![P]\!]}$ et $\sigma_{F^{ex}}$ en fonction du rayon discontinu équivalent pour les solutions d'équilibre correspondant aux profils de la figure C.8. Nous distinguons clairement deux parties dans ces courbes, parties correspondant aux deux types de solutions décrits dans le paragraphe précédent.

- ⋆ Pour les grands rayons
  Le saut de pression est inversement proportionnel au rayon de l'inclusion, la constante valant la tension de surface d'une interface plane ($\lim_{R\to\infty} \sigma_{[\![P]\!]} = \sigma$) ce qui est cohérent avec la théorie de Laplace. Cette constante représente bien une énergie libre en excès ($\sigma_{F^{ex}} \simeq \sigma_{[\![P]\!]}$)

- ⋆ Pour les faibles rayons (*i.e.* $R_\rho/h \lesssim 4$)
  Le saut de pression dévie de la relation de Laplace. Ainsi, et contrairement à la théorie de Laplace, $[\![P]\!]$ ne diverge pas à l'approche de $R = 0$ mais tend vers zéro. La figure représentant les tensions interfaciales montre alors que cette valeur du saut de pression peut toujours être reliée à une énergie libre en excès, cette dernière tendant elle aussi vers zéro à l'approche de $R = 0$.

Cette dernière propriété permet au modèle de décrire de manière cohérente les disparition et apparition de phase associées aux phénomènes physiques de nucléation et collapse. Il est important de préciser que le modèle ne permet pas de reproduire la véritable physique de ces phénomènes qui nécessite la prise en compte, pour le moins, des effets compressibles des phases et d'une valeur physiquement réaliste de l'épaisseur de l'interface. Nous montrons par ailleurs les propriétés suivantes

- ⋆ La valeur φ_0 vaut quasiment 1 dès que le rayon de l'inclusion dépasse environ 6 fois l'épaisseur h. Sinon elle varie continûment de 1 à 0 comme précédemment illustré sur la figure C.8.
- ⋆ Le rayon de l'interface est directement proportionnel à l'inverse du paramètre $\mathfrak{g}$ comme suggéré dans notre analyse de l'équation différentielle.
- ⋆ Les deux rayons discontinus définis R_ρ et Rs_ρ sont équivalents pour la gamme de conditions d'équilibre $\mathfrak{g}$ considérées ce qui prouve la cohérence de notre description avec une description discontinue même pour des inclusions de faible masse (ou rayon)

Sur les figures C.9, nous avons représenté les mêmes quantités discontinues dans le cas où la fonction d'interpolation n'est pas choisie égale au polynôme P_5 de degré 5 que nous préconisons mais au polynôme P_3 de degré 3 (*cf.* équation (III.19b)). Dans ce cas les résultats diffèrent comme suit

- ⋆ Le rayon discontinu équivalent R_ρ (*cf.* figure 4.9) diverge lorsque la masse de l'inclusion ($R_{s\rho}$) tend vers zéro. Ce comportement est fréquemment observé dans les modèles à interface diffuse[5] sans qu'il ne lui soit attribué une signification claire. Dans notre cas, nous ne souhaitons pas reproduire ce comportement car aucune physique ne lui est associée.
- ⋆ En ce qui concerne les saut de pression et les valeurs de la tension interfaciale, les résultats sont un peu moins satisfaisants que dans le cas P_5 étant donné que les courbes dévient de la relation de Laplace, que l'on souhaite reproduire jusqu'à approcher les faibles rayons, pour des rayons plus importants.

Ainsi nous pouvons conclure que les résultats obtenus avec notre modèle sont pour partie dus à notre choix concernant la fermeture thermodynamique. En outre, ces résultats satisfaisants semblent se dégrader si l'on s'écarte des choix préconisés. Ceci justifie *a posteriori* le choix de poursuivre numériquement l'étude faite analytiquement en section 4.3.2 et utilisant des fonctions continues par morceaux comme approximation de la fermeture thermodynamique.

Conclusion

L'étude de l'équilibre sous hypothèse de symétrie sphérique du système nous a permis de caractériser la description des interfaces courbes à l'aide de notre modèle de champ de phase pour les écoulements liquide vapeur avec changement de phase.

Notre premier constat repose sur une analyse des équations d'équilibre de notre modèle. Elle montre que la fermeture thermodynamique que nous proposons conduit à la résolution d'une unique équation différentielle en le champ de phase paramétrée par le seul nombre adimensionnel $\mathfrak{g}$ traduisant les conditions d'équilibre. Cette équation

- ⋆ a toujours pour solution $\varphi = 0$ ou $\varphi = 1$ en $r = \infty$ ce qui assure une description fidèle des états extérieurs d'une inclusion
- ⋆ peut se simplifier pour obtenir des solutions analytiques d'équilibre , et ce quelle que soit la physique des phases décrites (notamment le contraste de masse volumique, résultat qui n'est pas possible si d'autres choix concernant la fermeture thermodynamique sont faits)

[5] Existence d'un rayon minimal de nucléation, *e.g.* [43, 89]

Nous avons pu résoudre numériquement à l'aide d'une discrétisation spatiale de type différence finie la solution d'équilibre dans le cas d'un domaine sphérique fermé. Pour les grands rayons nous avons montré que le profil de φ à la traversée de l'interface a une épaisseur caractéristique de l'ordre du paramètre h ce qui est avantageux du point de vue numérique. Étant donnés les phénomènes physiques que le modèle doit décrire (*cf.* notre étude du chapitre I), la relation de Laplace doit être vérifiée tant que le rayon de courbure est grand devant l'épaisseur de l'interface. Nous avons montré que notre modèle permet effectivement de satisfaire une telle relation. En outre nous avons montré que le comportement de notre modèle aux faibles rayons est avantageusement différent du modèle discontinu classique ou bien que d'autres modèles à interface diffuse. En effet, le modèle permet de décrire les inclusions sphériques à la limite $R \to 0$ sans que ni le saut de pression ni le rayon discontinu équivalent ne divergent. Ceci permet de reproduire si ce n'est quantitativement, du moins qualitativement, les phénomènes de nucléation et de collapse qui sont des limites naturelles de la description d'une inclusion sphérique lorsque son rayon tend vers zéro.

V Dynamique des fluides

Au chapitre 5 nous déduisons les équations de la dynamique du fluide décrit par notre modèle thermodynamique de champ de phase. Nous précisons la modélisation des processus de retour à l'équilibre (introduction des phénomènes dissipatifs). Puis nous commentons les différents termes et couplages du système d'équation et proposons une forme adimensionnelle pour ce dernier. Nous montrons comment l'usage d'un modèle thermodynamique de champ de phase permet d'introduire une régularisation des différents "termes sources" utilisés pour la résolution numérique des équations de bilan basées sur un modèle discontinu de l'interface. En outre nous montrons comment notre modèle de champ de phase permet d'introduire un mécanisme dissipatif additionnel localisé au sein de la zone interfaciale et associé à la dynamique de changement de phase. Nous étudierons les conséquences de ce mécanisme additionnel sur la modélisation de la dynamique du changement de phase au chapitre VII.

V.1 Cas non-dissipatif et compressible

Dans un premier temps nous considérons la dynamique d'un fluide compressible[6] décrit par un modèle de champ de phase. Cette étude permet de suggérer une expression pour le travail appliqué sur un volume fluide. Elle sera utilisée par la suite (*cf.* section V.2) lors de l'étude de la dynamique dissipative anisotherme et quasi-compressible du fluide.

La déduction des équations du mouvement dans l'hypothèse non dissipative isotherme se base sur l'application du principe variationnel de d'Alembert-Lagrange. Elle est détaillée dans la section 5.1 du corps de texte. Nous reprenons dans ce résumé uniquement les étapes principales de la démonstration. Précisons que dans cette étude, et pour rester le plus général possible, nous envisageons la dépendance de la description thermodynamique en fonction du gradient $\nabla\varphi$ (plutôt qu'en la norme $(\nabla\varphi)^2$ comme précédemment) et posons

$$\vec{\Psi} \triangleq \frac{\partial f}{\partial \nabla\varphi}$$

Nous considérons ainsi une description Lagrangienne du champ de déplacement des particules du fluide de position $\vec{x}$. Nous introduisons la variation δ du mouvement fluide, paramétrée par ϵ. La première étape consiste à relier les variations des différentes variables de description aux deux variations primaires et indépendantes considérées, à savoir $\delta\vec{x}$ et $\delta\varphi$ (variation de position et variation d'état). Nous en déduisons les relations (classiques) suivantes

- ⋆ équation de continuité (*cf.* la démonstration de la relation (5.4))

$$\delta\rho = -\rho\nabla\cdot(\delta\vec{x})$$

- ⋆ relation liant les variations de $\nabla\varphi$ aux autres variations (*cf.* la démonstration de la relation (5.5))

$$\delta\nabla\varphi = \nabla(\delta\varphi) - \left(\nabla(\delta\vec{x})\right)\,\nabla\varphi$$

le deuxième terme correspondant à un produit matrice vecteur. Nous sommes alors en mesure d'étudier la variation $\delta\mathscr{L}$ du lagrangien $\mathscr{L}$ défini par

$$\mathscr{L} \triangleq \int_{t_i}^{t_f}\int_{\Omega}\rho\left(\frac{V^2}{2} - f\right)d\mathcal{V}\,dt$$

où

- ⋆ f est l'énergie libre massique du fluide
- ⋆ $\Omega(t)$ est un volume arbitraire de particules fluides se déplaçant avec le fluide (*i.e.* composé à chaque instant des mêmes particules)

[6] La variable φ étant interprétée comme le paramètre d'ordre, on peut penser à une généralisation de notre modèle au cas compressible, les fonctions g_{liq} et g_{vap} n'étant plus linéaires en P. On n'étudie pas ici les modifications à envisager en ce qui concerne les variations en φ d'une telle fermeture thermodynamique. En effet le résultat recherché est indépendant de tout choix analytique pour le potentiel thermodynamique compressible.

- ⋆ $d\mathcal{V}$ est la contraction du volume élémentaire en trois dimensions $d\mathcal{V} = dx_1\, dx_2\, dx_3$
- ⋆ $\dfrac{V^2}{2} \hat{=} \dfrac{1}{2}\vec{V}\cdot\vec{V}$ est l'énergie cinétique par unité de masse
- ⋆ et t_i et t_f sont les temps initial et final pour lesquels les variations sont supposées nulles (conformément aux hypothèses de travail nécessaires à l'application du principe d'Hamilton utilisé dans cette étude)

Nous en déduisons les équations de la dynamique suivantes

- ⋆ Équation de bilan de masse

$$\frac{d\rho}{dt} = -\rho\nabla\cdot(\vec{V})$$

- ⋆ Équation de bilan de quantité de mouvement

$$\rho\,\frac{d\vec{V}}{dt} = -\nabla\cdot\left(\rho\vec{\Psi}\otimes\nabla\varphi\right) - \nabla P \tag{V.26}$$

où le terme $\nabla\cdot\left(\rho\vec{\Psi}\otimes\nabla\varphi\right)$ du tenseur des contraintes non-dissipatif est un tenseur capillaire de type de Korteweg.

- ⋆ Condition d'équilibre thermodynamique

$$\tilde{\mu} = 0 \tag{V.27}$$

Cette équation est cohérente avec la condition d'équilibre (III.9c) déduite lors de notre analyse de la stabilité thermodynamique des états d'équilibre en section 3.2.2.

- ⋆ Les conditions limites :
  - spécification d'une force surfacique travaillant selon les variations de la variable champ de phase φ sur la frontière $\partial\Omega$ du volume Ω :

$$\rho\,\vec{\Psi} \tag{V.28}$$

  - taux de travail surfacique associé au produit scalaire du déplacement virtuel de la frontière $\delta\vec{x}$ avec le tenseur des contraintes non-dissipatif généralisé (*cf.* équation (V.26))

$$\left(P\,\mathcal{I} + \rho\,\vec{\Psi}\otimes\nabla\varphi\right) \tag{V.29}$$

Nous montrons que ces conditions aux limites peuvent s'interpréter en terme d'angle de contact ϑ entre l'interface et la frontière $\partial\Omega$. Il s'agit de la fermeture généralement utilisée pour la formulation discontinue du problème, *i.e.*

$$\frac{\nabla\varphi}{|\nabla\varphi|}\cdot\vec{n} = cos(\vartheta)$$

Notons dès à présent que *via* l'introduction des phénomènes dissipatifs, il est possible d'introduire une relaxation thermodynamiquement cohérente vers cette condition d'équilibre permettant de reproduire la physique d'un angle de contact dynamique et du phénomène d'hystérésis d'angle de contact.

L'équation de bilan de quantité de mouvement (V.26) est cohérente avec l'équation d'équilibre (III.9b). En effet nous montrons en utilisant les différentielles de l'énergie libre que le tenseur des contraintes peut se ré-écrire de sorte que l'équation (V.26) s'écrive

$$\frac{d\vec{V}}{dt} = \tilde{\mu}\,\nabla\varphi - \nabla g$$

et donc, en utilisant la relation d'équilibre (V.27), nous montrons que l'enthalpie libre massique est une première intégrale du mouvement de notre fluide. Remarquons que d'un point de vue numérique, il peut être alors plus avantageux de résoudre en g (qui est uniforme à l'équilibre) plutôt qu'en pression P, ce qui ne sera plus vrai pour le cas anisotherme.

V.2 Cas dissipatif anisotherme

Nous considérons désormais la fermeture anisotherme quasi-compressible de notre modèle. Les équations de la dynamique correspondantes sont déduites de l'application des premier et second principes de la thermodynamique. Nous reprenons ici les principales étapes de cette démonstration.

Premier principe Nous introduisons pour ce faire le travail $\mathcal{W}$ des efforts non dissipatifs sur un volume fluide Ω (dont l'expression nous est suggérée par l'étude compressible et conservative précédente) ainsi que le flux de chaleur $\vec{q}$ à travers la frontière $\partial\Omega$. Le premier principe s'écrit alors

$$\frac{d}{dt}\int_\Omega \rho\left(\tilde{u}+V^2\right)d\mathcal{V} = -\int_{\partial\Omega}\left(\vec{q}\cdot\vec{n}+\mathcal{W}\right)dS$$

où $\tilde{u}$ est l'énergie interne massique du fluide (*cf.* (5.29)). Nous en déduisons l'expression (5.33) pour l'équation d'évolution de l'entropie de notre fluide

$$\rho T\frac{ds}{dt} = -\rho\tilde{\mu}\frac{d\varphi}{dt} - \vec{V}\cdot\left(\rho\frac{d\vec{V}}{dt}+\nabla P+\nabla\cdot\left(\rho\vec{\Psi}\otimes\nabla\varphi\right)\right)-\nabla\cdot\vec{q}$$

Second principe Introduisons $\mathcal{R}_s$ la source d'entropie définie par

$$\mathcal{R}_s \triangleq \rho\frac{ds}{dt}+\nabla\cdot\vec{q_s}$$

où $\vec{q_s}$ est un flux d'entropie que nous définissons classiquement (*e.g.* [107]) par $\vec{q_s}\triangleq\vec{q}/T$. Le second principe de la thermodynamique stipule la positivité de $\mathcal{R}_s$

$$\mathcal{R}_s \geq 0 \tag{V.30}$$

et nous montrons comment, dans le cadre d'une description thermodynamique de type champ de phase, l'inégalité (V.30) peut s'écrire

$$-\rho\tilde{\mu}\frac{d\varphi}{dt}+\bar{\bar{\tau}}^D:\nabla\vec{V}-\frac{\vec{q}}{T}\cdot\nabla T\geq 0 \tag{V.31}$$

où $\bar{\bar{\tau}}^D$ est le tenseur des contraintes dissipatives introduit dans l'équation de bilan de quantité de mouvement, *i.e.* (*cf.* équation (5.38))

$$\rho\frac{dV}{dt} = -\nabla P-\nabla\cdot\left(\rho\vec{\Psi}\otimes\nabla\varphi\right)+\nabla\cdot\bar{\bar{\tau}}^D$$

L'inégalité (V.31) est la somme de trois termes. Les deux derniers termes sont classiquement rencontrés en mécanique des fluides et correspondent aux dissipations mécanique et thermique ; le premier est une contribution qui est clairement associée à notre introduction de la variable champ de phase dans la description thermodynamique, en effet nous y retrouvons le produit du terme $\tilde{\mu}$, dérivée variationnelle du potentiel thermodynamique par rapport à φ, avec le terme $d\varphi/dt$, qui selon le sens donné à φ représente le taux de changement de phase local.

Fermeture dissipative Afin de satisfaire l'inégalité (V.31), nous considérons l'approximation linéaire de la thermodynamique des processus irréversibles. Dans ce contexte, comme l'a montré Roshchin and Truskinovsky [114], nous disposons d'un ensemble de 14 paramètres cinétiques pour définir le triplet $(\bar{\bar{\tau}}^D,\vec{q},d\varphi/dt)$. Étant donné le manque de connaissance concernant la nature des processus dissipatifs se produisant à l'interface, il n'est pas possible de renseigner ces paramètres, nous considérons par la suite une fermeture simple pour ce triplet. En particulier pour assurer la positivité des trois termes de l'inégalité, nous considérons trois processus dissipatifs indépendants, assurant chacun la positivité d'un des termes. Ainsi nous considérons

- ⋆ une viscosité de type Newton, *i.e.* nous définissons $\bar{\bar{\tau}}^D$ par

$$\bar{\bar{\tau}}^D \triangleq \eta(\nabla\vec{V}+\nabla\vec{V}^T)-\eta\frac{2}{3}\nabla\cdot\vec{V}\,\mathcal{I}$$

  où η est la viscosité dynamique du fluide qui peut dépendre de φ afin de retrouver les valeurs physiques au sein des phases. Nous n'étudierons pas les conséquences de ce choix.

⋆ une loi de type pour Fourier pour la conduction

$$\vec{q} = -k\nabla T$$

où k est la conductivité thermique du fluide qui peut dépendre de φ afin de retrouver les valeurs physiques au sein des phases. Nous étudions les conséquences du choix d'une conductivité variable $k(\varphi)$ sur la dynamique du changement de phase dans le chapitre 7.

⋆ une relaxation de type Ginzburg-Landau vers la condition d'équilibre $\tilde{\mu} = 0$

$$\frac{d\varphi}{dt} = -\kappa\tilde{\mu}$$

où κ est une mobilité, cette équation est communément appelée équation d'Allen-Cahn dans la communauté des modèles de champ de phase.

Cette fermeture des processus dissipatifs nous permet de retrouver au sein des phases (où φ est constant et où ainsi la contribution de la relaxation de Ginzburg-Landau est nulle), les modèles de Newton et de Fourier classiquement utilisés pour décrire les phases liquide et vapeur.

Équations du mouvement dissipatives Les processus dissipatifs ayant été précisés, nous sommes à même d'écrire le système complet d'équations du mouvement de notre fluide

$$\frac{d\varphi}{dt} = -\kappa\,\tilde{\mu} \tag{V.32a}$$

$$\frac{d\rho}{dt} = -\rho\,\nabla\cdot\vec{V} \tag{V.32b}$$

$$\rho\,\frac{d\vec{V}}{dt} = -\nabla P - \left(\rho\,\vec{\Psi}\otimes\nabla\varphi\right) + \vec{F}_g + \nabla\cdot\left(\eta(\nabla\vec{V} + \nabla\vec{V}^T) - \eta\,\frac{2}{3}\,\nabla\cdot\vec{V}\,\mathcal{I}\right) \tag{V.32c}$$

$$\rho\,T\,\frac{ds}{dT} = \nabla\cdot(k\,\nabla T) - \rho\,\kappa\,\tilde{\mu}^2 - \vec{V}\cdot\left[\nabla\cdot\left(\eta(\nabla\vec{V} + \nabla\vec{V}^T) - \eta\,\frac{2}{3}\,\nabla\cdot\vec{V}\,\mathcal{I}\right)\right] \tag{V.32d}$$

où nous avons introduit la force gravitationnelle $\vec{F}_g = -\rho\vec{g_0}$. Nous remarquons que l'ensemble de ces équations ne font pas intervenir explicitement les variables principales choisies pour le modèle (à savoir $(P, T, \varphi, \vec{V})$). Par la suite nous étudions la forme de ces équations ré-écrites en fonction de ces seules variables afin de mieux analyser les différents termes de chaque équation ainsi que les couplages existant entre ces dernières.

V.3 Étude du système d'équations

Équation d'évolution en température Nous montrons dans la section 5.3.1 comment l'équation d'évolution de l'entropie (V.32d) peut en fait être ré-écrite comme suit

$$\rho c_P\frac{dT}{dt} = \rho\,T\left(\underbrace{\frac{\partial\mu}{\partial T}\frac{d\varphi}{dt} + \frac{\partial\vec{\Psi}}{\partial T}\cdot\frac{d\nabla\varphi}{dt}}_{\text{champ de phase}} + \frac{\partial v}{\partial T}\frac{dP}{dt}\right) + \bar{\bar{\tau}}^D : \nabla\vec{V} \quad \underbrace{-\rho\tilde{\mu}\,\frac{d\varphi}{dt}}_{\text{champ de phase}} \quad -\nabla\cdot\vec{q} \tag{V.33}$$

Les premiers termes "champ de phase" seront rapprochés d'une régularisation du terme source de chaleur latente associé à la transition de phase. Le dernier terme "champ de phase" correspond à la dissipation induite par le mécanisme de relaxation de Ginzburg-Landau. Dans le corps du texte, nous soulignons l'importance de la présence des différents termes associés à l'introduction de la variable champ de phase. En effet ils assurent la cohérence thermodynamique de notre modèle. Nous constatons que l'équation (V.33) diffère (toutes choses étant supposées égales en ce qui concerne la fermeture thermodynamique) de celle utilisée communément dans les modèles de type champ de phase pour l'étude de la transition de phase solide-liquide. A cela deux raisons principales. La première concerne un choix différent pour le flux d'entropie $\vec{q_s}$ qui n'est alors plus égal à sa forme classique $\vec{q}/T$ sans qu'une justification claire de cette différence ne soit fournie (*e.g.* Charach and Fife [33]). La seconde concerne la négligence volontaire de certains termes fortement non-linéaires (comme $\tilde{\mu}\,(d\varphi/dt) = \tilde{\mu}^2$) dans le système d'équations résolu numériquement de manière à augmenter l'efficacité des solveurs utilisés (*e.g.* Karma and Rappel [73]). Concernant notre modèle, nous souhaitons conserver dans un premier temps la cohérence du système d'équations résolues.

Théorème Pi de Vaschy-Buckingham Dans la section 5.3.2, nous définissons les échelles physiques principales propres à la description de l'ébullition nucléée et celles qu'il est nécessaire de considérer en supplément dans le cadre de notre modélisation de type champ de phase. Elles sont au nombre de 14, utilisant 4 unités physiques indépendantes (à savoir m, s, K, kg) et nous introduisons ainsi les 10 nombres adimensionnels pertinents pour une simulation de la croissance d'une bulle à l'aide de notre modèle champ de phase

- ⋆ Reynolds : $Re = \dfrac{U\,L\,\rho_0}{\eta}$
- ⋆ Stefan : $St = \dfrac{c_{P0}\,\Delta T}{\mathcal{L}}$
- ⋆ $\gamma = \dfrac{\sigma}{L\rho_0\,c_{P0}\,\Delta T}$
- ⋆ Atwood: $At = \delta v \rho_0$, $At \in [0;1[$
- ⋆ Froude : $Fr = \dfrac{U^2}{g_0\,L}$
- ⋆ Weber : $We = \dfrac{\rho_0\,U^2\,L}{\sigma}$
- ⋆ $\varepsilon = \dfrac{h}{L}$
- ⋆ Peclet: $Pe = \dfrac{\rho_0\,U\,L\,c_{P0}}{k}$
- ⋆ $\theta = \dfrac{T_{ref}}{\Delta T}$
- ⋆ $\kappa^* = \dfrac{\kappa\,\sigma\,L}{U\,h\,\rho_0}$

Commentons brièvement les nombres adimensionnels qui ne sont pas classiques

- ⋆ Le nombre γ est nécessaire dans notre modélisation du processus d'ébullition car les échelles thermodynamiques "thermique" et "mécanique" sont couplées, ce qui n'est pas classiquement considéré dans la description du processus d'ébullition, *e.g.* Mikic et al. [93].

- ⋆ Le nombre θ mesure la surchauffe ou le sous-refroidissement du fluide, il est typiquement grand devant 1.

- ⋆ Le nombre ε est une mesure de l'épaisseur de l'interface devant la longueur macroscopique L caractéristique du problème étudié ; cette dernière dépend *a priori* du problème de changement de phase étudié mais on peut la supposer égale à la longueur capillaire.

- ⋆ Le nombre κ^* caractérise la dissipation interfaciale lors du processus de changement de phase comme nous le montrerons au chapitre VII, il est choisi en accord avec la relation cinétique que l'on souhaite reproduire.

Écriture finale du système d'équations Dans la suite de la section 5.3.3, nous analysons successivement les différents termes du système d'équations adimensionnel (5.46) et introduisons une fermeture simplifiée pour les aspects thermiques de notre modèle. Cette fermeture suppose une linéarité en température de la pression de saturation $P_{sat}(T)$ ce qui permet de simplifier l'écriture des termes des équations impliquant la fonction μ, tout en introduisant les principales grandeurs nécessaires à la description de l'ébullition, à savoir la chaleur latente et la capacité thermique des phases. Puis nous considérons une dépendance isotrope en $(\nabla\varphi)^2$ et négligeons le coefficient d'expansion thermique des phases. Nous introduisons aussi les variables suivantes qui, utilisées à la place de la pression, induisent des simplifications des calculs analytiques ou numériques (mais sans pour autant causer de perte du point de vue de la physique décrite).

- ⋆ $\mathcal{G} \triangleq P + \left(W + (\varepsilon^2/2)\,(\nabla\varphi)^2\right)(\varepsilon\,We)^{-1}$ est l'enthalpie libre volumique isotherme du fluide et est ainsi uniforme à l'équilibre. L'utilisation de cette variable a le mérite de simplifier l'expression du tenseur des contraintes tout en réduisant le nombre de non-linéarités dans l'expression de $\tilde{\mu}$.

- ⋆ $\tilde{P} \triangleq P + \varepsilon^2\,(\nabla\varphi)^2$ est uniforme à l'équilibre d'une interface plane et permet de simplifier l'écriture d'un problème mono-dimensionnel.

Ainsi le système d'équations du mouvement prend la forme suivante

$$\frac{d\varphi}{dt} = -\kappa \left[\frac{d\nu}{d\varphi} \left((At\,\varepsilon\,We)\,\mathcal{G} - \frac{\varepsilon}{St\,\gamma\,\theta}\,T \right) + v \left(\frac{dW}{d\varphi} - \varepsilon^2 \Delta\varphi \right) \right] \tag{V.34a}$$

$$\nabla \cdot \rho\vec{V} = \rho^2\,At\,\frac{\partial \nu(\varphi)}{\partial t} \tag{V.34b}$$

$$\rho\,\frac{d\vec{V}}{dt} = -\nabla\mathcal{G} + \frac{\left(\frac{dW}{d\varphi} - \varepsilon^2\Delta\varphi\right)}{\varepsilon\,We}\,\nabla\varphi + \frac{\nabla\cdot\bar{\bar{\tau}}^D}{Re} + \frac{\rho\,\vec{g}}{Fr} \tag{V.34c}$$

$$\rho\,\frac{dT}{dt} = \frac{\nabla\cdot(k\nabla T)}{Pe} - \frac{\rho\,(1+T/\theta)}{St}\frac{d\nu}{d\varphi}\frac{d\varphi}{dt} + \gamma\,We\left(\frac{\bar{\bar{\tau}}^D\,:\,\nabla V}{Re} - \frac{\rho\vec{g}\cdot\vec{V}}{Fr}\right) + \frac{\gamma}{\varepsilon\,\kappa}\rho\left(\frac{d\varphi}{dt}\right)^2 \tag{V.34d}$$

Les propriétés d'un tel système d'équations sont les suivantes

- ⋆ La pression modifiée $\mathcal{G}$ n'apparaît pas dans l'équation d'évolution de la température. L'équation d'Allen-Cahn ainsi que l'équation bilan de quantité de mouvement sont linéaires en $\mathcal{G}$.
- ⋆ La température T n'apparaît pas dans le bilan de quantité de mouvement, apparaît linéairement dans l'expression de $\tilde{\mu}$ (*cf.* l'équation d'Allen-Cahn) ainsi que dans l'équation d'évolution pour la température (dans les termes convectif et diffusif).
- ⋆ La variable φ définit à elle seule la masse volumique (puisque nous négligeons la compressibilité ainsi que l'expansion thermique du fluide). Ainsi l'équation de bilan de masse montre que la divergence de la quantité de mouvement $\rho\vec{V}$ est directement associée au taux de transfert de phase ($\partial\varphi/\partial t$).
- ⋆ Le second terme du membre de droite de l'équation d'évolution de la température ($\rho\ (1+T/\theta)\ /St$) est une régularisation du terme source de chaleur latente, localisé au sein de la zone interfaciale (où $(d\nu/d\varphi) \neq 0$) et associé au taux de transfert de phase ($d\varphi/dt$). Il est à comparer avec des termes sources équivalents utilisés pour la résolution numérique des problèmes à frontière libre, *e.g.* Juric and Tryggvason [69].

Nous introduisons aussi la forme simplifiée du système d'équations dans le cas où les phases sont considérées comme "solides" pour lequel nous avons supposé que la masse volumique est uniforme

$$\frac{d\varphi}{dt} = -\kappa \left[-\frac{d\nu}{d\varphi}\,\frac{\varepsilon}{St\,\gamma\,\theta}\,T + \frac{dW}{d\varphi} - \varepsilon^2\Delta\varphi \right] \tag{V.35a}$$

$$\frac{dT}{dt} = \frac{\nabla\cdot(k\nabla T)}{Pe} - \frac{\rho\,(1+T/\theta)}{St}\frac{d\nu}{d\varphi}\frac{d\varphi}{dt} + \frac{\gamma}{\varepsilon\,\kappa}\left(\frac{d\varphi}{dt}\right)^2 \tag{V.35b}$$

ainsi que dans le cas isotherme

$$\frac{d\varphi}{dt} = -\kappa \left[\frac{d\nu}{d\varphi}(At\,\varepsilon\,We)\,\mathcal{G} + v \left(\frac{dW}{d\varphi} - \varepsilon^2\Delta\varphi \right) \right] \tag{V.36a}$$

$$\nabla\cdot\rho\vec{V} = \rho^2\,At\,\frac{\partial\nu(\varphi)}{\partial t} \tag{V.36b}$$

$$\rho\,\frac{d\vec{V}}{dt} = -\nabla\mathcal{G} + \frac{\left(\frac{dW}{d\varphi} - \varepsilon^2\Delta\varphi\right)}{\varepsilon\,We}\,\nabla\varphi + \frac{\nabla\cdot\bar{\bar{\tau}}^D}{Re} + \frac{\rho\,\vec{g}}{Fr} \tag{V.36c}$$

Ces sous-systèmes d'équations, obtenus en faisant des hypothèses simplificatrices de la description physique de notre fluide, seront utilisés dans nos études analytiques (*cf.* section 7) et numériques (*cf.* section VIII) ultérieures car ils permettent d'analyser certains sous-problèmes et couplages de manière indépendante.

Analyse de la relaxation de type Ginzburg-Landau avec notre fermeture thermodynamique Considérons l'expression particulière du mécanisme de relaxation (équation (V.34a)) induite par le choix de notre fermeture

thermodynamique

$$\frac{d\varphi}{dt} = -\kappa \left[\underbrace{\frac{dv}{d\varphi}\left((At\,\varepsilon\,We)\,\mathcal{G} - \frac{\varepsilon}{St\,\gamma\,\theta}\,T \right)}_{\text{saturation}} + \underbrace{v\,\left(\frac{dW}{d\varphi} - \varepsilon^2 \Delta\varphi \right)}_{\text{profil}} \right]$$

Ainsi le changement de phase, *i.e.* le déplacement de l'interface aussi bien que les variations de la variable champ de phase au sein de la zone interfaciale (terme de gauche de l'équation) est gouverné par deux contributions :

- ⋆ La première (terme "saturation") concerne un retour à l'équilibre thermodynamique diphasique "classique" imposant au sein de la zone interfaciale (où $(dv/d\varphi) \neq 0$) que le fluide (*i.e.* les phases liquide et vapeur de part et d'autre de l'interface) soit à saturation ($\mathcal{G} \propto T$). Ce terme peut être comparé à ses équivalents dans les méthodes de relaxation numérique et/ou pénalisation permettant d'imposer numériquement la condition limite $T_{interface} = T_{sat}$.
- ⋆ La seconde (terme "profil") concerne la régularisation de l'interface, en effet on identifie facilement ce terme avec l'équation différentielle (III.14) satisfaite à l'équilibre d'une interface plane et permettant d'obtenir un profil de φ d'épaisseur ε.

Cette analyse de la dynamique de φ avec notre modèle permet d'illustrer comment ce dernier permet à la fois de retrouver un changement de phase "macroscopique" tout en contrôlant la dynamique interne à la zone interfaciale qui permet de maintenir une épaisseur caractéristique proche de la valeur d'équilibre.

Forme adimensionnelle en vue de l'étude de la limite "interface discontinue" de notre modèle Les systèmes d'équations (V.34, V.35, V.36) sont rendus adimensionnels en vue de la résolution d'un problème à frontière libre mais ne permettent pas, de part le grand nombre de paramètres (10 nombres adimensionnels) d'obtenir une analyse claire de la modélisation champ de phase de la dynamique de changement de phase. Pour cette dernière étude, nous proposons donc une forme plus adéquate des équations adimensionnelles pour laquelle les grandeurs physiques utilisées pour la description des phases sont trivialisées (égales à 1). Cette démarche est détaillée en début de section 5.3.4. Les nombres adimensionnels pertinents pour l'étude asymptotique de la zone interfaciale que nous avons retenus sont donc l'épaisseur adimensionnelle de l'interface ε et les 2 paramètres des phénomènes dissipatifs (le nombre de Reynolds Re est considéré comme ∞ dans cette étude), à savoir le nombre de Péclet Pe et la mobilité adimensionnelle κ^*. Concernant cette dernière, nous considérons l'équivalence $\kappa^* \sim \alpha\varepsilon^{-2}$ lors du passage à la limite des faibles ε ; nous considérerons les conséquences de cette hypothèse en section VII.5. Nous étudions alors une solution mono-dimensionnelle de type onde progressive de vitesse $\mathcal{D}$ selon un axe arbitraire X perpendiculaire à l'interface, l'abscisse x étant normalisée par la longueur capillaire l

$$l \triangleq \frac{\sigma}{\rho \mathcal{L}}$$

Le système d'équations du mouvement s'écrit[7](nous notons $\cdot_{,x} \triangleq (\partial \cdot / \partial x)$)

$$\frac{\varepsilon^2}{\alpha}\,(\mathcal{D} - V)\,\varphi_{,x} = \varepsilon\,\frac{dv}{d\varphi}\left(\tilde{P} - T\right) + v\,\left(\frac{dW}{d\varphi} - \varepsilon^2 \varphi_{,xx}\right) + \frac{dv}{d\varphi}\left(W - \frac{\varepsilon^2}{2}\varphi_{,x}^2\right) \tag{V.37a}$$

$$(\rho V)_{,x} = -\rho^2\,\frac{\partial v}{\partial \varphi}\,(\mathcal{D} - V)\,\varphi_{,x} \tag{V.37b}$$

$$(V - \mathcal{D})\,\rho V_{,x} = -\tilde{P}_{,x} \tag{V.37c}$$

$$(V - \mathcal{D})\,\rho\,T_{,x} = \frac{(k\,T_{,x})_{,x}}{Pe} - (V - \mathcal{D})\,\rho\,(1 + T)\,\frac{dv}{d\varphi}\,\varphi_{,x} + (\mathcal{D} - V)^2\,\frac{\rho\varepsilon}{\alpha}\,(\varphi_{,x})^2 \tag{V.37d}$$

Nous montrons au chapitre VII que ce système est compatible avec le modèle incompressible discontinu dans la limite asymptotique des faibles ε.

[7]L'écriture du membre de gauche de l'équation de bilan de quantité de mouvement (V.37c) repose sur l'identité suivante et n'est valable que pour un système mono-dimensionnel $\left(\varphi_{,x}^2/2\right)_{,x} = \varphi_{,xx}\,\varphi_{,x}$

Conclusion Dans ce chapitre nous avons déduitle système d'équations du mouvement d'un fluide quasi-compressible en se basant sur des principes clairs, assurant ainsi sa cohérence thermodynamique. Nous avons interprété physiquement l'ensemble des termes issus de l'introduction de la variable champ de phase et de son gradient comme variables thermodynamiques. Nous avons ainsi montré que l'ensemble de la physique liée au changement de phase est reproduite. En outre nous avons défini les mécanismes dissipatifs au sein de la zone interfaciale et introduit un mécanisme de type relaxation de Ginzburg-Landau qui est spécifique à la modélisation de type champ de phase. Nous étudierons au chapitre VII comment ce mécanisme permet de définir la relation cinétique de la transition de phase liquide-vapeur dans le cas non-visqueux. Finalement nous avons proposé une écriture adimensionnelle simple du système d'équations permettant d'illustrer les principaux couplages entre les équations.

VI Stabilité des états homogènes

Dans ce chapitre, nous étudions la stabilité des états homogènes décrits par notre modèle de champ de phase. Notre but est de démontrer que les états liquide et vapeur sont effectivement les seuls états monophasiques admissibles pour le fluide. En outre nous étudions l'influence du modèle champ de phase sur la définition des domaines de stabilité de ces phases. Étant donnée notre hypothèse quasi-compressible, les phases liquide et vapeur sont décrites par des équations d'état incompressibles (g_{liq} et g_{vap}). Ainsi dans le cadre d'une modélisation classique ces phases devraient exister pour toute valeur de pression et température (condition de Gibbs-Duhem classique). Dans le cadre d'une modélisation champ de phase, cette physique se traduit par la stabilité thermodynamique inconditionnelle des états $\varphi = 0$ et $\varphi = 1$. En particulier nous déterminons dans le cadre de cette étude comment de telles propriétés d'un modèle champ de phase reposent sur le choix fait pour la dépendance en φ de la description thermodynamique. Nous montrons que le choix que nous proposons permet effectivement de satisfaire les objectifs susmentionnés.

VI.1 Étude bibliographique

Notre première contribution à l'analyse de la stabilité des états homogènes est une étude bibliographique des études de ce problème dans la famille des modèles à interface diffuse (*cf.* section 6.1 du corps de texte).

Nous distinguons dans un premier temps les modèles à interface diffuse dits classiques des modèles à interface diffuse utilisant la variable champ de phase comme paramètre d'ordre. Afin d'analyser ces résultats, nous considérons que la fermeture thermodynamique peut-être formellement divisée en deux parties, une première portant la non-convexité qui induit la dynamique de séparation des phases et une seconde consistant en une interpolation en fonction du paramètre d'ordre de la description thermodynamique des différentes phases. Nous verrons par la suite que le choix de la fonction d'interpolation conditionne plus particulièrement les propriétés de stabilité des états homogènes.

Modèles classiques Pour la première catégorie de modèles, regroupant les modèles de type van der Waals et les modèles de type Cahn-Hilliard, les précédentes analyses de stabilité ont considéré majoritairement le cas d'une fonction d'interpolation linéaire en le paramètre d'ordre. Nous montrerons que cette linéarité n'est pas compatible avec notre interprétation de la variable champ de phase.

Modèles champ de phase ou apparentés Roshchin and Truskinovsky [114] étudie la condition de stabilité d'un état homogène dans le cas d'une description de type champ de phase d'un fluide. Pour autant l'influence de la fermeture thermodynamique sur cette condition n'est pas considèrée, point qui apparaît comme crucial dès lors que des applications "quantitatives" du modèle sont visées. Umantsev [141] propose une analyse plus poussée de l'influence de la fonction d'interpolation pour un modèle de type champ de phase (isobare). Umantsev [141] montre en particulier l'influence de cette fonction sur les domaines de stabilité des états monophasiques. Pour autant, le choix retenu ne permet pas d'assurer la stabilité inconditionnelle des états $\varphi = 0$ et $\varphi = 1$. Ce constat justifie la nécessité de poursuivre cette analyse plus avant.

En outre, nous constatons que les précédentes études ne considèrent pas la stabilité éventuelle d'autres états homogènes (différents de $\varphi = 0$ ou $\varphi = 1$). Nous considérons que le modèle (et en particulier la fermeture thermodynamique) ne doit pas conduire à l'existence de tels états pour lesquels aucune physique n'est associée. Finalement nous souhaitons aussi considérer dans cette étude l'influence des phénomènes dissipatifs sur la dynamique de croissance d'une instabilité d'un état homogène, cette analyse permettant d'appréhender la dynamique de séparation des phases à l'aide de notre modèle.

VI.2 Perturbation d'un état homogène

Dans cette partie, nous considérons l'étude analytique de l'évolution d'une perturbation d'un état homogène ($\nabla\varphi = \vec{0}$) à l'équilibre (*cf.* les équations d'équilibre (III.9)) sans mouvement. On considère alors un système mono-dimensionnel selon une abscisse arbitraire x. Cet état est caractérisé par deux paramètres principaux qui sont ainsi les paramètres de cette étude, à savoir

- ⋆ la valeur de l'écart de l'enthalpie libre massique par rapport à sa valeur à saturation, g^{*hs};

- ⋆ la valeur de la variable champ de phase φ^{hs}.

Ces deux paramètres sont tels que l'état est à l'équilibre et donc en particulier satisfont la relation (*cf.* équation (6.2))

$$\frac{\lambda}{h^2}\frac{dW}{d\varphi}^{hs} - \frac{d\rho}{d\varphi}^{hs} g^{*hs} = 0$$

dont les solutions ont été étudiées en section 3.4.1 en fonction de la fonction d'interpolation ν. Nous rappelons dans la suite les principaux enseignements de cette étude nous concernant présentement. Les deux paramètres g^{*hs} et φ^{hs} doivent ou non être considérés comme indépendants, selon le choix fait pour ν et l'état considéré. En effet si la fonction d'interpolation pour la masse volumique est choisie comme étant les polynômes P_3 ou P_5, les valeurs $\varphi = 0$ et $\varphi = 1$ sont solutions d'équilibre quelle que soit la valeur de g^{*hs}. En effet ces fonctions entraînent la propriété suivante pour l'enthalpie libre massique : 0 et 1 sont toujours des extrema locaux. Hors de ce cas, (*i.e.* $\varphi^{hs} \neq 1/2 \pm 1/2$ et/ou 0 et 1 pas toujours extrema locaux) il existe une relation (pas obligatoirement bijective) liant les deux valeurs et nous considérerons arbitrairement g^{*hs} comme étant l'unique paramètre pertinent (en effet il se rapporte à des grandeurs physiques tandis que la valeur de φ^{hs} est purement abstraite). Nous avons alors $\varphi^{hs}(g^{*hs})$. Pour éviter toute ambiguïté nous considérons dans un premier temps les deux paramètres comme indépendants.

Notons dès à présent une conséquence importante de cette propriété du potentiel thermodynamique : il existe des états d'équilibre différents de 0 ou 1, et ce quel que soit le choix de la fermeture thermodynamique champ de phase. Les états monophasiques correspondant ont donc une équation d'état différente de celle visée pour les états liquide ou vapeur. Nous ne souhaitons pas observer ces états "parasites" et le modèle se doit donc d'assurer qu'ils sont instables.

VI.3 Stade d'évolution linéaire d'une perturbation

Ecriture matricielle du système d'équations pour les amplitudes de la perturbation Nous considérons désormais que l'état d'équilibre homogène considéré est soumis à une perturbation infinitésimale et nous linéarisons le système d'équations du mouvement autour de l'état d'équilibre. Nous obtenons alors le système d'équations suivant pour la perturbation (*cf.* l'obtention du système (6.3))

$$-\rho^{hs} V'_{,x} = \frac{d\rho}{d\varphi}^{hs} \varphi'_{,t} \tag{VI.38a}$$

$$V'_{,t} = -s^{hs} T'_{,x} - g'_{,x} + \left(\frac{\eta}{\rho}\right)^{hs} V'_{,xx} \tag{VI.38b}$$

$$(\rho c_P)^{hs} T'_{,t} = k^{hs} T'_{,xx} + \frac{T^{hs}}{\rho^{hs}}\frac{dP_{sat}}{dT}\frac{d\rho}{d\varphi}^{hs} \varphi'_{,t} \tag{VI.38c}$$

$$\frac{\rho^{hs}}{\kappa}\varphi'_{,t} = -\frac{\partial\rho\mu}{\partial\varphi}\varphi' - \frac{\partial\rho\mu}{\partial g^*}g^{*'} + \lambda\varphi'_{,xx} \tag{VI.38d}$$

Posons alors la perturbation comme étant une onde progressive, *i.e.* comme étant proportionnelle à $e^{\omega t + \mathbf{I}k_x x}$, où le nombre d'onde k_x est un réel, *i.e.* $\Im(k_x) = 0$ et où ω est la fréquence angulaire. L'état homogène hs considéré dans cette étude est considéré comme inconditionnellement stable si et seulement si pour toute valeur de k_x, la fréquence angulaire ω a une partie réelle (taux de croissance) strictement négative, *i.e.* $\Re(\omega) < 0$. Le système d'équations (6.5) pour les 4 amplitudes de cette perturbation (correspondant aux 4 variables principales (g, T, φ, V)) se déduit facilement du système (VI.38).

Particularité de la fermeture quasi-compressible Nous remarquons que la structure du système d'équations est fortement influencée par l'hypothèse de quasi-compressibilité (nous la comparons avec un système d'équation équivalent obtenu dans un cas compressible comme le considère Roshchin and Truskinovsky [114] par exemple). En effet l'amplitude de la perturbation en vitesse V' se déduit trivialement de l'amplitude de la perturbation en champ de phase φ', selon la relation (6.6)

$$V' = \frac{\mathbf{I}\omega}{k_x\rho^{hs}}\frac{d\rho}{d\varphi}^{hs} \varphi'$$

Ceci est dû à l'expression particulière de l'équation de bilan de masse : puisque les phases sont incompressibles, la divergence du champ de quantité de mouvement est directement et uniquement associée au changement de phase. Ceci modifie aussi la structure de la relation de dispersion traduisant la stabilité d'une perturbation : la perturbation V' sont simplement proportionnelles à ω fois la perturbation φ', ce qui trivialise la détermination de V', ainsi plutôt qu'un polynôme de degré 4 en ω, nous obtenons un polynôme de degré 3 par élimination de la solution triviale $\omega = 0$.

Relation de dispersion et condition de stabilité Il s'agit alors de déterminer les solutions non trivialement nulles pour les amplitudes de la perturbation. Pour ce faire nous étudions le déterminant du système écrit sous forme matricielle. Il s'agit de la relation de dispersion, reliant k_x et ω qui s'écrit (*cf.* équation (6.9))

$$\det M(\omega, k_x) = \mathbf{I} k_x^2 \rho^{hs} \left(\omega \, \frac{T^{hs}}{\rho^{2\,hs}} \left(\frac{dP_{sat}}{dT} \right)^2 \left(\frac{d\rho}{d\varphi}^{hs} \right)^2 + \left(\omega \, (\rho c_P)^{hs} + k_x^2 \, k^{hs} \right) \det {}_{isoth}(\omega, k_x) \right) \tag{VI.39}$$

où

$$\begin{aligned} \det {}_{isoth}(\omega, k_x) \;\hat{=}\; & \begin{vmatrix} \left(\omega \dfrac{\rho^{hs}}{\kappa} + \lambda \, k_x^2 + \dfrac{\lambda}{h^2} \dfrac{d^2 W}{d\varphi^2}^{hs} - \dfrac{d^2 \rho}{d\varphi^2}^{hs} \, g^{*\,hs} \right) & -\dfrac{d\rho}{d\varphi}^{hs} \\ \dfrac{\omega}{\rho^{hs}} \dfrac{d\rho}{d\varphi}^{hs} \left(\left(\dfrac{\eta}{\rho} \right)^{hs} + \dfrac{\omega}{k_x^2} \right) & 1 \end{vmatrix} \\ = \; & \omega^2 \left[\left(\frac{d\rho}{d\varphi}^{hs} \right)^2 \frac{1}{k_x^2 \rho^{hs}} \right] + \omega \left[\frac{\rho^{hs}}{\kappa} - \left(\frac{d\rho}{d\varphi}^{hs} \right)^2 \left(\frac{\eta}{\rho^2} \right)^{hs} \right] \\ & + \lambda \left[k_x^2 + \frac{1}{h^2} \frac{d^2 W}{d\varphi^2}^{hs} - \frac{d^2 \rho}{d\varphi^2}^{hs} \frac{g^{*\,hs}}{\lambda} \right] \end{aligned} \tag{VI.40}$$

$\det {}_{isoth}(\omega, k_x)$ est un polynôme de degré 2 en ω et $\det {}_{isoth}(\omega, k_x) = 0$ correspond en fait à la relation de dispersion obtenue dans le cas isotherme comme montré en section 6.3.2.

Il s'agit donc désormais d'étudier les racines du polynôme $\det M$.

VI.4 Étude générale de la relation de dispersion

Dans un premier temps nous considérons l'étude générale de la relation de dispersion d'un modèle champ de phase quasi-compressible. Cette étude permet de dégager les principales propriétés de ce modèle et de mettre en évidence l'influence de la partie champ de phase de la fermeture thermodynamique sur la description des états monophasiques, ce qui servira à jutifier le choix fait dans notre modèle par la suite.

Condition de stabilité dans le cas dissipatif anisotherme Notons tout d'abord que dans ce cas, il n'est pas possible de déduire la relation de dispersion pour l'évolution de la perturbation puisque sa connaissance repose sur la résolution du polynôme de degré 3 en ω $\det M = 0$. Pour autant, il est possible d'obtenir analytiquement les conditions pour lesquelles les solutions sont stables en utilisant le critère de Routh-Hurwitz rappelé en note 6 de la page 142.

L'expression du critère de stabilité nous amène à l'introduction d'une notion de région spinodale associé à la convexité du potentiel thermodynamique vis à vis des variations en φ. Ainsi nous définissons la longueur d'onde de coupure k^c par (*cf.* équation (6.14))

$$(k^c)^2 = -\frac{\rho^{hs}}{\lambda} \frac{\partial \mu}{\partial \varphi}^{hs}_{|P,T} \tag{VI.41}$$

Les états appartenant à la région spinodale ($\frac{\partial \mu}{\partial \varphi}^{hs}_{|P,T} < 0$) sont conditionnellement instables (*i.e.* instable pour toute perturbation dont la longueur d'onde est à k^c qui est réel) tandis que les états hors de cette région sont inconditionnellement stables (k^c imaginaire pur). Une simple analogie $\varphi \leftrightarrow \rho$ permet de relier formellement la quantité k^c à l'inverse de la compressibilité χ_T dont la positivité est une condition classique de stabilité d'une phase.

Il ressort de cette étude que les propriétés de stabilité d'un état d'équilibre vont dépendre de la relation (g^{*hs}, φ^{hs}) et donc du choix pour la fonction d'interpolation.

Dans la suite de cette étude nous considérons différents cas physiques pour lesquels la relation de dispersion est suffisamment dégénérée pour pouvoir déduire analytiquement plus d'informations concernant l'évolution linéaire de la perturbation d'un état monophasique à l'équilibre.

Cas isotherme Nous montrons tout d'abord que dans ce cas la résolution du système d'équations linéarisé des amplitudes des variables perturbées est simplifiée. En effet il se ramène à la résolution du polynôme $\det_{isoth} = 0$ défini par (VI.40) qui est de degré 2 en ω.

La structure (signe des parties réelle $\Re$ et imaginaire $\Im$) des deux branches ω_+ et ω_- de la relation de dispersion peut ainsi aisément s'établir et est résumée dans la table de vérité ci-dessous (*cf.* l'établissement de la table 6.1).

$(k^c)^2$	> 0 *i.e.* *hs* dans la région spinodale					< 0		
ϑ^{isoth}_{diss}	$> \vartheta^c$		$< \vartheta^c$			$> \vartheta^c$		$< \vartheta^c$
$\left(k^c_{disp}\right)^2$	< 0		> 0			> 0		< 0
k_x	$< k^c$	$> k^c$	$< k^c$	$\in [k^c : k^c_{disp}]$	$> k^c_{disp}$	$< k^c_{disp}$	$> k^c_{disp}$	$\forall$
$\Im(\omega_\pm)$	$= 0$				$\neq 0$	$\neq 0$	$= 0$	$\neq 0$
$\Re(\omega_+)$	> 0	< 0	> 0	< 0				

Table C.3: Nature dispersive et dissipative de la perturbation dans le cas isotherme

Les paramètres k^c_{disp} et ϑ^c apparaissant dans cette table sont donnés par (*cf.* équations (6.12, 6.18, 6.19))

$$\left(k^c_{disp}\right)^2 \triangleq (k^c)^2 \left(1 - \vartheta^{isoth\,2}_{diss} \left(\frac{d\rho}{d\varphi}^{hs}\right)^{-2} \frac{\rho^{hs}}{4\,\sigma\,h}\right)^{-1} \quad ; \quad \vartheta^{isoth}_{diss} = \frac{\rho^{hs}}{\kappa} + \left(\frac{d\rho}{d\varphi}^{hs}\right)^2 \left(\frac{\eta}{\rho^2}\right)^{hs} \quad ; \quad \vartheta^c \triangleq 2\sqrt{\frac{\sigma\,h}{\rho^{hs}}} \left|\frac{d\rho}{d\varphi}^{hs}\right|$$

Notons que ϑ^{isoth}_{diss} est une mesure des processus dissipatifs isothermes et vaut zéro dans la limite conservative ce qui entraîne $k^c_{disp} = k^c$.

Influence des processus dissipatifs La remarque précédente nous amène naturellement à considérer l'influence des processus dissipatifs sur la stabilité des états d'équilibre. Nous montrons que dans le cas conservatif ($\kappa = \infty$, $k^{hs} = \eta^{hs} = 0$), la relation de dispersion est constituée de trois branches, la première étant trivialement $\omega = 0$ et les deux autres étant de signe opposé mais de même module, ce dernier ayant été déterminé analytiquement (*cf.* équation (6.22)). Par contre la fréquence de coupure $k^c_{diss=0}$ (qui comme k^c dans le cas non-dissipatif définit une région spinodale) a une expression différente de k^c (*cf.* équation (6.20))

$$\left(k^c_{diss=0}\right)^2 \triangleq (k^c)^2 - \frac{T^{hs}}{\lambda \rho^{3\,hs} c_P^{hs}\, h\, \sigma} \left(\frac{dP_{sat}}{dT}\right)^2 \left(\frac{d\rho}{d\varphi}^{hs}\right)^2$$

Il est alors facile de montrer que la condition de stabilité dans le cas non-dissipatif est moins restrictive que dans le cas conservatif, résultat cohérent avec ceux de Ngan and Truskinovsky [99] ou encore ceux de Umantsev [141]. En outre nous montrons que cette propriété est liée à la seule nullité de la conductivité thermique et nous montrons que la région spinodale ainsi définie est une région adiabatique, *i.e.* liée au signe de

$$\lambda \left(k^c_{diss=0}\right)^2 = -\rho^{hs} \frac{\partial \mu}{\partial \varphi}^{hs}_{|P,s}$$

Tout comme dans le cas isotherme nous établissons par analogie ($\varphi \leftrightarrow \rho$) le lien avec la condition de positivité de la compressibilité adiabatique χ_s.

La suite de cette étude détermine l'influence du choix de la thermodynamique de type champ de phase sur la maîtrise des possibles états d'équilibre pour le fluide.

VI.5 Cas d'une interpolation linéaire des fonctions d'état

Afin d'illustrer notre propos justifiant le choix d'un polynôme d'ordre élevé pour l'interpolation des fonctions d'état, nous considérons (section 6.4) dans un premier temps le cas d'une interpolation de la masse volumique (fonction $\rho(\varphi)$) par une fonction linéaire. Ce cas permet d'illustrer la relation de dispersion dans le cas instable, cas que l'on souhaite retrouver pour les états ne correspondant ni à $\varphi = 0$ ni à $\varphi = 1$. Les conclusions principales suivantes peuvent être retenues.

- ⋆ Outre le fait que la valeur de la variable champ de phase à l'équilibre n'est pas égale à 0 ou 1, cette valeur (et par là même les propriétés physiques des états monophasiques) est dépendante du paramètre h, paramètre permettant d'imposer une valeur arbitraire à l'épaisseur de l'interface.
- ⋆ Les états monophasiques pseudo-liquide et pseudo-vapeur ont des domaines de métastabilité qui sont eux-même h-dépendants, leur étendue étant une fonction strictement décroissante de ce paramètre.

Ces conclusions suffisent à justifier le fait de ne pas considérer une interpolation linéaire pour $\rho(\varphi)$, la propriété de stabilité des états liquide et vapeur que l'on souhaite décrire n'étant assurée qu'à saturation.

VI.6 Cas d'une interpolation non-linéaire

On considère les cas particuliers où la fonction $\rho(\varphi)$ est bâtie à l'aide des polynômes P_3 ou P_5, les résultats suivants étant valides dès que la fonction d'interpolation choisie est équivalente à ces polynômes autour de 0 ou 1 et régulière ailleurs. Dans ce cas nous avons établi (*cf.* section 3.4.1) que les états uniformes $\varphi = 0$ et $\varphi = 1$ sont des états d'équilibre pour tout couple pression-température mais que ce ne sont pas les seuls pour des conditions pression, température, données.

États vapeur et liquide Nous montrons dans un premier temps que pour les cas particuliers $\varphi = 0$ ou 1 le système d'équations gouvernant l'évolution d'une perturbation d'un état homogène à l'équilibre est modifié en profondeur, les couplages entre les variables étant moindres. Ainsi la relation de dispersion est simplifiée (par comparaison avec l'expression générale de $\det M$, équation (6.9)) et s'écrit (*cf.* la démonstration de l'équation (6.24))

$$\left((\rho\, c_P)^{hs}\,\omega + k^{hs}\,k_x^2\right)\left(\frac{\rho^{hs}\,\omega}{\lambda\,\kappa} - (k^c)^2 + k_x^2\right) = 0 \tag{VI.42}$$

Il est trivial de déterminer les racines d'un tel polynôme, elles confèrent les propriétés suivantes à l'évolution d'une perturbation.

- ⋆ Toute perturbation instable n'affecte, lors de l'étape linéaire, que la variable champ de phase, les autres perturbations (des champs "physiques" de température, vitesse, pression) étant identiquement nulles (propriété valable dès que 0 et 1 sont des extrema locaux de la fonction d'interpolation).
- ⋆ Contrairement au cas plus général, il n'y a aucun effet à considérer le cas non-conductif sur la condition de stabilité, par contre dans le cas non-dissipatif l'état ne peut qu'être marginalement stable et dans le cas où la mobilité κ est infinie elle est toujours atténuée ($\omega \leq 0$) (propriétés valables dès que 0 et 1 sont des extrema locaux de la fonction d'interpolation).
- ⋆ Pour le cas dissipatif $\kappa < \infty$,
  - dans le cas P_5
    les états liquide et vapeur sont inconditionnellement stables
  - dans le cas P_3
    les états liquide et vapeur sont conditionnellement stables et les domaines de métastabilité sont dépendant du paramètre h pour des conditions (P, T) données

Ce dernier résultat est suffisant pour écarter de notre attention le choix P_3. Le premier résultat concernant P_5 peut s'étendre à toutes les fonctions d'interpolation pour lesquelles les valeurs 0 et 1 sont des points d'inflexion.

Ainsi nous avons montré que dans le cas P_5 nous retrouvons effectivement les propriétés souhaitées pour le modèle champ de phase qui consiste à associer sans condition les états liquide et vapeur à des valeurs discrètes de la variable φ ce qui permet de contrôler leurs propriétés physiques.

Nous montrons par la suite qu'il est en outre possible d'introduire un pseudo-domaine de métastabilité contrôlé en jouant sur les coefficients de la fonction d'interpolation dès lors que cette dernière est au moins de degré 5. Cette propriété peut être intéressante si on souhaite introduire une limite de métastabilité d'un état monophasique sans pour autant introduire les conditions classiques de déséquilibre, notamment concernant notre cas sans introduire de compressibilité.

Stabilité des états autres que 0 **ou** 1 Dans cette étude (section 6.5.2) nous étudions la stabilité des solutions d'équilibre correspondant à des valeurs de φ différentes de 0 ou 1. Nous montrons que dans le cas P_5, et contrairement au cas P_3, ces solutions correspondent à des états instables. Cette propriété du modèle est primordiale puisqu'elle permet d'assurer qu'aucun autre état que les états liquide et vapeur ne sont viables. En effet nous ne saurions associer aucune physique à cet état monophasique supplémentaire.

VI.7 Conclusion

Dans ce chapitre nous avons étudié analytiquement l'évolution linéaire d'une perturbation d'un état homogène à l'équilibre. Il s'agissait de montrer qu'avec le modèle proposé seuls les états liquide et vapeur sont stables.

Nous avons établi que ce résultat est effectivement retrouvé avec la formulation proposée qui préconise entre autre l'utilisation de polynômes de degré au moins 5 comme fonction d'interpolation. Nous avons clairement montré que ce résultat est fortement dépendant du choix fait pour cette fonction d'interpolation et notamment que d'autres choix classiquement faits dans les modèles de champ de phase (polynômes de degré 3 ou fonction linéaire) induisent des propriétés néfastes au modèle. En particulier ces choix différents ne permettent pas de contrôler les états monophasiques qui sont soit de domaine de métastabilité dépendant du paramètre h, soit de propriété physique non maîtrisée.

Une étude aussi détaillée et complète des conséquences des choix faits pour les fonctions de champ de phase utilisées dans la fermeture thermodynamique sur la modélisation des états d'équilibre stables n'avait pas été, à notre connaissance, réalisée.

VII Étude analytique de la dynamique de changement de phase

Dans ce chapitre nous considérons l'étude analytique de la dynamique de changement de phase dans le cadre formel d'un problème mono-dimensionnel. Le système étudié se compose donc des équations (V.37). Cette étude est organisée comme suit. Dans un premier temps nous étudions les relations principales d'une modélisation de type interface discontinue de la dynamique de changement de phase, en particulier nous nous intéressons à la relation cinétique induite par la création d'entropie à l'interface. Ce formalisme établi, nous étudions la description diffuse de l'interface en dynamique et déterminons à l'aide de la méthode des développements asymptotiques raccordés la description discontinue équivalente. Nous montrons ainsi comment notre modèle de type champ de phase est cohérent avec la description classique de la dynamique de changement de phase et permet, de par la prise en compte du mécanisme dissipatif de relaxation de Ginzburg-Landau, de contrôler la relation cinétique. Les effets visqueux sont négligés dans cette étude.

VII.1 Modélisation de type interface-discontinue

Cette partie de notre étude s'intéresse à la modélisation discontinue de la transition de phase liquide-vapeur. Nous étudions les conditions de saut s'appliquant à la traversée d'une interface. En particulier nous montrons comment on peut définir pression et température de l'interface hors équilibre. Nous relions ces valeurs à la création d'entropie à l'interface grâce à l'utilisation du formalisme de la relation cinétique, *e.g.* Truskinovsky [134]. Nous noterons par la suite par les exposants $^{\pm}$ les valeurs prises par une variable de part et d'autre d'une interface discontinue, nous définissons alors le saut $[\![Y]\!]$ et la valeur interfaciale $\{Y\}$ de cette variable Y par

$$\begin{aligned} [\![Y]\!] &\triangleq Y^+ - Y^- \\ \{Y\} &\triangleq \frac{Y^+ + Y^-}{2} \end{aligned}$$

Relations de Rankine-Hugoniot Nous considérons une onde progressive de célérité constante $\mathcal{D}$. Par intégration des équations de Navier Stokes à la traversée d'un volume fluide, on obtient les relations de Rankine-Hugoniot suivantes

$$[\![\rho(\mathcal{D}-V)]\!] = 0 \tag{VII.43a}$$

$$[\![P]\!] + [\![\rho(\mathcal{D}-V)^2]\!] = 0 \tag{VII.43b}$$

$$\rho(\mathcal{D}-V)\left[\!\left[\frac{V^2}{2}+e\right]\!\right] - [\![q]\!] - [\![PV]\!] = 0 \tag{VII.43c}$$

$$\left[\!\left[\frac{q}{T}\right]\!\right] - \rho(\mathcal{D}-V)[\![s]\!] = \mathcal{R}_s \tag{VII.43d}$$

où V est la vitesse, q le flux de chaleur, e et s les énergie et entropie massiques et $\mathcal{R}_s$ la production d'entropie à l'interface qui satisfait le second principe de la thermodynamique, *i.e.*

$$\mathcal{R}_s \geq 0$$

Il est important à ce stade de préciser que, en ce qui concerne la résolution d'un problème de transition de phase à l'aide de ce formalisme, il est nécessaire de préciser (*i.e.* de fermer) la valeur de $\mathcal{R}_s$ de sorte que le problème soit correctement posé. L'étude de cette fermeture fait l'objet des développements suivants. Introduisons pour ce faire le taux de transfert de masse Γ défini par

$$\Gamma \triangleq \frac{\mathcal{D}-\{V\}}{\{1/\rho\}}$$

Nous montrons tout d'abord que les relations de saut classiques concernant la vitesse et la pression sont satisfaites, *i.e.* que

$$[\![V]\!] = -\Gamma\left[\!\left[\frac{1}{\rho}\right]\!\right] \tag{VII.44a}$$

$$[\![P]\!] = -\Gamma^2\left[\!\left[\frac{1}{\rho}\right]\!\right] \tag{VII.44b}$$

En utilisant des relations thermodynamiques nous montrons que $\mathcal{R}_s$ s'exprime comme suit

$$\mathcal{R}_s\{T\} = \Gamma\left(\llbracket g\rrbracket + \llbracket T\rrbracket\{s\} + \frac{\llbracket (V-\mathcal{D})^2\rrbracket}{2}\right) - \llbracket q\rrbracket + \left\llbracket \frac{q}{T}\right\rrbracket\{T\}$$

Dans la suite, et sauf précision contraire, on se limitera pour le modèle discontinu à l'étude des transitions de phase isothermes $\llbracket T\rrbracket = 0$ ou adiabatiques $q = 0$, pour lesquelles il est alors naturel d'introduire la force motrice $\mathscr{G}$ suivante

$$\mathscr{G} \;\hat{=}\; \llbracket g\rrbracket + \llbracket T\rrbracket\{s\} + \frac{\llbracket (V-\mathcal{D})^2\rrbracket}{2} \tag{VII.45}$$

telle que $\mathcal{R}_s$ se rapporte au produit de cette force par le flux caractéristique de la transition de phase Γ

$$\mathcal{R}_s\{T\} = \Gamma\mathscr{G} \tag{VII.46}$$

La relation cinétique que nous cherchons à caractériser s'écrit naturellement comme $\mathscr{G}(\Gamma)$. On distingue différents modèles classiques pour cette relation, à savoir un modèle d'équilibre pour lequel $\mathcal{R}_s = 0$ et un modèle pour faibles déséquilibres, la théorie de croissance normale, pour lequel $\mathcal{R}_s \propto \Gamma^2$. Or nous montrons que pour un fluide faiblement compressible (faible variation de ρ au sein des phases par rapport à l'écart de masse volumique entre ces dernières) et pour lequel les variations de chaleur sensibles sont négligeables devant la chaleur latente, il vient

$$\mathscr{G} \simeq \Big(\{P\} - P_{eq}\Big)\llbracket 1/\rho\rrbracket - \Big(\{T\} - T_{eq}\Big)\llbracket s\rrbracket \tag{VII.47}$$

où P_{eq} et T_{eq} sont un couple de pression température à saturation de référence. Il est alors trivial de montrer que la théorie de croissance normale implique la relation de fermeture suivante

$$\Big(\{P\} - P_{eq}\Big)\llbracket 1/\rho\rrbracket - \Big(\{T\} - T_{eq}\Big)\llbracket s\rrbracket \propto \Gamma$$

qui se réduit à la relation de Clapeyron à l'équilibre ($\Gamma = 0$).

Nous avons ainsi démontré les relations fondamentales du modèle discontinu de la transition de phase liquide-vapeur. Notre but est désormais de déduire des relations équivalentes à l'aide de notre modèle de champ de phase afin de caractériser sa relation cinétique.

VII.2 Développements asymptotiques raccordés

En vue de la résolution du système d'équations caractérisant une transition de phase mono-dimensionnelle nous utilisons la technique des développements asymptotiques raccordés qui considère une séparation d'échelle entre un domaine intérieur (correspondant à la zone interfaciale) et un domaine extérieur (correspondant aux domaines phasiques de part et d'autre de l'interface). Cette séparation d'échelle est caractérisée par le petit paramètre adimensionnel ε défini page 295. Nous sommes alors en mesure de déduire les ordres dominants des solutions en terme de développement limité en puissance de ε, *i.e.* les premiers termes de

$$Y = Y_0 + \varepsilon Y_1 + O(\varepsilon^2)$$

Néanmoins, afin de résoudre le problème complet, il est à la fois utile[8] et intéressant de se limiter dans un premier temps à deux cas particuliers, à savoir le cas pour lequel la masse volumique est uniforme et le cas isotherme. En effet ces sous-cas permettent de comprendre le lien particulier existant entre les variables physiques (pression, température, vitesse) et artificielle (champ de phase) et les couplages entre les équations principales. Ces résolutions guident alors la résolution du problème complet.

[8] Utile d'un point de vue mathématique, étant donné que la structure des équations de chaque cas est simplifiée et permet une résolution plus aisée des sous-systèmes d'équations.

VII.3 Transition de phase et masse volumique uniforme

Il s'agit ici de résoudre le couplage entre l'équation d'Allen-Cahn avec l'équation d'entropie écrite en tant qu'évolution du champ de température. Ce système s'écrit pour le problème intérieur (*cf.* système (7.11))

$$\alpha\,\varepsilon\,\mathcal{D}\,\varphi' = \varepsilon\,\partial_\varphi \nu(\varphi)\,T - \left(\partial_\varphi W(\varphi) - \varphi''\right) \tag{VII.48a}$$

$$\varepsilon\,\mathcal{D}\,T' = \frac{(k\,T')'}{Pe} + \mathcal{D}\,\varepsilon\,(1+T)\,\partial_\varphi \nu(\varphi)\,\varphi' - \mathcal{D}^2\,\frac{\varepsilon}{\alpha}\,(\varphi')^2 \tag{VII.48b}$$

où $\partial_\varphi \cdot$ est une notation abrégée de $\partial \cdot / \partial\varphi$. Il s'agit en fait d'une version thermodynamiquement cohérente du modèle utilisé pour l'étude de la transition solide/liquide.

Champ de phase et température Le premier résultat issu de la résolution des équations correspond aux profils des variables principales à l'ordre dominant en ε (obtenu en résolvant le système d'équations (VII.48) pour lequels seuls les termes dominants en ε sont retenus).
Nous montrons alors que le champ de phase φ_0 satisfait l'équation satisfaite à l'équilibre plan, *i.e.*

$$\partial_\varphi W(\varphi_0) - \varphi_0'' = 0 \tag{VII.49}$$

et le profil est donc en tangente hyperbolique.
La température au sein de la zone interfaciale est uniforme à l'ordre dominant, son niveau peut alors être déterminé en intégrant sur $\mathbb{R}$ le produit de l'équation d'Allen-Cahn à l'ordre supérieur en ε par une solution de sa partie homogène (en l'occurrence $\varphi_0'(x)$), il vient ainsi (*cf.* équation (7.13))

$$[\![T]\!]_0 = 0 \qquad T_0^i \triangleq T_0(x_i) = \{T\}_0 = -\frac{[\![\varphi]\!]\,\mathcal{D}}{\alpha}$$

Ainsi la transition de phase décrite par notre modèle a pour limite discontinue (quand $\varepsilon \to 0$) une transition de phase isotherme pour laquelle l'interface a un profil d'équilibre. Nous avons pu déterminer alors les ordres supérieurs des profils ; la contribution au profil de champ de phase à cet ordre est non nulle uniquement en présence de transfert de masse et d'une relaxation de type Ginzburg-Landau (*cf.* équation (7.14)). La température est discontinue à l'ordre supérieur dès que les flux de chaleur de part et d'autre de l'interface sont non nuls et le saut de température à la traversée de l'interface est associé à la non-uniformité de la conductivité thermique au sein de la zone interfaciale (*cf.* équation (7.18)).

Relation cinétique Nous avons alors analysé ces résultats sous le regard du formalisme de la relation cinétique. A l'ordre dominant, la production d'entropie interfaciale s'écrit (*cf.* équation (7.23))

$$\mathcal{R}_{s\,0} = \frac{Pe\,\mathcal{D}^2}{\alpha}$$

Elle est donc associée au mécanisme dissipatif de relaxation de Ginzburg-Landau. A ce titre il s'agit donc d'une dissipation purement interfaciale et $\mathcal{R}_{s0}$, en tant que quantité en excès est, conformément au second principe, bien strictement positive. En outre elle est quadratique en le taux de transfert de masse ce qui rejoint l'hypothèse faite dans la théorie de la croissance normale. A l'ordre supérieur, la création d'entropie est en partie due à la dissipation de type conductive. La contribution interfaciale est, selon le choix fait pour la dépendance de la conductivité thermique en φ, soit supérieure, soit inférieure à la contribution des phases. La quantité en excès $\mathcal{R}_{s1}$ associée à la conduction n'est pas signée et s'écrit

$$\mathcal{R}_{s\,1} = \Phi_{th}^2 \left(\frac{1}{k}\right)_0^{\bar{e}x} + \Phi_{th}\,Pe\,\mathcal{D}\left(\frac{1}{2}\left(\frac{1}{k}\right)_0^{\bar{e}x} + \left(\frac{\nu}{k}\right)_0^{\bar{e}x}\right) - \frac{Pe^2\,\mathcal{D}^2}{2}\left(\frac{\nu}{k}\right)_0^{\bar{e}x}$$

Conclusion Nous avons ainsi pu analyser le couplage entre thermique et champ de phase dans le cadre théorique d'une transition de phase mono-dimensionnelle et sous l'angle du formalisme de la relation cinétique. Cette étude permet de mettre en évidence le rôle du mécanisme dissipatif de type Ginzburg-Landau sur la modélisation du changement de phase.

VII.4 Transition de phase isotherme

Nous étudions ici la réduction isotherme de notre modèle. Dans ce cas le système d'équations pour la région intérieure s'écrit

$$\begin{aligned}
\alpha\,\varepsilon\,(\mathcal{D}-V)\,\varphi' &= \varepsilon\,\partial_\varphi\nu\tilde{P} + v\,\left(\partial_\varphi W - \varphi''\right) + \partial_\varphi\nu\left(W - \frac{(\varphi')^2}{2}\right)\\
(\rho V)_{,x} &= -\rho^2\,\partial_\varphi\nu\,(\mathcal{D}-V)\,\varphi_{,x}\\
(V-\mathcal{D})\,\rho V_{,x} &= -\tilde{P}_{,x}
\end{aligned}$$

Champ de phase, pression et vitesse De la même manière que dans le cas précédent où la masse volumique était supposée uniforme, il est possible de résoudre analytiquement les premiers ordres en ε des solutions intérieures. Nous retiendrons quelques résultats en particulier.

Le profil de la variable champ de phase est à l'ordre dominant le profil d'équilibre plan (solution de l'équation différentielle (VII.49)) tandis que la pression et la vitesse satisfont les relations classiques de saut à la traversée de l'interface, c'est à dire

$$\begin{aligned}
[\![V_0]\!] &= -\Gamma\,[\![1/\rho]\!]\\
[\![P_0^{ext}]\!] &= -\Gamma^2\,[\![1/\rho]\!]
\end{aligned}$$

Relation cinétique Nous montrons qu'il est possible dans ce cadre isotherme de définir une relation cinétique exprimant la force motrice $\mathscr{G}$ en fonction du taux de transfert de masse et ainsi de définir une création d'entropie interfaciale (*cf.* équation (VII.46)). A l'ordre dominant cette création d'entropie est quadratique en Γ et inversement proportionnelle au coefficient cinétique de Ginzburg-Landau α , *i.e.*

$$\mathcal{R}_{s0}\,T_{eq} = \frac{\Gamma^2}{\alpha}\,\mathcal{A}_1$$

où $\mathcal{A}_1$ est une constante définie par (7.30) et dépendant des fonctions thermodynamiques de la variable champ de phase. Nous avons relié cette relation à l'écart du niveau de pression de l'interface par rapport à la pression d'équilibre. A l'ordre dominant, la relation cinétique est donc encore une fois associée au mécanisme dissipatif de Ginzburg-Landau et cohérente avec la théorie de "croissance normale".

Les résultats précédents nous permettent de mieux analyser les résultats obtenus dans le cas complet ainsi que de simplifier sa résolution.

VII.5 Transition de phase liquide-vapeur anisotherme

Le système d'équations à résoudre pour le problème extérieur s'écrit

$$\alpha\,\varepsilon^2\,(\mathcal{D}-V)\,\varphi_{,x} = \varepsilon\,\frac{d\nu}{d\varphi}\left(\tilde{P} - T\right) + v\,\left(\frac{dW}{d\varphi} - \varepsilon^2\varphi_{,xx}\right) + \frac{d\nu}{d\varphi}\left(W - \frac{\varepsilon^2}{2}\varphi_{,x}^2\right) \tag{VII.50a}$$

$$(\rho V)_{,x} = -\rho^2\,\frac{\partial\nu}{\partial\varphi}\,(\mathcal{D}-V)\,\varphi_{,x} \tag{VII.50b}$$

$$(V-\mathcal{D})\,\rho V_{,x} = -\tilde{P}_{,x} \tag{VII.50c}$$

$$(V-\mathcal{D})\,\rho\,T_{,x} = \frac{(k\,T_{,x})_{,x}}{Pe} - (V-\mathcal{D})\,\rho\,(1+T)\,\frac{d\nu}{d\varphi}\,\varphi_{,x} + (\mathcal{D}-V)^2\,\frac{\rho\varepsilon}{\alpha}\,(\varphi_{,x})^2 \tag{VII.50d}$$

Solution à l'ordre dominant En s'inspirant des développements précédents, nous montrons que les solutions à l'ordre dominant s'écrivent comme suit

$$\varphi_0(\bar{x}) = 1/2 + (\llbracket\varphi\rrbracket/2)\ \tanh(3\ \bar{x}) \tag{VII.51a}$$
$$\tilde{P}_0(\bar{x}) = \{P_0\} + \{v_0\}\,\Gamma^2 - v(\varphi_0(\bar{x}))\,\Gamma^2 \tag{VII.51b}$$
$$V_0(\bar{x}) = \mathcal{D} - \Gamma\, v(\varphi_0(\bar{x})) \tag{VII.51c}$$
$$\{P_0\} = T_0^i + \Gamma\,\frac{\mathcal{A}_1}{\alpha} \tag{VII.51d}$$
$$\llbracket T_0\rrbracket = 0 \tag{VII.51e}$$
$$\{T_0\} = T_0^i \tag{VII.51f}$$
$$\llbracket q_0\rrbracket = Pe\,\Gamma\left(1 + T_0^i\right)\,\llbracket\varphi\rrbracket + \Gamma^2\,|\mathcal{A}_1| \tag{VII.51g}$$

En particulier le profil de champ de phase est toujours le profil à l'équilibre plan, le saut de température est nul, et les sauts de vitesse et pression sont cohérents avec les relations discontinues. Les valeurs de la température et de la pression à l'interface s'écarte de la valeur à saturation en présence de changement de phase. Ce phénomène est dû à la dissipation de Ginzburg-Landau. Le saut de flux de chaleur à l'interface comprend deux contributions en Γ et Γ^2, il peut ainsi être nul même en présence de changement de phase (changement de phase isotherme obtenu dans notre étude isotherme). Nous avons aussi pu déterminer certains résultats à l'ordre supérieur qui sont utilisés par la suite dans l'étude de la relation cinétique du modèle.

Relation cinétique Utilisant les développements précédents, il est possible de déduire l'expression des premiers ordres du développement limité en ε de la création d'entropie interfaciale qui s'écrit comme suit

$$\mathcal{R}_s = \Gamma^2\,\frac{Pe}{\alpha}\mathcal{A}_1\frac{1}{1+\{T_0\}} + \varepsilon\,\left(Pe\,\Gamma\left(1+T_0^i\right)\ \llbracket\varphi\rrbracket + \Gamma^2\,|\mathcal{A}_1|\right)\left(\Phi_{th}\left(\frac{1}{k}\right)_0^{\bar{ex}} + Pe\,\Gamma\left(1+T_0^i\right)\left(\frac{\nu}{k}\right)_0^{\bar{ex}}\right) + O\varepsilon^2$$

Ainsi à l'ordre dominant, le modèle est équivalent à la théorie de "croissance normale" qui suppose que la création d'entropie à l'interface est quadratique en le transfert de masse. Cette contribution est uniquement associée au mécanisme dissipatif de Ginzburg-Landau. A l'ordre supérieur la contribution est fonction de grandeurs en excès qui concernent la modélisation du transfert de chaleur conductif.

Une limite discontinue pour les transitions fortement hors équilibre Dans la section 7.6, nous étudions une autre limite discontinue de notre modèle obtenue en considérant une variation différente de la mobilité dans la limite $\varepsilon \to 0$: $\bar{\alpha} = \alpha/\varepsilon$ est considéré comme fini dans cette limite. Nous n'étudions cette limite que dans le cas très simple où le modèle se réduit à sa part champ de phase (ni thermique ni mécanique). Nous montrons alors qu'à l'ordre dominant en ε (limite discontinue) la relation cinétique n'est pas équivalente à la théorie de "croissance normale". Par contre nous montrons qu'elle s'y réduit dans la limite des faibles taux de transfert de masse ($\Gamma \to 0$) ce qui est physiquement cohérent.

Cette étude montre ainsi que les modèles champ de phase dotés du mécanisme dissipatif de relaxation de Ginzburg-Landau ne se réduisent pas à une régularisation de la théorie de "croissance normale" qui n'est valable que pour les transitions de phase proche de l'équilibre.

Conclusion

Cette étude nous a permis d'analyser notre modèle dans une situation hors équilibre. Nous avons en effet pu, grâce à l'utilisation de la technique des développements asymptotiques raccordés, déduire des solutions approchées des profils des variables au sein de la zone interfaciale pour une dynamique de changement de phase de type onde progressive mono-dimensionnelle. En particulier nous avons montré que les résultats obtenus sont cohérents avec les résultats discontinus, et en ce qui concerne la variable champ de phase, proche de ceux à l'équilibre. Nous avons déterminé la relation cinétique de notre modèle, qui comme nous l'avons montré en début de chapitre est une relation essentielle pour la caractérisation de la dynamique de changement de phase. Cette dernière est cohérente avec la théorie de "croissance normale" dans la limite des faibles épaisseurs d'interface. Nous avons aussi montré que ce résultat dépend d'une hypothèse faite sur la variation de la mobilité dans la limite des faibles épaisseurs. La création d'entropie a été clairement analysée comme héritant de deux contributions. La première

est due uniquement à la dissipation de type Ginzburg-Landau et est à l'origine du terme dominant, la seconde se rapporte au phénomène de conduction thermique et induit un saut de température au second ordre en ε. Cette dernière contribution est dépendante du choix fait pour l'interpolation de la conductivité thermique par la fonction champ de phase $k(\varphi)$.

Il serait intéressant de compléter cette analyse par la prise en compte du mécanisme dissipatif de viscosité, ce qui complique l'analyse. En outre nous soulignons la nécessité de faire le lien entre les modèles de différente nature concernant la relation cinétique (comme les modèles de résistance d'interface, comme ceux de type couche de Knudsen [28]). De manière générale la connaissance de la relation cinétique pour le mécanisme d'ébullition n'est pas satisfaisante comme souligné par Anderson et al. [2]. Finalement nous soulignons que notre analyse de la modélisation champ de phase par le biais du formalisme de relation cinétique apporte un éclairage nouveau et enrichissant pour cette famille de modèles en permettant de relier la modélisation des phénomènes dissipatifs et la relation hors équilibre entre température et pression d'interface.

VIII Étude numérique du modèle

Dans ce chapitre nous étudions la résolution numérique du système d'équations du mouvement de notre modèle de champ de phase. Le but est de développer un algorithme de résolution et d'étudier la cohérence entre les simulations et les résultats analytiques obtenus dans les chapitres précédents. En particulier nous étudions comment notre modèle permet

- ⋆ de contrôler la stabilité des phases liquide et vapeur (*cf.* notre étude du chapitre VI) ;
- ⋆ de reproduire une relation cinétique ainsi que de retrouver les conditions de saut classiques à la traversée d'une interface (*cf.* notre étude du chapitre VII) ;
- ⋆ de traiter un écoulement capillaire en présence de courbure (*cf.* notre étude du chapitre IV).

Nous considérons la résolution de trois systèmes d'équations différents, suivant ainsi l'approche du chapitre précédent. Nous commençons par considérer la partie purement thermique de notre modèle de transition de phase en supposant la masse volumique comme uniforme (*cf.* section VIII.1), *i.e.* en ne prenant pas en compte de mécanique. Puis nous étudions le couplage entre transition de phase et mécanique des fluides à l'aide du modèle isotherme (*cf.* section VIII.2). Enfin nous étudions le modèle de champ de phase pour la transition de phase liquide-vapeur (*cf.* section VIII.3). Précisons que la présentation des notations et principaux schémas numériques utilisés par la suite est proposée en annexe C.

VIII.1 Transition de phase sans écoulement

Algorithme, couplage et approximations Afin de trouver un compromis entre efficacité de la résolution numérique et précision du résultat, nous avons, à l'aide de tests numériques, déterminé un schéma de résolution partiellement implicite du système d'équations s'écrivant

$$\frac{\varphi^{n+1}-\varphi^n}{Dt} = -\kappa\left[-\frac{dv}{d\varphi}^n \frac{\varepsilon}{St\,\gamma\,\theta}T^{n+1} + \frac{dW}{d\varphi}^n + \left(\varphi^{n+1}-\varphi^n\right)\left(-\frac{d^2v}{d\varphi^2}^n \frac{\varepsilon}{St\,\gamma\,\theta}T^n + \frac{d^2W}{d\varphi^2}^n\right) - \varepsilon^2\Delta\varphi^{n+1}\right] \quad \text{(VIII.52a)}$$

$$\frac{T^{n+1}-T^n}{Dt} = \frac{\nabla\cdot\left(k\nabla T^{n+1}\right)}{Pe} - \frac{\rho\,(1+T^n/\theta)}{St}\left[\frac{dv}{d\varphi}^n \frac{\varphi^{n+1}-\varphi^n}{Dt}\right] + \frac{\gamma\,\kappa}{\varepsilon}(\tilde{\mu}^n)^2 \quad \text{(VIII.52b)}$$

Remarquons que cette écriture linéaire en les inconnues (T^{n+1},φ^{n+1}) permet d'envisager une résolution efficace.

Changement de phase stationnaire L'étude de la dynamique de changement de phase stationnaire pour un système mono-dimensionnel est présentée en section 8.1.1. Pour ce faire nous imposons un flux de chaleur constant aux frontières du domaine simulé. Cette étude montre que

- ⋆ la vitesse de propagation de l'interface est conforme à l'estimation théorique, *i.e.* à la formule

$$\Gamma_{theor} = [\![\varphi]\!]\,\frac{St\,[\![q]\!]}{Pe}$$

- ⋆ les profils de la variable de champ de phase et de température varient à la traversée de l'interface conformément aux ordres dominants des développements asymptotiques déterminés au chapitre VII
- ⋆ la température de l'interface est cohérente avec l'estimation théorique de type "théorie de la croissance normale" valable pour les faibles transferts de masse considérés
- ⋆ l'influence de l'interpolation des conductivités thermiques par φ sur la dissipation au sein de l'interface et par là même sur le saut de température est qualitativement cohérente avec la prédiction théorique

Ainsi nous validons notre algorithme de résolution dans ce cas stationnaire.

Changement de phase instationnaire Nous étudions en section 8.1.2 le problème mono-dimensionnel de la mise en contact "brutale" d'une phase liquide surchauffée avec un solide à saturation, cas test instationnaire pour lequel une solution analytique est connue dans l'hypothèse d'une transition de phase proche de l'équilibre (*cf.* Lemonnier et al. [85]).

Au travers de cette étude nous étudions plus particulièrement la capacité de l'algorithme à prendre en compte un phénomène instationnaire. Les résultats numériques sont proches du résultat théorique comme l'atteste la figure 8.10.

Séparation de phase Nous présentons en section 8.1.5 les résultats d'une simulation d'un système diphasique pour lequel la variable champ de phase est initialement aléatoirement réparti spatialement. L'évolution du calcul montre la formation de domaines phasiques où la valeur de la variable champ de phase est uniformément égale aux valeurs théoriques. Ces domaines sont séparés par une zone de transition d'épaisseur constante et de l'ordre de grandeur de l'épaisseur théorique. Au cours de la simulation on peut observer un grand nombre de transitions de topologie ce qui atteste de la capacité du modèle, tout comme de la méthode numérique, de prendre en compte ces phénomènes.

Courbure et transition de phase Nous présentons en section 8.1.6 les simulations de changement de phase pour un domaine bidimensionnel et sous deux conditions limites différentes. Dans chaque cas un "noyau" solide à la température d'équilibre préexiste au centre d'un domaine carré et baigne dans un liquide à une température initialement uniforme et inférieure à la température d'équilibre. Dans le premier cas un flux de chaleur nul est imposé à la frontière extérieure. Ainsi le noyau solide grandit dans un premier temps avant que la température du liquide ne rejoigne la température d'équilibre. Tant que le noyau solide n'a pas une forme circulaire, la température de l'interface n'est pas uniforme et la transition de phase se poursuit. Dans le second cas une température uniforme inférieure à la température d'équilibre est imposée sur la frontière du domaine. La dynamique de croissance du grain solide est alors bien différente. En particulier la vitesse de l'interface s'accélère au fur et à mesure qu'elle se rapproche de la frontière. En outre on observe que les protubérances de l'interface ont tendance à s'exacerber ce qui correspond au phénomène de croissance dendritique, aussi connu sous le nom d'instabilité de Mullins-Sekerka.

L'ensemble de ces comportements sont satisfaisants qualitativement.

Conclusion Nous avons montré à l'aide des différentes études numériques que l'algorithme développé pour la résolution de notre modèle de champ de phase à masse volumique uniforme permettait de reproduire la physique du changement de phase et la dynamique de l'interface incluant des transitions de topologie ; Nous retiendrons plus particulièrement qu'il est nécessaire pour cela de résoudre de manière fortement couplée (implicite) le couplage entre équation d'entropie et d'Allen-Cahn mais qu'il est possible (et avantageux) de linéariser certains termes de ce couplage pour les évaluer implicitement.

VIII.2 Transition de phase isotherme

La méthode de projection La résolution du modèle isotherme repose sur l'utilisation d'une méthode de projection pour le traitement des équations de bilan de masse et de quantité de mouvement. Cette méthode de projection peut être utilisée grâce à l'hypothèse de quasi-compressibilité. Dans un premier temps nous présentons comment nous avons pu adapter la méthode de projection, classiquement utilisée pour la résolution d'écoulements pour lesquels la masse volumique est uniforme. Supposons tout d'abord dans un souci de simplicité que l'avancée en temps du champ de phase est connue. Ainsi en utilisant une écriture discrète approchée de l'équation de bilan de masse, on peut écrire la divergence du champ de quantité de mouvement

$$\nabla \cdot \rho \vec{V}^{n+1} = -\frac{d\rho}{d\varphi}^{n} \frac{\varphi^{n+1} - \varphi^{n}}{Dt}$$

En prenant la divergence de l'équation de bilan de quantité de mouvement et en utilisant l'identité ci-dessus, il est aisé de montrer que

$$\frac{d\rho}{d\varphi}^{n} \frac{\varphi^{n+1} - \varphi^{n}}{Dt^2} - \frac{\nabla \cdot (\rho V)^{n}}{Dt} + \nabla \cdot (\rho V \cdot V)^{n} = \Delta \mathcal{G}^{n+1} - \nabla \cdot \left(\frac{\left(\frac{dW}{d\varphi}^{n} - \varepsilon^2 \Delta \varphi^{n} \right)}{\varepsilon We} \nabla \varphi^{n} \right)$$

Nous disposons alors d'une équation de type Poisson en la variable $\mathcal{G}^{n+1}$ et indépendante du champ de vitesse V^{n+1}. Une fois cette équation résolue, il est alors possible de calculer V^{n+1} en utilisant l'équation de bilan de quantité de mouvement sous son écriture originelle. En outre l'équation d'Allen-Cahn peut s'écrire

$$\begin{aligned}\frac{\varphi^{n+1}-\varphi^n}{Dt}+\vec{V}^n\cdot\nabla\varphi^n &= -\kappa\left[\frac{d\nu}{d\varphi}^n(At\,\varepsilon\,We)\,\mathcal{G}^{n+1}+\frac{d^2\nu}{d\varphi^2}^n\left(\varphi^{n+1}-\varphi^n\right)(At\,\varepsilon\,We)\,\mathcal{G}^n\right.\\ &\quad\left.+v^n\left(\frac{dW}{d\varphi}^n+\frac{d^2W}{d\varphi^2}^n\left(\varphi^{n+1}-\varphi^n\right)-\varepsilon^2\Delta\varphi^{n+1}\right)\right]\end{aligned}$$

et elle est ainsi linéaire en $(\varphi^{n+1},\mathcal{G}^{n+1})$. Ceci permet d'envisager un algorithme d'une seule étape implicite basé sur la résolution du système d'équations de Poisson et d'Allen-Cahn, toutes deux linéaires en $(\varphi^{n+1},\mathcal{G}^{n+1})$. Cet algorithme ou sa version en deux temps, résolution d'Allen-Cahn avec pression explicite, puis de Poisson, sont utilisés par la suite afin de résoudre des problèmes de changement de phase isothermes.

Calculs mono-dimensionnels Nous présentons en section 8.2.2 un cas test de changement de phase isotherme. Le système considéré est ouvert, mono-dimensionnel et symétrique ; il est initialement rempli de vapeur en son centre et de liquide en périphérie. Sur les frontières on impose un débit constant de liquide. L'augmentation de la masse du système à volume constant est donc à l'origine d'un changement de phase qui se poursuit jusqu'à disparition complète de la phase vapeur au profit de la phase liquide. Les résultats numériques montrent la cohérence des profils obtenus avec les résultats analytiques démontrés au chapitre VII. En particulier nous retrouvons bien les sauts de pression et de vitesse classiques et le profil de la variable champ de phase est proche de celui à l'équilibre, les deux phase existant étant effectivement les états $\varphi = 0$ et $\varphi = 1$. En outre nous montrons que la variation du niveau de pression de l'interface avec la dissipation de Ginzbirg-Landau est conforme à la prédiction théorique.

Simulation de la dynamique isotherme d'une bulle Nous étudions ici la dynamique d'une bulle sous l'action de la pesanteur et des forces capillaires. Pour ce faire nous considérons l'écoulement d'une bulle initialement hémisphérique en paroi basse d'une boîte close bi-dimensionnelle et soumise à un champ de gravité uniforme. La vitesse est imposée nulle sur toutes les frontières du domaine. Notons que le problème reste mathématiquement bien posé dès lors que nous écrivons le couplage entre les équations d'Allen-Cahn et l'équation de Poisson. Ce n'est plus vrai si l'on écrit la seule équation de Poisson dans le cas d'une modélisation discontinue de l'interface séparant deux phases incompressibles (indétermination du niveau de pression). La condition limite en champ de phase est un flux en paroi nul, ou encore un angle de contact de $\pi/2$. notons que la discrétisation spatiale du domaine simulé est faible (60×60 éléments). Quelques instantanés de la simulation sont reproduits sur la figure C.10. Ils représentent en couleur la variable champ de phase qui est claire pour $\varphi = 1$ (vapeur) et sombre pour $\varphi = 0$ (liquide). La ligne noire continue correspond à l'isovaleur $\varphi = 0.5$ et peut représenter la position de l'interface. Les flèches noires représentent le champ de quantité de mouvement. Le changement de norme de celui-ci à la traversée de l'interface illustre le fait que la dynamique de changement de phase est négligeable devant les déplacements de l'interface associés aux autres effets mécaniques, à savoir pesanteur et capillarité, *i.e.* $[\![\rho]\!]\{V\} \gg \{\rho\}[\![V]\!]$ (notons que le changement de phase global est nul). Dans une première phase le centre de gravité s'élève sous l'action de la pesanteur ce qui a pour effet de modifier la courbure locale de la bulle et de diminuer sa surface de contact avec la paroi. Celle-ci va alors s'annuler la bulle ayant alors un pied comme pincé. Sous l'action des forces capillaires ce pied va être élastiquement ramené vers le centre de gravité de la bulle de manière à ce que celle-ci adopte une forme plus circulaire. Puis la bulle atteint le sommet du domaine simulé. Elle s'étale alors en un film continu couvrant le sommet de la boîte. L'interface de ce film d'abord mouvementée se stabilise progressivement. L'ensemble de cette dynamique est qualitativement cohérente. Elle atteste de la validité de l'algorihtme proposé à prendre en compte une dynamique complexe d'un écoulement liquide-vapeur à l'échelle de la bulle.

VIII.3 Transition de phase anisotherme

Simulations mono-dimensionnelles Dans un premier temps nous résolvons un problème de changement de phase mono-dimensionnel dans un système fermé. L'algorithme utilisé s'inspire des développements effectués dans les études précédentes. Il est basé sur l'utilisation d'une méthode de projection ainsi que d'une écriture

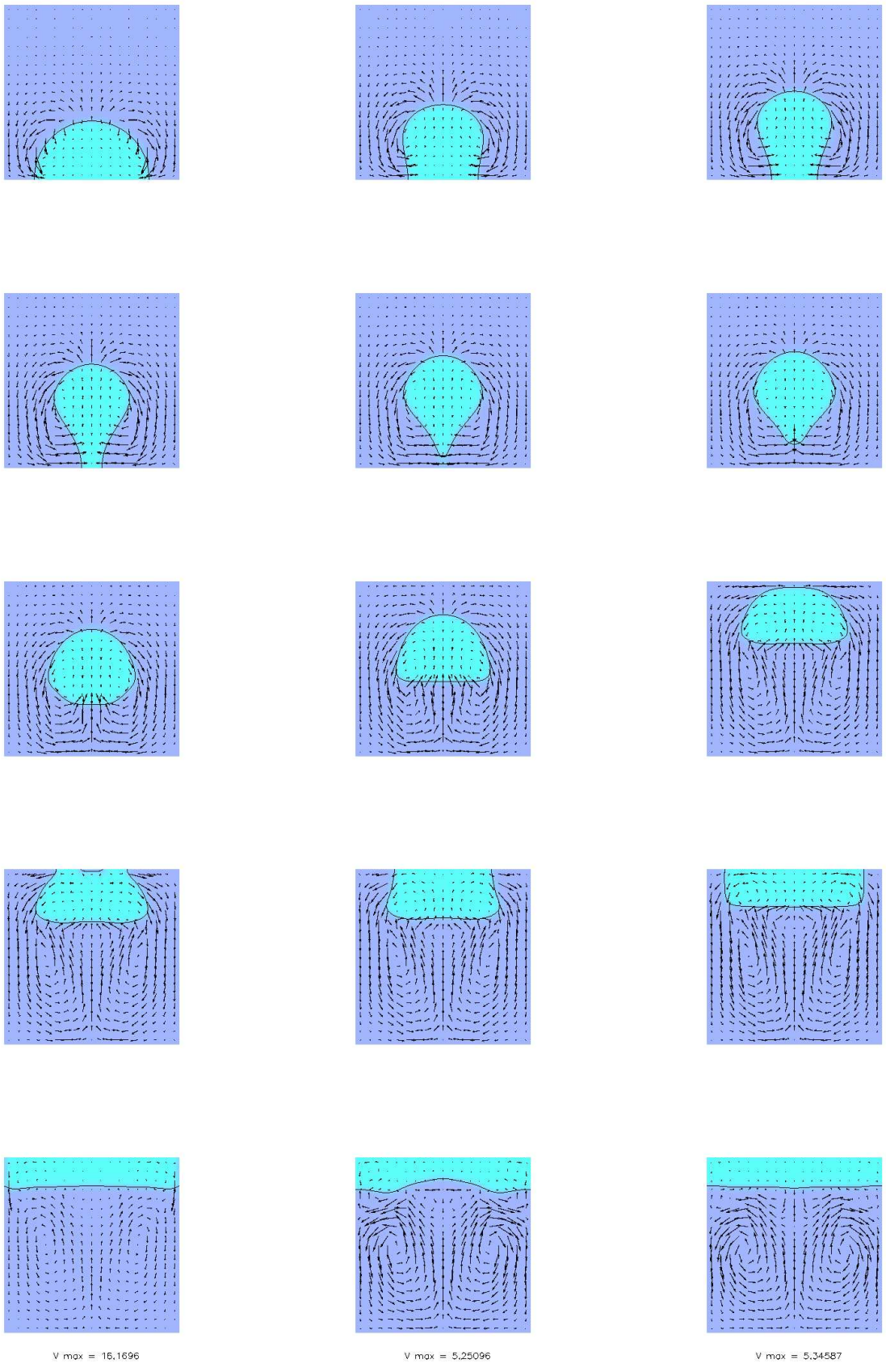

Figure C.10: Ascension d'une bulle dans une boîte fermée en isotherme

linéarisée de l'avancée en temps des termes de couplages non-linéaires implicites entre les équations de température et d'Allen-Cahn. Le système fermé et chauffé voit ses niveaux de température et pression augmenter tout comme dans la situation physique d'un auto-cuiseur. Nous avons alors montré que pression et température suivent la courbe de saturation. Ce cas test permet d'illustrer comment notre modèle, bien que considérant les phases liquide et vapeur comme incompressibles, donne une signification physique claire au niveau de pression.

Dans un second temps nous étudions un phénomène de condensation dans un système semi-ouvert (vapeur à saturation) en contact avec une paroi refroidie par un flux de chaleur constant. Les figures C.11 montrent les profils des variables principales à différents instants. Le champ de température illustre le saut de flux de chaleur qui existe à la traversée de l'interface dû au changement de phase tandis que la température est continue, résultats cohérents avec notre étude analytique à l'ordre dominant du chapitre VII. Le profil de champ de phase est proche d'un profil à l'équilibre et la vitesse de déplacement de l'isovaleur $\varphi = 0.5$ est tout à fait cohérente avec la valeur du flux de chaleur imposé. Les profils de vitesse et pression sont cohérents avec les prédictions théoriques.

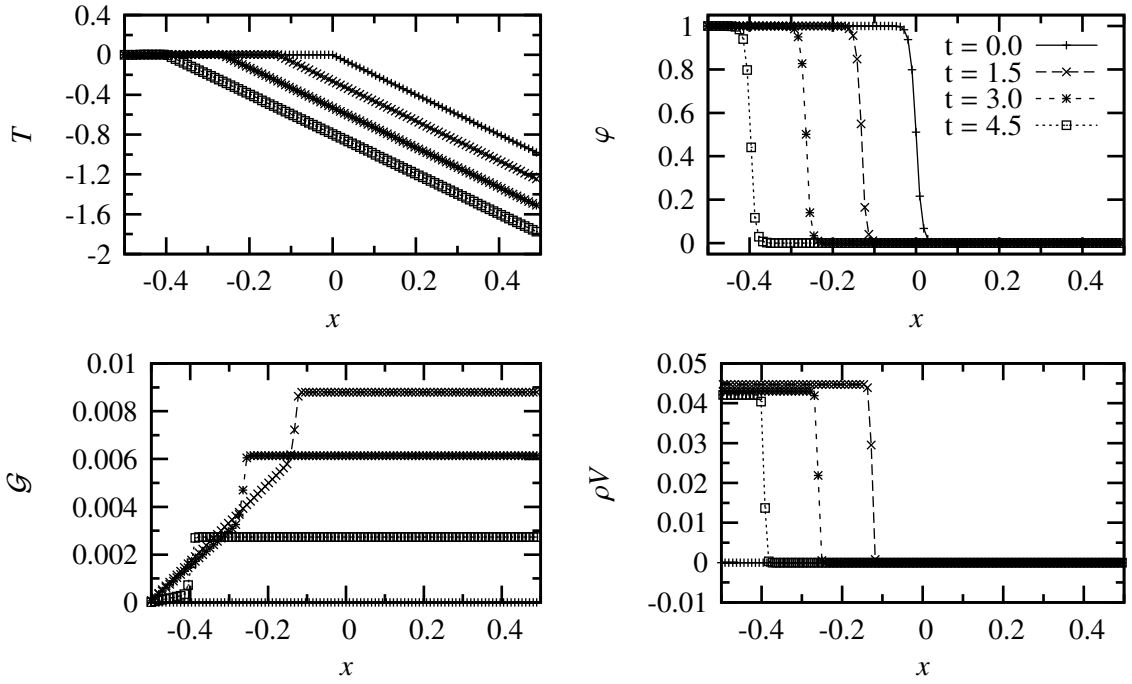

Figure C.11: Changement de phase en milieu ouvert

L'algorithme développé dans cette étude permet donc de prendre en compte la dynamique de changement de phase liquide-vapeur pour un système mono-dimensionnel.

Simulations bidimensionnelles Nous avons donc naturellement tenté d'appliquer cet algorithme à la résolution d'un problème bi-dimensionnel, mais nous nous sommes heurtés à une difficulté numérique majeure. Dans la suite nous présentons les résultats obtenus ainsi que l'analyse que nous en avons fait. Cette dernière nous a permis d'identifier l'origine de la difficulté et d'envisager des perspectives de travail afin de surmonter ce problème.

Afin d'illustrer la difficulté numérique nous considérons un problème similaire au problème mono-dimensionnel de condensation résolu précédemment. Nous introduisons alors une discrétisation bi-dimensionnelle du domaine, le problème restant physiquement purement mono-dimensionnel. Au cours de la simulation et dès les toutes premières itérations un courant d'origine parasite composé de cellules centrées sur la zone interfaciale s'établit. L'intensité de ces courants croît exponentiellement au fur et à mesure des itérations jusqu'à devenir dominant et finalement déstabiliser la résolution. L'origine de ces courants est purement numérique. Notre analyse présentée en section 8.3.3 a permis d'identifier le terme capillaire comme en étant responsable. Mais ce terme existait déjà pour les simulations isothermes présentées en section VIII.2. L'origine de l'instabilité provient en fait plus précisément du couplage entre ce terme capillaire et la détermination de la dynamique de changement de phase anisotherme. Nous avons pu forcer artificiellement ce couplage à être satisfait avec une très grande précision ce

qui a effectivement permis de détruire cette instabilité. Pour autant la méthode utilisée ne peut se généraliser à des écoulements physiquement bi-dimensionnels.

Le couplage mis en cause et la nature rotationnelle de l'écoulement parasite mettent directement en cause un des ingrédients majeurs de notre algorithme à savoir l'utilisation d'une méthode de projection. Ainsi nous proposons comme perspective d'étude de développer un algorithme basé sur une formulation de type vorticité.

VIII.4 Conclusion

Nous avons montré à l'aide de résolutions numériques que le modèle de champ de phase développé peut aisément se résoudre à l'aide d'algorithmes simples. Ces algorithmes utilisent une écriture linéarisée de certains termes afin de diminuer les temps de calcul. Nous nous sommes assurés que la physique du changement de phase ainsi que de l'écoulement diphasique ne s'en trouve pas affectée. En particulier nous avons observé une bonne cohérence entre les profils numériques des variables principales du modèle et leurs analogues analytiques qui ont été démontré au chapitre précédent. Malheureusement nous n'avons pas pu mettre au point d'algorithme permettant la résolution d'un écoulement anisotherme bi-dimensionnel. Nous avons néanmoins analysé la cause de cette limitation ; elle provient d'une instabilité numérique provoquée par le couplage, *via* la méthode de projection, entre la dynamique de changement de phase et le terme de force capillaire. Ainsi nous avons proposé comme perspective l'utilisation d'une approche basée sur une formulation de type vorticité.

IX Conclusion et perspectives

L'étude des phénomènes prépondérants au sein des écoulements bouillants et plus particulièrement près des conditions de crise d'ébullition reste un problème scientifique d'actualité. Ainsi le mécanisme de la crise d'ébullition demeure aujourd'hui encore largement mal compris et ce malgré plus de soixante-dix années de recherche. Afin d'analyser le niveau de compréhension du phénomène, nous avons proposé au chapitre 1 une analyse de la compréhension actuelle de la crise d'ébullition en considérant les différentes théories existant. Cette étude révèle un manque de connaissance expérimentale, et par conséquence de modèles, des mécanismes de base de l'ébullition nucléée à fort flux de chaleur. Des avancées dans ce domaine sont des pré-requis à toute tentative de modéliser la crise d'ébullition de manière réaliste. Néanmoins, parmi l'ensemble des points restant à éclaircir, nous avons pu identifier un mécanisme potentiellement relié à la crise d'ébullition : la *croissance "irrégulière" d'une bulle*. En effet, à fort flux de chaleur pariétal, une bulle attachée en paroi peut s'étaler le long de cette dernière plutôt que de s'en détacheret être ainsi à l'origine de l'assèchement d'une paroi chaude, ce dernier déclenchant la transition de régime d'ébullition. La croissance, l'étalement et le détachement d'une bulle en paroi sont gouvernés par la courbure locale de la forme de la bulle ainsi que par les transferts de masse, quantité de mouvement et d'énergie localisés à l'interface. Par conséquent, la simulation numérique est l'outil le plus pertinent pour réaliser l'étude de cette dynamique de croissance de bulle. Notons que les compressibilités des phases vapeur et liquide ne sont pas considérés comme des mécanismes fondamentaux en ce qui concerne la dynamique d'étalement. Ainsi il est envisageable de supposer ces phases comme incompressibles. Cette hypothèse induit une simplification du traitement numérique des équations du mouvement, simplification dont nous souhaitons bénéficier.

Au chapitre 2 nous étudions les méthodes numériques existantes à même d'étudier les écoulements bouillants. Nous portons alors notre attention vers les méthodes dites d'interface diffuse. Ces méthodes sont basées sur une modélisation de l'interface comme une zone de transition volumique au travers de laquelle l'ensemble des variables physiques sont continues. Ainsi le système d'équations du mouvement, valable en tout point de l'espace, décrit de manière thermodynamiquement cohérente la dynamique des interfaces. Cette zone de transition devant être résolue par quelques éléments du maillage il est nécessaire que l'épaisseur de l'interface soit un paramètre libre dans la modélisation, tout paramètre physique de la description du système liquide vapeur étant donné. Il a été montré que le modèle de van der Waals, qui est le modèle à interface diffuse classiquement dédié à la description de la transition de phase liquide-vapeur, n'offre pas cette souplesse. Les modèles à interface diffuse de type de champ de phase sont largement utilisés pour la simulation numérique de la transition de phase solide-liquide. Le principe de cette modélisation repose sur l'introduction d'une variable de description thermodynamique abstraite du système, nommément le champ de phase. Grâce à cette formulation, il est possible de régulariser la zone interfaciale indépendamment (et donc artificiellement) de la description de la physique de la transition de phase. Nous avons montré que les modèles de champ de phase existants ne sont pas adaptés à l'étude de la transition de phase liquide-vapeur à l'échelle de la croissance de bulle. Nous proposons par la suite une formulation de champ de phase plus adéquate.

Au chapitre 3, nous avons développé la partie thermodynamique de notre modèle de champ de phase. Nous avons tout d'abord montré comment, grâce à l'hypothèse de quasi-compressibilité introduite initialement par Lowengrub and Truskinovsky [89], on modélise la transition entre deux phases de masse volumique différente bien que toutes deux incompressibles. Nous avons alors étudié l'introduction de la variable champ de phase dans une description thermodynamique. Nous avons précisé son rôle : la variable de champ de phase n'a d'autre signification que de varier à la traversée de l'interface et nous supposons alors *(i)* qu'elle prend une valeur caractéristique et arbitraire au sein des phases et *(ii)* qu'elle varie continûment entre ces deux valeurs à la traversée de l'interface. Nous avons alors exprimé analytiquement ces différentes propriétés en étudiant les conditions d'équilibre d'un fluide de type champ de phase. Ces dernières comprennent une relation supplémentaire (par rapport aux relations d'équilibre classiques) qui assure la nullité de la dérivée variationnelle de l'enthalpie libre massique par rapport à la variable champ de phase φ. Nous avons proposé une fermeture thermodynamique permettant de satisfaire les contraintes que l'on impose au modèle. L'écriture de l'enthalpie libre se base sur l'interpolation des enthalpies libres des phases liquide et vapeur par une fonction non linéaire de la variable φ (*cf.* (III.18)). Cette fonction d'interpolation est à la base de notre modèle de champ de phase. La formulation retenue comprend en plus de cette interpolation des enthalpies libres phasiques une partie dédiée à la description de la structure de l'interface à l'équilibre plan ; cette partie s'exprime comme le produit par le volume spécifique de la somme d'une fonction double-puits en la variable φ et d'une dépendance en $(\nabla\varphi)^2$. Cette expression pour l'enthalpie libre permet de satisfaire la propriété suivante : l'épaisseur de l'interface à l'équilibre plan est

indépendante des paramètres physiques (*i.e.* en particulier les conditions d'équilibre, en l'occurrence la courbe de saturation, la masse volumique des phases ainsi que leur capacité calorifique ou bien le coefficient de tension de surface) ce qui était un des buts recherchés. Nous avons étudié au chapitre 6 la stabilité des états d'équilibre homogènes et nous avons montré qu'il est nécessaire que la fonction d'interpolation satisfasse à 6 conditions analytiques (polynôme de degré 5) pour contrôler les propriétés physiques des phases liquide et vapeur qui sont associées à des valeurs fixes de φ. Ces valeurs son en outre les seules qui correspondent à des états monophasiques inconditionnellement stables à toute perturbation (stabilité linéaire). Cette propriété ne peut pas être satisfaite par des polynômes de degré inférieur à 5. En outre nous avons montré qu'il est possible de reproduire une valeur physique de la limite de métastabilité en choisissant de manière adéquate la fonction d'interpolation de degré 5. Cette étude de la modélisation thermodynamique de type champ de phase a permis d'associer un sens clair à chaque élément du potentiel thermodynamique, et finalement de pouvoir aisément maîtriser les propriétés en résultant.

Nous avons alors étudié l'équilibre d'inclusions sphériques au chapitre 4. L'expression particulière de notre modèle permet à l'équation d'équilibre sous hypothèse de symétrie sphérique d'être suffisamment simple pour en déduire des solutions analytiques approchées. Nous avons montré que le modèle discontinu équivalent à notre formulation diffuse est cohérent avec la relation de Laplace tant que le rayon de l'inclusion est 4 fois supérieur à l'épaisseur de l'interface à l'équilibre plan. Ce résultat est satisfaisant pour les études envisagées et ceci montre que le modèle propose effectivement une régularisation thermodynamiquement cohérente de la formulation discontinue. Lorsque le rayon de l'inclusion devient inférieur à l'épaisseur caractéristique de l'interface, la tension de surface associée à l'interface ainsi que le saut de pression à sa traversée tendent vers zéro. Cette décroissance du saut de pression permet au modèle de prendre en compte les apparitions/disparitions d'inclusions, ce qui n'est pas possible à l'aide de la formulation discontinue classique. Notons que nous avons mis en évidence que la description des inclusions de faible rayon est sensible au choix fait pour la fonction d'interpolation.

Le système d'équations de la dynamique du fluide correspondant à notre modèle thermodynamique a été démontré au chapitre 5. Cette démonstration a été réalisée en deux étapes. Dans un premier temps nous avons étudié formellement un modèle champ de phase pour une thermodynamique compressible et isotherme. A l'aide du principe fondamental de d'Alembert-Lagrange nous avons déduit la forme conservative du système d'équations du mouvement. Nous avons ainsi pu identifier la partie capillaire du tenseur des contraintes et déduire une expression pour le travail des efforts conservatifs. Dans un deuxième temps, nous avons utilisé les résultats précédents lors de l'application des principes fondamentaux de la thermodynamique. Ceci nous a permis de déduire le système d'équations du mouvement pour notre modèle quasi-compressible et anisotherme. Outre les mécanismes de dissipation de conduction de type Fourier et de viscosité de type Newton, le modèle prend en compte un mécanisme de relaxation de type Ginzburg-Landau vers la condition d'équilibre additionnelle de notre modèle champ de phase. Ce mécanisme permet d'introduire une cinétique propre à la variable champ de phase, cinétique qui a été étudiée au chapitre 7. Par conséquent, le système d'équations se compose des équations de bilan de masse, quantité de mouvement, d'entropie et d'une équation non-classique de type Allen-Cahn (*cf.* le système d'équations (V.34)). Nous avons alors démontré une écriture des équations du mouvement contenant un nombre réduit de non-linéarités et reproduisant l'ensemble des phénomènes majeurs de la dynamique de croissance d'une bulle.

Le chapitre 7 a été consacré à l'étude des solutions hors équilibre. Dans un premier temps nous avons proprement introduit le formalisme de la relation cinétique pour un modèle discontinu équivalent à notre formulation. Nous avons montré en particulier que les relations hors équilibre de type Gibbs-Thomson et Clapeyron généralisées peuvent être aisément reliées au modèle de type "croissance normale" pour la création d'entropie interfaciale. Nous avons alors étudié la situation hors-équilibre d'une transition de phase de type onde progressive mono-dimensionnelle à l'aide de développements asymptotiques raccordés, les solutions étant apprchées par des développements limités en le petit paramètre donné par le rapport entre l'épaisseur caractéristique de l'interface et la longueur caractéristique de la région extérieure. Les profils des variables principales au sein de la région intérieure aux premier et second ordre en ce paramètre ont été montrés ainsi que la relation cinétique correspondante permettant une analyse claire de ces résultats : elle satisfait la théorie de "croissance normale" valable pour des faibles déséquilibres, la relaxation de Ginzburg-Landau constituant le mécanisme dissipatif dominant. Aux ordres supérieurs le saut de température n'est plus nul ce qui est associé à une dissipation de type conductive au sein de la zone interfaciale. Nous avons en outre établi qu'un tel résultat est lié au choix particulier fait classiquement pour l'échelle de la mobilité qui est le coefficient dissipatif de la relaxation de Ginzburg-Landau, un

choix différent modifie la relation cinétique qui n'est plus cohérente avec la théorie de "croissance normale" qu'à la limite des faibles transferts de masse et s'en écarte pour des situations plus franchement hors équilibre, ce qui est physiquement satisfaisant.

Le chapitre 8 fut dédié à la résolution numérique du système d'équations du mouvement. Le but est de développer un algorithme de résolution permettant de prendre en compte les couplages essentiels de notre modèle entre thermique, mécanique et dynamique de champ de phase. Nous avons présenté des algorithmes à même de résoudre ces couplages dans deux cas simplifiés à savoir les cas *(i)* à masse volumique uniforme (sans écoulement) et *(ii)* isotherme. Ces algorithmes sont basés sur une linéarisation de l'avancée en temps de certains termes de couplage ce qui permet d'obtenir des résultats précis en un temps de calcul raisonnable. Les résultats obtenus sont cohérents avec les résultats analytiques obtenus précédemment. En outre nous avons validé qualitativement des simulations bidimensionnelles. Ces résultats prouvent la capacité du modèle à être utilisé comme base d'une méthode numérique. Un algorithme de résolution du système complet a été déduit de ces études préliminaires. Cet algorithme permet effectivement de résoudre une dynamique de changement de phase comme l'attestent les résultats obtenus pour un système mono-dimensionnel. Néanmoins des instabilités numériques s'établissent dès lors que le système étudié est bidimensionnel. Ces instabilités ne nous ont pas permis d'étudier des dynamiques de bulles non-isothermes. Nous avons analysé l'origine de ces instabilités et montré leur origine purement numérique mais n'avons pas pu les passer outre.

L'ensemble de cette étude doit être vu comme une tentative d'utiliser les modèles de champ de phase pour l'étude des phénomènes d'ébullition. Cette étude propose dans un premier temps une justification claire de la nécessité de l'utilisation de la simulation numérique afin d'améliorer notre connaissance des écoulements bouillants et plus particulièrement du phénomène de crise d'ébullition. En outre elle a permis d'identifier clairement les phénomènes primordiaux qu'une telle méthode se doit de reproduire. Dans un deuxième temps nous avons développé un modèle de type interface diffuse utilisant un ensemble de paramètres et de fonctions au rôle clairement identifié et permettant notamment *(i)* de reproduire les caractéristiques principales des écoulements bouillants tout en *(ii)* contrôlant les caractéristiques de la zone de transition interfaciale. Dans cette étude nous avons porté une attention particulière aux conséquences de l'introduction d'une variable de type champ de phase dans le modèle thermodynamique sur la description de la transition de phase liquide-vapeur. Nous avons aussi produit une analyse détaillée du modèle discontinu équivalent, ce qui a permis de montrer que notre modèle propose une régularisation thermodynamiquement cohérente du modèle discontinu classique avec des phases incompressibles. Finalement notre étude numérique, bien qu'infructueuse sur la fin, a permis de déterminer les principales étapes de résolution du système complet, et d'envisager ainsi l'étude numérique des écoulements bouillants.

Notre étude a révélé que la connaissance des phénomènes d'ébullition prenant place dans une région très proche de la paroi et en des conditions de fort flux pariétal est primordiale en vue d'accroître notre niveau de compréhension des mécanismes fondamentaux de la crise d'ébullition. L'observation expérimentale de ces phénomènes proche paroi (où nucléation et croissance de bulle se produisent) dans des conditions proches du flux critique devraient apporter une information sur l'origine exacte des crises d'assèchement telles qu'observées dans [130] et qui sont des événements précurseurs de la crise d'ébullition elle-même. Cette remarque suggère l'utilisation de techniques expérimentales permettant l'observation simultanée de la nature des contacts fluide/paroi (en utilisant une caméra infrarouge par exemple), et de la dynamique de croissance de bulle (en utilisant une visualisation latérale).

Notre étude des méthodes numériques a distingué deux catégories de méthodes de résolution d'un problème à frontière libre permettant un suivi implicite de l'interface : les méthodes dites "level-set", basées sur une modélisation de type discontinue, et les modèles d'interface diffuse, famille à laquelle notre modèle appartient. Or on peut considérer que la variable de champ de phase est similaire à la variable indicatrice de phase, ou fonction couleur, utilisée dans les méthodes "level set". Ceci permet d'introduire un premier lien formel entre les deux familles de méthodes. Il est intéressant alors de souligner que les équations de relaxation de la fonction distance, classiquement utilisées dans les méthodes level set, ont de grandes similarités avec notre équation d'Allen-Cahn. Dans une étude des méthodes numériques pour la résolution de modèles à interface diffuse de type champ de phase, Glasner [57] propose ainsi de travailler sur une fonction de type distance plutôt que directement sur la variable champ de phase. Ce changement de variable rapproche encore plus les deux formalismes. De

notre point de vue il serait bénéfique pour les deux familles de méthode d'étudier plus en profondeur le lien formel qui les relie afin de conjuguer les avantages réciproques.

Le modèle champ de phase développé dans cette étude a été délibérément dédié à la description de phases incompressibles. Pour autant il est nombre de situations physiques pour lequel cette hypothèse ne serait pas justifiée. A ce titre il serait de tout premier intérêt d'étudier une formulation prenant en compte la compressibilité des phases. La formulation quasi-compressible que nous proposons serait alors une réduction naturelle de cette formulation. Nous pensons que la base de cette formulation compressible devrait s'écrire comme une interpolation des équations d'état des phases. Notons que, dès lors que la compressibilité est non nulle, l'enthalpie libre n'est plus linéaire en pression. Les conséquences de cette non linéarité sur le contrôle des propriétés de régularisation (profil des variables à la traversée de la zone interfaciale) devra plus particulièrement être étudiée. Il est intéressant de souligner que notre modèle, puisque considérant les phases comme incompressibles peut s'appliquer à l'étude de la transition de phase solide-liquide avec convection. De manière plus générale, il serait intéressant d'étudier dans quelle mesure la structure de notre modèle champ de phase peut être utilisée pour différents systèmes multi-phasiques ou multi-composants d'équations d'état arbitraires. En particulier, le cas des fluides non miscibles semble suffisamment similaire à notre cas si on établit un parallèle entre notre équation d'entropie et une équation de diffusion de masse.

La relation cinétique de notre modèle a été déduite en utilisant la méthode des développements asymptotiques. Cette méthode permet d'obtenir des solutions analytiques approchées pour une transition de phase mono-dimensionnelle dans la limite où le petit paramètre considéré tend vers zéro. Il serait intéressant d'étudier cette relation cinétique plus systématiquement en utilisant une résolution numérique par exemple.

Il est important de noter que la fonction d'interpolation utilisée dans la formulation thermodynamique de note modèle joue un rôle important en ce qui concerne l'équilibre des inclusions sphériques. Lorsqu'elle n'est pas choisie comme un polynôme de degré 5, le rayon discontinu équivalent diverge quand la masse équivalente de l'inclusion tend vers zéro (*cf.* section IV.4). Par conséquent cette dernière caractéristique n'est nullement associée aux méthodes d'interface diffuse en général bien qu'elle se retrouve dans une majorité de modèles. Une meilleure compréhension de l'origine de ce phénomène passe ainsi par une étude de l'influence qu'a la fonction d'interpolation sur l'équation d'équilibre sous hypothèse de symétrie sphérique. Concernant toujours l'influence de la fonction d'interpolation sur les propriétés du modèle, nous avons introduit une manière d'introduire dans le modèle une limite de métastabilité phénoménologique (*cf.* section VI.6). Nous avons montré que pour obtenir cette propriété, il est suffisant d'utiliser un polynôme de degré 5 dont les coefficients dépendent de l'épaisseur de l'interface. Ainsi le modèle champ de phase possède une propriété supplémentaire intéressante par rapport au modèle discontinu équivalent. Il serait alors nécessaire d'étudier les conséquences de ce choix sur les autres propriétés du modèle pour s'assurer qu'elles sont conservées.

La méthode de projection est couramment utilisée dans les méthodes numériques dédiées à l'étude des écoulements diphasiques, même en présence de changement de phase, dès lors que les phases sont incompressibles. Néanmoins, notre étude numérique a montré que l'utilisation de cette méthode pour l'étude de transition de phase bidimensionnelles en présence de phénomènes capillaires, est à l'origine de difficultés numériques importantes. Ainsi pour ce type d'écoulement, il serait intéressant de développer un algorithme utilisant une méthode de résolution alternative pour le couplage bilan de quantité de mouvement, bilan de masse. On peut notamment penser à l'utilisation de méthodes basées sur une formulation en vorticité. Une autre perspective serait d'utiliser une simplification des termes non-linéaires des équations. Sacrifiant ainsi à la cohérence thermodynamique des équations, il est possible d'envisager un gain sur le plan de la résolution numérique. Cette approche pragmatique a d'ores et déjà été mise en pratique pour d'autre modèles de champ de phase, *e.g.* Karma and Rappel [73].

Bibliography

[1] R.F. Almgren. Second-order phase-field asymptotics for unequal conductivities. *SIAM J. Appl. Math.*, 59: 2086–2107, 1999.

[2] D. M. Anderson, P. Cermelli, E. Fried, M.E. Gurtin, and G.B. McFadden. General dynamical sharp-interface conditions for phase transformations in viscous heat-conducting fluids. *submitted to J. Fluid Mech.*

[3] D.M. Anderson and S.H. Davis. Local fluid and heat flow near contact lines. *J. Fluid Mech.*, 268:231–265, 1994.

[4] D.M. Anderson, G.B. McFadden, and A.A. Wheeler. Diffuse-interface models in fluid mechanics. *Ann. Rev. Fluid Mech.*, 30:139–165, 1998.

[5] D.M. Anderson, G.B. Mc Fadden, and A.A. Wheeler. A phase-field model of solidification with convection. *Physica D*, 135:175–194, 2000.

[6] D.M. Anderson, G.B. Mc Fadden, and A.A. Wheeler. A phase-field model with convection: sharp-interface asymptotics. *Physica D*, 151:305–331, 2001.

[7] H. Auracher and W. Marquardt. Heat transfer characterisitcs and mechanisms along entire boiling curves under steady-state and transient conditions. *Int. J. Heat Fluid Flow*, 25:223–242, 2004.

[8] V.E. Badalassi, H.D. Ceniceros, and S. Banerjee. Computation of multiphase system with phase field models. *J. Comp. Physics*, 190:371–397, 2003.

[9] I.C. Bang, S.H. Chang, and W.-P. Baek. Visualization of the subcooled flow boiling of R-134a in a vertical rectangular channel with an electrically heated wall. *Int. J. Heat and Mass Transfer*, 47:4349–4363, 2004.

[10] P. Bates and F. Chen. Periodic traveling waves for a non-local integro-differential model. *Electronic J. of Differential Equations*, 26:1–19, 1999.

[11] C. Beckermann, H.-J. Diepers, I.Steinbach, A. Karma, and X. Tong. Modeling melt convection in phase-field simulations of solidification. *J. Comp. Physics*, 154:468–496, 1999.

[12] R.J. Benjamin and A.R. Balakrishnan. Nucleation site density in pool boiling of saturated pure liquids: effect of surface microroughness and surface and liquid physical properties. *Exp. Thermal and Fluid Science*, 15:32–42, 1997.

[13] S. Benzoni-Gavage, R. Danchin, S. Descombes, and D. Jamet. Structure of Korteweg models and stability of diffuse interfaces. *Interfaces Free Boundaries*, 7:371–414, 2005.

[14] G. Berthoud. Etude du flux critique en chauffage transitoire. Technical Note DEN/DTN/SE2T/2006-01, CEA, 2006.

[15] A.L. Biance, C. Clanet, and D. Quéré. Leidenfrost drops. *Phys. Fluids*, 15(6):1632–7, 2003.

[16] J. Blum, T. Lüttich, and W. Marquardt. Temperature wave propagation as a route from nucleate to film boiling. In G.P. Celata, P. Di Marco, and R.K. Shah, editors, *2nd Internatinal Symposium on two-phase flow modelling and experimentation*, volume 1, pages 137–144. Edizioni ETS, Pisa, 1999.

[17] W.J. Boettinger, J.A. Warren, C. Beckermann, and A. Karma. Phase-field simulation of solidification. *Annual Review of Materials Research*, 32:163–194, 2002.

[18] J. U. Brackbill, D. B. Kothe, and C. Zemach. A continuum method for modeling surface tension. *J. Comput. Phys.*, 100(2):335–354, 1992. ISSN 0021-9991. doi: http://dx.doi.org/10.1016/0021-9991(92)90240-Y.

[19] P. Bricard. Modélisation du mécanisme de crise d'ébullition par assèchement d'un site de nucléation. Technical Report 96NB00119, EDF, 1996.

[20] P. Bricard, P. Péturaud, and J.M. Delhaye. Understanding and modelling DNB in forced convective boiling: Modelling of a mechanism based on nucleation site dryout. *Multiphase Science and Technology*, 9:329–379, 1997.

[21] M. Buchholz, T. Lüttich, H. Auracher, and W. Marquardt. Experimental investigation of local processes in pool boiling along the entire boiling curve. *Int. J. Heat Fluid Flow*, 25:243–261, 2004.

[22] YU.A. Buyevich and B.W. Webbon. Dynamics of vapour bubbles in nucleate boiling. *Int. J. Heat and Mass Transfer*, 39(12):2409–2426, 1996.

[23] G. Caginalp. Dynamical renormalization group calculation of a two-phase sharp interface model. *Physical Review E*, 6:R6267–R6270, 1999.

[24] G. Caginalp and E.A. Socolovsky. Computation of sharp phase boundaries by spreading: the planar and spherically symmetric cases. *J. Comput. Phys.*, 95:85–100, 1991.

[25] J.W. Cahn. On spinodal decomposition. *Acta Mettalurgica*, 9:795–801, 1961.

[26] J.W. Cahn and J.E. Hilliard. Free energy of a nonuniform system. I. interfacial free energy. *J. Chemical Physics*, 28(2):258–267, 1958.

[27] I. Calmet and J. Magnaudet. Large-eddy simulation of high-schmidt number mass transfer in a turbulent channel. *Phys. Fluids*, 9(2):438–455, 1997.

[28] Van P. Carey. *Liquid-vapor phase-change phenomena*. Taylor and Francis, 1992.

[29] F. Caro. *Modélisation et simulation numérique des transitions de phase liquide-vapeur*. Thèse de doctorat, Ecole Polytechnique, 2004.

[30] G.P. Celata. Critical heat flux in subcooled flow boiling. *Heat and Technology*, 16(1):11–27, 1998.

[31] G.P. Celata, M. Cumo, A. Mariani, and G. Zummo. Visual investigation of boiling crisis in subcooled flow boiling. *The Arabian Journal for Science and Engineering*, 27(2C):67–89, 2002.

[32] Y-P Chang. Some possible critical conditions in nucleate boiling. *J. Heat Transfer, transactions of the ASME*, May:89–100, 1963.

[33] C. Charach and P.C. Fife. On thermodynamically consistent schemes for phase field equations. *Open Systems and Information Dynamics*, 5:99–123, 1998.

[34] C. Charach, C.K. Chen, and P.C. Fife. Developments in phase-field modeling of thermoelastic and two-component materials. *J. Stat. Physics*, 95:1141–1164, 1999.

[35] R. Chella and J. Viñals. Mixing of a two-phase fluid by cavity flow. *Physical Review E*, 53(4):3832–3840, 1996.

[36] H-Y Chen, D. Jasnow, and J. Viñals. Interface and contact-line motion in a two phase fluid under shear flow. *Physical Review letters*, 85(8):1686–1689, 2000.

[37] H.J. Chung and H.C. No. Simultaneous visualization of dry spots and bubbles for pool boiling of r-113 on a horizontal heater. *Int. J. Heat and Mass Transfer*, 46:2239–2251, 2003.

[38] M. Conti. Density change effects on crystal growth from the melt. *Physical Review E*, 64:051601, 2001.

[39] M. Conti. Pressure effects for crystal growth in a closed system. *Physical Review E*, 70:031602, 2004.

[40] M.G. Cooper and A.J.P. Lloyd. The microlayer in nucleate boiling. *Int. J. Heat Mass Transfer*, 12: 895–913, 1969.

[41] A. Danescu. Generalized stefan models accounting for a discontinuous temperature field. *Continuum Mech. Thermodyn.*, 16:427–439, 2004.

[42] J.M. Delhaye. Jump conditions and entropy sources in two-phase systems. Local instant formulation. *Int. J. Multiphase Flow*, 1:395–409, 1974.

[43] F. Dell'Isola, H. Gouin, and G. Rotoli. Nucleation of spherical shell-like interfaces by second gradient theory: numerical simulations. *Eur. J. Mech. B/Fluids*, 15(4):545–568, 1996.

[44] F. Demiray and J. Kim. Heat-transfer from a single nucleation site during saturated pool boiling of fc-72 using an array of 100 micron heaters. In *Proceedings of the AIAA/ASME Thermophysics and heat transfer conference, St. Louise, M.O.*, June 2002.

[45] V.K. Dhir. Boiling heat transfer. *Ann. Rev. Fluid Mech.*, 30:365–401, 1998.

[46] D.A. Edwards, H. Brenner, and D.T. Wasan. *Interfacial transport processes and rheology*. Butterworth-Heinemann, 1991.

[47] H. Emmerich. *The diffuse interface approach in material science. Thermodynamic concepts and applil-cations of phase-field models*. Springer,Berlin, 2003.

[48] D. Enright, R. Fedkiw, J. Ferziger, and I. Mitchell. A hybrid particle level set method for improved interface capturing. *J. Comp. Phys.*, 183:83–116, 2002.

[49] G.B. Mc Fadden, A.A. Wheeler, and D.M. Anderson. Thin interface asymptotics for an energy/entropy approach to phase-field models with unequal conductivities. *Physica D*, 144:154–168, 2000.

[50] M.P. Fiori and A.F. Bergles. Model of critical heat flux in subcooled flow boiling. In *Proceedings of the 4th Heat Transfer Conference, Versailles*, volume 9, 1970.

[51] R. Folch, J. Casademunt, A. Hernández-Machado, and L. Ramírez-Piscina. Phase-field model for Hele-Shaw flows with arbitrary viscosity contrast. I. Theoretical approach. *Physical Review E*, 60(2):1724–1733, 1999.

[52] R. Folch, J. Casademunt, A. Hernández-Machado, and L. Ramírez-Piscina. Phase-field model for Hele-Shaw flows with arbitrary viscosity contrast. II. Numerical study. *Physical Review E*, 60(2):1734–1740, 1999.

[53] C. Fouillet. *Généralisation à des mélanges binaires de la méthode du second gradient et application à la simulation numérique directe de l'ébullition nucléée*. Thèse de doctorat, Université Paris VI, 2003.

[54] C. Fouillet and D. Jamet. Generalization of the second gradient method to binary mixtures and investigation of the direct numerical simulation of nucleate boiling flows. In *Proceedings of the 11th international topical meeting on nuclear thermal-hydraulics (NURETH 11)*, number 364, October 2005.

[55] W. Fritz. Berechnung des maxiamlvolume von dampfblasen. *Phys. Z.*, 36:379–388, 1935.

[56] Gaertner. Photographic study of nucleate pool boiling on a horizontal surface. *J. Heat Transfer, transactions of the ASME*, 65(02):17–29, 1965.

[57] K. Glasner. Nonlinear preconditioning for diffuse interfaces. *J. Comp. Physics*, 174:695–711, 2001.

[58] S.J. Ha and H.C. No. A dry-spot model of critical heat flux applicable to both pool boiling and subcooled forced convection boiling. *Int. J. Heat and Mass Transfer*, 43:241–250, 2000.

[59] S.J. Ha and H.C. No. A dry-spot model of critical heat flux in pool boiling and forced convection boiling. *Int. J. Heat and Mass Transfer*, 41(2):303–311, 1997.

[60] Y. He, M. Shoji, and S. Maruyama. Numerical study of high heat flux pool boiling heat transfer. *Int. J. Heat and Mass Transfer*, 44:2357–2373, 2001.

[61] T. Hibiki and M. Ishii. Active nucleation site density in boiling systems. *Int. J. Heat and Mass Transfer*, 46:2587–2601, 2003.

[62] D. Jacqmin. Contact-line dynamics of a diffuse fluid interface. *J. Fluid Mech.*, 402:57–88, 2000.

[63] D. Jacqmin. Calculation of two-phase navier-stokes flows using phase-field modeling. *J. Comp. Physics*, 155:96–127, 1999.

[64] Jakob. *Heat transfer part 1*. John Wiley NY, 1950.

[65] D. Jamet. A solid-liquid diffuse interface model based on an entropy order parameter. *in preparation*.

[66] D. Jamet. *Etude des potentialités de la théorie du second gradient pour la simulation numérique directe des écoulements liquide-vapeur avec changement de phase*. Thèse de doctorat, Ecole Centrale Paris, 1998.

[67] D. Jamet, O. Lebaigue, N. Coutris, and J.M. Delhaye. The second gradient method for the direct numerical simulation of liquid-vapor flows with phase change. *J. Comp. Physics*, 169:624–651, 2001.

[68] D. Jamet, D. Torres, and J.U. Brackbill. On the theory and computation of surface tension: the elimination of parasitic currents through energy conservation in the second-gradient method. *J. Comp. Physics*, 182: 262–276, 2002.

[69] D. Juric and G. Tryggvason. Computations of boiling flows. *Int. J. Multiphase Flow*, 24(3):387–410, 1998.

[70] S.G. Kandlikar. A theoretical model to predict pool boiling CHF incorporating effects of contact angle and orientation. *J. Heat Transfer, transactions of the ASME*, 123:1071–1079, 2001.

[71] S.G. Kandlikar and M.E. Steinke. Contact angles and interface behavior during rapid evaporation of liquid on a heated surface. *Int. J. Heat and Mass Transfer*, 45:3771–3780, 2002.

[72] A. Karma and W.-J. Rappel. Phase-field method for computationnaly efficient modeling of solidification with arbitrary interface kinetics. *Physical Review E*, 53(4):R3017–R3019, 1996.

[73] A. Karma and W.-J. Rappel. Quantitative phase-field modeling of dendritic growth in two and three dimensions. *Physical Review E*, 57(4):4323–4349, April 1998.

[74] Y. Katto. Critical heat flux. *Int. J. Multiphase Flow*, (20 Suppl.):53–90, 1994.

[75] Y. Katto and S. Otokuni. Behavior of vapor masses on a vertical flat surface of comparatively large height near critical heat flux conditions in saturated pool boiling. *Int. J. Heat and Mass Transfer*, 37:255–263, 1994.

[76] D.B.R Kenning. Optical studies of boiling heat transfer: insights and limitations. *Int. J. Heat Fluid Flow*, 25:209–222, 2004.

[77] J. Kim, K. Kang, and J. Lowengrub. Conservative multigrid methods for Cahn-Hilliard fluids. *J. Comp. Physics*, 193:511–543, 2004.

[78] G.J. Kirby, R. Staniforth, and J.H. Kinneir. A visual study of forced convection boiling - part 2. Flow patterns and burnout for a round test section. Technical Report AEEW-R-506, Winfrith, 1967.

[79] N.I. Kolev. How accurately can we predict nucleate boiling? *Exp. Thermal and Fluid Science*, 10: 370–378, 1995.

[80] D.J. Korteweg. Sur la forme que prennent les équations du mouvement des fluides si l'on tient compte des forces capillaires causées par des variations de densité considérables mais continues et sur la théorie de la capillarité dans l'hypothèse d'une variation continue de la densité. *Arch. Néerl. Sci. Exactes Nat.*, 6:1–24, 1901.

[81] A.P. Krekhov and L. Kramer. Phase separation in the presence of spatially periodic forcing. *Physical Review E*, 70, 2004.

[82] S.S. Kutateladze. A hydrodynamic theory of changes in the boiling process under free convection conditions. *Izv. Akademia nauk Otledarie Tkh. (AEC-TR-1441)*, 4:529–536, 1951.

[83] H-G. Lee, J.S. Lowengrub, and J. Goodman. Modeling pinchoff and reconnection in a Hele-Shaw cell. I. The models and their calibration. *Phys. Fluids*, 14(2):492–513, 2002.

[84] J.G. Leidenfrost. On the fixation of water in diverse fire (first publication in 1756). *Int. J. Heat and Mass Transfer*, 9:1153–1166, 1966.

[85] H. Lemonnier, D. Jamet, and O. Lebaigue. *Validation of advanced computational methods for multiphase flow*. Begell House, 2005.

[86] J.H. Lienhard and V.K. Dhir. Hydrodynamic prediction of peak pool-boiling heat fluxes from finite bodies. *J. Heat Transfer, transactions of the ASME*, may:152–158, 1973.

[87] J.H. Lienhard and V.K. Dhir. Extended hydrodynamic theory of the peak and minimum pool boiling heat fluxes. CR 2270, NASA, 1973.

[88] X.-D. Liu, R. Fedkiw, and M.Kang. A boundary condition capturing method for Poisson's equation on irregular domains. *J. Comp. Phys.*, 160:151–178, 2000.

[89] J. Lowengrub and L. Truskinovsky. Quasi-incompressible Cahn-Hilliard fluids and topological transitions. *Proc. R. Soc. Lond. A*, 454:2617–2654, 1998.

[90] C.H.P. Lupis. *Chemical thermodynamics of materials*. North-Holland, New-York, 1983.

[91] B. Mathieu. *Etudes physique, expérimentale et numérique des mécanismes de base intervenant dans les écoulements diphasiques*. Thèse de doctorat, Université de Provence, 2003.

[92] B. Mathieu, O. Lebaigue, and L. Tadrist. Influence of a dynamic contatc line model on the characteristics of nucleate wall boiling computed with a dns approach. In *Proceedings of the 5th international conference on Multiphse flow, ICMF'04, Yokohama Japan*, number paper n°439, 2004.

[93] B.B. Mikic, W.M. Rohsenow, and P. Griffith. On bubble growth rates. *Int. J. Heat and Mass Transfer*, 13: 657–666, 1970.

[94] N. Moelans, B. Blanpain, and P. Wollants. A phase-field model for the simulation of grain growth in materials containing finely dispersed incoherent second-phase particles. *Acta Materialia*, 53:1171–1781, 2005.

[95] R. Moissis and P.J. Berenson. On the hydrodynamic transitions in nucleate boiling. *J. Heat Transfer, transactions of the ASME*, 85:221–229, 1963.

[96] S.A. Mokrushin. The boiling crisis in nucleate pool boiling of liquids. *Heat transfer Soviet Research*, 20 (1):65–68, 1988.

[97] B.T. Nadiga and S. Zaleski. Investigations of a two-phase fluid model. *Euro. J. Mech. B/Fluid*, 15(2): 885–896, 1996.

[98] B. Nestler, A. Wheeler, L. Ratke, and C. Stöcker. Phase-field model for solidification of a monotectic alloy with convection. *Physica D*, 141:133–154, 2000.

[99] S-H Ngan and L. Truskinovsky. Thermal trapping and kinetics of martensitic phase boundaries. *Mechanics and Physics of Solids*, 47:141–172, 1999.

[100] V. S. Nikolayev, D. A. Beysens, G.-L. Lagier, and J. Hegseth. Growth of a dry spot under a vapor bubble at high heat flux and high pressure. *Int. J. Heat and Mass Transfer*, 44:3499–3511, 2001.

[101] V.S. Nikolayev and D.A. Beysens. Boiling crisis and non-equilibirum drying transition. *Europhysics Letters*, 47(3):345–351, 1999.

[102] S. Nishio, T. Gotoh, and N. Nagai. Observation of boiling structures in high heat-flux boiling. *Int. J. Heat and Mass Transfer*, 41:3191–3201, 1998.

[103] S. Nukiyama. The maximum and minimum values of the heat Q transmitted from metal to boiling water under atmospheric pressure (english translation of the original paper published in Journal Japan Soc. Mech. Engrs vol. 37 ,367-374 (1934)). *Int. J. Heat and Mass Transfer*, 9:1419–1433, 1966.

[104] A. Onuki. Dynamic van der Waals theory of two-phase fluids in heat flow. *Physical Review Letters*, 94: 054501, 2005.

[105] H. Paillere, C. Viozat, A. Kumbaro, and I. Toumi. Comparison of low Mach number models for natural convection problems. *Heat and mass transfer*, 36:567–573, 2000.

[106] H.J. Palmer. The hydrodynamic stability of rapidly evaporating liquids at reduced pressure. *J. Fluid Mech.*, 75:487–511, 1976.

[107] P. Papon and J. Leblond. *Thermodynamique des états de la matière*. Hermann, 1990.

[108] R.L. Pego. Front migration in the nonlinear Cahn-Hilliard equation. *Proc. Roy. Soc. Lond. A*, 422:261–278, 1989.

[109] O. Penrose and P.C. Fife. Thermodynamically consistent models of phase-field type for the kinetics of phase transitions. *Physica D*, 43:44–62, 1990.

[110] O. Penrose and P.C. Fife. On the relation between the standard phase-field model and a "thermodynamically consistent" phase-field model. *Physica D*, 69:107–113, 1993.

[111] Y. Pomeau. Recent progress in the moving contact line problem: a review. *C.R. Mécanique*, 330:207–222, 2002.

[112] T. Qian, X.-P. Wang, and P. Sheng. Molecular scale contact line hydrodynamics of immiscible flows. *Physical Review E*, 68, 2003.

[113] Y. Rocard. *Thermodynamique*. Masson Paris, 1967.

[114] A.B. Roshchin and L.M. Truskinovsky. Model of a weakly non-local relaxing compressible medium. *PMM U.S.S.R.*, 53(6):715–20, 1989.

[115] J.S. Rowlinson and B. Widom. *Molecular theory of capillarity*. Clarendon press, 1982.

[116] T.D. Rule and J. Kim. Heat transfer behavior on small horizonal heaters during pool boiling of FC-72. *J. Heat Transfer, transactions of the ASME*, 121:386–393, 1999.

[117] P. Sadavisan, C. Unal, and R. Nelson. Perspective : Issues in CHF modeling - The need for new experiments. *J. Heat Transfer, transactions of the ASME*, 117:558–567, 1995.

[118] A. Sakurai. Mechanisms of transitions to film boiling at CHFs in subcooled and pressurized liquids due to steady and increasing heat inputs. *Nuclear Eng. Design*, 197:301–356, 2000.

[119] R. Salmon. Hamiltonian fluid mechanics. *Ann. Rev. Fluid Mech.*, 20:225–256, 1988.

[120] K. Sefiane, D. Benielli, and A. Steinchen. A new mechanism for pool boiling crisis, recoil instability and contact angle influence. *Colloids surf.*, 142:361–373, 1998.

[121] P. Seppecher. *Etude d'une modélisation des zones capillaires fluides: interfaces et lignes de contact*. Thèse de doctorat, Université Paris VI, 1987.

[122] J. Serrin. *Mathematical Principles of Classical Fluid Dynamics*, volume VIII/1 of *Handbuch der Physik*. Springer-Verlag, Berlin,Gottingen, Heidelberg, 1959.

[123] J.A. Sethian. Evolution, implementation and application of level set and fast marching methods for advancing fronts. *J. Comp. Physics*, 169:503–555, 2001.

[124] Y.D. Shikhmurzaev. Moving contact lines in liquid/liquid/solid systems. *J. Fluid Mech.*, 334:211–249, 1997.

[125] Y.D. Shikhmurzaev. On the initial stage of the bubble growth on a plate. In *Proc. of the second int. symp. on two-phase flow modelling and experimentation*, volume 2, pages 907–914, 1999.

[126] S. Shin and D. Juric. Modeling three-dimensional multiphase flow using a level contour reconstruction method for front tracking without connectivity. *J. Comp. Phys.*, 180:427–470, 2002.

[127] M. Slemrod. Admissibility criteria for propagating phase boundaries in a van der waals fluid. *Arch. Nat. Mech. Anal.*, 81(4):301–315, 1983.

[128] G. Son, N. Ramanujapu, and V.K. Dhir. Numerical simulation of bubble merger process on a single nucleation site during pool nucleate boiling. *Int. J. Heat and Mass Transfer*, 124:51–62, 2002.

[129] K. Stephan. *Heat transfer in condensation and boiling*. Springer Verlag, 1992.

[130] T.G. Theofanous, T.N. Dinh, J.P. Tu, and A.T. Dinh. The boiling crisis phenomenon part I: nucleation and nucleate boiling heat transfer. *Exp. Thermal and Fluid Science*, 26:775–792, 2002.

[131] T.G. Theofanous, T.N. Dinh, J.P. Tu, and A.T. Dinh. The boiling crisis phenomenon part II: dryout dynamics and burnout. *Exp. Thermal and Fluid Science*, 26:793–810, 2002.

[132] G.E. Thorncroft, J.F. Klausner, and R. Mei. Bubbles forces and detachment models. *Multiphase Science and Technology*, 13(3 and 4):35–76, 2001.

[133] X. Tong, C. Beckermann, A. Karma, and Q. Li. Phase-field simulations of dendritic crystal growth in a forced flow. *Physical Review E*, 63, 2001.

[134] L. Truskinovsky. Equilibrium phase interfaces. *Sov. Phys. Dokl.*, 27(7):551–553, 1982.

[135] L. Truskinovsky. Critical nuclei in the van der waals model. *Sov. Phys. Dokl*, 28(3):248–250, 1983.

[136] L. Truskinovsky. Dynamics of non-equilibrium phase boundaries in the heat-conductive nonlinear elastic medium. *J. Appl. Math. & Mech. (PMM)*, 51(6):777–784, 1987.

[137] L. Truskinovsky. Nonequilibrium phase boundaries in the earth's mantle. *Dokl. Akad. Nauk. SSSR*, 303 (6):1337–1342, 1988.

[138] L. Truskinovsky. Kinks versus shocks. In J.E. Dunn, R. Fosdick, and M. Slemrod, editors, *Shock induced transitions and phase structure in general media*, pages 185–229. Springer-Verlag, 1993.

[139] L. Truskinovsky. About the "normal growth" approximation in the dynamical theory of phase transitions. *Cont. Mech. Thermodyn.*, 6:185–208, 1994.

[140] G. Tryggvason, B. Brunner, A. Esmaeeli, D. Juric, N. Al-Rahawi, W. Tauber, J. Han ans S. Has, and Y.-H. Jan. A front-tracking method for the computations of multiphase flow. *J. Comp. Phys.*, 204:708–759, 2001.

[141] A. Umantsev. Thermodynamic stability of phases and transition kinetics under adiabatic conditions. *J. Chemical Physics*, 96(1):605–617, 1992.

[142] J.D. van der Waals. Thermodynamische Theorie der Kapillarität unter Voraussetzung stetiger Dichteanderung. *Z. Phys. Chem.*, 13:657–725, 1894. Traduction française dans *Arch. Néerl. Sci. Exactes Nat.*, 28:121-209.

[143] M. van Dyke. *Perturbation methods in fluid mechanics*, chapter V. The method of matched asymptotic expansions. The parabolic press, Stanford,California, 1975.

[144] N.G. van Kampen. Condensation of a classical gas with long range attraction. *Physical Review*, 135: A362–A369, 1964.

[145] H.J. van Ouwerkerk. Burnout in pool boiling. the stability of boiling mechanisms. *Int. J. Heat and Mass Transfer*, 15:25–34, 1972.

[146] S.-L. Wang, R.F. Sekerka, A.A. Wheeler, B.T. Murray, S.R. Coriell, R.J. Braun, and G.B. McFadden. Thermodynamically-consistent phase-field models for solidification. *Physica D*, 69:189–200, 1993.

[147] S.W.J. Welch and J. Wilson. A volume of fluid based method for fluid flows withphase change. *J. Comp. Physics*, 160:662–682, 2000.

[148] J.W. Westwater and J.G. Santangelo. Photographic study of boiling. *Industrial and engineering chemistry*, 47(8):1605–1610, 1955.

[149] N. Yaddanapudi and J. Kim. Single bubble heat transfer in saurated pool boiling of FC-72. *Multiphase Science and Technology*, 12(3 and 4):47–63, 2000.

[150] V.V. Yagov. The mechanism of the pool boiling crisis. *Thermal Engineering*, 50(3):175–183, 2003.

[151] Z.L. Yang, T.N. Dinh, R.R. Nourgaliev, and B.R. Sehgal. Numerical investigation of bubble growth and detachment by the lattice-Boltzmann method. *Int. J. Heat and Mass Transfer*, 44:195–206, 2001.

[152] C.-L. Yu and R.B. Mesler. A study of nucleate boiling near the peak heat flux through measurements of transient surface temperature. *Int. J. Heat and Mass Transfer*, 20:827–840, 1977.

[153] P. Yue, J.J. Feng, C. Liu, and J. Shen. A diffuse-interface method for simulating two-phase flows of complex fluids. *J. Fluid Mech.*, 515:293–317, 2004.

[154] L. Zhang and M. Shoji. Nucleation site interaction in pool boiling on the artificial surface. *Int. J. Heat and Mass Transfer*, 46:513–522, 2003.

[155] Y.-H. Zhao, T. Masuoka, and T. Tsuruta. Unified theoretical prediction of fully developed nucleate boiling and critical heat flux based on a dynamic microlayer model. *Int. J. Heat and Mass Transfer*, 45:3189–3197, 2002.

[156] N. Zuber. On the stability of boiling heat transfer. *J. Heat Transfer, transactions of the ASME*, 80(2): 711–720, 1958.

[157] N. Zuber. Nucleate boiling. the region of isolated bubbles and the similarity with natural convection. *Int. J. Heat and Mass Transfer*, 6:53–78, 1963.

Résumé

Dans cette étude nous considérons l'ébullition en paroi sous les angles de la modélisation et de la simulation numérique. Dans un premier temps nous proposons une revue bibliographique au sujet du régime d'ébullition nucléée à fort flux de chaleur pariétal et analysons plus particulièrement la compréhension du phénomène de crise d'ébullition de type caléfaction. Nous en déduisons une motivation pour l'étude de la dynamique de croissance de bulle au moyen de la simulation numérique. L'essentiel du travail concerne alors le développement d'un modèle de type champ de phase pour l'étude des écoulements liquide-vapeur avec changement de phase. Nous proposons une fermeture thermodynamique quasi-compressible dont les propriétés sont adaptées aux simulations envisagées. Le système d'équations du mouvement qui s'en déduit constitue une régularisation thermodynamiquement cohérente de la description discontinue du système diphasique, ce qui est l'avantage des modèles à interfaces diffuses. Nous démontrons que la formulation retenue permet de définir l'épaisseur de la zone régularisée indépendamment de la description thermodynamique des phases, ce qui est intéressant numériquement. Nous établissons la relation cinétique et analysons ainsi la modélisation champ de phase des mécanismes dissipatifs. Finalement nous étudions la résolution numérique du modèle à l'aide de simulations de transition de phase en configuration simple et de dynamique de bulle en isotherme.

Mots-clé

Changement de phase liquide-vapeur, ébullition nucléée, simulation numérique, interface diffuse, champ de phase, quasi-compressible, crise d'ébullition.

Abstract

This study concerns both the modeling and the numerical simulation of boiling flows. First we propose a review concerning nucleate boiling at high wall heat flux and focus more particularly on the current understanding of the boiling crisis. From this analysis we deduce a motivation for the numerical simulation of bubble growth dynamics. The main and remaining part of this study is then devoted to the development and analyze of a phase field model for the liquid-vapor flows with phase change. We propose a thermodynamic quasi-compressible formulation whose properties match the one required fot the numerical study envizaged. The system of governing equations is a thermodynamically consistent regularization of the sharp interface model, that is the advantage of the diffuse interface models. We show that the thickness of the interface transition layer can be defined independently from the thermodynamic description of the bulk phases, a property that is numerically attractive. We derive the kinetic relation that allows to analyze the consequences of the phase field formulation on the model of the dissipative mechanisms. Finally we study the numerical resolution of the model with the help of simulations of phase transition in simple configurations as well as of isothermal bubble dynamics.

Keywords

Phase change, nucleate boiling, numerical simulation, diffuse interface, phase field, quasi-compressible, boiling crisis.